The Institute for Solid State Physics
The University of Tokyo

Activity Report 2022

Ⓒ 2023 The Institute for Solid State Physics, The University of Tokyo

ISSP

Activity Report
2022

Contents

	Pages
Preface	1
Research Highlights	2 - 33
Joint Research Highlights	34 - 51
Progress of Facilities	52 - 59
Conferences and Workshops	60 - 63
Publications	64 - 96
Subjects of Joint Research	97 - 149

Preface

We would like to present the annual activity report of the Institute for Solid State Physics (ISSP) for the academic year 2022. ISSP was established in 1957 as a joint usage/research institute affiliated with the University of Tokyo. In every era, we strive to lead the frontiers of condensed matter physics and materials science and contribute to the development of science and technology from a basic research perspective. In this report, we present a selection of research outcomes produced by ISSP members and other researchers from our community who participated in joint research programs.

The first section of the report includes 32 research highlights from ISSP groups, and the second section contains 16 highlights from joint research conducted by outside researchers with the assistance of ISSP members using the joint-use program. The third section details the development of the following facilities: Supercomputer Center, Neutron Science Laboratory, International MegaGauss Science Laboratory, Center of Computational Materials Science, Laser and Synchrotron Research Center, and Synchrotron Radiation Laboratory. The fourth section provides a summary of seven conferences/workshops held by ISSP in 2022. The publication and joint-use research topics lists conclude the document.

These activities demonstrate ISSP's position as the global center of excellence in condensed matter physics and materials science and we appreciate the ongoing support and cooperation of the community to continue our activities.

July 2023

HIROI Zenji
Director of the Institute for Solid State Physics
The University of Tokyo

Research Highlights

Ambipolar Nickel Dithiolene Complex Semiconductors: from One to Two-Dimensional Electronic Structures Based upon Alkoxy Chain Lengths

Mori and Ozaki Groups

Molecular semiconductors, which are mainly based on π-conjugated organic molecules are crucial materials in fundamental research and electronics because they are flexible, light-weight, and can be solution-processed in a cost-effective, energy-saving manner. Among them, materials that can transport both holes and electrons are required for next-generation devices, such as organic light-emitting transistors and organic solar cells. Hence, materials that physically combine hole- and electron-transporting semiconductors in mixed or bi-layered forms have been used as dual transporters. However, poor interfacial contact between the two materials, where charge recombination or separation occurs, often leads to poor quantum efficiencies and reproducibilities. Instead, single-component ambipolar semiconductors that can transport both holes and electrons are promising materials capable of overcoming these obstacles. Polymer-based materials, such as donor–acceptor copolymers, exhibited ambipolar semiconducting characteristics. However, the structural inhomogeneity based on the inevitable wide-ranged molecular weight distribution severely hampered access to the structural insights and the conduction mechanism, hampering the establishment of the materials designing guidelines. Therefore, we focused on the single-molecular-weight ambipolar organic semiconductors that offer excellent tunability of electronic structures and crystallinity to access the structural insights and conduction mechanism.

Our groups have designed and synthesized d/π-conjugated molecules, Ni(4OR) [R = Me, Et, Pr] (Fig. 1) [1,3], in which the nickel element with d electrons plays a central role. These molecules are highly stable and do not react easily with water or oxygen, and are also attractive because they can be easily synthesized using nickel, which is a relatively inexpensive metallic material. In addition to the electronic structure and properties, molecular semiconductors with excellent carrier transport properties requires seemingly contradictory properties: high crystallinity to enable highly ordered and highly dimensional stacking states, and high solubility to realize excellent thin-film processability. The research group searched for new materials that fulfil these conditions among combinations of d/π-conjugated backbone and side chains, and found a group of d/π-conjugated molecules that achieve both.

Unexpectedly, it was found that slight differences in the number of carbons on the side chains dramatically changed the stacking structure in single crystals. Those with one carbon substituent exhibited a one-dimensional stacking pattern, while those with two or three carbons exhibited a herringbone-type stacking pattern with a two-dimensional electronic structure, which is advantageous for stable device operation (Fig. 1). The latter stacking pattern was reproduced in thin films with a thickness of several tens of nanometres, which were constructed by solution coating, and highly ordered crystalline thin films were successfully realized. Field-effect transistor devices in which the resulting thin films were inserted as semiconductor layers exhibited ambipolar charge transport properties and showed high levels of both carrier mobility (up to 10^{-2} $cm^2V^{-1}s^{-1}$) and on-off ratio (10^5). These performances were demonstrated in an open environment without the strict exclusion of water and oxygen, enabling the realization of a new ambipolar semiconductors with high stability, solution-dispensable and high mobility.

In summary, novel molecular ambipolar semiconductors, Ni(4OR) [R = Me, Et, Pr], which are inexpensive and easy to synthesize, resistant to reaction with water and oxygen, and possible to solution process, have been developed and exhibited excellent carrier mobility and on-off ratio. The availability of structural information at the atomic level has enabled detailed electronic structure and conduction mechanism analysis, and has revealed molecular design guidelines for superior semiconductors, which have not been established for polymer materials. In the future, it is

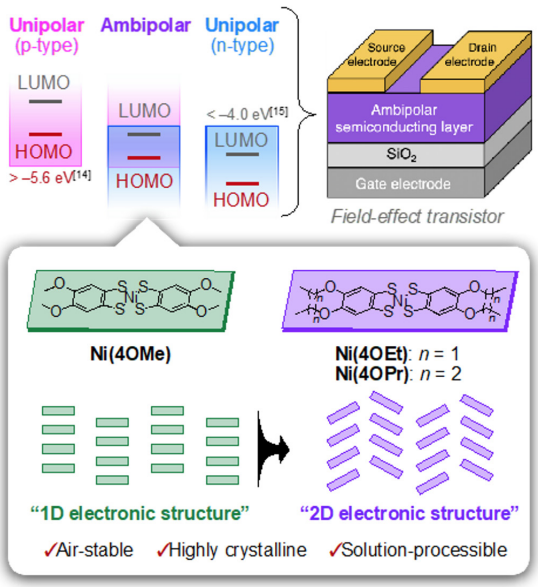

Fig. 1. (Top) Electronic structure requirements for ambipolar semiconductors used in field-effect transistors (FET), where the electronic structure requirements imposed on p-type/n-type semiconductors must be compatible with each other. (Bottom) Schematic diagram of the structural formula of the novel complex developed in this study and its molecular stacking pattern. Single crystal X-ray structure analysis revealed a dramatic modulation of the molecular stacking pattern associated with a slight extension of the side chains, and theoretical calculations confirmed the acquisition of dimensionality (D) from 1D to 2D.

expected that d/π-conjugated molecules will be developed by utilizing the high degree of structural freedom based on the combination of the central metal and ligand towards high transport properties through a higher-dimensional electronic structure based on changes in stacking pattern according to the number of carbons on the side chains. Such a detailed material design strategy using molecular materials can be extended not only to electrically conductive materials but also to various applications such as magnetic materials and photo-functional materials and is expected to make a significant contribution to the development of next-generation organic electronic devices.

References

[1] M. Ito, T. Fujino, L. Zhang, S. Yokomori, T. Higashino, R. Makiura, K. J. Takeno, T. Ozaki, and H. Mori, J. Am. Chem. Soc. **145**, 2127 (2023).

[2] D. Zhang, S. Yokomori, R. Kameyama, C. Zhao, A. Ueda, L. Zhang, R. Kumai, Y. Murakami, H. Meng, and H. Mori, ACS Appl. Mater. Interfaces **13**, 989 (2021).

[3] S. Yokomori, S. Dekura, A. Ueda, R. Kumai, Y. Murakami, and H. Mori, J. Mater. Chem. **9**, 10718 (2019).

Authors

M. Ito, T. Fujino, L. Zhang, S. Yokomori, T. Higashino, R. Makiura, K. J. Takeno, T. Ozaki, and H. Mori

Quantized Thermoelectric Hall Effects in Nodal-Line Semimetals at the High-Magnetic-Field Quantum Limit

Osada Group

The "quantized thermoelectric Hall effect (QTHE)" has been established theoretically and experimentally in 3D Dirac/Weyl semimetals with nodal points, at the high-magnetic-field quantum limit (QL). Reflecting their characteristic $N = 0$ chiral Landau subband (Fig. 1(a)), their thermoelectric Hall conductivity α_{xy} takes a constant value (Fig. 1(b)), which is independent of magnetic field and carrier number, resulting in the boundless linear increase of the Seebeck coefficient $S_{xx} \sim \alpha_{xy} / \sigma_{xy}$. This feature brings about high-performance thermoelectricity. The more remarkable QTHE was proposed in the 2D massless Dirac fermion system with nodal points at the QL. In this case, α_{xy} takes a quantized constant value of $(4 \log 2)\, k_B\, e / h$, which is independent of temperature, magnetic field, and carrier density, so that the boundless increase of S_{xx} can be expected even at low temperatures. Here, we have theoretically and experimentally investigated the possible QTHE in the 3D topological semimetals with straight nodal lines at the QL.

First, we exhibited that the QTHE can more generally appear even in a part of the 3D nodal-line semimetals in addition to the nodal-point semimetals [1]. We considered the 3D semimetals with straight parallel nodal lines. For example, they can be realized as multilayer systems where 2D massless Dirac fermion layers stack with weak interlayer coupling. When the magnetic field is applied parallel to the straight nodal lines, the $N = 0$ ground Landau subband (Fig. 1(c)), which consists of the $N = 0$ Landau level of each 2D layer, plays the similar role as the pair of the $N = 0$ chiral Landau subbands in Dirac/Weyl semimetals, and also causes the similar QTHE (Fig. 1(d)). The constant value of α_{xy} contains the dispersion parameter, and it is proportional to temperature but independent of carrier density.

We quantitatively discussed the possible QTHE in graphite as an example of the nodal-line semimetal [1]. In 3D graphite, the conduction and valence bands quadratically touch along the H-K-H edge of the Brillouin zone, forming nodal lines. Based on the Landau subband configuration obtained from the Slonczewski-Weiss-McClure model (Fig. 1(e)), we calculated α_{xy} as a function of magnetic field and confirmed the QTHE plateau formation with the value $\alpha_{xy}^{(\mathrm{sheet})} \sim 0.036\ [\mathrm{K}^{-1}]\ T\,(k_B\, e / h)$ per bilayer at the quasi-QL $|B_z| > 8$ T, where only two ground subbands ($N' = -1, 0$) locate at the Fermi level (Fig. 1(f)).

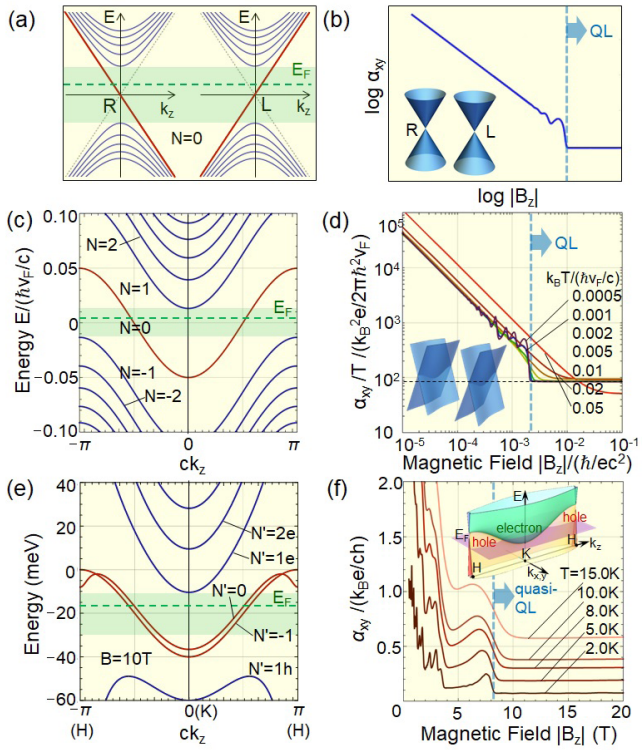

Fig. 1. Landau subband configuration and thermoelectric Hall conductivity α_{xy} in (a)(b) Dirac/Weyl semimetals, (c)(d) straight nodal-line semimetals, and (e)(f) graphite. The plateau due to the QTHE appears in the QL region [1].

Next, we performed the thermoelectric measurement on graphite to confirm the QTHE [2]. The resistivity (ρ_{xx}, ρ_{xy}) and thermopower (S_{xx}, S_{xy}) were measured simultaneously to compute α_{xy}. We could successfully obtain the plateau of α_{xy} at the quasi-QL (Fig. 2), which quantitatively agrees with our calculation. In graphite, the Hall conductivity σ_{xy} is not simply proportional to $1/B$ but shows complicated B-dependence, so that the boundless increase of S_{xx} cannot be observed.

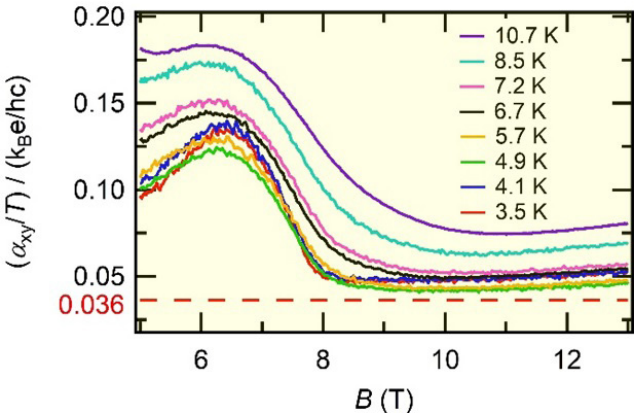

Fig. 2. Thermoelectric Hall conductivity α_{xy} measured in bulk graphite. The QTHE plateau corresponding to the calculation (Fig. 1(f)) can be seen above 8 T [2].

In addition, we theoretically investigated the quantum size effect on the QTHE in thin-film graphite [1]. When the thickness of graphite is decreased, the Landau subbands is discretized into many levels by the quantization of the inter-layer wave number. This causes the dimensional crossover of the QTHE from 3D to 2D.

References

[1] T. Osada, T. Ochi, and T. Taen, J. Phys. Soc. Jpn. **91**, 063701 (2022).

[2] A. Kiswandhi, T. Ochi, T. Taen, M. Sato, K. Uchida, and T. Osada, Phys. Rev. B **107**, 195106 (2023).

Authors

T. Osada, A. Kiswandhi, T. Ochi, M. Sato, K. Uchida, and T. Taen

Topological Thermal Hall Effect of Magnons in Magnetic Skyrmion Lattice

Yamashita Group

Currently, research on the effects of emergent magnetic fields created by spin structures in solids is attracting much attention. This is because such emergent magnetic fields directly affect the wave function of electrons, giving rise to more drastic effects on electrons than those caused by an external magnetic field. One of the most celebrated examples is the emergent magnetic field produced by a magnetic skyrmion – a vortex texture of spins in a magnetic solid (see Fig. 1(a)). For conduction electrons in a metal, it is well known that the topological Hall effect is given by the emergent magnetic field of the magnetic skyrmions of which the field strength is equivalent to several hundred tesla in external magnetic field. On the other hand, it has been unknown how the emergent field acts on charge-neutral heat carriers in insulators, such as magnons and phonons.

In this study [1], we investigated in detail the thermal transport properties in GaV_4Se_8, a ferromagnetic insulator in which a magnetic cycloidal phase at zero-field below the Curie temperature is transformed into a magnetic skyrmion phase by applying a magnetic field (Fig. 1(c)). We find that, whereas the thermal Hall effect is absent both in the cycloidal and the forced-ferromagnetic phases, a clear thermal Hall effect appears in the magnetic skyrmion phase (Fig. 1(b)). A color plot of the thermal Hall conductivity (κ_{xy}) demonstrates the position of the magnetic skyrmion phase in the B–T phase diagram as shown in Fig. 1(c). In addition, the thermal Hall signal is increased by increasing the domain volume of the magnetic skyrmion phase by cooling the sample under a magnetic field through the structural phase transition. These results indicate that the observed thermal Hall signal is caused by the emergent magnetic field of the magnetic skyrmion lattice.

We confirm that this is indeed the case by theoretically calculating the heat transport of the magnons in the magnetic skyrmion lattice. We find that the calculated magnon bands, which are folded by the lattice of the magnetic skyrmions, acquire non-trivial Chern number. In particular, as shown by the Fig. 2(a), the magnon bands around the top of the lowest

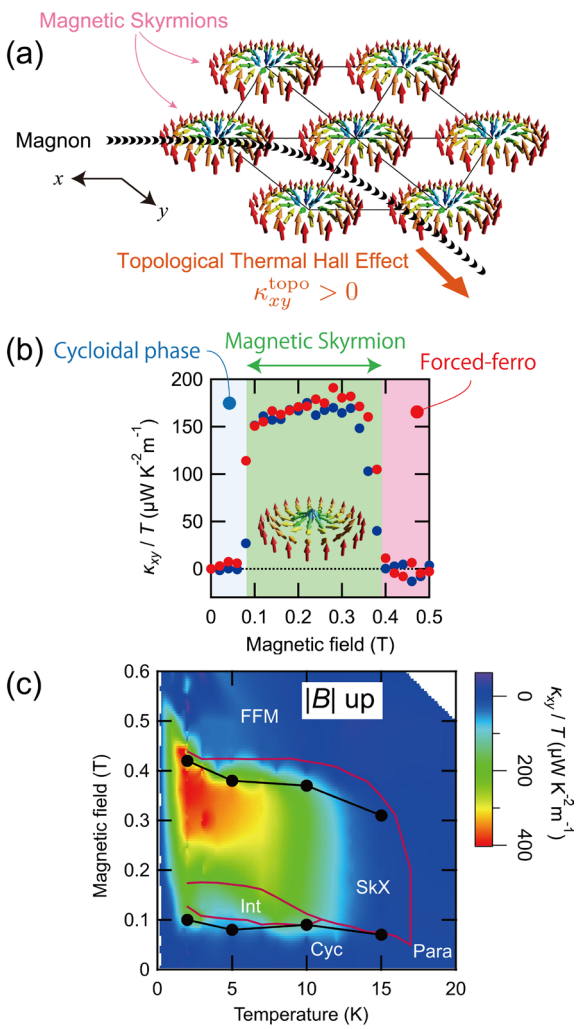

Fig. 1. (a) A schematic illustration of the topological thermal Hall effect of magnons in the lattice of magnetic skyrmions. The flow of the magnons is bent by the emergent magnetic field produced by the vortex spin texture of the magnetic skyrmions. (b) The magnetic field dependence of the thermal Hall conductivity (κ_{xy}). A finite κ_{xy} sharply appears in the magnetic skyrmion phase (green shared area), but disappears in the cycloidal (blue) and the forced-ferromagnetic (pink) phases. (c) A color plot of κ_{xy}/T observed in the magnetization process ("|B| up").

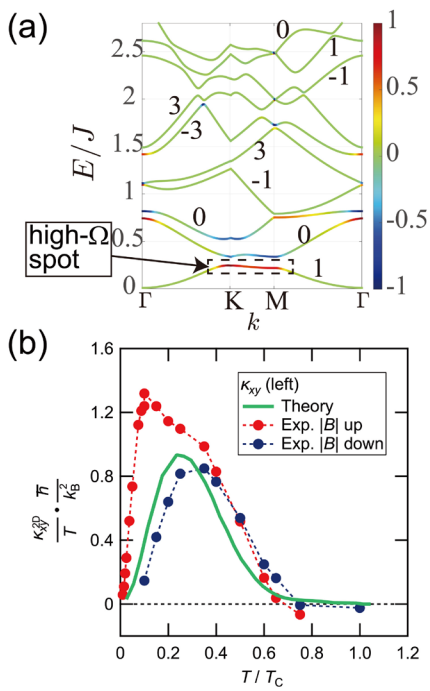

Fig. 2. (a) Energy bands of the magnons in the lattice of magnetic skyrmions along high-symmetry points. Color denotes the Berry curvature that is normalized in each band. (b) Temperature dependence of κ_{xy}/T by calculation (solid line) and experiments (symbols). Experimental data obtained at 0.36 T in the magnetizing (|B| up) and 0.2 T in the demagnetizing (|B| down) processes are shown in red and blue circles, respectively. To fit with the theoretical result, the horizontal axis of the experimental data is normalized by the Curie temperature T_C = 20 K. See [1] for more details.

magnon band have a large Berry curvature ("high-Ω spot" in Fig. 2(a)), giving rise to the topological thermal Hall effect of the magnons. Based on this magnon band calculation, we estimate the temperature dependence of κ_{xy}, and find that our calculation well reproduces the experimental result observed in the demagnetization process (see the green solid line and the blue data in Fig. 2(b)). On the other hand, κ_{xy} observed in the magnetization process shows a very different temperature dependence that persists at lower temperature than κ_{xy} in the demagnetization process (red data in Fig. 2(b)). This unexpected hysteresis might indicate that the lattice of the magnetic skyrmion is more disordered in the magnetization process, suggesting a difference in the skyrmion lattice depending on whether it is formed from the forced-ferromagnetic phase or the cycloidal phase. Although this possibility should be scrutinized by future measurements of the skyrmion lattice, this hysteresis in κ_{xy} shows a high sensitivity of the thermal Hall measurements for the skyrmion lattice structure not attainable by other measurements.

Reference
[1] M. Akazawa, H.-Y. Lee, H. Takeda, Y. Fujima, Y. Tokunaga, T. Arima, J. H. Han, and M. Yamashita, Phys. Rev. Research **4**, 043085 (2022).

Authors
M. Akazawa, H.-Y. Lee[a], H. Takeda, Y. Fujima[b], Y. Tokunaga[b], T. Arima[b], J. H. Han[c], and M. Yamashita
[a]Korea University
[b]University of Tokyo
[c]Sungkyunkwan University

Enhanced Bulk Photovoltaic Effect in Strained 3R-MoS_2

Ideue Group

Bulk photovoltaic effect, which indicates the generation of spontaneous photocurrent in uniform materials instead of conventional p-n junctions, is attracting considerable interest due to its microscopic origins related to the electronic band topology or geometry as well as its potential to achieve a high solar energy conversion efficiency. So far, bulk photovoltaic effect has been reported in a variety of noncentrosymmetric quantum materials and several strategies to enhance the photocurrent magnitude are also developed. Among them, strain application is a simple method for controlling the crystal structures or electronic states and thus an effective way for realizing the enhanced photovoltaic signals.

In this work, we studied the effect of uniaxial strain on the bulk photovoltaic effect in van der Waals layered semiconductor 3R-MoS_2. Without strain, 3R-MoS_2 has a noncentrosymmetric trigonal crystal structure (Fig.1 (a)). Although it exhibits the photoconductivity, which indicates the enhancement of conductivity under the illumination of light, zero-bias photocurrent is negligibly small (Fig. 1 (b)). By transferring the exfoliated flake of 3R-MoS_2 on a pre-patterned substrate consisting of two parallel steps and pushing it so that flake stretches and gets in contact with the bottom substrate part, we applied the uniaxial strain on 3R-MoS_2 (Fig. 1 (c)). In strained samples, symmetry of the crystal is reduced and electronic polarization appears (inset of Fig. 1 (c)). We found that zero-bias photocurrent is largely enhanced in such strained samples (Fig. 1 (d)). We confirmed that photocurrent appears when the light is illuminated at the center of the device away from the electrodes and flows only

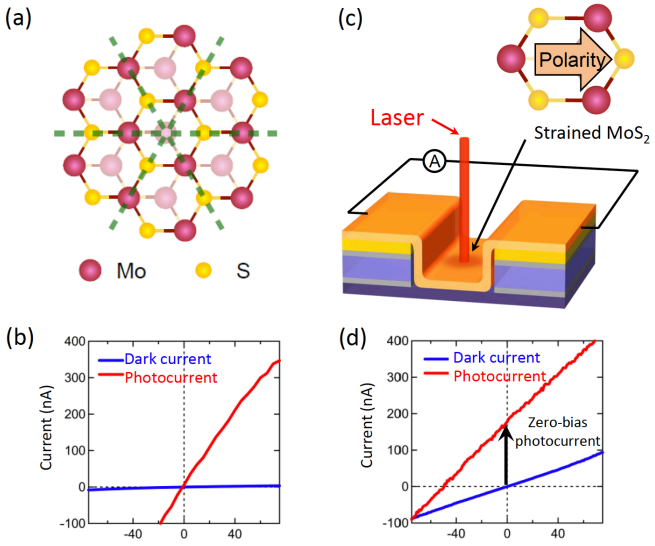

Fig. 1. (a)Crystal structure (top view) of 3R-MoS_2. Green dashed lines indicate the mirror planes. (b) The *I-V* characteristic of an unstrained 3R-MoS_2 device. (c) Schematic of photocurrent measurement in a strained 3R-MoS_2 device. (d) The *I-V* characteristic of a strained 3R-MoS_2 device.

along the direction parallel to the electronic polarization. It is also observed that the magnitude of the zero-bias photocurrent increases in a nonlinear manner with the value of uniaxial strain. These results implies that the observed zero-bias photocurrent is the intrinsic bulk photovoltaic effect and the emergence of the electronic polarization is essential to enhance the bulk photovoltaic effect.

We further studied the detailed light power dependence and photon energy dependence of the bulk photovoltaic effect. The light power dependence of the photocurrent shows the characteristic crossover, evolving from a linear relation to a nonlinear manner while increasing the light intensity. The photon energy dependence of the zero-bias photocurrent exhibits the non-monotonic behavior differently from the absorption spectrum. These behaviors can be well explained by the shift current, which is one of the origins of bulk photovoltaic effect related to the geometrical properties (Berry connection or shift vector) of the wave function and arises from the shift of the wave packet under the optical transition.

In summary, we have demonstrated the gigantic enhancement of bulk photovoltaic effect by uniaxial strain in van der Waals layered semiconductor 3R-MoS_2. This work clarifies the important role of symmetry reduction and the induced electric polarization for the large photocurrent generation, enriching our knowledge concerning the microscopic mechanism of bulk photovoltaic effect in non-centrosymmetric systems. Present results also indicate that strain application is a powerful method to control the symmetries, geometric properties of the electronic wave function, and resultant physical properties of flexible layered materials.

Reference
[1] Y. Dong, M. Yang, M. Yoshii, S. Matsuoka, S. Kitamura, T. Haswgawa, N. Ogawa, T. Morimoto, T. Ideue, and Y. Iwasa, Nat. Nanotechnol. **18**, 36 (2023).

Authors
Y. Dong[a], M. Yang[b,c], M. Yoshii[a], S. Matsuoka[a,d], S. Kitamura[a], T. Haswgawa[a], N. Ogawa[b], T. Morimoto[a], T. Ideue, and Y. Iwasa[a,b]
[a]The University of Tokyo
[b]RIKEN Center for Emergent Matter Science (CEMS)
[c]The University of Warwick
[d]Nagasaki University

Spin Hall Magnetoresistance in Quasi-Two-Dimensional Antiferromagnetic-Insulator /Metal Bilayer Systems

Kato Group

Recently, a novel type of magnetoresistance, called spin Hall magnetoresistance (SMR), has been attracting much attention. SMR was first observed in a normal metal (NM)/ ferromagnetic insulator bilayer [1] and subsequently in a NM/antiferromagnetic insulator (AFI) bilayer [2]. Because SMR reflects information on the FI magnetization or AFI Néel vector, it can be utilized for detecting the orientation of ordered spins in magnetic materials. Although the existing theory [1,3] succeeds in explaining the qualitative features of SMR measurements, it could not explain the temperature dependence of the SMR signal. Recently, a microscopic theory using Green's function has been constructed [4]. This microscopic theory describes SMR in terms of local spin susceptibilities of the FI(AFI). It can include dynamic processes such as magnon absorption and emission responsible for a nontrivial sign change in the SMR signal, which are neglected in the semiclassical theory.

In this study, we numerically calculated SMR by using a quantum Monte Carlo method [5] for a NM/AFI bilayer (see Fig. 1 (a)). We utilized an improved method for accurately obtaining the integral of the local spin susceptibilities from the QMC data without using numerical analytic continuation. We evaluated the detailed temperature dependence of SMR for S = 1/2 and S = 1 spin systems on a two-dimensional square lattice and a quasi-two-dimensional cubic lattice with a finite number of layers.

Figure 1 (b) shows the spin conductance, which is proportional to the SMR signal, for the S = 1/2 quasi-two-dimensional quantum Heisenberg model on a $16 \times 16 \times W$ (W = 2, 4, 6) cubic lattice. As the thickness W increases, the ordering temperature (indicated by the green arrows) increases. The spin conductance induced below the transition temperature becomes large while it vanishes above the transition temperature. We find that the peak of the spin conductance is greatly enhanced compared with that for a single-layer spin system (not shown). Although the maximum of the spin conductance increases with increasing thickness W, the difference between the results for W = 4 and 6 is much smaller than that for W = 2 and 4. Figure 1 (c) shows the SMR signal for the S = 1 quasi-two-dimensional quantum Heisenberg model on a $16 \times 16 \times W$ (W = 2, 4, 6) cubic lattice. As the thickness W increases, the ordering temperature (indicated by the green arrows) raises and the SMR signal becomes large. Above the transition temperature, the SMR signal becomes small but remains finite, in contrast with the case of S = 1/2. We showed that this feature can be understood well by the high-temperature expansion. As the temperature decreases below the ordering temperature, the SMR signal increases, takes a maximum roughly at three-fifths of the ordering temperature, and then decreases. The maximum value of the signal is rather larger than in the case of S = 1/2. At sufficiently low temperatures, the SMR signal becomes negative, as predicted by the spin-wave approximation. We also discussed the effect of the disordered exchange interactions.

In our study, we succeeded in clarifying the qualitative features of SMR based on the numerical results. These qualitative features are expected to be observed experimentally. Our simulation using a simplified model is expected to be a useful starting point for understanding SMR in quasi-two-dimensional quantum spin systems.

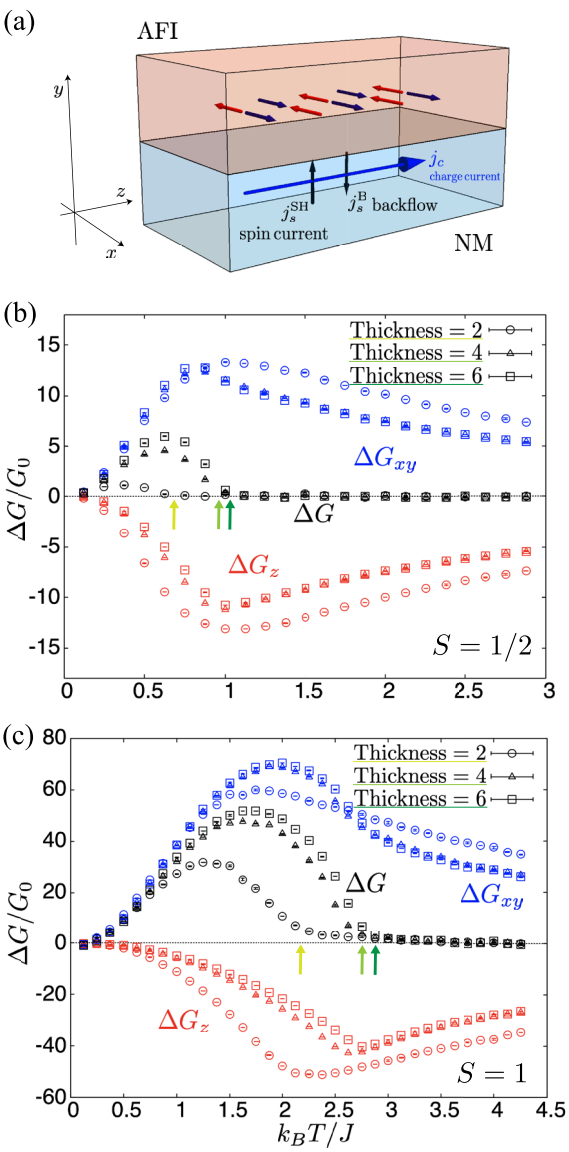

Fig. 1. (a) Illustration of spin Hall magnetoresistance. Spin absorption at the interface changes according to the orientation of the Néel vector of the antiferromagnetic insulator, and the magnitude of the magnetoresistance changes. (b,c) Temperature dependences of spin conductance ΔG are shown for (b) S = 1/2 and (c) S = 1 quantum Heisenberg model. The two contributions, ΔG_{xy} and ΔG_z, are plotted separately.

References

[1] H. Nakayama *et al.*, Phys. Rev. Lett. **110**, 206601 (2013).
[2] D. Hou *et al.*, Phys. Rev. Lett. **118**, 147202 (2017).
[3] Y. T. Chen *et al.*, Phys. Rev. B **87**, 144411 (2013).
[4] T. Kato, Y. Ohnuma, and M. Matsuo, Phys. Rev. B **102**, 094437 (2020).
[5] T. Ishikawa, M. Matsuo, and T. Kato, Phys. Rev. B **107**, 054426 (2023).

Authors
T. Ishikawa, M. Matsuo, and T. Kato

Shear-Strain Controlled High-Harmonic Generation in Graphene

Kato and Akiyama Groups

Two-dimensional (2D) Dirac electrons in single-layer graphene have attracted much attention for their novel linear and nonlinear optical properties. One-atom-thick graphene exhibits universal frequency-independent light absorption, $\pi\alpha$ = 2.3%, where $\alpha = e^2/\hbar c \approx 1/137$ is the fine structure constant [1]. Ultrafast carrier dynamics on massless bands provide a variety of high-speed broadband optical responses. Further studies have targeted artificial control, modulation, or switching of these properties for potential applications in graphene-based optical devices. However, the robustness of optical transition probability $\pi\alpha$ inherent to 2D Dirac electrons makes the external control of optical responses highly challenging.

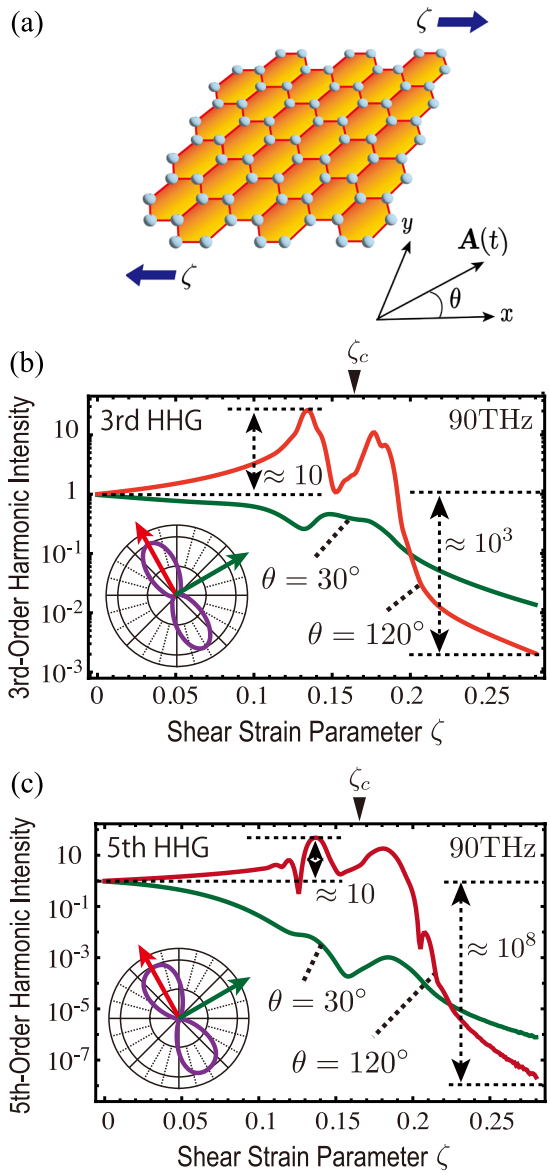

Fig. 1. (a) Schematic figure of lattice structure of graphene under shear strain. The amplitude of the shear strain is represented by ζ and the vector potential of the incident light is denoted as $A(t)$, whose tilt angle measured from the armchair axis is described by θ (see the inset). (b) Shear strain dependence of the third- and fifth-order harmonics. The red and green lines indicate the high-harmonic intensities for the incident-light angles $\theta = 120^\circ$ and $\theta = 30^\circ$, respectively. The polarization angle dependences of the third and fifth harmonics for $\zeta = 0.12$ are shown in the insets. The critical strength of the shear strain for a band gap to form is described by ζ_c.

A graphene sheet has high flexibility and a shear strain of up to 27% can be reversibly applied to it [2]. This strain effect should be useful for control of the nonlinear optical responses of graphene. In this study [3], we theoretically demonstrated a significant enhancement or quenching of HHG over several orders of magnitude in graphene by tuning the shear strain and the incident-light polarization angle (Fig. 1 (a)).

We show the shear-strain dependences of the third and fifth harmonics in Fig. 1 (b) and (c). The red and green lines indicate the dependences for the different incident-light polarization angles, $\theta = 120^\circ$ and $\theta = 30^\circ$, respectively (for definition of theta, see Fig. 1 (a)). These two angles are regarded as the specific ones because they can yield the maximum and minimum intensities of the emitted harmonics (see insets in Fig. 1 (b) and (c)). Fig. 1 (b) and (c) show that, for $\theta = 120^\circ$, the third-order (fifth-order) harmonics are largely enhanced by around one order of magnitude at $\zeta \approx 0.13$ and 0.18, while they are quenched rapidly by around third (eight) orders of magnitude at $0.2 < \zeta < 0.27$ (red line), where ζ is the amplitude of the shear strain. The plots for $\theta = 30^\circ$ do not show this nonmonotonic behaviour; they only show an approximately monotonic decrease with increasing shear strain. By using linear response theory, we showed that the HHG enhancement came from the resonances at which the incident-light photon energy matches the saddle-point energy or the band gap [3]. In addition, the dipole moment near the saddle point (or the band gap) plays an important role in the polarization angle dependence of this enhancement. Strong quenching of HHG was induced by rapid growth of the band-gap energy with increasing shear strain.

In conclusion, we theoretically investigated the linear and nonlinear optical responses of graphene distorted by shear strain. Using the tight-binding model, we clarified that tuning both the shear strain and the polarization angle of the incident THz light enables a significant enhancement or quenching of HHG. Our findings suggest the possibility of using shear strain to control HHG in graphene and pave the way for optical nanotechnology of single-layer materials.

References

[1] R. R. Nair, P. Blake, A. N. Grigorenko, K. S. Novoselov, T. J. Booth, T. Stauber, N. M. Peres, and A. K. Geim, Science **320**, 1308 (2008).
[2] Z. Peng, X. Chen, Y. Fan, D. J. Srolovitz, and D. Lei, Light: Sci. Appl. **9**, 190 (2020).
[3] T. Tamaya, H. Akiyama, and T. Kato, Phys. Rev. B **107**, L081405 (2023).

Authors
T. Tamaya, H. Akiyama, and T. Kato

Visualizing Magnetization c Domain Structure with Heat Injection Using Atomic Force Microcopy

Otani Group

Magnetic imaging plays a crucial role in studying the magnetism of materials. Its significance has been growing with the rapid development of topological magnetic materials. For instance, the magnetic domain structure of the antiferromagnetic Weyl semimetal Mn_3Sn [1] is intriguing from the magnetothermoelectric application point of view.

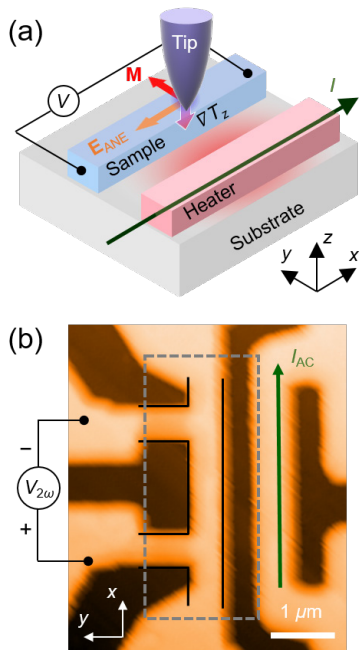

Fig. 1. (a) Conceptual drawing of magnetic imaging. (b) Device structure and electric configuration of the measurement.

However, the methods with enough high spatial resolution usually require costly instruments. Here, we report a simple magnetic imaging method using an atomic force microscope (AFM) with a sub-100-nm resolution, in which we measure the locally induced anomalous Nernst effect (ANE).

Figure 1(a) illustrates the concept of our method. The Joule effect of the heater causes a non-equilibrium temperature distribution in the sample nanowire. An AFM tip contact creates a local vertical temperature gradient $\nabla_z T$ in a sample. The ANE is expressed as $E_{\mathrm{ANE}} = S_{\mathrm{ANE}}(\boldsymbol{m} \times \nabla T)$, where E_{ANE}, S_{ANE}, $\boldsymbol{m}$ are the electric field induced by ANE, the magnitude of ANE, and the unit vector of the magnetization, respectively. If the magnetization under the tip points to the wire width direction (the y-direction), the ANE causes a voltage along the x-direction. Therefore, the tip-induced ANE voltage represents the y-component of the local magnetization.

We demonstrate this method on the ferromagnetic Weyl semimetal Co_2MnGa that exhibits large ANE ($S_{\mathrm{ANE}} \sim 5\ \mu$V/K)

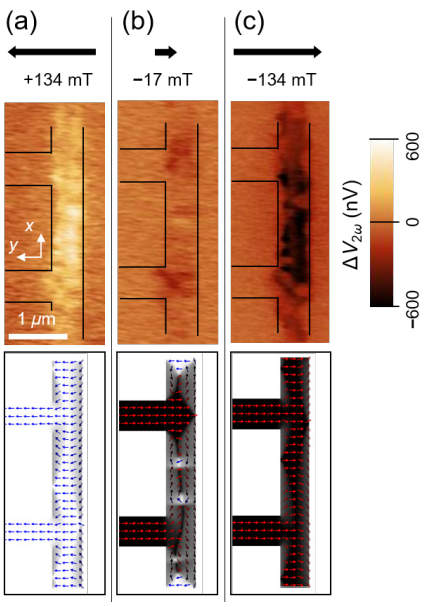

Fig. 2. The results of anomalous Nernst voltage mapping with (a) +134 mT, (b) −17 mT and (c) −134 mT.

[2]. The topographic image of the sample and the electric measurement configuration are shown in Fig. 1(b). We apply an alternating current to the heater and measure the voltage across the sample wire at the second harmonic frequency. We map the voltage during the scan with the contact mode. We conduct the experiment in an atmosphere at room temperature. The result of the voltage mapping Figure 2(a), (b), and (c) represents the results under the external magnetic field along the y-direction of +134 mT, −17 mT, and −134 mT, respectively. With +134 mT, a uniformly positive voltage is obtained. The magnitude of the signal is proportional to the square of the current. The signal reverses its sign with −134 mT. These results indicate that the voltage is attributable to the ANE. With −17 mT, a pair of bright and dark spots (positive and negative voltage) appeared near the center of the sample wire. This reflects the presence of a 180° magnetic domain wall. The bottom row of Fig. 2 shows the results of micromagnetic simulation in the Co_2MnGa with each magnetic field obtained by OOMMF. One can see a good agreement between the experimental and simulation results. We estimated the spatial resolution to ~ 80 nm from the edge response of the ANE voltage. Using same technique, we saw a magnetic signal on the permalloy ($Ni_{80}Fe_{20}$) nanowire. Therefore, our method applies to the antiferromagnetic Weyl semimetal Mn3Sn ($S_{\mathrm{ANE}} \sim 0.5\ \mu$V/K).

We develop a simple method for magnetic imaging [3]. Our method only requires a conventional atomic force microscope with a high spatial resolution. Moreover, our technique can apply to antiferromagnetic Weyl semimetals that exhibit the anomalous Nernst effect.

References

[1] S. Nakatsuji and R. Arita, Annu. Rev. Condens. Matter Phys. **13**, 119 (2022).
[2] A. Sakai *et al.*, Nat. Phys. **14**, 1119 (2018).
[3] N. Budai, H. Isshiki, R. Uesugi, Z. Zhu, T. Higo, S. Nakatsuji, and Y. Otani, Appl. Phys. Lett. **122**, (2023).

Authors
H. Isshiki, and Y. Otani

Microscopic Views of Quantum Phase Transition in Disorder-Controlled 2D Superconductors

Hasegawa Group

Disorder-induced superconductor-insulator transition (SIT) in the two-dimensional (2D) systems has been a subject of extensive studies as one of typical examples of quantum phase transitions (QPT). Recent advancements in fabricating highly crystalline 2D systems revealed the unexpected quantum phases, such as anomalous metallic state and quantum Griffiths phase, around QPT. The origins of the new quantum phases are still uncovered partly because of lack of microscopic pictures. Here, by performing scanning tunnelling spectroscopy (STM) at low temperature (0.36 K) on highly-crystalline monoatomic-layer superconductors, we elucidated these quantum phases in real space microscopically.

In the present work we used one of the Pb-monolayer superconducting phases called striped incommensurate (SIC) phase formed on vicinal Si(111) substrates. On the vicinal substrates single-layer-height steps, which work as a disorder [1,2], are regularly aligned, and the density of steps can be

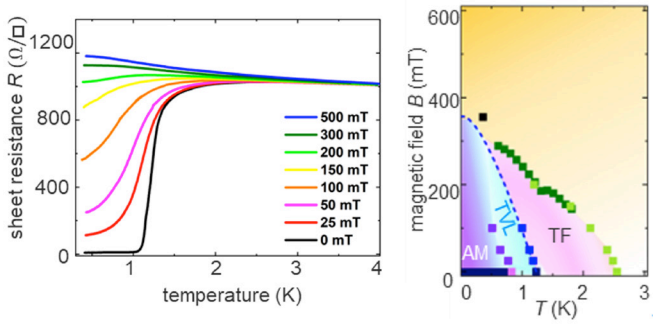

Fig. 1. (left) Temperature dependence of sheet resistance R measured on the 1.1°-tilted vicinal sample under out-of-plane magnetic fields of 0, 25, 50, 100, 150, 200, 300 and 500 mT. (right) B-T phase diagram obtained from the data shown in the left panel. AM: anomalous metallic phase, TVL: thermal vortex liquid phase, TF: thermal-fluctuation-induced metallic phase..

controlled precisely with the miscut angle. We investigated how the disorder in the superconducting layers affects the presence of the quantum phases.

First we performed *in situ* (in ultrahigh vacuum) transport measurements on the SIC phases formed on 1.1°-tilted vicinal substrates (Fig. 1). The terrace spacing for the vicinal substrate is 16 nm, shorter than the coherence length of the system (38 nm). The superconducting critical temperatures T_c of the vicinal samples are 1.21 K, slightly lower than the flat sample (1.53 K). Under out-of-plane magnetic fields below the critical field B_{c2}, the sample exhibits non-zero resistance near zero temperature, indicating the presence of anomalous (quantum) metallic phase, which is often explained with the quantum motion of vortices. From the Arrhenius plots of the sheet resistance R, we determined the crossover temperature between the regions where the quantum and thermal vortex motions are dominant.

Outside of the superconducting regime, metallic phases ($dR/dT > 0$) are observed. Whereas the thermal-fluctuation-induced metallic (paraconductivity) phases are found above T_c, the quantum-fluctuation (QF)-induced metallic phase, which appears above B_{c2} near $T = 0$, appears only on the flat sample, was not observed on the vicinal sample. The absence of the QF-induced metallic phase on the step-abundant sample is consistent with the fact that the QF-induced metallic phase, which is often attributed to quantum Griffith phase, is only observed on highly-crystalline monolayer samples.

Then, we performed STM observation at low temperature (T = 0.36 K). Figure 2 shows the results taken on the vicinal sample. Figure 2(a) is an STM image showing equally-spaced steps on the surface. Figure 2(b)-2(l) are maps showing the spatial distribution of the superconducting gap under various out-of-plane magnetic fields B. At B = 120 mT, individual oval vortices elongated along the steps are observed. The oval shape is due to the Josephson coupling at the steps and explained as Josephson-Abrikosov vortices [2]. By increasing B to 180 mT, vortices are significantly overlapped each other but still individual vortices are recognized, but at B = 270 mT individual vortices are not observable any more. B_{c2} can be estimated from the gap evolution with B outside of the vortices and found B_{c2} = 355 mT, which is consistent with that obtained by the transport measurement (Black square in the phase diagram of Fig. 1 corresponds to the B_{c2} by STM.). In the range of 270 mT < B < B_{c2}, the density of vortices should increase with B and in fact averaged gap depth decreases, but individual vortices cannot be seen. The indistinct vortices are, therefore, due to liquidation of vortices. Above B_{c2}, we still observed the gap remaining, and the pseudo gap disappears around B = 500 mT.

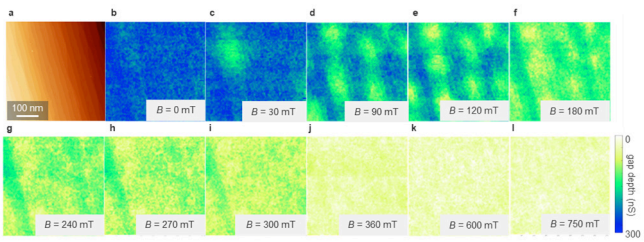

Fig. 2. (a) STM image taken on Pb monoatomic-layer SIC phase formed on 1.1°-tilted vicinal Si(111) substrate. (b-l) Superconducting gap depth maps under various out-of-plane magnetic fields on the same area as (a).

According to the phase diagram obtained by the transport measurement (right panel of Fig. 1), under 30 mT < B < 120 mT finite resistance is observed and thus anomalous metallic phase should be there at T = 0.36 K. However, in STM, we observed individual vortices, indicating the presence of short-range order of the vortex arrangement, at least. The regime is, therefore, the quantum creep phase, and the finite resistance is likely generated due to the vortex motions induced by infinitesimal current for the transport measurement.

We performed the same measurements on the flat sample and basically the same results were obtained in the low B range. Curiously, however, the vortex liquid phase was not observed on the flat sample. The vortex liquidation, which we believe induced by the quantum fluctuation, occurs only under the presence of phase fluctuation induced by the disorder.

Under B higher then B_{c2}, we observed a pseudo gap on both flat and vicinal samples. This implies that the localized Cooper pairs are formed, presumably by quantum fluctuation, regardless of the degree of disorder. Depending on the degree of disorder, however, the amount of the localization is different, making the system metallic or insulating depending on the amount of disorder.

References

[1] S. Yoshizawa *et al*., Phys. Rev. Lett. **113**, 247004 (2014).
[2] Y. Sato *et al*., Phys. Rev. Lett **130**, 106002 (2023).

Authors
Y. Sato, M. Haze, S. Yoshizawa[a], T. Uchihashi[a] and Y. Hasegawa
[a]National Institute for Materials Science

Machine Learning for Structural Phase Mapping

Lippmaa Group

Structural phase analysis in thin film materials development is usually done by ex-situ x-ray diffraction (XRD) after the film growth is finished. The XRD analysis typically takes longer than the film synthesis and the XRD analysis provides an average composition of the whole film volume without being able to distinguish which phases that occur at the surface or at the substrate interface. An alternative structure analysis method is in-situ reflection high-energy electron diffraction (RHEED), which provides structural information on the surface of the film in real time during growth. While this makes RHEED an attractive alternative to XRD, manual

analysis of RHEED patterns to determine the phase composition is generally time-consuming and thus rarely used for contemporaneous structure analysis with film growth.

We have developed a machine learning workflow to automatically detect and locate various diffraction features in complex diffraction patterns. We use the U-Net neural network segmentation algorithm to quickly determine where diffraction spots and streaks occur in a diffraction pattern, as illustrated in Fig. 1. The neural network has to be trained before such image segmentation is possible. For this purpose, we collect a large number of visually different diffraction patterns and hand-label those training patterns, manually marking the position of each diffraction spot and streak. The training image set is then used to train the U-Net to recognize the desired features in typical RHEED patterns. As shown in Fig. 1, U-Net can reliably distinguish between overlapping spots and streaks and can find even very weak features that are difficult to detect by eye.

The U-Net segmentation tool produces mask patterns. As the next step in the workflow, the original image intensity distribution is examined in each mask area. For example, it is possible to integrate the intensity in the vertical direction in each mask area and examine the resulting cross-section plots by peak fitting to determine accurate horizontal diffraction feature positions. The feature spacing corresponds to the distance between neighboring reciprocal space points and can thus be used to calculate the in-plane lattice parameter. In case the surface contains a mixture of phases, multiple spot or streak periodicities will appear on the surface. An iterative approach was developed to extract all base periodicities from a complex image, providing a list of periodicities. The total diffraction intensity corresponding to each bas distance is then used to calculate the phase composition ratios.

A series of thin film FeO_x samples was synthesized over a broad range of film growth temperatures and ambient oxygen pressures. The RHEED patterns of all films were analyzed using the automated composition analysis workflow. This produced for each synthesis phase space point a descriptor containing information on the phase lattice parameters and the associated relative diffraction intensities. Clustering was then used to form a phase map as shown in Fig. 2, where a pie diagram at each synthesis point represents the relative intensities of each clustered lattice parameter.

The mapping result shows that hematite Fe_2O_3 (green) dominates the film composition in the 600 to 800 °C range, while magnetite Fe_3O_4 (pink) appears at both lower and higher temperatures. This result was verified by later x-ray

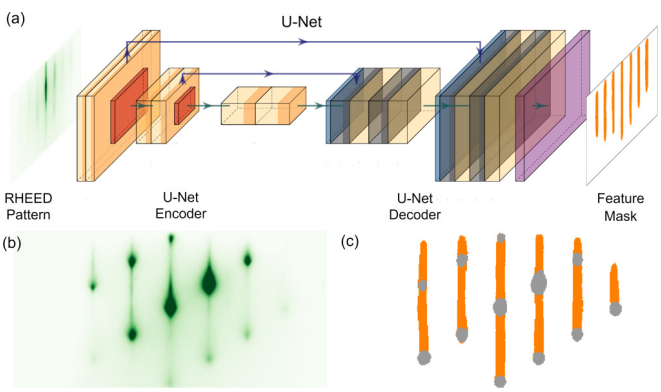

Fig. 1. (a) Schematic diagram of the U-Net model used for semantic segmentation of RHEED patterns. (b) and example pattern of a hematite film. (c) Masks for diffraction spots (gray) and streaks (orange) generated by the neural network model.

Fig. 2. A phase diagram constructed by automated RHEED pattern analysis for FeO_x phase formation in thin films grown at various oxygen pressures and temperatures. The marker colors correspond to various lattice periodicities. The center region is mostly hematite (green), while magnetite (pink) appears at both low and high growth temperatures.

diffraction analysis. Under thermodynamic equilibrium conditions, a monotonic change from magnetite at higher growth temperatures to hematite at lower temperatures would have been expected. The non-monotonic phase composition variation shows the importance of kinetic effects in thin film growth.

The RHEED phase mapping thus produces an equivalent result to XRD analysis, but RHEED mapping can be done in-situ in near-real-time. The machine learning workflow thus creates a new way to use RHEED for automated phase formation analysis and real-time phase evolution tracking during thin film growth.

Reference

[1] H. Liang, V. Stanev, A. G. Kusne, Y. Tsukahara, K. Ito, R. Takahashi, M. Lippmaa, and I. Takeuchi, Phys. Rev. Materials **6**, 063805 (2022).

Authors
H. Liang[a], V. Stanev[a,b], A. G. Kusne[a,c], Y. Tsukahara[d], K. Ito[d], R. Takahashi[d], M. Lippmaa, and I. Takeuchi[a]
[a]University of Maryland
[b]AstraZeneca
[c]NIST
[d]Nihon University

Elucidation of the Atomic-Scale Processes of Dissociative Adsorption and Spillover of Hydrogen on the Single Atom Alloy Catalyst Pd/Cu(111)

Yoshinobu and Ozaki Groups

The utilization of hydrogen in industry has become more important for our modern society because many indispensable processes consist of chemical reactions involving hydrogen: synthesis of chemical feedstocks such as methanol and ammonia, petroleum refining, energy sources through fuel cell systems, and so forth. In these reactions, dissociation of molecular hydrogen is an essential elementary step in hydrogenation reactions, where the active sites for hydrogen dissociation are necessary. In recent years, single atom alloy catalysts (SAACs) have been attracting much attention due to their excellent properties, such as high activity/selectivity and resistance to deactivation via coke formation or CO poisoning. In SAACs, active metal atoms are highly diluted and atomically dispersed on an inert but selective metal surface. Several previous studies have shown that the Pd/

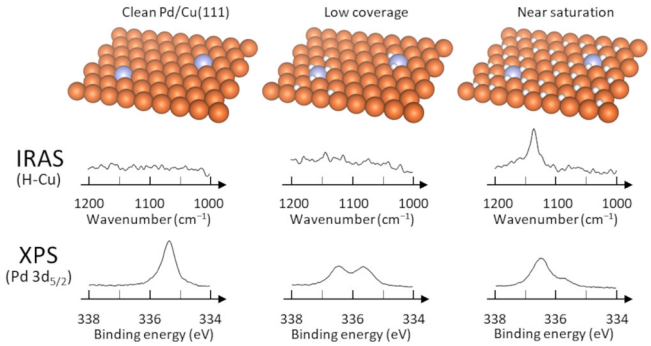

Fig. 1. (Up) Schematic models of the dissociative adsorption and spillover of hydrogen on Pd/Cu(111) as a function of coverage (Middle) Vibrational spectra of the Cu-H stretching mode (Bottom) Photoelectron spectra of Pd3d$_{5/2}$

Cu SAAC shows excellent activity for hydrogen dissociation and hydrogenation reactions. On the Pd/Cu SAACs, the hydrogen spillover from Pd sites onto Cu host surfaces is a vital process for selective hydrogenation because it has been considered that the reaction proceeds on the Cu surface which weakly interacts with the product molecules.

We investigated the dissociative adsorption of hydrogen and the subsequent spillover process on the Pd/Cu(111) surface using infrared reflection absorption spectroscopy (IRAS), temperature programmed desorption (TPD), and high-resolution X-ray photoelectron spectroscopy (HR-XPS), as well as density functional (DFT) calculations [1]. The hydrogen spillover onto Cu(111) was successfully observed in real time using time-resolved IRAS measurements. The chemical shifts of Pd 3d$_{5/2}$ indicate that molecular hydrogen is dissociated and adsorbed at the Pd site. In addition, "two-step" chemical shifts of the Pd 3d$_{5/2}$ binding energy were observed as a function of hydrogen exposure. The DFT calculation revealed that the "two-step" chemical shifts originate from the charge transfer (CT) from Pd to hydrogen; initially hydrogen atoms are directly adsorbed at the Pd site, and thereafter a significant amount of additional hydrogen atoms are adsorbed at the Cu sites in which CT occurs in an indirect manner. Based on the present experimental and theoretical results, we propose the following mechanism of the hydrogen dissociation and spillover process on Pd-Cu(111) : (i) a hydrogen molecule is dissociated at a Pd site, and the hydrogen atoms are adsorbed on the Pd site, (ii) the number of hydrogen atoms on the Pd site increases up to three, and (iii) the additional hydrogen atoms spill over onto the Cu surface.

Reference
[1] W. Osada, S. Tanaka, K. Mukai, M. Kawamura, Y.H. Choi, F. Ozaki, T. Ozaki, and Jun Yoshinobu, Phys. Chem. Chem. Phys. **24**, 21705 (2022).

Authors
W. Osada, S. Tanaka, K. Mukai, M. Kawamura, Y.H. Choi, F. Ozaki, T. Ozaki, and J. Yoshinobu

Thought Experiment of the Activity of an Oxide Electrode

Sugino Group

While a great deal of attention has been given to the computational design of functional materials, the degree of freedom is overwhelming when dealing with the heterogeneous interfaces of defective materials. Typical example is the defective oxides interfaced with solutions used for the electrocatalysis application. Recent experiments show that both zirconia and titania cathodes provide enhanced electromotive force of fuel cells when they contain nitrogen impurities and oxygen vacancies, but the microscopic structure of the electrode-electrolyte interface is not well understood. In this context, we use the large supercomputers such as Fugaku and the recently developed programs such as abICS [1] to perform ab initio Monte Carlo (MC) and molecular dynamics simulations to model the interface by sampling unprecedentedly large degrees of freedom. Note that abICS does not simply generate the ab initio trajectories, but also help enhance the sampling by machine learning the generated trajectories to significantly speed up the simulation. We used them to address the problem of understanding the reason for the improved fuel cell efficiency. In our approach, we first simulated the zirconia surface and then the zirconia-water interface.

Our previous simulation has revealed that an oxygen vacancy can be stabilized when doped with two times denser nitrogen impurities because of the charge compensation effect. The surface simulation showed that the vacancies are distributed not only at the surface but also in the subsurface regions, while the nitrogen impurities do not favor the surface sites. Based on this result, we reduced the size of the model surface so that we can examine all possible configurations of the ORR intermediates, i.e., O_2*, O_2H*, OH*, and O*, where * means adsorbed species. The resulting adsorption energies were used to obtain the free energy profile. The result showed that an oxygen molecule can be efficiently reduced to form water molecules on the vacancy site, with the activity comparable to that of the platinum electrode [2]. The activity was estimated thermodynamically using the empirical assumption that the barrier existing between the reaction intermediates does not play a role. Importantly, the estimated activity was found to be comparable to that of the non-defective surface. This result should be interpreted with caution. Considering the low availability of the active defects, we can conclude that the overall rate of ORR is likely to be higher for the non-defective surface, although we cannot rule out the possibility that we have missed important configurations due to the finite cell size and time used for the simulation. The apparent inconsistency with experiments that the efficiency of the fuel cell is increased by introducing the defects can be explained if the carrier supply is significantly increased by doping. This will be the case if defect induced

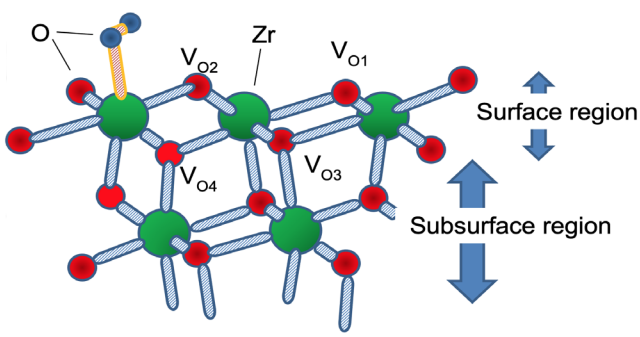

Fig. 1. (Schematic view) Part of the 2 × 1 slab model of the defective tetragonal ZrO_2(101) surface where one O_2 molecule (blue spheres) is adsorbed on a surface Zr atom (green) surface. We have examined all possible paths for the oxygen reduction reaction where the adsorbed O_2 is reduced to form a water molecule. The defect site was modeled by removing a surface O atom, VO1 and VO2, and substituting a subsurface O atom with a N impurity.

gap states are extended in the sample. With this in mind, we are now theoretically investigating the electrostatic potential profile to see how the carrier path can be facilitated.

In the above surface simulation, we have neglected the solvation effect. Water molecules can be adsorbed on the zirconia surface as a molecule or as dissociated species, OH* and H*, blocking the incoming oxygen molecule to be adsorbed. This possibility was investigated using the machine-learned potential developed with abICS. Based on many nanosecond trajectories, we found that water molecules do not favor the surface vacancy site, while they favor reactive Zr sites when no defects are introduced. This is likely to be an indirect indication that the blocking effect is significantly different between the defective and pristine surfaces. Further simulations are now in progress to make a conclusion about the solvation effect.

References
[1] https://www.pasums.issp.u-tokyo.ac.jp/abics/
[2] S. Muhammady, J. Haruyama, S. Kasamatsu, and O. Sugino, J. Phys. Chem. C**126**, 15662 (2022).

Authors
S. Muhammady, A. Nakanishi, A. F. Flaviano, J. Haruyama, S. Kasamatsu[a], and O. Sugino.
[a]Yamagata University

Study on the Channel Gating Mechanism of Channelrhodopsin C1C2

Akiyama and Inoue Groups

Channelrhodopsins (ChRs) are members of microbial rhodopsins that function as light-gated cation channels. ChRs are composed of seven transmembrane (TM) helices and an all-*trans*-retinal chromophore which is covalently bound to the seventh TM helix via a protonated Schiff base linkage. Light absorption induces the isomerization of the retinal chromophore from the all-*trans* to the 13-*cis* form leading to the subsequent conformation change of the protein moiety opening the ion-transport channel connecting the extracellular and cytoplasmic solvents. Recently, ChRs are being used widely in optogenetics to control neural activity in an animal body. Whereas high-functional ChR proteins are being strongly demanded to realize efficient and low-invasive optogenetics, the lack of understanding of its channel-gating mechanism is inhibiting rational and precise protein engineering to improve the functionality of ChRs. The structural information of the open state of ChR

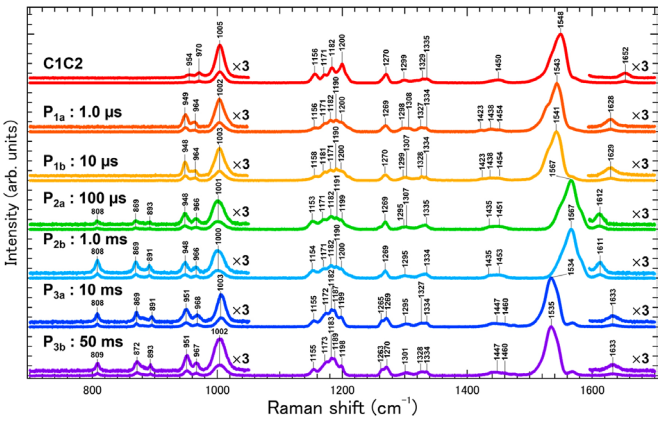

Fig. 1. Time-resolved resonance Raman spectra of each state of C1C2

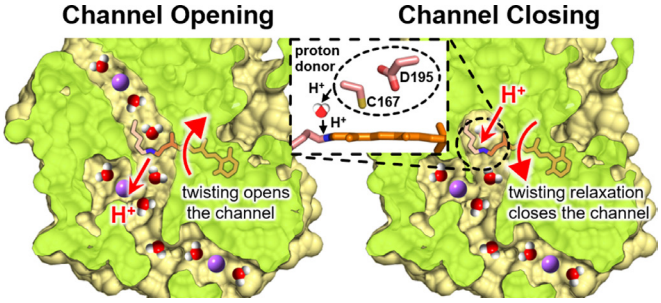

Fig. 2. Channel gating mechanism of C1C2

is indispensable to clarify the mechanism. However, it was difficult due to the inhibition of the channel opening by the tight packing of protein molecules in the crystal phase for the X-ray crystallographic analysis.

To overcome this difficulty, we studied the channel opening and closing processes of C1C2, one of the best characterized ChRs whose three-dimensional structure was first solved, by time-resolved resonance Raman spectroscopy, laser flash photolysis, and laser electrophysiology. Especially, time-resolved resonance Raman spectroscopy can selectively obtain detailed information on the chemical bonds of the retinal chromophore based on its vibrational modes. However, time-resolved resonance Raman spectroscopy generally requires a large amount of protein sample which is difficult to prepare for C1C2. We avoided this problem by developing a new Raman microspectroscopy system using semiconductor lasers, acoustic-optics modulators (AOM), an optical objective lens, and an automated optical stage. As a result, we succeeded in obtaining the resonance Raman spectra of the initial and all photointermediate states of C1C2 and revealed the enhancement of the hydrogen-out-of-plain mode of the retinal chromophore after the photoexcitation of C1C2 indicating the polyene chain of the retinal is more twisted compared with the dark state. The twisting of the retinal is maximized in the full-open state of C1C2. Hence, the channel gate in C1C2 is opened by the steric repulsion between the retinal chromophore and transmembrane helices as previously suggested by the quantum-mechanics/molecular-mechanics calculation [1] and time-resolved X-ray crystallographic study [2] on the pre-opened state. On the other hand, the shift and broadening of the C=N stretching vibration band revealed the switching of the hydrogen-bonding partner of the retinal Schiff base from the counterion to a water molecule during the channel opening. Furthermore, the laser flash photolysis and laser electrophysiology measurements revealed that, while the channel opening kinetics did not alter between H_2O and D_2O solvents, the rate of channel closing was significantly slowed in D_2O compared to H_2O. This result indicates that the protonation of the retinal chromophore relaxes the twisted polyene chain leading to the channel closing.

This study provided a new understanding of the channel gating mechanism of ChR in which the channel opening is induced by the retinal twisting and the closing rate is regulated by the proton transfer between the protein moiety and the chromophore [3]. The development of novel functional ChRs based on this understanding in the near future is highly expected.

References
[1] C. Cheng, M. Kamiya, M. Takemoto, R. Ishitani, O. Nureki, N. Yoshida, and S. Hayashi, Biophys. J. **115**, 1281 (2018).
[2] K. Oda, T. Nomura, T. Nakane, K. Yamashita, K. Inoue, S. Ito, J. Vierock, K. Hirata, A. D. Maturana, K. Katayama, T. Ikuta, I. Ishigami,

T. Izume, R. Umeda, R. Eguma, S. Oishi, G. Kasuya, T. Kato, T. Kusakizako, W. Shihoya, H. Shimada, T. Takatsuji, M. Takemoto, R. Taniguchi, A. Tomita, R. Nakamura, M. Fukuda, H. Miyauchi, Y. Lee, E. Nango, R. Tanaka, T. Tanaka, M. Sugahara, T. Kimura, T. Shimamura, T. Fujiwara, Y. Yamanaka, S. Owada, Y. Joti, K. Tono, R. Ishitani, S. Hayashi, H. Kandori, P. Hegemann, S. Iwata, M. Kubo, T. Nishizawa, and O. Nureki, eLife **10**, e6238 (2021).
[3] K. Shibata, K. Oda, T. Nishizawa, Y. Hazama, R. Ono, S. Takaramoto, R. Bagherzadeh, H. Yawo, O. Nureki, K. Inoue, and H. Akiyama, J. Am. Chem. Soc., doi: 10.1021/jacs.3c01879 (2023).

Authors
K. Shibata, K. Oda[a], T. Nishizawa[a], Y. Hazama, R. Ono, S. Takaramoto, R. Bagherzadeh, H. Yawo, O. Nureki[a], K. Inoue, and H. Akiyama
[a]The University of Tokyo

Non-Invertible Duality Transformation Between SPT and SSB Phases

Oshikawa Group

Symmetry-Protected Topological (SPT) phases are one of the central issues in contemporary quantum many-body physics. While the concept of SPT phases was established after the discovery of topological insulators, which are the free electron version of SPT phases, a prototypical example of the bosonic SPT phases, the Haldane gap phase, was found much earlier. In 1992, Kennedy and Tasaki constructed a non-local unitary transformation that maps between a $\mathbb{Z}_2\times\mathbb{Z}_2$ spontaneously symmetry breaking phase and the Haldane gap phase on an open spin chain [1,2]. This gave a unified understanding of the exotic natures of Haldane gap phase, narrowly missing the clear recognition of concept of the SPT phases.

Since the discovery of the concept of the SPT phases in 2009, significant progress has been made on many fronts. In particular, systematic classifications in general dimensions have been studied, uncovering the deep relation to topological quantum field theory and algebraic topology. Given the history, it would be worthwhile to revisit the Kennedy-Tasaki transformation, which played a significant role in understanding the Haldane gap phase 30 years ago, from the modern perspective.

To this end, in this work [3] we demonstrate that the Kennedy-Tasaki transformation can be defined on closed chains by sacrificing unitarity, or by expanding the Hilbert space by including "twist" sectors corresponding to different boundary conditions. This is shown for both the original Kennedy-Tasaki transformation on S = 1 chain and for its generalization on S = 1/2 chain. In both cases, the closed chain version of the Kennedy-Tasaki transformation is a non-unitary transformation and satisfy the non-invertible fusion rules, as in the famous Kramers-Wannier duality transformation. Such non-invertible duality transformations generalizing the Kramers-Wannier duality have been extensively discussed in recent years, both in (1 + 1) and higher dimensions. When the system is invariant under the duality transformation, the operator representing the transformation becomes a non-invertible symmetry of the system. Indeed, we reveal the close connection between the Kramers-Wannier and Kennedy-Tasaki dualities; in particular, we show that Kennedy-Tasaki duality can be constructed in terms of the Kramers-Wannier duality in field theory and on S = 1/2 chain.

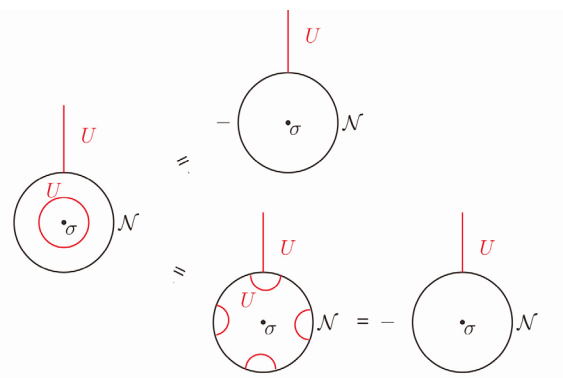

Fig. 1. A graphical illustration for the fusion rule between the Kramers-Wannier duality $\mathcal{N}$ and the global spin-flip operator U in the twisted sector, which is implemented by the twist operator σ. This type of relations is also relevant for Kennedy-Tasaki transformation.

Although the Kennedy-Tasaki transformation on S = 1 chain and that on S = 1/2 chain can be shown to be equivalent, the construction on S = 1/2 chain is more convenient for further applications, because the degrees of freedom charged under two $\mathbb{Z}_2$'s are decoupled; the first and the second groups of S = 1/2 are charged under separate $\mathbb{Z}_2$'s respectively. Moreover, the decoupling between degrees of freedom admits a more convenient interpretation of twisted gauging, similarly to the Kramers-Wannier duality transformation which implements gauging of the $\mathbb{Z}_2$ global symmetry. This interpretation also facilitates the construction of new models with interesting topological features. In particular, we utilize Kennedy-Tasaki transformation on S = 1/2 chain to systematically construct a series of gapless SPT phases, not only those have been recently explored, but also uncovering new ones. Our work opens up a new approach to the study of gapless SPT phases, which are at the forefront of the current quantum many-body problem.

References
[1] T. Kennedy and H. Tasaki, Phys. Rev. B **45**, 304 (1992); Commun. Math. Phys. **147**, 431 (1992).
[2] M. Oshikawa, J. Phys. Condens. Matter **4**, 7469 (1992).
[3] L. Li, M. Oshikawa, and Y. Zheng, arXiv:2301.07899 (2023).

Authors
L. Li, M. Oshikawa, and Y. Zheng[a]
[a]Kavli IPMU (and ISSP)

Pressure-Induced Superconductivity up to 9 K in the Quasi-One-Dimensional KMn_6Bi_5

Uwatoko Group

Unconventional superconductivity beyond the Bardeen-Cooper-Schrieffer theory usually emerges on the border of long-range antiferromagnetic order as exemplified by the cuprate, iron-pnictide, and heavy-fermion superconductors. In these cases, the enhanced magnetic fluctuations are believed to be the binding glue of Cooper pairs. As such, it is expected to find unconventional superconductivity in the vicinity of the antiferromagnetic quantum critical point (QCP), which can be achieved by employing external tuning parameters such as chemical doping and applying physical pressure. By following this approach, we discovered the first Mn-based superconductor MnP by suppressing its helimagnetic order via the application of high pressure, even though the Mn-based superconductor is rare owing to the strong magnetic pair-breaking effect. Its superconducting transition temperature Tc ≈ 1 K is low and the superconductivity

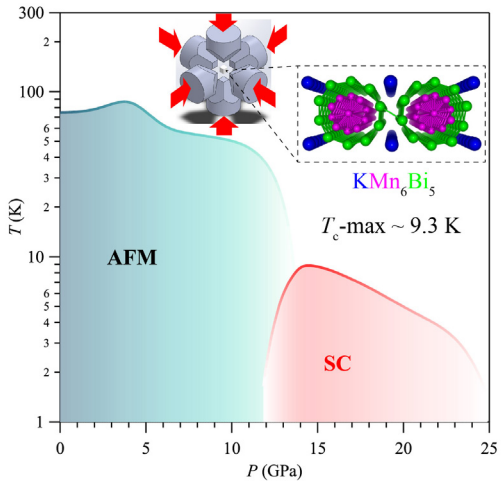

Fig. 1. Temperature-pressure phase diagram of KMn_6Bi_5. Inset shows the Q1D crystal structure of KMn_6Bi_5.

only appears in a narrow pressure range around Pc ≈ 8 GPa where the helimagnetic order just vanishes. Since then, we have been devoted to find more Mn-based superconductors with higher T_c. In this regard, we pay special attention to the ternary or complex Mn-based magnetic materials with low-dimensional structures, in which the enhanced magnetic fluctuations are expected to promote stronger superconducting pairing and thus higher T_c in comparison to the three-dimensional MnP. After seven-year endeavor, we recently discovered the first ternary Mn-based superconductor KMn_6Bi_5 [1].

KMn_6Bi_5 is a newly synthesized ternary compound with a quasi-one-dimensional (Q1D) monoclinic structure featured by the presence of infinite $[Mn_6Bi_5]^-$ columns along the b-axis as shown in the inset of Fig. 1. These columns are composed of an outer nanotube of Bi atoms surrounding an inner Mn–Mn bonded metallic core. At ambient pressure (AP), KMn_6Bi_5 undergoes an antiferromagnetic transition at $T_N \approx 75$ K, which is manifested as a pronounced anomaly in resistivity and magnetic susceptibility. Curie–Weiss fitting to the paramagnetic susceptibility above T_N yield a relatively small effective moment of Mn, i.e., 1.4-1.6 μB, signaling an itinerant nature of the magnetism similar to MnP. First-principles calculations have revealed that the density of states at the Fermi level are dominated by the Mn-3d electrons and the helical antiferromagnetic structures are stable.

By measuring resistance and ac magnetic susceptibility under hydrostatic pressures up to 14.2 GPa in a cubic anvil cell apparatus, we find that its antiferromagnetic order is first enhanced moderately and then suppressed completely at a critical pressure of $P_c \approx 13$ GPa, around which bulk superconductivity emerges and exhibits a domelike $T_c(P)$ with the maximal $T_c^{onset} \approx 9.3$ K achieved at 14.2 GPa. As shown in Fig. 1, the close proximity of superconductivity to a magnetic instability in the temperature-pressure phase diagram of KMn_6Bi_5 resembling many unconventional superconducting systems mentioned above suggests an unconventional magnetism-mediated paring mechanism. Its unconventional nature is also substantiated by the observations of strange-metal behavior in the normal-state resistance near P_c and an unusually large $\mu_0H_{c2}(0T)$ exceeding the Pauli limit. Since the theoretical calculations on KMn_6Bi_5 suggest dominant contributions of Mn-3d orbital electrons to the density of states at Fermi level, it becomes the first ternary Mn-based superconductor with a relatively high T_c of 9.3 K, which is one order of magnitude higher than that of MnP (~1 K). In contrast to the binary MnP, the flexibility of the crystal structure and chemical compositions in the ternary AMn_6Bi_5 (A = alkali metal) can open a new avenue for finding more Mn-based superconductors.

Reference

[1] Z. Y. Liu, Q. X. Dong, P. T. Yang, P. F. Shan, B. S. Wang, J. P. Sun, Z. L. Dun, Y. Uwatoko, G. F. Chen, X. L. Dong, Z. X. Zhao, and J.-G. Cheng, Phys. Rev. Lett. **128**, 187001 (2022).

Authors

Z. Y. Liu[a,b], Q. X. Dong[a,b], P. T. Yang[a,b], P. F. Shan[a,b], B. S. Wang[a,b], J. P. Sun[a,b], Z. L. Dun[a,b], Y. Uwatoko, G. F. Chen[a,b], X. L. Dong[a,b], Z. X. Zhao[a,b], and J.-G. Cheng[a,b]
[a]Chinese Academy of Sciences
[b]University of Chinese Academy of Sciences

Pressured-Induced Superconducting Phase with Large Upper Critical Field and Concomitant Enhancement of Antiferromagnetic Transition in $EuTe_2$

Uwatoko Group

The interplay between static magnetism and conduction electrons has been a core topic in modern condensed matter physics spanning a broad spectrum of interesting phenomena including the Kondo physics and heavy fermions, dilute magnetic semiconductors, giant/colossal magnetoresistance, and spintronics. Recently, the addition of nontrivial band topology to this topic leads to more exotic topological quantum phenomena such as quantum anomalous Hall effect and the intrinsic large anomalous Hall effect. When the conduction electrons condense into Cooper pairs and coexist with static magnetism in the magnetic superconductors, unconventional pairing states with intriguing superconducting properties can emerge as exemplified by the U- and Eu-based magnetic superconductors. Due to the antagonistic nature between magnetism and superconductivity, however, the magnetic superconductors are rare, and the concurrence of abovementioned phenomena in a single material is even scarce. Recently, we reported on a rare case that manifests an intimated interplay among static magnetism, conduction electrons, and possible exotic superconductivity through pressure regulations on an antiferromagnetic (AF) semiconductor $EuTe_2$ [1].

At ambient pressure (AP), $EuTe_2$ crystallizes in a $CuAl_2$-type tetragonal structure with space group I4/mcm. As seen in the inset of Fig. 1, each Eu^{2+} ion is surrounded by eight Te atoms, which form the $[Te_2]^{2-}$ dimers stacking along the c-axis. Upon cooling down at zero field, $EuTe_2$ exhibits a semiconducting behavior in resistivity and the Eu^{2+} moments develop a type-A AF order below $T_N = 11$ K, having the c-axis-oriented ferromagnetic (FM) Eu^{2+} layers coupled antiferromagnetically. When an external magnetic field is applied along c-axis, the type-A AF order can be tuned into a canted AF state through a spin-flop transition at $\mu_0H_1 = 2.3$ T and then a fully spin-polarized state at $\mu_0H_2 = 7.6$ T. Interestingly, these field-induced transitions have a profound impact on the transport properties of $EuTe_2$; i.e., ρ(T) under $\mu_0H > \mu_0H_1$ is altered from semiconducting to metallic-like behavior below a characteristic temperature $T_m >> T_N$, resulting in a large negative MR with over five orders of drop in resistivity at low temperatures. According to the density-

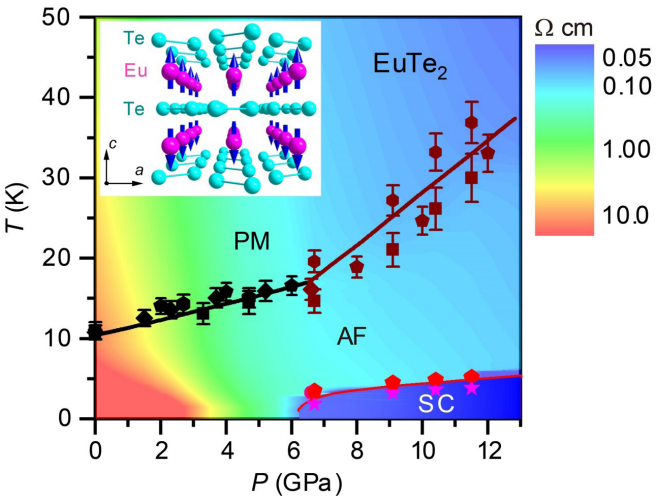

Fig. 1. Temperature-pressure phase diagram of $EuTe_2$. Inset shows the crystal and magnetic structures of $EuTe_2$ at ambient pressure.

functional-theory calculations, the charge carriers near the Fermi level originate mainly from the Te-5p orbitals and the small energy gap of $E_a \approx 16$ meV at zero field can be closed by lifting the band degeneracy of the Te-5p orbitals in the spin-flop state with a net FM component. This explains the field-induced metallic state and thus the large negative MR below T_m. These results thus demonstrated an intimated interplay between the static magnetism of Eu^{2+} sublattice and the charge carries from Te-5p orbitals in $EuTe_2$.

Considering the fact that many Te-containing materials become superconducting at ambient and/or high pressures, we are motived to pursue whether $EuTe_2$ can be driven into a magnetic superconductor upon compression. So, we investigate the effect of pressure on the transport and magnetic properties of $EuTe_2$ single crystals by using a cubic anvil cell apparatus. The main results are summarized in the temperature–pressure phase diagram of $EuTe_2$ in Fig. 1. We find that the application of high-pressure drives $EuTe_2$ from an AF semiconductor showing a large negative MR into a magnetic superconductor with a large upper critical field comparable to the Pauli paramagnetic limit. Interestingly, the emergence of superconductivity above the critical pressure of $P_c \approx 6$ GPa is accompanied with a concomitant enhancement of T_N, which experiences a quicker rise with the slope increased dramatically from $dT_N/dP = 0.85(14)$ K/GPa for $P \leq Pc$ to 3.7(2) K/GPa for $P \geq Pc$. Moreover, the superconductivity can survive in the spin-flop state with a net FM component of the Eu^{2+} sublattice under moderate fields $\mu_0 H \geq 2$ T, implying a possible exotic pairing state. Our findings establish the pressurized $EuTe_2$ as a rare magnetic superconductor, and these new results under high pressures have enriched the physics pertinent to the interplay between static magnetism and conduction electrons in this interesting compound.

Reference

[1] P. T. Yang, Z. Y. Liu, K. Y. Chen, X. L. Liu, X. Zhang, Z. H. Yu, H. Zhang, J. P. Sun, Y. Uwatoko, X. L. Dong, K. Jiang, J. P. Hu, Y. F. Guo, B. S. Wang, and J.-G. Cheng, Nature Commun. **13**, 2975 (2022)

Authors

P. T. Yang[a,b], Z. Y. Liu[a], K. Y. Chen[a,b], X. L. Liu[c], X. Zhang[c], Z. H. Yu[c], H. Zhang[a,b], J. P. Sun[a,b,d], Y. Uwatoko, X. L. Dong[a,b,d], K. Jiang[a,b,d], J. P. Hu[a,b], Y. F. Guo[c] B. S. Wang[a,b,d], and J.-G. Cheng[a,b]

[a]Chinese Academy of Sciences

[b]University of Chinese Academy of Sciences

[c]Shanghai Tech University

[d]Songshan Lake Materials Laboratory

Pressure Induced Superconductivity and Multiple Structural Transitions in CsCl-Type Cubic CeZn Single Crystal

Uwatoko Group

The CsCl-type compound crystallizing in cubic structure with chemical formula *ReTm* (where *Re* = rare earth elements such as La, Ce, Pr…etc., and *Tm* = typical metal elements such as Ag, Zn, Cd, …etc.) have been known for last three decades due to their strong correlation between charge, spin, and lattice degrees of freedom. These compounds undergo a cubic-to-tetragonal structural transition on cooling, followed by a magnetically ordered state at a lower temperature.

Among these, CeZn is distinct because the magnetic and structural transitions are coupled, revealing a first-order nature of the transition. CeZn exhibits antiferromagnetic (AFM) order below the Neel temperature, $T_N \sim 30$ K, and a concurrent crystal structural change from cubic to a tetragonal structure [1,2]. So far, the electrical, magnetic, and structural properties of CeZn have been investigated by substituting Cu in place of Zn, $CeZn_{1-x}Cu_x$ [3], and applying pressure up to 2.9 GPa [1]. On applying pressure, the AFM ordering changes to ferromagnetic (FM) ordering above 1 GPa, and the coupled magnetic and crystal structural transitions become separated. The neutron diffraction study [2] pointed that the crystal structure altered from cubic to rhombohedral structure in the FM state. With further increase in pressure, the Curie temperature, T_C, of the FM state was found to decrease with pressure, while the structural transition temperature increases and reaches room temperature around 3.0 GPa. However, further investigation of the lattice structure and electronic properties of CeZn at higher pressure has remained unexplored.

CeZn single crystals were synthesized by melting Ce and Zn with a 1:1 ratio as starting material in a tungsten crucible sealed inside a quartz tube under vacuum. Resistivity under high pressure was measured using a clamp type piston cylinder cell and a palm cubic anvil cell. The single crystal X-ray diffraction was carried out by using Rigaku XtaLab HyPix-6000 diffractometer with Mo-Kα radiation (λ = 0.71073 Å).

Figure 1 shows the temperature dependence of the electrical resistivity ρ of a CeZn single crystal at some

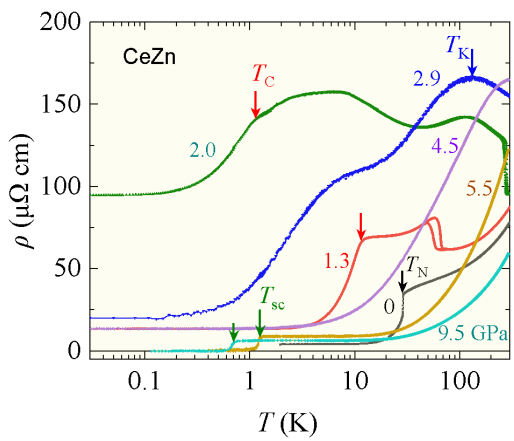

Fig. 1. Temperature dependence of electrical resistivity ρ, of CeZn single crystal at some selected pressures. Black and red arrows show the magnetic transition temperatures, T_N and T_C, respectively. Blue arrow indicates Kondo temperature (T_K), and green arrows indicate superconductivity transition temperature (T_{sc}).

selected pressures from 300 K down to 30 mK. At ambient pressure, ρ(T) monotonically decreases with temperature and drops suddenly below T_N = 29.0 K. It is clear from Fig. 1 that the coupled structural and magnetic transition become separated on increasing pressure above 1.0 GPa, in agreement with the earlier report [1,2]. At 1.3 GPa, the bend at the lower temperature side is assigned to the pressure-induced FM state, while the thermal hysteresis appearing at the high temperature side is attributed to the crystal structural transition. On increasing pressure to 2.0 GPa, FM state shifts towards lower temperature and the crystal structural transition temperature almost reaches to 280 K. Here, it is worthy to note that, in contrast to earlier result [1], in the present case, the crystal structural transition exceeds room temperature at lower pressure. This is clear by the absence of hysteretic behavior in ρ(T) below 300 K even at 2.9 GPa. This difference is attributed to the higher quality of sample used in the present study than the earlier polycrystalline samples [1]. Moreover, at 2.9 GPa, the signature of T_C disappears, and another big hump appears around 100 K, implying the pronounced Kondo effect. Up to 5.0 GPa, ρ(T) shows a normal metallic behavior in the measured temperature range. Surprisingly, on slightly increasing the pressure to 5.5 GPa as shown in Fig. 1, ρ(T) displays a pronounced drop below ~1.3 K and reaches zero around 0.8 K, signaling the occurrence of a superconducting state, which survives even up to 9.5 GPa.

To find the microscopic origin of these anomalies, we performed single crystal X-ray diffraction of CeZn at selected pressures at room temperature. From the X-ray diffraction analysis, we deduce that the crystal structure of CeZn sequentially evolves with increasing pressure from a cubic structure (at ambient pressure) to tetragonal (at 2.8 GPa), orthorhombic (at 4.2 GPa) and finally to monoclinic (at 8.2 GPa). To find a correlation between the crystal structure and the underlying electronic properties with increasing pressure, we have constructed a temperature (T)—pressure (P) phase diagram of CeZn, as shown in Fig. 2. The coupled magnetic transition, PM to AFM state, and the structural transition, cubic to tetragonal structure due to the magnetic striction, at T_N decreases hardly up to 1.0 GPa [1,2]. Above 1.0 GPa, the pressure induced an another cubic-to-tetragonal structural transition caused by the band Jahn-Teller effect [4]. The T–P phase diagram reveals that the electronic properties of CeZn also change simultaneously across the structural transitions. First, the ground state changes AFM to FM due to the cubic-to-tetragonal structural transition with pressure. T_C decreases rapidly to 1.1 K in the tetragonal structure as pressure increases to 2.0 GPa, implying a possible existence of a quantum critical point. Secondly, at the tetragonal-to-orthorhombic structural transition, CeZn transforms into a nonmagnetic simple metallic state. Finally, superconductivity emerges below T_{sc} ~ 1.3 K around 5.5 GPa possibly when the crystal structure changes from orthorhombic to monoclinic. The superconducting states survive up to 9.5 GPa in the monoclinic crystal structure. Here, it is worth noting that the T–P diagram of CeZn is different from that of the other Ce-based superconductors, in which superconductivity appears very close to the magnetic quantum critical point, whereas superconductivity in CeZn appears far away from the magnetic state. These results may suggest that the emergence of superconductivity in CeZn under pressure is related to the change in crystal structure implying a nonmagnetic origin of the Cooper pair formation.

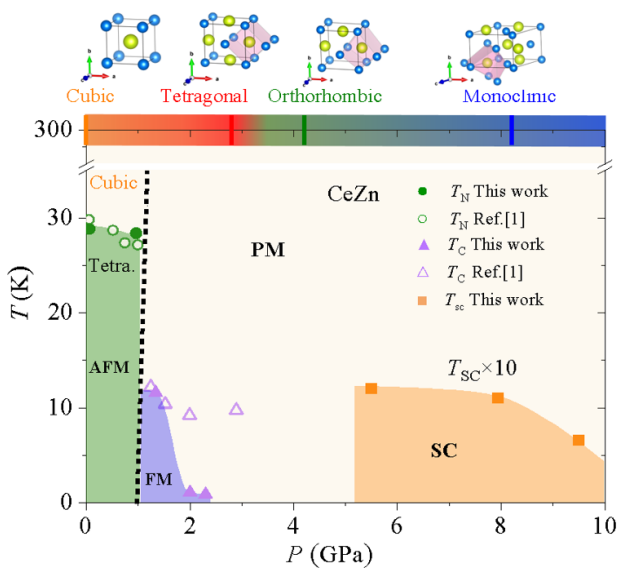

Fig. 2. Temperature–pressure phase diagram of CeZn. T_N, T_C, and T_{sc} are the Néel temperature, the Curie temperature and the superconducting transition temperature determined from the resistivity data, respectively. For clarity, T_{sc} has been multiplied by a factor of 10. The stars indicate the pressure value at which the single crystal X-ray diffraction measurements are performed. The tetragonal structure in the AFM region is obtained from Ref. [2]. The cubic to the tetragonal structure boundary line has been used from Ref. [1].

In summary, we have performed systematic electrical resistivity and single crystal X-ray diffraction measurement of CeZn under high pressure up to 9.5 GPa. We find that CeZn exhibits multiple crystal structural transitions under pressure. Simultaneously, across these crystal structural transitions, the signature of modification of the underlying electronic properties of CeZn is also detected. Also, we would like to add that further investigation of how crystal structural change with decreasing temperature at a fixed pressure is required for detailed understanding about the relationship between the crystal structure and electronic properties.

References

[1] H. Kadomatsu, H. Tanaka, M. Kurisu, and H. Fujiwara, Phys. Rev. B **33**, 4799 (1986).
[2] T. Shigeoka, Y. Uwatoko, H. Fujii, L. Rebelsky, S. M. Shapiro, and K. Asai, Phys. Rev. B **42**, 8394 (1990).
[3] Y. Uwatoko, Y. Fujii, M. Nishi, K. Motoya, and Y. Ito, J. Magn. Magn. Mater. **76**, 411 (1988).
[4] H. Ihrig, D.T. Vigren, J.Kübler, and S. Methfessel, Phys. Rev. B **8**, 4525 (1973).

Authors
X. Shen[a], H. Ma, D. Bhoi, J. Gouchi, Y. Uwatoko, A. Dalan[b], Y. Kawamura[b], H. Sato[c], I. Umehara[a] , and M. Uehara[a]
[a]Yokohama National University
[b]Muroran Institute of Technology
[c]Rigaku Corporation, Akishima

Large Magnetic-Field-Induced Volume Change in Sintered Chromium Tellurides

Okamoto Group and X-Ray Diffraction Section

There is a long history in the study of magnetic-field-induced strains in ferromagnets. The most classical examples are iron and nickel, which show linear strains of several ppm to several tens of ppm by applying a magnetic field. The fact that their shapes can be changed by applying a magnetic field means that it can be used as an actuator that converts input energy or signal into mechanical movement. The small

magnetostrictions in iron and nickel are insufficient for this application, but in 1960s, giant magnetostrictive materials such as Terfenol-D, exhibiting a large strain exceeding 2000 ppm, have been developed and used as a material for magnetostrictive actuators. In such magnetostrictions in ferromagnetic metals, the volume change is small. In contrast, there are a few materials that exhibit a large volume change in magnetic fields (forced volume magnetostriction), such as invar alloys. Invar alloys exhibit very small thermal expansion over a wide temperature range due to the magnetovolume effect, which also plays an important role in the manifestation of the large volume change in magnetic fields.

We have discovered large magnetic-field-induced volume changes in Cr-based magnets such as $LiInCr_4S_8$ and $AgCrS_2$, which were hardly recognized as candidates for magnetostrictive materials [1,2]. Large volume increases reaching $\Delta V/V$ = 700 ppm under a magnetic field of 9 T were observed in $LiInCr_4S_8$ just below the Néel temperature of T_N = 24 K and in $AgCrS_2$ at T_N = 42 K. Unlike invar alloys, these Cr-based magnets are antiferromagnetic insulators, suggesting that the large volume increases are caused by a complex interplay between the characteristic features of Cr spins, such as magnetic ordering accompanied by structural distortion, strong spin–lattice coupling, and geometrical frustration. However, the large volume changes were realized only at low temperature due to the low Néel temperatures, which is a disadvantage as a volume function. Therefore, we focused on Cr_3Te_4, which shows a ferromagnetic transition at a high temperature of T_C = 330 K. Cr_3Te_4 is ferromagnetic unlike the above Cr sulfides but is promising if the characteristic features of Cr-based magnets are utilized. In fact, we found that Cr_3Te_4 sintered samples, shown in the inset of Fig. 1(c), show magnetic-field-induced strains accompanied by large volume changes in a wide temperature region including room temperature [3].

Figure 1 shows the linear strains in magnetic fields of a Cr_3Te_4 sintered sample measured at various temperatures. The strains in Cr_3Te_4 can be understood as the summation of two components that are isotropic strain with the volume change and anisotropic strain with the shape change shown in Fig. 1(a). The latter shows small values up to several tens of ppm, which correspond to the ferromagnetic magnetization curve, suggesting that Cr_3Te_4 showed usual behavior as a ferromagnet. In contrast, as shown in Fig. 1(b), the volume changes in magnetic fields are very large reaching $\Delta V/V$

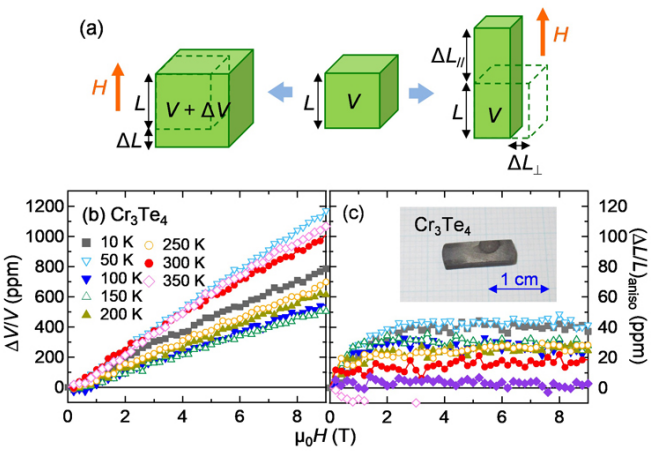

Fig. 1. (a) Isotropic (left) and anisotropic (right) magnetic-field-induced strains. (b) The volume changes in magnetic fields of a Cr_3Te_4 sintered sample measured at various temperatures. (c) The anisotropic strains in magnetic fields, corresponding to $\Delta L_\perp$ in the right panel of (a), of a Cr_3Te_4 sintered sample. The inset shows the Cr_3Te_4 sintered sample.

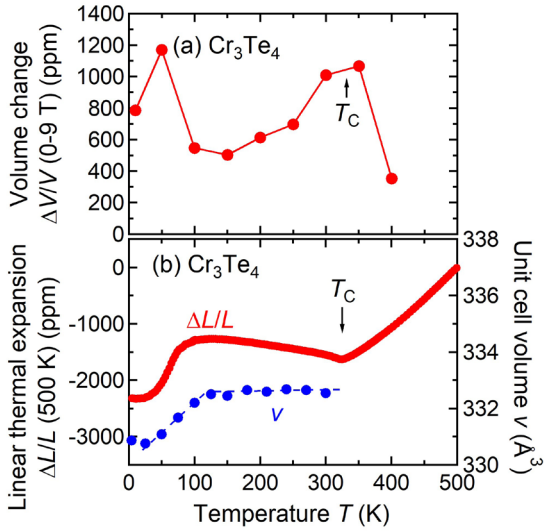

Fig. 2. (a) The volume changes of a Cr_3Te_4 sintered sample by applying a magnetic field of 9 T. (b) Linear thermal expansion with the reference temperature of 500 K (left) and unit cell volume determined by powder X-ray diffraction experiments (right) of a Cr_3Te_4 sintered sample.

=1200 ppm at a magnetic field of 9 T. This value is nearly twice as large as the maximum value of volume changes observed in Cr-based magnets as well as comparable to those of invar alloys. It is notable that a magnetic field of 9 T induced a significant volume change over 1000 ppm at room temperature and that the volume changes over 500 ppm throughout the entire temperature range below 350 K, as shown in Fig. 2(a).

The magnetic-field-induced volume changes in the Cr_3Te_4 sintered sample are particularly large near the Curie temperature, suggesting that the ferromagnetic order plays an essential role for the manifestation of the large volume increase. As shown in the linear thermal expansion shown in Fig. 2(b), a Cr_3Te_4 sintered sample showed a negative thermal expansion in a wide temperature range of 120–330 K below T_C, where the volume increases with decreasing temperature. This result indicates that Cr_3Te_4 gradually changes from paramagnetic to ferromagnetic ordered states with decreasing temperature, implying that the ferromagnetic order is enhanced by applying a magnetic field in this temperature region, resulting in the large magnetic-field-induced volume change.

The thermal expansion of the Cr_3Te_4 sintered sample has another feature that the volume change associated with the ferromagnetic order does not match the volume change of a unit cell. As seen in the Fig 1(b), there is no temperature region where the unit cell volume increases with decreasing temperature. This discrepancy suggests that the negative thermal expansion in the Cr_3Te_4 sintered sample is due to the "mictrostructural effects", discussed in β-eucryptite and Ca_2RuO_4, etc.[4,5] In Cr_3Te_4, the large magnetic-field-induced volume change and negative thermal expansion have the same origin that is the volume change at the ferromagnetic order, strongly suggesting that the microstructural effects play an important role in the emergence of the large magnetic-field-induced volume change. This is a different mechanism from the strong magnetovolume effect for invar alloys and might be a novel magneto-volume phenomenon occurring in Cr-based magnets.

References
[1] T. Kanematsu, M. Mori, Y. Okamoto, T. Yajima, and K. Takenaka, J. Phys. Soc. Jpn. **89**, 073708 (2020).
[2] T. Kanematsu, Y. Okamoto, and K. Takenaka, Appl. Phys. Lett. **118**, 142404 (2021).
[3] Y. Kubota, Y. Okamoto, T. Kanematsu, T. Yajima, D. Hirai, and K. Takenaka, Appl. Phys. Lett. **122**, 042404 (2023).
[4] F. H. Gillery and E. A. Bush, J. Am. Ceram. Soc. **42**, 175 (1959).
[5] K. Takenaka, Y. Okamoto, T. Shinoda, N. Katayama, and Y. Sakai, Nat. Commun. **8**, 14102 (2017).

Authors
Y. Okamoto, Y. Kubota[a], T. Kanematsu[a], T. Yajima, D. Hirai[a], and K. Takenaka[a]
[a]Nagoya University

Rotations of Methane Molecules in Amorphous and Crystalline Hydrates

Yamamuro Group

Methane hydrate has been studied extensively not only as a future energy resource but also from the interest in quantum and classical rotations of methane molecules. The crystalline methane hydrate (c-MH) forms a host water lattice of type I with two dodecahedral (12-hedral) and six tetradecahedral (14-hedral) cages per unit cell (space group: *Pm*3*n*), and each cage contains one methane molecule [1]. The chemical formula of c-MH is $CH_4 \cdot 5.75H_2O$. The "amorphous" MH (a-MH) was first prepared with a vapor-deposition method by our group [2]. The radial distribution functions derived from the neutron diffraction data demonstrated that the methane molecules are accommodated in the cage-like spaces even in amorphous structures. It is also known that the a-MH crystallizes into the c-MH around 175 K [3].

In this study, we have investigated the rotations of methane molecules in a-MH and c-MH. Our main interest is how the rotation of methane molecules is affected by the cage (like) structure, e.g., size and symmetry. The a-MH was prepared by depositing the mixture of CH_4 and D_2O gases onto the substrate cooled at 5 K using a custom-made cryostat [4], and c-MH was obtained by annealing the sample at 170 K under 0.1 MPa of CH_4 gas. Their quasi-elastic neutron scattering (QENS) and inelastic neutron scattering (INS) data were collected at 5 to 80 K using AGNES spectrometer at JRR-3, Tokai, Japan.

Figure 1 shows clear QENS broadening due to the

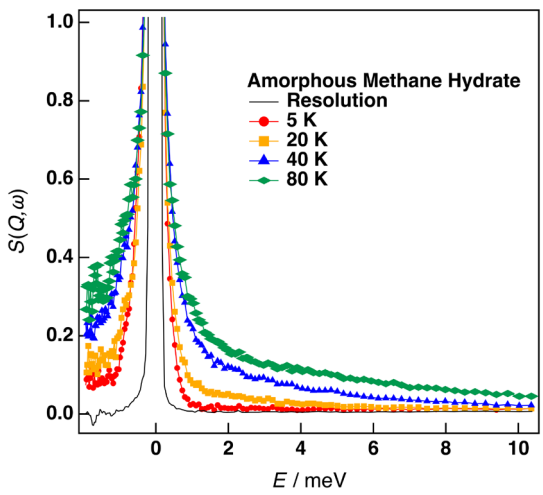

Fig. 1. Quasielastic neutron scattering spectra of amorphous methane hydrate. The data from all detectors are summed up. The average Q value is about 1.7 Å^{-1}.

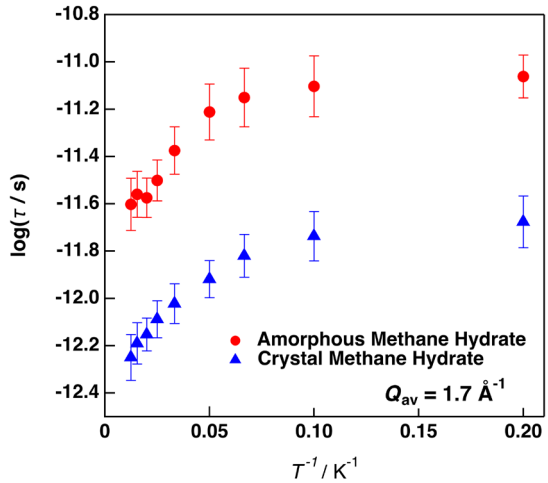

Fig. 2. Arrhenius plots of the relaxation times at Q_{av} = 1.7 Å^{-1} for the CH_4 rotation in amorphous and crystalline hydrates.

rotational motion of CH_4 accommodated in a-MH. It is worth noting that the QENS appeared even at 5 K. The data were well fitted to the combination of Delta and Lorentz functions as usual and the relaxation time τ was calculated from the peak width of the Lorentz function. Similar QENS data were observed also in c-MH. Figure 2 shows the Arrhenius plots for both a-MH and c-MH. There is a clear bending of the τ line around 20 K for both samples and the slope (activation energy ΔE_a) on the low-temperature side is very small (ΔE_a < 0.2 kJ/mol). We guess that there is a crossover between the classical (high-T) and quantum (low-T) rotations around 20 K; there is no temperature dependence of τ in a pure tunneling process. The a-MH has longer τ than that of c-MH. This is probably because the cage space in a-MH is narrower than that of c-MH. Additional neutron diffraction and calorimetric experiments are now going on to explain the QENS data more quantitatively.

References
[1] D. W. Davidson *et al.*, Nature **311**, 142 (1984).
[2] T. Kikuchi *et al.*, J. Phys. Soc. Jpn. **81**, 094604 (2012).
[3] M. Z. Faizullin *et al.*, Chem. Eng. Sci. **130**, 135 (2015).
[4] O. Yamamuro *et al.*, J. Chem. Phys. **115**, 9808 (2001).

Authors
M. Zhang, H. Akiba, and O. Yamamuro

Spin Excitation in a Chiral-Polar-Corundum Compound Ni_2InSbO_6

Masuda Group

In some types of non-centrosymmetric magnets, spin moments are incommensurately arranged to balance Dzyaloshinskii–Moriya (DM) and Heisenberg interactions.

This leads to helimagnetic spin textures and spin soliton lattice which exhibit distinctive magnetoelectric response and promising potential for applications in spintronics. A chiral-polar-corundum compound Ni_2InSbO_6 is an example for a proper-screw type spin structure realized by chirality-induced DM interaction [1], as shown in Fig. 1(a). In conventional helimagnets, a spin soliton lattice is induced in the magnetic field applied in the spin rotation plane. In contrast in Ni_2InSbO_6, the soliton lattice was proposed by a unique scenario. Suppose that additional DM interac-

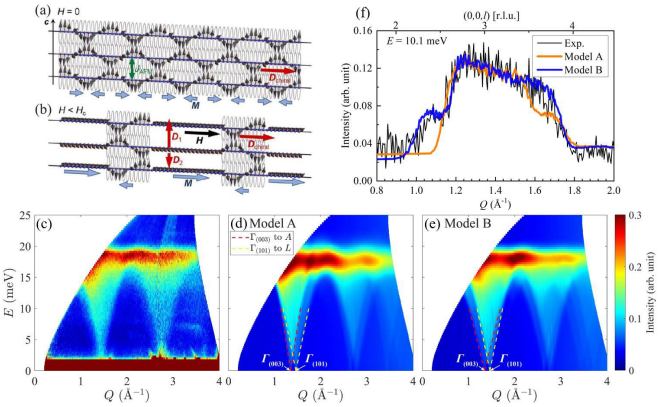

Fig. 1 Schematic of (a) proper-screw type helical spin structure and (b) spin soliton lattice in Ni_2InSbO_6. The figures were adopted from Ref. [1]. (c) INS spectrum measured with E_i = 30.5 meV at T = 10 K. (d),(e) Powder averaged LSWT calculation of INS spectra using the best fit parameters for model A in (d) and model B in (e). Modes of spin wave excitation from $\Gamma_{(003)}$ to $A_{(00\ 3/2)}$ and from $\Gamma_{(101)}$ to $L_{(1/2\ 0\ 1/2)}$ points are described by red and yellow dashed lines, respectively. (f) 1D-cut of powder spectrum at E = 10.1 meV for experiment (black), model A (orange) and model B (blue).

tions with the staggered vector component $\boldsymbol{D}_1$ and $\boldsymbol{D}_2$ along the polar c axis are assumed, as shown in Fig. 1(b). At zero magnetic field, localized magnetization components M are induced by $\boldsymbol{D}_1$ and $\boldsymbol{D}_2$ interacting between neighboring Ni^{2+} ions along the c axis, indicated by the light blue arrows in Fig. 1(a). In the magnetic field applied perpendicular to the spin rotation plane, they shrink or expand to minimize Zeeman energy, and hence the spin soliton lattice is realized. In previous Raman study [2], however, the spectrum was analyzed by the spin model assuming that the first and second neighbor Heisenberg interactions J_1 and J_2 were equal, corresponding that $\boldsymbol{D}_1$ and $\boldsymbol{D}_2$ were equal. The assumption was contradictory to the scenario based on the staggered DM vectors. Thus, in this work, we collected magnetic spectrum in wide momentum-energy space on Ni_2InSbO_6 by inelastic neutron scattering (INS) technique to identify the precise spin Hamiltonian and validate the mechanism of the spin soliton lattice [3].

The INS powder spectrum is shown in Fig. 1(c). Well-defined spin wave excitation is observed with the band energy of 20 meV at 10 K. Two spin models of antiferromagnetic Heisenberg Hamiltonian considering the first to fourth nearest neighbor interactions J_1 to J_4 are used to analyze the spectrum by the linear spin-wave theory (LSWT). The calculated spectra of model A with constraints $J_1 = J_2$ and $J_3 = J_4$ according to the previous Raman study [2] and model B without the constraints according to the crystallographic consideration are shown in Figs. 1(d) and 1(e), respectively. χ^2 and correlation coefficient R for model A were 8.8 and 0.928, and those for model B are 6.1 and 0.953, meaning that model B is more probable. Indeed, one-dimensional cuts of the experiment and calculations at the energy of 10.1 meV in Fig. 1(f) suggest that the model B reproduces the experiment better. The difference is, in fact, caused by the fast and low spin wave velocities along the c axis for model A and B, respectively. The spin model of Ni_2InSbO_6, thus, turns out to be a coupled two-dimensional lattice stacked along the c axis with intraplane interaction J_1 = 6.05 meV and interplane interaction J_1 = 0.95 meV. Since DM interaction is proportional to the corresponding exchange interaction, $\boldsymbol{D}_1$ and $\boldsymbol{D}_2$ are different as well, which validates the mechanism of spin soliton lattice [1].

References

[1] Y. Araki, T. Sato, Y. Fujima, N. Abe, M. Tokunaga, S. Kimura, D. Morikawa, V. Ukleev, Y. Yamasaki, C. Tabata, H. Nakao, Y. Murakami, H. Sagayama, K. Ohishi, Y. Tokunaga, and T. Arima, Phys. Rev. B **102**, 054409 (2020).

[2] M. A. Prosnikov, A. N. Smirnov, V. Y. Davydov, Y. Araki, T. Arima, and R. V. Pisarev, Phys. Rev. B **100**,144417 (2019).

[3] Z. Liu, Y. Araki, T. Arima, S. Itoh, S. Asai, and T. Masuda, Phys. Rev. B **107**, 064428 (2023).

Authors

Z. Liu, Y. Araki[a], T. Arima[a], S. Itoh[b,c], S. Asai, and T. Masuda

[a]The University of Tokyo

[b]Institute of Materials Structure Science, High Energy Accelerator Research Organization

[c]J-PARC Center

Spin Dynamics in Equilateral Triangular Spin Tube Material $CsCrF_4$

Masuda Group

Frustrated magnetism has attracted significant attention due to their potential to exhibit unique magnetic phases resulting from the competition between various interactions. Lattices composed of triangles as basic units, such as the triangular lattice, Kagome lattice, and Pyrochlore lattice, serve as representative examples of frustrated magnet systems. Triangular spin tube has been extensively studied theoretically as a one-dimensional frustrated system, where triangles are arranged in a single direction. In the Heisenberg equilateral triangular spin tube system, the spin correlation decays exponentially, and the ground state is a dimerized nonmagnetic state with a spin gap [1]. Furthermore, the presence of a Tomonaga-Luttinger liquid with chiral order has been predicted under the influence of anisotropy and a magnetic field [2].

In real materials, the presence of intertube interactions, albeit small, leads to the emergence of various magnetically ordered states [3]. As shown in Fig. 1(a), $CsCrF_4$ consists of Cr^{3+} ions forming equilateral triangular spin tubes with S = 3/2 spins. Magnetic susceptibility and heat capacity measurements did not exhibit any sign of phase transitions [4]. Nevertheless, neutron diffraction experiments unveiled the presence of a long-range order characterized by a 120-degree structure, along with successive phase transitions

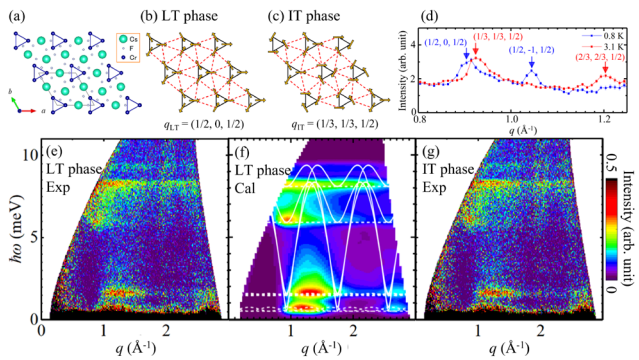

Fig. 1.(a) Crystal structure of $CsCrF_4$. Cr ions form equilateral triangular spin tubes with S = 3/2 spins along the crystallographic c axis. (b) Magnetic structure of $CsCrF_4$ in the LT phase. (c) Magnetic structure of $CsCrF_4$ in the IT phase. (d) Elastic part of INS spectra measured with E_i = 3.1 meV. (e) INS spectra measured with E_i = 15.3 meV at 0.8 K (LT phase). (f) Powder averaged INS spectra in LT phase calculated by linear spin-wave theory. The white solid and dashed curves are dispersion relations calculated along the c* and a* axes, respectively. (g) INS spectra measured with E_i = 15.3 meV at 3.1 K (IT phase).

where the propagation vector changes from q_{LT} in Fig. 1(b) to q_{IT} in Fig. 1(c) [5]. So far, the spin dynamics of this material have remained unexplored. In the present research, inelastic neutron scattering (INS) experiments were conducted using powder samples to determine the spin Hamiltonian and shed light on the successive phase transitions.

The experiment was conducted using the HRC spectrometer installed at J-PARC/MLF [6]. As shown in Fig. 1(d), magnetic Bragg peaks with q_{LT} were observed at 0.8 K and those with q_{IT} were observed at 3.1 K in the elastic part of the neutron spectra [5]. The observed and calculated INS spectra in the LT phase are shown in Figs. 1(e) and 1(f), respectively. For the latter, we used linear spin-wave theory on the basis of Heisenberg model of a triangular spin tube, including small DM interaction and a small single-ion anisotropy. The experiment was reasonably reproduced by the calculation. The spectrum in wide-energy range is explained by the quasi-one-dimensional nature of the spin tube in the c^* direction. The analysis highlighted the significant roles of the DM interaction and single-ion anisotropy in low-energy range.

Furthermore, as depicted in Fig. 1(g), the INS spectrum in the IT phase was measured. Surprisingly, despite the change in the propagation vector in the diffraction profiles in Fig. 1(d), the INS spectrum in the IT phase exhibited a striking resemblance to the LT phase in level of powder-averaged spectra. The same analysis method utilized for the LT phase was applied to analyze the INS spectrum in the IT phase. However, the INS spectra in the IT phase could not be reproduced, indicating that the successive phase transition is not driven by variations in the spin Hamiltonian parameters.

To gain further insights, a phase diagram of the ground state was calculated for the coupled spin tubes system. The parameter values of the spin Hamiltonian estimated by the present INS experiment lie near the boundary between the magnetic phases with the structures of q_{IT} and q_{LT}. This finding implies that the internal energy of the magnetic structures in the LT and IT phases is similar. Considering that large spin entropy can favor the selection of the magnetic structure, it is proposed that the gain in spin entropy serves as the origin of the successive phase transition. Notably, this study provides the first evidence that, despite disparities in the static structures, the dynamic structures exhibit similarity under such circumstances.

References

[1] K. Kawano, and M. Takahashi, J. Phys. Soc. Jpn. **66**, 4001 (1997).
[2] T. Sakai, M. Sato, K. Okunishi, Y. Otsuka, K. Okamoto, and C. Itoi, Phys. Rev. B **78**, 184415 (2008).
[3] K. Seki and K. Okunishi, Phys. Rev. B **91**, 224403 (2015).
[4] H. Manaka, Y. Hirai, Y. Hachigo, M. Mitsunaga, M. Ito, and N. Terada, J. Phys. Soc. Jpn. **78**, 093701 (2009).
[5] M. Hagihala, S. Hayashida, M. Avdeev, H. Manaka, H. Kikuchi, and T. Masuda, npj Quantum Mater. **4**, 14 (2019).
[6] H. Kikuchi, S. Asai, H. Manaka, M. Hagihala, S. Itoh, and T. Masuda, Phys. Rev. B **107**, 184404 (2023).

Authors

H. Kikuchi, S. Asai, H. Manaka[a], M. Hagihala[b], S. Itoh[b], and T. Masuda

[a]Kagoshima University

[b]Institute of Materials Structure Science, High Energy Accelerator Research Organization

Spin Fluctuations in Spin-Hedgehog-Anti-Hedgehog Lattice State in $MnSi_{1-x}Ge_x$

Nakajima Group

Couplings between topological magnetic orders and conduction electrons have been of increasing interest in recent condensed matter physics research [1,2]. One of the most well-known examples is the magnetic skyrmion lattice (SkL) discovered in a chiral cubic helimagnet MnSi [1]. The SkL is composed of topologically-nontrivial vortex like spin objects, which have finite scalar spin chirality, $S_i \cdot (S_j \times S_k)$, owing to the non-coplanar arrangements of the magnetic moments. The scalar spin chirality acts as an effective magnetic field for conduction electrons, and thus induces an unconventional Hall effect, which is known as Topological Hall Effect (THE). Another example of topological magnetic orders is a spin-hedgehog-anti-hedgehog (SHAH) lattice state discovered in MnGe [3], which is isostructural to MnSi. The spin arrangement of SHAH lattice is described by a superposition of three proper-screw-type magnetic modulations with the q-vectors of $(q,0,0)$, $(0,q,0)$ and $(0,0,q)$. By calculating spatial distribution of the scalar spin chirality in the SHAH lattice, one can find that the spin texture can be viewed as periodic arrays of effective magnetic monopoles and antimonopoles. Although the effective magnetic fields in the SHAH lattice are cancelled to be zero in zero magnetic field, an application of an external magnetic fields and resulting distortion of the SHAH lattice can induce a finite THE. In addition to the THE mechanism for the long-range-ordered non-coplanar magnetic orders, a recent theoretical study [4] has pointed out that 'fluctuating' short range magnetic order with scalar spin chirality can induce skew scattering, which leads to Hall effect with opposite sign to that induced by the long-range non-coplanar orders.

In the present study, we investigate $MnSi_{1-x}Ge_x$, which exhibits a variety of Hall effects depending on temperature, magnetic field, and amount of the chemical substitution [5]. Specifically, we focus on $x = 0.8$ and 0.6 samples; the former exhibits the same SHAH lattice state as that in the $x = 1$ sample, while the latter shows another SHAH lattice state composed of four q-vectors, specifically (q,q,q), $(q,-q,-q)$, $(-q,q,-q)$ and $(-q,-q,q)$ [5]. To understand the origins of the Hall effects in these systems, it is necessary to experimen-

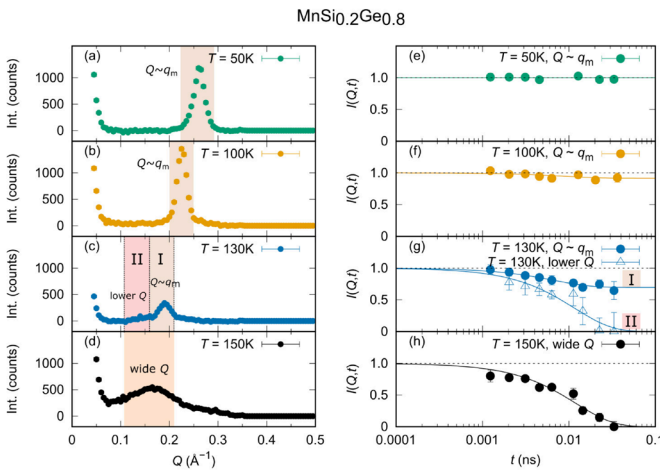

Fig. 1. (a)–(d) Q-dependence of intensity in the $x = 0.8$ sample measured at four representative temperatures. (e)–(h) Intermediate scattering function of $I(Q,t)$ deduced from the selected Q-range given in (a)–(d).

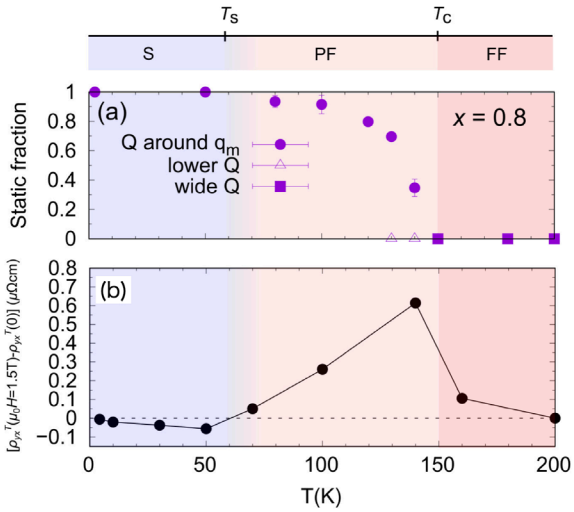

Fig. 2. Temperature dependence of (a) the volume fraction of the static spin component and (b) the topological Hall resistivity at $\mu_0 H$ = 1.5 T, measured in the x = 0.8 sample.

tally study the magnetic structures and their fluctuations by neutron scattering.

Figure 1 shows the results of the neutron scattering measurements on the x = 0.8 sample. The data was obtained at VIN ROSE (BL06) beamline in Materials and Life-science experimental Facility (MLF) of J-PARC. We used the powder sample of $MnSi_{1-x}Ge_x$ with x = 0.8 used in the previous study in Ref. 5. Figures 1(a)–1(d) show the neutron diffraction profiles in the low-Q region. At low temperatures, a sharp magnetic Bragg peak was observed at around Q = 0.26 Å^{-1}. As the temperature was increased, the intensity of the Bragg peak was reduced, and its position was shifted toward lower Q region. Finally, the Bragg peak disappeared above the critical temperature of 150 K, and instead, a broad diffuse scattering was observed at around Q = 0.15 Å^{-1}.

Figures 1(e)–1(h) show the intermediate correlation function $I(Q,t)$ deduced from the neutron resonance spin echo spectroscopy at VIN ROSE. The Q ranges used for the data reduction are indicated by colored area in Figs. 1(a)–1(d). At 50 K, the $I(Q,t)$ remains very close to unity even at 0.03 ns, which is the upper limit of the time window of the present experiment, indicating that there is no spin fluctuations and that the magnetic moments are static. However, near the critical temperature, we observed the $I(Q,t)$ curve shows the exponential decay, meaning that the spins are fluctuating with the characteristic time of approximately 0.01 ns. In Fig. 2(a), we show the fraction of the fluctuating spin components deduced form the neutron spin echo experiment as function of temperature, revealing that the spin fluctuations remain above 60 K. This shows a good agreement with the sign change of the additional Hall resistivity shown in Fig. 2(b); the additional component of the Hall resistivity changes from negative to positive at around 60 K. These observations demonstrated that the dominant contribution of the additional Hall resistivity changes from the static emergent magnetic field from the long-range-ordered SHAH lattice to the skew scattering due to the fluctuating spin cluster with scalar spin chirality as the temperature is increased. We also performed the neutron spin echo measurements on the x = 0.6 sample in the same manner as that for the x = 0.8 sample, and carried out inelastic neutron scattering experiments for both the x = 0.6 and 0.8 samples at HRC (BL12) in MLF of J-PARC. More detailed analysis will be published elsewhere [6].

References

[1] S. Muhlbauer *et al.*, Science **323**, 915 (2009).
[2] N. Nagaosa and Y. Tokura, Nat. Nanotech. **8**, 899 (2013).
[3] N. Kanazawa *et al.*, Phys. Rev. Lett. **106**, 156603 (2011).
[4] H. Ishizuka and N. Nagaosa, Sci. Adv. **4**, eaap9962 (2018).
[5] Y. Fujishiro *et al.*, Nat. Commun. **10**, 1059 (2019).
[6] S. Aji *et al.*, arXiv:2305.01172

Authors

S. Aji[a], T. Oda[a], Y. Fujishiro[b], N. Kanazawa[a], H. Saito[a], H. Endo[c], M. Hino[d], S. Itoh[c], T. Arima[a,b], Y. Tokura[a,b], and T. Nakajima[a,b]
[a]University of Tokyo
[b]RIKEN Center for Emergent Matter Science
[c]KEK
[d]Kyoto University

Quasi-Elastic Neutron Scattering Study on Stretched Polymer Gels

Mayumi Group

Hydrogels, cross-linked polymer networks containing water, are expected to be applied for biomaterials and the mechanical toughness of polymer gels needs to be improved. The reason for the brittleness of polymer gels is the heterogeneous strain distribution caused by their inhomogeneous network structure. When a polymer gel is stretched, local stress concentrates on at short strands between cross-links. The stress-concentrated strands are highly stretched and become potential fracture onsets, which dominates the macroscopic fracture properties of polymer gels.

In this study, the segment/monomer dynamics of polymer

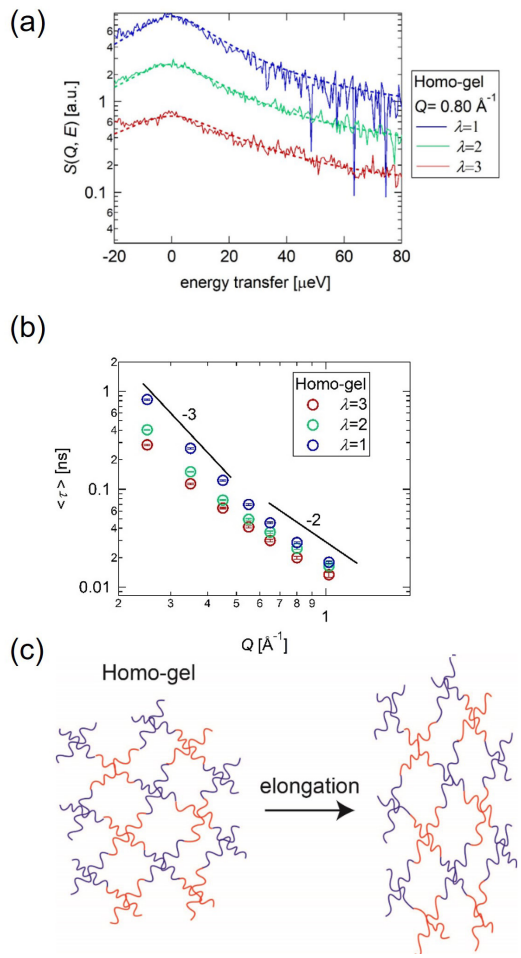

Fig. 1 (a) Dynamic structure factor $S(Q, \omega)$ of Homo-gel at λ =1, 2, 3, (b) Q dependence of average relaxation time for Homo-gel at λ =1, 2, 3, (c) Schematic illustration of deformation mechanism for Homo-gel.

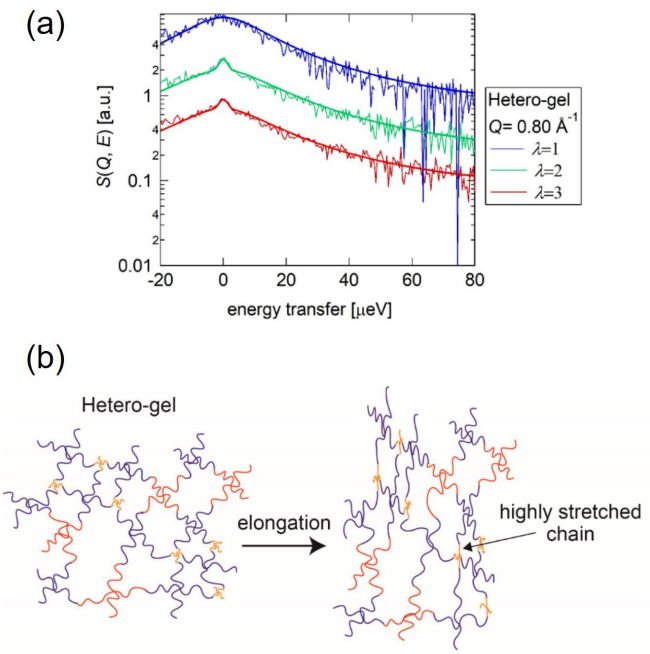

Fig. 2 (a) Dynamic structure factor $S(Q, \omega)$ of Hetero-gel at λ =1, 2, 3, (b) Schematic illustration of deformation mechanism for Hetero-gel.

gels under uniaxial deformation is investigated by means of quasi-elastic neutron scattering (QENS) [1]. In order to clarify the effect of heterogeneity in polymer network structure, we prepared two types of polymer gels with controlled heterogeneities: a homogeneous Tetra-PEG gel prepared by end-cross-linking of Tetra-arm prepolymers (Homo-gel) [2], and heterogeneous Tetra-PEG gel (Hetero-gel) containing a small amount of Tetra-PEG prepolymers with shorter arms [3]. Hetero-gel shows a more brittle fracture behavior than Homo-gel, which suggests a stress-concentration occurs in Hetero-gel under deformation.

Figures 1 (a) shows $S(Q, \omega)$ for Homo-gel under uniaxial deformation (λ = 1, 2, 3) at Q = 0.8 Å^{-1}. The dynamic structure factors were fitted with a KWW function. As shown in Figure 1 (b), the average relaxation times (τ) of Homo-gel decrease with increasing stretching, and the segment/monomer dynamics in the gel are accelerated by stretching. Stretching exponent β for the homogeneous gel is not changed with stretching, suggesting that the local deformation in the gel is kept homogeneous (Fig. 1 (c)).

Figures 2 (a) shows $S(Q, \omega)$ of Hetero-gel under uniaxial deformation (λ = 1, 2, 3) at Q = 0.8 Å^{-1}. A sharp elastic peak corresponding to slow chain dynamics with a broad base was observed under deformation (λ = 2, 3), while only a broad peak was seen for the un-deformed state (λ =1). This means that the slow chain dynamics appears only for the deformed Hetero-gel. The elastic component can be ascribed to a slow chain dynamics of highly stretched short strands (Fig. 2 (b)). When Hetero-gel is stretched, the short strands oriented to the stretching direction are strongly stretched and the chain dynamics of the highly deformed chains is suppressed, which causes a more brittle macroscopic fracture compared with that in the case of Homo-gel.

References
[1] K. Aomura, Y. Yasuda, T. Yamada, T. Sakai, and K. Mayumi, Soft Matter, **19**, 147 (2023).
[2] T. Sakai, T. Matsunaga, Y. Yamamoto, C. Ito, R. Yoshida, S. Suzuki, N. Sasaki, M. Shibayama, and U. I. Chung, Macromolecules **41**, 5379 (2008).
[3] S. Kondo, H. Sakurai, U. I. Chung, and T. Sakai, Macromolecules **46**, 7027 (2013).

Authors
K. Aomura, Y. Yasuda[a], T. Yamada[b], T. Sakai[a], and K. Mayumi
[a]The University of Tokyo
[b]Neutron Science and Technology Center, Comprehensive Research Organization for Science and Society (CROSS)

Detection of the Spatial Modulation of the FFLO State in High Magnetic Fields

Kindo and Kohama Groups

Superconductivity appears as a result of forming pairs of itinerant electrons by an attractive force. In the case of conventional superconductivity, the electron pairs are composed of electrons with momenta $\boldsymbol{k}$ and $-\boldsymbol{k}$. In 1964, Fulde & Ferrell [1] and Larkin & Ovchinnikov [2] proposed that an imbalanced pairing of up-/down-spin electrons with momenta $\boldsymbol{k}$ and $-\boldsymbol{k}+\boldsymbol{q}$, known as the FFLO state, can be realized in high fields where Zeeman splitting energy exceeds the superconducting energy gap. In the FFLO state, the finite total momentum of the pair $\boldsymbol{q}$ modifies the order parameter of the superconductivity and yields the term $\cos(\boldsymbol{qr})$, which results in spatial oscillations of the superconductivity in real space. Although the spatial modulation of the order parameter is one of the most decisive pieces of evidence of the FFLO state, it has never been experimentally observed.

In order to detect the spatial modulation, we carried out multi-directional ultrasound measurements of one of the FFLO candidates, an organic superconductor κ-(BEDT-TTF)$_2$Cu(NCS)$_2$, in pulsed magnetic fields [3]. Figure 1 shows the magnetic-field dependence of sound velocity at 1.6 K when polarization vectors of sound waves $\boldsymbol{u}$ are along the crystal axes parallel to the conducting plane, b and c. Magnetic fields are applied parallel to the c axis. From the results of previous studies of this material, the field where the Zeeman energy reaches the superconducting energy gap is expected to be about 21 T, and also, the superconductivity is completely suppressed above 25 T. Namely, the FFLO state can be stable in the field range of 21–25 T. Indeed, as clearly seen from

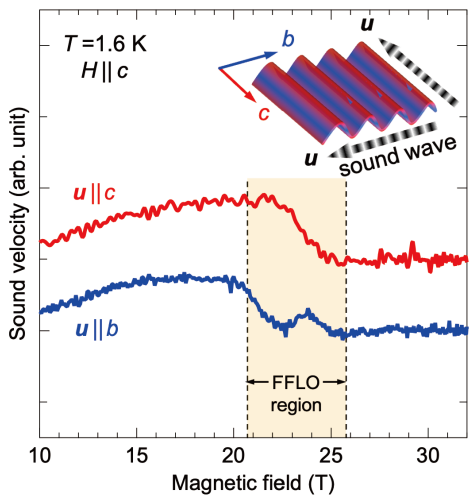

Fig. 1. Anisotropic acoustic response in the FFLO state.Magnetic field dependence of sound velocity at 1.6 K for $\boldsymbol{u}||b$ (blue) and $\boldsymbol{u}||c$ (red) in a magnetic field along the c axis. Only in the FFLO region between 21–25 T, the sound-wave-direction-dependent response is observed. The schematics in the inset show the spatial modulation of the FFLO state composed of superconductivity (red) and normal state (blue). The striped arrows signify the sound-wave directions, which are parallel to the polarization vector $\boldsymbol{u}$.

our results, only in this field region, a distinct difference appears between the two datasets. It is natural because the spatial modulation produced by the $\boldsymbol{q}$ vector, as shown in the inset of Fig. 1, must make the superconducting state anisotropic. Since only the $\boldsymbol{u}\|b$ data shows the enhancement of the sound velocity, the emergent superlattice of the spatial modulation should be parallel to the b axis. This means that $\boldsymbol{q}$ should orient along the b axis. In the case of κ-(BEDT-TTF)$_2$Cu(NCS)$_2$, it is expected that antiferromagnetic spin fluctuations along some nesting vectors mediate the pairing of the superconductivity, and one of the most predominant nesting direction points towards the $\boldsymbol{b}$ axis. It seems reasonable because an energy gain by better nesting stabilizes the FFLO state in a low-dimensional superconducting state. This agreement experimentally unveil the nature of the FFLO state occurred in the low-dimensional superconductivity.

Nowadays the concept of the unique pairing of the FFLO state has been widely investigated in various physics not only condensed matter physics but also elemental particle physics and so on. The present results demonstrate that the spatial modulation of the FFLO state can be discussed by the emergent anisotropy of the acoustic properties. Our findings will facilitate a deeper understanding of the FFLO state.

References

[1] P. Fulde and R. A. Ferrell, Phys. Rev. **35**, A550 (1964).
[2] A. I. Larkin and Y. N. Ovchinnikov, Zh. Eksp. Teor. Fiz. **47**, 1136 (1964).
[3] S. Imajo, T. Nomura, Y. Kohama, and K. Kindo, Nat. Commun. **13**, 5590 (2022).

Authors

S. Imajo, T. Nomura, Y. Kohama, and K. Kindo

Signature of Spin-Triplet Exciton Condensations in $LaCoO_3$ at Ultrahigh Magnetic Fields up to 600 T

Y. H. Matsuda Group

Bose–Einstein condensation of electron-hole pairs, exciton condensation, has been effortfully investigated since predicted 60 years ago. Irrefutable evidence has still been lacking due to experimental difficulties in verifying the condensation of the charge-neutral and non-magnetic spin-singlet excitons. On the other hand, condensation of spin-triplet excitons is a promising frontier because spin supercurrent and spin-Seebeck effects will be observable. A canonical cobaltite $LaCoO_3$ under very high magnetic fields is a propitious candidate, yet to be verified. In this study, we unveil the exotic phase diagram of $LaCoO_3$ up to 600 T generated using the electromagnetic flux compression method and the state-of-the-art magnetostriction gauge. We found continuous magnetostriction curves and a bending structure, which suggest the emergence of two distinct spin-triplet exciton condensates. By constructing a phenomenological model, we showed that quantum fluctuations of excitons are crucial for the field-induced successive transitions. The spin-triplet exciton condensation in a cobaltite, which is three-dimensional and thermally equilibrated, opens a novel venue for spintronics technologies with spin-supercurrent such as a spin Josephson junction.

$LaCoO_3$ has been claimed to be a promising candidate when placed under very high magnetic fields exceeding

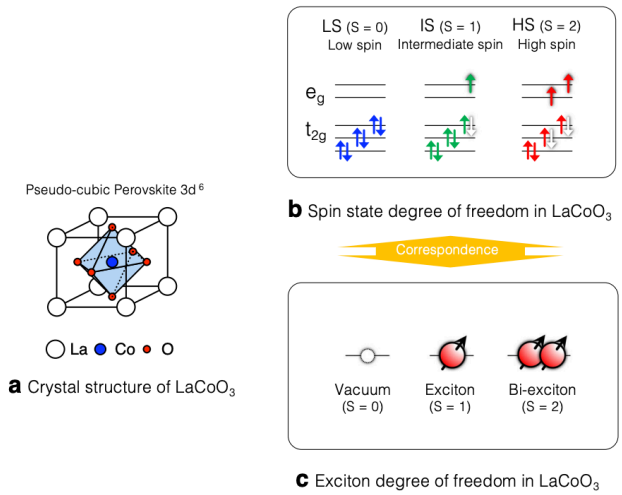

Fig. 1. Schematic illustrations describing the correspondence between spin-states and exciton states in $LaCoO_3$.

100 T. $LaCoO_3$ is an archetypal compound having a variety of spin-states, such as low-spin (LS: S = 0), intermediate spin (IS: S = 1) and high spin (HS: S = 2) states (See Fig. 1), which are viewed as vacuum, an exciton, and bi-exciton states, respectively (See Fig. 1). The spin-triplet exciton condensation will emerge when the magnetic field eliminates the spin-gap and changes the vacuum state (LS) to a magnetic exciton state (IS) or bi-exciton state (HS).

Previously in $LaCoO_3$, the field-induced phase transitions are uncovered below 30 K (α phase) and above 30 K (β phase), which extend beyond 100 T, using magnetization [1] and magnetostriction measurements [2] up to 200 T generated by single turn coil (STC) method. The two phases are considered superlattice formation (i.e., solidification) of the excitons, bi-excitons, and vacuum based on the observa-

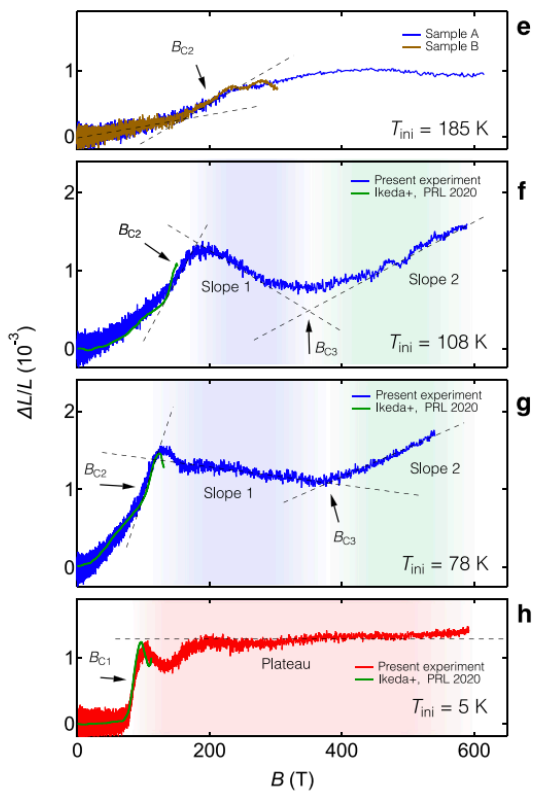

Fig. 2. Result of magnetostriction measurement of $LaCoO_3$ shown as a function of time, along with the magnetic field profiles generated using the EMFC method. The initial sample temperatures T_{ini} are varied from 5 K to 185 K

tion of plateaux of magnetostrictions. Considering that the magnetization below 200 T is far from the full polarization of the spin-states, further orderings of excitons are expected to appear above 200 T.

The experimental investigation has been challenging due to the need for very high magnetic fields beyond 100 T which is necessitated by the large spin-gap of ~100 K. Besides, one needs to probe the exciton states at such high magnetic fields. As solutions to these difficulties, recently, we reported the generation of 1200 T with electromagnetic flux compression (EMFC) method using a newly installed capacitor banks system in ISSP [3]. Furthermore, we succeeded in implementing a state-of-the-art high-speed 100 MHz strain gauge using fiber Bragg grating (FBG) and optical filter method, which have enabled us to measure magnetostriction in the μs-pulsed 1000 T environment [4]. Magnetostriction is a crucial probe of the exciton states because the density of excitons is coupled to the lattice volume of $LaCoO_3$, where exciton and bi-exciton states have larger ionic volumes with the occupation of eg orbitals that is spatially more extended than t2g orbitals as can be seen in the correspondence of spin-states and exciton states. Solidifications and Bose-Einstein condensations of excitons result in plateaus and slope of exciton density. Thus, we expect that they also result in plateaus and slope in magnetostriction curves at very low temperatures. Note that the correspondences are analogs to the magnetization plateaus and slopes in magnon solids and superfluids, respectively.

The results of magnetostriction measurements up to 600 T are presented in Fig 2. The new features indicating magnetic field induced phase transitions are observed. We summarize the obtained results in the present and previous studies on a magnetic field – temperature plane as shown in Fig. 3.

In addition to the data up to 600 T for the α phase and the β phase, we found novel phase termed γ phase. The variety of phases indicates the exotic ordering of the exciton degree of freedom in $LaCoO_3$. We qualitatively discuss the possibility of two kinds of spin-triplet exciton condensation realized in $LaCoO_3$ corresponding to the β phase and the γ phase. We attributed the origin of the α phase to be a crystallization of excitons. The study indicates the complicated interactions and symmetry breakings are in play in $LaCoO_3$

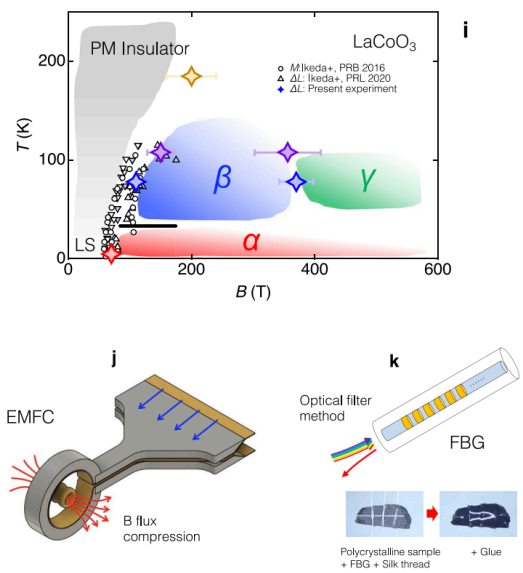

Fig. 3. Summary of the magnetostriction measurement of $LaCoO_3$ on a magnetic field-temperature plane up to 600 T along with the previously obtained data using magnetization and magnetostriction measurements

placed at ultrahigh magnetic fields [5].

References

[1] A. Ikeda, T. Nomura, Y. H. Matsuda, A. Matsuo, K. Kindo, and K. Sato, Phys. Rev. B **93**, 220401(R) (2016).
[2] A. Ikeda, Y. H. Matsuda, and K. Sato, Phys. Rev. Lett. **125**, 177202 (2020).
[3] D. Nakamura, A. Ikeda, H. Sawabe, Y. H. Matsuda, and S. Takeyama, Rev. Sci. Instrum. **89**, 095106 (2018)
[4] A. Ikeda, T. Nomura, Y. H. Matsuda, S. Tani, Y. Kobayashi, H. Watanabe, and K. Sato, Rev. Sci. Instrum. **88**, 083906 (2017).
[5] A. Ikeda, Y. H. Matsuda, K. Sato, Y. Ishii, H. Sawabe, D. Nakamura, S. Takeyama, and J. Nasu, Nat. Commun. **14**, 1744 (2023).

Authors
A. Ikeda[a], J. Nasu[b], and Y. H. Matsuda
[a]University of Electro-Communications
[b]Tohoku University

Closing the Hybridization Charge Gap in the Kondo Semiconductor SmB_6 with an Ultrahigh Magnetic Field

Y. Matsuda Group

In materials with strong electron correlation, the nontrivial energy-band structure beyond the single-electron picture gives rise to exotic properties. SmB_6 is a typical Kondo semiconductor, whose hybridization gap has been estimated to be 5–20 meV. In addition to the strong electron correlation in SmB_6, the valence fluctuation of the Sm ion and possible topological surface state induce a complicated energy band structure. Under sufficiently high magnetic fields, the energy bands are shifted by the Zeeman effect and the evolution in magnetoresistance gives information to understand the complicated electronic states. However, an ultra-high magnetic fields above 100 T is required to achieve the field-induced semiconductor–metal (S–M) transition, which leads to the difficulty in observing the details of the evolution of the magnetoresistance up to the S–M transition in SmB_6 with high sensitivity.

In this research, we utilized the electromagnetic flux-compression (EMFC) technique [1] to generate ultra-high magnetic fields up to 320 T. The high-frequency electrical resistivity was measured using a contactless radio-frequency impedance measurement method developed by the authors [2], which demonstrates the observation of the upper critical magnetic field in cuprate superconductor [3] and the S–M phase transition in narrow-gap semiconductor [4]. The measurement SmB_6 sample (typically $1 \times 1 \times 0.05$ mm^3) was mounted on a self-resonant spiral probe coil with the diameter of 1 mm so that the ⟨100⟩ axis was parallel to the magnetic field. A radio-frequency voltage tuned around 700 MHz was applied to the probe coil and the reflected signal was acquired by the digital oscilloscope. The amplitude of reflected signal was obtained by the numerical lock-in method, and then converted to electrical resistivity by using the temperature dependence of signals measured just before applying the pulsed magnetic field.

Figure 1 shows the magnetic field dependence of the high-frequency electrical resistivity at 6.5 K, 16 K and 24 K (initial temperature just before applying the pulsed magnetic field) obtained from independent EMFC experiments up to 320 T [5]. The AC (50 kHz) magnetoresistances up to 55 T generated by the non-destructive pulsed magnet are also presented for comparison (black curves). At 16 K and 24 K, the data obtained by the EMFC and non-destructive magnet

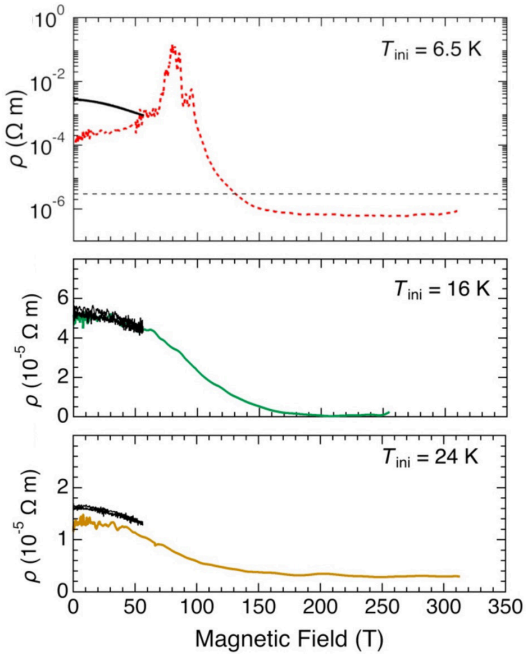

Fig. 1. Magnetic field dependence of the electrical resistivity at 6.5 K, 16 K, and 24 K. The AC magnetoresistances with 50 kHz up to 55 T generated by the non-destructive pulsed magnet are also presented for comparison (black curves).

experiments coincide well each other, indicating the high reliability of the results of EMFC experiments. The high-frequency resistivity gradually decreases with increasing the magnetic field and the field-induced S–M transition appears around 180 T by closing the hybridization gap in SmB_6. On the other hand, at 6.5 K, the resistivity obtained by the EMFC experiments significantly increases up to ~80 T, different from the result of non-destructive magnet experiment. This indicates a significant frequency dependence of electrical resistivity at low temperatures, and the scattering process for the carriers changes around 80 T at low temperatures. This is also suggested by an anomaly of temperature dependence of the electrical resistivity around 12.5 K under zero magnetic field.

Figure 2 presents the phase diagram of SmB_6 constructed based on the experimental findings in the present research

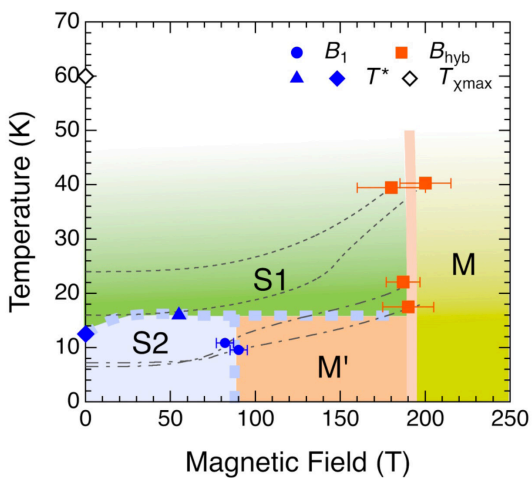

Fig. 2. Temperature–magnetic field phase diagram of SmB_6. B_1 (closed circle) and B_{hyb} (closed square) are taken from the results of the EMFC experiments. critical temperature T^* (closed triangle and diamond) is taken from the nondestructive magnet and PPMS experiments. The thin dashed-dotted and dotted curves indicate the temperature evolution during the magnetic-field pulse. Each state is separated by bold guidelines for a clear view, whose identifications are described in the main text.

[5]. Four black dashed-dotted and dotted curves represent the temperature evolution in the sample during the independent EMFC experiments, which arises from the extremely short pulse of the magnetic field generated by the EMFC technique.

By connecting the boundary points (the fields exhibiting the anomalies in the resistivity), four independent states (S1, S2, M′, and M) are defined in the phase diagram. Semiconducting state S1 is phenomenologically characterized by frequency-independent magnetoresistance and metallization at B_{hyb} ~ 180 T. The high-field M phase is likely to be a normal paramagnetic metal. The low-temperature semiconducting state S2 exhibits frequency-dependent magnetoresistance, and becomes metallic in the low-frequency transport at B_1 although the hybridization gap is still open. We suggest that the observed transition at B_1 relates with the energy scale of quasiparticles such as the spin polaron in the in-gap state.

References

[1] D. Nakamura *et al*., Rev. Sci. Instrum. **89**, 95106 (2018).
[2] D. Nakamura, M. M. Altarawneh, and S. Takeyama, Meas. Sci. Technol. **29**, 035901 (2018).
[3] D. Nakamura *et al*., Sci. Rep. **9**, 16949 (2019).
[4] D. Nakamura *et al*., Phys. Rev. Lett. **127**, 156601 (2021).
[5] D. Nakamura *et al*., Phys. Rev. B **105**, L241105 (2022).

Authors
D. Nakamura[a], A. Miyake, A Ikeda[b], M. Tokunaga, F. Iga[c], and Y. H. Matsuda
[a]RIKEN Center for Emergent Matter Science
[b]University of Electro-Communications
[c]Ibaraki University

Gradual Charge Order Melting in $Bi_{0.5}Ca_{0.5}MnO_3$ Induced by Ultrahigh Magnetic Fields

Y. H. Matsuda Group

Perovskite-type manganite series $AMnO_3$ (A = non magnetic ion) is the long standing one of the central subjects in condensed matter physics. Because of the coupling among the spin, charge, and orbital degrees of freedom, a lot of abundant exotic physical phenomena appear.

Electronic ground state of perovskite-type manganites is determined by the balance of the several interactions such as the Jahn-Teller coupling, on-site and inter-site Coulomb repulsion, superexchange interaction, and double exchange interaction.

Magnetic field effect on the ground state is significantly important subject in the perovskite-type manganites. The melting of the charge ordered (CO) state by applying magnetic fields is one of the central issues. This CO melting phenomenon sometimes accompanies the giant resistance change which is known as the colossal magnetoresistance.

The CO state in the perovskite-type manganites including Bi ions as A site ($Bi_{1-x}AE_xMnO_3$; AE = Ca or Sr) is more stable than that in the manganites including rare earth ions as A site ($Ln_{1-x}AE_xMnO_3$; Ln = rare earth element). The transition temperature of CO in $Bi_{0.5}Ca_{0.5}MnO_3$ (T_{CO} = 322 K) is higher than that in most of the rare earth systems with x = 0.5. The detailed investigation of the magnetic field effect on the CO phase in perovskite-type manganites with Bi ions would be interesting. However, the ultrahigh magnetic fields exceeding 100 T are needed for that investigation [1,2].

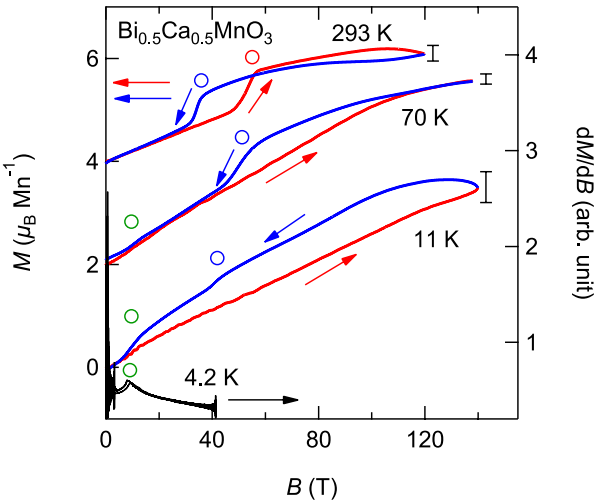

Fig. 1. Magnetization curves at 293 K (up to 120 T), 70 K (140 T), and 11 K (140 T). Red and blue lines represent the field ascending and descending processes, respectively. Black line is the dM/dB at 4.2 K up to 40 T measured by the nondestructive method. Critical fields are marked by red and blue open circles in the field ascending (B_c^{up}) and descending processes (B_c^{down}), respectively. Green open circles mark the critical field of the metamagnetic transition which appears around 10 T below T_N. The estimated error bar is shown for each measurement.

In this research [3], we tried to reveal the magnetic properties of $Bi_{0.5}Ca_{0.5}MnO_3$ under ultrahigh magnetic fields by means of the magnetization measurements up to 140 T over a wide temperature range from 11 to 293 K. We prepared the single crystals by Bi_2O_3 flux method, and the sample characterization was performed by XRD, SEM, and magnetic susceptibility measurement by MPMS. The powder sample prepared by crushing and grinding the obtained crystals was used for the magnetization measurements.

We revealed that the CO in $Bi_{0.5}Ca_{0.5}MnO_3$ can be melted by applying the magnetic field at the room temperature (293 K) (Fig. 1). It is observed as the metamagnetic transition. At low temperatures, the CO melting phase transition in the field ascending process becomes broad. However, the CO reformation can be observed clearly in the field descending process (Fig. 1). This asymmetric broadening phenomenon can be understood by the gradual CO melting induced by the ultrahigh magnetic fields.

This asymmetric broadening of the CO melting is possibly explained by the spatial inhomogeneity of charge distribution. In perovskite-type manganites, a spatial inhomogeneity of charge distribution the one of the attractive subjects and the important factor for the electronic ground state and phase transitions. The spatial inhomogeneity will be

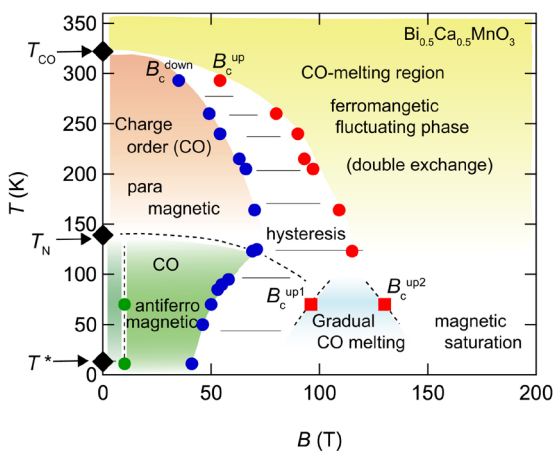

Fig. 2. B-T phase diagram constructed. Electronic and magnetic states in the low-field region have been reported in several previous studies.

frozen by decreasing temperature, therefore the phase transition can be broad in the field ascending process. On the other hand, the spatial inhomogeneity will become less because the electron becomes itinerant in the CO melting region under the ultrahigh magnetic field. As a result, the metamagnetic transition can be sharp in the field descending process.

Another possible reason related to the slow dynamics is the critical slowing down owing to the quantum criticality of antiferromagnetic order.

Finally, we constructed the B-T phase diagram of $Bi_{0.5}Ca_{0.5}MnO_3$ (Fig. 2).

For further investigation of the unusual CO melting phenomenon, the magnetostriction, resistivity, and XRD measurement under ultrahigh magnetic fields will be performed.

References

[1] A. Kirste *et al.*, Phys. Rev. B **67**, 134413 (2003).
[2] S. Takeyama *et al.*, J. Phys. Soc. Jpn. **81**, 014702 (2011).
[3] Y. Ishii, A. Ikeda, M. Tokunaga, K. Kindo, A. Matsuo, and Y. H. Matsuda, J. Phys. Soc. Jpn. 92, 074702 (2023).

Authors

Y. Ishii, A. Ikeda[a], M. Tokunaga, K. Kindo, A. Matsuo, and Y. H. Matsuda
[a]University of Electro-Communications

Metastable Quantum Phase in Adiabatic Condition with the Spin-Lattice Separation

Y. H. Matsuda, Kohama, and Kindo Group

Several low-dimensional spin systems exhibit exotic magnetization processes such as magnetization plateaux as a result of the appearance of exotic quantum phases. The spin-ladder materials are intriguing because they possess intermediate properties between one- and two-dimensions. The two-leg spin-ladder compound 3, 3′, 5, 5′-tetrakis(N-tert-butylaminoxyl)biphenyl: $C_{28}H_{42}N_4O_4$ (BIP-TENO) was synthesized as the first S = 1 two-leg spin ladder, where S is the spin quantum number. In BIP-TENO, the nontrivial 1/4 magnetization plateau was observed in the magnetic field range from 42 to 66 T and theoretically analyzed [1]. To explain the 1/4 plateau, the authors of Ref. [1] introduced the second-nearest-neighbor (diagonal direction) and third-nearest-neighbor (leg direction) exchange interactions and found that the third-nearest-neighbor exchange interaction is more essential for the appearance of the 1/4 plateau. They obtained the magnetization by a numerical diagonalization. Although further successive phase transitions to the 1/2 and 3/4 plateau states are theoretically predicted [1], they were never experimentally observed because the required magnetic field is as strong as 150 T, which is only available employing a destructive manner [2]. In the present study, the entire magnetization process of BIP-TENO is investigated in ultrahigh magnetic fields of up to 150 T using the single-turn coil that is one of the destructive means for ultrahigh magnetic field generation. It is unveiled that 1/3 and 2/3 plateaus appear in addition to the previously discussed 1/4, 1/2, and 3/4 plateaus. Moreover, the 1/3 and 2/3 plateaus are found to appear only when the magnetic field is swept in a microsecond timescale. The adiabatic condition is likely to be necessary for its observation, suggesting that the newly observed plateaus are metastable states.

The single crystals of BIP-TENO were used. The typical dimensions of the crystal used are 2 ~ 4 × 0.5 × 0.2 mm^3 and the direction of the long side is parallel to the c-axis. Three or four single crystals were used for the magnetization measurement to obtain the larger signal. In the pulsed-field experiments, magnetic fields (B) were applied parallel to the c-axis of the crystal that is parallel to the leg direction of the spin ladder. The ultrahigh magnetic fields were generated using the single-turn coil. The magnetization was measured using a self-compensated parallel-type pickup coil. The sample temperature was lowered by directly immersing the sample in liquid helium or by putting the sample in flowing cold helium gas.

Figure 1 shows the magnetization process measured at 4.2 K with the single-turn coil up to approximately 100 T (a red curve) [3]. The pulse duration is about 7 μs. In the figure, the previously reported magnetization curve at 1.3 K [1] is also shown for comparison (a green curve). A nondestructive magnet with a 5 ms duration was used in this measurement.

The 1/4 plateau is observed in both (red and green) curves. The striking difference is seen in the length of the plateau: the plateau ends at around 50 T and a new plateau appears after that in the red curve, while it continues to around 70 T. One may wonder whether this distinct difference can be caused by the temperature difference because the fast magnetic field changes potentially induce the temperature change due to the magnetocaloric effect. Hence, we investigated the magneto-caloric effect and found that although temperature decreases by several degrees with increasing the magnetic field in adiabatic conditions, the plateau lasts at least up to 60 T and no new plateau emerges at around 50 T [3]. This fact excludes the possibility that the different temperatures cause the different magnetization processes.

The measurement of the magnetostriction solved this mysterious question. We found that the leg direction of the crystal shrinks when the spin gap closes. The fiber Bragg grating method was utilized. The shrinkage of the lattice also causes a dissipation process and causes some heat production, which was detected in our magnetocaloric effect.

Figure 2 shows the shrinkage of the lattice when a pulsed magnetic field is applied as a function of time [3]. The lattice shrinks when a magnetic field is applied slowly

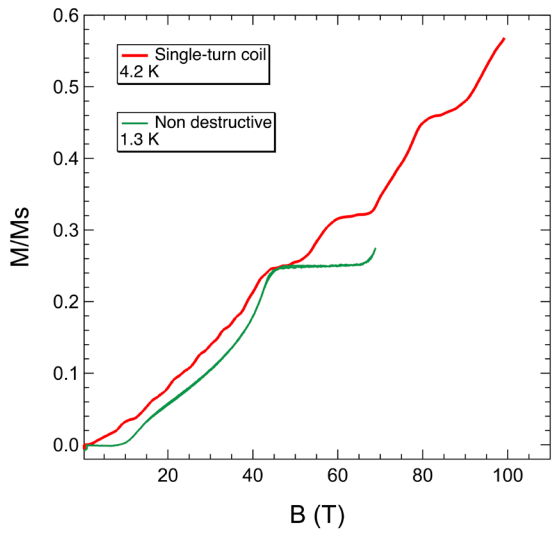

Fig. 1. Magnetization process of a single crystal of BIP-TENO measured within 7 μs using the single-turn coil (red curve). The green curve shows the magnetization process of BIP-TENO measured in a non- destructive pulsed magnetic field with a duration of 5 ms.

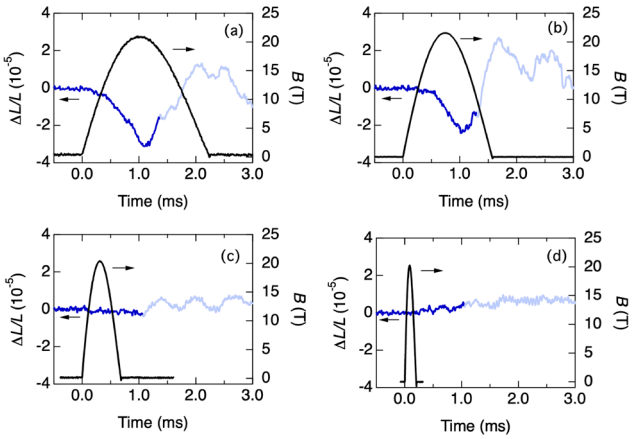

Fig. 2. The magnetostriction ΔL / L and the magnetic field are plotted as a function of time. The striction is seen in high magnetic fields as shown in (a) and (b), while it is absent when the magnetic field pulse is short as shown in (c) and (d).

(Fig. 2 (a)). However, the response of the lattice is delayed for the shorter field pulse (Fig. 2 (b)), and then, interestingly, the lattice doesn't move if the magnetic field pulse is short enough (Fig. 2 (c.) (d)). The threshold time is around 1 ms, which gives the answer to why the two different magnetization processes are observed with fast and slow magnetic field pulses.

The red curve in Fig. 1 is a magnetization process for the spins at the original lattice sites. The length of the 1/4 plateau suggests the strength of the interaction given by the zero-field crystal lattice. The new plateau following the 1/4 plateau seems to be assigned to the 1/3 plateau which has been proposed to emerge in a recent theoretical study [4]. The longer 1/4 plateau seen in the green curve in Fig. 1 is explained by an enhancement in the exchange interaction along the leg direction due to the contraction of the leg direction by a magnetic field.

In summary, the slow contraction of the crystal in the leg direction by the application of a magnetic field stabilizes the 1/4 plateau and hinders the following 1/3 plateau. The novel 1/3 plateau is a metastable state where the crystal lattice maintains the original form within a short time in the range of microseconds. This metastable quantum phase is a result of the spin-lattice separation and has hardly ever been observed before.

References

[1] T. Sakai, N. Okazaki, K. Okamoto, K. Kindo, Y. Narumi, Y. Hosokoshi, K. Kato, K. Inoue, and T. Goto, Phys. B: Condens. Matter **329**, 1203 (2003).
[2] N. Miura, T. Osada, and S. Takeyama, J. Low Temp. Phys. **133**, 139 (2003).
[3] K. Nomura, Y. H. Matsuda, A. Ikeda, Y. Kohama, H. Tsuda, N. Amaya, T. Ono, and Y. Hosokoshi, Phys. Rev. B **105**, 214430 (2022).
[4] H. Kohshiro, R. Kaneko, S. Morita, H. Katsura, and N. Kawashima, Phys. Rev. B **104**, 214409 (2021).

Authors

K. Nomura, Y. H. Matsuda, A. Ikeda[a], Y. Kohama, H. Tsuda[b], T. Ono[c], and Y. Hosokoshi[c]
[a]The University of Electro-Communications
[b]National Institute of Advanced Industrial Science and Technology
[c]Osaka Metropolitan University

Field-Induced Insulating State in a Topological Insulator BiSb Alloy

Tokunaga Group

Applying high-enough magnetic fields on metals realizes the quantum limit states, in which all the carriers are accommodated in the lowest Landau level. Since the carriers are confined in the smallest cyclotron orbit, the kinetic degree of freedom normal to the field is suppressed in this state. Thus, the ratio between Coulomb interaction and bandwidth, a measure of electron correlation, grows as the field increases. Such strong correlation in the quantum limit state can realize anomalous quantum state, like the fractional quantum Hall effect in two-dimensional electron systems. On the other hand, it is an open question what kind of quantum states can be realized by the effect of a strong correlation in the quantum limit state of a three-dimensional system [1]. In particular, quantum limit states of semimetals in which electrons and holes coexist are ideal platforms for realizing novel quantum states.

In this context, we focused on narrow gap semiconductors in which the gap can be closed by external magnetic fields, as illustrated in Fig. 1. Continuous valence and conduction bands at a zero magnetic field split into discrete Landau sub-bands in finite magnetic fields. These Landau sub-bands can be continuously shifted by a magnetic field with the Zeeman and cyclotron energies. We can close the gap in some materials at a specific field, causing semiconductor-semimetal transition at a critical field of B_c. The realized semimetallic state is a spin-polarized quantum limit state. We can expect the emergence of a novel quantum state above B_c.

As a target, we focus on a BiSb alloy. The BiSb alloys have attracted renewed interest after recognized as the first example of topological insulators [2]. Applying a magnetic field to this system can close the gap due to the level crossing of spin-split Landau levels in the conduction and valence bands. We found that further magnetic field application realizes an insulating state in this realized field-induced semimetallic state.

Figure 2 shows longitudinal magnetoresistance in a single crystal of $Bi_{1-x}Sb_x$ (x = 0.10) at various temperatures

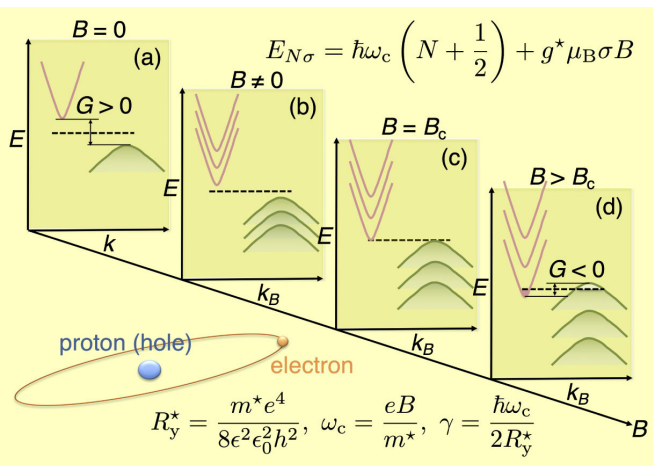

Fig. 1. Schematic of field-induced semiconductor-semimetal transition. Application of magnetic field changes continuous dispersion at a zero magnetic field (a) to discrete Landau sub-bands (b). In some materials, we can close the gap at a critical field of B_c (c) and realize a spin-polarized quantum limit state in a semimetallic phase (d). As illustrated in the inset, the electron-hole system in semimetals can reproduce an electron-proton system in an extremely high magnetic field.

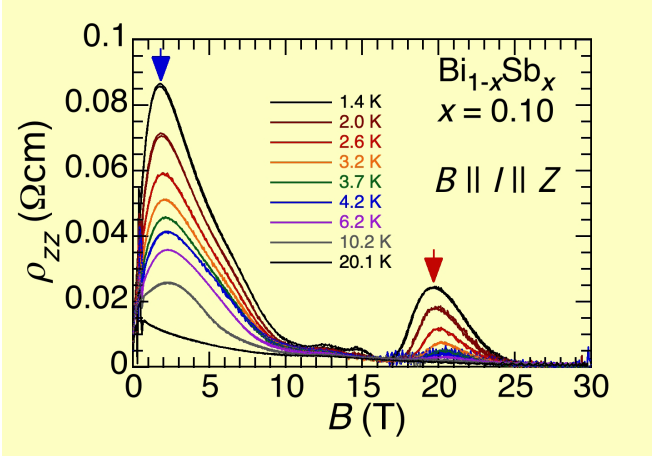

Fig. 2. Longitudinal magnetoresistance of $Bi_{1-x}Sb_x$ (x = 0.10) in a field along the three-fold rotational axis of the crystal. A semiconductor-semimetal transition is induced at 11 T. Additional insulating behavior appears at a field ~ 20 T below a temperature of 4 K, as marked with a red arrow.

[3]. Here, magnetic fields and electric currents are applied along the three-fold rotational axis of the crystal. In this field direction, Zeeman energy in the valence band is significantly larger than the cyclotron energy, so the application of the field higher than 11 T causes a semiconductor-semimetal transition at this field. Our results of magnetoresistance show metallic behavior above 11 T while causing insulating again at around 20 T and temperatures below 4 K.

This field-induced semimetallic state is a spin-polarized quantum limit state, in which we expect a strong correlation effect. The correlation effect in such an electron-hole system has been expected to host the BEC or BCS state of excitons (excitonic phase) at the vicinity of the zero-gap state. Estimation from our experimental results revealed that the binding energy between an electron and a hole becomes 0.3 meV, which is comparable to the thermal energy of 4 K. In addition, interparticle distance becomes also comparable with the thermal de Broglie length below 3 K. These estimations suggest possible emergence of the excitonic phase in BiSb.

The electron-hole systems of semimetals in magnetic fields can reproduce the electron-proton system under extremely high magnetic fields [4]. Suppose the effect of a magnetic field is measured by the ratio of cyclotron energy to Rydberg energy. In that case, the magnetic field effect is amplified in semimetals with small effective mass and large relative permittivity. Applying a magnetic field of 20 T to this BiSb alloy results in this ratio γ of ~ 4000, corresponding to a situation in which a magnetic field of one billion Tesla is applied to hydrogen atoms. What happens when the number of positive and negative carriers is continuously increased from zero under such conditions? Our results in a semimetal may reproduce the quantum state exhibited by hydrogen atoms in a billion Tesla magnetic field.

References

[1] B. I. Halperin, Jpn. J. Appl. Phys. **26**, 1913 (1987).
[2] D. Hsieh *et al.*, nature **452**, 970 (2008).
[3] Y. Kinoshita *et al.*, Phys. Rev. B **107**, 125140 (2023).
[4] Y. Kuramoto, *Hankinzokuchu no Densi-Seikou Soukan to Chouonpa no Kyodai Ryousigensui* (in Japanese) (Kyoritsu 1982).

Authors
Y. Kinoshita, T. Fujita, R. Kurihara, A. Miyake, Y. Izaki[a], Y. Fuseya[b], and M. Tokunaga
[a]Tokyo Institute of Technology
[b]University of Electro-Communications

Correlation-Driven Organic 3D Topological Insulator with Relativistic Fermions

Kohama and Kindo Group

Topological insulators (TIs) are a new class of materials that possess both bulk insulating and exotic surface/edge states. Conventionally, realizing a TI state usually requires a strong spin–orbit coupling (SOC) of heavy elements, leading to a band inversion and an insulating bulk gap. Consequently, it is challenging to observe a TI state and its unique physical features in light-atom materials, such as carbon-based systems, because of their weaker SOC. Recent theoretical studies propose a new pathway to realize a TI state via strong electron correlation, where the Coulomb interaction induces the bulk gap [1, 2]. Such correlation-driven TIs hold great scientific significance as they expand the scope of materials capable of forming TI states and potentially introduce new functions unique to correlated systems. An organic conductor α-(BETS)$_2$I$_3$ is a theoretical candidate for such correlation-driven TIs [3]. Nonetheless, experimental evidence to determine the accurate electronic state of this compound has been scant.

In our recent work [4], we performed magnetotransport measurement for α-(BETS)$_2$I$_3$ using pulsed high fields up to 60 T to clarify the low-temperature electronic state of this compound. Fig. 1a shows the longitudinal magnetoresistance (MR) measured at several temperatures. As shown in Fig. 1a, a large negative MR is observed below 4 K. This negative longitudinal MR resembles the MR induced by the "chiral anomaly" which is typically observed in three-dimensional (3D) Dirac or Weyl semimetals under parallel electric and magnetic fields (Fig. 1b). This result implies the presence of 3D relativistic particles (Weyl particles) in α-(BETS)$_2$I$_3$. The chiral-anomaly-induced negative MR is expected to be proportional to the square of the magnetic field. As shown in Fig. 1c, the inverse value of MR (written as MG in this report) at low temperatures is well-fitted by a quadratic function across a broad range of magnetic fields.

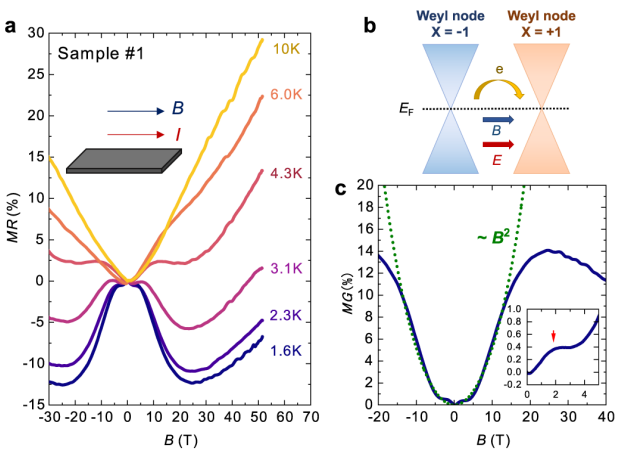

Fig. 1. **a** Longitudinal MR of α-(BETS)$_2$I$_3$ (I // B). The magnetic-field dependence of MR was measured at several temperatures. The quadratic negative magnetoresistance can be observed below 4 K. **b** Schematic of the charge flow induced by chiral magnetic effect (CME). In a magnetic field, the positive magnetoconductance (MG) due to the chiral anomaly flows between two Weyl nodes with different chirality $x = \pm 1$. **c** MG at 1.6 K. The green dashed line denotes the fitting curve MG = $C_a B^2$ with $C_a = 4.92 \times 10^{-4}$. Below 15 T, MG follows B^2 dependence, indicating the CME-induced MR. Inset: Expanded figure of MG at 1.6 K. The hump-like positive MG can be observed below 5 T, implying weak localization.

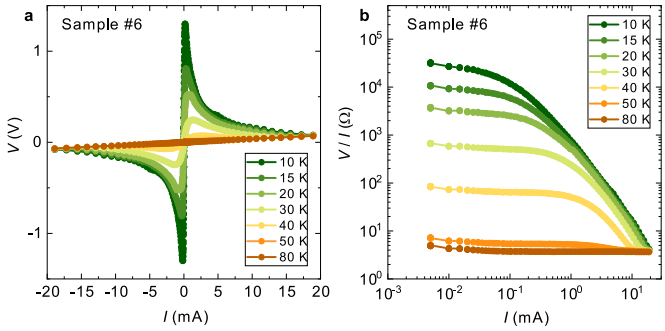

Fig. 2. **a** Current–voltage (I – V) characteristic measured at several temperatures using the four-terminal dc method with constant currents. A nonlinear conduction effect is observed in the wide current range. **b** Current dependence of the sample resistance (V/I). In the low current region, V/I is a constant value followed by Ohm's law. As the applied current increases, the sample resistance decreases by several orders of magnitude.

Moreover, unlike the longitudinal MR, the transverse MR of this compound exhibits positive [4], which is also consistent with the characteristics of the 3D-Dirac/Weyl system. Our findings suggest that the band structure of α-(BETS)$_2$I$_3$ has a Dirac-type dispersion with a very small gap, coinciding with the correlation-induced TI state theorized for this compound.

Next, we measured the current-voltage (I-V) character of this compound to observe a unique functionality of the correlation-driven TI state. As shown in Fig. 2a and 2b, we found that this compound shows a significant negative-differential resistance at low temperatures where a resistance (V/I) reduces by 3~4 orders of magnitude upon current application. This indicates that the low-temperature insulating state of this compound can be switched to a metallic state under external currents. Such metal-insulator switching due to current application is a phenomenon often seen in materials becoming insulating due to electron correlation [5] and is not a characteristic of conventional TIs.

Our experimental results provide evidence for the theoretical prediction that α-(BETS)$_2$I$_3$ is a TI. This is the first discovery of a TI composed of organic materials. Furthermore, this TI state can be manipulated into other electronic states using external fields, which has a potential for industrial application. We desire to deepen our understanding of the physical properties of organic TIs and advance further material development through research on analog compounds.

References

[1] S. Raghu, X. L. Qi, C. Honerkamp *et al.*, Phys. Rev. Lett. **100**, 156401 (2008).
[2] D. Ohki, K. Yoshimi, and A. Kobayashi, Phys. Rev. B. **105**, 205123 (2022).
[3] S. Kitou, T. Tsumuraya, H. Sawahata *et al.*, Phys. Rev. B **103,** 035135 (2021).
[4] T. Nomoto, S. Imajo, H. Akutsu *et al.*, Nat. Commun. **14**, 2130 (2023).
[5] F. Sawano, I. Terasaki, H. Mori *et al.*, Nature **437**, 522 (2005).

Authors

T. Nomoto, S. Imajo, H. Akutsu[a], Y. Nakazawa[a], and Y. Kohama
[a]Osaka University

Rise of Nonlinear Soft X-Ray Spectroscopy

I. Matsuda Group

X-ray spectroscopy has been a powerful technique to probe electronic states in materials. The light-matter interaction is based on a linear-response but it becomes non-linear when the intensity of incident light is significantly high. Recently, developments of X-ray free electron laser (XFEL) have led to our observation of the second harmonic generation, one of the well known non-linear optical phenomena, with soft X-ray (SX-SHG)[1]. A SX-SHG event occurs only when the inversion symmetry of the targeted system is broken and the signal is element-specific. These unique characters have pushed to apply SX-SHG for spectroscopy of materials science. However, it is often difficult to acquire a pure SX-SHG beam from a sample when the intensity is as small as second-harmonic radiation, generated on off-axis at the undulators. Such signal contamination is harmful for discussing genuine properties of SHG from any target sample. To overcome the situation, we developed and installed a new ellipsometry method for soft X-ray SHG experiment, as shown in Fig.1, to suppress the contribution of second-harmonic light from the XFEL beamline [2]. By the collaboration with RIKEN, we have also developed an experimental chamber of SX-SHG and opened for the SACLA users. We have successfully detected the broken inversion symmetry in the polar metal phase of $LiOsO_3$ with an enhanced feature above the Li K-edge that reflects the degree of Li atom displacement [3]. In a noncentrosymmetric crystal of $LiNbO_3$, elemental contributions by lithium and niobium were apparently distinguished by energy dependent SX-SHG measurements [4]. We have also probed the lithium mobility at a solid electrolyte surface to develop the Li-ion battery [5].

These research have applied the novel measurement method for investigation of crystallographic or electronic properties. The sensitivity to magnetism has remained elusive. Though a magnetic moment as an axial vector does not break the bulk inversion symmetry, it lowers the symmetry at interfaces, and thus should make additional contributions to SHG. While X-ray linear spectroscopies such as X-ray magnetic circular dichroism are useful to element-selectively study the magnetic properties of a material, it averages inevitably information over a certain depth along the incident light. To meet the demand of frontier technology, such as spintronics, that utilizes magnetic materials with complicated multilayered structure, it is, thus, useful to develop an element-selective method that can exclusively probe interface magnetism. We developed a magnetization induced SHG for soft X-ray (SX-MSHG) measurement system and made a demonstration for an Fe-based multilayer samples with broken inversion symmetry [6]. At the Fe M-edge resonance condition, we observed, as shown in Fig. 2, a clear dependence of SX-MSHG on the direction of applied magnetic field, even though the field was along the hard magnetization axis and thus the magnetization was only a small fraction of the saturation value. The results indicate high sensitivity of the measurement likely due to inner-shell resonance. By further deepening the understanding of its unique characteristics, SX-MSHG could be developed into a solid technique to element-selectively probe interface magnetism.

Through the technical efforts, research of the nonlinear optical effect in the soft X-ray region has evolved into a method of nonlinear soft X-ray spectroscopy. The unique characters of both the interface- and element-selectivity are useful for unveiling electronic and magnetic properties of the complicated compounds that provide various functionalities. Nonlinear X-ray spectroscopy is expected to become one of the standard analysis methods for materials science.

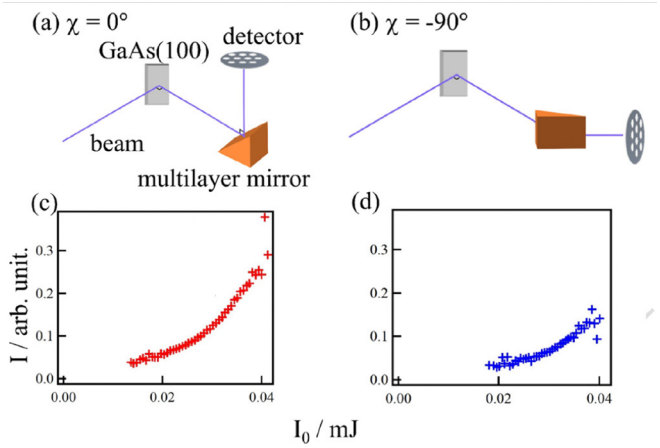

Fig. 1. Soft X-ray SHG data of GaAs(100) taken at the As M absorption edge, recorded with the ellipsometry method. The incident photon (I_0) beam was set at hν = 75 eV and the SHG signal (I) was detected at 2hν = 150 eV. The measurement geometries for the ellipsometry rotation angles at (a) χ = 0° and (b) −90°. Intensity curves of the SHG signals are shown in (c) and (d) that were taken by (a) and (b), respectively.

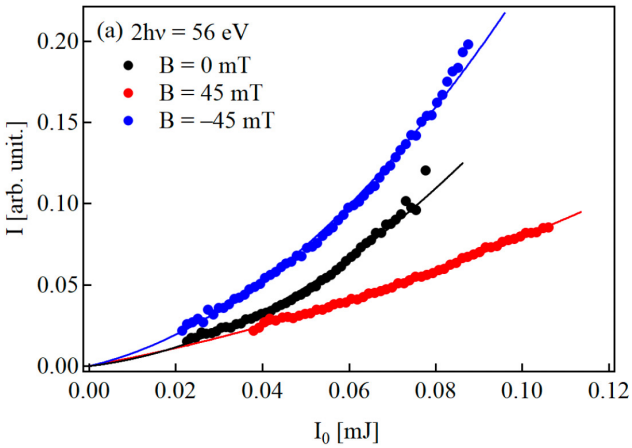

Fig. 2. SX- magnetization induced SHG (MSHG) from the $[Au/Fe/MgO]_4$ sample. 2hν intensity plot with respect to the incident beam intensity I_0 at 2hν = 56 eV under magnetic field as indicated. Photon energy of 56 eV corresponds to the Fe M-edge resonance. Solid curves represent the results of fitting with nonlinear curves.

References

[1] Sh. Yamamoto, T. Omi, H. Akai, Y. Kubota, Y. Takahashi, Y. Suzuki, Y. Hirata, K. Yamamoto, R. Yukawa, K. Horiba, H. Yumoto, T. Koyama, H. Ohashi, S. Owada, K. Tono, M. Yabashi, E. Shigemasa, S. Yamamoto, M. Kotsugi, H. Wadati, H. Kumigashira, T. Arima, S. Shin, and I. Matsuda, Phys. Rev. Lett. **120**, 223902 (2018).

[2] T. Sumi, M. Horio, T. Senoo, T. Wada, Y. Tsujikawa, X. Zhang, P. Manset, M. Araki, Y. Hirata, W. S. Drisdell, J. W. Freeland, A. Amado, M. Zuerch, Y. Kubota, S. Owada, K. Tono, M. Yabashi, C. P. Schwartz, and I. Matsuda, e-J. Surf. Sci. Nanotechnol. **20**, 25 (2022).

[3] E. Berger, S. Jamnuch, C. B. Uzundal, C. Woodahl, H. Padmanabhan, A. Amado, P. Manset, Y. Hirata, Y. Kubota, S. Owada, K. Tono, M. Yabashi, C. Wang, Y. Shi, V. Gopalan, C. P. Schwartz, W. S. Drisdell, I. Matsuda, J. W. Freeland, T. A. Pascal, and M. Zuerch, Nano Letters **21**, 6095 (2021).

[4] C. B. Uzundal, S. Jamnuch, E. Berger, C. Woodahl, P. Manset, Y. Hirata, T. Sumi, A. Amado, H. Akai, Y. Kubota, S. Owada, K. Tono, M. Yabashi, J. W. Freeland, C. P. Schwartz, W. S. Drisdell, I. Matsuda, T. A. Pascal, A. Zong, and M. Zuerch, Phys. Rev. Lett. **127**, 237402 (2021).

[5] C. Woodahl, S. Jamnuch, A. Amado, C. B. Uzundal, E. Berger, P. Manset, Y. Zhu, Y. Li, D. D. Fong, J. G. Connell, Y. Hirata, Y. Kubota, S. Owada, K. Tono, M. Yabashi, S. Tepavcevic, I. Matsuda, W. S. Drisdell, C. P. Schwartz, J. W. Freeland, T. A. Pascal, A. Zong, and M. Zuerch, Nat. Mater. (2023). https://doi.org/10.1038/s41563-023-01535-y

[6] T. Sumi, M. Horio, T. Senoo, Y. Kubota, G. Yamaguchi, T. Wada, M. Miyamoto, K. Yamaguchi, Y. Tsujikawa, Y. Sato, M. Niibe, Y. Hirata, Y. Miyauchi, D. Oshima, T. Kato, S. Owada, K. Tono, M. Yabashi, and I. Matsuda, Appl. Phys. Lett. **122**, 171601 (2023).

Author
I. Matsuda

Real-Time Observation of the Woodward-Hoffmann Rules for 1,3-Cyclohexadiene by Femtosecond Soft X-Ray Transient Absorption

Itatani Group

The stereochemistry of pericyclic reactions is explained by orbital symmetry conservation, referred to as the Woodward-Hoffmann (WH) rules. Although these rules have been verified by the structures of reactants and products, the temporal evolution of the orbital symmetry during the reaction has not been clarified. Herein, we used femtosecond soft X-ray transient absorption spectroscopy to elucidate the thermal pericyclic reaction of 1,3-cyclohexadiene (CHD) molecules, *i.e.*, its isomerization to 1,3,5-hexatriene. In the present experimental scheme, the ring-opening reaction is driven by the thermal vibrational energy injected by photoexcitation to the Rydberg states at 6.2 eV and subsequent femtosecond relaxation to the ground state of CHD molecules. The direction of the ring opening, which can be conrotatory or disrotatory, was the primary focus (see Fig. 1), and the WH rules predict the disrotatory pathway in the thermal process.

We focused on the *K*-edge absorption of the carbon atom from the 1s orbital to vacant molecular orbitals around 285 eV, because the *K*-edge absorption energy depends on the local environment of a carbon atom and could be sensitive to the transient molecular structure [1]. We expect to identify the transient molecular structures by the *K*-edge absorption. The BiB_3O_6-based optical parametric chirped pulse amplifier is used to produce carrier-envelope phase-stable intense infrared pulses (center wavelength 1.6 μm, pulse energy 1 mJ, pulse duration 10 fs at 1 kHz). This output is focused into Ne-filled gas cell to produce soft-X-ray continua covering the carbon *K*-edge, and the transmitted spectrum through the CHD-filled gas cell is measured by a grating spectrometer. The second harmonic (wavelength 400 nm) from the Ti:sapphire laser amplifier is used to pump the CHD molecules by two-photon absorption. Figure 2 shows the stationary carbon *K*-edge absorption spectrum of CHD (upper panel) and the time-resolved difference spectra (ΔA) at the designated delay time (lower panel).

The ultrafast relaxation from the Rydberg states to the ground state with a time constant of 26 ± 7 fs is identified by the disappearance of the bleaching of peak X observed at 0 fs. Another interesting feature in the time-resolved ΔA spectra is that the induced absorption band temporally appears between 340 and 600 fs at a higher absorption energy than peak X indicated by the arrows in Fig. 2. A theoretical investigation predicts that the transient molecular structures along the disrotatory pathway have higher *K*-edge absorption than peak X, while those along the conrotatory pathway have lower. Therefore, we attributed the observed induced absorption to the structural change in the disrotatory pathway, which is consistent with the prediction by the W-H rules. The observed dynamics show that the CHD ring starts to open approximately 340 fs later upon photoexcitation. This agrees with the observations by time-resolved photoelectron and high-harmonic spectroscopies [2, 3].

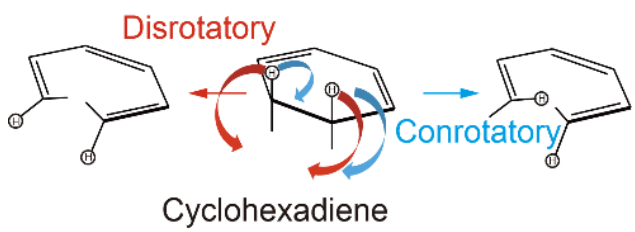

Fig. 1. Two ring-opening pathways of 1,3-cyclohexadiene (CHD) molecules

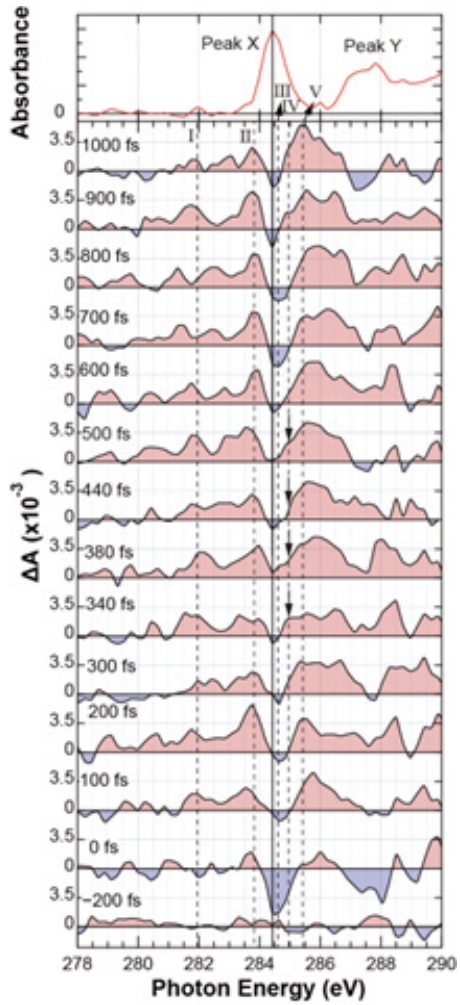

Fig. 2. Stational absorption spectrum and time-resolved ΔA spectra.

References
[1] T. Sekikawa *et al*., Phys. Chem. Chem. Phys. **25**, 8497 (2023).
[2] R. Iikubo *et al*., Faraday Discuss. **194**, 147 (2016).
[3] K. Kaneshima *et al*., Opt. Express **26**, 31030 (2018).

Authors
T. Sekikawa[a], N. Saito, Y. Kurimoto[a], N. Ishii[b], T. Mizuno, T. Kanai, J. Itatani, K. Saita[a], and T. Taketsugu[a]
[a]Hokkaido University
[b]National Institute for Quantum Science and Technolgy

Testing Electron-phonon Coupling for Superconductivity in Kagome Metal CsV_3Sb_5

Okazaki and Kondo Groups

In crystalline materials, electron-phonon coupling (EPC) is a ubiquitous many-body interaction that drives conventional Bardeen-Cooper-Schrieffer superconductivity. Recently, in a new kagome metal CsV_3Sb_5, superconductivity that possibly intertwines with time-reversal and spatial symmetry-breaking orders is observed [see phase diagram in Fig. 1a]. Density functional theory (DFT) calculation [1] predicted a weak EPC strength, λ, supporting an unconventional pairing mechanism in CsV_3Sb_5. However, experimental determination of λ is still missing, hindering a microscopic understanding of the intertwined ground state of CsV_3Sb_5. In this study, using 7-eV laser-based angle-resolved photoemission spectroscopy (ARPES) and Eliashberg function analysis, we experimentally extract the orbital- and momentum-dependent λ by determining the EPC-induced kinks in the electronic band structure.

We first present the Fermi surface (FS) topology of CsV_3Sb_5 in Fig. 1b. In agreement with DFT study and previous ARPES studies [1, 2], the Sb 5*p*-band forms a circular FS, marked as α, at the BZ center and the V 3d-bands yield hexagonal and triangular FSs, marked as β and δ in Fig. 1b, respectively. Figure 1c shows a typical ARPES intensity plot of the α band corresponding to the black cut shown in Fig. 1b. By fitting momentum distribution curves (MDCs) with a Lorentzian function as the yellow and black curves shown in Fig. 1c, the band dispersion $\omega(\boldsymbol{k})$ is extracted as the red curve in Fig. 1c and the single-particle self-energy, $\Sigma(\omega = E - E_F)$, is quantitively extracted in Fig. 1d. At $E_B \sim$ 32 meV, a peak in the real part $\mathrm{Re}\Sigma(\omega)$ and a step jump in the imaginary part $\mathrm{Im}\Sigma(\omega)$ prove a strong coupling between electrons and bosonic modes [3], which are manifested as a kink in the band structure. As the kink is persistent above the CDW transition temperature and any magnetic orders are absent, we attribute it to EPC.

Next, we study the orbital-dependence of EPC by comparing the kinks on the α and β bands. As in Fig. 1e, $\mathrm{Re}\Sigma(\omega)$ of the β band which is derived from V 3*d* orbitals shows a peak near $E_B \sim 12$ meV, suggesting a strong

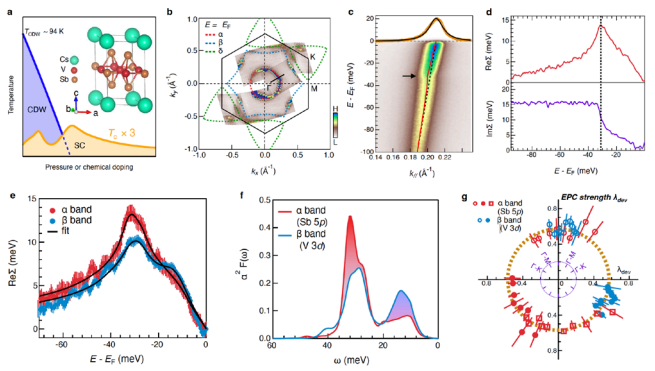

Fig. 1. Orbital and momentum dependence of EPC in CsV_3Sb_5 kagome superconductor. (a) Phase diagram and crystal structure (inset). (b) Fermi surface mapping with ARPES intensity integrated within $E_F \pm$ 5 meV. (c) ARPES intensity plot for a black cut in (b). (d) Extracted self-energy from the ARPES intensity plot shown in (c). (e) Real-part self-energy for the α and β bands along the Γ-K direction. (f) Extracted Eliashberg function for the α and β bands by fitting $\mathrm{Re}\Sigma(\omega)$ in (e). (g) EPC strength λ_{dev} at different momenta on the α and β Fermi surfaces.

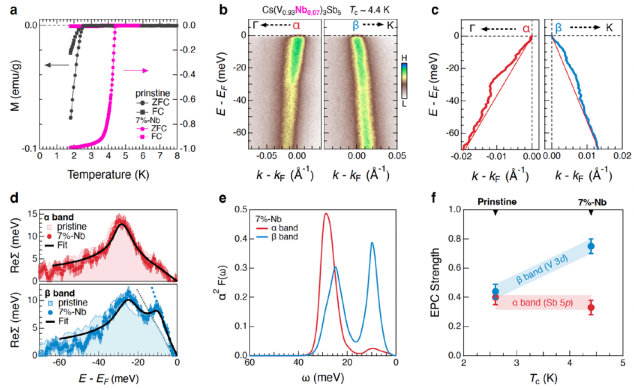

Fig. 2. Orbital and energy selective enhancement of EPC in 7%-Nb doped CsV_3Sb_5. (a) Temperature dependence of magnetic susceptibility. Both zero-field cooling (ZFC) and field cooling (FC) curves are presented. (b) ARPES intensity plots of the α and β bands along the Γ-K direction. (c) Extracted band dispersions. (d) Extracted real-part self-energy for the α (top panel) and β (bottom panel) bands. Colored shadows are the corresponding $\mathrm{Re}\Sigma(\omega)$ for pristine CsV_3Sb_5. The dashed lines in bottom panel represent the slope of $\mathrm{Re}\Sigma(\omega)$ at E_F. (e) Extracted Eliashberg function. (f) EPC strength estimated from the Eliahsberg function and plotted as a function of T_c.

d-electron-phonon coupling near 12 meV. In contrast, $\mathrm{Re}\Sigma(\omega)$ of the α band only shows a broad shoulder. Through a fit to the extracted $\mathrm{Re}\Sigma(\omega)$ following the maximum energy method [3], we extract the Eliashberg function, $\alpha^2F(\omega)$. The extracted $\alpha^2F(\omega)$ for the α and β bands are plotted in Fig. 1f. The orbital dependence of the EPC is mirrored in the different shapes of $\alpha^2F(\omega)$, where phonon modes near 32 meV are accounted for 70% of the total EPC strength on the α band, λ_p, but less than 50% for the EPC strength on the β band, λ_d. Interestingly, due to the spectral weight redistribution in $\alpha^2F(\omega)$ [shaded area in Fig. 1f], λ_p and λ_d calculated by $2\int_0^{\omega_{max}}\left[\frac{\alpha^2F(\omega)}{\omega}\right]d\omega$ are similar with $\lambda_{p,d} \sim$ 0.45 ± 0.05. Theoretically, λ can approximately be derived from a simpler approach following $\lambda_{dev} = \partial\mathrm{Re}\Sigma(\omega)\partial\omega|_{\omega = E_F} \cong \lambda$, when *T* is far lower than the Debye temperature. At *T* = 6 K, this method yields $\lambda_{dev} \sim 0.6 \pm 0.1$. By scanning the kinks along with the FSs, the extracted $\lambda_{dev}(\boldsymbol{k})$ for the α and β bands of two independent samples are summarized in Fig. 1g, which shows a nearly isotropic behavior within experimental uncertainties.

The orbital- and momentum-dependent results demonstrate that λ in CsV_3Sb_5 falls in the intermediate range of 0.45 – 0.6, which is about 2 times larger than the previous DFT predicted $\lambda_{DFT} \sim 0.25$ [1]. Using McMillan's formula and taking the lower and upper limits of the experimentally estimated λ and the logarithmic mean phonon frequency ~17.1 meV obtained by $2/\lambda\int_0^{\infty} ln\omega\left[\frac{\alpha^2F(\omega)}{\omega}\right]d\omega$, we derive T_c in a range from 0.8 K to 3 K. The upper limit is comparable to the experimentally determined T_c in CsV_3Sb_5 (Fig. 2a).

As T_c of CsV_3Sb_5 can be increased with chemical substitutions or external pressure (Fig. 1a). We thus continue to examine the EPC strength in 7% Nb-doped $Cs(V_{0.93}Nb_{0.07})_3Sb_5$ with $T_c \sim 4.4$ K. Electronic kinks are observed on both the α and β bands as shown in Fig. 2b for the ARPES intensity plots and Fig. 2c for the extracted band dispersions. Figure 2d shows the extracted $\mathrm{Re}\Sigma(\omega)$ on the α and β bands of $Cs(V_{0.93}Nb_{0.07})_3Sb_5$. Remarkably, we observe that while $\mathrm{Re}\Sigma(\omega)$ on the α band is similar in $Cs(V_{0.93}Nb_{0.07})_3Sb_5$ and CsV_3Sb_5, on the β band, it shows a strong enhancement in the Nb-doped sample, especially near $E_B \sim 10$ meV. Based on the extracted $\alpha^2F(\omega)$, shown in

Fig. 2e, we find that $\lambda_d \sim 0.75 \pm 0.05$ is enhanced by about 50% in $Cs(V_{0.93}Nb_{0.07})_3Sb_5$ (Fig. 2f). Importantly, the enhanced λ_d is expected to elevate T_c up to 4.5 K, which is comparable to the experimental value of 4.4 K. Such synchronous enhancements of λ_d and T_c may indicate that the V 3*d*-electron–phonon couplings are the main driver of the superconductivity in CsV_3Sb_5.

In summary, by investigating the electronic kinks, we determined the intermediate EPC that is twice larger than the DFT calculation in the kagome superconductors CsV_3Sb_5 and $Cs(V_{0.93}Nb_{0.07})_3Sb_5$. Our results provide an important clue to understand the pairing mechanism in CsV_3Sb_5. The orbital and momentum dependence of the electronic kinks and their strengthening with the promoted T_c prove that the EPC in CsV_3Sb_5 is strong enough to support T_c comparable to the experiment value and hence cannot be excluded as a possible pairing mechanism.

References

[1] H. Tan *et al.*, Phys. Rev. Lett. **127**, 046401 (2021).
[2] B. Ortiz *et al.*, Phys. Rev. Lett. **125**, 247002 (2020).
[3] Y. Zhong *et al.*, Nat. Commun. **14**, 1945 (2023).

Authors

Y. Zhong, S. Li[a], H. Liu[b], Y. Dong, K. Aido, Y. Arai, H. Li[a], W. Zhang[c], Y. Shi[b], Z. Wang[d], S. Shin, H. N. Lee[a], H. Miao[a], T. Kondo, and K. Okazaki
[a]Oak Ridge National Laboratory
[b]Chinese Academy of Sciences
[c]Sophia University
[d]Boston College

Joint Research Highlights

Anomalous Electromagnetic Response in the Spin-Triplet Superconductor UTe_2

Unconventional superconductivity with a spin-triplet pairing state has attracted considerable interest because of its unusual nontrivial superconducting order parameters and magnetic response, which are quite different from those of conventional Bardeen-Cooper-Schrieffer superconductors. In particular, the spin-triplet pairing state protected by a topological invariant provides a good opportunity to seek exotic quasiparticles such as Majorana fermions. The recent discovery of unconventional superconductivity in UTe_2 has provided a new opportunity in the research of spin-triplet pairing states in solid state physics [1]. One of the most important challenges for studying the superconducting state of UTe_2 is to clarify its thermodynamic behavior and its magnetic response.

In this study [2], to further understand the spin-triplet superconductivity in UTe_2 from a thermodynamic point of view, we investigate the magnetic field and the temperature dependence of dc magnetization, heat capacity down to 80 mK in magnetic fields up to 14 T. Our high-resolution magnetization measurements done by the Faraday magnetometer for $H \parallel a$ (the magnetic easy axis, Fig. 1(a) and (c)) and for $H \parallel b$ (hard axis, Fig. 1(b) and (d)) reveal multiple

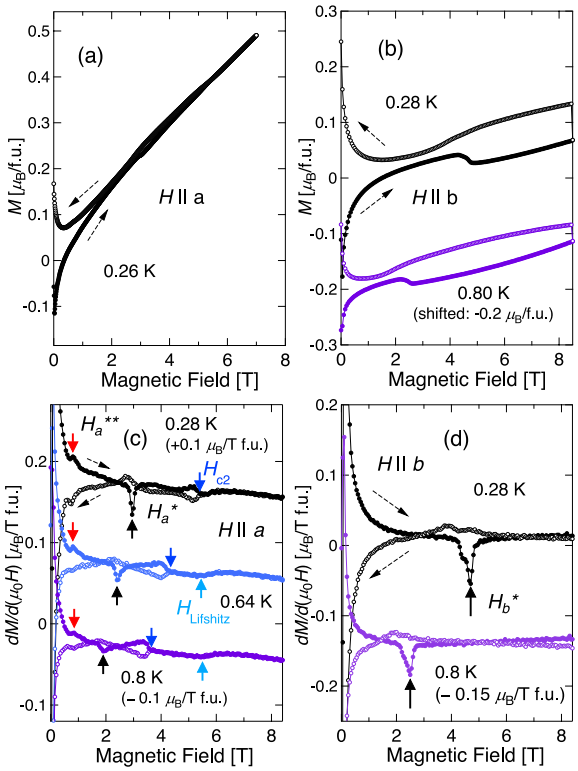

Fig. 1. (a,b) Magnetization curves $M(H)$ of UTe_2 in $H \parallel a$ (a) and in $H \parallel b$ (b). (c,d) The differential of magnetization curves dM/dH in $H \parallel a$ (c) and in $H \parallel b$ (d). The dashed arrows indicate the field sweep direction.

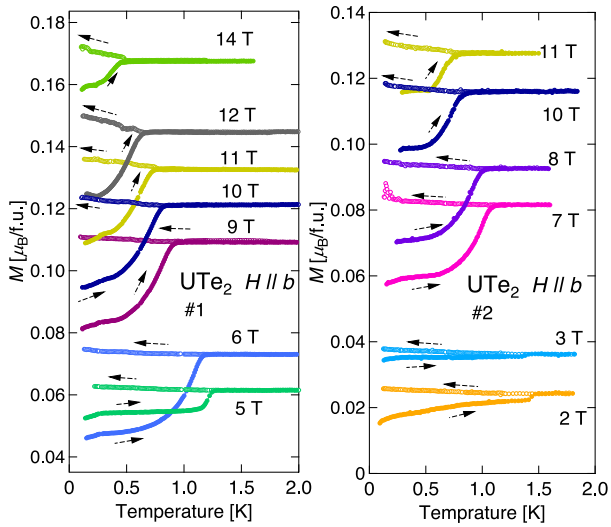

Fig. 2. Temperature dependence of magnetization $M(T)$ at different magnetic fields applied along the b axis of UTe_2 sample #1 (left) and #2 (right). The solid and the open symbols show the data obtained in the warming up process after zero-field cooling and that obtained in subsequent cooling process, respectively.

anomalies (H_a^{**}, H_a^*, and H_b^*) in the field dependence of the magnetization $M(H)$ below the upper critical field (H_{c2}). These anomalies are also observed in our ac susceptibility measurements done down to 30 mK [2].

We further find the temperature dependence of the magnetization, $M(T)$, is changed at the anomaly. Figure 2 shows $M(T)$ observed in two different crystals at different magnetic fields applied along the b axis. As shown in Fig. 2, the difference between zero-field cooling and field-cooling processes in the superconducting state below H_b^* becomes smaller as approaching H_b^* and then larger with strong irreversibility above H_b^*.

These anomalies observed both in $M(H)$ and $M(T)$ in the superconducting phase are attributed to strong pinning effects on vortices in the spin-triplet superconducting state of UTe_2. In addition, we find a broad steplike anomaly just above H_{c2} for the magnetic easy axis ($H \parallel a$). Given that this anomaly does not depend on the temperature and is observed above the superconducting transition temperature, we suggest that this is caused by the Lifshitz transition of this compound.

The anomalous vortex states in UTe_2 suggested by our magnetization measurements are also consistent with recent NMR measurements [3] showing gradual decrease of the NMR Knight shift and shoulder-like anomalies in the NMR spectra. These anomalies observed for 6–10 T indicate the presence of inhomogeneous internal fields, which could be brought by a gradual change of the d-vector of the spin-triplet state in vortices. We suggest that depinning of the d-vector above H_b^* that is pinned to $d \parallel H$ at lower fields might be related to these anomalies observed in our magnetization and the NMR measurements.

References
[1] D. Aoki, K. Ishida, and J. Flouquet, J. Phys. Soc. Jpn. **88**, 022001 (2019).
[2] Y. Shimizu, S. Kittaka, Y. Kono, T. Sakakibara, K. Machida, A. Nakamura, D. Li, Y. Homma, Y. J. Sato, A. Miyake, M. Yamashita, and D. Aoki, Phys. Rev. B **106**, 214525 (2022).
[3] G. Nakamine, K. Kinjo, S. Kitagawa, K. Ishida, Y. Tokunaga, H. Sakai, S. Kambe, A. Nakamura, Y. Shimizu, Y. Homma, D. X. Li, F. Honda, and D. Aoki, J. Phys. Soc. Jpn. **90**, 064709 (2021).

Authors
Y. Shimizu[a], S. Kittaka[b], Y. Kono[b], T. Sakakibara, K. Machida[c], A. Nakamura[a], D. Li[a], Y. Homma[a], Y. J. Sato[a], A. Miyake, M. Yamashita, and Dai Aoki[a]
[a]Institute for Materials Research (IMR), Tohoku University
[b]Chuo University
[c]Ritsumeikan University

PI of Joint-use project: Y. Shimizu
Host lab: Yamashita Group

Theory of Energy Splitting of Chiral Phonons

Chirality is a property manifesting that the system's structure cannot overlap with its mirror image by using any combination of translation and rotation alone, and chiral materials exhibit many interesting cross correlations in their electromagnetic and/or thermal properties. This is due to the property that polar-vector inputs can induce axial-vector outputs and *vice versa* in those systems in addition to ordinary responses, and this cross-correlated response is governed by a "order parameter" represented by an electric toroidal multipole of some rank [1]. Many of the preceding studies on the chiral systems have focused on their electronic properties, since the cross correlated electromagnetic responses are mainly governed by those degrees of freedom.

We have conducted a project to theoretically investigate the effects of chiral structure on phonon properties with mainly targeting tellurium and its related systems [2]. It has been known that these systems have a special quantum number related to their chirality, and it is crystal angular momentum (CAM) m. The main issue is how to characterize an energy splitting of chiral phonons with different CAM values ($m = \pm 1$). Chiral phonons have an elliptic polarization of atomic displacement that rotates clockwise or anticlockwise depending on the sign of CAM m.

For studying this problem, we have first performed a model building within the harmonic approximation for the lattice deformation energy and constructed a related dynamical matrix, the eigenvalues of which determine phonon energies. We have found an important constraint for the dynamical matrix that guarantees the stability of the atomic equilibrium positions in the given chiral structure. Taking account of this constraint, we have shown that the sound velocity of chiral phonons is identical independent of the sign of CAM m, and this disproves some precedent discussions expecting different velocities. Energy splitting $\Delta\omega$ between the $m = \pm 1$ CAM modes is remarkable for optical phonons, and it is linear in the phonon momentum k_z along the chiral axis as $\Delta\omega = \Gamma\, k_z\, m$ around $k_z = 0$. We have derived a simple formula for the coefficient Γ of this linear splitting represented in terms of microscopic stiffness constants in the dynamical matrix. This is a pseudo-scalar and corresponds to an electric toroidal monopole of the system.

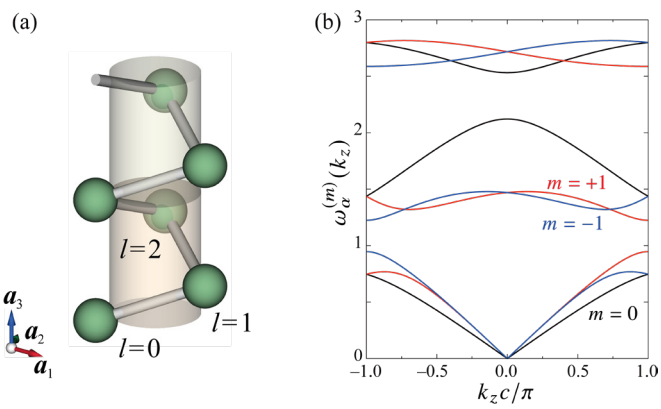

Fig. 1. (a) Structure of tellurium-like lattice. (b) Phonon energy dispersion in tellurium-like lattice for wave vector k = (0,0,k_z). m is the value of CAM. (Taken from Ref.[2]).

In order to check this and further study the effects of chiral structure on phonon energy dispersion, we have also proposed a lattice model for which one can control its lattice chirality continuously. Its one limit is a set of three decoupled chiral tellurium-like lattices, while the other limit is a non-chiral coupled system with mirror symmetry. We have confirmed the above findings for the chiral system and found that the chirality-related energy splitting of optical phonons continuously vanish as we control the system towards the non-chiral limit. This type of energy splitting between two optical phonon modes had been recently observed by Raman scattering experiment, and the assignment of CAM quantum number was simultaneously performed to those two modes using the polarization selection rule [3], which is consistent with the theoretical predictions. We are planning to continue the study on chiral phonons and clarify other interesting properties related to several galvano-electric and galvano-magnetic responses.

References
[1] S. Hayami, M. Yatsuhiro, Y. Yanagi, and H. Kusunose, Phys. Rev. B **98**, 165110 (2018).
[2] H. Tsunetsugu and H. Kusunose, J. Phys. Soc. Jpn. **92**, 023601 (2023).
[3] K. Ishito *et al.*, Nat. Phys. **19**, 35 (2023).

Authors
H. Tsunetsugu and H. Kusunose[a]
[a]Meiji University

PI of Joint-use project: H. Kusunose
Host lab: Tsunetsugu Group

Mechanical Conformation Control of Cyclized Binaphthyl at the Air–Water Interface

Biological activity is maintained by various molecular machines working in the body. The complex structure of molecular machines makes it difficult to elucidate their behavior. Molecular machines function through a combination of various molecular conformation changes. Detailed analysis of simple molecular conformation changes is expected to provide a deeper understanding of the operating mechanisms of complex molecular machines. The air-water interface is a suitable field for controlling molecular machines because mechanical compression can be applied with the help of movable barriers of the Langmuir–Blodgett (LB) system, comparable to those that can change the conformation of proteins. In addition, a lipid matrix, which is a medium analogous to biological membranes, can be prepared at the air-water interface.

Molecular conformations can be identified using several spectroscopic methods. We have confirmed the conformational change of binaphthyl derivatives at the air-water interface. The circular dichroism (CD) spectra can be obtained for these molecules at low concentrations and the spectra sensitively reflect conformational changes [1, 2]. In this work, we have controlled the molecular conformations of monobinaphthyldurene (MBD) in a lipid matrix similar to biological systems [3].

Figure 1 shows the chemical structure of MBD and three conformers of 1-MBD, 2-MBD, and flat-MBD, which is indicated by density functional theory (DFT) calculations, having different dihedral angles of φ between the two naphthyl moieties. The conformer 2-MBD is 2.8 kcal mol^{-1} higher in energy than the more stable 1-MBD, while flat-MBD is not favored energetically. DFT calculations also indicate that 2-MBD has a larger dihedral angle than 1-MBD, which causes the CD peak of 2-MBD to shift to a longer wavelength.

MBD was mixed with linear stearic acid (SA) or unsaturated oleic acid (OA) as matrices and then spread at the air–water interface. The mechanical properties of the mixed monolayers with MBD were characterized by surface pressure–molecular area (π-A) isotherms. The monolayers were transferred onto quartz substrates at different surface pressures to analyze the molecular aggregations and conformations by using CD spectra and Fourier transform infrared reflection absorption spectroscopy (FT-IR-RAS), atomic force microscopy (AFM). It suggested that MBD mixes more effectively with OA than with SA and dissolves in the lipid matrices upon mechanical compression.

The π–A isotherms suggest high miscibility of MBD with OA. It was also supported by FT-IR-RAS and AFM. The CD peak of the mixed monolayer with SA did not change with surface pressure. On the other hand, the mixed monolayer with OA shifted to longer wavelength with increasing surface pressure. Thus, the conformation of MBD changes from 1-MBD to 2-MBD in the mixed monolayer of OA; in contrast, 1-MBD is stable in SA. The higher-energy conformer 2-MBD is stabilized by the dissolution in the highly miscible lipids of OA.

As summarized in Figure 2, MBD confirmations could be controlled from 1-MBD to 2-MBD by mechanical stimulus in highly miscible lipids of OA. In contrast, the most stable 1-MBD conformation could not be transformed during mechanical compression in poorly miscible lipids of SA. It was found that different behaviors of molecular machines showed in their different local environments.

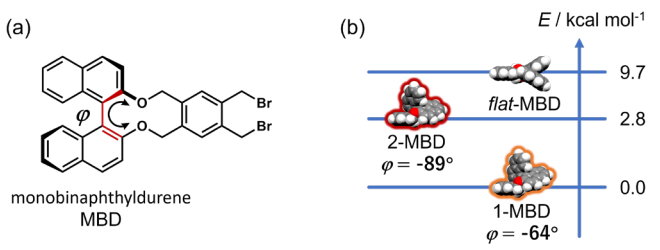

Fig. 1. (a) Molecular structure of MBD having a dihedral angle φ between two naphthyl rings of 1,1′-binaphthyl; (b) relative energies of MBD conformers.

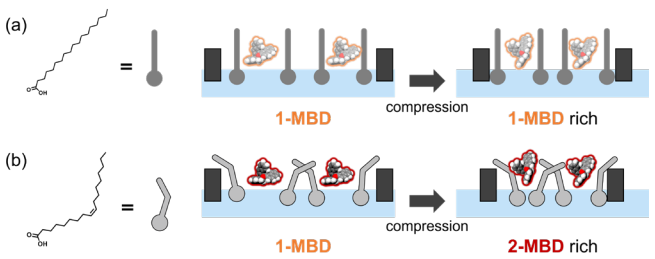

Fig. 2. Schematic Illustration of Aggregated States Involving MBD and Lipid Matrices. (a) Mixed with stearic acid. 1-MBD persists during mechanical compression; (b) mixed with oleic acid. MBD dissolves in oleic acid, accompanied by a conformational change from 1-MBD to 2-MBD.

References

[1] D. Ishikawa, T. Mori, Y. Yonamine, W. Nakanishi, D. L. Cheung, J. P. Hill, and K. Ariga, Angew. Chem. Int. Ed. **54**, 8988 (2015).
[2] M. Ishii, T. Mori, W. Nakanishi, J. P. Hill, H. Sakai, and K. Ariga, ACS Nano **14**, 13294 (2020).
[3] M. Ishii, T. Mori, W. Nakanishi, J. P. Hill, H. Sakai, and K. Ariga, Langmuir **38**, 6481 (2022).

Authors

M. Ishii[a,b], T. Mori, W. Nakanishi[b], J. P. Hill[b], H. Sakai[a], and K. Ariga[b]
[a]Tokyo University of Science
[b]National Institute for Materials Science

PI of Joint-use project: K. Ariga
Host lab: Lippmaa Group

Drude Weights in One-Dimensional Systems with a Single Defect

Ballistic transport of a quantum system can be characterized by Drude weight, which quantifies the response of the system to a uniform electric field in the infinitely long timescale. The Drude weight is often discussed in terms of the Kohn formula, which gives the Drude weight by the derivative of the energy eigenvalue of a finite-size system with the periodic boundary condition in terms of the Aharonov-Bohm flux. Recently, the Kohn formula is generalized to nonlinear responses [1,2]. In particular, for the S = 1/2 XXZ chain, analytic expressions of the nonlinear Drude weights are obtained utilizing the Bethe Ansatz exact solution. However, the nonlinear Drude weight determined by the Kohn formula often diverges in the thermodynamic limit. In order to elucidate the issue, in this work [3] we examine a simple example of a one-dimensional tight-binding model in the presence of a single defect at zero temperature. This problem can be formulated in terms of the scattering matrix of the defect. While the bulk energy density and the "defect energy" are

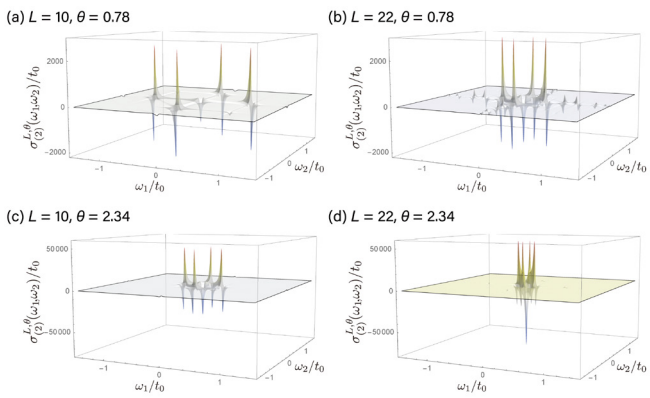

Fig. 1. Second-order optical conductivity of the impurity model for system size L=10, 22 with the Aharonov-Bohm flux θ, as a function of the two frequencies ω_1 and ω_2. Several peaks are observed near zero frequencies.

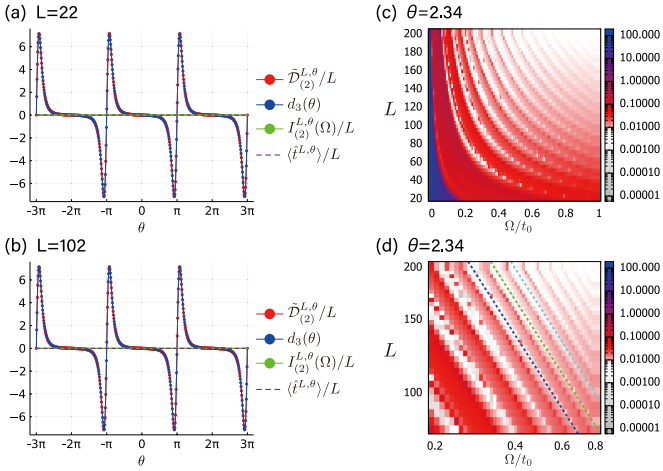

Fig. 2. Comparison between the Kohn formula $\tilde{\mathcal{D}}_{(2)}$ and the optical conductivity integrated over a window of low frequencies $I_{(2)}$, for the second-order Drude weight. While the Kohn formula depends strongly on the Aharonov-Bohm flux θ, the integrated conductivity (almost) vanishes for the entire range of θ. The latter corresponds to the vanishing bulk Drude weight expected in the thermodynamic limit.

non-universal and independent of the Aharonov-Bohm flux, the flux dependence appears in the O(1/L) correction, where L is the system size, which is a universal function of the scattering matrix. This is also consistent with the Conformal Field Theory. Using this formulation, we find that its linear and non-linear Drude weights given by the Kohn formula (i) depend on the Aharonov-Bohm flux and (ii) diverge proportionally to a power of the system size. Since the effect of the Aharonov-Bohm flux on the bulk transport property should vanish in the thermodynamic limit, the dependence on the Aharonov-Bohm flux signals that the non-linear Drude weights thus obtained may not describe the bulk property.

We argue that the problem can be attributed to different order of limits. The Drude weight according to the Kohn formula indicates the response of a finite-size system to an adiabatic insertion of the Aharonov-Bohm flux. While it is a well-defined physical quantity for a finite-size system, its thermodynamic limit does not always describe the ballistic transport of the bulk. The pathological behaviors such as the divergence of the nonlinear Drude weights mentioned above are indications of the discrepancy between the bulk transport property and the thermodynamic limit of the Kohn formula.

In order to clarify the issue, we propose to call the thermodynamic limit of the Kohn formula, namely the Drude weight defined by taking the adiabatic limit before the thermodynamic limit as "Kohn Drude weight". The ballistic transport of the bulk is rather characterized by the "bulk Drude weight" defined by taking the thermodynamic limit first before the adiabatic (zero-frequency) limit. While the potential issue of the order of limits has been sometimes discussed within the linear response, the discrepancy between the two limits is amplified in nonlinear Drude weights. We demonstrate that, the low-energy excitations of O(1/L) in the finite system of size L, which are excluded from the Kohn–Drude weight, contribute to the bulk Drude weight. This removes the pathological behaviors, making the bulk Drude weight finite and also independent of the Aharonov-Bohm flux.

References

[1] H. Watanabe and M. Oshikawa, Phys. Rev. B **102**, 165137 (2020).
[2] H. Watanabe, Y. Liu, and M. Oshikawa, J. Stat. Phys. **181**, 2050 (2020).
[3] K. Takasan, M. Oshikawa, and H. Watanabe, Phys. Rev. B **107**, 075141 (2023).

Authors
K. Takasan[a], M. Oshikawa, and H. Watanabe[a]
[a]University of Tokyo

PI of Joint-use project: K. Takasan
Host lab: Oshikawa Group

Perfect Co^{2+}-Based $J_{eff} = 1/2$ Kagomé Magnets

Kagomé lattice antiferromagnets have attracted significant interest in condensed matter physics due to their exotic magnetic properties, such as geometric frustration and the emergence of topologically ordered ground states. Our research aims to contribute to understanding the J_{eff} = 1/2 kagomé physics, which has not been comprehensively explored experimentally or theoretically. In this study, we report the synthesis, crystal structure, and magnetic properties of two cobalt-based kagomé magnets, namely $Co_3V_2O_7(OH)_2{\cdot}2H_2O$ and $BaCo_3(VO_4)_2(OH)_2$. These compounds can be considered as Co analogs of the extensively studied quantum kagomé magnets volborthite $Cu_3V_2O_7(OH)_2{\cdot}2H_2O$ and vesignieite $BaCu_3(VO_4)_2(OH)_2$. The titled Co^{2+}-based kagomé materials were synthesized utilizing the hydrothermal technique. For a comprehensive understanding of the specific synthesis procedures employed in this study, please refer to the associated publication [1].

As illustrated in Figure 1, the temperature-dependent magnetic susceptibility of $Co_3V_2O_7(OH)_2{\cdot}2H_2O$ and $BaCo_3(VO_4)_2(OH)_2$ under low magnetic fields of 10 mT displays anomalies indicative of an antiferromagnetic transition. However, this characteristic behavior vanishes when the applied magnetic field is elevated to 0.1 T. This observation can be corroborated by the isothermal magnetization process at 2 K, depicted in Figure 2(a), where the antiferromagnetic ground state is suppressed by a field-induced phase transition at considerably lower magnetic fields (75 mT for $Co_3V_2O_7(OH)_2{\cdot}2H_2O$ and 16 mT for $BaCo_3(VO_4)_2(OH)_2$, respectively). Moreover, the M^2 vs. H/M plot [Figure 2(b)] reveals a curve characteristic of metamagnetism. In the high-field region beyond the metamagnetic transition field, the M^2 vs. H/M plot exhibits linearity, signifying that the order parameter within the framework of Landau theory corresponds to the spontaneous magnetization M_0 (associated with the value of the intercept) and exhibits a metamagnetic feature [2].

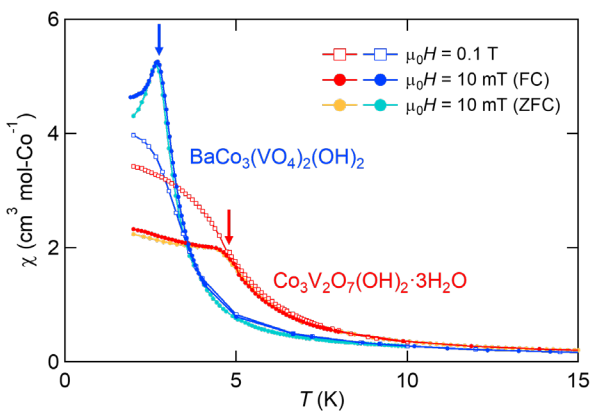

Fig. 1. Temperature dependence of magnetic susceptibility (χ) in Co^{2+}-based kagomé magnets, measured under magnetic fields of 0.1 T and 10 mT.

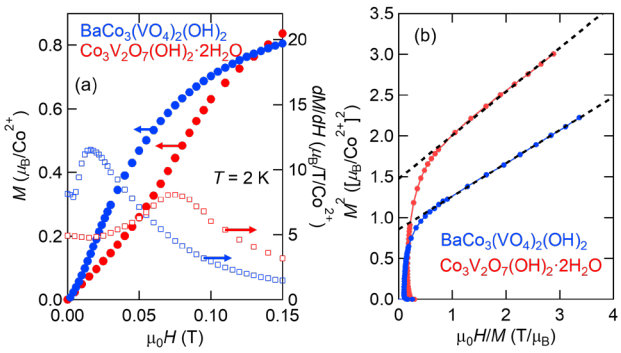

Fig. 2. (a) Low-field (< 0.15 T) magnetization curves (M) and their derivatives (dM/dH) obtained at 2 K for Co^{2+}-based kagome magnets. A metamagnetic-like transition is discerned at $\mu_0 H$ = 75 mT for $Co_3V_2O_7(OH)_2{\cdot}2H_2O$ and $\mu_0 H$ = 16 mT for $BaCo_3(VO_4)_2(OH)_2$. (b) The M^2 vs. $\mu_0 H/M$ plot

Nevertheless, the spontaneous magnetization M_0 is approximately half of the powder-averaged saturation magnetization of 2 μ_B anticipated for Co^{2+} and cannot be elucidated by simple in-plane ferromagnetism, as typically observed in metamagnetic transitions. Theoretical investigations suggest that antisymmetric exchange mediated by the Dzyaloshinsky-Moriya (DM) interaction may engender such moments by causing a slight out-of-plane tilt of the spins [3,4]. The DM interaction prompts the spins within each triangle of the kagomé lattice to adopt an "umbrella" configuration [5]. If the Co^{2+} ion exhibits a J_{eff} = 1/2 effective spin, the powder-averaged g factor is approximately 4. The angle θ, representing the spin tilt induced by the DM interaction, is nearly equal to arctan[(g-2)/g]. Consequently, the emergent ferromagnetic moment in Co^{2+} spin is approximately 45% of the saturation magnetization, which explains the magnetic moment that emerges due to the metamagnetic transition, constituting nearly half of the saturation field.

Based on these observations, the origin of the metamagnetic transition in Co^{2+} kagomé systems can be elucidated as portrayed in Figure 3. The relatively substantial DM interaction provokes each triangular spin of the kagomé lattice to adopt a significantly tilted umbrella structure, generating a ferromagnetic moment of about M_0 ~ 1 μ_B on each kagomé plane. The coupling between kagomé planes is characterized by weak antiferromagnetic interactions between layers of ferromagnetic moments under a feeble applied magnetic field. Furthermore, the antiferromagnetic coupling becomes destabilized by weak magnetic fields on the order of tens of millitesla, culminating in "halfway-saturated ferromagnetism."

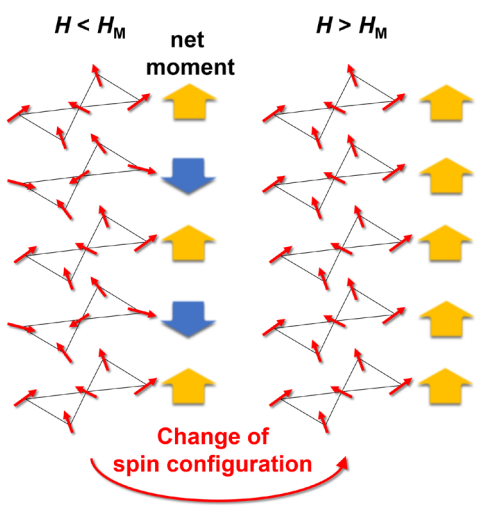

Fig. 3. Schematic representation of the spin configuration transition in Co^{2+}-based kagomé magnets, wherein antiferromagnetically aligned canted moments transform into ferromagnetically aligned ones.

Our study highlights the importance of synthesizing and characterizing new materials with kagomé lattice structures to broaden the understanding of the J_{eff} = 1/2 kagomé physics. Furthermore, the Co^{2+} kagomé magnets presented here serve as a platform for further investigations of the interplay between crystal-field, superexchange, spin-orbit coupling, and DM interactions in kagomé systems.

References

[1] Y. Haraguchi, T. Ohnoda, A. Matsuo, K. Kindo, and H. Aruga Katori, Physical Review B **106**, 214421 (2022).
[2] S. K. Banerjee, Phys. Lett. **12**, 16 (1964).
[3] I. E. Dzyaloshinskii, J. Phys. Chem. Solids **4**, 241 (1958).
[4] T. Moriya, Phys. Rev. **120**, 91 (1960).
[5] M. Elhajal, B. Canals, and C. Lacroix, Phys. Rev. B **66**, 014422 (2002).

Authors
Y. Haraguchi[a], T. Ohnoda[a], A. Matsuo, K. Kindo, and H. Aruga Katori[a]
[a]Tokyo University of Agriculture and Technology

PI of Joint-use project: Y. Haraguchi
Host lab: Hiroi Group and Electromagnetic Measurements Section

Unconventional Superconductivity Robust Against Impurities in a Newly Discovered Kagome Lattice Superconductor

One of the strategies in the search for quantum phenomena such as non-trivial magnetism and superconductivity is to focus on the symmetry of crystal structures of materials. The kagome lattice consisting of corner-sharing triangles and hexagonal holes (Fig. 1(a)) has attracted much attention because materials with kagome lattice structures exhibit various exotic properties, such as quantum spin liquids, Dirac/Weyl physics, and unconventional superconductivity, driven by its geometry. In this context, the discovery of superconductivity in AV_3Sb_5 (A = K, Rb, Cs) with a perfect kagome lattice in 2020 has received significant attention [1]. In these materials, charge density wave (CDW)

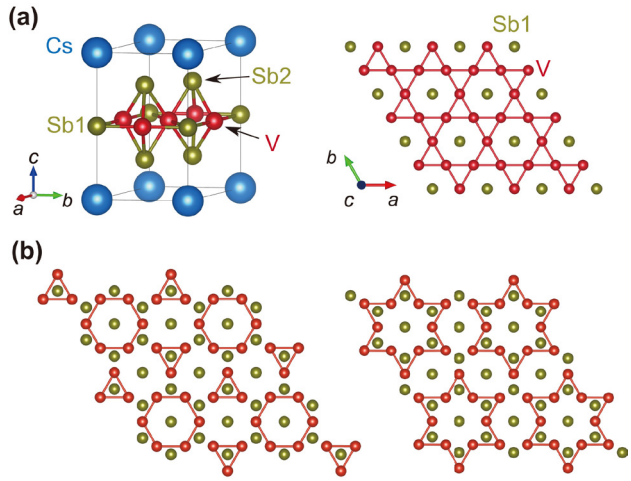

Fig. 1. (a) Crystal structure of CsV_3Sb_5. V-Sb1 plane viewed from the c-axis direction (right). Whereas the V atoms form a two-dimensional kagome network, the Sb1 atoms are located at the hexagonal centers.(b) CDW pattern in CsV_3Sb_5. V and Sb1 atoms form the so-called star of David (right) and inverse star of David (left) patterns. These patterns alternate in the interplane direction.

orders with a so-called (inverse) star-of-David pattern of electronic hopping have been observed above the superconducting transition temperature (Fig. 1(b)) [2]. Very interestingly, it has been reported that these CDW states break time-reversal and rotational symmetries. In addition, high-pressure studies have revealed that the CDW phase is suppressed by applying pressure, accompanied by the emergence of a superconducting dome, indicating the close relationship between the CDW and superconductivity [3,4]. Therefore, one of the most crucial unresolved issues is identifying the symmetry of the superconductivity that develops inside the CDW phase. However, the mechanism of superconductivity in AV_3Sb_5 and its relationship with the CDW state have remained elusive [2].

Here, we focus on the effect of impurities on the superconducting state to elucidate the mechanism of superconductivity in AV_3Sb_5. Based on the Bardeen-Cooper-Schrieffer (BCS) theory, which is the standard theory of superconductivity, the conventional superconducting state arises from the pairing of two electrons induced by electron-phonon interactions. In this case, the introduction of nonmagnetic impurities generally has little effect on the superconducting transition temperature (T_c) and the superconducting gap structure [5]. However, it is well known that unconventional superconducting states, as observed in high-T_c cuprates and heavy-fermion superconductors, are significantly suppressed by nonmagnetic impurities.

In this study, we systematically investigated the impurity effects of CsV_3Sb_5 on the superconducting transition temperature and the superconducting gap structure [6]. The introduction of non-magnetic impurities into crystals was achieved by using electron irradiation, enabling precise control of the impurity concentration in the CsV_3Sb_5 single-crystal samples. We examined the change in the superconducting transition temperature by measuring the resistivity of the impurity-controlled samples at ambient and high pressure. We also performed magnetic penetration depth measurements, which reflect the superconducting gap structure. As a result, we found that the superconducting transition temperature of CsV_3Sb_5 is rapidly suppressed at a low impurity concentration but starts to saturate at moderate impurity concentrations (Fig. 2(a)). This behavior differs from those of both conventional BCS superconductors and unconventional superconductors such as high-T_c cuprates. In addition, our magnetic penetration depth measurements

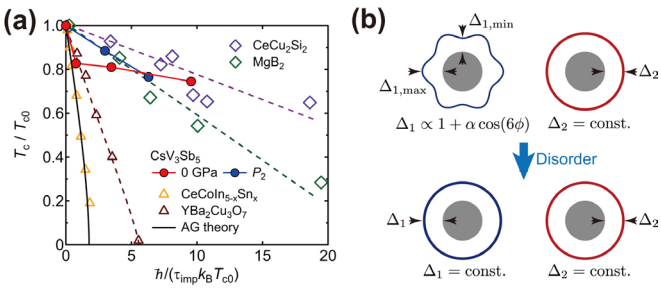

Fig. 2. (a) Suppression of the superconducting transition temperature T_c in CsV_3Sb_5 as a function of pair breaking parameter (corresponding to the amount of impurities). Red circles represent the transition temperature under ambient pressure (0 GPa), and blue circles represent the transition temperature at P_2. (b) Changes in the superconducting gap structure in CsV_3Sb_5 by impurities. The gap structure is anisotropic before the introduction of impurities, but as the impurity concentration is increased, the gap size averages out and eventually the two gaps become isotropic and almost the same size. This behavior is consistent with the theoretical expectation in the bond-order fluctuation superconducting mechanism [6].

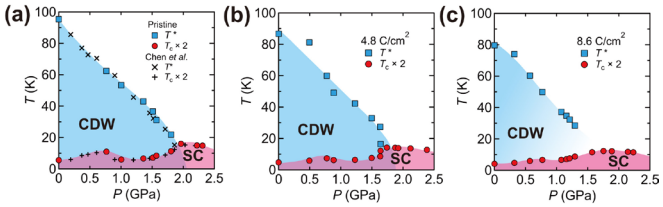

Fig 3. *P-T* phase diagrams of the (a) pristine, (b) 4.8, and (c) 8.6 C/cm^2 irradiated samples. For clarity, T_c is doubled. The phase diagram of the pristine sample includes data from Chen *et al* [3]. The CDW (superconducting (SC)) phase is shaded in blue (red).

reveal that with increasing impurities, an anisotropic fully-gapped state changes to an isotropic full-gap state without showing impurity-induced Andreev bound states, which excludes any of sign-changing symmetries (Fig. 2(b)). Furthermore, transport measurements under pressure show that the double superconducting dome in the pressure-temperature phase diagram survives against sufficient impurities (Fig. 3). These results support that CsV_3Sb_5 is a non-chiral, anisotropic *s*-wave superconductor with no sign change both at ambient and under pressure. The present findings support a new type of unconventional superconductivity originated from bond-order fluctuations in the CDW state of CsV_3Sb_5, where the gap function is non-sign-changing *s*-wave [7].

Our present study will pave the way to understanding the unique electronic and superconducting states in kagome lattice materials.

References

[1] B. R. Ortiz *et al.*, Phys. Rev. Lett. **125**, 247002 (2020).
[2] T. Neupert *et al.*, Nat. Phys. **18**, 137 (2022).
[3] K. Y. Chen *et al.*, Phys. Rev. Lett. **126**, 247001 (2021).
[4] R. Gupta *et al.*, Commun. Phys. **5**, 232 (2022).
[5] P. W. Anderson, J. Phys. Chem. Solids **11**, 26 (1959).
[6] M. Roppongi *et al.*, Nature Communications **14**, 667 (2023).
[7] R. Tazai *et al.*, Sci. Adv. **8**, eabl4108 (2022).

Authors

M. Roppongi[a], K. Ishihara[a], K. Hashimoto[a], and T Shibauchi[a], and Y. Uwatoko
[a]The university of Tokyo

PI of Joint-use project: K. Hashimoto
Host lab: Uwatoko Group

Heavy-Fermion Antiferromagnet $Yb_4Ru_7As_6$ with the $U_4Re_7Si_6$ Type Cubic Structure

Yb–T–X (T: transition metal, X: pnictogen) ternary compounds have been studied intensively in terms of novel phenomena in the vicinity of the magnetic quantum critical point (QCP). For example, $YbNi_4P_2$ is reported to be close to the ferromagnetic QCP, exhibiting the ferromagnetic transition (FM) at 0.17 K [1]. The field-induced non-Fermi liquid behavior of $Yb_2Fe_{12}P_7$ has also attracted attention [2].

To our knowledge, no ternary compound of Yb–Ru–As has been reported. In this study, we have investigated ternary Yb–Ru–As compounds and found a compound $Yb_4Ru_7As_6$, which crystallizes in the $U_4Re_7Si_6$-type cubic structure, showing a weak ferromagnetic (FM) behavior below T_0~ 4.0 K and antiferromagnetic (AFM) ordering at T_N = 2.5 K with the moderately enhanced electronic specific heat coefficient of 120 Yb-mJ/K^{2}mol [3].

Single crystals of $Yb_4Ru_7As_6$ were grown by the Bi-flux method, and obtained crystals are shown in the inset of Fig. 1. The crystal structure of $Yb_4Ru_7As_6$ is determined to be the cubic $U_4Re_7Si_6$-type structure (No.229, $Im\bar{3}m$) using a XtaLAB HyPix-600HE diffractometer. Note that the local symmetry of Yb atom is similar to rare earth metals in skutterudite. Fig. 1 shows the temperature dependence of the electrical resistivity ρ of $Yb_4Ru_7As_6$ for the current J along the [100] direction. With decreasing temperature, ρ monotonically decreases with a shoulder-like structure below 10 K. At low temperatures, two inflection points at T_0~4 K and T_N~2.5 K in ρ are observed, as shown in the inset of Fig. 1. The residual resistivity ratio is about 40, indicating a high-quality sample.

Magnetic properties are isotropic reflecting the cubic structure. With decreasing temperature, magnetic susceptibility M/H increases and follows the Curie–Weiss law at temperatures higher than 150 K. The estimated effective magnetic moments are 4.28–4.45 μ_B/Yb, which is close to the expected value of Yb^{3+} ionic state: 4.54 μ_B/Yb. Fig. 2 shows the temperature dependences of M/H for $H \parallel [100]$ below 10 K measured at several magnetic fields. M/H at 5 mT shows a ferromagnetic increment in the temperature range between 6 and 4 K, and a small peak at 2.5 K. Note that no detectable hysteresis loop is observed in magnetization at 1.8 K, as shown in the inset of Fig. 2. With increasing temperature, the peak temperature decreases to 2.25 K at 1.0 T and disappears above 2.0 T, meaning that the peak in M/H corresponds to the AFM transition.

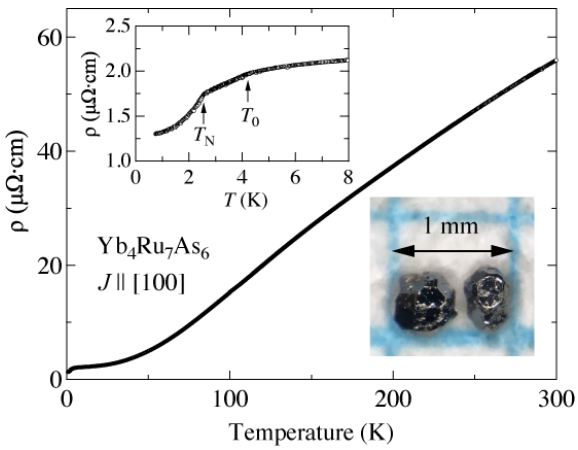

Fig. 1. Temperature dependence of ρ of $Yb_4Ru_7As_6$. The magnification of the low temperature part and photograph of single crystals are shown in inset.

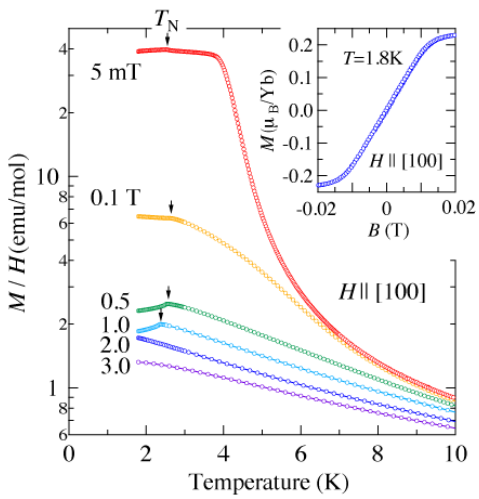

Fig. 2. M/H for $H \parallel [100]$ below 10 K at several magnetic fields. Inset shows the magnetization curve for $H \parallel [100]$ at 1.8 K in low magnetic fields.

The specific heat C shows an upturn below 7.5 K and λ type sharp peak at 2.5 K, corresponding to the short-range magnetic correlation and/or the Kondo effect, and the long-range magnetic ordering, respectively. In addition, a tiny anomalous behavior is observed at T_0~4 K, which corresponds to the temperature where the anomaly in ρ and the occurrence of the FM behavior emerge as mentioned above. It means that T_0 can be attributed to a temperature characterizing the FM behavior. T_N is shifted to lower temperatures under magnetic fields and seems to disappear at 2.5 T. On the other hand, the tiny anomaly at T_0 becomes obscure in the magnetic fields.

The characteristic temperature where the FM behavior in M/H is observed corresponds to the beginning of the short-range ordering as observed in the temperature dependence of C, implying that one of the possibilities of the FM in $Yb_4Ru_7As_6$ is considered a concomitant phenomenon of the AFM ordering with a canted magnetic moment arrangement from the <100> direction. The canted AFM can be realized in the condition of magnetic interaction and magnetocrystalline anisotropy favoring the non-antiparallel arrangement of magnetic moments. Since there is no inversion symmetry at the center between the nearest neighbor magnetic Yb sites, the Dzyaloshinskii–Moriya interaction can be one of the possible origins of FM behavior, for example. To elucidate the origin of T_0, resistivity measurements in magnetic fields are in progress, and further experiments with microscopic probes are needed.

References

[1] C. Krellner, S. Lausberg, A. Steppke, M. Brando, L. Pedrero, H. Pfau, S. Tencé, H. Rosner, F. Steglich, and C. Geibel, New J. Phys. **13**, (2011) 103014.
[2] R.E. Baumbach, J.J. Hamlin, L. Shu, D.A. Zocco, J.R. O'Brien, P.-C. Ho, and M.B. Maple, Phys. Rev. Lett. **105**, 106403 (2010).
[3] Y. Hirose, K. Arakawa, Y. Kato, Y. Uwatoko, H. Ma, J. Gouchi, F. Honda, and R. Settai, J. Magn. Magn. Mater. **556**, 169327 (2022).

Authors
Y. Hirose[a], K. Arakawa[a], Y. Kato[a], Y. Uwatoko, H. Ma, J. Gouchi, and F. Honda[b], R. Settai[a]
[a]Niigata University
[b]Kyushu University

PI of Joint-use project: Y. Hirose
Host lab: Uwatoko Group

Structural Instability and Electronic Properties of CeCoSi under Pressure

We have clarified structural and electronic properties under pressure at low temperatures on CeCoSi, which has been attracted attention for its novel long-range order. CeCoSi crystallizes into the tetragonal crystal structure (No. 129, P4/nmm), which lacks local inversion symmetry at Ce site. CeCoSi exhibits a long-range ordering below T_0 ~ 12 K at ambient pressure, which is proposed to be odd-parity multipole orderings. The T_0 strongly enhances with increasing pressure and reaches 37 K at 1.7 GPa, followed by a rapid suppression. The phase below T_0 is phase II and the phase II disappears above 2.2 GPa. CeCoSi also undergoes structural transition at P_s ~ 4.9 GPa at 300 K and becomes phase IV [1]. The rapid change of T_0, followed by the emergence of phase IV indicates that Ce-4f electronic state significantly altered under pressure. In order to reveal

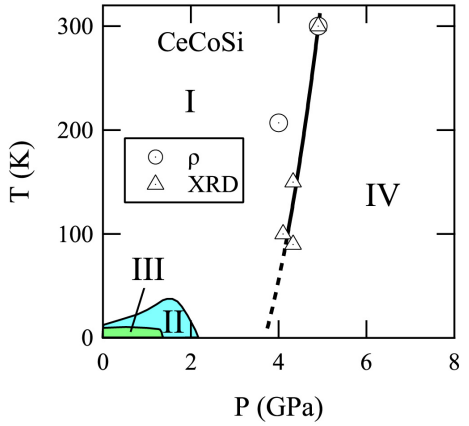

Fig. 1. Temperature Pressure phase diagram of CeCoSi. The bordering temperature and pressure are defined from resistivity (circle) and from XRD (triangle) measurements. The borders among phase I, II, III are in literature.

the electronic and structural properties of CeCoSi in the above whole temperature and pressure range and to clarify the relationship between phase II and IV, electrical resistivity of CeCoSi in the pressure range of 0 ~ 8 GPa and in the temperature range of 2.5 ~ 300 K and X-ray diffraction in 0 ~ 6 GPa and in 6 ~ 300 K have been performed.

CeCoSi single crystals were grown with a Ce/Co eutectic flux method. The electrical resistivity on CeCoSi has been performed by cubic anvil pressure system with a standard four terminal method. X-ray diffraction (XRD) on powdered CeCoSi has been performed with GM refrigerator incorporated with diamond anvil pressure cell [2].

Figure 1 shows the phase diagram depicted based on the results of electrical resistivity and XRD under pressure. The anomaly of electrical resistivity is observed as drop of resistivity by the temperature or pressure, whereas additional peaks and peak splittings are observed in the XRD pattern. This study reveals that the boundary of phase IV and phase I is not directly connected to phase II or phase III.

The temperature dependence of resistivity exhibits a peak due to the Kondo scattering of the conduction electrons. The temperature of this peak rapidly increases with increasing pressure, which corresponds the rapid enhancement of Kondo temperature under pressure. Although CeCoSi is reported as localized electronic state at ambient pressure, the results of resistivity suggest that CeCoSi becomes itinerant electronic state around 2 GPa. XRD indicates that the ratio of lattice parameters *c/a* of CeCoSi linearly decreases with pressure up to ~ 4 GPa, which is just below P_s. In contrast, *c/a* of LaCoSi and PrCoSi decreases linearly below 2 GPa but they level off above 2 GPa. These results suggest that the valence of Ce on CeCoSi gradually increases from 3+ above 2 GPa. Also, the resistivity shows a drop to exhibit a metallic temperature dependence when crossing the phase IV.

These results strongly suggest that CeCoSi is localized character at ambient pressure and it gradually becomes itinerant character around 2 GPa and the valence of Ce gradually changes above 2 GPa. In addition, the Ce-4f electronic states changes drastically when crossing the boundary of phase I and IV, implying the valence change by the structural transition. Although phase II and IV is not directly influenced to each other, our results strongly suggest that both the rapid change of T_0 and emergence of phase IV can be ascribed to the valence instability of Ce-4f electron.

References
[1] Y. Kawamura *et al*., J. Phys. Soc. Jpn. **89**, 054702 (2020).
[2] Y. Kawamura *et al*., J. Phys. Soc. Jpn. **91**, 064714 (2022).

Authors
Y. Kawamura[a], K. Ikeda[a], J. Hayashi[a], K. Takeda[a], C. Sekine[a], T. Matsumura[b], J. Gouchi, Y. Uwatoko, T. Tomita, H. Takahashi[c], and H. Tanida[d]
[a]Muroran Institute of Technology
[b]Hiroshima University
[c]Nihon University
[d]Toyama Prefectural University

PI of Joint-use project: Y. Kawamura
Host lab: Uwatoko Group

Sub-Micron Particle Size Effects on Metastable Phases for a Photoswitchable Co-Fe Prussian Blue Analogue

The $K_{0.3}Co[Fe(CN)_6]_{0.77}\cdot nH_2O$ compound undergoes a charge transfer coupled spin transition (CTCST), where spin configurations change between a paramagnetic Co^{II} (S = 3/2)-Fe^{III} (S = 1/2) high temperature (HT) state and a diamagnetic Co^{III} (S = 0) -Fe^{II} (S = 0) low temperature (LT) state. The compound having average particle size of 500 nm exhibits a unique intermediate **(IM)** phase that depend on the cooling rate. The IM phase corresponds to a mixture of IM-A (HT+LT fraction mixture) and IM-B (LT state), which have ~50 nm and ~200 nm coherent domain sizes, receptivity [1]. (Fig. 1) Moreover, several hidden metastable HT states

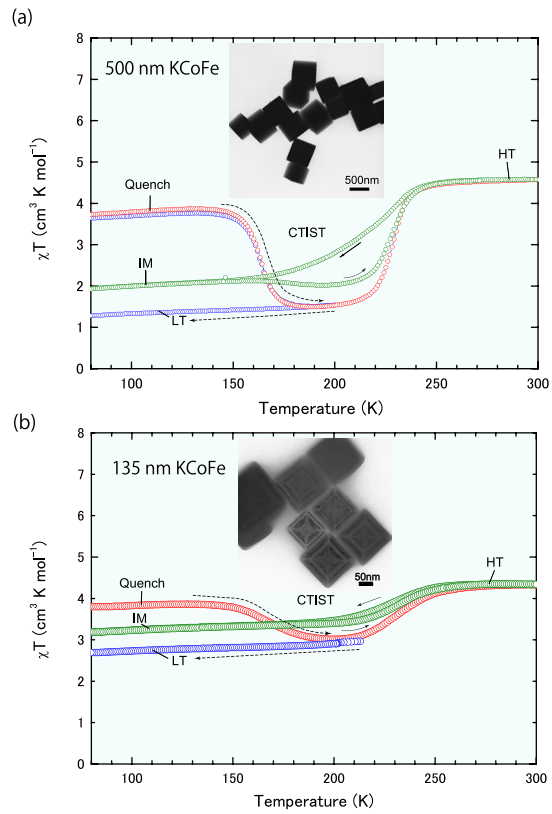

Fig. 1. Magnetic susceptibility curves of $K_{0.3}Co[Fe(CN)_6]_{0.77}\cdot nH_2O$ for (a) 500 nm and (b) 135 nm particles. The thermally accessed Quench (Q) phase and Low-temperature (LT) phase are depicted as red and blue curves, respectively. The thermal procedure to reach the LT phase is indicated by dotted arrow. The IM phase is obtained by slow cooling (at 1 K/min). Differences in the thermal response as a function of particle size are observed in the hysteresis, becoming narrower with decreasing particle size. Insets: TEM images of the particles showing their clear cubic shapes.

emerge as a function of thermal and photo stimuli in the compound, namely: (1) a quench (**Q**) state generated from the HT state by flash cooling, (2) a **LTPX** state obtained by photoexcitation from the LT state derived by thermal relaxation from the Q state, and (3) an **IMPX** state accessed by photo-irradiation from the IM state [1, 2]. (Fig. 2(a))

A sample with smaller particle size 135 nm, which were designed on the scale of the coherent LT domains in the IM phase of the 500 nm sample [3], was investigated for by means of thermal and photo controlled PXRD and complementary magnetic susceptibility measurements, and an unusual IM phase and metastable HT phases in 135 nm particles of $K_{0.3}Co[Fe(CN)_6]_{0.77}\cdot nH_2O$ were compared to those of a similar sample with 500 nm particle size in the paper (Fig. 2). The incomplete character of the thermally-induced CTCST between Co^{II} (S = 3/2)-Fe^{III} (S = 1/2) and Co^{III} (S = 0)-Fe^{II} (S = 0) pairs becomes even less complete when the particle size is reduced from 500 nm to 135 nm. The HT spin Co^{II}-Fe^{III} states become predominant and the PXRD profiles suggest a multiphasic behavior, with a peak broadening larger than the one observed for the 500 nm sample. This behavior is attributed to HT domains or clusters made of a limited number of Co^{II}-Fe^{III} pairs that become constrained within the Co^{III}-Fe^{II} lattice at low temperature, which compose a multitude of Co^{II}-Fe^{III} clusters having different sizes and experiencing different elastic strains from the dominant Co^{III}-Fe^{II} phase. The multiple state in IM phase can be then viewed as a response of an inhomogeneous diluted system. In addition, the disordered character generated by CTCST in the 135 nm sample reflects to LT state obtained by thermal relaxation from a single Q phase and photo-excited states from IM and LT states, these metastable phases are always multiple states. (Fig. 2(b))

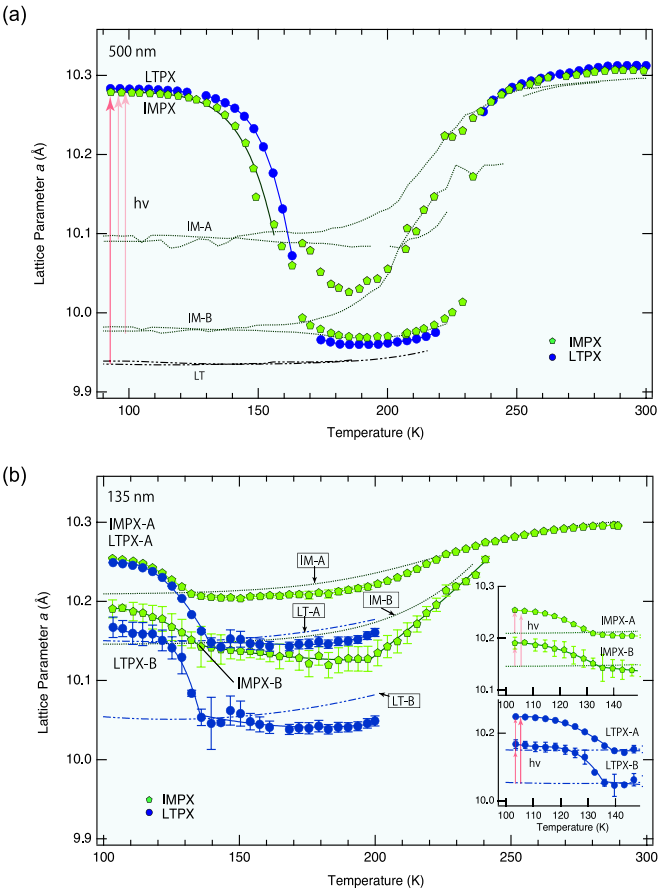

Fig. 2. Thermal decay of the lattice parameter *a* for photo-excited states IMPX (filled pentagons) and LTPX (filled circles) produced from IM and LT states, at 90 K for the 500 nm sample and at 100 K for the 135 nm sample. (a) Data related to the 500 nm sample extracted by the Le Bail method. The original IM state and LT state, which are the starting phases before 690 nm light irradiations, are indicated by the dotted and dot-dash lines, respectively. (b) Similar plots for the 135 nm sample extracted from (400) PXRD peaks. Inset: Expanded figures between 100 K and 150 K for temperature dependent photo-excited lattice parameters, IMPX-A & B (filled pentagons) and LTPX-A & B (filled circles) from the respective original states, IM-A &B (dotted lines) and LT-A & B (dot-dash lines).

Determination of the linear thermal expansion coefficients (LTEC) and pressure- dependent CTCST temperatures for the two (500 nm and 135 nm) particle sizes gave insights on the intrinsic stretchability and external compressibility, which were indicated that the bulk sample has higher flexibility at the CTCST, while the lattice change at the CTCST becomes less sensitive to external circumstances upon size reduction. We attributed these behaviors to the decrease of the cooperative electron-phonon coupling in small particles due to the enhancement of lattice defects which alters the elasticity of the small particles. The weak character of the elastic energy barriers produced during photoexcitation, combined with the disorder of elastic forces in the lattice, prevents the complete photoexcitation and the collective lattice change in the 135 nm sample. As a result, in the $K_{0.3}Co[Fe(CN)_6]_{0.77}\cdot nH_2O$ compound, photo-excitation under common values of power density does not change from the multiphasic IM state and/or LT state to a single metastable HT phase, through sub-micron scale particle size reduction [4].

References

[1] C. Chong, M. Itoi, K. Boukheddaden, E. Codjovi, A. Rotaru, F. Varret, F. A. Frye, D. R. Talham, I. Maurin, D. Chernyshov, and M. Castro, Phys. Rev. B. **84**, 144102 (2011).
[2] M. Itoi, I. Maurin, F. Varret, F. A. Fry, D. R. Talham, D. Chernyshov, and K. Boukheddaden, Phys. Rev. B. **88**, 094104 (2013).
[3] M. J. Andrus, Y. M. Calm, E. S. Knowles, M. F. Dumont, K. A. Abboud, M. W. Meisel, and D. R. Talham, Polyhedron **64,** 289 (2013).
[4] M. Itoi, I. Maurin, K. Boukheddaden, M. J. Andrus, D. R. Talham, E. Elkaim, and Y. Uwatoko, J. Appl. Phys. **131**, 085110 (2022)

Authors
M. Itoi[a], I. Maurin[b,c], K. Boukheddaden[d], M. J. Andrus[e], D. R. Talham[e], E. Elkaim[f], and Y. Uwatoko
[a]Nihon University School of Medicine
[b]Ecole Polytechnique
[c]Institut NEEL
[d]Université de Versailles-Saint-Quentin
[e]University of Florida
[f]Synchrotron SOLEIL

PI of Joint-use project: M. Itoi
Host lab: Uwatoko Group

Conformation of Ultra-Long Chain Fatty Acid in Lipid Bilayer

Phospholipids are the most abundant lipids in biological membranes and have a polar head group and two hydrocarbon tails (fatty acids). Phospholipids, more than 1000 molecular species, are biosynthesized by a combination of a head group and two hydrocarbon tails. Each tail typically contains between 14 and 22 carbon atoms. Fatty acids containing more than 22 carbons are called very-long-chain fatty acids, such as docosahexaenoic acid (DHA, C22:6). Moreover, much longer chains containing more than 32 carbons were found at the sn-1 position of phosphatidylcholine in photoreceptors, fibroblasts, and keratinocytes. These fatty acids are called ultra-long-chain fatty acids (ULCFAs). It is considered that ULCFAs are stored as a precursor of

bioactive lipid mediators and derivatives of C32:6 and C34:6 are neuroprotective in retina. However, the physicochemical properties of ULCFAs and the biological roles of ULCFAs-containing phospholipids are still unclear. In order to clarify the physicochemical properties of ULCFAs, we have simulated a single ULCFA in a lipid bilayer by all-atom molecular dynamics using the ISSP supercomputer [1,2].

We found that ULCFAs have large conformational fluctuations. Figure 1 shows the conformations of dotriacontahexaenoic acid containing phosphatidylcholine (dTSPC, C32:6-C18:0) in membrane of distearoyl phosphatidylcholine (DSPC, C18:0-C18:0) [1]. The ultra-long chain has a turned conformation in the upper leaflet, a L-shaped conformation between the two leaflets, and an elongated conformation deeply inserting in the lower (opposite) leaflet. The L-shaped conformation is taken most frequently. There are no free-energy barriers among these conformations and the transit time between turned and elongated conformations is ~ 10 ns. Moreover, we revealed that ULCFAs can sense the density differences between the two leaflets and respond to these changes. As the number ratio of lipids in the opposite leaflet increases, the ratio of the elongated shape linearly decreases. This change in ULCFA conformations reduces the lipid-density difference between the two leaflets. We have examined three types of phospholipids (DSPC, SDPC, C18:0-C22:6, and SOPC, C18:0-C18:1) for host membranes and three types of ULCFAs (dTSPC, HSPC, C26:4-C18:0, and LSPC, C32:0-C18:0) [1,2]. HSPC is constructed by truncating the long hydrocarbon chain of dTSPC at C26, and LSPC is constructed by the saturation of the long hydrocarbon chain of dTSPC. In all cases, ULCFAs have this sensing capability. Therefore, we concluded that it is a unique property of ULCFAs. This response may be essential for the functions of ULCFAs in living cells.

Moreover, we added cholesterols to membranes [2]. The flip—flop of cholesterols is ~1 μs and is much faster than those of phospholipids (hours or days). The flip—flop of cholesterols can also reduce the lipid-density difference. After the equilibration of cholesterols, the probability distribution of ULCFA conformations is back to that for no-lipid-density-difference membranes. Thus, we consider that ULCFAs initially respond to the density difference and, later, cholesterol removes the difference in living cells.

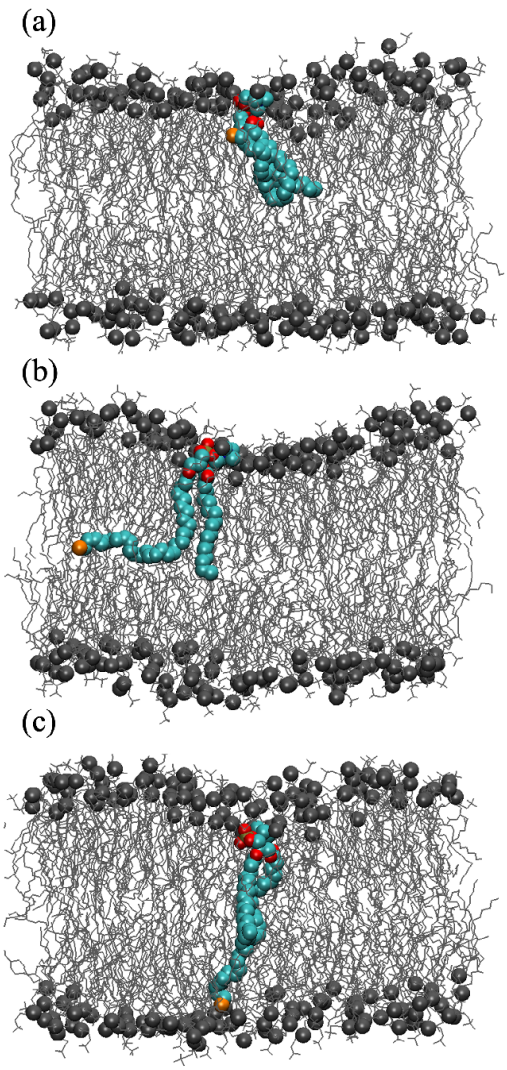

Fig. 1. Snapshots of a Ultra-Long Chain Fatty Acid, dTSPC, in bilayer membrane. (a) Turned conformation. (b) L-shaped conformation. (c) Elongated conformation. dTSPC are represented by colored spheres. Host lipid (DSPC) molecules are shown in gray (spheres represent the phosphate atoms). Water molecules are not shown for clarity.

References
[1] K. Kawaguchi, K. M. Nakagawa, S. Nakagawa, H. Shindou, H. Nagao, and H. Noguchi, J. Chem. Phys. **153**, 165101 (2020).
[2] K. Kawaguchi, H. Nagao, H. Shindou, and H. Noguchi, J. Phys. Chem. B **126**, 9316 (2022).

Authors
K. Kawaguchi[a] and H. Noguchi
[a]Kanazawa University

PI of Joint-use project: K. Kawaguchi
Host lab: Noguchi Group

Unified View of High-T_c Superconductivity and Quantum Spin Liquids Revealed by *Ab initio* Supercomputer Simulations

Since the discovery of superconductivity in 1986 in copper oxides with quasi-two-dimensional perovskite structure, more than 35 years have already passed. However, its mechanism has not converged to consensus in the community because of the difficulty in treating strongly correlated electron systems, to which the cuprates belong.

Recently, numerical methods to study the strongly correlated electron systems have largely been developed [1], in which effective Hamiltonians derived by an *ab initio* framework starting from given crystal structure without resorting to adjustable parameters are solved by accurate quantum many-body solvers. The solutions of effective Hamiltonians for a number of copper oxide compounds correctly reproduce *d*-wave superconducting ground states [2,3]. From the relation between the *ab initio* parameters and the obtained superconducting order parameters, the principal component that controls the strength of the superconductivity was found. The results further show that the diverse materials dependence is well captured as shown in Fig. 1 for the superconducting critical temperature T_c. It was also clarified how the superconductivity can be enhanced in the present mechanism beyond the existing materials.

The *ab initio* solution also offers insights into electron fractionalization. It was found that an electron that is an elementary particle in vacuum is emergently splintered in strongly correlated electron systems. Thus generated particles are mutually tunneling quantum mechanically, in other words, hybridizing each other. The fractionalization

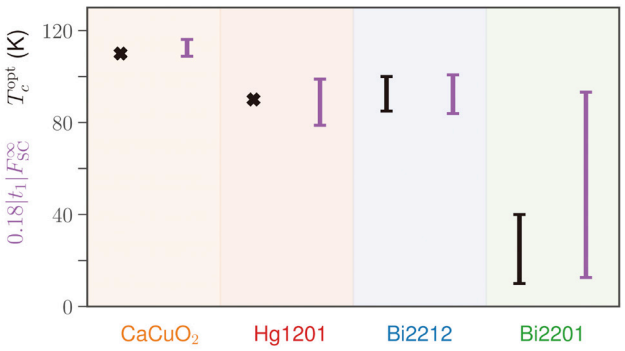

Fig. 1. Comparison of experimentally optimal critical temperature, T_c^{opt} (black symbols) and the scaling formula 0.16 $t_1 F_{SC}^{\infty}$ (purple symbols) obtained from the *ab initio* parameter t_1 (nearest neighbor electron transfer) and the calculated order parameter F_{SC}^{∞} [3]. Calculated results reproduce experimental trend of T_c quantitatively for carrier doped $CaCuO_2$, $HgBa_2CuO_4$ (Hg1201), $Bi_2Sr_2CaCu_2O_8$ (Bi2212), and $Bi_2Sr_2CuO_6$ (Bi2201) .

well accounts for spectroscopic data otherwise puzzling, by combining experimental and computational results with the help of machine learning in the analyses of angle resolved photoemission and the resonant inelastic X-ray scattering results [4-7].

Another challenge of condensed matter physics is the nature of quantum fluids, especially, the quantum spin liquid since the first proposal half a century ago [8]. It was shown with the aid of supercomputers that the quantum spin liquid phase indeed exists and the spin excitations are well described by the fractionalized spinons in gapless quantum spin liquids, where the spinon has the Dirac-type gapless excitation and an observable spin excitation is represented by the two composite excitations of the spinon [9,10]. *Ab initio* calculations of molecular solid called dmit salts indeed demonstrated that this picture holds and the experimental phase diagram of the dmit salts is reproduced [10] as shown in Fig. 2 and the quantum spin liquid established in a theoretical touchstone model, J_1-J_2 Heisenberg Hamiltonian on the square lattice also shows essentially the same structure of the fractionalized excitation [9]. These findings were made it possible by the progress in quantum many-body solver using the neural network [11].

The electron fractionalization found in the cuprate superconductors and the fractionalization of an electronic spin into two spinons look quite different at a glance. However, the

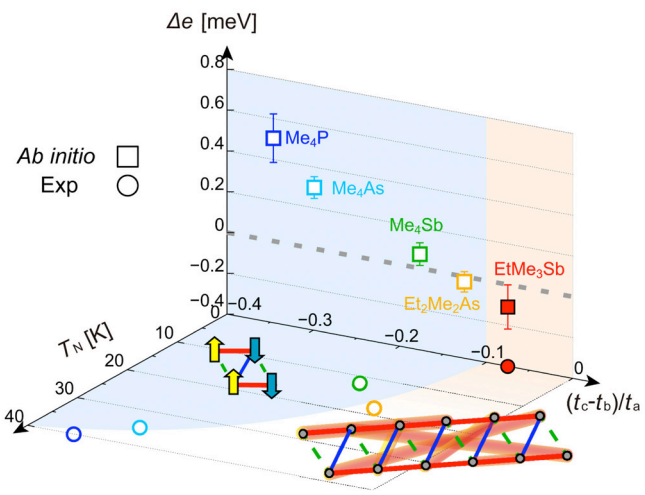

Fig. 2. Ground-state phase diagram revealed by *ab initio* simulations (vertical plane), which shows agreement with the experimental phase diagram (bottom plane) for molecular solid, dmit salts with five different cations [10].

essence of the superconducting state as well as the quantum spin liquid lies in the way of constructing quantum mechanically entangled state, the element of which is commonly the paired state of two electrons with further entanglement of the pairs. Indeed, the wavefunctions have a common structure of the pair-product functions at the core. The quantum entanglement by the spin singlet constituting the quantum spin liquid and by the exciton leading to the electron fractionalization are represented in the extended Hilbert space in a unified fashion and the singlet and exciton take on different aspect of the same entanglement [4].

Acknowledgements

This report is based on the collaborations with Michael Schmid, Jean-Baptiste Morèe, Youhei Yamaji, Motoaki Hirayama, Yusuke Nomura, Di-Jing Huang, Atsushi Fujimori, Teppei Yoshida, Kota Ido, Takahiro Misawa, and Kazuyoshi Yoshimi.

References

[1] M. Imada and T. Miyake, J. Phys. Soc. Jpn. **79,** 112001 (2010).
[2] J.-B. Morèe, M. Hirayama, M. T. Schmid, Y. Yamaji, and M. Imada, Phys. Rev. B **106**, 235150 (2022).
[3] M. T. Schmid, J.-B. Morèe, Y. Yamaji, and M. Imada, arXiv:2303.06672.
[4] M. Imada, J. Phys. Soc. Jpn. **90**, 111009 (2021).
[5] M. Imada, J. Phys. Soc. Jpn. **90**, 074702 (2021).
[6] A. Singh, H. Y. Huang, J. D. Xie, J. Okamoto, C. T. Chen, T. Watanabe, A. Fujimori, M. Imada, D. J. Huang, Nat. Commun. **13**, 7906 (2022).
[7] Y. Yamaji, T. Yoshida, A. Fujimori, M. Imada, Phys. Rev. Research **3**, 043099 (2021).
[8] P. Fazekas and P. W. Anderson, Phil. Mag. **30**, 423 (1974).
[9] Y. Nomura and M. Imada, Phys. Rev. X **11**, 031034 (2021).
[10] K. Ido, K. Yoshimi, T. Misawa, and M. Imada, npj Quantum Mater. **7**, 48 (2022).
[11] Y. Nomura, A. S. Darmawan, Y. Yamaji and M. Imada, Phys. Rev. B **96**, 205152 (2017).

Authors
M. Imada[a,b,c]
[a] Waseda University
[b]Sophia University
[c]Toyota Physical and Chemical Research Institute

PI of Joint-use project: M. Imada
Host lab: Supercomputer Center

Acceleration of First-Principles Statistical Thermodynamics Framework abICS Using an On-Lattice Neural Network Model and Active Learning

In 2019, ab Initio Configuration Sampling toolkit, or abICS for short, was developed as an ISSP Software Advancement Project for directly combining first-principles relaxation and total energy calculations with replica exchange Monte Carlo (RXMC) sampling [1]. The motivation was that effective models such as cluster expansion, which are used to speed up the usual Metropolis Monte Carlo sampling for analyzing order/disorder in alloy systems, are limited in describing complex many-component systems with sufficient accuracy. Our aim at that time was to enable direct sampling on first-principles energies by employing highly parallel sampling methods such as RXMC in combination with massively parallel supercomputing resources. A few years later, some of the authors found that an on-lattice neural network model overcomes many issues found in previous effective models if sufficient training data is provided in an active learning setting [2,3]. This led to the

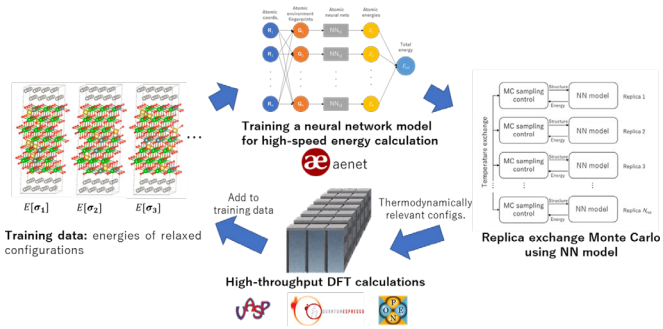

Fig. 1. Overview of the active learning procedure using abICS

proposal of last year's Software Advancement Project, which we outline in this report.

The abICS framework developed in this project uses Python as a glue language to piece together the necessary components (Fig. 1). It is registered on PyPI (Python Package Index; pypi.org) and can be installed easily in most environments through the command "`pip install --user abics`". A typical use case is outlined as follows:

1. Random configurations on a lattice are relaxed and their total energies are calculated using the first-principles code of choice. We support VASP, Quantum Espresso, and OpenMX.
2. A neural network model is trained on data from step 1 to predict relaxed energies from configurations on the non-relaxed lattice. We currently use aenet code [4] for the neural network training.
3. RXMC or population annealing MC (PAMC) calculation is performed using the neural network model from step 2. Two sampling modes are available: canonical sampling with a fixed number of atoms or grand canonical sampling which allows for changes in the composition. For the neural network evaluation, we provide a file IO-based interface to aenet, and we also provide an interface to aenet-lammps [5] python interface which does not rely on file IO and is thus usually faster.
4. A subset of samples from step 3 are relaxed and their total energies are calculated using first-principles calculation. If the results deviate considerably from the neural network prediction, the data is added to the training data set and the procedure is repeated from step 2.

The overall procedure is controlled by an input file in TOML format, which is an easy-to-read software configuration format that is being used in many projects [6]. The parameters for the first-principles calculations and neural network training/evaluation are controlled by separate files following formats of the specified solver.

We believe that abICS will be a game-changer in modeling order/disorder in many-component crystalline systems as we have already demonstrated for partially hydrated Sc-doped $BaZrO_3$ [3]. Please do not refrain from contacting us if you find any difficulties in using or extending this software.

References
[1] S. Kasamatsu and O. Sugino, J. Phys.: Condens. Matter **31**, 085901 (2019).
[2] S. Kasamatsu *et al*., J. Chem. Phys. **157**, 104114 (2022).
[3] K. Hoshino, S. Kasamatsu *et al*., Chem. Mater. **35**, 2289 (2023).
[4] N. Artrith *et al*., Phys. Rev. B **96**, 014112 (2017).
[5] M. S. Chen *et al*., J. Chem. Phys. **155**, 074801 (2021).
[6] https://github.com/toml-lang/toml

Authors
S. Kasamatsu[a], T. Aoyama, Y. Motoyama, K. Yoshimi, and O. Sugino
[a]Yamagata University

PI of Joint-use project: S. Kasamatsu
Host lab: Supercomputer Center

Topological Hall Effect Induced by Non-Coplanar Magnetic Structure in van der Waals Magnets

Antiferromagnets with broken time-reversal symmetry (TRS) have been attracting remarkable attention since the discovery of the large Hall effect in the kagome antiferromagnet Mn_3Sn [1], which exhibits a coplanar 120-degree spin order on the kagome lattice. From the viewpoint of symmetry, this magnetic structure is compatible with the in-plane ferromagnetic order, and thus accounts for the large Hall effect despite the extremely small net magnetization. These properties would be applicable for novel information storage/processing devices with small stray fields and faster spin dynamics. Thus far, the number of this class of materials has been limited, and further exploration of TRS-broken antiferromagnets is highly demanded.

In the present study, we focus on the van der Waals materials composed of triangular lattice layers of magnetic ions, $CoTa_3S_6$ (CTS) and $CoNb_3S_6$ (CNS), which have been recently reported to show large Hall effect in the antiferromagnetic ordered phases [2,3]. However, the magnetic structures of these compounds were not investigated in detail. We thus performed polarized neutron scattering experiments on these compounds at the POlarized Neutron Triple-Axis spectrometer (PONTA) installed in the 5G beamline of the Japan Research Rector 3 (JRR-3), in order to elucidate the magnetic structure relevant to the large Hall effect [4].

Single crystals of CTS and CNS were synthesized by the chemical vapor transport method. As for CTS, we observed the large spontaneous Hall effect in zero magnetic field, as shown in Fig. 1(a), as if the conduction electrons were subject to a magnetic field along the c axis of the crystal. We mounted a single crystal of CTS on a standard ^{4}He closed-cycle refrigerator with the (H,K,0) scattering plane, and measured magnetic reflections with polarized neutrons. Figures 2(a) and 2(b) show the scattering profiles of the magnetic Bragg peaks at (1/2,0,0) and (1/2,1/2,0) at the lowest temperature. The incident neutrons were polarized along the c axis of the crystal, that was perpendicular to the scattering plane. By using a spin flipper and an analyzer of a magnetic Heusler-alloy crystal, we measured the intensities of the scattered neutrons in the non-spin-flip (NSF) and spin-flip (SF) channels, which correspond to the Fourier-transformed magnetic moments parallel to the c axis and that perpendicular to both the c axis and the scattering vector, respectively. We found that the reflection at (1/2, 1/2, 0) contains both the NSF and SF signals, suggesting that the system has non-coplanar magnetic structure. By representation analysis, we obtained possible bases of the magnetic structure, and found that the observed SF and NSF intensities can be reproduced by the all-in-all-out type magnetic structure constructed by a linear combination of the possible bases, as shown in Figs. 2(c) and 2(d). This magnetic structure breaks the time-reversal symmetry, and thus has the two domains, each of which is interconverted to the other by the time-reversal operation. Therefore, these two domains are

compatible with the ferromagnetic state with up and down magnetic moments, respectively, and exhibit the large Hall effect with opposite signs. We also investigated the magnetic structure of CNS in the same manner, and found that this system also has the all-in-all-out type non-coplanar magnetic structure. We also performed time-of-flight neutron diffraction measurements on CTS in Material and Life-science experimental Facility (MLF) of J-PARC, and also carried out first-principles calculations based on the density functional theory. Both confirmed the all-in-all-out magnetic structure. We note here that this magnetic structure has finite scalar spin chirality, $S_i \cdot (S_j \times S_k)$, which can induce a fictitious magnetic field acting only on the conduction electrons by adding quantum-mechanical Berry phase to their wavefunctions. The present results indicate that the scalar spin chirality mechanism can offer a promising route to realize giant spontaneous Hall response even in compensated antiferromagnets.

References

[1] S. Nakatsuji *et al*., Nature **527**, 215 (2015).
[2] N. J. Ghimire *et al*., Nature Commun. **9**, 3280 (2018).
[3] P. Park *et al*., npg Quantum Materials **7**, 42 (2022).
[4] H. Takagi *et al*., Nature Physics (advanced online publication) (2023).

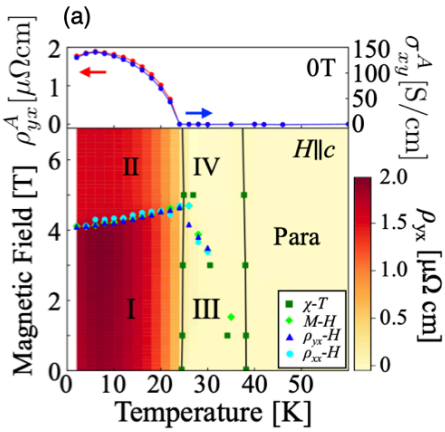

Fig. 1. (upper panel) Temperature dependence of the Hall resistivity and conductivity of CTS measured in zero field. (lower panel) Color map of thethe Hall resistivity superposed on the magnetization-temperature phase diagram of CTS.

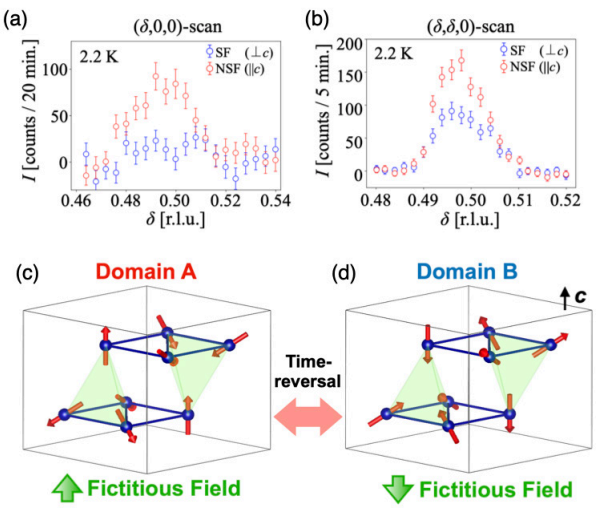

Fig. 2. [(a),(b)] Polarized neutron scattering profiles of CTS. [(c),(d)] Two domains of all-in-all-out magnetic structure.

Authors
H. Takagi[a], R. Takagi[a,b,c], S. Minami[a], T. Nomoto[a], K. Ohishi[d], M.-T. Suzuki[e,f], Y. Yanagi[e,g], M. Hirayama[a,c], N. D. Khanh[c], K. Karube[c], H. Saito[a], D. Hashizume[c], R. Kiyanagi[h], Y. Tokura[a,c], R. Arita[a,c], T. Nakajima[a,c], and S. Seki[a,b,c]
[a]The university of Tokyo
[b]PRESTO, Japan Science and Technology Agency (JST)
[c]RIKEN Center for Emergent Matter Science (CEMS)
[d]Comprehensive Research Organization for Science and Society (CROSS)
[e]Tohoku University
[f]Osaka University
[g]Toyama Prefectural University
[h]J-PARC Center

PI of Joint-use project: S. Seki
Host lab: Neutron Science Laboratory

Large Anomalous Hall Effect Induced by Field-Tunable Weyl Points in Antiferromagnetic Degenerate Semiconductor $EuMg_2Bi_2$

Weyl magnets, which have the topologically nontrivial band crossing points, have recently attracted significant attention because of the unconventional physical properties, such as large anomalous Hall effects (AHE). The typical materials have a semimetallic band structure where many bands cross the Fermi energy (E_F), resulting in complicated band structures and Fermi surfaces that hinder a simple understanding of their Weyl physics. In this study, we report on the field-tunable Weyl points in the degenerate antiferromagnetic semiconductor $EuMg_2Bi_2$, which has a simple and small Fermi surface. $EuMg_2Bi_2$ has a $CaAl_2Si_2$-type structure, which consists of the alternative stacking of the Eu magnetic layer and the Mg_2Bi_2 buckled-honeycomb layer (Fig. 1(a)). The former layer exhibits the A-type antiferromagnetic (A-AFM) order below $T_N \sim 6.7$ K at zero field. When the field is applied along the c -axis, Eu spins start canting toward the c-axis and are fully polarized above $B_c \sim 4$ T at 2 K. The latter layer forms the semiconducting band with the direct band gap at the Γ point, resulting in the simple Fermi surface. Therefore, it is expected that, in the magnetic field, the spin-polarized band crossing points (Weyl points) are formed while maintaining a simple band structure due to the spin splitting caused by the exchange interaction with local Eu spins. To reveal the impacts of the Eu magnetism on the band structure of $EuMg_2Bi_2$, we synthesized the large single crystal (Fig. 1(b)) and performed the various measurements and the first-principles calculations.

Figure 1(c) shows the field dependence of the Hall resistivity ρ_{yx} at 2 K for the field along the c-axis. Although, ρ_{yx} is almost linear with respect to field above B_c, it deviates from the straight line below B_c and shows a hump structure at approximately 2.5 T. This signals the AHE coupled with Eu magnetic order. To extract the anomalous component ρ^A_{yx}, we estimate the ordinary component $\rho^N_{yx} = R_H B$ from the data above B_c. We obtained the anomalous component as $\rho^A_{yx} = \rho_{yx} - \rho^N_{yx}$ which is roughly proportional to magnetization. At $B > B_c$, the anomalous Hall angle $\Theta_{AH} = \sigma^A_{xy}/\sigma_{xx}$, where $\sigma^A_{xy} = \rho^A_{yx}/(\rho^2_{xx} + \rho^2_{yx})$ and $\sigma_{xx} = \rho_{xx}/(\rho^2_{xx} + \rho^2_{yx})$ exhibits the nearly constant value (~ 0.07), which is comparable to those reported for other Weyl ferromagnets $Co_3Sn_2S_2$ (~ 0.2 at 150 K) [2], Fe_3GeTe_2 (~ 0.09 at 2 K) [3], and GdPtBi (~ 0.15 at 2.5 K) [4]. Such a large Θ_{AH} indicates that $EuMg_2Bi_2$ has band crossing points near E_F in the forced-ferromagnetic (f-FM) phase as a source of the Berry

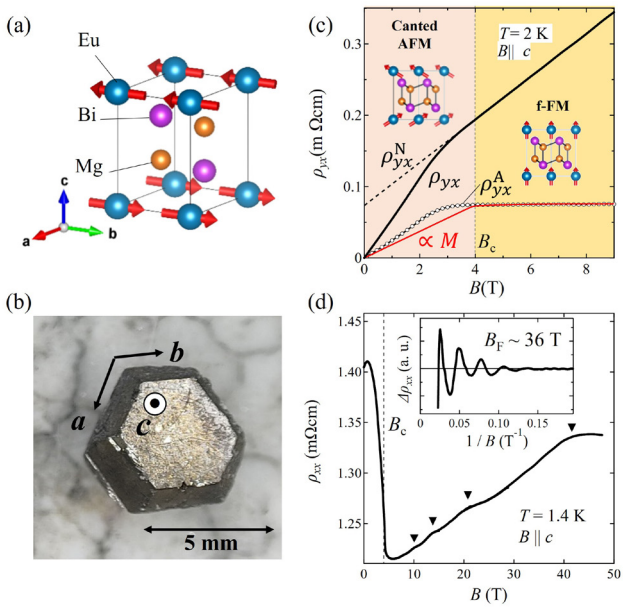

Fig. 1. (a) The crystal structure of $EuMg_2Bi_2$. (b) The photograph of the single crystal of $EuMg_2Bi_2$. (c) The field dependence of ρ_{yx} and its anomalous part ρ_{yx}^{A} at 2 K. The black dotted line corresponds to the ordinary part ρ_{yx}^{N} obtained from the liner fit to the experimental data above B_c. Note here that the ρ_{yx}^{N} is vertically shifted to demonstrate the fitted result at the high-field region. The red curve represents the field dependence of the magnetization M at 2 K. Insets show the magnetic structure of Eu spins at canted-antiferromagnetic (AFM) and forced-ferromagnetic (f-FM) phases. (d) Field dependence of ρ_{xx} at T = 1.4 K up to B ~ 50 T. Triangles denote the oscillatory component. The inset shows the oscillatory component $\Delta\rho_{xx}$.

curvature.

To obtain the detailed information of the Fermi surface, we measured the several physical properties up to ~ 55 T using the nondestructive mid-pulse magnet. Figure 1(d) shows the field dependence of the resistivity ρ_{xx}. As denoted by black triangles, we observed clear oscillatory structure. These oscillations are periodic with respect to $1/B$ [see inset of Fig. 1(d)], which indicates the quantum oscillation arising from the Landau quantization. By Onsager's theorem, we can estimate the cross-section S_F (~ 0.352 nm^{-2}) of the Fermi surface from the oscillation frequency B_F (~ 36 T), which allows us to determine the position of E_F in combination with the first-principles calculation shown below.

Figure 2(a) shows the calculated band structure around the Γ point for A-AFM phase. The two valence bands I and II cross each other on the Γ−A line, leading to a Dirac-like point located far from the E_F. When the field is applied along the c-axis, both bands exhibit a spin splitting because of the exchange interaction with the local Eu spins to form the multiple Weyl points. The position of the Weyl points shifts with increasing the magnitude of the spin splitting. Intriguingly, in the f-FM phase, one of the Weyl points are formed in the vicinity of E_F (Fig. 2(b)), which is determined to be ~ 110 meV from the comparison between the experimental and theoretical values of S_F and carrier density obtained from the Hall coefficient [1]. To clarify the intrinsic AHE due to the Berry curvature of the Weyl point, we calculated the E_F dependence of the anomalous Hall conductivity σ_{xy}^{A} in the f-FM phase. The calculated σ_{xy}^{A} shows a peak near the experimental E_F value where the Weyl point exists, and a good quantitative agreement with the experimental result obtained by the carrier-tuned samples. This strongly indicates that the observed large AHE in $EuMg_2Bi_2$ is due to the Berry curvature at the Weyl point induced by the magnetic field.

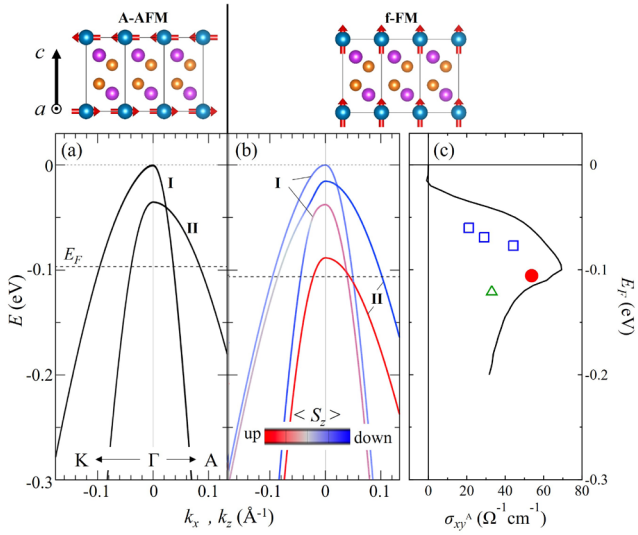

Fig. 2. (a, b) Valence band structures around the Γ point near E_F (lower panels) for various magnetic states (upper panels). Red and blue colors of band dispersions represent spin up and spin down, respectively. The dotted lines denote the Fermi energy E_F determined from the quantum oscillation frequency B_F at T = 1.4 K. (c) Anomalous Hall conductivity σ_{xy}^{A} as a function of E_F. The solid black curve represents the calculated result for the f-FM phase. The solid red circle denotes the experimental data (2 K, 9 T) for pristine $EuMg_2Bi_2$, while the open blue squares and open green triangle denote those for the annealed crystals and In-doped crystal, respectively.

Thus, our findings have clarified the unambiguous relationship between the emergent Weyl points and the anomalous Hall effect in a simple band structure, providing a guiding principle for future material design.

References

[1] M. Kondo *et al*., Physical Review B **107**, L121112 (2023).
[2] E. Liu *et al*., Nat. Phys. **14**, 1125 (2018).
[3] K. Kim *et al*., Nat. Mater. **17**, 794 (2018).
[4] T. Suzuki *et al*., Nat. Phys. **12**, 1119 (2016).

Authors

M. Kondo[a], M. Ochi[a], R. Kurihara[b], A. Miyake, Y. Yamasaki[c, d], M. Tokunaga, H. Nakao[e], K. Kuroki[a], T. Kida[f], M. Hagiwara[f], H. Murakawa[a], N. Hanasaki[a], and H. Sakai[a]
[a]Osaka University
[b]Tokyo University of Science
[c]NIMS
[d]CEMS, RIKEN
[e]KEK
[f]AHMF, Osaka University

PI of Joint-use project: H. Sakai
Host lab: Tokunaga Group

High Upper Critical Field of 120 T and Small Anisotropy in Highly Hydrogen-Substituted SmFeAsO Epitaxial Film

Among iron-based bulk superconductors, the highest critical temperature (T_c) of 55 K has been recorded for the 1111-type SmFeAsO. The superconductivity emerges by electron doping through partial substitution of F^- or H^- in the O^{2-} sites. Recently, we succeeded in fabrication of H-substituted SmFeAsO epitaxial thin films using topochemical reaction with binary dihydrides. The H-substituted SmFeAsO films exhibit not only high T_c, but also high critical current density (J_c), which is comparable with those of high J_c films of 122-type $BaFe_2As_2$ that is regarded as the most promising candidate among iron-based superconduc-

tors for practical application. Other than T_c and J_c, the upper critical field ($\mu_0 H_{c2}$) and its anisotropic parameter ($\gamma \equiv H_{c2\parallel}/H_{c2\perp}$, where the directions of the applied external magnetic fields are parallel ($\mu_0 H \parallel$) and perpendicular ($\mu_0 H \perp$) to the *ab* plane of SmFeAsO.) are also the important properties for evaluation of superconductors and their applications. In this study, the electronic transport properties of the highly H-substituted SmFeAsO epitaxial film were investigated to determine the low-temperature and high-field limits of its $\mu_0 H_{c2}$ ($\mu_0 H_{c2}(0)$) and γ under extremely high magnetic fields generated by nondestructive (60 T) and single-turn (130 T) pulsed magnets at the ISSP.

To experimentally determine $\mu_0 H_{c2}(0)$ for $\mu_0 H \parallel ab$, we performed radio-frequency (rf) impedance measurement with the single-turn magnet up to 130 T at 2.2 K (Fig. 1). The sample resistance (R) was roughly proportional to the inverse ratio of the amplitude of the reflection rf signal to the incident rf excitation with a field-independent background (Γ^{-1}). Even though Γ^{-1} remained constant with the wire resistance due to two-wire configuration between 0 and ~100 T, Γ^{-1} steeply increased at higher fields. An enlarged view of the high-field region in Fig. 1(a) is shown in Fig. 1(b). From the least-squares fits, clear saturation of Γ^{-1} was observed above ~125 T. By taking $\mu_0 H$ where Γ^{-1} became 80% of the saturated Γ^{-1} as $\mu_0 H_{c2}$, $\mu_0 H_{c2}$ of H-substituted SmFeAsO at 2.2 K was estimated to be 120 T for $\mu_0 H \parallel ab$. Because the experimentally confirmed $\mu_0 H_{c2}$ at 2.2 K should be almost the same as its low-temperature limit $\mu_0 H_{c2}(0)$, we concluded that $\mu_0 H_{c2}(0)$ of H-substituted SmFeAsO film reaches 120 T. This is the first experimental determination of $\mu_0 H_{c2}$ for 1111-type SmFeAsO at the low-temperature and high-field limits, and it is the highest value among those of other iron-based superconductors.

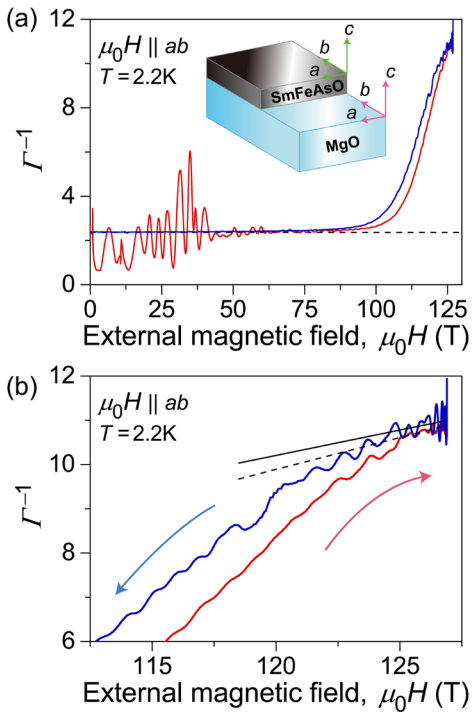

Fig. 1. Impedance measurement under high magnetic fields of up to 130 T at 2.2 K. The magnetic field was generated by the single-turn magnet and applied within the *ab* plane. (a) Γ^{-1} in the field region from 0 to 130 T. The inset shows relationship between the crystallographic orientation and the sample configuration of the H-substituted SmFeAsO epitaxial film on a MgO single-crystal substrate. (b) Enlarged image of (a) in the high-field region. The constant background is indicated by a black dashed line in (a). The red and blue arrows in (b) denote the directions of the field sweep. The black dashed and solid lines in (b) are the least-squares fits of the normal-state resistance in the up and down sweeps.

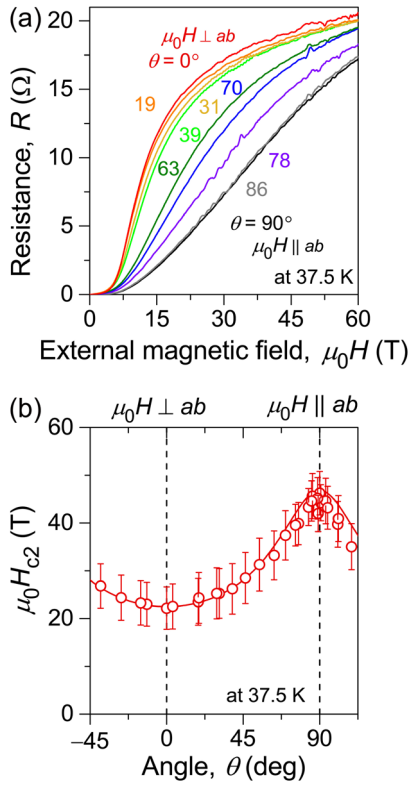

Anisotropic parameter of $\mu_0 H_{c2}$ (γ) in the H-substituted SmFeAsO epitaxial film. (a) R–$\mu_0 H$ curves under $\mu_0 H$ of up to 60 T at 37.5 K as a function of the angle (θ). (b) Angular dependence of $\mu_0 H_{c2}$ at 37.5 K. The red curve is the fit obtained by two-band analysis.

Next, to determine γ, the H-substituted SmFeAsO epitaxial film was mounted on a rotator probe, where the angle between the field direction and the *c* axis of the film was defined as θ, and $\mu_0 H$ was applied with the nondestructive pulsed magnet up to 60 T. Figure 2(a) shows the R–$\mu_0 H$ curves at 37.5 K with different field angles θ. With increasing θ, the jump in the R–$\mu_0 H$ curve gradually shifted to the higher field side. This experiment revealed that although there is a non-negligible angle dependence in $\mu_0 H_{c2}$, γ seems to be very small despite the layered structure of H-substituted SmFeAsO, which consists of individual SmO insulating and FeAs conductive layers. The θ dependence of $\mu_0 H_{c2}$ was estimated from the θ-dependent R (Fig. 2(b)), revealing that the γ around T_c is ~2. This small γ is comparable with those of MgB_2 and 122-type $BaFe_2As_2$, and almost half of that of F-substituted SmFeAsO ($\gamma > 4$). The small γ value of H-substituted SmFeAsO mainly originates from realization of three-dimensional superconductivity owing to high H incorporation.

In summary, we clarified the remarkable and unique characteristics in the H-substituted SmFeAsO epitaxial film such as the high $\mu_0 H_{c2}(0)$ of 120 T and relatively isotropic γ (~2) under extremely high magnetic fields generated by nondestructive and single-turn pulsed magnets at the ISSP [1]. Owing to the high and nearly isotropic $\mu_0 H_{c2}$, as well as the high T_c and high J_c, H-substituted SmFeAsO is a promising candidate for superconducting applications, such as the wires and tapes for cables and high-field electromagnets.

Reference

[1] K. Hanzawa, J. Matsumoto, S. Iimura, Y. Kohama, H. Hiramatsu, and H. Hosono, Phys. Rev. Mater. **6**, L111801 (2022).

Authors
K. Hanzawa[a], J. Matsumoto[a], S. Iimura[a, b], Y. Kohama, H. Hiramatsu[a], and H. Hosono[a, b]
[a]Tokyo Institute of Technology
[b]NIMS

PI of Joint-use project: H. Hiramatsu
Host lab: Kohama Group

Time-Resolved Angle-Resolved Photoemission Spectroscopy on $Ta_2Ni_{0.9}Co_{0.1}Se_5$

Ultrafast optical response of $Ta_2Ni_{0.9}Co_{0.1}Se_5$ has been studied by means of time-resolved angle-resolved photoemission spectroscopy (tr-ARPES). The Ti:Sapphire laser pulse with hν = 1.55 eV was used for the pump light and its higher harmonics with hν = 21.7 eV was employed for the probe light. The temporal resolution of the tr-ARPES is about 80 fs. $Ta_2Ni_{0.9}Co_{0.1}Se_5$ has a quasi one-dimensional crystal structure (Ta chain and Ni chain run along the a axis) and is one of the excitonic insulator (EI) candidates where the transition temperature is reduced by Co substitution in Ta_2NiSe_5. Under the sufficient incident fluence (1.9 mJ cm^{-2}), the conduction band is clearly observed above the Fermi level and the energy gap between the conduction and valence bands is closed at the delay time about 150 fs [1]. This observation suggests a photoinduced phase transition from the EI state to a semimetal state. The observed band dispersions of the semimetal phase roughly agree with the generalized gradient approximation (GGA) calculation which fails to reproduce the band gap at the ambient condition.

In Fig. 1, the tr-ARPES spectra of the semimetal phase are differentiated two times with respective to energy and are smoothed [2]. In this measurement, the Fermi surfaces are observed even before the arrival of the pump pulse (-400 fs). k_x represents a momentum along the Ta/Ni chain direction along which the valence and the conduction bands exhibit large dispersions. The k_x dispersions appreciably depend on k_y which is a momentum perpendicular to the Ta/Ni chains. The crosses indicate the band positions extracted from the momentum distribution curves (MDCs). The agreement between the band positions and the band structure calculations is not perfect, but the positions of the valence and conduction bands are roughly reproduced. Most probably, the electron-hole interaction, which is not exactly included in GGA, is screened out by the photoexcited carriers. In the photoinduced semimetal phase, the conduction and valence bands provide quasi one-dimensional Fermi surfaces with similar momentum positions suggesting a quasi one-dimensional line-node semimetal.

In most of the tr-ARPES measurements, the EI gap of $Ta_2Ni_{0.9}Co_{0.1}Se_5$ remains before the pump pulse arrival and is gradually suppressed after the pump pulse excitation. Such spectral behavior is clearly demonstrated in Fig. 2, where the energy distribution curves (EDCs) are numerically deconvoluted and divided by Fermi-Dirac distribution functions in order to extract the intrinsic spectral function [3]. With the fluence of 3.00 mJcm^{-2} and at the delay time of 70 fs, the valence band top does not reach the Fermi level creating a partial gap or a pseudogap, and the transition from the EI state to the semimetal state is not completed. While the conduction band crossing the Fermi level is observed with the shorter delay time (down to 50-70 fs) and/or the

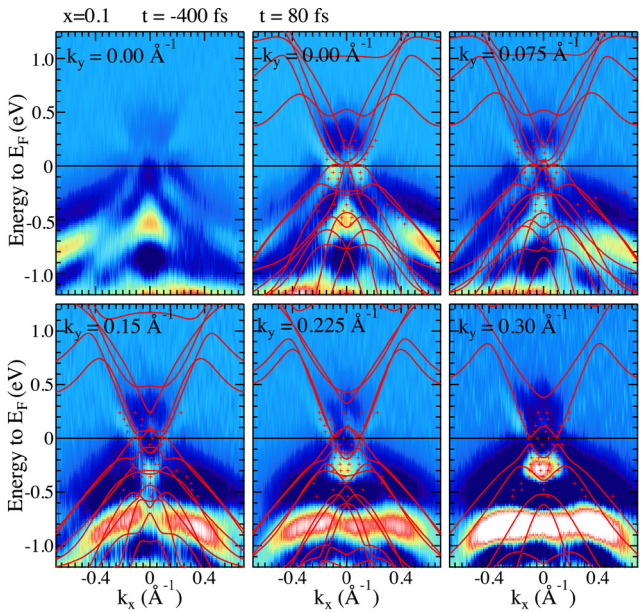

Fig. 1. The second derivatives of the tr-ARPES spectra with respective to energy as functions of k_x for $Ta_2Ni_{0.9}Co_{0.1}Se_5$, which are taken at 100 K with pump-probe delay of -400 fs (only k_y = 0.00 Å^{-1}) and about 100 fs (k_y = 0.00, 0.075, 0.15, 0.225, and 0.30 Å^{-1}). The symbols indicate the band positions extracted from MDCs. The solid curves indicate calculated GGA band dispersions for Ta_2NiSe_5.

lower fluence (down to 0.32 mJ cm^{-2}), the valence band top stays well below the Fermi level up to the fluence of 1.39 mJ cm^{-2} even at the delay time of 150-170 fs. Only with the highest fluence (3.00 mJ cm^{-2}) and the delay time of 150-170 fs, the gap (or pseudogap) at the Fermi level is closed. Such different optical responses of the valence and conduction bands cannot be explained by the canonical EI scenario, suggesting a vital role of electron-lattice coupling. One can speculate that the fluctuations of the Ni-Se bond, which can be coupled to the negative charge-transfer energy state (d^9L state) of Ni (L represents a Se 4p hole), remain at the 50-70 fs delay time and suppress the valence band shift. Around the delay time of 150-170 fs, the lattice fluctuations

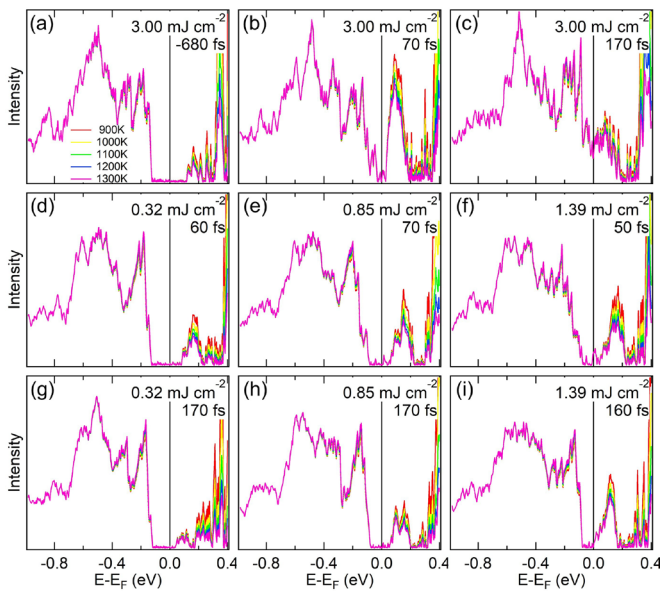

Fig. 2. EDCs (integrated in the k_x range between 0.05 and -0.05 Å^{-1}) deconvoluted and divided by the Fermi-Dirac distribution functions at the delay time of (a) -680 fs, (b) 70 fs, and (c) 170 fs for the fluence of 3.00 mJ cm^{-2}. Deconvoluted EDCs at 50-70 fs for the fluence of (d) 0.32 mJ cm^{-2}, (e) 0.85 mJ cm^{-2}, and (f) 1.39 mJ cm^{-2}. Deconvoluted EDCs at 150-170 fs for the fluence of (g) 0.32 mJ cm^{-2}, (h) 0.85 mJ cm^{-2}, and (i) 1.39 mJ cm^{-2}.

are screened out due to the photoexcited holes resulting in the semimetal phase with the substantial energy overlap between the conduction and valence bands. Such electron-lattice coupling is expected to be weak for the Ta-Se bond where the extended Ta 5d orbitals form the conduction band.

References

[1] T. Mitsuoka, T. Suzuki, H. Takagi, N. Katayama, H. Sawa, M. Nohara, M. Watanabe, J. Xu, Q. Ren, M. Fujisawa, T. Kanai, J. Itatani, S. Shin, K. Okazaki, and T. Mizokawa, J. Phys. Soc. Jpn. **89**, 124703 (2020).
[2] T. Mitsuoka, Y. Takahashi, T. Suzuki, M. Okawa, H. Takagi, N. Katayama, H. Sawa, M. Nohara, M. Watanabe, J. Xu, Q. Ren, M. Fujisawa, T. Kanai, J. Itatani, K. Okazaki, S. Shin, and T. Mizokawa, J. Phys. Soc. Jpn. **92**, 023703 (2023).
[3] Y. Takahashi, T. Suzuki, M. Hattori, M. Okawa, H. Takagi, N. Katayama, H. Sawa, M. Nohara, Y. Zhong, K. Liu, T. Kanai, J. Itatani, S. Shin, K. Okazaki, and T. Mizokawa, J. Phys. Soc. Jpn. in press.

Authors
T. Mizokawa[a], T. Mitsuoka[a], Y. Takahashi[a], M. Hattori[a], M. Okawa[a], T. Suzuki, and K. Okazaki
[a]Waseda University

PI of Joint-use project: T. Mizokawa
Host lab: Okazaki Group

Progress of Facilities

Supercomputer Center

The Supercomputer Center (SCC) is a part of the Materials Design and Characterization Laboratory (MDCL) of ISSP. Its mission is to serve the whole community of computational condensed-matter physics of Japan, providing it with high performance computing environment. In particular, the SCC selectively promotes and supports large-scale computations. For this purpose, the SCC invites proposals for supercomputer-aided research projects and hosts the Steering Committee, as mentioned below, that evaluates the proposals.

The ISSP supercomputer system consists of two subsystems: System B, which was last replaced in Oct. 2020, is intended for larger total computational power and has more nodes with relatively loose connections whereas System C is intended for higher communication speed among nodes. System B (ohtaka) consists of 1680 CPU nodes of AMD EPYC 7702 (64 cores) and 8 FAT nodes of Intel Xeon Platinum 8280 (28 cores) with total theoretical performance of 6.881 PFlops. System C was replaced in June 2022 and the current system (kugui) consists of 128 nodes of AMD EPYC 7763 (64 cores) and 8 ACC nodes of AMD EPYC 7763 (64 cores) NVIDIA A100 40GB for HGX with total theoretical performance of 0.973 PFLOPS.

In addition to the hardware administration, the SCC puts increasing effort on the software support. Since 2015, the SCC has been conducting “Project for advancement of software usability in materials science (PASUMS).” In this project, for enhancing the usability of the ISSP supercomputer system, we conduct several software-advancement activities: developing new application software that runs efficiently on the ISSP supercomputer system, adding new functions to existing codes, help releasing private codes for public use, creating/improving manuals for public codes, etc. Two target programs were selected for fiscal year 2022: (1) abICS (proposal made by S. Kasamatsu (Yamagata U.)), and (2) H-wave (proposal made by A. Kobayashi (Nagoya U.)). In addition, since 2021, we have been maintaining the data repository service for secure storage and enhanced usability of results of numerical calculation.

All staff members of university faculties or public research institutes in Japan are invited to propose research projects (called User Program). The proposals are evaluated by the Steering Committee of SCC. Pre-reviewing is done by the Supercomputer Project Advisory Committee. In fiscal year 2022, totally 337 projects were approved including the ones under the framework of Supercomputing Consortium for Computational Materials Science (SCCMS), which specially supports FUGAKU and other major projects in computational materials science. The total points applied and approved are listed on Table. 1 below.

The research projects are roughly classified into the following three (the number of projects approved, not including SCCMS):

First-Principles Calculation of Materials Properties (151)
Strongly Correlated Quantum Systems (25)
Cooperative Phenomena in Complex, Macroscopic Systems (141)

In all the three categories, most proposals involve both methodology and applications. The results of the projects are reported in 'Activity Report 2022' of the SCC. Every year 3-4 projects are selected for “invited papers” and published at the beginning of the Activity Report. In the Activity Report 2022, the following three invited papers are included:

Class	Max Points		Application	Number of Projects	Total Points			
					Applied		Approved	
	System B	System C			System B	System C	System B	System C
A	100	50	any time	28	2.8k	1.4k	2.8k	1.4k
B	800	100	twice a year	94	65.9k	6.7k	38.6k	5.5k
C	8k	500	twice a year	176	1092.9k	47.4k	566.8k	35.7k
D	10k	500	any time	6	30.5k	0.9k	23.4k	0.8k
E	24k	1.5k	twice a year	13	273.0k	18.0k	185.5k	14.4k
S			twice a year	0	0k	0k	0k	0k
SCCMS				20	52.3k	5.2k	52.3k	5.2k
Total				337	1517.4k	79.6k	869.4k	62.9k

Table 1. Research projects approved in Academic Year 2022.
The maximum points allotted to the project of each class are the sum of the points for the two systems; Computation of one node for 24 hours corresponds to one point for the CPU nodes of System B and System C. A FAT node of System B and an ACC node of System C require 4 and 2 points, respectively, for 24 hours.

1. "Training method for refinement of machine-learning interatomic potential and its applications", Kohei SHIMAMURA, Akihide KOURA, and Fuyuki SHIMOJO (Kumamoto Univ.)
2. "First principles calculation of copper-oxide superconductors exhibiting electron fractionalization", Masatoshi IMADA (Waseda Univ.)
3. "Molecular dynamics study of ultra-long chain fatty acid in lipid bilayer", Kazutomo KAWAGUCHI (Kanazawa Univ.) and Hiroshi NOGUCHI (ISSP)

Neutron Science Laboratory

The Neutron Science Laboratory (NSL) has been playing a central role in neutron scattering activities in Japan since 1961 by performing its own research programs as well as providing a strong General User Program (GUP) for the university-owned various neutron scattering spectrometers installed at JRR-3 (20 MW) operated by Japan Atomic Energy Agency (JAEA) in Tokai, Ibaraki (Fig. 1). In 2003, the Neutron Scattering Laboratory was reorganized as the Neutron Science Laboratory to further promote the neutron science with use of the instruments in JRR-3. Under GUP supported by NSL, 12 university-group-owned spectrometers in the JRR-3 reactor are available for a wide scope of research on material science. The submitted proposals were about 300 and the visiting users reached over 6000 person-day in FY2010. In 2009, NSL and Neutron Science Division (KENS), High Energy Accelerator Research Organization (KEK) built a chopper spectrometer, High Resolution Chopper Spectrometer, HRC, at the beam line BL12 of MLF/J-PARC (Materials and Life Science Experimental Facility, J-PARC) (Fig. 2). HRC covers wide energy transfer (100 μeV < $\hbar\omega$ < 0.5 eV) and momentum transfer (0.03 Å^{-1} < Q < 30 Å^{-1}) ranges, and therefore becomes complementary to the existing inelastic spectrometers at JRR-3. HRC has accepted general users through the J-PARC proposal system since FY2011.

Triple axis spectrometers, HRC, a four-circle diffractometer, and a high resolution powder diffractometer are utilized mainly for a conventional solid state physics and a variety of research fields on hard-condensed matter, while in the field of soft-condensed matter science, researches are mostly carried out by using a small angle neutron scattering (SANS-U) and/or neutron spin echo (iNSE) instruments. The upgraded time-of-flight (TOF) inelastic scattering spectrometer, AGNES, is available both for hard- and soft-matter science. Our GUP has produced 2088 publications and 289 dissertations until April 24, 2023. Their lists for the last 10 years are given in Activity Report on Neutron Scattering Research which is available in ISSP and NSL web pages.

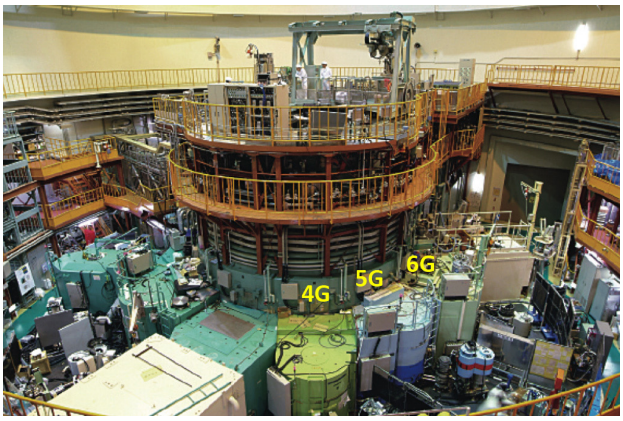

Fig. 1. Reactor hall of JRR-3. Three triple axis spectrometers are shown in the photo.

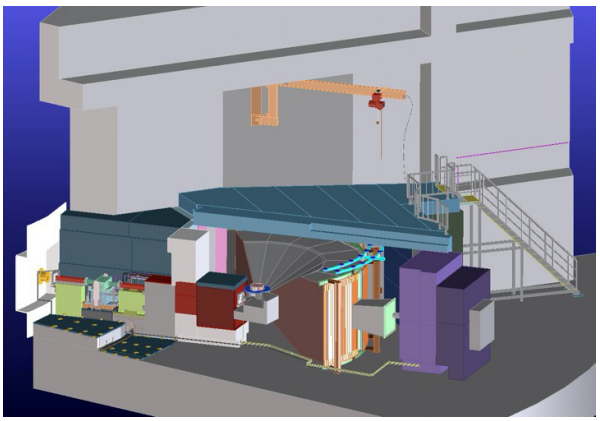
Fig. 2. Schematic view of HRC.

Since the Great East Japan Earthquake on March 11, 2011, JRR-3 were closed for about 10 years mainly from safety issues. Hence, our domestic activity was only on HRC. To keep the activity of reactor-neutron science in Japan, NSL has managed User-Program Supports for Overseas Experiments from FY2012 to FY2020. 398 people (for 297 proposals) have performed their experiments in various foreign facilities and published 118 papers (as of February 28, 2022). The lists for this program are also available in Activity Report on Neutron Scattering Research mentioned above.

As for international cooperative programs, NSL operates the U.S.-Japan Cooperative Program on neutron scattering, providing further research opportunities to material scientists who utilize the neutron scattering technique for their research interests. In 2010, relocation of the U.S.-Japan triple-axis spectrometer, CTAX, was completed, and it is now open to Japanese users. NSL has another agreement with Australian Centre for Neutron Scattering (ANSTO), which was the main foreign facility for the User-Program Supports for Overseas Experiments.

It was long-awaited news that JRR-3 restarted in February 2021 after long shutdown and the normal GUP came back from July 2021. During the shutdown period, we made a lot of efforts on upgrading the instruments and neutron beam circumstances. Specific actions taken include: the installation of focusing collimation systems, such as focusing monochromator and focusing analyzer, and super-mirror collimators. The neutron guides in the beam-hall have also been upgraded by replacing the existing ones with super-mirror guides. These upgrades have resulted in increase in neutron beam flux several times. For example, the neutron intensity of AGNES (high resolution cold neutron spectrometer) increased seven times. The sample environments such as cryostat and pressure cells have also been upgraded. We had conducted 84 experiments for 155 proposals in 2021 (reactor operation: 4 cycles, 92 days) and 123 experiments for 166 proposals in 2022 (reactor operation: 7 cycles, 152 days). For these experiments, more than 40 papers, including those under review, have been obtained as of October 14, 2022.

International MegaGauss Science Laboratory

The objective of this laboratory (Fig. 1) is to study the physical properties of solid-state materials (such as metals, semiconductors, insulators, superconductors, and magnetic materials) in a high magnetic field of 100 T or even higher. Such a high magnetic field can control material phases and functions. Our pulsed magnets, at the moment, can generate up to 87 Tesla (T) by non-destructive manner, and up to 1200 T by destructive manner. The world record indoor magnetic field 1200 T was achieved in 2018. The laboratory is open for scientists in domestic as well as from overseas. Lots of fruitful results have come out not only from the collaborative researches but also from our in-house activities.

Fig. 1. The building C of the IMGSL.

Our interests cover the study on quantum phase transitions (QPT) induced by high magnetic fields. Field-induced QPT has been explored in various materials such as quantum spin systems, strongly correlated electron systems and other magnetic materials. One of our ultimate goals is to provide the joint-research users with a 100 T millisecond-long pulse using a non-destructive magnet, and to offer versatile high-precision physical measurements. Measurable physical quantities or properties are magneto-optical spectra, magnetization, magnetostriction, electrical transport, specific heat, nuclear magnetic resonance, and ultrasound propagation. They can be carried out with sufficiently high accuracy. Another ultimate goal is to extend the magnetic field region and discover novel phenomena happening only in extremely strong magnetic fields exceeding 100 T. Recent technical developments allow us to even measure magnetostriction and ultrasound propagation in the destructive magnetic fields over 100 T, that can directly reach potential structural changes in the ultrahigh magnetic fields. Recent discovery of magnetic field induced insulator-metal transitions of strongly correlated materials in 500 T would open new direction of the megagauss field research, namely exploration of field-induced novel phases in materials with strong interactions comparable to thermal energy of a room temperature.

A 210 MJ flywheel generator (Fig. 2), which is the world's largest DC power supply (recorded in the Guinness Book of World Records) was installed in the DC flywheel generator station at our laboratory, and used as an energy source of super-long pulse magnets. The magnet technologies are intensively devoted to the quasi-steady long pulse

	Alias	Type	B_{max}	Pulse width Bore	Power source	Applications	Others
Building C Room 101-113	ElectroMagnetic Flux Compression	Destructive	1200 T	3μs (100-1200T) 10 mm	5 MJ, 50 kV 2 MJ, 50 kV	Magneto-Optical Magnetization	5 K – room temperature
	Horizontal Single-turn Coil	Destructive	300 T 200 T	6μs 5 mm 10 mm	0.2 MJ, 50 kV	Magneto-Optical measurements Magnetization	5 K – room temperature
	Vertical Single-turn Coil	Destructive	300 T 200 T	8μs 5 mm 10 mm	0.2 MJ, 40 kV	Magneto-Optical Magnetization	2 K – room temperature
Building C Room 114-120	Mid-pulse Magnet	Non-destructive	60 T 70 T	40 ms 18 mm 40 ms 10 mm	0.9 MJ, 10 kV	Magneto-Optical measurements Magnetization Magneto-Transport Hall resistance Polarization Magneto-Striction Magneto-Imaging Torque Magneto- Calorimetry Heat Capacity	Independent Experiment in 5 site Lowest temperature 0.1 K
Building C Room 121	PPMS	Steady	14 T			Resistance Heat Capacity	Down to 0.3 K
	MPMS	Steady	7 T			Magnetization	
Building K	Short-Pulse Magnet	Non-destructive	87 T (2-stage pulse) 86 T	5 ms 10 mm 5 ms 18 mm	0.5 MJ, 20 kV	Magnetization Magneto-Transport	2 K – room temperature
	Long-Pulse Magnet	Non-destructive	43.5 T	1 s 30 mm	210 MJ, 2.7 kV	Resistance Magneto-Calorimetry	2 K – room temperature

Table 1. Available Pulse Magnets, Specifications

Fig. 2. Upper: The K-building for the flywheel generator (left-hand side) and a long pulse magnet station (right-hand side). Lower: The flywheel giant DC generator which is 350 tons in weight and 5 m high (bottom). The generator, capable of a 51 MW output power with the 210 MJ energy storage, is planned to energize the long pulse magnet generating 100 T without destruction.

magnet (an order of 1-10 sec) energized by the giant DC power supply. The giant DC power source will also be used for the giant outer-magnet coil to realize a 100 T nondestructive magnet by inserting a conventional pulse magnet coil in its center bore. Recently, the super-long pulsed magnet has been intensively used to investigate thermal properties such as specific heat and magnetocaloric effects.

Magnetic fields exceeding 100 T can only be obtained with destruction of a magnet coil. The ultrahigh magnetic fields are obtained in a microsecond time scale. The project, financed by the Ministry of Education, Culture, Sports, Science and Technology aiming to generate 1000 T with the electromagnetic flux compression (EMFC) system (Fig. 3), has been completed. Our experimental techniques using the destructive magnetic fields have intensively been developed. The system which is unique to ISSP in the world scale is comprised of a power source of 5 MJ main condenser bank and 2 MJ condenser bank. Two magnet stations are constructed and both are energized from each power source. Both systems are fed with another 2 MJ condenser bank used for a seed-field coil of which magnetic flux is to be compressed. The 2 MJ EMFC system can generate 450 T. The 5 MJ system is used for generation of

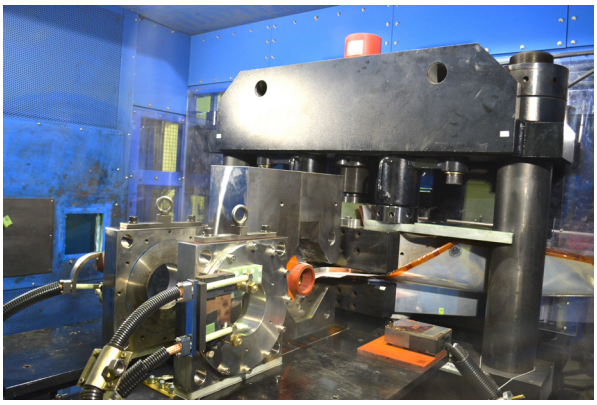

Fig. 3. View of the coil setup of the electromagnetic flux compression inside of an anti-explosive house. The world's strongest indoor magnetic field 1200 T was achieved in 2018.

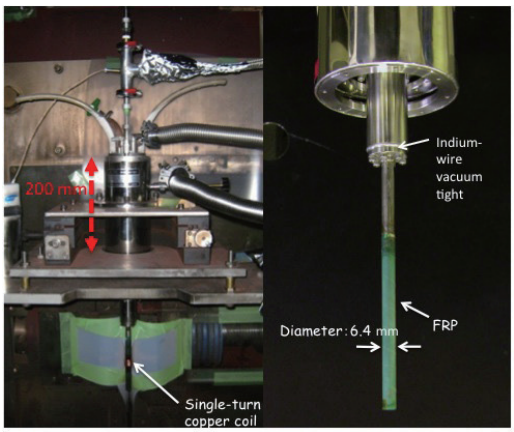

Fig. 4. Schematic picture of the V-type single-turn coil equipped with a 40 kV, 200 kJ fast capacitor bank system. The liquid-helium-bath cryostat with a plastic tail is also shown.

1000 T-class magnetic field. For the research in magnetic field range of 100 - 300 T, we have two single-turn coil (STC) systems that have a fast-capacitor bank system of 200 kJ for each. One is the horizontal type (H-type) and the other is a vertical type (V-type, Fig. 4). Various kinds of laser spectroscopy experiments such as the cyclotron resonance and the Faraday rotation are possible using the H-type STC, while a stable low temperature condition of 2 K is available for the V-type STC.

Center of Computational Materials Science

With the advancement of hardware and software technologies, large-scale numerical calculations have been making important contributions to materials science and will have even greater impact on the field in the near future. CCMS is a specialized research center established in 2011 for promoting computer-aided materials science with massively parallel computers, such as the Fugaku supercomputer, which has been developed in Kobe as the core of a billion-dollar national project. Activities of CCMS are divided into the following three categories: (1) highly efficient and large-scale use of the Fugaku supercomputer and its application to grand-challenge problems in computational materials science, (2) activities as the center for the community of computational condensed matter physics and materials science, and (3) the matching program for computational materials science in industry and academia.

For the first category, each group in CCMS is carrying out various individual research projects in its own expertise to efficiently utilize large-scale parallel computers. For example, the Ozaki group has been developing efficient and accurate methods and software packages to extend the applicability of DFT to more realistic systems, and investigated the structural and electronic properties of various 2D materials in successful collaboration with experimental groups and industrial companies. There are other activities such as development of Tensor Network (TN) based numerical methods and Markov-chain Monte Carlo methods by the Kawashima group and the Todo group.

As for the activities in the second category, apart from major annual conferences and formal international meetings, the CCMS provided a series of lectures and training sessions at Kashiwa. For example, training sessions "Kashiwa Hands-

On" for getting accustomed to various application programs, such as Hphi, TeNeS, mVMC, DSQSS, and MateriApps LIVE!, as shown in Fig. 1, have been held monthly. Each session is designed for more than 10 trainees and takes 4-5 hours. We also coordinate the use of the computational resources available to our community, and support community members through various activities such as administrating the website "MateriApps" for information on application software in computational science as shown in Fig. 2.

For the third category, in order to foster young people with a high level of expertise in computational materials science and to support their career paths, the consortium project, Professional Development Consortium for Computational Materials Scientists (PCoMS), was established cooperatively with Tohoku Univ., Institute for Molecular Science, and Osaka Univ in 2015. From 2020, CCMS has continued to develop this consortium project by building a cooperative framework with industrial companies, called MP-CoMS. In the MP-CoMS, we have two activities: advanced human resource development and matching program. The former offers advanced lectures by university faculty members on computational science for researchers, graduate students, and postdoctoral fellows, and providing opportunities for human resource exchange across industry-academia boundaries. The latter intends bridging doctoral students, postdoctoral fellows with participating companies who have a background in computational science and materials science, and in every year about 10 Ph. D students experience the internship researches in the participating company.

These activities are supported by funds for the MP-CoMS and governmental projects including the Program for Promoting Researches on the Supercomputer Fugaku.

Fig. 1. Software in the CCMS community

Fig. 2. MateriApps Website

The following is the selected list of meetings organized by CCMS in recent years:

- 2022/5/12, 13 The ISSP Supercomputer Usage/ CCMS Joint Workshop.
- 2022/4/7-2022/7/28 On-line lecture series for advanced computational science and technology B (2022).
- 2022/6/8,9 Matching Workshop for industries & graduate students/postdocs.
- 2022/9/9,16,22,30 MP-CoMS on-line lecture series for fundamentals and applications of materials informatics.
- 2022/10/26 The 14th workshop for the computational materials science in the post Fugaku era.
- 2023/2/24 The 15th workshop for the innovation in materials development through integration of computational and metrology science.
- 2023/3/29 DxMT workshop: frontiers in development of machine learning potentials

In addition to the events listed above, we organized regular hands-on program for various application, such as Hφ and mVMC.

Laser and Synchrotron Research Center (LASOR Center)

Laser and synchrotron research center (LASOR Center) was established in October 2012 to push the frontiers of the photon and materials science. LASOR has 10 groups in 2022, which is the biggest division in ISSP. Most of the research activities on the development of new lasers with an extreme performance and the application to materials science are studied in specially designed buildings D and E with large clean rooms and the isolated floor from the vibrations in Kashiwa Campus. We also have a clean room for a laser processing platform in Kashiwa II Campus. On the other hand, the experiments utilizing the synchrotron radiation are performed at SPring-8 and SACLA (Hyogo). Recently new beamline is under development at Nano Terasu in Sendai.

The development of new laser light sources in the vacuum ultraviolet to soft x-ray region has revolutionized materials research, represented by photoelectron spectroscopy with the highest energy resolution, ultrafast time-domain spectroscopy, and ultrafast nonlinear spectroscopy. Materials science research powered by lasers thus has entered a new era. The ultra-short and high-power lasers are more and more attractive light source for both basic science

Fig. 1. Optical frequency comb

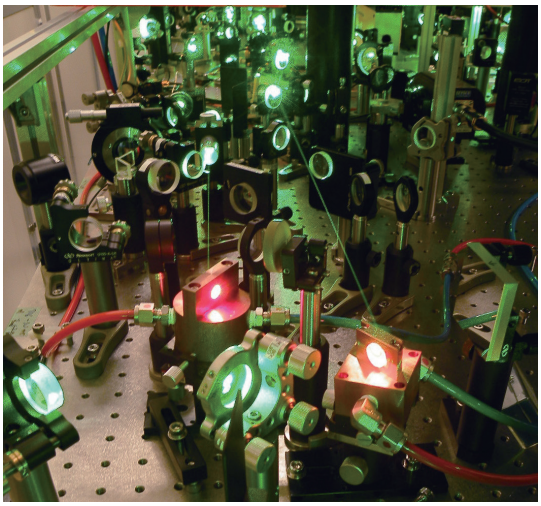

Fig. 2. Close look of a high-peak-power ultrashort-pulse laser

and industry. The state-of-the-art laser source and spectroscopy are intensively explored.

Another stream pursued at ISSP is the synchrotron-based research. The drastic advance in brilliance of the synchrotron radiation has also opened a new field of its own in photon science. The soft-X-ray beam-line in SPring-8 (BL07LSU) has been implemented with the longest undulator in the world: The end stations illuminated by the brilliant soft-X-rays are used to output innovative achievements based on high-resolution spectroscopy data. In 2018, Japanese government has made a statement to construct a new synchrotron facility in Tohoku (Nano Terasu). LASOR has decided to subjectively contribute to this facility from the design to the operation, and Nano Terasu is now under construction.

Lasers and synchrotrons have developed independently; now both light sources cover a wide photon-energy range with an overlap in the vacuum-ultraviolet to soft-X-ray regions. Foreseeing their common interests in research fields and technologies, ISSP integrated the two streams, namely the extreme lasers and synchrotron radiations, into the common platform. Through the mutual interactions between the forefronts of lasers and synchrotrons, LASOR will be the center of innovations in light and materials science, with the aid of world-wide joint research and close collaborations with other divisions in ISSP such as New Materials Science, Nanoscale Science, and Condensed Matter Theory.

The mission of LASOR is to cultivate and propel the following three scientific fields:

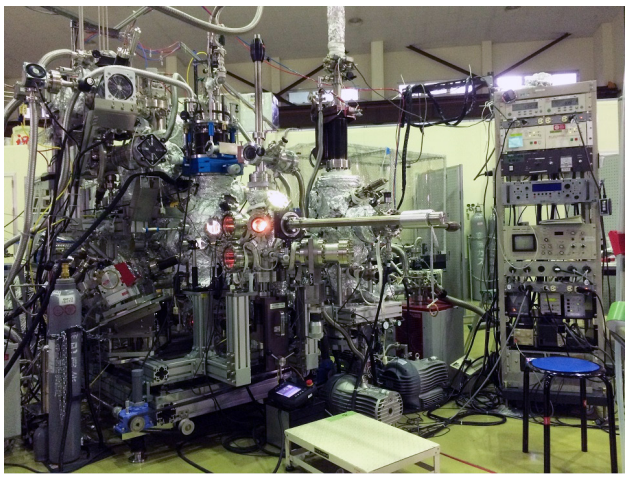

Fig. 3. Spin-resolved photo-emission spectroscopy.

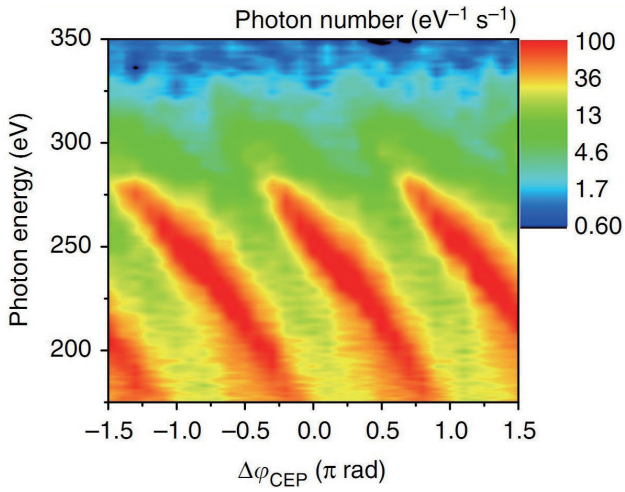

Fig. 4. Phase-dependence of high harmonic spectra in soft X rays.

1. Laser Science,
2. Synchrotron radiation Science,
3. Extreme Spectroscopy,

• Laser science group

We were committed to continuing to develop various state-of-the-art laser systems such as high-power solid-state or gas lasers, high-intensity lasers, ultra-short pulse lasers down to attosecond time scale (Peta-Hz linewidth), ultrastable lasers with 1-Hz linewidth, optical frequency combs, mid-infrared lasers, THz light source, and semiconductor lasers.

High-power and ultrashort pulse laser technology has progressed for these 10 years. It opened two directions of research. One is a coherent extreme ultraviolet light source realized by a high-harmonic generation (HHG) scheme. The average power of HHG became high enough to use it for a photoemission spectroscopy. The photon energies of 7 eV to 60 eV are now available. They can be either very narrow band width or ultrashort pulse. The other is an industrial science such as a laser processing. Pulse duration variable, 100-W average power, femtosecond laser is now available in LASOR for any collaborative research including companies. We have a laser processing platform for both industrial and scientific applications.

We also aim to develop novel laser spectroscopy and coherent non-linear optical physics, enabled via emerging lasers and optical science/technology, and extensively study basic light-matter physics, optical materials science, and applied photonics. Such researches include ultrafast spectroscopy for excited state dynamics, terahertz magnetic-field spectroscopy for spin dynamics, quantitative micro-spectroscopy on semiconductor lasers and nano-structure photonics devices, such as quantum wire lasers, gain-switch semicon-

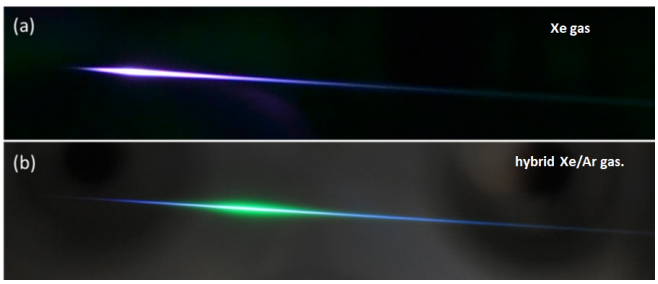

Fig. 5. Generation of 7-eV, femtosecond light with (a) Xe and (b) Xe/Ar gases.

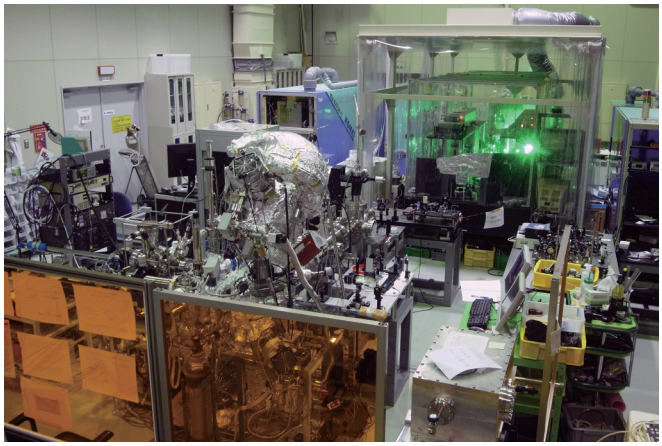

Fig. 6. Pump-probed photoemission system using 60-eV laser

ductor laser, multi-junction solar cells, and bio-luminescent systems.

• Synchrotron radiation science group

By inheriting and developing the synchrotron techniques cultivated for more than 20 years, we continuously develop world cutting-edge spectroscopies such as time-resolved photoemission /diffraction, ultrahigh resolution soft X-ray emission, 3D (depth + 2D microscopy) nano ESCA and X-ray magneto-optical effect and provide these techniques both for basic material science and for applied science, which contributes to the device applications in collaboration with outside researchers. In order to pioneer new spectroscopies for the next-generation light sources, we upgrade fast polarization switching of the undulator light source in cooperation with SPring-8. In addition, we promote frontier works on the use of X-ray free electron lasers, SACLA with high spatial and temporal coherence comparable to optical lasers in collaboration with scientists of laser light sources and spectroscopies.

• Extreme spectroscopy group

The advent of laser-based light sources in the soft-X-ray region is opening a new stage in the field that has been cultivated by the synchrotron radiations. One of the milestones is to develop a laser-based light source of ~7 eV for the sub-meV-resolution photoemission spectroscopy. In these five years, available photon energy became 11 eV with help of Yb-fiber laser technology. It has high photon flux (10^{14} photons/sec) with sub picosecond time resolution.

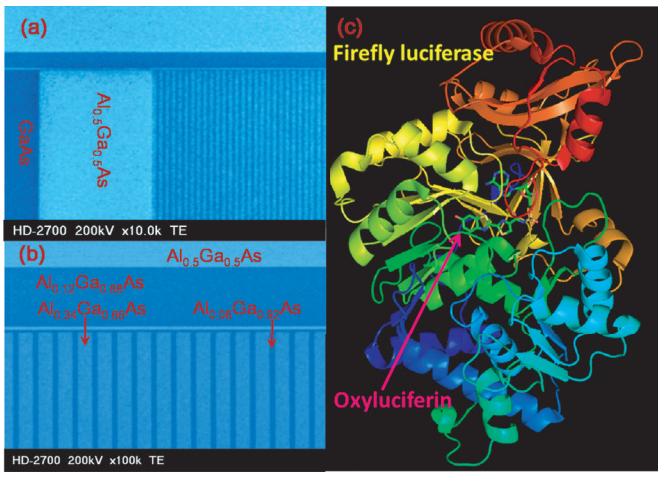

Fig. 7. Photonics devices under study: (left panel) semiconductor quantum wires and (right panel) firefly-bioluminescence system consisting of light emitter (oxyluciferin) and enzyme (luciferase)

Laser-based spin-resolved ARPES is realizing in LASOR with 11 eV laser. This technology would open brand-new spectroscopy. High-harmonic generation based photoemission spectroscopy in the 20-60 eV region is another direction to be pursued. Time-domain spectroscopy in the femtosecond region was achieved. Combined with the picosecond time-domain spectroscopy utilizing the pulsed light delivered from synchrotrons, we investigate the electronic structures and dynamics of matter in bulk, on surface, and into the nano-scale. The ultimate objective is to expand the soft-X-ray operando methodologies by lasers. Diffractions, magneto-optical effects, and inelastic scatterings now done at synchrotrons will be performed by lasers, to access the real-time dynamics of chemical reactions and phase transitions down to the femtoseconds.

State-of-the-art laser based organism spectroscopy is new direction in LASOR. ISSP research area is shifting from simple material and science to complex one including living body and functional material with excited state physics.

Synchrotron Radiation Laboratory

The Synchrotron Radiation Laboratory (SRL) was established in 1975 as a research division dedicated to solid state physics using synchrotron radiation. Currently, SRL is composed of three research sites, the Sendai office, the Harima office and the E-building of the Institute for Solid State Physics.

• Synchrotron soft X-ray experimental stations at Sendai office and Harima office

In 2006, the SRL staffs joined the Materials Research Division of the Synchrotron Radiation Research Organization (SRRO) of the University of Tokyo, and they played an essential role in constructing a high brilliant and polarization-controlled 25-m long soft X-ray undulator beamline, BL07LSU, in SPring-8. The construction was completed in 2009 and SRL established the Harima branch laboratory in SPring-8. The beamline was equipped with electromagnetic phase shifters that allow fast switching of the circularly (left, right) and linearly (vertical, horizontal) polarized photons, covering the photon energy range from 250 eV to 2 keV. At the downstream of the beamline, a lot of experimental stations have been developed for frontier spectroscopy researches. In 2022, four endstations, ambient pressure X-ray photoemission (APXPS) (Fig. 1a), soft X-ray imaging (ptychography) (Fig. 1b), three-dimensional nanoESCA (3DnanoESCA) (Fig. 1c), high resolution soft X-ray emission spectroscopy (HORNET) (Fig. 1d) stations were maintained by the SRL staffs and open for the joint-research program. The APXPS system achieved the 100 Torr XPS measurement and is used for various catalytic reactions including CO_2 reduction; the soft X-ray imaging station established a new soft X-ray ptychography system using a total-reflection Wolter mirror with a resolution of approximately 50 nm. Long working distance of the system enables stereo imaging with a large rotation angle; the 3Dnano-ESCA station reached the spatial resolution of 70 nm and is equipped with a sample holder with a 5-terminal electrode dedicated for the analysis of secondary battery materials, high electron mobility transistors etc.; the HORNET station provides spectra with the energy resolution around 70 meV at 400 eV and enables real ambient pressure experiments

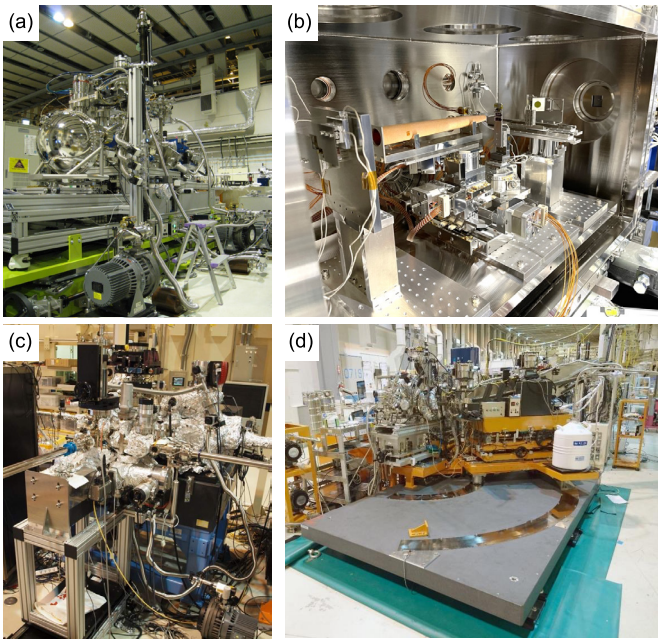

Fig. 1 Soft X-ray experimental stations dedicated for the joint-research program at SPring-8 (a) Ambient pressure photoemission (APXPS) (b) Soft X-ray imaging (c) 3DnanoESCA (d) Soft X-ray emission (HORNET). APXPS, 3DnanoESCA and HORNET stations have been transferred to the new 3GeV synchrotron facility NanoTerasu at the end of FY2022.

on various targets including solution and its interface with solids and gases. In the first half of the 2022 cycle, 21 user groups made their experiments. The joint-research program at SPring-8, which lasted for 13 years, was terminated in August 2022, and the management of the beamline was transferred to the RIKEN SPring-8 Center. In November 2022, the Sendai office was established in the Aobayama campus of Tohoku University under the auspices of a new SRRO launched in April 2022 comprising six departments of the University of Tokyo. At the end of FY2022, the APXPS, XES, and 3DnanoESCA stations have been moved to the new 3GeV synchrotron facility NanoTerasu in Sendai, which will start operation in FY2024. The Harima office at SPring-8 continues and the development of the soft X-ray imaging station is cooperated with the RIKEN SPring-8 Center.

- **High-resolution Laser SARPES and ARTOF systems at E-building**

High-resolution Laser Spin- and Angle-Resolved Photoemission Spectroscopy (SARPES) is a powerful technique to investigate the spin-dependent electronic states in solids. In FY2014, LASOR and SRL staffs constructed a new SARPES apparatus (Fig. 2a), which was designed to provide high-energy and angular resolutions and high efficiency of spin detection using a laser light at E-building. The achieved energy resolution of 1.7 meV in SARPES spectra is the highest in the world at present. From FY2015, the new SARPES system has been opened for the joint-research program. The Laser-SARPES system consists of an analysis chamber, a carousel chamber connected to a load-lock chamber, and a molecular beam epitaxy chamber, which are kept ultra-high vacuum (UHV) environment and are connected to UHV gate valves. The electrons are excited with 6.994 eV photons, yielded by 6th harmonic of a Nd:YVO_4 quasi-continuous wave laser with a repetition rate of 120 MHz, and 10.7 eV photons, driven by the third harmonic radiation at 347 nm of an Yb:fiber chirped pulse amplifier laser, which was developed by Kobayashi's lab in LASOR. The hemispherical electron analyzer is a custom-made Scienta Omicron DA30-L, modified for installing the spin detectors. The spectrometer is equipped with two high-efficient spin detectors orthogonally placed each other, associating very low energy electron diffraction, which allows us to analyze the three-dimensional spin polarization of electrons. At the exit of the hemispherical analyzer, a multi-channel plate and a CCD camera are also installed, which enables us to perform the angle-resolved photoelectron spectroscopy with two-dimensional (energy-momentum) detection. The laser-SARPES with 7 eV laser can provide both high-resolution spin-integrated and spin-resolved photoemission spectra in various types of solids, such as spin-orbit coupled materials and ferromagnetic materials. In addition, using the 10.7 eV makes it possible to follow their ultrafast spin dynamics in the time domain by pump-probe scheme. A spectroscopy system using a dichroic mirror (SiO_2/HfO_2 multilayer) was introduced for a stable switching of the 7 eV and 10.7 eV lasers.

The time-resolved soft X-ray spectroscopy (TR-SX) station was moved from SPring-8 BL07LSU to the E-building in 2020. The measurement chamber is equipped with a unique electron spectrometer, the two-dimensional (2D) angle-resolved time-of-flight (ARTOF) analyzer (Fig. 2b). The system is currently operational for measurements of 2D angle-resolved photoemission spectroscopy with pulsed laser of 6 eV photon energy supplied by Itatani's lab in LASOR. Time-resolved measurements can also be conducted with temporal resolution of 600 fs. An ultra high-speed reading and visualization program is currently in development to enhance usability.

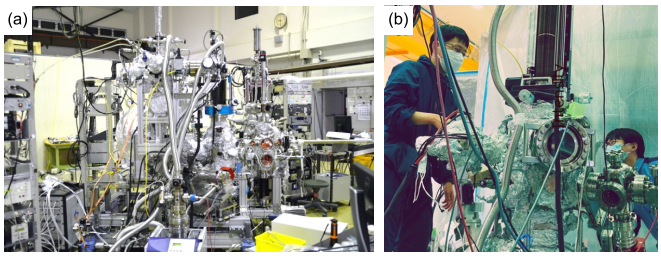

Fig. 2 (a) Laser-SARPES system and (b) ARTOF system at E-building.

Conferences and Workshops

Research Front of Neutron Scattering
- Achievements from the User-program Support for Overseas Experiments and Latest Results from JRR-3 -

April 18-20, 2022
O. Yamamuro, T. Masuda, T. Nakajima, and K. Mayumi

After the great east Japan earthquake in 2011, the Japan Research Rector-3 (JRR-3), which was the largest neutron science facility before J-PARC started, stopped the operation. Since then, the Neutron Science Laboratory of the Institute for Solid State Physics (ISSP-NSL) had supported research groups conducting neutron scattering experiments in overseas facilities. In this workshop, 8 users presented their results obtained in the overseas experiments. In 2021, JRR-3 finally restarted, and ISSP-NSL also restarted the joint-use program on neutron research in JRR-3. In this workshop, the instrument scientists of the neutron scattering instruments in JRR-3 gave talks on the current status of their instruments, and the users of the joint-use program in FY2021 also presented the latest results. The workshop was held only online. There were approximately 50-100 participants on each day. These presentations were accompanied by active discussions, which would contribute to the development of the neutron scattering community in Japan.

Computational Materials Science —New Perspectives—

May 12-13, 2022
H. Noguchi, T. Ozaki, N. Kawashima, O. Sugino, T. Fukushima, K. Ido, M. Kawamura, J. Haruyama, M. Fukuda, S. Morita, F. Oba, T. Ono, H. Watanabe, and Y. Higuchi

This workshop was organized for the computational condensed matter research community, especially for the users of the ISSP supercomputers, to exchange the most recent information on the computational condensed matter research and on the high-performance computation of related research areas. This was held as a series of annual workshops of ISSP supercomputer that has been held every year. This year, it was held in a hybrid style for the first time. Most of talks were presented on-site and also broadcasted online. The posters were presented online. The selected topics include the progress made in the elements strategy projects, the emergent data-driven material research, and the project for advancement of software usability in materials science (PASUMS) that developed the unified platform of experiment-data analysis for 2D material structure and implemented the ESM RISM method in Quantum ESPRESSO in 2021. In addition to 14 invited talks and 32 poster presentations, two special lectures for material informatics were given by Dr. Yoshihiko Takano and Prof. Haruki Watanabe.

Development of 1000-Tesla Science

June 10-11, 2022
Y. Matsuda

This workshop was organized to newly explore ultrahigh magnetic field science in a 1000 T range and have researchers exchange current interests and the latest achievements in the research area. Since the world record of 1200 T in 2018, several scientific results have been obtained such as field-induced insulator-metal phase transition in strongly correlated materials and structural phase transitions in frustrated spin systems. On top of that, several novel measurement techniques such as magneto-striction, electrical impedance in radio-frequency range, and sound velocity have been developed for the destructive ultrahigh magnetic fields, leading to the exploration of a new research area using 1000 T. Researchers from different areas like solid state physics, chemistry, bioscience, particle physics, and plasma science got together. A variety of topics were discussed from the viewpoint of the potential novel effects and phenomena. Among those topics, the magnetic field effect on the ferroelectric phase transition was intensively discussed. Although the phonon has generally been thought to be insensitive to the magnetic field, the strong magnetic field can affect the phonon mode even through direct Lorentz force to the charged ions. The potential magnetic field effect on the ferroelectric material sounded to be one of the most interesting themes in the 1000 T research.

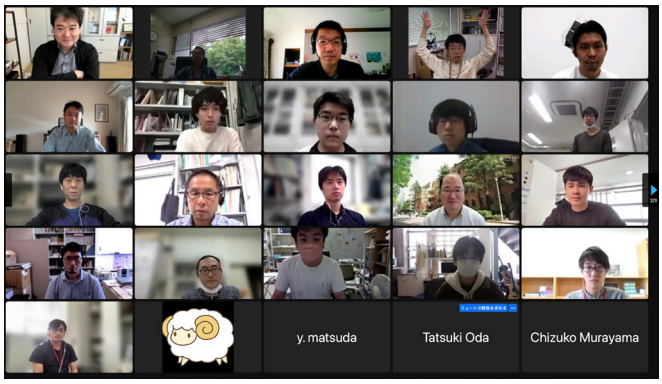

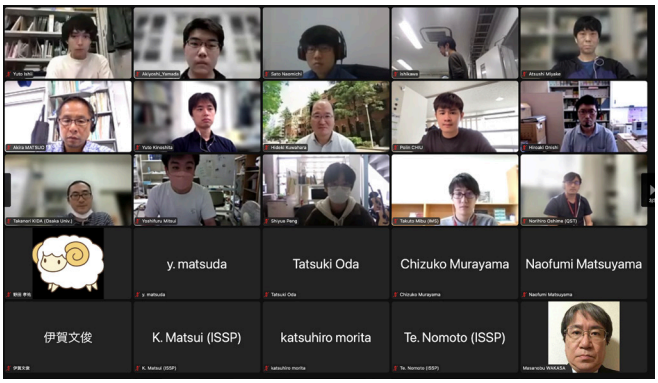

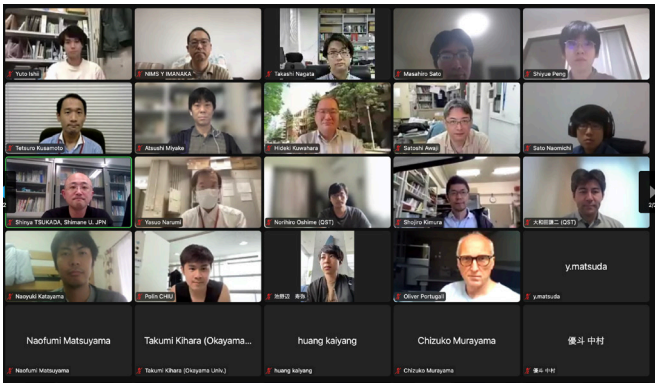

Frontiers of Protein Sciences: Close Collaboration between Theory and Experiment

July 26-27, 2022
H. Noguchi, K. Inoue, and Y. Shigeta

Recent developments in supercomputers and experimental methods have combined to make significant progress in the field of analyses on structures and functions of proteins and organelles in living organisms. In order to exchange information on the latest results and discuss future prospects for joint theoretical, computational, and experimental research in protein science, this ISSP regular workshop was organized in the hybrid type (in person and online) format. In this workshop, 20 lectures were given in a wide range of biophysics fields for both theoretical and experimental studies. Active discussions were also held in 16 poster presentations. The workshop attracted a great deal of attention, with 102 participants registered, including online participants, 26 on-site participants on the first day and 29 on the second day (total of 32), and the maximum number of simultaneous online participants was 67.

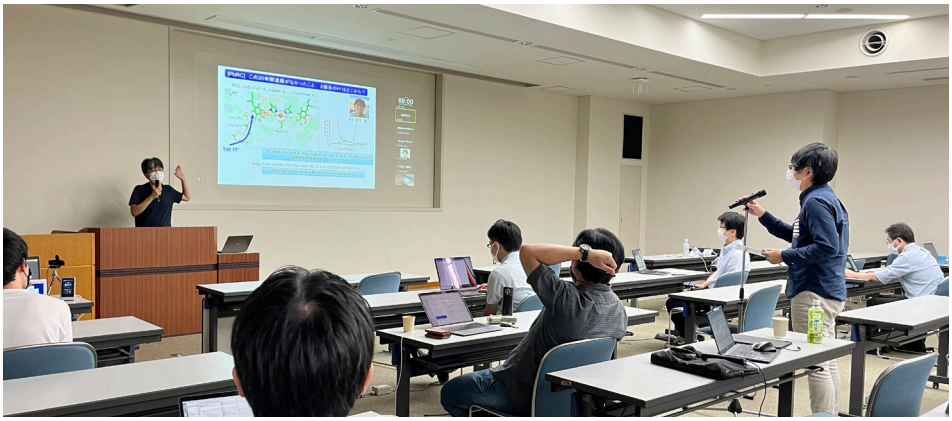

Exchange Meeting for Young Women Condensed Matter Physicists 2022

November 15, 2022
S. Miwa, T. Ideue, K. Inoue, M. Oshikawa, Y. Kohama, T. Nakajima,
H. Noguchi, T. Fujino, I. Matsuda, and M. Lippmaa.

This workshop was organized to support women researchers in the research field of condensed matter physics. This workshop is part of the events of the ISSP Women's Week 2022. In order to organize this workshop, we set up a working group consisting of ISSP professors selected from each division/group/laboratory. We discussed a lot about the style of the workshop and decided that the main purpose of this workshop is to interact with each other. The workshop consists of oral and poster presentations and panel discussions. We invited 25 young women researchers, including assistant professors, postdocs, and graduate students. The presentations cover a wide range of topics in the research fields of physics, chemistry, and biology. All of the presentations were held on the 6th floor of the ISSP main building and were successfully concluded. Especially, in the poster session, not only the female participants but also the members of ISSP joined the discussion and it was very exciting. The number of participants was 63, including 43 on-site and 20 online registrations.

Recent Developments and Future Prospects of Chiral Materials

December 22-24, 2022

H. Kusunose, H. Tsunetsugu, J. Kishine, Y. Togawa, H. Yamamoto, and T. Satoh

Chirality is a significant concept that bridges across multi-scale research fields such as physics, chemistry, biology, and astronomy. Recently, there has been growing interest in the nontrivial couplings among electromagnetic fields, electronic spins and orbitals, phonons, heat current, etc. in chiral systems. In these circumstances, we organized this workshop aimed at stimulating a renaissance in materials science from the perspective of chirality. The specific focused topics include chiral magnetism, chiral phonon, cross-correlated phenomena inherent from chirality, visualization of chirality, chirality-induced spin selectivity (CISS). The workshop was held for three days in a hybrid style, and featured 17 invited talks, 20 contributed talks, and 23 poster presentations, most of which were given on-site. Pre-registrations reached 200 people from a wide range of research fields and generations, and there were 500 participants throughout the workshop (164 on-site, and 336 on-line). The workshop provided an excellent opportunity for researchers from various backgrounds to share the basic concept of chirality, update their understanding of chirality, and promote a cultural exchange that could lead to new collaborations in the near future.

Frontiers of Anyons and Fractional Statistical Particle Studies in Solids

February 13–14, 2023

M. Udagawa, Y. Otani, T. Osada, M. Oshikawa, Y. Kasahara, M. Hashisaka, and M. Yamashita

Anyons, following fractional statistics in two-dimensional systems, are not only interesting in their own right, but are also attracting a great deal of attention as emergent particles in solids that enable topological quantum computing. This workshop was organized to gather researchers studying anyons and Majorana fermions in various systems, including 2D quantum Hall systems, 1D quantum nanowires, topological superconductors, and Kitaev spin liquids. In this workshop, various topics are discussed, such as the progress of braiding experiments in fractional quantum Hall systems, Majorana fermions in topological superconducting states and the challenges of detecting Majorana zero modes in 1D quantum wire experiments, the progress of experiments on the Kitaev candidate α-$RuCl_3$, the mathematics of quantum calculations using non-Abelian anyons, and the challenges for preventing errors in the quantum calculations. We invited 4 keynote speakers for the tutorial presentations and 11 invited speakers to cover the research in these areas, in addition to 11 contributed poster presentations. The meeting was held in a hybrid format, combining a face-to-face meeting in the Media Hall in Kashiwa Campus Library and a Zoom meeting. A total of about 120 people attended the on-site meeting, and nearly 160 people participated online.

Publications (2022.1 - 2023.4)

Division of Condensed Matter Science

Mori group

We have successfully developed and unveiled unprecedented functional properties for the molecular materials and systems. The major achievements in 2022 are (1) to develop the doped EDOT(3,4-ethylenedioxythiophene)-based oligomer conductors, (2) to discover novel anhydrous molecular superproton conductivity of imidazolium dihydrogen phosphate, and (3) to develop ambipolar nickel dithiolene complex semiconductors.

1. Terahertz Radiation with Multi-Narrowband Components via Photoinduced Melting of Charge Order in an Electronic-Type Ferroelectric Organic α-(BEDT-TTF)$_2$I$_3$: Y. Kinoshita, H. Yamakawa, T. Miyamoto, K. Yamamoto, H. Mori, H. Okamoto and N. Kida, J. Phys. Soc. Jpn. 91, 094705 (2022).
2. *Charge and spin interplay in a molecular-dimer-based organic Mott insulator: N. Drichko, S. Sugiura, M. Yamashita, A. Ueda, S. Uji, N. Hassan, Y. Sunairi, H. Mori, E. I. Zhilyaeva, S. Torunova and R. N. Lyubovskaya, Phys. Rev. B 106, 064202 (2022).
3. †Proton–electron-coupled functionalities of conductivity, magnetism, and optical properties in molecular crystals: H. Mori, S. Yokomori, S. Dekura and A. Ueda, Chem. Commun. 58, 5668 (2022).
4. Conjugation length effect on the conducting behavior of single-crystalline oligo(3,4-ethylenedioxythiophene) (n EDOT) radical cation salts: R. Kameyama, T. Fujino, S. Dekura and H. Mori, Phys. Chem. Chem. Phys. 24, 9130 (2022).
5. *Band-filling effects in single-crystalline oligomer models for doped PEDOT: 3,4-ethylenedioxythiophene (EDOT) dimer salt with hydrogen-bonded infinite sulfate anion chains: R. Kameyama, T. Fujino, S. Dekura, S. Imajo, T. Miyamoto, H. Okamoto and H. Mori, J. Mater. Chem. C 10, 7543 (2022).
6. †Molecular Arrangement Control of [1]Benzothieno[3,2- b][1]benzothiophene (BTBT) via Charge-Assisted Hydrogen Bond: R. Akai, K. Oka, S. Dekura, H. Mori and N. Tohnai, BCSJ 95, 1178 (2022).
7. Isotropic Anhydrous Superprotonic Conductivity Cooperated with Installed Imidazolium Molecular Motions in a 3D Hydrogen-Bonded Phosphate Network: S. Dekura, M. Mizuno and H. Mori, Angew Chem Int Ed 61, e202212872(1-7) (2022).
8. †*Ambipolar Nickel Dithiolene Complex Semiconductors: From One- to Two-Dimensional Electronic Structures Based upon Alkoxy Chain Lengths: M. Ito, T. Fujino, L. Zhang, S. Yokomori, T. Higashino, R. Makiura, K. J. Takeno, T. Ozaki and H. Mori, J. Am. Chem. Soc. 145, 2127 (2023).
9. †Neutral Radical Molecular Conductors Based on a Gold Dimethoxybenzenedithiolene Complex with and without Crystal Solvent: S. Yokomori, S. Dekura, A. Ueda, T. Higashino and H. Mori, Chem. Lett. 52, 25 (2023).
10. †*Precise Control of the Molecular Arrangement of Organic Semiconductors for High Charge Carrier Mobility: R. Akai, K. Oka, S. Dekura, K. Yoshimi, H. Mori, R. Nishikubo, A. Saeki and N. Tohnai, J. Phys. Chem. Lett. 14, 3461 (2023).
11. 水素を使いこなすためのサイエンス ハイドロジェノミクス : 森 初果 , (共立出版 , ISBN 978-4-320-04498-2, 2022).

Osada group

We have theoretically and experimentally established that the quantum thermoelectric Hall effect (QTHE) appears even in the 3D semimetals with straight nodal lines. It corresponds to the QTHE in 3D Dirac/Weyl semimetals with nodal points. In the QTHE, the plateau-like constant thermoelectric Hall conductivity α_{xy} is observed at the high-magnetic-field quantum limit. When the magnetic field is parallel to the nodal lines, the n=0 ground Landau subband of the nodal line semimetal plays the similar role as the pair of the n=0 chiral Landau subbands of Dirac/Weyl semimetals. We successfully observed the QTHE, which quantitatively agrees with the theoretical calculation, in bulk graphite with straight nodal lines. We also discussed the

* Joint research among groups within ISSP.

dimensional crossover of the QTHE from 3D to 2D in graphite thin-films.

1. Observation of possible nonlinear anomalous Hall effect in organic two-dimensional Dirac fermion system: A. Kiswandhi and T. Osada, J. Phys.: Condens. Matter **34**, 105602(1-7) (2022).

2. Thermoelectric Hall Effect at High-Magnetic-Field Quantum Limit in Graphite as a Nodal-Line Semimetal: T. Osada, T. Ochi and T. Taen, J. Phys. Soc. Jpn. **91**, 063701(1-4) (2022).

3. Weak localization on moire superlattice in twisted double bilayer graphene: M. Kashiwagi, T. Taen, K. Uchida, K. Watanabe, T. Taniguchi and T. Osada, Jpn. J. Appl. Phys. **61**, 100907(1-5) (2022).

4. 有機ディラック電子系におけるトポロジカル輸送現象：長田 俊人，固体物理 **57**, 227-240 (2022).

5. 有機ディラック電子系における非線形トポロジカル輸送現象： 長田　俊人，キスワンディ　アンディカ，日本物理学会誌 **77**, 233-238 (2022).

6. Quantized thermoelectric Hall plateau in the quantum limit of graphite as a nodal-line semimetal: A. Kiswandhi, T. Ochi, T. Taen, M. Sato, K. Uchida and T. Osada, Phys. Rev. B **107**, 195106(1-5) (2023).

Yamashita group

We have been studying (1) quantum criticality in heavy-fermion materials by ultralow temperature cryostat, (2) thermal-Hall conductivity of exotic excitations in frustrated magnets and (3) a new technique for the study of strongly-correlated electron systems. In this year, we have performed (1) ultralow-temperature resistivity measurements of UTe_2, (2) thermal-Hall measurements of AFM skyrmions in $MnSc_2S_4$, (3) spontaneous thermal Hall measurements of candidate materials of chiral superconductivity, and (4) NMR measurements of $EuIn_2As_2$.

1. Anomalous electromagnetic response in the spin-triplet superconductor UTe_2: Y. Shimizu, S. Kittaka, Y. Kono, T. Sakakibara, K. Machida, A. Nakamura, D. Li, Y. Homma, Y. J. Sato, A. Miyake, M. Yamashita and D. Aoki, Phys. Rev. B **106**, 214525 (2022).

2. *Charge and spin interplay in a molecular-dimer-based organic Mott insulator: N. Drichko, S. Sugiura, M. Yamashita, A. Ueda, S. Uji, N. Hassan, Y. Sunairi, H. Mori, E. I. Zhilyaeva, S. Torunova and R. N. Lyubovskaya, Phys. Rev. B **106**, 064202 (2022).

3. Resistivity and thermal conductivity of an organic insulator β'–$EtMe_3Sb[Pd(dmit)_2]_2$: M. Yamashita, Y. Sato, Y. Kasahara, S. Kasahara, T. Shibauchi and Y. Matsuda, Scientific Reports **12**, 9187 (2022).

4. Field-induced topological Hall effect in antiferromagnetic axion insulator candidate $EuIn_2As_2$: J. Yan, Z. Z. Jiang, R. C. Xiao, W. J. Lu, W. H. Song, X. B. Zhu, X. Luo, Y. P. Sun and M. Yamashita, Phys. Rev. Research **4**, 013163 (2022).

5. Planar thermal Hall effects in the Kitaev spin liquid candidate $Na_2Co_2TeO_6$: H. Takeda, J. Mai, M. Akazawa, K. Tamura, J. Yan, K. Moovendaran, K. Raju, R. Sankar, K.-Y. Choi and M. Yamashita, Phys. Rev. Research **4**, L042035 (2022).

6. Topological thermal Hall effect of magnons in magnetic skyrmion lattice: M. Akazawa, H.-Y. Lee, H. Takeda, Y. Fujima, Y. Tokunaga, T.-H. Arima, J. H. Han and M. Yamashita, Phys. Rev. Research **4**, 043085 (2022).

Ideue group

We have investigated the optical and magnetic properties of layered van der Waals crystals. By applying strain, we have successfully controlled the symmetry of 3R-MoS_2 and demonstrated the giant enhancement of bulk photovoltaic effect reflecting the polar structure. In addition, we have clarified that photovoltaic property along the out-of-plane direction is affected by the stacking sequence of two-dimensional semiconductors. We have also reported the effective modulation of magnetic properties such as transition temperature and magnetic anisotropy by applying pressure or electrolyte gating.

1. 空間反転対称性の破れた結晶における整流現象：井手上　敏也，板橋　勇輝，岩佐　義宏，日本物理学会誌 **77**, 475-480 (2022).

2. Spontaneous-polarization-induced photovoltaic effect in rhombohedrally stacked MoS_2: D. Yang, J. Wu, B. T. Zhou, J. Liang, T. Ideue, T. Siu, K. M. Awan, K. Watanabe, T. Taniguchi, Y. Iwasa, M. Franz and Z. Ye, Nat. Photon. **16**, 469-474 (2022).

3. Magnetic Anisotropy Control with Curie Temperature above 400 K in a van der Waals Ferromagnet for Spintronic Device: Z. Li, M. Tang, J. Huang, F. Qin, L. Ao, Z. Shen, C. Zhang, P. Chen, X. Bi, C. Qiu, Z. Yu, K. Zhai, T. Ideue, L.

† Joint research with outside partners.

Wang, Z. Liu, Y. Tian, Y. Iwasa and H. Yuan, Advanced Materials **34**, 2201209 (2022).

4. Giant bulk piezophotovoltaic effect in 3R-MoS_2: Y. Dong, M.-M. Yang, M. Yoshii, S. Matsuoka, S. Kitamura, T. Hasegawa, N. Ogawa, T. Morimoto, T. Ideue and Y. Iwasa, Nat. Nanotechnol. **18**, 36-41 (2023).

5. Continuous manipulation of magnetic anisotropy in a van der Waals ferromagnet via electrical gating: M. Tang, J. Huang, F. Qin, K. Zhai, T. Ideue, Z. Li, F. Meng, A. Nie, L. Wu, X. Bi, C. Zhang, L. Zhou, P. Chen, C. Qiu, P. Tang, H. Zhang, X. Wan, L. Wang, Z. Liu, Y. Tian, Y. Iwasa and H. Yuan, Nat. Electron. **6**, 28-36 (2023).

Division of Condensed Matter Theory

Tsunetsugu group

We have collaborated with the visiting professor, Dr. Hiroaki Kusunose, and investigated fundamental properties of phonons in chiral crystals. The main issue is how to characterize the splitting in the phonon energy dispersion between two chiral modes with different crystal angular momentum (CAM), which is specific to the systems with chiral crystal structure. Examining necessary conditions for their dynamical matrix, we have proved that the sound velocity is identical for the two chiral modes with CAM +1 and –1, which invalidates precedent some discussions expecting its splitting. The effects of chiral structure are manifested in a linear energy splitting of the optical phonon modes and we have derived a simple formula for its linear coefficient represented in terms of parameters in the microscopic model. This is a pseudo-scalar and related to electric toroidal monopole G_0 of the system.

1. *Stimulated Rayleigh Scattering Enhanced by a Longitudinal Plasma Mode in a Periodically Driven Dirac Semimetal Cd_3As_2: Y. Murotani, N. Kanda, T. N. Ikeda, T. Matsuda, M. Goyal, J. Yoshinobu, Y. Kobayashi, S. Stemmer and R. Matsunaga, Phys. Rev. Lett. **129**, 207402 (2022).

2. Diabatic and adiabatic transitions between Floquet states imprinted in coherent exciton emission in monolayer WSe_2: K. Uchida, S. Kusaba, K. Nagai, T. N. Ikeda and K. Tanaka, Science Advances **8**, eabq7281 (2022).

3. Criticality and rigidity of dissipative discrete time crystals in solids: K. Chinzei and T. N. Ikeda, Phys. Rev. Research **4**, 023025 (2022).

4. Floquet-Landau-Zener interferometry: Usefulness of the Floquet theory in pulse-laser-driven systems: T. N. Ikeda, S. Tanaka and Y. Kayanuma, Phys. Rev. Research **4**, 033075 (2022).

5. †Theory of Energy Dispersion of Chiral Phonons: H. Tsunetsugu and H. Kusunose, J. Phys. Soc. Jpn. **92**, 023601 (2023).

6. ユニークな四極子秩序の安定化機構の発見：服部 一匡，石飛 尊之，常次 宏一，固体物理 **57**, 255-266 (2022).

Kato group

The main research subject of Kato Lab. is transport properties in mesoscopic and spintronic devices. We studied (1) heat transport through a two-level system under continuous quantum measurement, (2) spin pumping from ferromagnetic insulators to unconventional superconductors and anisotropic Dirac systems, (3) non-adiabatic corrections in electronic transport through a quantum dot, (4) spin Hall magnetoresistance in metals coupled with two-dimensional spin systems, (5) high-harmonic generation in distorted graphens, and (6) nonequilibrium noise in the BCS-BEC crossover.

1. Kondo Effect and Phase Measurement in Double Quantum Dot in Parallel: Y. Zhang, R. Sakano and M. Eto, J. Phys. Soc. Jpn. **91**, 014703(1-10) (2022).

2. Nonadiabatic Correction and Adiabatic Criteria of Noninteracting Quantum Dot Systems: M. Hasegawa and T. Kato, J. Phys. Soc. Jpn. **91**, 074705(1-8) (2022).

3. Current noise and Keldysh vertex function of an Anderson impurity in the Fermi-liquid regime: A. Oguri, Y. Teratani, K. Tsutsumi and R. Sakano, Phys. Rev. B **105**, 115409(1-37) (2022).

4. Ferromagnetic resonance modulation in d-wave superconductor/ferromagnetic insulator bilayer systems: Y. Ominato, A. Yamakage, T. Kato and M. Matsuo, Phys. Rev. B **105**, 205406(1-7) (2022).

5. Heat transport through a two-level system under continuous quantum measurement: T. Yamamoto, Y. Tokura and T. Kato, Phys. Rev. B **106**, 205419 (2022).

* Joint research among groups within ISSP.

6. Spin pumping into anisotropic Dirac electrons: T. Funato, T. Kato and M. Matsuo, Phys. Rev. B **106**, 144418(1-10) (2022).

7. Einstein–de Haas Nanorotor: W. Izumida, R. Okuyama, K. Sato, T. Kato and M. Matsuo, Phys. Rev. Lett. **128**, 017701(1-6) (2022).

8. †*TeNeS: Tensor network solver for quantum lattice systems: Y. Motoyama, T. Okubo, K. Yoshimi, S. Morita, T. Kato and N. Kawashima, Computer Physics Communications **279**, 108437 (2022).

9. Fluctuation theorem for spin transport at insulating ferromagnetic junctions: T. Sato, M. Tatsuno, M. Matsuo and T. Kato, Journal of Magnetism and Magnetic Materials **546**, 168814(1-6) (2022).

10. †*MateriApps LIVE! and MateriApps Installer: Environment for starting and scaling up materials science simulations: Y. Motoyama, K. Yoshimi, T. Kato and S. Todo, SoftwareX **20**, 101210 (2022).

11. Effect of vertex corrections on the enhancement of Gilbert damping in spin pumping into a two-dimensional electron gas: M. Yama, M. Matsuo and T. Kato, Phys. Rev. B **107**, 174414 (2023).

12. *Shear-strain controlled high-harmonic generation in graphene: T. Tamaya, H. Akiyama and T. Kato, Phys. Rev. B **107**, L081405 (2023).

13. Spin Hall magnetoresistance in quasi-two-dimensional antiferromagnetic-insulator/metal bilayer systems: T. Ishikawa, M. Matsuo and T. Kato, Phys. Rev. B **107**, 054426 (2023).

14. Nonequilibrium noise as a probe of pair-tunneling transport in the BCS–BEC crossover: H. Tajima, D. Oue, M. Matsuo, T. Kato and D. Abbott, PNAS Nexus **2**, pgad045 (2023).

15. 電子スピンにより駆動するナノモーター：泉田 渉，奥山 倫，加藤 岳生，松尾 衛，固体物理 **57**, 547-554 (2022).

16. 一歩進んだ理解を目指す物性物理学講義：加藤 岳生，(サイエンス社，東京，2022).

17. 電磁気学入門 (物理学レクチャーコース): 加藤 岳生，(裳華房，東京，2022).

Division of Nanoscale Science

Katsumoto group

We have experimentally found that an increase in the curvature of the electron orbit increases the portion of non-adiabatic transition at the orbital corner. This is used in the realization of a "half-mirror" device in which the wave function is equally distributed between two edge states. By using the recursive Green function method, the experiment was successfully reproduced. A Mach-Zehnder (MZ) interferometer consisting of such half mirrors showed high visibility of over 60%. Moreover, the coherence length of over 0.6 mm is an order of magnitude compared to MZ interferometers using ordinary edge states. This surprisingly high coherence is attributed to the closeness of the two edge states.

1. Joule heating and the thermal conductivity of a two-dimensional electron gas at cryogenic temperatures studied by modified 3ω method: A. Endo, S. Katsumoto and Y. Iye, Journal of Applied Physics **132**, 104302 (2022).

2. Anisotropic Behavior of the Thermoelectric Power and the Thermal Conductivity in a Unidirectional Lateral Superlattice: A Typical Anisotropic System Exhibiting Two Distinct Nernst Coefficients: A. Endo, S. Katsumoto and Y. Iye, J. Phys. Soc. Jpn. **92**, 044705 (2023).

3. Half-Mirror for Electrons in Quantum Hall Copropagating Edge Channels in a Mach-Zehnder Interferometer: T. Shimizu, J.-I. Ohe, A. Endo, T. Nakamura and S. Katsumoto, Phys. Rev. Applied **19**, 034085 (2023).

Otani group

This year, our research on antiferromagnetic spintronics advanced as we successfully manipulated the cluster magnetic octupole state in M_3X (X=Mn or Sn) thin films and achieved complete switching of the state using epitaxial thin films through spin-orbit torque. We also explored the spin Hall effect in the Weyl ferromagnet Co_2MnGa and identified that the anomalous Nernst effect could contribute up to 75% of the total measured signal. Additionally, we investigated efficient pattern recognition with neuromorphic computing by utilizing the magnetic field-induced dynamics of skyrmions. Our research extended to magnon-phonon coupling as well, where we developed a theoretical formulation for the interaction between surface acoustic waves and spin waves in ferromagnetic thin films. Furthermore, we observed intriguing behaviors in voltage signals under out-of-plane

† Joint research with outside partners.

external magnetic fields caused by surface acoustic wave-driven ferromagnetic resonance. Our studies on molecular chirality and metallic thin films demonstrated the chirality-induced magnetoresistance due to thermally driven spin polarization. Finally, our international collaborative investigations uncovered thickness-dependent reconfigurable spin-wave dynamics in $Ni_{80}Fe_{20}$ nanostripe arrays. We also explored the role of spin-orbit coupling in ultrafast spin dynamics in nonmagnet/ferromagnet heterostructures. These findings offer valuable insights into the fundamental mechanisms of spintronics and pave the way for developing novel technologies and applications in this rapidly-evolving field.

1. Efficient orbital torque in polycrystalline ferromagnetic−metal/Ru/Al_2O_3 stacks: Theory and experiment: L. Liao, F. Xue, L. Han, J. Kim, R. Zhang, L. Li, J. Liu, X. Kou, C. Song, F. Pan and Y. Otani, Phys. Rev. B **105**, 104434 (2022).

2. Perspectives on spintronics with surface acoustic waves: J. Puebla, Y. Hwang, S. Maekawa and Y. Otani, Appl. Phys. Lett. **120**, 220502 (2022).

3. *Chirality-Induced Magnetoresistance Due to Thermally Driven Spin Polarization: K. Kondou, M. Shiga, S. Sakamoto, H. Inuzuka, A. Nihonyanagi, F. Araoka, M. Kobayashi, S. Miwa, D. Miyajima and Y. Otani, J. Am. Chem. Soc. **144**, 7302-7307 (2022).

4. *Perpendicular full switching of chiral antiferromagnetic order by current: T. Higo, K. Kondou, T. Nomoto, M. Shiga, S. Sakamoto, X. Chen, D. Nishio-Hamane, R. Arita, Y. Otani, S. Miwa and S. Nakatsuji, Nature **607**, 474-479 (2022).

5. Pattern recognition with neuromorphic computing using magnetic field–induced dynamics of skyrmions: T. Yokouchi, S. Sugimoto, B. Rana, S. Seki, N. Ogawa, Y. Shiomi, S. Kasai and Y. Otani, Sci. Adv. **8**, eabq5652 (2022).

6. *Determination of spin Hall angle in the Weyl ferromagnet Co_2MnGa by taking into account the thermoelectric contributions: H. Isshiki, Z. Zhu, H. Mizuno, R. Uesugi, T. Higo, S. Nakatsuji and Y. Otani, Phys. Rev. Materials **6**, 084411 (2022).

7. Interaction between surface acoustic waves and spin waves in a ferromagnetic thin film: K. Yamamoto, M. Xu, J. Puebla, Y. Otani and S. Maekawa, Journal of Magnetism and Magnetic Materials **545**, 168672 (2022).

8. Orbital angular momentum for spintronics: J. Kim and Y. Otani, Journal of Magnetism and Magnetic Materials **563**, 169974 (2022).

9. Electric field induced parametric excitation of exchange magnons in a CoFeB/MgO junction: A. Deka, B. Rana, R. Anami, K. Miura, H. Takahashi, Y. Otani and Y. Fukuma, Phys. Rev. Research **4**, 023139 (2022).

10. Efficient and controllable magnetization switching induced by intermixing-enhanced bulk spin–orbit torque in ferromagnetic multilayers: K. Zhang, L. Chen, Y. Zhang, B. Hong, Y. He, K. Lin, Z. Zhang, Z. Zheng, X. Feng, Y. Zhang, Y. Otani and W. Zhao, Applied Physics Reviews **9**, 011407 (2022).

11. Thickness-Dependent Reconfigurable Spin-Wave Dynamics in $Ni_{80}Fe_{20}$ Nanostripe Arrays: P. K. Pal, S. Sahoo, K. Dutta, A. Barman, S. Barman and Y. Otani, Adv Materials Inter **9**, 2201333 (2022).

12. Voltage Signals Caused by Surface Acoustic Wave Driven Ferromagnetic Resonance Under Out-of-Plane External Fields: Y. Hwang, J. Puebla, K. Kondou and Y. Otani, Adv Materials Inter **9**, 2201432 (2022).

13. Giant effective Zeeman splitting in a monolayer semiconductor realized by spin-selective strong light–matter coupling: T. P. Lyons, D. J. Gillard, C. Leblanc, J. Puebla, D. D. Solnyshkov, L. Klompmaker, I. A. Akimov, C. Louca, P. Muduli, A. Genco, M. Bayer, Y. Otani, G. Malpuech and A. I. Tartakovskii, Nat. Photon. **16**, 632 (2022).

14. Role of Spin–Orbit Coupling on Ultrafast Spin Dynamics in Nonmagnet/Ferromagnet Heterostructures: S. N. Panda, B. Rana, Y. Otani and A. Barman, Adv Quantum Tech **5**, 2200016 (2022).

15. *High-resolution magnetic imaging by mapping the locally induced anomalous Nernst effect using atomic force microscopy: N. Budai, H. Isshiki, R. Uesugi, Z. Zhu, T. Higo, S. Nakatsuji and Y. Otani, Appl. Phys. Lett. **122**, 102401 (2023).

16. *Temperature-induced anomalous magnetotransport in the Weyl semimetal Mn_3Ge: M. Wu, K. Kondou, T. Chen, S. Nakatsuji and Y. Otani, AIP Advances **13**, 045102 (2023).

17. Emergence of spin–charge conversion functionalities due to spatial and time-reversal asymmetries and chiral symmetry: K. Kondou and Y. Otani, Front. Phys. **11**, 1140286 (2023).

Hasegawa group

Disorder-induced superconductor-insulator transition (SIT) in the two-dimensional (2D) systems has been a subject of extensive studies as one of the quantum phase transitions (QPT). Recent advancements in the fabrication of highly crystalline 2D system revealed the presence of anomalous metallic state and quantum Griffiths phase around QPT. The origins of such new phases are

* Joint research among groups within ISSP.

still under debate partly because of lack of microscopic understanding. In 2022, we performed scanning tunnelling spectroscopy (STM) on highly-crystalline Pb monoatomic-layer superconductors formed on vicinal substrates with various miscut angles to investigate these phases microscopically and to reveal how their presences are affected by the introduction of disorder. Our results revealed the presence of stable vortices in the regime of the quantum metallic state. The vortex liquid phase, which was expected in the metallic regime, was observed in a small portion of the regime only on vicinal substrates, suggesting that the metallic resistance is driven by infinitesimal current in the transport measurements. A pseudogap was also observed above the critical magnetic fields presumably due to the localization of the Cooper pairs induced by quantum fluctuation.

1. †Multiband superconductivity in strongly hybridized 1T'−WTe_2/$NbSe_2$ heterostructures: W. Tao, Z. J. Tong, A. Das, D.-Q. Ho, Y. Sato, M. Haze, J. Jia, Y. Que, F. Bussolotti, K. E. Johnson Goh, B. Wang, H. Lin, A. Bansil, S. Mukherjee, Y. Hasegawa and B. Weber, Phys. Rev. B **105**, 094512 (1-14) (2022).

2. Numerical simulations for ferromagnetic resonance of nano-size island structures probed by radio-frequency scanning tunneling microscopy: Y. Sato, M. Haze, H.-H. Yang, K. Asakawa, S. Takahashi and Y. Hasegawa, Jpn. J. Appl. Phys. **61**, 025001 (1-6) (2022).

3. Squeezed Abrikosov-Josephson Vortex in Atomic-Layer Pb Superconductors Formed on Vicinal Si(111) Substrates: Y. Sato, M. Haze, R. Nemoto, W. Qian, S. Yoshizawa, T. Uchihashi and Y. Hasegawa, Phys. Rev. Lett. **130**, 106002 1-6 (2023).

4. スパースモデリングを活用した走査トンネル顕微鏡像解析：土師 将裕，吉田 靖雄，長谷川 幸雄，表面と真空 **65**, 78-83 (2022).

Lippmaa group

We are developing a machine learning approach to the analysis of reflection high-energy electron diffraction images. The purpose is to capture in real time, during thin film growth, the phase composition of a thin film surface. A neural network is thus used to extract diffraction features from the diffraction patterns, followed by periodicity and intensity analysis to extract composition information. Besides inorganic thin films grown by pulsed laser deposition, we study organic molecular layer formation on the water surface and the formation of Langmuir-Blodgett films.

1. Mechanical Tuning of Aggregated States for Conformation Control of Cyclized Binaphthyl at the Air–Water Interface: M. Ishii, T. Mori, W. Nakanishi, J. P. Hill, H. Sakai and K. Ariga, Langmuir **38**, 6481 (2022).

2. Critical Role of Terminating Layer in Formation of 2DEG State at the $LaInO_3$/$BaSnO_3$ Interface: S. Kim, M. Lippmaa, J. Lee, H. Cho, J. Kim, B. Kim and K. Char, Adv. Mater. Interfaces **9**, 2201781 (1-7) (2022).

3. Effects of shape and solute-solvent compatibility on the efficacy of chirality transfer: Nanoshapes in nematics: A. Nemati, L. Querciagrossa, C. Callison, S. Shadpour, D. P. N. Gonçalves, T. Mori, X. Cui, R. Ai, J. Wang, C. Zannoni and T. Hegmann, Sci. Adv. **8**, eabl4385 (2022).

4. Application of machine learning to reflection high-energy electron diffraction images for automated structural phase mapping: H. Liang, V. Stanev, A. G. Kusne, Y. Tsukahara, K. Ito, R. Takahashi, M. Lippmaa and I. Takeuchi, Phys. Rev. Materials **6**, 063805 (1-9) (2022).

5. Coordination Amphiphile: Design of Planar-Coordinated Platinum Complexes for Monolayer Formation at an Air-Water Interface Based on Ligand Characteristics and Molecular Topology: J. Adachi, M. Naito, S. Sugiura, N.-T. Le, S. Nishimura, S. Huang, S. Suzuki, S. Kawamorita, N. Komiya, J. P. Hill, K. Ariga, T. Naota and T. Mori, BCSJ **95**, 889 (2022).

6. Vortex Flow-controlled Circularly Polarized Luminescence of Achiral Pt(II) Complex Aggregates Assembled at the Air-Water Interface (Small Methods 12/2022): T. Maeda, T. Mori, M. Ikeshita, S. C. Ma, G. Muller, K. Ariga and T. Naota, Small Methods **6**, 2270071 (2022).

7. *Semiconducting Electronic Structure of the Ferromagnetic Spinel $HgCr_2Se_4$ Revealed by Soft-X-Ray Angle-Resolved Photoemission Spectroscopy: H. Tanaka, A. V. Telegin, Y. P. Sukhorukov, V. A. Golyashov, O. E. Tereshchenko, A. N. Lavrov, T. Matsuda, R. Matsunaga, R. Akashi, M. Lippmaa, Y. Arai, S. Ideta, K. Tanaka, T. Kondo and K. Kuroda, Phys. Rev. Lett. **130**, 186402 (1-6) (2023).

8. 機械学習による意思決定とデータ解釈：物質合成パラメータの最適化と in situ 測定結果の自動解析：大久保 勇男 and M. Lippmaa,「ケモインフォマティクスにおけるデータ収集の最適化と解析手法」5, (株式会社技術情報協会，Tokyo, 2023), 359-366.

† Joint research with outside partners.

Yoshinobu group

We conducted several research projects in the fiscal year 2022: (1) The surface chemistry of hydrogen, formic acid and CO_2 on Pd-Cu(111), Cu(997), Cu(977) and Pd-Cu(977) surfaces was studied by SR-PES, IRAS, HREELS and TPD. (2) The adsorption/desorption of CH_4 on Pt(997) was studied by TPD, IRAS, SR-XPS and van der Waals DFT. (3) The dry reforming process of CH_4 with CO_2 on Pt(997) was studied by AP-XPS at SPring-8. (4) The reaction dynamics of CO + O -> CO_2 on Pt(111) was studied by ab-initio molecular dynamics (AIMD) with van der Waals DFT. (5) The reaction of MoS_2 basal plane and the edge of MoS_2 in vacuum and under hydrogen pressure was studied by AP-XPS at SPring-8 and DFT calculations. (6) Hydrogenation of CO_2 using a hydrogen-permeable PdCu alloy membrane, and (7) The newly constructed narrow band and broad band THz pulse system has been applied to the surface chemistry on Pt(111).

1. *Stimulated Rayleigh Scattering Enhanced by a Longitudinal Plasma Mode in a Periodically Driven Dirac Semimetal Cd_3As_2: Y. Murotani, N. Kanda, T. N. Ikeda, T. Matsuda, M. Goyal, J. Yoshinobu, Y. Kobayashi, S. Stemmer and R. Matsunaga, Phys. Rev. Lett. **129**, 207402 (2022).

2. †Substrate-Selective Intermolecular Interaction and the Molecular Self-Assemblies: 1,3,5-Tris(4-bromophenyl)benzene Molecules on the Ag(111) and Si(111) (√3 × √3)-Ag Surfaces: N. Tsukahara and J. Yoshinobu, Langmuir **38**, 8881 (2022).

3. Adsorption, Desorption, and Decomposition of Formic Acid on Cu(977): The Importance of Facet of the Step: W. Osada, S. Tanaka, K. Mukai, Y. H. Choi and J. Yoshinobu, J. Phys. Chem. C **126**, 8354 (2022).

4. *Elucidation of the atomic-scale processes of dissociative adsorption and spillover of hydrogen on the single atom alloy catalyst Pd/Cu(111): W. Osada, S. Tanaka, K. Mukai, M. Kawamura, Y. Choi, F. Ozaki, T. Ozaki and J. Yoshinobu, Phys. Chem. Chem. Phys. **24**, 21705-21713 (2022).

5. †*Materials Science Research by Ambient Pressure X-ray Photoelectron Spectroscopy Systems at Synchrotron Radiation Facilities in Japan: Applications in Energy, Catalysis, and Sensors: S. Yamamoto, Y. Takagi, T. Koitaya, R. Toyoshima, M. Horio, I. Matsuda, H. Kondoh, T. Yokoyama and J. Yoshinobu, Synchrotron Radiation News **35**, 19-25 (2022).

6. †*Functionalization of the MoS_2 basal plane for activation of molecular hydrogen by Pd deposition: F. Ozaki, S. Tanaka, W. Osada, K. Mukai, M. Horio, T. Koitaya, S. Yamamoto, I. Matsuda and J. Yoshinobu, Applied Surface Science **593**, 153313 (2022).

7. †*Hydrogen absorption and diffusion behaviors in cube-shaped palladium nanoparticles revealed by ambient-pressure X-ray photoelectron spectroscopy: J. Tang, O. Seo, D. S. R. Rocabado, T. Koitaya, S. Yamamoto, Y. Nanba, C. Song, J. Kim, A. Yoshigoe, M. Koyama, S. Dekura, H. Kobayashi, H. Kitagawa, O. Sakata, I. Matsuda and J. Yoshinobu, Applied Surface Science **587**, 152797 (2022).

8. *Tracking Ultrafast Change of Multiterahertz Broadband Response Functions in a Photoexcited Dirac Semimetal Cd_3As_2 Thin Film: N. Kanda, Y. Murotani, T. Matsuda, M. Goyal, S. Salmani-Rezaie, J. Yoshinobu, S. Stemmer and R. Matsunaga, Nano Letters **22**, 2358 (2022).

9. †Enhanced Rashba Splitting of Au(111) Surface States with Hydrogen-Bonded Melamine-Based Organic Framework: R. Moue, Y. Kokubo, K. Mukai, H. Mizushima, Y. Fukushima, K. Kawaguchi, T. Kondo, A. Harasawa, J. Yoshinobu, K. Mase, S. Shin and K. Kanai, Adv Materials Inter **9**, 2201102 (2022).

10. Termination of graphene edges created by hydrogen and deuterium plasmas: T. Ochi, M. Kamada, T. Yokosawa, K. Mukai, J. Yoshinobu and T. Matsui, Carbon **203**, 727 (2023).

11. The quantitative study of methane adsorption on the Pt(997) step surface as the initial process for reforming reactions: Y. H. Choi, S. E. M. Putra, Y. Shiozawa, S. Tanaka, K. Mukai, I. Hamada, Y. Morikawa and J. Yoshinobu, Surface Science **732**, 122284 (2023).

12. †*In-Situ Electrical Detection of Methane Oxidation on Atomically Thin IrO_2 Nanosheet Films Down to Room Temperature: Y. Ishihara, T. Koitaya, W. Sugimoto, S. Yamamoto, I. Matsuda, J. Yoshinobu and R. Nouchi, Advanced Materials Interfaces (2023), accepted for publication.

13. Hydrogenomics: Efficient and Selective Hydrogenation of Stable Molecules Utilizing Three Aspects of Hydrogen: K. Fukutani, J. Yoshinobu, M. Yamauchi, T. Shima and S. Orimo, Catal Lett **152**, 1583 (2022).

14. “ 水素 " を使いこなすためのサイエンス ハイドロジェノミクス : 折茂 慎一 , 福谷 克之 , 藤田健 一（編）, (共立出版 , 東京都文京区 , 2022).

* Joint research among groups within ISSP.

Functional Materials Group

Akiyama group

In 2022, we studied ultra-fast gain-switching in 30GHz-modulation-bandwidth 1270nm DFB-type single-mode laser diodes (LDs) with and without chirp compensation, and realized gain-switched 5.3 ps short pulses near the Fourier transform limit. We made processing twice in a year on gain-switched 1030-1060nm InGaAs LDs with revised designs and procedures, and installed them into our original 10 ps LD-seed-pulse prototype modules. We studied on heat-recovery (HERC) solar cells, in collaboration with AIST team, and found output-power equivalence of two- and four-terminal photovoltaic-thermoelectric hybrid tandems. Time-resolved resonant Raman spectroscopy on channel rhodopsin with semiconductor-laser-based light sources has been performed in collaboration with Inoue-group within ISSP, and the first collaboration journal paper on this subject was accomplished. Collaboration work and papers with Hiyama-team in Gunma University were accomplished on quantitative spectroscopy on bioluminescence quantum yield of new luciferin analogs and on photo-cleavage/photo-bleaching quantum yields of D-luciferin and coumarin-caged-luciferins.

1. Theoretical modeling and ultra-thin design for multi-junction solar cells with a light-trapping front surface and its application to InGaP/GaAs/InGaAs 3-junction: L. Zhu, Y. Wang, X. Pan and H. Akiyama, Opt. Express **30**, 35202 (2022).

2. Diagnosis and Breakeven Analysis of GaInNAs Subcell Incorporated in Monolithic Lattice-Matched Five-Junction Solar Cell: L. Zhu, S. Huang and H. Akiyama, IEEE J. Photovoltaics **12**, 1487 (2022).

3. Differences in radiation damage to carrier lifetimes in the neutral and depletion regions of InGaP and GaAs solar cells: T. Nakamura, M. Imaizumi, S.-I. Sato, T. Ohshima, H. Akiyama and Y. Okada, Journal of Applied Physics **132**, 115701 (2022).

4. Gain-switching in $CsPbBr_3$ microwire lasers: J. Tian, G. Weng, Y. Liu, S. Chen, F. Cao, C. Zhao, X. Hu, X. Luo, J. Chu, H. Akiyama and S. Chen, Commun Phys **5**, 160 (2022).

5. †Photo-bleaching of firefly luciferin with UV irradiation: R. Kumagai, R. Ono, H. Akiyama, H. Itabashi and M. Hiyama, Chemical Physics Letters **792**, 139414 (2022).

6. A new lock-in amplifier-based deep-level transient spectroscopy test and measurement system for solar cells: Y. Jia, X. Ding, R. Wang, Y. Wang, S. Zheng, X. Hu, G. Weng, S. Chen, T. Sakurai and H. Akiyama, Solar Energy **244**, 507 (2022).

7. Carrier dynamics of AlGaAs/AlAs asymmetric double quantum wells with different barrier thickness: Y. Liu, G. Weng, F. Cao, Y. Wang, W. Wan, C. Wang, H. Nakamae, C. Kim, X. Hu, X. Luo, S. Luo, S. Chen, J. Chu and H. Akiyama, Opt. Mater. Express **12**, 1291 (2022).

8. Defect-induced current coupling in multi-junction solar cells revealed by absolute electroluminescence imaging: Y. Wang, L. Li, Y. Jia, X. Hu, G. Weng, X. Luo, S. Chen, Z. Zhu, J. Chu and H. Akiyama, Progress in Photovoltaics **30**, 1410 (2022).

9. Revealing Sub-Cell Degradation of Multi-Junction Solar Cells by Absolute Electroluminescence Imaging: Y. Wang, L. Li, X. Hu, Y. Jia, G. Weng, X. Luo, S. Chen and H. Akiyama, Proc. of 2022 IEEE 49th Photovoltaics Specialists Conference **54**, 0468-0471 (2022).

10. *Shear-strain controlled high-harmonic generation in graphene: T. Tamaya, H. Akiyama and T. Kato, Phys. Rev. B **107**, L081405 (2023).

11. Output-power equivalence of two- and four-terminal photovoltaic-thermoelectric hybrid tandems: J. Sakuma, K. Kamide, T. Mochizuki, H. Takato and H. Akiyama, Appl. Phys. Express **16**, 014003 (2023).

12. Optimisation of Sb2S3 thin-film solar cells via Sb_2Se_3 post-treatment: R. Wang, D. Qin, X. Ding, Q. Zhang, Y. Wang, Y. Pan, G. Weng, X. Hu, J. Tao, J. Chu, H. Akiyama and S. Chen, Journal of Power Sources **556**, 232451 (2023).

13. †Photo-cleaving and photo-bleaching quantum yields of coumarin-caged luciferin: R. Kumagai, R. Ono, S. Sakimoto, C. Suzuki, K.-I. Kanno, H. Aoyama, J. Usukura, M. Kobayashi, H. Akiyama, H. Itabashi and M. Hiyama, Journal of Photochemistry and Photobiology A: Chemistry **434**, 114230 (2023).

14. †Quantum yield of near-infrared bioluminescence with firefly luciferin analog: AkaLumine: R. Ono, K. Osawa, Y. Takahashi, Y. Noguchi, N. Kitada, R. Saito-Moriya, T. Hirano, S. A. Maki, K. Shibata, H. Akiyama, K.-I. Kanno, H. Itabashi and M. Hiyama, Journal of Photochemistry and Photobiology A: Chemistry **434**, 114270 (2023).

† Joint research with outside partners.

Sugino group

We have developed the exchange-correlation functional of the density functional theory for solids based on machine learning. We also studied activity of the oxygen reduction reaction occurring on the defective zirconia electrode. We further studied the cuprate superconductor using an advanced exchange-correlation functional. We also did collaborating works on the many-body greens function method, a topological material, and so on.

1. †Development of the Bethe-Salpeter method considering second-order corrections for a *GW* electron-hole interaction kernel: S. Yamada, Y. Noguchi, K. Ishii, D. Hirose, O. Sugino and K. Ohno, Phys. Rev. B **106**, 045113 (2022).

2. †*Homotopic analysis of quantum states in two-dimensional polymorphs by a herringbone lattice model: Y. Ando, X. Zhang, Y. Tsujikawa, Y. Sato, M. Horio, J. Haruyama, O. Sugino, T. Kondo and I. Matsuda, Phys. Rev. B **106**, 195106 (2022).

3. †Effect of Nitrogen Doping and Oxygen Vacancy on the Oxygen Reduction Reaction on the Tetragonal Zirconia(101) Surface: S. Muhammady, J. Haruyama, S. Kasamatsu and O. Sugino, J. Phys. Chem. C **126**, 15662 (2022).

4. First-principles electronic structure investigation of $HgBa_2Ca_{n-1}Cu_nO_{2n+2+x}$ with the SCAN density functional: A. N. Tatan, J. Haruyama and O. Sugino, AIP Advances **12**, 105308 (2022).

5. †Machine-learning-based exchange correlation functional with physical asymptotic constraints: R. Nagai, R. Akashi and O. Sugino, Phys. Rev. Research **4**, 013106 (2022).

6. †Surface facet dependence of Ru and Ru-based alloy oxidation resistance using ab initio thermodynamics calculation: S. M. Aspera, E. F. Arguelles, R. L. Arevalo, B. Chantaramolee, H. Nakanishi and H. Kasai, Surface Science **724**, 122129 (2022).

7. †Roadmap on Machine Learning in Electronic Structure: R. Nagai, R. Akashi and O. Sugino, Electron. Struct. **1**, 37-38 (2022).

8. †*Suppression of atomic displacive excitation in photo-induced A_{1g} phonon mode of bismuth unveiled by low-temperature time-resolved x-ray diffraction: Y. Kubota, Y. Tanaka, T. Togashi, T. Ebisu, K. Tamasaku, H. Osawa, T. Wada, O. Sugino, I. Matsuda and M. Yabashi, Appl. Phys. Lett. **122**, 092201 (2023).

Oka group

Oka group has worked on Nonequilibrium quantum materials including Floquet engineering of Dirac semimetals, spin systems, and many-body systems.

1. Magnetic Hedgehog Lattice in a Centrosymmetric Cubic Metal: S. Okumura, S. Hayami, Y. Kato and Y. Motome, J. Phys. Soc. Jpn. **91**, 093702 (2022).

2. Lindbladian dynamics of the Sachdev-Ye-Kitaev model: A. Kulkarni, T. Numasawa and S. Ryu, Phys. Rev. B **106**, 075138 (2022).

3. Phase degree of freedom and topology in multiple-Q spin textures: K. Shimizu, S. Okumura, Y. Kato and Y. Motome, Phys. Rev. B **105**, 224405 (2022).

4. Microwave Dynamical Conductivity in the Quantum Hall Regime: T. Arakawa, T. Oka, S. Kon and Y. Niimi, Phys. Rev. Lett. **129**, 046801 (2022).

5. Confinement phase in carbon-nanotubes and the extended massive Schwinger model: T. Oka, J. Phys. A: Math. Theor. **55**, 504001 (2022).

6. Universal dynamics of heavy operators in boundary CFT2: T. Numasawa and I. Tsiares, J. High Energ. Phys. **2022**, 156 (2022).

7. Four coupled SYK models and nearly AdS_2 gravities: phase transitions in traversable wormholes and in bra-ket wormholes: T. Numasawa, Class.Quant.Grav. **398**, 04001 (2022).

8. Mott memristors based on field-induced carrier avalanche multiplication: F. Peronaci, S. Ameli, S. Takayoshi, A. S. Landsman and T. Oka, Phys. Rev. B **107**, 075154 (2023).

Inoue group

In 2022, we reported the first three-dimensional structure of *Psp*R, which is a light-driven outward H^+ pump without the typical

* Joint research among groups within ISSP.

cytoplasmic H^+ donor, by X-ray crystallography. A new type of outward H^+ pumping rhodopsins (SacR) was found from Saccharibacteria, a lineage of candidate phyla radiation (CPR). Interestingly, SacR has a fenestration close to the head group of the retinal chromophore in the protein body. We revealed exogenous retinal is taken up into the protein body through this fenestration. Moreover, a new microbial rhodopsin class fused with a bestrophin channel, named Bestrhodopsin, was discovered from diverse algae. The ion flux through the pore in the bestrophin part is regulated by surrounding rhodopsin parts in a light-dependent manner. Interestingly, bestrhodopsin exhibits pure all-*trans*-to-11-*cis* isomerization which was not known for microbial rhodopsins but is typical among animal rhodopsins. The kinetic study of schizorhodopsin (SzR) revealed that the kinetic isotope effect of many photo intermediate-conversion processes involving retinal deprotonation and reprotonation and activation enthalpy and entropy are much lower than that of other microbial rhodopsins. The photoreaction cycle of a new channelrhodopsin, ChRmine was also reported.

1. Structural characterization of proton-pumping rhodopsin lacking a cytoplasmic proton donor residue by X-ray crystallography: K. Suzuki, M. D. C. Marín, M. Konno, R. Bagherzadeh, T. Murata and K. Inoue, J. Biol. Chem. **298**, 101722 (2022).

2. Diverse heliorhodopsins detected via functional metagenomics in freshwater *Actinobacteria* , *Chloroflexi* and *Archaea*: A. Chazan, A. Rozenberg, K. Mannen, T. Nagata, R. Tahan, S. Yaish, S. Larom, K. Inoue, O. Béjà and A. Pushkarev, Environmental Microbiology **24**, 110-121 (2022).

3. Saccharibacteria harness light energy using type-1 rhodopsins that may rely on retinal sourced from microbial hosts: A. L. Jaffe, M. Konno, Y. Kawasaki, C. Kataoka, O. Béjà, H. Kandori, K. Inoue and J. F. Banfield, ISME J, published on the web (2022).

4. Rhodopsin-bestrophin fusion proteins from unicellular algae form gigantic pentameric ion channels: A. Rozenberg, I. Kaczmarczyk, D. Matzov, J. Vierock, T. Nagata, M. Sugiura, K. Katayama, Y. Kawasaki, M. Konno, Y. Nagasaka, M. Aoyama, I. Das, E. Pahima, J. Church, S. Adam, V. A. Borin, A. Chazan, S. Augustin, J. Wietek, J. Dine, Y. Peleg, A. Kawanabe, Y. Fujiwara, O. Yizhar, M. Sheves, I. Schapiro, Y. Furutani, H. Kandori, K. Inoue, P. Hegemann, O. Béjà and M. Shalev-Benami, Nat. Struct. Mol. Biol. **29**, 592-603 (2022).

5. Kinetic study on the molecular mechanism of light-driven inward proton transport by schizorhodopsins: Y. Kawasaki, M. Konno and K. Inoue, Biochimica et Biophysica Acta (BBA) - Biomembranes published on the web, 184016 (2022).

6. Structural basis for channel conduction in the pump-like channelrhodopsin ChRmine: K. E. Kishi, Y. S. Kim, M. Fukuda, M. Inoue, T. Kusakizako, P. Y. Wang, C. Ramakrishnan, E. F. X. Byrne, E. Thadhani, J. M. Paggi, T. E. Matsui, K. Yamashita, T. Nagata, M. Konno, S. Quirin, M. Lo, T. Benster, T. Uemura, K. Liu, M. Shibata, N. Nomura, S. Iwata, O. Nureki, R. O. Dror, K. Inoue, K. Deisseroth and H. E. Kato, Cell **185**, 672 (2022).

7. Converting a Natural-Light-Driven Outward Proton Pump Rhodopsin into an Artificial Inward Proton Pump: M. D. C. Marín, M. Konno, H. Yawo and K. Inoue, J. Am. Chem. Soc. **TBA**, jacs.2c12602 (2023).

8. Twisting and Protonation of Retinal Chromophore Regulate Channel Gating of Channelrhodopsin C1C2: K. Shibata, K. Oda, T. Nishizawa, Y. Hazama, R. Ono, S. Takaramoto, R. Bagherzadeh, H. Yawo, O. Nureki, K. Inoue and H. Akiyama, J. Am. Chem. Soc. **TBA**, jacs.3c01879 (2023).

9. Phototrophy by antenna-containing rhodopsin pumps in aquatic environments: A. Chazan, I. Das, T. Fujiwara, S. Murakoshi, A. Rozenberg, A. Molina-Márquez, F. K. Sano, T. Tanaka, P. Gómez-Villegas, S. Larom, A. Pushkarev, P. Malakar, M. Hasegawa, Y. Tsukamoto, T. Ishizuka, M. Konno, T. Nagata, Y. Mizuno, K. Katayama, R. Abe-Yoshizumi, S. Ruhman, K. Inoue, H. Kandori, R. León, W. Shihoya, S. Yoshizawa, M. Sheves, O. Nureki and O. Béjà, Nature **615**, 535-540 (2023).

10. Difference FTIR Spectroscopy of Jumping Spider Rhodopsin-1 at 77 K: S. Hanai, T. Nagata, K. Katayama, S. Inukai, M. Koyanagi, K. Inoue, A. Terakita and H. Kandori, Biochemistry **62**, 1347-1359 (2023).

11. Reversible Photoreaction of a Retinal Photoisomerase, Retinal G-Protein-Coupled Receptor RGR: N. Morimoto, T. Nagata and K. Inoue, Biochemistry **62**, 1429-1432 (2023).

12. Time-resolved detection of light-induced conformational changes of heliorhodopsin: Y. Nakasone, Y. Kawasaki, M. Konno, K. Inoue and M. Terazima, Phys. Chem. Chem. Phys. **25**, 12833-12840 (2023).

13. Biophysical characterization of microbial rhodopsins with DSE motif: M. D. C. Marín, A. L. Jaffe, P. T. West, M. Konno, J. F. Banfield and K. Inoue, Biophys. Physicobiol. **20**, e201023 (2023).

14. Protein dynamics of a light-driven Na^+ pump rhodopsin probed using a tryptophan residue near the retinal chromophore: A. Otomo, M. Mizuno, K. Inoue, H. Kandori and Y. Mizutani, Biophysics. Physicobiol. **20**, e201016 (2023).

15. Characterization of retinal chromophore and protonated Schiff base in Thermoplasmatales archaeon heliorhodopsin using solid-state NMR spectroscopy: S. Suzuki, S. Kumagai, T. Nagashima, T. Yamazaki, T. Okitsu, A. Wada, A. Naito,

† Joint research with outside partners.

K. Katayama, K. Inoue, H. Kandori and I. Kawamura, Biophysical Chemistry **296**, 106991 (2023).

16. ロドプシンを用いたオプトジェネティクスの最前線 : 井上 圭一 , 生物工学会誌 **100**, 420-424 (2022).

17. 特集によせて —Mehr Licht !—: 井上 圭一 , 生物工学会誌 **100**, 354 (2022).

18. アスガルドアーキアの持つ光受容膜タンパク質ロドプシン : 井上 圭一 , 極限環境生物学会誌 **22**, 13-23 (2022).

19. ロドプシンを用いた光受容と新奇シゾロドプシンファミリー : 井上 圭一 ,「未培養微生物研究の最新動向」, 青柳 秀紀 , (シーエムシー出版 , 2023), 74-81.

Quantum Materials Group

Oshikawa group

Ballistic transport can be characterized by Drude weight, which is given by Kohn formula. Recently, we have generalized the Kohn formula to all orders of the nonlinear conductivity. However, the nonlinear Drude weights obtained by the generalized Kohn formula often diverge in the thermodynamic limit. In order to clarify this remarkable behavior, we have studied ballistic transport and its characterizations in a very simple system of the one-dimensional tight-binding model with a single defect. We showed that, even in this simple model, we can observe the divergence of nonlinear Drude weights. We emphasize that these nonlinear Drude weights are obtained by the generalized Kohn formula, which corresponds to the adiabatic limit for a given system size. As a resolution, we demonstrated that, by taking the thermodynamic limit before the adiabatic limit, low-frequency contributions merge into the Drude weight, which does not diverge. The result also does not depend on the impurity strength, thus characterizes the ballistic transport in the bulk. We propose to distinguish the Drude weight obtained by taking the thermodynamic limit first as "bulk Drude weight", and the Drude weight given by the Kohn formula, which corresponds to taking the adiabatic limit first, as "Kohn Drude weight". While the potential issue of the order of limits has been sometimes discussed within the linear response, the discrepancy between the two limits is amplified in nonlinear Drude weights.

1. Boson-fermion duality with subsystem symmetry: W. Cao, M. Yamazaki and Y. Zheng, Phys. Rev. B **106**, 075150 (2022).

2. Duality viewpoint of criticality: L. Li and Y. Yao, Phys. Rev. B **106**, 224420 (2022).

3. Absence versus Presence of Dissipative Quantum Phase Transition in Josephson Junctions: K. Masuki, H. Sudo, M. Oshikawa and Y. Ashida, Phys. Rev. Lett. **129**, 087001 (2022).

4. Gappability Index for Quantum Many-Body Systems: Y. Yao, M. Oshikawa and A. Furusaki, Phys. Rev. Lett. **129**, 017204 (2022).

5. Kramers-Wannier-like Duality Defects in (3+1)D Gauge Theories: J. Kaidi, K. Ohmori and Y. Zheng, Phys. Rev. Lett. **128**, 111601 (2022).

6. Tensor network renormalization study on the crossover in classical Heisenberg and RP2 models in two dimensions: A. Ueda and M. Oshikawa, Phys. Rev. E **106**, 014104 (2022).

7. Fracton topological order at finite temperature: X. Shen, Z. Wu, L. Li, Z. Qin and H. Yao, Phys. Rev. Research **4**, L032008 (2022).

8. Non-invertible symmetries of $N = 4$ SYM and twisted compactification.: J. Kaidi, G. Zafrir and Y. Zheng, J. High Energ. Phys. **2022**, 53 (2022).

9. On lattice models of gapped phases with fusion category symmetries: K. Inamura, J. High Energ. Phys. **2022**, 36 (2022).

10. Topology and Edge State Meet an Exact Solution for Nonlinear Electric Circuits: M. Oshikawa, JPSJ News Comments **19**, 06 (2022).

11. Differentiable Programming of Isometric Tensor Networks: C. Geng, H.-Y. Hu and Y. Zou, Machine Learning: Science and Technology **3**, 015020 (2022).

12. The mishandling of scientifically flawed articles about radiation exposure, retracted for ethical reasons, impedes understanding of the scientific issues pointed out by Letters to the Editor: Y. Tanimoto, Y. Hamaoka, K. Kageura, S. Kurokawa, J. Makino and M. Oshikawa, Journal of Scientific Practice and Integrity **2022**, 38474 (2022).

13. Drude weights in one-dimensional systems with a single defect: K. Takasan, M. Oshikawa and H. Watanabe, Phys. Rev.

* Joint research among groups within ISSP.

B **107**, 075141 (2023).

14. Duality, criticality, anomaly, and topology in quantum spin-1 chains: H. Yang, L. Li, K. Okunishi and H. Katsura, Phys. Rev. B **107**, 125158 (2023).

Nakatsuji group

The myths of quantum mechanics render electronic, magnetic, and optical properties in materials that defy common sense while inspiring future technologies. Through decades of effort, researchers studying quantum materials have uncovered a wealth of fascinating properties, ranging from superconductivity that allows electric current to flow without any resistance to topological insulators whose surface states serve as superhighways for electrons to flow freely. Discoveries in the field of quantum materials offer a central thread linking the previously disparate fields, like condensed matter physics, high-energy physics, quantum computing, and cosmology. Moreover, the functionalities of quantum materials provide the basis for emerging transformational technologies, such as antiferromagnetic memory. Our vision is to lead the quest for functional quantum materials to bear a groundbreaking impact on fundamental science and benefit humanity in the future. The main research topics in our group are (1) Quantum transport in topological materials; (2) Coherent quantum transport in antiferromagnetic spintronics; (3) Strange metal and exotic superconductivity in strongly correlated electron systems; (4) Long-range quantum entanglement in topologically ordered states.

1. Phonon spectrum of $Pr_2Zr_2O_7$ and $Pr_2Ir_2O_7$ as evidence of coupling of the lattice with electronic and magnetic degrees of freedom: Y. Xu, H. Man, N. Tang, T. Ohtsuki, S. Baidya, S. Nakatsuji, D. Vanderbilt and N. Drichko, Phys. Rev. B **105**, 075137 (2022).

2. Pressure-induced changes of valence fluctuation in β-$YbAlB_4$ probed by x-ray absorption spectroscopy: Y. Sakaguchi, S. Ikeda, N. K. M. Mizumaki, K. Kuga, S. S. K. Sone, S. Nakatsuji and H. Kobayashi, Phys. Rev. B **105**, 155129 (2022).

3. Superconducting properties of the A15 structure compound V_3Ge: E. Ahmed, K. Kobayashi, N. Arakawa, Y. Okubo, A. Sakai, S. Nakatsuji, A. Iyo and T. Ebihara, Physica C **602**, 1354140 (2022).

4. *Perpendicular full switching of chiral antiferromagnetic order by current: T. Higo, K. Kondou, T. Nomoto, M. Shiga, S. Sakamoto, X. Chen, D. Nishio-Hamane, R. Arita, Y. Otani, S. Miwa and S. Nakatsuji, Nature **607**, 474-479 (2022).

5. Large Anomalous Nernst Effect and Nodal Plane in an Iron-based Kagome Ferromagnet: T. Chen, S. Minami, A. Sakai, Y. Wang, Z. Feng, T. Nomoto, M. Hirayama, R. Ishii, T. Koretsune, R. Arita and S. Nakatsuji, Science Advances **8**, 1480 (2022).

6. *Determination of spin Hall angle in the Weyl ferromagnet Co_2MnGa by taking into account the thermoelectric contributions: H. Isshiki, Z. Zhu, H. Mizuno, R. Uesugi, T. Higo, S. Nakatsuji and Y. Otani, Phys. Rev. Materials **6**, 084411 (2022).

7. Topological magnets—their basic science and potential applications: S. Nakatsuji, AAPPS Bulletin **32-25**, 1-13 (2022).

8. Piezomagnetic switching of anomalous Hall effect in an antiferromagnet at room temperature: M. Ikhlas, S. Dasgupta, F. Theuss, T. Higo, S. Kittaka, B. J. Ramshaw, O. Tchernyshyov, C. W. Hicks and S. Nakatsuji, Nature Physics **18**, 1-12 (2022).

9. Anisotropy-driven quantum criticality in an intermediate valence system: M. S. Grbic, E. C. T. O'Farrell, Y. Matsumoto, K. Kuga, M. Brando, R. Küchler, A. H. Nevidomskyy, M. Yoshida, T. Sakakibara, Y. Kono, Y. Shimura, M. L. Sutherland and M. T. &. S. Nakatsuji, Nature Communications **13**, 2141 (2022).

10. Magnetic field tuning of the valley population in the Weyl phase of $Nd_2Ir_2O_7$: I. Kapon, C. W. Rischau, B. Michon, K. Wang, B. Xu, Q. Yang, S. Nakatsuji and D. van der Marel, Physical Review Research **4**, 023056 (2022).

11. Ferrimagnetic compensation and its thickness dependence in TbFeCo alloy thin films: M. Ishibashi, K. Yakushiji, M. Kawaguchi, A. Tsukamoto, S. Nakatsuji and M. Hayashi, Applied Physics Letters **120**, 022405-1 and 4 (2022).

12. Topological Magnets: Functions Based on Berry Phase and Multipoles: S. Nakatsuji and R. Arita, Annu. Rev. Condens. Matter Phys. **13**, annurev-conmatphys-031620-103859 (2022).

13. Anomalous Hall antiferromagnets: L. Smejkal, A.-H. MacDonald, J. Sinova, S. Nakatsuji and T. Jungwith, Nature Review Materials **7**, 482–496 (2022).

14. *Ultrafast Dynamics of Intrinsic Anomalous Hall Effect in the Topological Antiferromagnet Mn_3Sn: T. Matsuda, T. Higo, T. Koretsune, N. Kanda, Y. Hirai, H. Peng, T. Matsuo, N. Yoshikawa, R. Shimano, S. Nakatsuji and R. Matsunaga, Phys. Rev. Lett. **130**, 126302 (2023).

† Joint research with outside partners.

15. *High-resolution magnetic imaging by mapping the locally induced anomalous Nernst effect using atomic force microscopy: N. Budai, H. Isshiki, R. Uesugi, Z. Zhu, T. Higo, S. Nakatsuji and Y. Otani, Appl. Phys. Lett. **122**, 102401 (2023).

16. *Octupole-driven magnetoresistance in an antiferromagnetic tunnel junction: X. Chen, T. Higo, K. Tanaka, T. Nomoto, H. Tsai, H. Idzuchi, M. Shiga, S. Sakamoto, R. Ando, H. Kosaki, T. Matsuo, D. Nishio-Hamane, R. Arita, S. Miwa and S. Nakatsuji, Nature **613**, 490-495 (2023).

17. *Temperature-induced anomalous magnetotransport in the Weyl semimetal Mn_3Ge: M. Wu, K. Kondou, T. Chen, S. Nakatsuji and Y. Otani, AIP Advances **13**, 045102 (2023).

18. Anomalous Hall Effect in Nanoscale Structures of the Antiferromagnetic Weyl Semimetal Mn_3Sn at Room Temperature: T. Matsuo, T. Higo, D. Nishio-Hamane and S. Nakatsuji, Jpn. J. Appl. Phys. (2022), in print.

Miwa group

We have studied the following topics this year: (1) Spin-torque control of chiral antiferromagnet Mn_3Sn, (2) Chirality-induced spin selectivity with no net current, and (3) x-ray magnetic circular dichroism on a magnetic interface. In topic (1), we find that current-induced full switching of octupole polarization by using strained Mn_3Sn thin film (Nature **607**, 404). This is a work in collaboration with Nakatsuji and Otani groups. In topic (2), we find that chiral molecule at the interface with metal possesses thermally-driven broken time-reversal symmetry. This is a work in collaboration with Otani group (J. Am. Chem. Soc. **144**, 7302). In topic (3), we find that electron correlation is a key to understanding interfacial magnetic anisotropy at Fe/MgO interface (ACS Appl. Electron. Mater. **4**, 1794).

1. Control of perpendicular magnetic anisotropy at the Fe/MgO interface by phthalocyanine insertion: S. Sakamoto, E. Jackson, T. Kawabe, T. Tsukahara, Y. Kotani, K. Toyoki, E. Minamitani, Y. Miura, T. Nakamura, A. Hirohata and S. Miwa, Phys. Rev. B **105**, 184414 (1-6) (2022).

2. Origin of enhanced interfacial perpendicular magnetic anisotropy in LiF-inserted Fe/MgO interface: S. Sakamoto, T. Nozaki, S. Yuasa, K. Amemiya and S. Miwa, Phys. Rev. B **106**, 174410 (1-6) (2022).

3. *Chirality-Induced Magnetoresistance Due to Thermally Driven Spin Polarization: K. Kondou, M. Shiga, S. Sakamoto, H. Inuzuka, A. Nihonyanagi, F. Araoka, M. Kobayashi, S. Miwa, D. Miyajima and Y. Otani, J. Am. Chem. Soc. **144**, 7302-7307 (2022).

4. *Perpendicular full switching of chiral antiferromagnetic order by current: T. Higo, K. Kondou, T. Nomoto, M. Shiga, S. Sakamoto, X. Chen, D. Nishio-Hamane, R. Arita, Y. Otani, S. Miwa and S. Nakatsuji, Nature **607**, 474-479 (2022).

5. Electron Correlation Enhances Orbital Polarization at a Ferromagnetic Metal/Insulator Interface: Depth-Resolved X-ray Magnetic Circular Dichroism and First-Principles Study: S. Sakamoto, M. Tsujikawa, M. Shirai, K. Amemiya and S. Miwa, ACS Appl. Electron. Mater. **4**, 1794-1799 (2022).

6. Magnetic anisotropy of Fe/MgO interfaces inserted with alkali halide layers: J. Chen, S. Sakamoto, H. Kosaki and S. Miwa, Phys. Rev. B **107**, 094420 (2023).

7. *Octupole-driven magnetoresistance in an antiferromagnetic tunnel junction: X. Chen, T. Higo, K. Tanaka, T. Nomoto, H. Tsai, H. Idzuchi, M. Shiga, S. Sakamoto, R. Ando, H. Kosaki, T. Matsuo, D. Nishio-Hamane, R. Arita, S. Miwa and S. Nakatsuji, Nature **613**, 490-495 (2023).

8. Observation of large spin conversion anisotropy in bismuth: N. Fukumoto, R. Ohshima, M. Aoki, Y. Fuseya, M. Matsushima, E. Shigematsu, T. Shinjo, Y. Ando, S. Sakamoto, M. Shiga, S. Miwa and M. Shiraishi, Proceedings of the National Academy of Sciences **102**, e2215030120 (2023).

9. Weyl 反強磁性体 Mn_3Sn のスピンダイナミクス : 三輪 真嗣 , 坂本 祥哉 , 飯浜 賢志 , 野本 拓也 , まぐね **17**, 233-240 (2022).

Division of Data-Integrated Materials Science

Fukushima group

Automatic exhaustive exploration of a large material space by high-performance supercomputers is crucial for developing new functional materials. We demonstrated the efficiency of high-throughput calculations using the all-electron Korringa–Kohn–Rostoker coherent potential approximation method with the density functional theory for the large material space consisting of quaternary high-entropy alloys, which are nonstoichiometric and substitutionally disordered materials. The exhaustive

* Joint research among groups within ISSP.

calculations were performed based on the AkaiKKR program package and supercomputer Fugaku, where the numerical parameters and self-consistent convergence are automatically controlled. The large material database including the total energies, magnetization, Curie temperature, and residual resistivity was constructed by our calculations. We used frequent itemset mining to identify the characteristics of parcels in magnetization and Curie temperature space. We also identified the elements that enhance the magnetization and Curie temperature and clarified the rough dependence of the elements through regression modeling of the residual resistivity.

1. Low-temperature acanthite-like phase of Cu_2S: electronic and transport properties: H. N. Nam, K. Suzuki, T. Q. Nguyen, A. Masago, H. Shinya, T. Fukushima and K. Sato, Phys. Rev. B **105**, 075205(1-11) (2022).

2. A first-principles study on the electrical conductivity of $Ag2S_{1-x}Se_x$ (x = 0, 0.25, 0.5): Electron-phonon coupling: 71. H. N. Nam, K. Suzuki, A. Masago, T. Q. Nguyen, H. Shinya, T. Fukushima and K. Sato, Appl. Phys. Lett. **120**, 143903(1-6) (2022).

3. Direct and inverse magnetocaloric effects in FeRh alloy: H. B. Tran, T. Fukushima, H. Momida, K. Sato, Y. Makino and T. Oguchi, Journal of Alloys and Compounds **926**, 166718(1-8) (2022).

4. *Automatic exhaustive calculations of large material space by Korringa-Kohn-Rostoker coherent potential approximation method — Applied to equiatomic quaternary high entropy alloys: T. Fukushima, H. Akai, T. Chikyow and H. Kino, Pays. Rev. Mater. **6**, 023802(1-19) (2022).

5. The role of electron–phonon scattering on thermoelectric properties of intermetallic compounds *X*Si (*X* = Co, Rh): H. N. Nam, K. Suzuki, A. Masago, H. Shinya, T. Fukushima and K. Sato, Japanese Journal of Applied Physics **62**, 020904(1-6) (2023).

6. *Physics-informed machine learning combining experiment and simulation for the design of neodymium-iron-boron permanent magnets with reduced critical-elements content: A. Kovacs, J. Fischbacher, H. Oezelt, A. Kornell, Q. Ali, M. Gusenbauer, M. Yano, N. Sakuma, A. Kinoshita, T. Shoji, A. Kato, Y. Hong, S. Grenier, T. Devillers, N. Dempsey, T. Fukushima, H. Akai, N. Kawashima, T. Miyake and T. Schrefl, Frontiers in Materials **9**, 1094055(1-19) (2023).

7. 半導体スピントロニクス材料のデザイン：佐藤 和則，真砂 啓，福島 鉄也，新屋ひ かり，「スピントロニクスのための計算機ナノマテリアルデザイン」，吉田博，(内田老鶴圃 , 2022), 167-188.

Materials Design and Characterization Laboratory

Hiroi group

Apart from rutile, which crystallizes in the rutile-type structure characteristic of many metal dioxides, three major polymorphs of titanium dioxide (TiO_2) are known: anatase, brookite, and the α-lead dioxide (α-PbO_2)-type high-pressure form. Ti ions are commonly found in octahedra composed of six oxide ions, and their crystal structures are distinguished according to the linkage pattern of the TiO_6 octahedra. Inorganic structural chemistry considers that, in the rutile and α-PbO_2 types, Ti ions occupy half of the octahedral voids in the hexagonal close packing of oxide ions, and the TiO_6 octahedra in each layer are joined via edge sharing to form linear and zigzag strands, respectively. Anatase and brookite, on the other hand, exhibit more complex three-dimensional edge-sharing octahedral connections, although their origins are not fully explained. I show that these configurations can be interpreted as distinct stacking structures of layers with α-PbO_2-type zigzag strands. Additionally, I characterize the crystal structures of four TiO_2 polymorphs in detail using stacking sequence descriptions based on anion close packings and explore their relationships in terms of inorganic structural chemistry. I note that the moderate covalent nature of the Ti–O bond and the local structural instability of d^0 ions result in an unusual variety of polymorphs in TiO_2.

1. Pyrochlore oxide $Hg_2Os_2O_7$ on verge of metal–insulator boundary: K. Kataoka, D. Hirai, A. Koda, R. Kadono, T. Honda and Z. Hiroi, J. Phys.: Condens. Matter **34**, 135602 (2022).

2. Successive phase transitions of the spin-orbit-coupled metal $Cd_2Re_2O_7$ probed by high-resolution synchrotron x-ray diffraction: D. Hirai, A. Fukui, H. Sagayama, T. Hasegawa and Z. Hiroi, J. Phys.: Condens. Matter **35**, 035403 (2022).

3. Dimer Crystallization Induced by Elemental Substitution in the Honeycomb Lattice of $Ru_{1-x}Os_xCl_3$: K. Kataoka, D. Wulferding, T. Yajima, D. Nishio-Hamane, D. Hirai, S. Lee, K.-Y. Choi and Z. Hiroi, J. Phys. Soc. Jpn. **91**, 014801 (2022).

4. Unusual Resistive Transitions in the Nodal-Line Semimetallic Superconductor NaAlSi: D. Hirai, T. Ikenobe, T. Yamada, H. Yamane and Z. Hiroi, J. Phys. Soc. Jpn. **91**, 024702 (2022).

5. Electronic states of metallic electric toroidal quadrupole order in $Cd_2Re_2O_7$ determined by combining quantum oscilla-

† Joint research with outside partners.

tions and electronic structure calculations: H. T. Hirose, T. Terashima, D. Hirai, Y. Matsubayashi, N. Kikugawa, D. Graf, K. Sugii, S. Sugiura, Z. Hiroi and S. Uji, Phys. Rev. B **105**, 035116 (2022).

6. Zigzag magnetic order in the Kitaev spin-liquid candidate material $RuBr_3$ with a honeycomb lattice: Y. Imai, K. Nawa, Y. Shimizu, W. Yamada, H. Fujihara, T. Aoyama, R. Takahashi, D. Okuyama, T. Ohashi, M. Hagihala, S. Torii, D. Morikawa, M. Terauchi, T. Kawamata, M. Kato, H. Gotou, M. Itoh, T. J. Sato and K. Ohgushi, Phys. Rev. B **105**, L041112 (2022).

7. High-Pressure Synthesis of Transition-Metal Oxyhydrides with Double-Perovskite Structures: T. Yajima, K. Takahashi, H. Nakajima, T. Honda, K. Ikeda, T. Otomo and Z. Hiroi, Inorg. Chem. **61**, 2010 (2022).

8. Inorganic Structural Chemistry of Titanium Dioxide Polymorphs: Z. Hiroi, Inorg. Chem. **61**, 8393 (2022).

9. Room temperature magnetic properties of Mn-Ga-B melt-spun ribbons: T. Saito and D. Nishio-Hamane, AIP Advances **12**, 035250 (2022).

10. Thermoelectric and magnetic properties of $(Fe,Co)_2TiSn$ Heusler compounds: T. Saito, S. Kamishima and D. Nishio-Hamane, Physica B: Condensed Matter **639**, 413984 (2022).

11. †*Dimensional reduction and incommensurate dynamic correlations in the S = 1/2 triangular-lattice antiferromagnet $Ca_3ReO_5Cl_2$: S. A. Zvyagin, A. N. Ponomaryov, J. Wosnitza, D. Hirai, Z. Hiroi, M. Gen, Y. Kohama, A. Matsuo, Y. H. Matsuda and K. Kindo, Nat Commun **13**, 6310 1-6 (2022).

12. The Role of Scandium Substitution in Babingtonite Group Minerals: M. Nagashima, D. Nishio-Hamane, T. Matsumoto and C. Fukuda, Minerals **12**, 333 (2022).

13. Surface Functionalization of Non-Woven Fabrics Using a Novel Silica-Resin Coating Technology: Antiviral Treatment of Non-Woven Fabric Filters in Surgical Masks: C. Tsutsumi-Arai, Y. Iwamiya, R. Hoshino, C. Terada-Ito, S. Sejima, K. Akutsu-Suyama, M. Shibayama, Z. Hiroi, R. Tokuyama-Toda, R. Iwamiya, K. Ijichi, T. Chiba and K. Satomura, IJERPH **19**, 3639 (2022).

14. *Large magnetic-field-induced strains in sintered chromium tellurides: Y. Kubota, Y. Okamoto, T. Kanematsu, T. Yajima, D. Hirai and K. Takenaka, Appl. Phys. Lett. **122**, 042404 (2023).

Kawashima group

We developed efficient methods, algorithms, parallelized programs, and sometimes new concepts, based on novel numerical techniques such as the tensor network (TN) method and quantum Monte Carlo (QMC). We then applied them to relevant physical problems. To list subjects of our research in 2022, (1) QMC study of Bose gases [Masaki-Kato, et al., JPSJ90], (2) Study of spin liquid in frustrated spin systems [Ogino, PRB106][Ido, et al., npj QM7], (3) Effect of boundary conditions in quantum spin clusters [Eguchi et al, JPSJ91], and (4) Development of open-source applications [Okubo et al, CPC279].

1. Energy Scale Deformation on Regular Polyhedra: T. Eguchi, S. Oga, H. Katsura, A. Gendiar and T. Nishino, J. Phys. Soc. Jpn. **91**, 034001 (2022).

2. Universal and non-universal correction terms of Bose gases in dilute region: a quantum Monte Carlo study: A. Masaki-Kato, Y. Motoyama and N. Kawashima, J. Phys. Soc. Jpn. **90**, 034711(1-8) (2022).

3. Ground-state phase diagram of a spin-1/2 frustrated *XXZ* ladder: T. Ogino, R. Kaneko, S. Morita and S. Furukawa, Phys. Rev. B **106**, 155106 (2022).

4. †*TeNeS: Tensor network solver for quantum lattice systems: Y. Motoyama, T. Okubo, K. Yoshimi, S. Morita, T. Kato and N. Kawashima, Computer Physics Communications **279**, 108437 (2022).

5. †*Unconventional dual 1*D*–2*D* quantum spin liquid revealed by ab initio studies on organic solids family: K. Ido, K. Yoshimi, T. Misawa and M. Imada, npj Quantum Mater. **7**, 48 (2022).

6. Cartesian Operator Factorization Method for Hydrogen: X. Lyu, C. Daniel and J. K. Freericks, Atoms **10**, 14 (2022).

7. *Data Analysis of *Ab initio* Effective Hamiltonians in Iron-Based Superconductors — Construction of Predictors for Superconducting Critical Temperature: K. Ido, Y. Motoyama, K. Yoshimi and T. Misawa, J. Phys. Soc. Jpn. **92**, 064702 (2023).

8. Non-monotonic behavior of the Binder parameter in discrete spin systems: H. Watanabe, Y. Motoyama, S. Morita and N. Kawashima, Prog. Theor. Exp. Phys. **2023**, 033A02 (2023).

* Joint research among groups within ISSP.

Uwatoko group

We have performed polycrystalline and single-crystal neutron diffraction experiments to determine the magnetic structure under ambient and high pressures on the $CePtSi_2$. We found incommensurate magnetic peaks with a magnetic propagation vector of (0.32,0,0.11) at ambient pressure below T_{SDW} ~ 1.25 K, which originate from a spin-density-wave order with the easy axis along the c axis and an averaged ordered moment of 0.45(5)μ_B. Applying pressures, the magnetic order disappears around 1.0 GPa, which is much lower than the critical pressure for the superconducting phase. The results suggest that other than magnetic fluctuations, may play a primary role in the superconducting pairing mechanism. We discovered the first ternary Mn-based superconductor KMn_6Bi_5 under high pressure. Bulk superconductivity emerges in the pressurized single-crystal KMn_6Bi_5 when its antiferromagnetic order disappears by pressure. The optimal $^{on}T_c$ reaches ~9.3 K at 14.2 GPa, and $\mu_0 H_{c2}(0)$ is found to exceed the Pauli paramagnetic limit. We investigated the superconductivity of $(TMTTF)_2TaF_6$ (TMTTF: tetramethyl-tetrathia-fulvalene) by conducting resistivity measurements under high pressure up to 8 GPa. A superconducting state in $(TMTTF)_2TaF_6$ emerged after a metal-insulator transition was suppressed with increasing external pressure. We discovered a superconducting state in $5 \leq P \leq 6$ GPa from T_c = 2.1 K to 2.8 K. In addition, when the pressures with maximum SC temperatures are compared between the PF_6 and the TaF_6 salts, we found that $(TMTTF)_2TaF_6$ has a 0.75 GPa on the negative pressure side in the *T-P* phase diagram of $(TMTTF)_2TaF_6$. We have performed systematic electrical resistivity and single crystal X-ray diffraction measurements of CsCl-type cubic compound CeZn under high pressure up to 9.5 GPa. Applying the pressure, the coupled magnetic and crystal structural transition becomes separated above 1.0 GPa and then the AFM order changes to ferromagnetic (FM). The FM ordering temperature decreases with further applying pressure and changes to a nonmagnetic state above ~3.0 GPa. In the nonmagnetic state, we discovered superconductivity below T_{sc} ~ 1.3 K over 5.5 GPa, which survives even up to 9.5 GPa.

1. Abrupt Change in Electronic States under Pressure in New Compound $EuPt_3Al_5$: T. Koizumi, F. Honda, Y. J. Sato, D. Li, D. Aoki, Y. Haga, J. Gouchi, S. Nagasaki, Y. Uwatoko, Y. Kaneko and Y. Ônuki, J. Phys. Soc. Jpn. **91**, 043704(1-5) (2022).

2. La-Substitution Effects on Multisite Ce Compound $CePtGe_2$: H. Muto, S. Onuma, T. Nakano, N. Takeda, J. Gouchi, Y. Uwatoko, K. Uhlírová, J. Prokleška and V. Sechovský, J. Phys. Soc. Jpn. **91**, 074712(1-4) (2022).

3. Structural Phase Transition and Possible Valence Instability of Ce-4*f* Electron Induced by Pressure in CeCoSi: Y. Kawamura, K. Ikeda, A. N. B. A. Dalan, J. Hayashi, K. Takeda, C. Sekine, T. Matsumura, J. Gouchi, Y. Uwatoko, T. Tomita, H. Takahashi and H. Tanida, J. Phys. Soc. Jpn. **91**, 064714(1-8) (2022).

4. *Magnetic field and pressure phase diagrams of the triangular-lattice antiferromagnet $CsCuCl_3$ explored via magnetic susceptibility measurements with a proximity-detector oscillator: K. Nihongi, T. Kida, Y. Narumi, J. Zaccaro, Y. Kousaka, K. Inoue, K. Kindo, Y. Uwatoko and M. Hagiwara, Phys. Rev. B **105**, 184416(1-7) (2022).

5. Pressure dependence of the magnetic ground state in $CePtSi_2$: S. E. Dissanayake, F. Ye, W. Tian, M. Matsuda, H. Muto, S. Suzuki, T. Nakano, S. Watanabe, J. Gouchi and Y. Uwatoko, Phys. Rev. B **105**, 245111(1-6) (2022).

6. Pressure effect in the antiperovskite phosphide superconductor $(SrP_{0.9}Pd_{0.1})_3P$: L. Shi, P. Yang, T. Wang, P. Shan, Z. Liu, S. Xu, K. Chen, N. Wang, L. Zhou, Y. Long, J. Sun, G. Mu, Y. Uwatoko, B. Wang and J. Cheng, Phys. Rev. B **105**, 214529(1-6) (2022).

7. Superconducting and structural properties of the noncentrosymmetric Re_6Hf superconductor under high pressure: S. Mariappan, M. Krishnan, D. Bhoi, H. Ma, J. Gouchi, K. Motla, R. P. Singh, P. Vajeeston, A. Sonachalam and Y. Uwatoko, Phys. Rev. B **105**, 224505(1-12) (2022).

8. Pressure-Induced Superconductivity up to 9 K in the Quasi-One-Dimensional KMn_6Bi_5: Z. Y. Liu, Q. X. Dong, P. T. Yang, P. F. Shan, B. S. Wang, J. P. Sun, Z. L. Dun, Y. Uwatoko, G. F. Chen, X. L. Dong, Z. X. Zhao and J. -G. Cheng, Phys. Rev. Lett. **128**, 187001(1-6) (2022).

9. Electronic properties of α -Mn-type non-centrosymmetric superconductor $Re_{5.5}Ta$ under hydrostatic pressure: S. Mariappan, D. Bhoi, M. Krishnan, S. Nagasaki, P. Vajeeston, R. K. Arushi, R. K. Kushwaha, R. P. Singh, A. Sonachalam and Y. Uwatoko, Supercond. Sci. Technol. **36**, 025002(1-16) (2022).

10. †Magnetization of Quaternary Heusler Alloy CoFeCrAl: S. Tsujikawa, I. Shigeta, J. Gouchi, T. Kanomata, R. Y. Umetsu, Y. Uwatoko and M. Hiroi, IEEE Trans. Magn. **58**, 1 (1-5) (2022).

11. Destabilization of the Charge Density Wave and the Absence of Superconductivity in ScV_6Sn_6 under High Pressures up to 11 GPa: X. Zhang, J. Hou, W. Xia, Z. Xu, P. Yang, A. Wang, Z. Liu, J. Shen, H. Zhang, X. Dong, Y. Uwatoko, J. Sun, B. Wang, Y. Guo and J. Cheng, Materials **15**, 7372(1-11) (2022).

12. Pressure-Induced Superconductivity of the Quasi-One-Dimensional Organic Conductor $(TMTTF)_2TaF_6$: M. Itoi, T. Nakamura and Y. Uwatoko, Materials **15**, 4638 (2022).

13. Pressure Induced Superconductivity and Multiple Structural Transitions in CsCl-Type Cubic CeZn Single Crystal: X.

† Joint research with outside partners.

Shen, H. Ma, D. Bhoi, J. Gouchi, Y. Uwatoko, A. Dalan, Y. Kawamura, H. Sato, I. Umehara and M. Uehara, Crystals **12**, 571(1-9) (2022).

14. Anharmonic phonon interactions and the Kondo effect in a FeSe/Sb_2Te_3/FeSe heterostructure: a proximity effect between ferromagnetic chalcogenide and di-chalcogenide: L. Ghosh, M. Alam, M. Singh, S. Dixit, S. V. Kumar, A. Verma, P. Shahi, Y. Uwatoko, S. Saha, A. Tiwari, A. Tripathi and S. Chatterjee, Nanoscale **14**, 10889-10902 (2022).

15. †Sub-micrometer particle size effects on metastable phases for a photoswitchable Co–Fe Prussian blue analog: M. Itoi, I. Maurin, K. Boukheddaden, M. J. Andrus, D. R. Talham, E. Elkaim and Y. Uwatoko, Journal of Applied Physics **131**, 085110(1-11) (2022).

16. Pressure-driven superconducting dome in the vicinity of CDW in the pyrite-type superconductor CuS_2: L. F. Shi, Z. Y. Liu, J. Li, X. X. Zhang, N. N. Wang, Q. Cui, K. Y. Chen, Q. Y. Liu, P. T. Yang, J. P. Sun, B. S. Wang, Y. Uwatoko, Y. Sui, H. X. Yang and J. -G. Cheng, Phys. Rev. Materials **6**, 014802(1-8) (2022).

17. Antiferromagnetic order in $Yb_4Ru_7As_6$ with the cubic $U_4Re_7Si_6$-type structure: Y. Hirose, K. Arakawa, Y. Kato, Y. Uwatoko, H. Ma, J. Gouchi, F. Honda and R. Settai, Journal of Magnetism and Magnetic Materials **556**, 169327(1-6) (2022).

18. Evidence for pressure induced unconventional quantum criticality in the coupled spin ladder antiferromagnet $C_9H_{18}N_2CuBr_4$: T. Hong, T. Ying, Q. Huang, S. E. Dissanayake, Y. Qiu, M. M. Turnbull, A. A. Podlesnyak, Y. Wu, H. Cao, Y. Liu, I. Umehara, J. Gouchi, Y. Uwatoko, M. Matsuda, D. A. Tennant, G.-W. Chern, K. P. Schmidt and S. Wessel, Nat Commun **13**, 3073(1-9) (2022).

19. Pressured-induced superconducting phase with large upper critical field and concomitant enhancement of antiferromagnetic transition in $EuTe_2$: P. T. Yang, Z. Y. Liu, K. Y. Chen, X. L. Liu, X. Zhang, Z. H. Yu, H. Zhang, J. P. Sun, Y. Uwatoko, X. L. Dong, K. Jiang, J. P. Hu, Y. F. Guo, B. S. Wang and J. -G. Cheng, Nat Commun **13**, 2975(1-9) (2022).

20. Pressure-induced monotonic enhancement of Tc to over 30 K in superconducting $Pr_{0.82}Sr_{0.18}NiO_2$ thin films: N. N. Wang, M. W. Yang, Z. Yang, K. Y. Chen, H. Zhang, Q. H. Zhang, Z. H. Zhu, Y. Uwatoko, L. Gu, X. L. Dong, J. P. Sun, K. J. Jin and J. -G. Cheng, Nat Commun **13**, 4367(1-8) (2022).

21. Emergence of Superconductivity on the Border of Antiferromagnetic Order in $RbMn_6Bi_5$ under High Pressure: A New Family of Mn-Based Superconductors: P.-T. Yang, Q.-X. Dong, P.-F. Shan, Z.-Y. Liu, J.-P. Sun, Z.-L. Dun, Y. Uwatoko, G.-F. Chen, B.-S. Wang and J.-G. Cheng, Chinese Phys. Lett. **39**, 067401 (2022).

22. Roles of surface and bulk states in giant magnetoresistance and anomalous hall effect in antiferromagnetically ordered $Bi_{1.9}Dy_{0.1}Te_3$ topological insulators: V. K. Gangwar, S. Kumar, M. Singh, D. Pal, L. Ghosh, P. Singh, Z. Yufeng, C. Chen, E. F. Schwier, K. Shimada, P. Shahi, Y. Uwatoko, S. Patil, A. K. Ghosh and S. Chatterjee, J. Mater. Chem. C **10**, 17281-17290 (2022).

23. Temperature-Pressure Phase Diagram and Possible Pressure-Driven New Electronic Phase in the Polar Metal $LiOsO_3$: J. -G. Cheng, J. -S. Zhou and Y. Uwatoko, ECS J. Solid State Sci. Technol. **11**, 023008(1-4) (2022).

24. Phthalocyanine-Based Radicals as Single-Component Molecular Conductors: R. Sato, J. Gouchi, Y. Uwatoko and M. Matsuda, Bull. chem. Soc. Jpn. **95**, 680-682 (2022).

25. Complex evolution of the magnetic transitions and unexpected absence of bulk superconductivity in chemically precompressed $NaMn_6Bi_5$: P. F. Shan, Q. X. Dong, P. T. Yang, L. Xu, Z. Y. Liu, L. F. Shi, N. N. Wang, J. P. Sun, Y. Uwatoko, G. F. Chen, B. S. Wang and J. -G. Cheng, Phys. Rev. B **107**, 094519(1-7) (2023).

Ozaki group

As a continuous research from the FY2021, we explored novel periodic structures of multi-sized hard spheres by a random structure searching method, and identified 60 putative densest ternary sphere packings (DTSPs), where the 59 packings have been discovered by our studies for the first time. We found that some of the discovered DTSPs are well-ordered, for example, the medium spheres in the (9-7-3) structure are placed in a straight line with comprising the unit cell, and that some of DTSPs correspond to real crystals. Our study suggests that the diverse structures of DTSPs can be effectively used as structural prototypes for searching ternary, quaternary, and quinary crystal structures. Using two DTSPs, the (13-2-1) and (13-3-1) structures, among the DTSPs as structure prototypes, we exhaustively searched quaternary metal hydrides for the 73 304 candidate hydrides, and identify 23 hydrides with static and dynamic stability, including $H_{12}ScY_2La$ and $H_{12}TiNi_3Ba$. The superconducting transition temperatures T_c, calculated by density functional theory for superconductors, are found to be 5.7 and 6.7 K for the selected two hydrides $H_{12}ScY_2Ca$ and $H_{12}ScY_2Sr$, respectively. We expect that the 23 candidates of hydrides screened by the exhaustive search for 73304 hydrides provide a guideline to narrow down the search space for trials in the experimental synthesis of quaternary metal hydrides.

* Joint research among groups within ISSP.

1. †*Structural and electronic evidence of boron atomic chains: Y. Tsujikawa, M. Horio, X. Zhang, T. Senoo, T. Nakashima, Y. Ando, T. Ozaki, I. Mochizuki, K. Wada, T. Hyodo, T. Iimori, F. Komori, T. Kondo and I. Matsuda, Phys. Rev. B **106**, 205406(1-9) (2022).

2. *Elucidation of the atomic-scale processes of dissociative adsorption and spillover of hydrogen on the single atom alloy catalyst Pd/Cu(111): W. Osada, S. Tanaka, K. Mukai, M. Kawamura, Y. Choi, F. Ozaki, T. Ozaki and J. Yoshinobu, Phys. Chem. Chem. Phys. **24**, 21705-21713 (2022).

3. Prediction of quaternary hydrides based on densest ternary sphere packings: R. Koshoji, M. Fukuda, M. Kawamura and T. Ozaki, Phys. Rev. Materials **6**, 114802 (2022).

4. Diverse densest ternary sphere packings: R. Koshoji and T. Ozaki, J. Phys. Commun. **6**, 075002 (2022).

5. Absolute Binding Energies of Core Levels in Solids from First Principles: T. Ozaki, Vacuum and Surface Science **65**, 236-241 (2022).

6. †*Ambipolar Nickel Dithiolene Complex Semiconductors: From One- to Two-Dimensional Electronic Structures Based upon Alkoxy Chain Lengths: M. Ito, T. Fujino, L. Zhang, S. Yokomori, T. Higashino, R. Makiura, K. J. Takeno, T. Ozaki and H. Mori, J. Am. Chem. Soc. **145**, 2127 (2023).

Noguchi group

We have studied (1) theoretical analysis of isotropic and anisotropic curvature-inducing proteins onto membranes, (2) reaction-diffusion waves on a deformable membrane tube,(3) conformations of ultra-long-chain fatty acids, (4) cavitation generated by a sound wave, and (5) assembly of peptide amphiphiles.

1. Hydrophobic immiscibility controls self-sorting or co-assembly of peptide amphiphiles: R. Wakabayashi, R. Imatani, M. Katsuya, Y. Higuchi, H. Noguchi, N. Kamiya and M. Goto, Chem. Commun. **58**, 585 (2022).

2. †Conformations of Three Types of Ultra-Long-Chain Fatty Acids in Multicomponent Lipid Bilayers: K. Kawaguchi, H. Nagao, H. Shindou and H. Noguchi, J. Phys. Chem. B **126**, 9316-9324 (2022).

3. Membrane shape deformation induced by curvature-inducing proteins consisting of chiral crescent binding and intrinsically disordered domains: H. Noguchi, J. Chem. Phys. **157**, 034901(1-8) (2022).

4. Excitable reaction-diffusion waves of curvature-inducing proteins on deformable membrane tubes: N. Tamemoto and H. Noguchi, Phys. Rev. E **106**, 024403 (2022).

5. Anisotropic, Degradable Polymer Assemblies Driven by a Rigid Hydrogen-Bonding Motif That Induce Shape-Specific Cell Responses: K. Fukushima, K. Matsuzaki, M. Oji, Y. Higuchi, G. Watanabe, Y. Suzuki, M. Kikuchi, N. Fujimura, N. Shimokawa, H. Ito, T. Kato, S. Kawaguchi and M. Tanaka, Macromolecules **55**, 15 (2022).

6. Nonequilibrium dynamics of a fluid vesicle: Turing patterns and traveling waves: H. Noguchi and N. Tamemoto, J. Phys.: Conf. Ser. **2207**, 012017 (2022).

7. †Binding of anisotropic curvature-inducing proteins onto membrane tubes: H. Noguchi, C. Tozzi and M. Arroyo, Soft Matter **18**, 3384-3394 (2022).

8. †Effects of vapor-liquid phase transitions on sound-wave propagation: A molecular dynamics study: Y. Asano, H. Watanabe and H. Noguchi, Phys. Rev. Fluids **7**, 064302 (2022).

9. Membrane domain formation induced by binding/unbinding of curvature-inducing molecules on both membrane surfaces: H. Noguchi, Soft Matter **19**, 679-688 (2023).

10. Disappearance, division, and route change of excitable reaction-diffusion waves in deformable membranes: H. Noguchi, Sci Rep **13**, 6207(1-8) (2023).

11. Binding of curvature-inducing proteins onto biomembranes: H. Noguchi, Int. J. Mod. Phys. B **36**, 2230002 (2022).

12. 曲率誘導タンパク質の反応拡散による生体膜のパターン形成：野口 博司，爲本 尚樹，生物物理 **62**, 338-340 (2022).

Yoshimi group

We have developed and enhanced the usability of programs adopted in the project for advancement of software usability in materials science (PASUMS). Our group's activity of 2022 include functional and usability enhancement of (1) abICS and (2) H-wave. We published five papers about the developed software packages (PHYSBO, TeNeS, 2DMAT, abICS and MateriApp-

† Joint research with outside partners.

sInstaller) in PASUMS. In addition, using the software packages developed by PASUMS, we have studied electronic properties of organic conductors such as β'-[Pd(dmit)$_2$]$_2$, α-(BEDT-TTF)$_2$I$_3$ and α-(BEDT-TSeF)$_2$I$_3$.

1. †Interaction-induced quantum spin Hall insulator in the organic Dirac electron system α-(BEDT-TSeF)$_2$I$_3$: D. Ohki, K. Yoshimi and A. Kobayashi, Phys. Rev. B **105**, 205123 (2022).

2. †Robust analytic continuation combining the advantages of the sparse modeling approach and the Padé approximation: Y. Motoyama, K. Yoshimi and J. Otsuki, Phys. Rev. B **105**, 035139 (2022).

3. †Facilitating *ab initio* configurational sampling of multicomponent solids using an on-lattice neural network model and active learning: S. Kasamatsu, Y. Motoyama, K. Yoshimi, U. Matsumoto, A. Kuwabara and T. Ogawa, J. Chem. Phys. **157**, 104114 (2022).

4. Bayesian optimization package: PHYSBO: Y. Motoyama, R. Tamura, K. Yoshimi, K. Terayama, T. Ueno and K. Tsuda, Computer Physics Communications **278**, 108405 (2022).

5. †Data-analysis software framework 2DMAT and its application to experimental measurements for two-dimensional material structures: Y. Motoyama, K. Yoshimi, I. Mochizuki, H. Iwamoto, H. Ichinose and T. Hoshi, Computer Physics Communications **280**, 108465 (2022).

6. sim-trhepd-rheed – Open-source simulator of total-reflection high-energy positron diffraction (TRHEPD) and reflection high-energy electron diffraction (RHEED): T. Hanada, Y. Motoyama, K. Yoshimi and T. Hoshi, Computer Physics Communications **277**, 108371 (2022).

7. †*TeNeS: Tensor network solver for quantum lattice systems: Y. Motoyama, T. Okubo, K. Yoshimi, S. Morita, T. Kato and N. Kawashima, Computer Physics Communications **279**, 108437 (2022).

8. †*Unconventional dual 1*D*–2*D* quantum spin liquid revealed by ab initio studies on organic solids family: K. Ido, K. Yoshimi, T. Misawa and M. Imada, npj Quantum Mater. **7**, 48 (2022).

9. Efficient ab initio many-body calculations based on sparse modeling of Matsubara Green's function: H. Shinaoka, N. Chikano, E. Gull, J. Li, T. Nomoto, J. Otsuki, M. Wallerberger, T. Wang and K. Yoshimi, SciPost Phys. Lect. Notes **63**, 1 (2022).

10. †*MateriApps LIVE! and MateriApps Installer: Environment for starting and scaling up materials science simulations: Y. Motoyama, K. Yoshimi, T. Kato and S. Todo, SoftwareX **20**, 101210 (2022).

11. *Data Analysis of Ab initio Effective Hamiltonians in Iron-Based Superconductors — Construction of Predictors for Superconducting Critical Temperature: K. Ido, Y. Motoyama, K. Yoshimi and T. Misawa, J. Phys. Soc. Jpn. **92**, 064702 (2023).

12. †Gap opening mechanism for correlated Dirac electrons in organic compounds α-(BEDT−TTF)$_2$I$_3$ and α-(BEDT−TSeF)$_2$I$_3$: D. Ohki, K. Yoshimi, A. Kobayashi and T. Misawa, Phys. Rev. B **107**, L041108 (2023).

13. †*Precise Control of the Molecular Arrangement of Organic Semiconductors for High Charge Carrier Mobility: R. Akai, K. Oka, S. Dekura, K. Yoshimi, H. Mori, R. Nishikubo, A. Saeki and N. Tohnai, J. Phys. Chem. Lett. **14**, 3461 (2023).

Okamoto group

The discovery of a new material has a potential to trigger the evolution of condensed matter physics. We aim at discovering new materials of crystalline solids that exhibit novel quantum phenomena and innovative electronic functions. In this year, we reported the results of our research on chromium tellurides and iridium and tungsten oxides. (1) We showed that sintered samples of Cr telluride Cr_3Te_4 and Cr_2Te_3 exhibit large magnetic-field-induced strains accompanied by large volume changes though the different mechanism from magnetostriction in ferromagnetic metals. In Cr_3Te_4, volume increases of 500-1170 ppm by applying a magnetic field of 9 T are observed over the entire temperature range below 350 K. (2) Physical properties of sintered samples of $Ca_2Ir_2O_7$, in which pentavalent Ir atoms with $5d^4$ electron configuration form a pyrochlore structure, have been studied. The obtained experimental data strongly suggest that $Ca_2Ir_2O_7$ is metallic below room temperature and exhibits no electronic or magnetic phase transitions above 0.12 K.

1. †Electronic Properties of Pyrochlore-Type $Ca_2Ir_2O_7$: Y. Nakayama, Y. Okamoto, D. Hirai and K. Takenaka, J. Phys. Soc. Jpn. **91**, 125002(1-2) (2022).

2. Electronic structure reconstruction by trimer formation in CsW_2O_6 studied by x-ray photoelectron spectroscopy: R. Nakamura, D. Takegami, A. Melendez-Sans, L. H. Tjeng, M. Okawa, T. Miyoshino, N. L. Saini, M. Kitamura, D. Shiga, H. Kumigashira, M. Yoshimura, K. -D. Tsuei, Y. Okamoto and T. Mizokawa, Phys. Rev. B **106**, 195104(1-6) (2022).

* Joint research among groups within ISSP.

3. *Large magnetic-field-induced strains in sintered chromium tellurides: Y. Kubota, Y. Okamoto, T. Kanematsu, T. Yajima, D. Hirai and K. Takenaka, Appl. Phys. Lett. **122**, 042404 (2023).

Neutron Science Laboratory

Yamamuro group

Our laboratory is studying chemical physics of complex condensed matters by using neutron scattering, X-ray diffraction, calorimetric, dielectric, and viscoelastic techniques. Our target materials are glasses, liquids, and various disordered systems. In 2022, we obtained great progress for structural studies on molecular liquids under high pressure. We have performed synchrotron-radiation X-ray diffraction works using a Paris-Edinburgh cell (< 5 GPa) and BL37XU, where focusing high energy X-ray is available, at SPring-8. A new anvil system workable at low temperature (200-300 K) was developed for our experiments. Neutron diffraction experiments were also conducted using the high-pressure instrument BL11, PLANET at J-PARC. The target materials are toluene, which is a typical van der Walls liquid and a series of polyalcohols, methanol CH_3OH, ethylene glycol $CH_2(OH)CH_2(OH)$, and glycerol $CH_2(OH)CH(OH)CH_2(OH)$. For toluene, we found that the intermolecular correlation is developed under high pressure, and that orientationally ordered structure is not changed much at low temperature. For glycerol and ethylene glycol, more compact intramolecular structures keeping hydrogen bonds were found under high pressure and their structures were not changed much at low temperature. Methanol exhibited intermediate pressure and temperature change between toluene and glycerol (and ethylene glycol). These results are partly confirmed by classical and the ab initio (Car-Parinello) MD simulations. The present results are completely new and will give a great impact on future research of glass transitions. Other than these results, we have obtained many interesting heat capacity and quasielastic neutron scattering (QENS) data on MOF (metal-organic-framework) and clathrate hydrate systems using our custom-made adiabatic calorimeters and the C3-1-1, AGNES spectrometer that we are managing at JRR-3, JAEA.

1. Intermolecular correlations of liquid and glassy CS_2 studied by synchrotron radiation x-ray diffraction: Y. Mizuno, Y. Zhao, H. Akiba, S. Kohara, K. Ohara, M. G. Tucker, M. T. McDonnell and O. Yamamuro, J. Chem. Phys. **156**, 034503 (2022).

2. Synergistic Stimulation of Metal-Organic Frameworks for Stable Super-cooled Liquid and Quenched Glass: Z. Yin, Y. Zhao, S. Wan, J. Yang, Z. Shi, S. -X. Peng, M. -Z. Chen, T. -Y. Xie, T. -W. Zeng, O. Yamamuro, M. Nirei, H. Akiba, Y. -B. Zhang, H. -B. Yu and M. -H. Zeng, J. Am. Chem. Soc. **144**, 13021-13025 (2022).

3. Structure of water-in-salt and water-in-bisalt electrolytes: M. A. González, H. Akiba, O. Borodin, G. J. Cuello, L. Hennet, S. Kohara, E. J. Maginn, L. Mangin-Thro, O. Yamamuro, Y. Zhang, D. L. Price and M. -L. Saboungi, Phys. Chem. Chem. Phys. **24**, 10727-10736 (2022).

4. Relative effects of polymer composition and sample preparation on glass dynamics: R. M. Elder, A. L. Forster, A. Krishnamurthy, J. M. Dennis, H. Akiba, O. Yamamuro, K. Ito, K. M. Evans, C. Soles and T. W. Sirk, Soft Matter **18**, 6511-6516 (2022).

5. Rotation of complex ions with ninefold hydrogen coordination studied by quasielastic neutron scattering and first-principles molecular dynamics calculations: Y. Ohmasa, S. Takagi, K. Toshima, K. Yokoyama, W. Endo, S. Orimo, H. Saitoh, T. Yamada, Y. Kawakita, K. Ikeda, T. Otomo, H. Akiba and O. Yamamuro, Phys. Rev. Research **4**, 033215 (2022).

6. Nanoscale structure of a hybrid aqueous–nonaqueous electrolyte: M. -L. Saboungi, O. Borodin, D. Price, B. Farago, M. A. González, S. Kohara, L. Mangin-Thro, A. Wildes and O. Yamamuro, J. Chem. Phys. **158**, 124502 (2023).

7. Reversible Transition between Discrete and 1D Infinite Architectures: A Temperature-Responsive Cu(I) Complex with a Flexible Disilane-Bridged Bis(pyridine) Ligand: Y. Zhao, T. Nakae, S. Takeya, M. Hattori, D. Saito, M. Kato, Y. Ohmasa, S. Sato, O. Yamamuro, T. Galica, E. Nishibori, S. Kobayashi, T. Seki, T. Yamada and Y. Yamanoi, Chemistry-A European Journal **29**, in press (2023).

8. The phase diagram of the API benzocaine and its highly persistent, metastable crystalline polymorphs: I. B. Rietveld, H. Akiba, O. Yamamuro, M. D. Barrio, R. Céolin and J. L. Tamarit, Pharmaceutics **15**, in press (2023).

Masuda group

The goal of our research is to discover a new quantum phenomenon and to reveal the mechanism of it. In this fiscal year we studied the following topics; magnetic diffuse and quasi-elastic scatterings in frustrated magnet $YBaCo_4O_7$, anomalous magnetic moment direction under magnetic anisotropy originated from crystalline electric field in van der Waals compounds

† Joint research with outside partners.

$CeTe_3$ and $CeTe_2Se$, damped dirac magnon in the metallic kagome antiferromagnet FeSn.

1. Anomalous Magnetic Moment Direction under Magnetic Anisotropy Originated from Crystalline Electric Field in van der Waals Compounds $CeTe_3$ and $CeTe_2Se$: D. Ueta, R. Kobayashi, H. Sawada, Y. Iwata, S.-I. Yano, S. Kuniyoshi, Y. Fujisawa, T. Masuda, Y. Okada and S. Itoh, J. Phys. Soc. Jpn. **91**, 094706(1-6) (2022).

2. Magnetic Diffuse and Quasi-Elastic Scatterings in Frustrated Magnet $YBaCo_4O_7$: M. Soda, M. Kofu, S. Ohira-Kawamura, S. Asai, T. Masuda, H. Yoshizawa and H. Kawano-Furukawa, J. Phys. Soc. Jpn. **91**, 094707(1-5) (2022).

3. Damped Dirac magnon in the metallic kagome antiferromagnet FeSn: S.-H. Do, K. Kaneko, R. Kajimoto, K. Kamazawa, M. B. Stone, J. Y. Y. Lin, S. Itoh, T. Masuda, G. D. Samolyuk, E. Dagotto, W. R. Meier, B. C. Sales, H. Miao and A. D. Christianson, Phys. Rev. B **105**, L180403(1-6) (2022).

4. Spin excitation in the coupled honeycomb lattice compound Ni_2InSbO_6: Z. Liu, Y. Araki, T.-H. Arima, S. Itoh, S. Asai and T. Masuda, Phys. Rev. B **107**, 064428(1-8) (2023).

Nakajima group

Nakajima group is studying magnetic materials with cross-correlated phenomena associated with the symmetry of the magnetic structures by means of neutron and X-ray scattering techniques. We are also responsible for a polarized-neutron triple-axis neutron spectrometer PONTA in the research reactor JRR-3 in Tokai, which restarted in 2021 after the long shutdown since the east Japan great earthquake in 2011. As the instrument team of PONTA, we have been supporting the users of the joint-use program, and have collaborated in their researches. One of the successful research collaborations is the magnetic structure analysis of the van der Waals magnet $CoTa_3S_6$. Prof. Seki's group in the University of Tokyo synthesized single crystals of this compound, and found that this compound exhibits a large spontaneous Hall effect without accompanying ferromagnetic moment. Temperature variations of the Hall resistivity and magnetic susceptibility indicate that the large Hall effect is induced by an antiferromagnetic order at low temperatures. We performed polarized neutron scattering experiment at PONTA, revealing that the spontaneous Hall effect arises from an all-in-all-out type non-coplanar magnetic order with broken time-reversal symmetry, which can be a source of the Hall effect.

1. †Square and rhombic lattices of magnetic skyrmions in a centrosymmetric binary compound: R. Takagi, N. Matsuyama, V. Ukleev, L. Yu, J. S. White, S. Francoual, J. R. L. Mardegan, S. Hayami, H. Saito, K. Kaneko, K. Ohishi, Y. Onuki, T.-H. Arima, Y. Tokura, T. Nakajima and S. Seki, Nat Commun 13, 1472 (2022).

2. Zoology of Multiple-*Q* Spin Textures in a Centrosymmetric Tetragonal Magnet with Itinerant Electrons: N. D. Khanh, T. Nakajima, S. Hayami, S. Gao, Y. Yamasaki, H. Sagayama, H. Nakao, R. Takagi, Y. Motome, Y. Tokura, T. Arima and S. Seki, Advanced Science 9, 2105452 (2022).

3. †Polarized neutron scattering study of the centrosymmetric skyrmion host material Gd_2PdSi_3: J. Ju, H. Saito, T. Kurumaji, M. Hirschberger, A. Kikkawa, Y. Taguchi, T.-H. Arima, Y. Tokura and T. Nakajima, Phys. Rev. B 107, 024405 (2023).

4. †Spontaneous topological Hall effect induced by non-coplanar antiferromagnetic order in intercalated van der Waals materials: H. Takagi, R. Takagi, S. Minami, T. Nomoto, K. Ohishi, M. -T. Suzuki, Y. Yanagi, M. Hirayama, N. D. Khanh, K. Karube, H. Saito, D. Hashizume, R. Kiyanagi, Y. Tokura, R. Arita, T. Nakajima and S. Seki, Nat. Phys., (advanced online publication) (2023).

5. †Crystal electric field level scheme leading to giant magnetocaloric effect for hydrogen liquefaction.: N. Terada, H. Mamiya, H. Saito, T. Nakajima, T. D. Yamamoto, K. Terashima, H. Takeya, O. Sakai, S. Itoh, Y. Takano, M. Hase and H. Kitazawa, Commun. Mater. 4, 13 (2023).

Mayumi group

Mayumi group has found that strain-induced crystallization occurs in simple polymer gels with homogeneous network structures. Also, we have performed quasi-elastic neutron scattering experiments on stretched polymer gels to detect the local strain distribution in the deformed polymer networks.

1. Quasi-elastic neutron scattering study on dynamics of polymer gels with controlled inhomogeneity under uniaxial deformation: K. Aomura, Y. Yasuda, T. Yamada, T. Sakai and K. Mayumi, Soft Matter **19**, 147-152 (2022).

2. †High-yield one-pot synthesis of polyrotaxanes with tunable well-defined threading ratios over a wide range: T. Noritomi, L. Jiang, H. Yokoyama, K. Mayumi and K. Ito, RSC Advances **12**, 3796–3800 (2022).

3. Tri-branched gels: Rubbery materials with the lowest branching factor approach the ideal elastic limit: T. Fujiyabu, N. Sakumichi, T. Katashima, C. Liu, K. Mayumi, U.-I. Chung and T. Sakai, Science Advances **8**, eabk0010 (2022).

* Joint research among groups within ISSP.

4. A neuromechanical model for Drosophila larval crawling based on physical measurements: X. Sun, Y. Liu, C. Liu, K. Mayumi, K. Ito, A. Nose and H. Kohsaka, BMC Biol **20**, 130 (2022).

5. Fabrication of Polyelectrolyte Sheets of Unimolecular Thickness via MOF-Templated Polymerization: A. Nishijima, Y. Hayashi, K. Mayumi, N. Hosono and T. Uemura, Macromolecules **56**, 3141–3148 (2023).

6. Phantom Chain Simulations for the Fracture of Energy-Minimized Tetra- and Tri-Branched Networks: Y. Masubuchi, Y. Doi, T. Ishida, N. Sakumichi, T. Sakai, K. Mayumi and T. Uneyama, Macromolecules **56**, 2217-2223 (2023).

International MegaGauss Science Laboratory

Kindo group

We have installed a super-capacitor bank for long pulsed magnet. The bank has a capability of generating magnetic field of 60 T with a duration of 1 to 2 seconds. The bank consists of three units. Each unit has the maximum energy of 60 MJ, 60 MJ and 30 MJ. The maximum current is 18 kA, 18 kA and 9 kA, respectively.

1. *Topological Phase Transitions and Critical Phenomena Associated with Unwinding of Spin Crystals by High Magnetic Fields: N. Kanazawa, Y. Fujishiro, K. Akiba, R. Kurihara, H. Mitamura, A. Miyake, A. Matsuo, K. Kindo, M. Tokunaga and Y. Tokura, J. Phys. Soc. Jpn. **91**, 1010021(14 pages) (2022).

2. †Anomalous low-temperature physical properties of the ytterbium-based Kondo-lattice compounds Yb_4TGe_8 (T = Cr, Mn, Fe, Co, and Ni): S. Yamanaka, M. Hikiji, C. Michioka, H. Ueda, A. Matsuo, K. Kindo, H. Yamaoka, N. Tsujii and K. Yoshimura, Phys. Rev. B **106**, 024402 (2022).

3. †Field-orientation dependence of quantum phase transitions in the S = 1/2 triangular-lattice antiferromagnet $Ba_3CoSb_2O_9$: K. Okada, H. Tanaka, N. Kurita, D. Yamamoto, A. Matsuo and K. Kindo, Phys. Rev. B **106**, 104415 (2022).

4. †Ground state of the S = 1/2 triangular lattice Heisenberg-like antiferromagnet $Ba_3CoSb_2O_9$ in an out-of-plane magnetic field: X. Z. Liu, O. Prokhnenko, M. Bartkowiak, A. Gazizulina, D. Yamamoto, A. Matsuo, K. Kindo, K. Okada, N. Kurita and H. Tanaka, Phys. Rev. B **105**, 214433 (2022).

5. *Magnetic field and pressure phase diagrams of the triangular-lattice antiferromagnet $CsCuCl_3$ explored via magnetic susceptibility measurements with a proximity-detector oscillator: K. Nihongi, T. Kida, Y. Narumi, J. Zaccaro, Y. Kousaka, K. Inoue, K. Kindo, Y. Uwatoko and M. Hagiwara, Phys. Rev. B **105**, 184416(1-7) (2022).

6. †*Nature of field-induced antiferromagnetic order in Zn-doped $CeCoIn_5$ and its connection to quantum criticality in the pure compound: M. Yokoyama, Y. Honma, Y. Oshima, Rahmanto, K. Suzuki, K. Tenya, Y. Shimizu, D. Aoki, A. Matsuo, K. Kindo, S. Nakamura, Y. Kono, S. Kittaka and T. Sakakibara, Phys. Rev. B **105**, 054515(9 pages) (2022).

7. Optical selection rules of the magnetic excitation in the S = 1/2 one-dimensional Ising-like antiferromagnet $BaCo_2V_2O_8$: S. Kimura, H. Onishi, A. Okutani, M. Akaki, Y. Narumi, M. Hagiwara, K. Okunishi, K. Kindo, Z. He, T. Taniyama and M. Itoh, Phys. Rev. B **105**, 014417(9 pages) (2022).

8. †Perfect kagome-lattice antiferromagnets with J_{eff} = 1/2 : The Co^{2+} analogs of the copper minerals volborthite and vesignieite: Y. Haraguchi, T. Ohnoda, A. Matsuo, K. Kindo and H. A. Katori, Phys. Rev. B **106**, 214421 (2022).

9. Persistence of fermionic spin excitations through a genuine Mott transition in κ-type organics: S. Imajo, N. Kato, R. J. Marckwardt, E. Yesil, H. Akutsu and Y. Nakazawa, Phys. Rev. B **105**, 125130 (2022).

10. *Quantum phase of the chromium spinel oxide $HgCr_2O_4$ in high magnetic fields: S. Kimura, S. Imajo, M. Gen, T. Momoi, M. Hagiwara, H. Ueda and Y. Kohama, Phys. Rev. B **105**, L180405 (2022).

11. Reentrant ferroelectric phase induced by a tilting high magnetic field in $Ni_3V_2O_8$: C. Dong, J. F. Wang, Z. Z. He, Y. T. Chang, M. Y. Shi, Y. R. Song, S. M. Jin, Y. Q. Du, Z. Y. Wu, X. T. Han, K. Kindo and M. Yang, Phys. Rev. B **105**, 024427(6 pages) (2022).

12. †Revised phase diagram of the high-T_c cuprate superconductor Pb-doped $Bi_2Sr_2CaCu_2O_{8+\delta}$ revealed by anisotropic transport measurements: K. Harada, Y. Teramoto, T. Usui, K. Itaka, T. Fujii, T. Noji, H. Taniguchi, M. Matsukawa, H. Ishikawa, K. Kindo, D. S. Dessau and T. Watanabe, Phys. Rev. B **105**, 085131(9 pages) (2022).

13. *Magnetically Hidden State on the Ground Floor of the Magnetic Devil's Staircase: S. Imajo, N. Matsuyama, T. Nomura, T. Kihara, S. Nakamura, C. Marcenat, T. Klein, G. Seyfarth, C. Zhong, H. Kageyama, K. Kindo, T. Momoi and

† Joint research with outside partners.

Y. Kohama, Phys. Rev. Lett. **129**, 147201 (2022).

14. Role of the Anion Layer's Polarity in Organic Conductors β″-(BEDT-TTF)$_2$*X*C$_2$H$_4$SO$_3$ (*X* = Cl and Br): H. Akutsu, M. Uruichi, S. Imajo, K. Kindo, Y. Nakazawa and S. S. Turner, J. Phys. Chem. C **126**, 16529 (2022).

15. Electronic Heat Capacity and Lattice Softening of Partially Deuterated Compounds of κ-(BEDT-TTF)$_2$Cu[N(CN)$_2$]Br: Y. Matsumura, S. Imajo, S. Yamashita, H. Akutsu and Y. Nakazawa, Crystals **12**, 2 (2022).

16. Superconductivity and Charge Ordering in BEDT-TTF Based Organic Conductors with β″-Type Molecular Arrangement: Y. Ihara and S. Imajo, Crystals **12**, 711 (2022).

17. †Birchite Cd$_2$Cu$_2$(PO$_4$)$_2$SO$_4$·5H$_2$O as a model antiferromagnetic spin-1/2 Heisenberg J_1–J_2 chain: M. Fujihala, H. O. Jeschke, K. Morita, T. Kuwai, A. Koda, H. Okabe, A. Matsuo, K. Kindo and S. Mitsuda, Phys. Rev. Materials **6**, 114408 (2022).

18. †Quantum paramagnetism in the hyperhoneycomb Kitaev magnet β−ZnIrO$_3$: Y. Haraguchi, A. Matsuo, K. Kindo and H. A. Katori, Phys. Rev. Materials **6**, L021401(6 pages) (2022).

19. *SmI$_3$: 4f^5 honeycomb magnet with spin-orbital entangled Γ_7 Kramers doublet: H. Ishikawa, R. Kurihara, T. Yajima, D. Nishio-Hamane, Y. Shimizu, T. Sakakibara, A. Matsuo and K. Kindo, Phys. Rev. Materials **6**, 064405 (2022).

20. †Magnetocaloric effect in the Ru-doped MnNiGe system: M. Ito, K. Onda, R. Kashima, A. Matsuo and K. Kindo, Journal of Magnetism and Magnetic Materials **546**, 168767 (2022).

21. †*Dimensional reduction and incommensurate dynamic correlations in the *S* = 1/2 triangular-lattice antiferromagnet Ca$_3$ReO$_5$Cl$_2$: S. A. Zvyagin, A. N. Ponomaryov, J. Wosnitza, D. Hirai, Z. Hiroi, M. Gen, Y. Kohama, A. Matsuo, Y. H. Matsuda and K. Kindo, Nat Commun **13**, 6310 (1-6) (2022).

22. *Emergent anisotropy in the Fulde–Ferrell–Larkin–Ovchinnikov state: S. Imajo, T. Nomura, Y. Kohama and K. Kindo, Nat Commun **13**, 5590 (2022).

23. *Quantum transport evidence of isolated topological nodal-line fermions: H. Kim, J. M. Ok, S. Cha, B. G. Jang, C. I. Kwon, Y. Kohama, K. Kindo, W. J. Cho, E. S. Choi, Y. J. Jo, W. Kang, J. H. Shim, K. S. Kim and J. S. Kim, Nat Commun **13**, 7188 (2022).

24. †Spin-glass transition in the spin–orbit-entangled *J*eff = 0 Mott insulating double-perovskite ruthenate: H. Yatsuzuka, Y. Haraguchi, A. Matsuo, K. Kindo and H. A. Katori, Sci Rep **12**, 2429(6 pages) (2022).

25. *Complex magnetic phase diagram with a small phase pocket in a three-dimensional frustrated magnet CuInCr$_4$S$_8$: M. Gen, H. Ishikawa, A. Ikeda, A. Miyake, Z. Yang, Y. Okamoto, M. Mori, K. Takenaka, H. Sagayama, T. Kurumaji, Y. Tokunaga, T. Arima, M. Tokunaga, K. Kindo, Y. H. Matsuda and Y. Kohama, Phys. Rev. Research **4**, 033148(1-13) (2022).

26. *Band-filling effects in single-crystalline oligomer models for doped PEDOT: 3,4-ethylenedioxythiophene (EDOT) dimer salt with hydrogen-bonded infinite sulfate anion chains: R. Kameyama, T. Fujino, S. Dekura, S. Imajo, T. Miyamoto, H. Okamoto and H. Mori, J. Mater. Chem. C **10**, 7543 (2022).

27. Molecular conductors from bis(ethylenedithio)tetrathiafulvalene with tris(oxalato)gallate and tris(oxalato)iridate: T. J. Blundell, A. L. Morritt, E. K. Rusbridge, L. Quibell, J. Oakes, H. Akutsu, Y. Nakazawa, S. Imajo, T. Kadoya, J.-I. Yamada, S. J. Coles, J. Christensen and L. Martin, Mater. Adv. **3**, 4724 (2022).

28. †*Quantum oscillations in the centrosymmetric skyrmion-hosting magnet GdRu$_2$Si$_2$: N. Matsuyama, T. Nomura, S. Imajo, T. Nomoto, R. Arita, K. Sudo, M. Kimata, N. D. Khanh, R. Takagi, Y. Tokura, S. Seki, K. Kindo and Y. Kohama, Phys. Rev. B **107**, 104421 (2023).

29. Thermodynamic properties of the Mott insulator-metal transition in a triangular lattice system without magnetic order: E. Yesil, S. Imajo, S. Yamashita, H. Akutsu, Y. Saito, A. Pustogow, A. Kawamoto and Y. Nakazawa, Phys. Rev. B **107**, 045133 (2023).

30. *Simultaneous measurement of specific heat and thermal conductivity in pulsed magnetic fields: T. Nomoto, C. Zhong, H. Kageyama, Y. Suzuki, M. Jaime, Y. Hashimoto, S. Katsumoto, N. Matsuyama, C. Dong, A. Matsuo, K. Kindo, K. Izawa and Y. Kohama, Rev. Sci. Instrum. **94**, 054901 (2023).

31. †Enhanced Superconducting Pairing Strength near a Pure Nematic Quantum Critical Point: K. Mukasa, K. Ishida, S. Imajo, M. Qiu, M. Saito, K. Matsuura, Y. Sugimura, S. Liu, Y. Uezono, T. Otsuka, M. Culo, S. Kasahara, Y. Matsuda, N. E. Hussey, T. Watanabe, K. Kindo and T. Shibauchi, Phys. Rev. X **13**, 011032 (2023).

---

* Joint research among groups within ISSP.

Tokunaga group

We newly developed a long-distance optical microscope that can be installed in PPMS. We successfully obtained surface morphology in a magnetic shape-memory alloy using this system. In addition to this, we used various techniques, *e.g.*, magnetization, magnetoresistance, dielectric constant, and magnetostriction, to study various magnetic materials, topological semimetals, superconductors, and semiconductors.

1. Elastic Soft Mode and Electric Quadrupole Response in Excitonic Insulator Candidate $(Ta_{0.952}V_{0.048})_2NiSe_5$: Contribution of Electron–Phonon Interaction: R. Kurihara, Y. Hirose, S. Sano, K. Mitsumoto, A. Miyake, M. Tokunaga and R. Settai, J. Phys. Soc. Jpn. **91**, 024601(1-7) (2022).

2. *Ferroelectric Transition of a Chiral Molecular Crystal BINOL 2DMSO: T. Nomura, T. Yajima, Z. Yang, R. Kurihara, Y. Ishii, M. Tokunaga, Y. H. Matsuda, Y. Kohama, K. Kimura and T. Kimura, J. Phys. Soc. Jpn. **91**, 064702(1-6) (2022).

3. †Magnetism of $Al_xFe_{2-x}GeO_5$ with Andalusite Structure: K. Kakimoto, S. Takada, H. Ohta, Y. Haraguchi, M. Hagihala, S. Torii, T. Kamiyama, H. Mitamura, M. Tokunaga, A. Hatakeyama and H. A. Katori, J. Phys. Soc. Jpn. **91**, 054704/1-7 (2022).

4. Magnetovolume Effect on the First-Order Metamagnetic Transition in UTe_2: A. Miyake, M. Gen, A. Ikeda, K. Miyake, Y. Shimizu, Y. J. Sato, D. Li, A. Nakamura, Y. Homma, F. Honda, J. Flouquet, M. Tokunaga and D. Aoki, J. Phys. Soc. Jpn. **91**, 063703(1-6) (2022).

5. *Topological Phase Transitions and Critical Phenomena Associated with Unwinding of Spin Crystals by High Magnetic Fields: N. Kanazawa, Y. Fujishiro, K. Akiba, R. Kurihara, H. Mitamura, A. Miyake, A. Matsuo, K. Kindo, M. Tokunaga and Y. Tokura, J. Phys. Soc. Jpn. **91**, 1010021(14 pages) (2022).

6. *Closing the hybridization charge gap in the Kondo semiconductor SmB_6 with an ultrahigh magnetic field: D. Nakamura, A. Miyake, A. Ikeda, M. Tokunaga, F. Iga and Y. H. Matsuda, Phys. Rev. B **105**, L241105(1-6) (2022).

7. *Enhancement of giant magnetoelectric effect in Ni-doped $CaBaCo_4O_7$: M. Gen, A. Miyake, H. Yagiuchi, Y. Watanabe, A. Ikeda, Y. H. Matsuda, M. Tokunaga, T. Arima and Y. Tokunaga, Phys. Rev. B **105**, 214412(1-9) (2022).

8. †Highly anisotropic geometrical Hall effect via f-d exchange fields in doped pyrochlore molybdates: H. Fukuda, K. Ueda, Y. Kaneko, R. Kurihara, A. Miyake, K. Karube, M. Tokunaga, Y. Taguchi and Y. Tokura, Phys. Rev. B **106**, 144431(1-7) (2022).

9. †Two Distinct Cu(II)–V(IV) Superexchange Interactions with Similar Bond Angles in a Triangular "CuV_2" Fragment: Y. Wang, M. Fukuda, S. Nikolaev, A. Miyake, K. J. Griffith, M. L. Nisbet, E. Hiralal, R. Gautier, B. L. Fisher, M. Tokunaga, M. Azuma and K. R. Poeppelmeier, Inorg. Chem. **61**, 10234-10241 (2022).

10. †Spin-orbit-derived giant magnetoresistance in a layered magnetic semiconductor $AgCrSe_2$: H. Takahashi, T. Akiba, A. H. Mayo, K. Akiba, A. Miyake, M. Tokunaga, H. Mori, R. Arita and S. Ishiwata, Phys. Rev. Materials **6**, 054602(1-6) (2022).

11. Long-distance polarizing microscope system combined with solenoid-type magnet for microscopy and simultaneous measurement of physical parameters: Y. Kinoshita, T. Miyakawa, X. Xu and M. Tokunaga, Review of Scientific Instruments **93**, 073702(1-7) (2022).

12. Extremely high upper critical field in $BiCh_2$-based (Ch: S and Se) layered superconductor $LaO_{0.5}F_{0.5}BiS_{2-x}Se_x$ (x = 0.22 and 0.69): K. Hoshi, R. Kurihara, Y. Goto, M. Tokunaga and Y. Mizuguchi, Sci Rep **12**, 288(1-8) (2022).

13. †Possible helimagnetic order in Co^{4+}-containing perovskites $Sr_{1-x}Ca_xCoO_3$: H. Takahashi, M. Onose, Y. Kobayashi, T. Osaka, S. Maeda, A. Miyake, M. Tokunaga, H. Sagayama, Y. Yamasaki and S. Ishiwata, APL Materials **10**, 111116(1-7) (2022).

14. †Field-induced multiple metal-insulator crossovers of correlated Dirac electrons of perovskite $CaIrO_3$: R. Yamada, J. Fujioka, M. Kawamura, S. Sakai, M. Hirayama, R. Arita, T. Okawa, D. Hashizume, T. Sato, F. Kagawa, R. Kurihara, M. Tokunaga and Y. Tokura, npj Quantum Mater. **7**, 13(1-6) (2022).

15. *Complex magnetic phase diagram with a small phase pocket in a three-dimensional frustrated magnet $CuInCr_4S_8$: M. Gen, H. Ishikawa, A. Ikeda, A. Miyake, Z. Yang, Y. Okamoto, M. Mori, K. Takenaka, H. Sagayama, T. Kurumaji, Y. Tokunaga, T. Arima, M. Tokunaga, K. Kindo, Y. H. Matsuda and Y. Kohama, Phys. Rev. Research **4**, 033148(1-13) (2022).

16. *Multipole polaron in the devil's staircase of CeSb: Y. Arai, K. Kuroda, T. Nomoto, Z. H. Tin, S. Sakuragi, C. Bareille, S. Akebi, K. Kurokawa, Y. Kinoshita, W. -L. Zhang, S. Shin, M. Tokunaga, H. Kitazawa, Y. Haga, H. S. Suzuki, S. Miyasaka, S. Tajima, K. Iwasa, R. Arita and T. Kondo, Nat. Mater. **21**, 410(1-7) (2022).

† Joint research with outside partners.

17. †Chirality-Dependent Magnetoelectric Responses in a Magnetic-Field-Induced Ferroelectric Phase of Pb(TiO) $Cu_4(PO_4)_4$: K. Kimura, T. Katsuyoshi, A. Miyake, M. Tokunaga, S. Kimura and T. Kimura, Adv Elect Materials **8**, 2200167(1-9) (2022).

18. †Coherent description of the magnetic properties of $SeCuO_3$ versus temperature and magnetic field: X. Rocquefelte, M. Herak, A. Miyake, W. Lafargue-Dit-Hauret, H. Berger, M. Tokunaga and A. Saúl, Phys. Rev. B **107**, 054407(1-8) (2023).

19. Field-induced reentrant insulator state of a gap-closed topological insulator ($Bi_{1-x}Sb_x$) in quantum-limit states: Y. Kinoshita, T. Fujita, R. Kurihara, A. Miyake, Y. Izaki, Y. Fuseya and M. Tokunaga, Phys. Rev. B **107**, 125140(1-9) (2023).

20. †Field-tunable Weyl points and large anomalous Hall effect in the degenerate magnetic semiconductor $EuMg_2Bi_2$: M. Kondo, M. Ochi, R. Kurihara, A. Miyake, Y. Yamasaki, M. Tokunaga, H. Nakao, K. Kuroki, T. Kida, M. Hagiwara, H. Murakawa, N. Hanasaki and H. Sakai, Phys. Rev. B **107**, L121112(1-7) (2023).

21. †Ising-type quasi-one-dimensional ferromagnetism with anisotropic hybridization in UNi_4P_2: A. Maurya, A. Miyake, H. Kotegawa, Y. Shimizu, Y. J. Sato, A. Nakamura, D. Li, Y. Homma, F. Honda, M. Tokunaga and D. Aoki, Phys. Rev. B **107**, 085142(1-6) (2023).

22. †*One-dimensional magnetism in synthetic Pauflerite, β−$VOSO_4$: D. L. Quintero-Castro, G. J. Nilsen, K. Meier-Kirchner, A. Benitez-Castro, G. Guenther, T. Sakakibara, M. Tokunaga, C. Agu, I. Mandal and A. A. Tsirlin, Phys. Rev. Materials **7**, 045003(1-7) (2023).

23. †Ordered and disordered variants of the triangular lattice antiferromagnet $Ca_3NiNb_2O_9$: Crystal growth and magnetic properties: D. Rout, R. Tang, M. Skoulatos, B. Ouladdiaf, Y. Kinoshita, A. Miyake, M. Tokunaga, S. Mahapatra and S. Singh, Phys. Rev. Materials **7**, 024419(1-14) (2023).

24. †Double dome structure of the Bose–Einstein condensation in diluted S = 3/2 quantum magnets: Y. Watanabe, A. Miyake, M. Gen, Y. Mizukami, K. Hashimoto, T. Shibauchi, A. Ikeda, M. Tokunaga, T. Kurumaji, Y. Tokunaga and T.-H. Arima, Nat Commun **14**, 1260(1-9) (2023).

Y. Matsuda group

Ultrahigh magnetic field research in the range of 500 T has been developing and the insulator-metal phase transition induced by such high magnetic fields is observed in VO_2 as well as in SmB_6. As for VO_2, the review article was published along with details of technical developments on the electromagnetic flux compression 1000 T field generator. Breathing pyrochlore compound possesses strong spin-lattice coupling and exhibits a variety of quantum phases in high magnetic fields; $CuInCr_4S_8$ has been studied with multi probes such as magnetization, striction, and dielectric constant. Several intriguing magnetic systems, a poler magnet $CaBaCo_4O_7$, a dimer magnet $Ni_2V_2O_7$, and a triangle lattice magnet $Ca_3ReO_5Cl_2$ have also studied in high magnetic fields. The review of the high magnetic field phases in solid and liquid oxygen has also been reported. The potential field-induced liquid-liquid phase transition is still uncovered and required to do continuous research. As new technical progress, a portable single-turn coil system termed PINK-01 was developed and applied to the X-ray free electron laser experiment. The X-ray diffraction up to 77 T has been performed and a structural transformation in a Mn-oxide was observed.

1. *Ferroelectric Transition of a Chiral Molecular Crystal BINOL 2DMSO: T. Nomura, T. Yajima, Z. Yang, R. Kurihara, Y. Ishii, M. Tokunaga, Y. H. Matsuda, Y. Kohama, K. Kimura and T. Kimura, J. Phys. Soc. Jpn. **91**, 064702(1-6) (2022).

2. †Magnetic-Field-Induced Insulator Metal Transition of W-doped VO_2 Observed by Electromagnetic Flux Compression at ISSP: Y. H. Matsuda, Y. Muraoka, D. Nakamura, A. Ikeda, Y. Ishii, X.-G. Zhou, H. Sawabe and S. Takeyama, J. Phys. Soc. Jpn. **91**, 101008(1-11) (2022).

3. *Closing the hybridization charge gap in the Kondo semiconductor SmB_6 with an ultrahigh magnetic field: D. Nakamura, A. Miyake, A. Ikeda, M. Tokunaga, F. Iga and Y. H. Matsuda, Phys. Rev. B **105**, L241105(1-6) (2022).

4. *Enhancement of giant magnetoelectric effect in Ni-doped $CaBaCo_4O_7$: M. Gen, A. Miyake, H. Yagiuchi, Y. Watanabe, A. Ikeda, Y. H. Matsuda, M. Tokunaga, T. Arima and Y. Tokunaga, Phys. Rev. B **105**, 214412(1-9) (2022).

5. †*Metastable magnetization plateaus in the S = 1 organic spin ladder BIP-TENO induced by a microsecond-pulsed megagauss field: K. Nomura, Y. H. Matsuda, A. Ikeda, Y. Kohama, H. Tsuda, N. Amaya, T. Ono and Y. Hosokoshi, Phys. Rev. B **105**, 214430(1-8) (2022).

6. †Unusual dimerization and magnetization plateaus in S = 1 skew chain $Ni_2V_2O_7$ observed at 120 T: J. J. Cao, Z. W. Ouyang, X. C. Liu, T. T. Xiao, Y. R. Song, J. F. Wang, Y. Ishii, X. G. Zhou and Y. H. Matsuda, Phys. Rev. B **106**, 184409(1-6) (2022).

* Joint research among groups within ISSP.

7. Generating 77 T using a portable pulse magnet for single-shot quantum beam experiments: A. Ikeda, Y. H. Matsuda, X. Zhou, S. Peng, Y. Ishii, T. Yajima, Y. Kubota, I. Inoue, Y. Inubushi, K. Tono and M. Yabashi, Appl. Phys. Lett. **120**, 142403 (5pages) (2022).

8. †*Dimensional reduction and incommensurate dynamic correlations in the S = 1/2 triangular-lattice antiferromagnet $Ca_3ReO_5Cl_2$: S. A. Zvyagin, A. N. Ponomaryov, J. Wosnitza, D. Hirai, Z. Hiroi, M. Gen, Y. Kohama, A. Matsuo, Y. H. Matsuda and K. Kindo, Nat Commun **13**, 6310(1-6) (2022).

9. *Complex magnetic phase diagram with a small phase pocket in a three-dimensional frustrated magnet $CuInCr_4S_8$: M. Gen, H. Ishikawa, A. Ikeda, A. Miyake, Z. Yang, Y. Okamoto, M. Mori, K. Takenaka, H. Sagayama, T. Kurumaji, Y. Tokunaga, T. Arima, M. Tokunaga, K. Kindo, Y. H. Matsuda and Y. Kohama, Phys. Rev. Research **4**, 033148(1-13) (2022).

10. †Solid and Liquid Oxygen under Ultrahigh Magnetic Fields: T. Nomura, Y. H. Matsuda and T. C. Kobayashi, Oxygen **2**, 152-163 (2022).

Kohama group

We have investigated various high-field properties. In magnetic materials, such as $CuInCr_4S_8$, $Ca_3ReO_5Cl_2$, $HaCr_2O_4$, BIP-TENO, and $SrCu_2(BO_3)_2$, the field induced phase transitions have been investigated by magnetization and calorimetry in non-destructive and destructive magnetic fields. In two dimensional conductors, $SrRuO_3$, alpha$(BETS)_2I_3$, and $SrAs_3$, we have investigated the topological properties. Here, the TDO and resistivity measurements have revealed rich transport phenomena in two dimensional materials. Using newly developed rf technique, we have determined the critical field of SmFeAsO at the low temperature limit. We have also succeeded to measure the thermal conductivity for the first time in pulsed magnet.

1. *Ferroelectric Transition of a Chiral Molecular Crystal BINOL 2DMSO: T. Nomura, T. Yajima, Z. Yang, R. Kurihara, Y. Ishii, M. Tokunaga, Y. H. Matsuda, Y. Kohama, K. Kimura and T. Kimura, J. Phys. Soc. Jpn. **91**, 064702(1-6) (2022).

2. High-Field Calorimetric Studies on Low-Dimensional and Frustrated Quantum Magnets: Y. Kohama, J. Phys. Soc. Jpn. **91**, 101004 (2022).

3. †*Metastable magnetization plateaus in the S=1 organic spin ladder BIP-TENO induced by a microsecond-pulsed megagauss field: K. Nomura, Y. H. Matsuda, A. Ikeda, Y. Kohama, H. Tsuda, N. Amaya, T. Ono and Y. Hosokoshi, Phys. Rev. B **105**, 214430(1-8) (2022).

4. *Quantum phase of the chromium spinel oxide $HgCr_2O_4$ in high magnetic fields: S. Kimura, S. Imajo, M. Gen, T. Momoi, M. Hagiwara, H. Ueda and Y. Kohama, Phys. Rev. B **105**, L180405 (2022).

5. *Magnetically Hidden State on the Ground Floor of the Magnetic Devil's Staircase: S. Imajo, N. Matsuyama, T. Nomura, T. Kihara, S. Nakamura, C. Marcenat, T. Klein, G. Seyfarth, C. Zhong, H. Kageyama, K. Kindo, T. Momoi and Y. Kohama, Phys. Rev. Lett. **129**, 147201 (2022).

6. Time-resolved measurements in pulsed magnetic fields: Y. Kohama, T. Nomura, S. Zherlitsyn and Y. Ihara, Journal of Applied Physics **132**, 070903 (2022).

7. High upper critical field (120 T) with small anisotropy of highly hydrogen-substituted SmFeAsO epitaxial film: K. Hanzawa, J. Matsumoto, S. Iimura, Y. Kohama, H. Hiramatsu and H. Hosono, Phys. Rev. Materials **6**, L111801 (2022).

8. †*Dimensional reduction and incommensurate dynamic correlations in the S = 1/2 triangular-lattice antiferromagnet $Ca_3ReO_5Cl_2$: S. A. Zvyagin, A. N. Ponomaryov, J. Wosnitza, D. Hirai, Z. Hiroi, M. Gen, Y. Kohama, A. Matsuo, Y. H. Matsuda and K. Kindo, Nat Commun **13**, 6310(1-6) (2022).

9. *Emergent anisotropy in the Fulde–Ferrell–Larkin–Ovchinnikov state: S. Imajo, T. Nomura, Y. Kohama and K. Kindo, Nat Commun **13**, 5590 (2022).

10. *Quantum transport evidence of isolated topological nodal-line fermions: H. Kim, J. M. Ok, S. Cha, B. G. Jang, C. I. Kwon, Y. Kohama, K. Kindo, W. J. Cho, E. S. Choi, Y. J. Jo, W. Kang, J. H. Shim, K. S. Kim and J. S. Kim, Nat Commun **13**, 7188 (2022).

11. High-mobility two-dimensional carriers from surface Fermi arcs in magnetic Weyl semimetal films: S. Kaneta-Takada, Y. K. Wakabayashi, Y. Krockenberger, T. Nomura, Y. Kohama, S. A. Nikolaev, H. Das, H. Irie, K. Takiguchi, S. Ohya, M. Tanaka, Y. Taniyasu and H. Yamamoto, npj Quantum Mater. **7**, 102 (2022).

12. *Complex magnetic phase diagram with a small phase pocket in a three-dimensional frustrated magnet $CuInCr_4S_8$: M. Gen, H. Ishikawa, A. Ikeda, A. Miyake, Z. Yang, Y. Okamoto, M. Mori, K. Takenaka, H. Sagayama, T. Kurumaji, Y. Tokunaga, T. Arima, M. Tokunaga, K. Kindo, Y. H. Matsuda and Y. Kohama, Phys. Rev. Research **4**, 033148(1-13)

† Joint research with outside partners.

(2022).

13. †*Quantum oscillations in the centrosymmetric skyrmion-hosting magnet $GdRu_2Si_2$: N. Matsuyama, T. Nomura, S. Imajo, T. Nomoto, R. Arita, K. Sudo, M. Kimata, N. D. Khanh, R. Takagi, Y. Tokura, S. Seki, K. Kindo and Y. Kohama, Phys. Rev. B **107**, 104421 (2023).

14. Rhombic skyrmion lattice coupled with orthorhombic structural distortion in $EuAl_4$: M. Gen, R. Takagi, Y. Watanabe, S. Kitou, H. Sagayama, N. Matsuyama, Y. Kohama, A. Ikeda, Y. Onuki, T. Kurumaji, T.-H. Arima and S. Seki, Phys. Rev. B **107**, L020410 (2023).

15. *Simultaneous measurement of specific heat and thermal conductivity in pulsed magnetic fields: T. Nomoto, C. Zhong, H. Kageyama, Y. Suzuki, M. Jaime, Y. Hashimoto, S. Katsumoto, N. Matsuyama, C. Dong, A. Matsuo, K. Kindo, K. Izawa and Y. Kohama, Rev. Sci. Instrum. **94**, 054901 (2023).

16. Nonreciprocal Phonon Propagation in a Metallic Chiral Magnet: T. Nomura, X. -X. Zhang, R. Takagi, K. Karube, A. Kikkawa, Y. Taguchi, Y. Tokura, S. Zherlitsyn, Y. Kohama and S. Seki, Phys. Rev. Lett. **130**, 176301 (2023).

17. フラットトップ磁場を用いたパルス磁場中 NMR 測定 : 井原 慶彦 , 小濱 芳允 , 固体物理 **58**, 89-98 (2023).

18. 新しいカイラル有機超伝導体 : 野村 肇宏 , 固体物理 **58**, 41-45 (2023).

19. Critical Current Measurements of HTS Tapes Using Pulsed Current in High Fields at Low Temperatures: Y. Tsuchiya, I. Sakai, K. Mizuno, Y. Kohama, Y. Yoshida and S. Awaji, IEEE Trans. Appl. Supercond. **33**, 1 (2023).

20. Correlation-driven organic 3D topological insulator with relativistic fermions: T. Nomoto, S. Imajo, H. Akutsu, Y. Nakazawa and Y. Kohama, Nat Commun **14**, 2130 (2023).

Laser and Synchrotron Research Center

Kobayashi group

We are studing a combination between an artificial intelligence and a laser material processing, aiming a construction of a theory.

1. *Stimulated Rayleigh Scattering Enhanced by a Longitudinal Plasma Mode in a Periodically Driven Dirac Semimetal Cd_3As_2: Y. Murotani, N. Kanda, T. N. Ikeda, T. Matsuda, M. Goyal, J. Yoshinobu, Y. Kobayashi, S. Stemmer and R. Matsunaga, Phys. Rev. Lett. **129**, 207402 (2022).

2. Autonomous parameter optimization for femtosecond laser micro-drilling: K. Bamoto, H. Sakurai, S. Tani and Y. Kobayashi, Opt. Express **30**, 243 (2022).

3. Ultrafast laser ablation simulator using deep neural networks: S. Tani and Y. Kobayashi, Sci Rep **12**, 5837 (2022).

Harada group

Application of soft X-ray emission spectroscopy has been significantly advanced, and research on the behavior of interfacial water on the surface of diverse polymer materials have been realized by developing the precise humidification system. As a representative example of this application hydrogen-bonded structure of water on the surface of PMEA, a material used for blood tubing in ECMO against COVID-19, was clarified by comparing infrared spectroscopy and DFT calculations, and a comparison of X-ray emission spectroscopy with AFM revealed that water molecules induce phase separation of polymers and change their biocompatibility. After more than a decade of debate, a theory explaining both the temperature and isotope dependence of soft X-ray emission spectra was completed, and the X-ray emission results of liquid water published since 2008 were finally validated. The electronic state changes of transition metals during charging and discharging of the cathode material $LiMn_2O_4$ and the anode material Fe_2O_3 of lithium-ion batteries were clarified using operando spectroscopy. The CREST project, which aims to integrate soft and hard X-ray imaging techniques with information science, has started, and we reported on high-resolution soft X-ray imaging using a Walter mirror in collaboration with Prof. Kimura's group.

1. †Interpretation of the X-Ray Emission Spectra of Liquid Water through Temperature and Isotope Dependence: O. Takahashi, R. Yamamura, T. Tokushima and Y. Harada, Phys. Rev. Lett. **128**, 086002(1-6) (2022).

2. †Identification of Valence Electronic States Reflecting the Hydrogen Bonding in Liquid Ethanol: R. Yamamura, K. Yamazoe, J. Miyawaki, Y. Harada and O. Takahashi, J. Phys. Chem. B **126**, 1101-1107 (2022).

* Joint research among groups within ISSP.

3. Infrared Spectra and Hydrogen-Bond Configurations of Water Molecules at the Interface of Water-Insoluble Polymers under Humidified Conditions: Y. Ikemoto, Y. Harada, M. Tanaka, S.-N. Nishimura, D. Murakami, N. Kurahashi, T. Moriwaki, K. Yamazoe, H. Washizu, Y. Ishii and H. Torii, J. Phys. Chem. B **126**, 4143-4151 (2022).

4. †Critical In-Plane Density of Polyelectrolyte Brush for the Ordered Hydrogen-Bonded Structure of Incorporated Water: K. Yamazoe, Y. Higaki, Y. Inutsuka, J. Miyawaki, A. Takahara and Y. Harada, Langmuir **38**, 3076-3081 (2022).

5. †Hydration Mechanism in Blood-Compatible Polymers Undergoing Phase Separation: D. Murakami, K. Yamazoe, S.-N. Nishimura, N. Kurahashi, T. Ueda, J. Miyawaki, Y. Ikemoto, M. Tanaka and Y. Harada, Langmuir **38**, 1090-1098 (2022).

6. † 磁場中共鳴非弾性軟 X 線散乱によるハーフメタル型ホイスラー合金のスピン偏極電子構造研究：藤原 秀紀，梅津 理恵，宮脇 淳，原田 慈久，菅 滋正，放射光 **35**, 78-87 (2022).

7. †Electronic Structure of Carbon Dioxide in Sylgard-184 Evaluated by Using X-ray Emission Spectroscopy: R. Matsuno, Y. Nutthon, A. Miyano, K. Ninomiya, M. Nishibori, H. Kiuchi, S. Fujikawa, Y. Harada and A. Takahara, Chem. Lett. **51**, 650-653 (2022).

8. †*Soft X-ray ptychography system using a Wolter mirror for achromatic illumination optics: T. Kimura, Y. Takeo, K. Sakurai, N. Furuya, S. Egawa, G. Yamaguchi, Y. Matsuzawa, T. Kume, H. Mimura, M. Shimura, H. Ohashi, I. Matsuda and Y. Harada, Opt. Express **30**, 26220 (2022).

9. †*Operando* resonant soft X-ray emission spectroscopy of the $LiMn_2O_4$ cathode using an aqueous electrolyte solution: D. Asakura, Y. Nanba, H. Niwa, H. Kiuchi, J. Miyawaki, M. Okubo, H. Matsuda, Y. Harada and E. Hosono, Phys. Chem. Chem. Phys. **24**, 19177-19183 (2022).

10. Editorial: Interfacial Water: A Physical Chemistry Perspective, Volume II: Y. Harada, Front. Chem. **10**, 896586(1-2) (2022).

11. †Conversion Reaction of Anode Material for Li-ion Battery Revealed by *Operando* Soft X-ray Emission Spectroscopy: D. ASAKURA, E. HOSONO and Y. HARADA, 電気化学 **90**, 4-9 (2022).

12. † 放射光を用いた固体高分子型燃料電池正極触媒のオペランド解析：尾嶋 正治，原田 慈久，燃料電池 **21**, 7-13 (2022).

I. Matsuda group

We have devoted ourselves to a project of developing the next-generation synchrotron radiation (SR) facility, NanoTerasu, at Sendai in Miyagi-prefecture. To focus on the project, we discontinued the joint-research at the beamline, SPring-8 BL07LSU, in August. Subsequently, we packed our instruments, two undulators, ambient-pressure XPS system and process-informatics robot units. Then, we successfully transferred them to the NanoTerasu beamlines by the end of the fiscal year. At the X-ray free electron laser (XFEL) beamline, SACLA BL-1, we have developed a new method of nonlinear X-ray spectroscopy and achieved fruitful science of the functional materials. Based on the SR and XFEL experiments, we have also succeeded in synthesizing boron nanomaterials and in unveiling their intriguing physical/chemical properties.

1. *Environmental effects on layer-dependent dynamics of Dirac fermions in quasicrystalline bilayer graphene: Y. Zhao, T. Suzuki, T. Iimori, H. -W. Kim, J. R. Ahn, M. Horio, Y. Sato, Y. Fukaya, T. Kanai, K. Okazaki, S. Shin, S. Tanaka, F. Komori, H. Fukidome and I. Matsuda, Phys. Rev. B **105**, 115304 (2022).

2. †*Homotopic analysis of quantum states in two-dimensional polymorphs by a herringbone lattice model: Y. Ando, X. Zhang, Y. Tsujikawa, Y. Sato, M. Horio, J. Haruyama, O. Sugino, T. Kondo and I. Matsuda, Phys. Rev. B **106**, 195106 (2022).

3. †*Structural and electronic evidence of boron atomic chains: Y. Tsujikawa, M. Horio, X. Zhang, T. Senoo, T. Nakashima, Y. Ando, T. Ozaki, I. Mochizuki, K. Wada, T. Hyodo, T. Iimori, F. Komori, T. Kondo and I. Matsuda, Phys. Rev. B **106**, 205406(1-9) (2022).

4. Element-selective magnetization states in a $Gd_{23}Fe_{67}Co_{10}$ alloy, probed by soft X-ray resonant magneto-optical Kerr effect: T. Sumi, T. Senoo, M. Horio, S. E. Moussaoui, E. Nakamura, K. Tanaka, A. Tsukamoto and I. Matsuda, Jpn. J. Appl. Phys. **62**, SB8001 (2022).

5. *Photoinduced transient states of antiferromagnetic orderings in $La_{1/3}Sr_{2/3}FeO_3$ and $SrFeO_{3-\delta}$ thin films observed through time-resolved resonant soft x-ray scattering: K. Yamamoto, T. Tsuyama, S. Ito, K. Takubo, I. Matsuda, N. Pontius, C. Schüßler-Langeheine, M. Minohara, H. Kumigashira, Y. Yamasaki, H. Nakao, Y. Murakami, T. Katase, T. Kamiya and H. Wadati, New J. Phys. **24**, 043012(1-9) (2022).

6. †Electronic Topological Transition of 2D Boron by the Ion Exchange Reaction: X. Zhang, Y. Tsujikawa, I. Tateishi, M.

† Joint research with outside partners.

Niibe, T. Wada, M. Horio, M. Hikichi, Y. Ando, K. Yubuta, T. Kondo and I. Matsuda, J. Phys. Chem. C **126**, 12802-12808 (2022).

7. †*Soft X-ray ptychography system using a Wolter mirror for achromatic illumination optics: T. Kimura, Y. Takeo, K. Sakurai, N. Furuya, S. Egawa, G. Yamaguchi, Y. Matsuzawa, T. Kume, H. Mimura, M. Shimura, H. Ohashi, I. Matsuda and Y. Harada, Opt. Express **30**, 26220 (2022).

8. The 2022 magneto-optics roadmap: A. Kimel, A. Zvezdin, S. Sharma, S. Shallcross, N. D. Sousa, A. García-Martín, G. Salvan, J. Hamrle, O. Stejskal, J. McCord, S. Tacchi, G. Carlotti, P. Gambardella, G. Salis, M. Münzenberg, M. Schultze, V. Temnov, I. V. Bychkov, L. N. Kotov, N. Maccaferri, D. Ignatyeva, V. Belotelov, C. Donnelly, A. H. Rodriguez, I. Matsuda, T. Ruchon, M. Fanciulli, M. Sacchi, C. R. Du, H. Wang, N. P. Armitage, M. Schubert, V. Darakchieva, B. Liu, Z. Huang, B. Ding, A. Berger and P. Vavassori, J. Phys. D: Appl. Phys. **55**, 463003 (2022).

9. †*Materials Science Research by Ambient Pressure X-ray Photoelectron Spectroscopy Systems at Synchrotron Radiation Facilities in Japan: Applications in Energy, Catalysis, and Sensors: S. Yamamoto, Y. Takagi, T. Koitaya, R. Toyoshima, M. Horio, I. Matsuda, H. Kondoh, T. Yokoyama and J. Yoshinobu, Synchrotron Radiation News **35**, 19-25 (2022).

10. †Surface Exchange Reaction of Mixed Conductive $La_{0.65}Ca_{0.35}FeO_{3-\delta}$ during Oxygen Evolution and Incorporation as Traced by Operando X-ray Photoelectron Spectroscopy: I. Kagomiya, T. Hirano, Y. Yagi, K.-I. Kakimoto, S. Yamamoto and I. Matsuda, ACS Appl. Mater. Interfaces **14**, 48194-48199 (2022).

11. Resolving decay-time dependent photoluminescence induced by phonon-dressed excitons in ZnO: R. Yukawa, S. Yamamoto, R. Arita, Y. Minami, K. Yamanoi, K. Ozawa, K. Sakamoto, T. Shimizu, N. Sarukura and I. Matsuda, Phys. Rev. Materials **6**, 104607 (2022).

12. †*Functionalization of the MoS_2 basal plane for activation of molecular hydrogen by Pd deposition: F. Ozaki, S. Tanaka, W. Osada, K. Mukai, M. Horio, T. Koitaya, S. Yamamoto, I. Matsuda and J. Yoshinobu, Applied Surface Science **593**, 153313 (2022).

13. †*Hydrogen absorption and diffusion behaviors in cube-shaped palladium nanoparticles revealed by ambient-pressure X-ray photoelectron spectroscopy: J. Tang, O. Seo, D. S. R. Rocabado, T. Koitaya, S. Yamamoto, Y. Nanba, C. Song, J. Kim, A. Yoshigoe, M. Koyama, S. Dekura, H. Kobayashi, H. Kitagawa, O. Sakata, I. Matsuda and J. Yoshinobu, Applied Surface Science **587**, 152797 (2022).

14. †Measurement of X-ray Magnetic Linear Dichroism by Rotating Polarization Angle of Soft X-ray Generated by a Segmented Cross Undulator: Y. Kudo, M. Horio, T. Sumi, T. Wada, Y. Hirata, T. Ohkochi, T. Kinoshita and I. Matsuda, e-J. Surf. Sci. Nanotechnol. **20**, 124-127 (2022).

15. Recovery Process from the Reversed Magnetization Simulated with a Square Lattice: T. Senoo, T. Sumi, M. Horio, A. Tsukamoto and I. Matsuda, e-J. Surf. Sci. Nanotechnol. **20**, 221-225 (2022).

16. Separating Non-linear Optical Signals of a Sample from High Harmonic Radiation in a Soft X-ray Free Electron Laser: T. Sumi, M. Horio, T. Senoo, T. Wada, Y. Tsujikawa, X. Zhang, P. Manset, M. Araki, Y. Hirata, W. S. Drisdell, J. W. Freeland, A. Amado, M. Zuerch, Y. Kubota, S. Owada, K. Tono, M. Yabashi, C. P. Schwartz and I. Matsuda, e-J. Surf. Sci. Nanotechnol. **20**, 31(1-5) (2022).

17. Electronic Structures of Polymorphic Layers of Borophane: I. Tateishi, X. Zhang and I. Matsuda, Molecules **27**, 1808(1-13) (2022).

18. Highly Dispersed Ni Nanoclusters Spontaneously Formed on Hydrogen Boride Sheets: N. Noguchi, S.-I. Ito, M. Hikichi, Y. Cho, K. Goto, A. Kubo, I. Matsuda, T. Fujita, M. Miyauchi and T. Kondo, Molecules **27**, 8261(1-12) (2022).

19. Structure of χ_3-Borophene Studied by Total-Reflection High-Energy Positron Diffraction (TRHEPD): Y. Tsujikawa, M. Shoji, M. Hamada, T. Takeda, I. Mochizuki, T. Hyodo, I. Matsuda and A. Takayama, Molecules **27**, 4219(1-8) (2022).

20. Carbon dioxide adsorption and conversion to methane and ethane on hydrogen boride sheets: T. Goto, S.-I. Ito, S. L. Shinde, R. Ishibiki, Y. Hikita, I. Matsuda, I. Hamada, H. Hosono and T. Kondo, Commun Chem **5**, 118(1-10) (2022).

21. Observing soft x-ray magnetization-induced second harmonic generation at a heterojunction interface: T. Sumi, M. Horio, T. Senoo, Y. Kubota, G. Yamaguchi, T. Wada, M. Miyamoto, K. Yamaguchi, Y. Tsujikawa, Y. Sato, M. Niibe, Y. Hirata, Y. Miyauchi, D. Oshima, T. Kato, S. Owada, K. Tono, M. Yabashi and I. Matsuda, Appl. Phys. Lett. **122**, 171601(1-5) (2023).

22. †*Suppression of atomic displacive excitation in photo-induced A_{1g} phonon mode of bismuth unveiled by low-temperature time-resolved x-ray diffraction: Y. Kubota, Y. Tanaka, T. Togashi, T. Ebisu, K. Tamasaku, H. Osawa, T. Wada, O. Sugino, I. Matsuda and M. Yabashi, Appl. Phys. Lett. **122**, 092201 (2023).

* Joint research among groups within ISSP.

23. †*Observing an ordered surface phase by B deposition on Cu(110): Y. Tsujikawa, X. Zhang, M. Horio, T. Wada, M. Miyamoto, T. Sumi, F. Komori, T. Kondo and I. Matsuda, Surface Science **732**, 122282 (2023).

24. †*Accelerated Synthesis of Borophane (HB) Sheets through HCl-Assisted Ion-Exchange Reaction with $YCrB_4$: X. Zhang, M. Hikichi, T. Iimori, Y. Tsujikawa, M. Yuan, M. Horio, K. Yubuta, F. Komori, M. Miyauchi, T. Kondo and I. Matsuda, Molecules **28**, 2985(1-15) (2023).

25. Prediction of a Cyclic Hydrogenated Boron Molecule as a Promising Building Block for Borophane: Y. Ando, T. Nakashima, H. Yin, I. Tateishi, X. Zhang, Y. Tsujikawa, M. Horio, N. T. Cuong, S. Okada, T. Kondo and I. Matsuda, Molecules **28**, 1225(1-13) (2023).

26. †*Developing a Simple Scanning Probe System for Soft X-ray Spectroscopy with a Nano-focusing Mirror: H. Ando, M. Horio, Y. Takeo, M. Niibe, T. Wada, Y. Ando, T. Kondo, T. Kimura and I. Matsuda, e-J. Surf. Sci. Nanotechnol., 2023-020 (2023), in print.

27. Probing lithium mobility at a solid electrolyte surface: C. Woodahl, S. Jamnuch, A. Amado, C. B. Uzundal, E. Berger, P. Manset, Y. Zhu, Y. Li, D. D. Fong, J. G. Connell, Y. Hirata, Y. Kubota, S. Owada, K. Tono, M. Yabashi, S. G. E. T. Velthuis, S. Tepavcevic, I. Matsuda, W. S. Drisdell, C. P. Schwartz, J. W. Freeland, T. A. Pascal, A. Zong and M. Zuerch, Nat. Mater. (2023), accepted for publication.

28. Enhanced Superconductivity and Rashba effect in a Buckled Plumbene-Au Kagome Superstructure: 9.-H. Chen, C.-H. Chen, G.-H. Chen, W.-C. Chen, P. Amrit, F.-X. Chen, P.-J. Chen, C.-K. Ku, C.-T. Lee, N. Kawakami, J.-Y. Li, I. Matsuda, W.-H. Chang, J.-J. Lin, C.-T. Wu, C.-Y. Mou, H.-T. Jeng, S.-J. Tang and C.-L. Lin, Advanced Science (2023), accepted for publication.

29. †*In-Situ Electrical Detection of Methane Oxidation on Atomically Thin IrO_2 Nanosheet Films Down to Room Temperature: Y. Ishihara, T. Koitaya, W. Sugimoto, S. Yamamoto, I. Matsuda, J. Yoshinobu and R. Nouchi, Advanced Materials Interfaces (2023), accepted for publication.

30. 物理科学，この１年　2022: 松田 巌 , 近藤 剛弘他 , (丸善出版 , 東京都千代田区 , 2022).

Itatani group

By using soft X-ray attosecond pulses, we have performed soft X-ray transient absorption spectroscopy of ring-opening reaction dynamics associated with photo-absorption of a ring-shaped molecule 1,3-cyclohexadiene. We found that the Woodward-Hoffmann rule for molecular orbital symmetry holds even in transient chemical reaction states for the first time. Development of a new soft X-ray beamline with a flat water jet was initiated to expand the variation of samples from gas phase to condensed matters. High harmonic generation in the flat water jet was also examined with intense MIR pulses, and we obtained a unique vibrational signal due to molecular vibration. Photoelectron re-scattering experiments associated with tunnel ionization were performed using carrier-envelope phase (CEP)-stable intense ultrashort pulses in the infrared region. The CEP dependence of the momentum distribution of photoelectrons due to backward re-scattering was measured for Kr atoms and CO_2 molecules with nearly equal ionization potentials, and the differential scattering cross sections were derived. We also successfully extracted the influence of the multi-center scattering effect in the case of CO_2 molecules. As for the light source R&D, we have developed a highly CEP-stable infrared light source in the 2 μm region, which is excited by a Yb solid-state laser operating at 100 kHz repetition rate.

1. *Photo-Excitation Band-Structure Engineering of 2*H*-$NbSe_2$ Probed by Time- and Angle-Resolved Photoemission Spectroscopy: M. Watanabe, T. Suzuki, T. Someya, Y. Ogawa, S. Michimae, M. Fujisawa, T. Kanai, J. Itatani, T. Saitoh, S. Shin and K. Okazaki, J. Phys. Soc. Jpn. **91**, 064703 (2022).

2. * パルス内差周波発生法と光パラメトリック増幅による位相安定高強度マルチテラヘルツパルス発生：神田 夏輝 , 石井 順久 , 板谷 治郎 , 松永 隆佑 , レーザー研究 **50**, 286 (2022).

3. †Ultrafast multidimensional spectroscopy with field resolution and noncollinear geometry at mid-infrared frequencies: T. Deckert, J. Allerbeck, T. Kurihara and D. Brida, New J. Phys. **24**, 023005 (1-9) (2022).

4. †Spin canting in nonlinear terahertz magnon dynamics revealed by magnetorefractive probing in orthoferrite: T. Kurihara, M. Bamba, H. Watanabe, M. Nakajima and T. Suemoto, arXiv **2202**, 11365 (2022).

5. †Ultrafast opto-protonics in a hydrogen-bonded π-molecular ferroelectric crystal: Y. Okimoto, P. Xia, J. Itatani, H. Matsushima, T. Ishikawa, S.-Y. Koshihara and S. Horiuchi, APL Materials **10**, 090702 (2022).

6. †*Quasi One-Dimensional Band Structure of Photoinduced Semimetal Phase of $Ta_2Ni_{1-x}Co_xSe_5$ (x = 0.0 and 0.1): T. Mitsuoka, Y. Takahashi, T. Suzuki, M. Okawa, H. Takagi, N. Katayama, H. Sawa, M. Nohara, M. Watanabe, J. Xu, Q. Ren, M. Fujisawa, T. Kanai, J. Itatani, K. Okazaki, S. Shin and T. Mizokawa, J. Phys. Soc. Jpn. **92**, 023703 (2023).

† Joint research with outside partners.

7. Comparative study of photoelectron momentum distributions from Kr and CO_2 near a backward rescattering caustic by carrier-envelope-phase mapping: T. Mizuno, T. Yang, T. Kurihara, N. Ishii, T. Kanai, O. I. Tolstikhin, T. Morishita and J. Itatani, Phys. Rev. A **107**, 033101 (2023).

8. Highly CEP-stable optical parametric amplifier at 2 μm with a few-cycle duration and 100 kHz repetition rate: T. Kurihara, T. Yang, T. Mizuno, T. Kanai and J. Itatani, Opt. Express **31**, 11649 (2023).

9. †Real-time observation of the Woodward–Hoffmann rule for 1,3-cyclohexadiene by femtosecond soft X-ray transient absorption: T. Sekikawa, N. Saito, Y. Kurimoto, N. Ishii, T. Mizuno, T. Kanai, J. Itatani, K. Saita and T. Taketsugu, Phys. Chem. Chem. Phys. **25**, 8497 (2023).

10. †*Direct observation of multiple conduction-band minima in high-performance thermoelectric SnSe: M. Okawa, Y. Akabane, M. Maeda, G. Tan, L.-D. Zhao, M. G. Kanatzidis, T. Suzuki, M. Watanabe, J. Xu, Q. Ren, M. Fujisawa, T. Kanai, J. Itatani, S. Shin, K. Okazaki, N. L. Saini and T. Mizokawa, Scripta Materialia **223**, 115081 (2023).

11. Intense infrared lasers for strong-field science: Z. Chang, L. Fang, V. Fedorov, C. Geiger, S. Ghimire, C. Heide, N. Ishii, J. Itatani, C. Joshi, Y. Kobayashi, P. Kumar, A. Marra, S. Mirov, I. Petrushina, M. Polyanskiy, D. A. Reis, S. Tochitsky, S. Vasilyev, L. Wang, Y. Wu and F. Zhou, Adv. Opt. Photon. **14**, 652 (2022).

12. 超高速光パルスによる強誘電体の光制御(「光と物質の量子相互作用ハンドブック」第３編 第９章): 沖本 洋一 , 板谷 治郎 , 堀内左 智雄 , (エヌ・ティー・エス , 東京都千代田区 , 2023).

Kondo group

We found evidence for the multipole polaron state in the devil's staircase of CeSb, and presented selective observation of surface and bulk bands in polar WTe_2. We also revealed band structure leading to a large anomalous Hall effect in the noncentrosymmetric antiferromagnet $CoNb_3S_6$.

1. *Multipole polaron in the devil's staircase of CeSb: Y. Arai, K. Kuroda, T. Nomoto, Z. H. Tin, S. Sakuragi, C. Bareille, S. Akebi, K. Kurokawa, Y. Kinoshita, W. -L. Zhang, S. Shin, M. Tokunaga, H. Kitazawa, Y. Haga, H. S. Suzuki, S. Miyasaka, S. Tajima, K. Iwasa, R. Arita and T. Kondo, Nat. Mater. **21**, 410(1-7) (2022).

2. Large anomalous Hall effect induced by weak ferromagnetism in the noncentrosymmetric antiferromagnet $CoNb_3S_6$: H. Tanaka, S. Okazaki, K. Kuroda, R. Noguchi, Y. Arai, S. Minami, S. Ideta, K. Tanaka, D. Lu, M. Hashimoto, V. Kandyba, M. Cattelan, A. Barinov, T. Muro, T. Sasagawa and T. Kondo, Phys. Review B **105**, 121102(1-7) (2022).

3. *Selective observation of surface and bulk bands in polar WTe_2 by laser-based spin- and angle-resolved photoemission spectroscopy.: Y. Wan, L. Wang, K. Kuroda, P. Zhang, K. Koshiishi, M. Suzuki, J. Kim, R. Noguchi, C. Bareille, K. Yaji, A. Harasawa, S. Shin, S.-W. Cheong, A. Fujimori and T. Kondo, Phys. Review B **105**, 085421 (2022).

4. *Visualization of optical polarization transfer to photoelectron spin vector emitted from a spin-orbit coupled surface state.: K. Kuroda, K. Yaji, R. Noguchi, A. Harasawa, S. Shin, T. Kondo and F. Komori, Phys. Review B **105**, 121106(1-6) (2022).

5. *Tunable vortex Majorana modes controlled by strain in homogeneous LiFeAs: W. Liu, Q. Hu, X. Wang, Y. Zhong, F. Yang, L. Kong, L. Cao, G. Li, Y. Peng, K. Okazaki, T. Kondo, C. Jin, J. Xu, H. -J. Gao and H. Ding, Quantum Front. **1**, 20 (2022).

6. *Semiconducting Electronic Structure of the Ferromagnetic Spinel $HgCr_2Se_4$ Revealed by Soft-X-Ray Angle-Resolved Photoemission Spectroscopy: H. Tanaka, A. V. Telegin, Y. P. Sukhorukov, V. A. Golyashov, O. E. Tereshchenko, A. N. Lavrov, T. Matsuda, R. Matsunaga, R. Akashi, M. Lippmaa, Y. Arai, S. Ideta, K. Tanaka, T. Kondo and K. Kuroda, Phys. Rev. Lett. **130**, 186402 (1-6) (2023).

7. *Nodeless electron pairing in CsV_3Sb_5-derived kagome superconductors: Y. Zhong, J. Liu, X. Wu, Z. Guguchia, J. -X. Yin, A. Mine, Y. Li, S. Najafzadeh, D. Das, C. Mielke, R. Khasanov, H. Luetkens, T. Suzuki, K. Liu, X. Han, T. Kondo, J. Hu, S. Shin, Z. Wang, X. Shi, Y. Yao and K. Okazaki, Nature **617**, 488-492 (2023).

8. *Testing electron-phonon coupling for the superconductivity in kagome metal CsV_3Sb_5: Y. Zhong, S. Li, H. Liu, Y. Dong, K. Aido, Y. Arai, H. Li, W. Zhang, Y. Shi, Z. Wang, S. Shin, H. N. Lee, H. Miao, T. Kondo and K. Okazaki, Nat. Commun. **14**, 1945 (2023).

Matsunaga group

We have studied light-matter interactions and light-induced nonequilibrium phenomena in solids by utilizing terahertz (THz) pulse. By using a phase-stable broadband multiterahertz pulses (10-45 THz, 40-180 meV, or 7-30 μm) with the pulse width of

* Joint research among groups within ISSP.

28 fs, we investigated dynamics of broadband response functions of a 3D Dirac semimetal Cd_3As_2 under intense periodic light wave with 30 THz frequency. We found a sharp increase of absorption at 28 THz and negative conductivity with optical gain at 31 THz. The drastic change of the spectrum can be explained by the stimulated Rayleigh scattering, which is remarkably enhanced at the frequency close to the longitudinal plasma resonance. The results suggest potential application for nondissipative slow light generation using conducting material at room temperature.

1. *Stimulated Rayleigh Scattering Enhanced by a Longitudinal Plasma Mode in a Periodically Driven Dirac Semimetal Cd_3As_2: Y. Murotani, N. Kanda, T. N. Ikeda, T. Matsuda, M. Goyal, J. Yoshinobu, Y. Kobayashi, S. Stemmer and R. Matsunaga, Phys. Rev. Lett. **129**, 207402 (2022).

2. * パルス内差周波発生法と光パラメトリック増幅による位相安定高強度マルチテラヘルツパルス発生：神田 夏輝 , 石井 順久 , 板谷 治郎 , 松永 隆佑 , レーザー研究 **50**, 286 (2022).

3. Topological Materials for Functional Optoelectronic Devices: H. Chorsi, B. Cheng, B. Zhao, J. Toudert, V. Asadchy, O. F. Shoron, S. Fan and R. Matsunaga, Advanced Functional Materials **32**, 2110655 (2022).

4. *Tracking Ultrafast Change of Multiterahertz Broadband Response Functions in a Photoexcited Dirac Semimetal Cd_3As_2 Thin Film: N. Kanda, Y. Murotani, T. Matsuda, M. Goyal, S. Salmani-Rezaie, J. Yoshinobu, S. Stemmer and R. Matsunaga, Nano Letters **22**, 2358 (2022).

5. *Semiconducting Electronic Structure of the Ferromagnetic Spinel $HgCr_2Se_4$ Revealed by Soft-X-Ray Angle-Resolved Photoemission Spectroscopy: H. Tanaka, A. V. Telegin, Y. P. Sukhorukov, V. A. Golyashov, O. E. Tereshchenko, A. N. Lavrov, T. Matsuda, R. Matsunaga, R. Akashi, M. Lippmaa, Y. Arai, S. Ideta, K. Tanaka, T. Kondo and K. Kuroda, Phys. Rev. Lett. **130**, 186402 (1-6) (2023).

6. *Ultrafast Dynamics of Intrinsic Anomalous Hall Effect in the Topological Antiferromagnet Mn_3Sn: T. Matsuda, T. Higo, T. Koretsune, N. Kanda, Y. Hirai, H. Peng, T. Matsuo, N. Yoshikawa, R. Shimano, S. Nakatsuji and R. Matsunaga, Phys. Rev. Lett. **130**, 126302 (2023).

7. *Pump-probe spectroscopy for non-equilibrium condensed matter: R. Matsunaga and K. Okazaki, Encyclopedia of Condensed Matter Physics, TBD (2023).

8. 「半金属」、光と物質の量子相互作用ハンドブック（監修 荒川泰彦）第 3 篇 第 11 章：松永 隆佑 , 森本 高裕 , (NTS, ., 2023).

Okazaki group

We have investigated the superconducting-gap structures of unconventional superconductors by using a low-temperature and high-resolution laser ARPES apparatus and transient electronic structures in photo-excited non-equilibrium states by using a time-resolved ARPES apparatus using EUV and SX lasers. In the academic year 2022, we have revealed the superconducting gap structures of CsV_3Sb_5-derived Kagome superconductors by high-resolution laser ARPES. In addition, we have developed a tunable mid-infrared pump system for HHG laser time-resolved ARPES.

1. *Photo-Excitation Band-Structure Engineering of 2*H*-$NbSe_2$ Probed by Time- and Angle-Resolved Photoemission Spectroscopy: M. Watanabe, T. Suzuki, T. Someya, Y. Ogawa, S. Michimae, M. Fujisawa, T. Kanai, J. Itatani, T. Saitoh, S. Shin and K. Okazaki, J. Phys. Soc. Jpn. **91**, 064703 (2022).

2. *Environmental effects on layer-dependent dynamics of Dirac fermions in quasicrystalline bilayer graphene: Y. Zhao, T. Suzuki, T. Iimori, H. -W. Kim, J. R. Ahn, M. Horio, Y. Sato, Y. Fukaya, T. Kanai, K. Okazaki, S. Shin, S. Tanaka, F. Komori, H. Fukidome and I. Matsuda, Phys. Rev. B **105**, 115304 (2022).

3. *Tunable vortex Majorana modes controlled by strain in homogeneous LiFeAs: W. Liu, Q. Hu, X. Wang, Y. Zhong, F. Yang, L. Kong, L. Cao, G. Li, Y. Peng, K. Okazaki, T. Kondo, C. Jin, J. Xu, H. -J. Gao and H. Ding, Quantum Front. **1**, 20 (2022).

4. †*Quasi One-Dimensional Band Structure of Photoinduced Semimetal Phase of $Ta_2Ni_{1-x}Co_xSe_5$ (x = 0.0 and 0.1): T. Mitsuoka, Y. Takahashi, T. Suzuki, M. Okawa, H. Takagi, N. Katayama, H. Sawa, M. Nohara, M. Watanabe, J. Xu, Q. Ren, M. Fujisawa, T. Kanai, J. Itatani, K. Okazaki, S. Shin and T. Mizokawa, J. Phys. Soc. Jpn. **92**, 023703 (2023).

5. *Coexistence of Bulk-Nodal and Surface-Nodeless Cooper Pairings in a Superconducting Dirac Semimetal: X. P. Yang, Y. Zhong, S. Mardanya, T. A. Cochran, R. Chapai, A. Mine, J. Zhang, J. Sánchez-Barriga, Z. -J. Cheng, O. J. Clark, J. -X. Yin, J. Blawat, G. Cheng, I. Belopolski, T. Nagashima, S. Najafzadeh, S. Gao, N. Yao, A. Bansil, R. Jin, T. -R. Chang, S. Shin, K. Okazaki and M. Z. Hasan, Phys. Rev. Lett. **130**, 046402 (2023).

6. *Nodeless electron pairing in CsV_3Sb_5-derived kagome superconductors: Y. Zhong, J. Liu, X. Wu, Z. Guguchia, J. -X. Yin, A. Mine, Y. Li, S. Najafzadeh, D. Das, C. Mielke, R. Khasanov, H. Luetkens, T. Suzuki, K. Liu, X. Han, T. Kondo,

† Joint research with outside partners.

J. Hu, S. Shin, Z. Wang, X. Shi, Y. Yao and K. Okazaki, Nature **617**, 488-492 (2023).

7. *Testing electron-phonon coupling for the superconductivity in kagome metal CsV_3Sb_5: Y. Zhong, S. Li, H. Liu, Y. Dong, K. Aido, Y. Arai, H. Li, W. Zhang, Y. Shi, Z. Wang, S. Shin, H. N. Lee, H. Miao, T. Kondo and K. Okazaki, Nat. Commun. **14**, 1945 (2023).

8. †*Direct observation of multiple conduction-band minima in high-performance thermoelectric SnSe: M. Okawa, Y. Akabane, M. Maeda, G. Tan, L.-D. Zhao, M. G. Kanatzidis, T. Suzuki, M. Watanabe, J. Xu, Q. Ren, M. Fujisawa, T. Kanai, J. Itatani, S. Shin, K. Okazaki, N. L. Saini and T. Mizokawa, Scripta Materialia **223**, 115081 (2023).

9. *Pump-probe spectroscopy for non-equilibrium condensed matter: R. Matsunaga and K. Okazaki, Encyclopedia of Condensed Matter Physics, TBD (2023).

Kimura group

In FY2022, the Kimura Lab. worked on the development of soft X-ray nanoimaging techniques using SPring-8 and SACLA. In experiments on SPring-8 BL07LSU, we developed a soft X-ray ptychography system using a total-reflection Wolter mirror to achieve absorption and phase imaging with a resolution of 50 nm, and succeeded in multi-wavelength imaging using mammalian cells. We also attempted to demonstrate femtosecond single-shot femtosecond spectromicroscopy imaging using a multi-aperture grating in experiments at SACLA BL1. Using a transmission type grating fabricated by electron beam lithography and a total reflection Walter mirror, we succeeded in single pulse measurement of the two-dimensional spectral distribution of an X-ray free electron laser emitted by self-amplified spontaneous emission.

1. Femtosecond X-ray Laser Reveals Intact Sea–Island Structures of Metastable Solid-State Electrolytes for Batteries: A. Suzuki, H. Tanaka, H. Yamashige, Y. Orikasa, Y. Niida, T. Kimura, K. Tono, M. Yabashi, T. Ishikawa, Y. Bessho, Y. Joti and Y. Nishino, Nano Lett. **22**, 4603 (2022).

2. †*Soft X-ray ptychography system using a Wolter mirror for achromatic illumination optics: T. Kimura, Y. Takeo, K. Sakurai, N. Furuya, S. Egawa, G. Yamaguchi, Y. Matsuzawa, T. Kume, H. Mimura, M. Shimura, H. Ohashi, I. Matsuda and Y. Harada, Opt. Express **30**, 26220 (2022).

3. An arrayed-window microfluidic device for observation of mixed nanoparticles with an X-ray free-electron laser: Y. Matsumoto, Y. Takeo, S. Egawa, G. Yamaguchi, S. Yokomae, M. Takei, H. Yumoto, T. Koyama, H. Ohashi, K. Tono, M. Yabashi, H. Mimura and T. Kimura, Opt Rev **29**, 7 (2022).

4. Fabrication of ultrashort sub-meter-radius x-ray mirrors using dynamic stencil deposition with figure correction: T. Shimamura, Y. Takeo, T. Kimura, F. Perrin, A. Vivo, Y. Senba, H. Kishimoto, H. Ohashi and H. Mimura, Review of Scientific Instruments **94**, 043102 (2023).

5. Design of soft x-ray fluorescence microscopy beyond 100-nm spatial resolution with ultrashort Kirkpatrick-Baez mirror: T. Shimamura, Y. Takeo, F. Moriya, T. Kimura, M. Shimura, Y. Senba, H. Kishimoto, H. Ohashi, K. Shimba, Y. Jimbo, H. Mimura, H. Mimura, C. Morawe and A. M. Khounsary, Advances in X-Ray/EUV Optics and Components XVII **12240**, 20-33 (2023).

6. †*Developing a Simple Scanning Probe System for Soft X-ray Spectroscopy with a Nano-focusing Mirror: H. Ando, M. Horio, Y. Takeo, M. Niibe, T. Wada, Y. Ando, T. Kondo, T. Kimura and I. Matsuda, e-J. Surf. Sci. Nanotechnol., 2023-020 (2023), in print.

* Joint research among groups within ISSP.

Subject of Joint Research

2022年度　共同利用課題一覧（前期）/ Joint Research List 2022 (First Term)

2022年度　共同利用課題一覧（後期）/ Joint Research List 2022 (Latter Term)

2022年度　中性子科学研究施設　共同利用課題一覧 / Joint Research List of Neutron Scattering Research Project 2022

2022年度　軌道放射物性研究施設　共同利用課題一覧 / Joint Research List of Synchrotron Radiation Research Project 2022

2022年度　スーパーコンピュータ共同利用課題一覧 / Joint Research List of Supercomputer System 2022

2022年度　CCMSスパコン共用事業枠課題一覧 / Supercomputing Consortium for Computational Materials Science Project List of Supercomputer System 2022

2022年度　共同利用課題一覧（前期）/ Joint Research List 2022 (First Term)

※実施課題一覧、所属は申請時のデータ

嘱託課題 / Comission Research Project

No.	課題番号	課題名	氏名	所属	分担者	Title	Name	Organization	Member of reseach project	担当所員
1	202111-CMBXX-0003	良質静水圧下での物性測定法の開発	村田 惠三	大阪公立大学		Development of a method for measuring physical properties under high-quality hydrostatic pressure	Keizo Murata	Osaka Metropolitan University		上床 美也
2	202111-CMBXX-0005	希土類化合物の良質試料作製	繁岡 透	山口大学		Preparation of high-quality samples of rare earth compounds	Toru Shigeoka	Yamaguchi University		上床 美也
3	202111-CMBXX-0006	圧力下NMR測定法に関する開発	藤原 直樹	京都大学		Development of NMR measurement method under high pressure	Naoki Fujiwara	Kyoto University		上床 美也
4	202111-CMBXX-0007	極低温下の磁気特性	鳥塚 潔	千葉工業大学		Development of magnetic measurement method	Kiyoshi Torizuka	Chiba Institute of Technology		上床 美也
5	202111-CMBXX-0009	希釈冷凍機温度での高圧発生装置の開発	松林 和幸	電気通信大学		Development of high pressure apparatus for low temperature	Kazuyuki Matsubayashi	The University of Electro-Communications		上床 美也
6	202111-CMBXX-0012	3d遷移化合物に関する圧力効果	鹿又 武	東北学院大学工学総合研究所		Effect of pressure on the 3d transition compounds	Takeshi Kanomata	Research Institute for Engineering and Technology, Tohoku Gakuin University		上床 美也
7	202111-CMBXX-0013	低次元有機物質の圧力下物性研究	糸井 充穂	東京都市大学		Study on pressure induced superconductivity of low dimension organic conductor	Miho Itoi	Tokyo City University		上床 美也
8	202111-CMBXX-0014	高圧下Ｘ線回折測定法の開発	江藤 徹二郎	久留米工業大学		Development of High Pressure X-ray diffraction measurements	Tetsujiro Eto	Kurume Institute of Technology		上床 美也
9	202112-CMBXX-0042	4Gにおける共同利用推進(C)	那波 和宏	東北大学		Research and Support of General-Use at 4G(C)	Kazuhiro Nawa	Tohoku University		眞弓 皓一
10	202112-CMBXX-0043	６G、T1-2、T1-3における共同利用推進(A)	藤田 全基	東北大学		Research and Support of General-Use at ６G, T1-2 and T1-3(A)	Masaki Fujita	Tohoku University		眞弓 皓一
11	202112-CMBXX-0045	６G、T1-2、T1-3における共同利用推進(C)	池田 陽一	東北大学金属材料研究所		Research and Support of General-Use at ６G, T1-2 and T1-3(C)	Yoichi Ikeda	Institute for materials research, Tohoku university		眞弓 皓一
12	202112-CMBXX-0046	６G、T1-2、T1-3における共同利用推進(D)	谷口 貴紀	東北大学		Research and Support of General-Use at ６G, T1-2 and T1-3(D)	Takanori Taniguchi	Tohoku University		眞弓 皓一
13	202112-CMBXX-0054	T2-2における共同利用推進(B)	坂倉 輝俊	東北大学多元物質科学研究所		Research and Support of General-Use at T2-2(B)	Terutoshi Sakakura	Institute of Multidisciplinary Research for Advanced Materials, Tohoku University		眞弓 皓一
14	202112-CMBXX-0056	C1-2における共同利用推進(A)	杉山 正明	京都大学		Research and Support of General-Use at C1-2(A)	Masaaki Sugiyama	Kyoto University		眞弓 皓一
15	202112-CMBXX-0057	C1-2、C2-3-1における共同利用推進	井上 倫太郎	京都大学		Research and Support of General-Use at C1-2 and C2-3-1	Rintaro Inoue	Kyoto University		眞弓 皓一
16	202112-CMBXX-0058	C1-2における共同利用推進(B)	守島 健	京都大学		Research and Support of General-Use at C1-2(B)	Ken Morishima	Kyoto University		眞弓 皓一
17	202112-CMBXX-0059	C1-2における共同利用推進(C)	Li Xiang	北海道大学大学院先端生命科学研究院		Research and Support of General-Use at C1-2(C)	Li Xiang	Faculty of Advanced Life Science, Hokkaido University		眞弓 皓一
18	202112-CMBXX-0060	C3-1-2における共同利用推進(A)	日野 正裕	京都大学		Research and Support of General-Use at C3-1-2(A)	Masahiro Hino	Kyoto University		眞弓 皓一

19	202112-CMBXX-0015	超強磁場におけるスピン格子強結合系の研究	池田 暁彦	電気通信大学		Study of the strongly spin-lattice-coupled systems in ultrahigh magnetic fields	Akihiko Ikeda	University of Electro-Communications		松田 康弘
20	202112-CMBXX-0016	高分解能光電子分光による強相関物質の研究	横谷 尚睦	岡山大学		Ultra-high resolution study on strongly correlated materials	Takayoshi Yokoya	Okayama University		近藤 猛
21	202112-CMBXX-0020	レーザースピン角度分解光電子分光による表面電子状態の研究	矢治 光一郎	物質・材料研究機構		SARPES studies of atomic layer materials at surfaces	Koichiro Yaji	National Institute for Materials Science		近藤 猛
22	202112-CMBXX-0021	有機化合物の光電子分光	金井 要	東京理科大学		Photoemission study on organic compounds	Kaname Kanai	Tokyo University of Science		近藤 猛
23	202112-CMBXX-0022	反強磁性を示す近似結晶の精密光電子分光測定	津田 俊輔	物質・材料研究機構		Laser-Photoemission Study on antiferromagnetic approximant crystals	Shunsuke Tsuda	National Institute for Materials Science		近藤 猛
24	202112-CMBXX-0023	光スピントロニクスに向けたスピン軌道ダイナミクスの研究	黒田 健太	広島大学		Studying spin-orbit dynamics for opt-spintronics	Kenta Kuroda	Hiroshima University		近藤 猛
25	202112-CMBXX-0033	軟Ｘ線発光×共鳴非弾性散乱分光の磁気円・線二色性測定システムの構築	菅 滋正	大阪大学産業科学研究所		Construction of a noble system for circular and linear dichroism in soft X-ray emission and RIXS spectroscopy	Shigemasa Suga	ISIR, Osaka University		原田 慈久
26	202112-CMBXX-0036	三次元nanoESCAによる実デバイスのオペランド電子状態解析	永村 直佳	物質・材料研究機構		Operando analysis of the electronic structure of actual devices by 3DnanoESCA	Naoka NAGAMURA	National Institute for Materials Science		原田 慈久
27	202112-CMBXX-0039	液体ジェットを用いた金属タンパク質中の金属反応中心の電子状態解析	藤井 健太郎	量子科学技術研究開発機構		Electronic structure analysis of metal reaction centers in metalloproteins using liquid jets	Kentaro Fujii	National Institutes for Science and Technology		原田 慈久
28	202203-CMBXX-0064	第一原理計算基統計熱力学計算フレームワークの高度化	笠松 秀輔	山形大学		First principles-based statistical thermodynamics framework	Shusuke Kasamatsu	Yamagata University		川島 直輝
29	202203-CMBXX-0067	トポロジカル絶縁体Bi2Te3薄膜におけるスピン軌道ダイナミクスの1研究	八田 振一郎	京都大学		Studying spin-orbit dynamics of topological insulator Bi2Te3 thin film	Shinichiro Hatta	Kyoto university		近藤 猛

一般課題 / General Research Project

No.	課題番号	課題名	氏名	所属	分担者	Title	Name	Organization	Member of reseach project	担当所員
1	202203-GNBXX-0080	配列制御された機能性有機分子結晶の電子特性解明	岡 弘樹	大阪大学	赤井 亮太	Elucidation of the electronic properties of the organic molecular crystals with the controlled molecular arrangements	Kouki Oka	Osaka University	Ryota Akai	森 初果
2	202205-GNBXX-0111	単一成分分子性導体における交換相互作用及び磁気特性に与えるアルキル基変調・伸長効果の研究	横森 創	立教大学		Study of effects of a modulation/extension of alkyl groups on magnetic properties and exchange interactions in single-component molecular conductors	So Yokomori	Rikkyo University		森 初果
3	202111-GNBXX-0021	重い電子系希土類化合物における異方的量子臨界現象の磁気的評価II	河野 洋平	中央大学	辻 貴丹 木元 大介 綱島 海斗 加藤 謙介 湯淺 翔平	Magnetic properties of anisotropic quantum critical phenomena in a heavy-fermion metal II	Yohei Kono	Chuo University	Kitami Tsuji KIMOTO Daisuke Tsunashima Kaito Kato Kensuke Shohei Yuasa	山下 穣
4	202111-GNBXX-0040	局所反転対称性の破れたCe系超伝導体における極低温磁化測定	清水 悠晴	東北大学金属材料研究所	佐藤 芳樹（東京理科大学）	High-resolution magnetization measurements on cerium-based superconductors without local-inversion symmetry	Yusei Shimizu	Tohoku University, Institute for Materials Research	Yoshiki Sato (Tokyo University of Science)	山下 穣

5	202111-GNBXX-0041	希釈冷凍機を用いたウラン系微小純良単結晶試料の高感度磁化測定	清水 悠晴	東北大学金属材料研究所	佐藤 芳樹（東京理科大学）	Magnetization measurements for tiny uranium-based single crystals using high-resolution capacitors in dilution refrigerator	Yusei Shimizu	Tohoku University, Institute for Materials Research	Yoshiki Sato (Tokyo University of Science)	山下 穣
6	202111-GNBXX-0071	新型ファラデー磁化測定セル及びdHvA用カンチレバーセルの開発	清水 悠晴	東北大学金属材料研究所	佐藤 芳樹（東京理科大学）	Development of new-type Faraday magnetization cell and cantilever torque cell for dHvA measurements	Yusei Shimizu	Tohoku University, Institute for Materials Research	Yoshiki Sato (Tokyo University of Science)	山下 穣
7	202112-GNBXX-0057	スピン軌道結合金属Cd2Re2O7の酸素NMRと電流誘起効果	瀧川 仁	高エネルギー加速器研究機構・物質構造科学研究所		Oxygen NMR and current-induced effects in the spin-orbit coupled metal Cd2Re2O7	Masashi Takigawa	High Energy Accelerator Research Organization, Institute of Materials Structure Science		山下 穣
8	202112-GNBXX-0068	カイラル構造を持つ磁性体の低温磁気特性	佐藤 芳樹	東京理科大学	清水 悠晴（東北大学金属材料研究所）	Low-temperature magnetic properties of chiral magnets	Yoshiki Sato	Tokyo University of Science	Yusei Shimizu (Tohoku University, Institute for Materials Research)	山下 穣
9	202206-GNBXX-0158	ウラン化合物超伝導体UTe2の極低温電子状態	芳賀 芳範	日本原子力研究開発機構	Opletal Petr	Low temperature electronic states of the uranium compound superconductor UTe2	Yoshinori Haga	Japan Atomic Energy Agency	Petr Opletal	山下 穣
10	202111-GNBXX-0005	基板における原子クラスター選別形成法の構築と,クラスター構造と磁性の関係の解明	塚原 規志	群馬工業高等専門学校		Establishment of selection method for atomic clusters on the substrate and elucidation of the relation between the cluster structure and its magnetic properties	Noriyuki Tsukahara	National Institute of Technology, Gunma College		吉信 淳
11	202111-GNBXX-0025	微傾斜Si(111)√3×√3-B基板上に成長したBi(110)超薄膜の電子状態	中辻 寛	東京工業大学	小森 文夫 長尾 俊佑 瓜生 瞳美	Electronic structure of Bi(110) thin films grown on vicinal Si(111) √3×√3-B substrates	Kan Nakatsuji	Tokyo Institute of Technology	Fumio Komori Shunsuke Nagao HITOMI URYU	吉信 淳
12	202111-GNBXX-0026	SiC基板上に成長したグラフェンへのFeインターカレーション	中辻 寛	東京工業大学	小森 文夫 竹村 晃一	Intercalation of Fe into graphene grown on a SiC substrate	Kan Nakatsuji	Tokyo Institute of Technology	Fumio Komori Koichi Takemura	吉信 淳
13	202111-GNBXX-0006	希土類金属間化合物および金属超伝導体の結晶育成と低温電子物性	海老原 孝雄	静岡大学	篠田 高志 エスティアク アフメド	Crystal Growth and Physical Properties at low temperatures in rare earth intermetallic compounds and metallic superconductors	Takao Ebihara	Shizuoka University	Takashi Shinoda Esteaque Ahmed	大谷 義近
14	202110-GNBXX-0001	量子ホール効果のための高移動度半導体試料作製と超低温での測定	福田 昭	兵庫医科大学		Development of the high mobility semiconductor samples for the quantum Hall state and their measurements in very low temperature	Akira Fukuda	Hyogo College of Medicine		勝本 信吾
15	202111-GNBXX-0003	二次元銅酸化物のホール係数測定 VI	神戸 士郎	山形大学	川村 桂太 南光 伸哉	Hall coefficient measurement of 2D cuprates VI	Shiro Kambe	Yamagata University	Keita Kawamura SHINYA NANKO	勝本 信吾
16	202112-GNBXX-0037	グラフェン/超伝導炭化物/SiCの低温電気伝導測定	乗松 航	名古屋大学		Electrical measurements of graphene/superconducting-carbide/SiC	Wataru Norimatsu	Nagoya University		勝本 信吾
17	202111-GNBXX-0007	ケージドATPの光解離特性	樋山 みやび	群馬大学	工藤 優斗	Study for Photodissociation Properties of Caged ATP	Miyabi Hiyama	Gunma University	kudo yuto	秋山 英文
18	202111-GNBXX-0008	新奇ケージドルシフェリン化合物の光解離測定	樋山 みやび	群馬大学	勝見 渓太	Study of photodissociation for a new caged compound	Miyabi Hiyama	Gunma University	katsumi keita	秋山 英文
19	202111-GNBXX-0009	生物発光のフィールド画像計測と個体数解析法の開発	樋山 みやび	群馬大学	高橋 由太翔	Field measurements of bioluminescence and numerical image analysis for individual discrimination	Miyabi Hiyama	Gunma University	Takahashi Yutaka	秋山 英文
20	202111-GNBXX-0014	水溶液におけるseMpaiの吸収特性	樋山 みやび	群馬大学	原田 昌拓	Absorption spectra of seMpai in aqueous solution	Miyabi Hiyama	Gunma University	masahiro harada	秋山 英文

21	202111-GNBXX-0017	GaAs:N中の等電子トラップからの発光エネルギーの揺らぎ	矢口 裕之	埼玉大学	矢野 裕子 伊藤 駿平	Fluctuations in the emission energy of isoelectronic traps in GaAs:N	Hiroyuki Yaguchi	Saitama University	Yuko Yano Shunpei Ito	秋山 英文
22	202111-GNBXX-0019	超低温トポケミカル合成したスピン軌道結合磁性体の物性研究	原口 祐哉	東京農工大学		Physical Properties of Spin-Orbit Coupled Magnets Synthesized by Ultralow Temperature Topochemical Manipulation	Yuya Haraguchi	Tokyo University of Agriculture and Technology		広井 善二
23	202111-GNBXX-0013	S置換したFeSeの高圧低温下NMR測定	藤原 直樹	京都大学	Yu Zhongyu	NMR studies on S-substituted FeSe at high pressures and low temperatures	Naoki Fujiwara	Kyoto University	Zhongyu Yu	上床 美也
24	202111-GNBXX-0016	(Ce1-xRx)PtGe2の単結晶育成と磁気的性質	中野 智仁	新潟大学 工学部	武藤 颯人	Single crystals growth of (Ce1-xRx)PtGe2 and thier magnetic properties	Tomohito NAKANO	Faculty of Engineering, Niigata University	Hayato Muto	上床 美也
25	202111-GNBXX-0030	擬三元化合物 Ce1- x La x NiC2の結晶育成と物質評価 4	繁岡 透	山口大学	内間 清晴（学校法人沖縄キリスト教学院・沖縄キリスト教短期大学）	Crystal growth and characterization of pseudo-ternary compounds Ce1- x La x NiC2 4	Toru Shigeoka	Yamaguchi University	Kiyoharu Uchima (Okinawa Christian Institute Okinawa christian junior College)	上床 美也
26	202111-GNBXX-0031	CeNiC2の結晶育成と物質評価 2	繁岡 透	山口大学	内間 清晴（学校法人沖縄キリスト教学院・沖縄キリスト教短期大学）	Crystal growth and characterization of CeNiC2 2	Toru Shigeoka	Yamaguchi University	Kiyoharu Uchima (Okinawa Christian Institute Okinawa christian junior College)	上床 美也
27	202111-GNBXX-0032	多型化合物RIr2Si2(R=希土類)の磁気特性7	内間 清晴	学校法人沖縄キリスト教学院・沖縄キリスト教短期大学	繁岡 透（山口大学）	Magnetic characteristics of polymorphic compounds RIr2Si2(R=Rare earth) 7	Kiyoharu Uchima	Okinawa Christian Institute Okinawa christian junior College	Toru Shigeoka (Yamaguchi University)	上床 美也
28	202111-GNBXX-0033	T型銅酸化物におけるスピン密度波秩序と超伝導の一軸圧力依存性	谷口 貴紀	東北大学		Spin density wave and superconductivity under axial high-pressure in T-type cuprate	Takanori Taniguchi	Tohoku University		上床 美也
29	202111-GNBXX-0036	T型銅酸化物における対密度波の磁場依存性	王 彤	東北大学		Pair density wave under magnetic field in T-type cuprate	Tong Wang	Tohoku University		上床 美也
30	202112-GNBXX-0048	磁気クラスター多極子秩序候補物質Ce3TiSb5の圧力下電気抵抗測定	篠﨑 真碩	島根大学	本山 岳	Electrical resistivity measurements of Ce3TiSb5 under high-pressure	Masahiro Shinozaki	Shimane University	Gaku MOTOYAMA	上床 美也
31	202112-GNBXX-0049	YbH2+x の高圧下での輸送現象	中村 修	岡山理科大学		Transport phenomena under high pressure of YbH2+x	Nakamura Osamu	Okayama University of Science		上床 美也
32	202112-GNBXX-0055	強誘電体および反強誘電体における圧力下量子臨界現象の研究	橋本 顕一郎	東京大学	劉 蘇鵬	Study of pressure-induced quantum critical phenomena in ferroelectric and antiferroelectric materials	Kenichiro Hashimoto	The University of Tokyo	SUPENG LIU	上床 美也
33	202112-GNBXX-0056	圧力媒体の特性の探索	村田 惠三	大阪公立大学		Search for New Properties of High Pressure Medium	Keizo Murata	Osaka Metropolitan University		上床 美也
34	202112-GNBXX-0061	ホイスラー化合物Fe3-xMnxSiの圧力下磁気相転移	廣井 政彦	鹿児島大学	赤石 幸起	Magnetic phase transitions under pressure in Heuser compounds Fe3-xMnxSi	Masahiko HIROI	Kagoshima University	Kouki Akaishi	上床 美也
35	202112-GNBXX-0062	不定比化合物GdCrxGe2化合物の単結晶育成	藤原 哲也	山口大学	五反田 礼	Single crystal growth of non stoichiometric compounds GdCrxGe2	Tetsuya Fujiwara	Yamaguchi University	Rei Gotanda	上床 美也
36	202112-GNBXX-0063	不定比化合物GdCrxGe2単結晶の磁化測定	藤原 哲也	山口大学	五反田 礼	Magnetization measurements of non stoichiometric GdCrxGe2 single crystals	Tetsuya Fujiwara	Yamaguchi University	Rei Gotanda	上床 美也
37	202112-GNBXX-0064	不定比化合物TbCrxGe2化合物の単結晶育成	藤原 哲也	山口大学	新谷 怜和	Single crystal growth of non stoichiometric compounds TbCrxGe2	Tetsuya Fujiwara	Yamaguchi University	reo niiya	上床 美也
38	202112-GNBXX-0065	不定比化合物TbCrxGe2単結晶の磁化測定	藤原 哲也	山口大学	新谷 怜和	Magnetization measurements of non stoichiometric TbCrxGe2 single crystals	Tetsuya Fujiwara	Yamaguchi University	reo niiya	上床 美也

39	202112-GNBXX-0066	Ni2In型強磁性体の自発磁化の圧力効果	安達 義也	山形大学		Pressure effects on the spontaneous magnetization for Ni2In-type ferromagnets	Yoshiya Adachi	Yamagata University		上床 美也
40	202112-GNBXX-0072	ウラン化合物の磁性の圧力効果	本多 史憲	九州大学アイソトープ統合安全管理センター		Effect of Pressure on the magnetism of uranium compounds	Fuminori Honda	Central Institute of Radioisotope Science and Safety Management, Kyushu University		上床 美也
41	202112-GNBXX-0075	高スピン分極ホイスラー合金における圧力誘起量子臨界現象の探索	重田 出	鹿児島大学	青島 英樹	Search for pressure-induced quantum critical phenomenon in highly spin polarized Heusler alloys	Iduru Shigeta	Kagoshima University	Aoshima Hideki	上床 美也
42	202204-GNBXX-0085	CeCoSiの高圧下における単結晶精密構造解析	川村 幸裕	室蘭工業大学	西山 紗恵	Structural refinement of CeCoSi single crystal under pressure	Yukihiro Kawamura	Muroran Institute of Technology	Sae Nishiyama	上床 美也
43	202204-GNBXX-0086	Eu3Bi2S4F4における圧力効果の研究 II	石垣 賢卯	東京理科大学		Research of Eu3Bi2S4F4 in high pressure II	Kento Ishigaki	Tokyo University of Science		上床 美也
44	202205-GNBXX-0108	単結晶X線構造解析による金属有機構造体へのイオン液体充填効果の解明	高 相圭	東京理科大学	大平 一路 常盤 和靖	Elucidating confinement effect of ionic liquids in metal-organic frameworks using single crystal X-ray diffraction analysis	Sang-Gyu Koh	Tokyo University of Science	Ichiro Ohira Kazuyasu Tokiwa	上床 美也
45	202206-GNBXX-0156	粉末X線回構造解析による金属有機構造体Cu3(btc)2へのイオン液体導入効果の解明	木下 健太郎	東京理科大学	高 相圭 大平 一路 甲斐 洋行	Elucidating the effect of introducing ionic liquids into the metal-organic framework Cu3(btc)2 by powder X-ray structural analysis	Kentaro Kinoshita	Tokyo University of Science	Sang-Gyu Koh Ichiro Ohira Hiroyuki Kai	上床 美也
46	202111-GNBXX-0010	新規トポロジカル磁性体の合成と磁気構造の解明	車地 崇	東京大学	有馬 孝尚 徳永 祐介	Magnetic structure analysis of novel topological magnets	Takashi Kurumaji	The University of Tokyo	Taka-hisa Arima Yusuke Tokunaga	益田 隆嗣
47	202112-GNBXX-0050	Ce5Si3-xGax及びCe5-xLaxSi3単結晶試料の極低温比熱測定	小林 理気	琉球大学	玉城 良仁	Low temperature specific heat measurement of Ce5Si3-xGax and Ce5-xLaxSi3 single crystals	Riki Kobayashi	University of the Ryukyus	Tamashiro Yoshihito	益田 隆嗣
48	202112-GNBXX-0051	高エネルギーX線ラウエによるCe5-xLaxSi3単結晶試料のアセンブル	小林 理気	琉球大学	玉城 良仁	Assembly of Ce5-xLaxSi3 single crystal sample by high energy X-ray Laue	Riki Kobayashi	University of the Ryukyus	Tamashiro Yoshihito	益田 隆嗣
49	202111-GNBXX-0020	次世代レーザーとレーザー加工の基礎技術研究	吉富 大	国立研究開発法人産業技術総合研究所	高田 英行 奈良崎 愛子 小川 博嗣 寺澤 英知 澁谷 達則 佐藤 大輔 黒田 隆之助 田中 真人	Basic research on next generation laser systems and laser machining technology	Dai Yoshitomi	National Institute of Advanced Industrial Science and Technology	Takada Hideyuki Aiko Narazaki Hiroshi Ogawa Eichi Terasawa Tatsunori Shibuya Daisuke Satoh Ryunosuke Kuroda Masahito Tanaka	小林 洋平
50	202111-GNBXX-0023	紫外光レーザー光源を用いた加工応用研究	藤本 靖	千葉工業大学		Research on laser processing application by ultraviolet laser light source	Yasushi Fujimoto	Chiba Institute of Technology		小林 洋平
51	202111-GNBXX-0028	レーザー誘起合金化のパルス時間幅依存性	富田 卓朗	徳島大学	河野 太洋	Pulse duration dependence of laser induced metal alloying	Takuro Tomita	Tokushima University	Taiyou Kawano	小林 洋平
52	202111-GNBXX-0034	金属ナノ構造の超高速発光による研究	末元 徹	電気通信大学		Studies on nanostructured metals by ultrafast luminescence spectroscopy	Suemoto Tohru	The University of Electro-Communications		小林 洋平
53	202112-GNBXX-0046	高分解能イメージングのためのファイバーレーザーの最適化	大間知 潤子	関西学院大学		Optimization of fiber laser for high-resolution imaging	Junko Omachi	Kwansei Gakuin University		小林 洋平
54	202112-GNBXX-0070	超短パルスYbファイバーレーザー光源を用いた生体組織の分子振動イメージング	長島 優	浜松医科大学		Molecular vibrational imaging of biological tissues using Yb fiber-based ultrashort pulse laser source	Yu Nagashima	Hamamatsu University School of Medicine		小林 洋平

55	202112-GNBXX-0076	熱可塑性高分子におけるレーザー誘起構造変化	山口 誠	秋田大学	高林 圭佑	Laser-induced structural changes in thermoplastic polymers	Yamaguchi Makoto	Akita University	Keisuke Takabayashi	小林 洋平
56	202112-GNBXX-0047	バルク敏感高分解能スピン分解角度分解光電子分光によるハーフメタル強磁性体La1-xSrxMnO3のNQP 状態の観測	横谷 尚睦	岡山大学	片岡 範行 瀬戸口 太朗	Observation of NQP state in half metal ferromagnet La1-xSrxMnO3 by bulksensitive high-resolution spin and angle resolved photoemissionspectroscopy	Takayoshi Yokoya	Okayama university	Noriyuki Kataoka Taro Setoguchi	近藤 猛
57	202112-GNBXX-0069	Zr3SnC2のスピン分解角度分解光電子分光	伊藤 孝寛	名古屋大学	杉本 卓史 三田 愛也	Spin- and Angle-resolved photoemission study of Zr3SnC2	Takahiro Ito	Nagoya University	takafumi sugimoto Mita Manaya	近藤 猛
58	202110-GNBXX-0002	超高分解能PEEMによる反強磁性相のトポロジカルボルテックス分域の観測	溝川 貴司	早稲田大学	大川 万里生	Observation of topological vortex domains in antiferromagnets by means of ultrahigh resolution PEEM	Takashi Mizokawa	Waseda University	Mario Okawa	岡崎 浩三
59	202111-GNBXX-0029	赤外パルスレーザーにより励起したSmSにおける光誘起ダイナミクス	中村 拓人	大阪大学	渡邊 浩 陳 奕同	Photo-induced dynamics on SmS excited by infrared-pulse laser	Takuto Nakamura	Osaka University	Hiroshi Watanabe Yitong CHEN	岡崎 浩三
60	202111-GNBXX-0035	カロリメトリによる金属試料の赤外吸収率測定	末元 徹	電気通信大学	森野 春樹	Measurement of infrared absorptivity on metal samples by calorimetry	Suemoto Tohru	The University of Electro-Communications	Haruki Morino	岡崎 浩三
61	202112-GNBXX-0067	励起子絶縁体Ta2NiSe5及び鉄系超伝導体FeSeにおける光誘起相転移の研究	久保田 雄也	理化学研究所		Investigation of the photo-induced phase transitions in an excitonic insulator Ta2NiSe5 and an Fe-based superconductor FeSe	Yuya Kubota	RIKEN		岡崎 浩三
62	202203-GNBXX-0082	二次高調波発生で調べる反強磁性体秩序における反対称スピン軌道相互作用	黒田 健太	広島大学	大和田 清貴 岩田 拓万	Investigation of antisymmetric spin-orbit coupling in antiferromagnets by second harmonic generation	Kenta Kuroda	Hiroshima University	Kiyotaka Ohwada Takuma Iwata	松永 隆佑

物質合成・評価設備Gクラス / Materials Synthesis and Characterization G Class Research Project

No.	課題番号	課題名	氏名	所属	分担者	Title	Name	Organization	Member of reseach project	実験室
1	202112-MCBXG-0030	極性と幾何学的フラストレーションを有する磁性体の電気磁気効果	有馬 孝尚	東京大学	木村 真栄 徳永 祐介 石崎 大悟	Magnetoelectric Effect in Polar Magnets with Geometrical Frustration	Taka-hisa Arima	The University of Tokyo	Shin-Ei Kimura Yusuke Tokunaga Daigo Ishizaki	X線測定室
2	202112-MCBXG-0033	Co基ホイスラー合金におけるマルテンサイト変態材料の探索	重田 出	鹿児島大学	青島 英樹	Search for materials with the Martensitic transformation in Co-based Heusler alloys	Iduru Shigeta	Kagoshima University	Aoshima Hidekiy	X線測定室
3	202111-MCBXG-0008	超臨界水熱合成における多段反応器の利用	秋月 信	東京大学	王 咏旭	Use of multi-stage reactors for supercritical hydrothermal synthesis	Makoto Akizuki	The University of Tokyo	YONGXU WANG	電子顕微鏡室
4	202111-MCBXG-0013	セラミックスナノ粒子の連続製造技術開発	陶 究	産業技術総合研究所		Development of continuous process for ceramics nanoparticles production	Kiwamu Sue	AIST		電子顕微鏡室
5	202112-MCBXG-0021	耐熱材料の微細組織解析	御手洗 容子	東京大学	松永 紗英 石田 雄士	Microstructure analysis of high-temperature materials	Yoko Mitarai	The University of Tokyo	Sae Matsunaga Yuji Ishida	電子顕微鏡室
6	202110-MCBXG-0001	Nd1-x(Sr1-yCay)xFeO3 (0.1≦x≦0.9, y=0.9) の高温における磁性と熱電特性に関する研究	中津川 博	横浜国立大学	鎌谷 雄大	Magnetism and thermoelectric properties at high temperature in Nd1-x(Sr1-yCay)xFeO3 (0.1≦x≦0.9, y=0.9)	Hiroshi Nakatsugawa	Yokohama National University	Yudai Kamatani	電磁気測定室
7	202110-MCBXG-0006	新規トポロジカル磁性体の合成と物性開拓	車地 崇	東京大学	有馬 孝尚 徳永 祐介	Materials development for novel topological magnets	Takashi Kurumaji	The University of Tokyo	Taka-hisa Arima Yusuke Tokunaga	電磁気測定室

8	202111-MCBXG-0002	高圧下で超伝導-絶縁体転移を示すロジウムスピネルの放射光X線構造研究	片山 尚幸	名古屋大学	小島 慶太	Synchrotron X-ray diffraction study on Rhodium Spinel compounds which exhibit a superconductivity to insulator transition under pressure	Naoyuki Katayama	Nagoya University	Keita Kojima	電磁気測定室
9	202111-MCBXG-0005	二次元銅酸化物の磁化率測定 II	神戸 士郎	山形大学	川村 桂太 南光 伸哉	Magnetic susceptibility measurement of 2D cuprates II	Shiro Kambe	Yamagata University	Keita Kawamura SHINYA NANKO	電磁気測定室
10	202111-MCBXG-0015	3d電子系におけるスピン軌道結合磁性の開拓	原口 祐哉	東京農工大学		Exploring spin-orbit coupled magnetism in 3d electron systems	Yuya Haraguchi	Tokyo University of Agriculture and Technology		電磁気測定室
11	202111-MCBXG-0017	スピン液体"擬態"物質における磁気秩序の観測の試み	原口 祐哉	東京農工大学		An attempt to observe magnetic ordering in spin liquid "mimicries"	Yuya Haraguchi	Tokyo University of Agriculture and Technology		電磁気測定室
12	202112-MCBXG-0022	奇パリティ磁気多極子秩序を持つ物質の単結晶育成と物性評価	阿部 伸行	日本大学	岩崎 義己	Crystal growth and physical properties measurement in odd parity multipole ordering materials	Nobuyuki Abe	Nihon University	IWASAKI Yoshiki	電磁気測定室
13	202112-MCBXG-0028	鉄ペロブスカイトにおける電気磁気熱量効果の開発	有馬 孝尚	東京大学	車地 崇 池田 凜太郎 徳永 祐介	Exploration of electromagnetocaloric effect in perovskite ferrites	Taka-hisa Arima	The University of Tokyo	Takashi Kurumaji rintaro ikeda Yusuke Tokunaga	電磁気測定室
14	202112-MCBXG-0031	ホイスラー化合物での反強磁性の研究	廣井 政彦	鹿児島大学		Study on antiferromagnetism in Heusler compounds	Masahiko HIROI	Kagoshima University		電磁気測定室
15	202112-MCBXG-0032	高スピン分極ホイスラー合金の磁気特性のスピンゆらぎ理論による解析に関する研究	重田 出	鹿児島大学	青島 英樹	Study on analysis of magnetic properties for highly spin polarized Heusler alloys by the spin fluctuation theory	Iduru Shigeta	Kagoshima University	Aoshima Hideki	電磁気測定室
16	202111-MCBXG-0014	第13族元素を充填した新規スクッテルダイト型熱電材料の高圧合成	関根 ちひろ	室蘭工業大学	淡路 功太 新井 聖也 寺坂 聡志 長瀬 竜也	High-pressure synthesis of new skutterudite-type thermolectric materials filled with group 13 element	Chihiro Sekine	Muroran Institute of Technology	Awaji Kouta SEIYA ARAI Satoshi Terasaka Tatsuya Nagase	高圧合成室
17	202112-MCBXG-0035	高温高圧下におけるFe-Si-H三元系における水素原子の占有サイトと水素誘起体積膨張係数の解明	鍵 裕之	東京大学	森 悠一郎 飯塚 理子（早稲田大学）	Site occupancy of hydrogen and hydrogen-induced volume expansion rate in Fe-Si-H ternary system at high pressure and high temperature	Hiroyuki Kagi	The University of Tokyo	Mori Yuichiro Riko Iizuka-Oku (Waseda University)	高圧合成室
18	202112-MCBXG-0024	ハニカム格子を持つRuBr3とRuI3の高圧合成	今井 良宗	東北大学	佐藤 楓貴	High pressure synthesis of RuBr3 and RuI3 with the honeycomb structure	Yoshinori Imai	Tohoku university	Fuki Sato	X線測定室、高圧合成室

物質合成・評価設備Uクラス / Materials Synthesis and Characterization U Class Research Project

No.	課題番号	課題名	氏名	所属	分担者	Title	Name	Organization	Member of reseach project	実験室
1	202203-MCBXU-0042	六方晶ペロブスカイト型イリジウム酸化物Ba4BiIr3O12の単結晶育成	松平 和之	九州工業大学	井上 正弥	Single Crystal Growth of 12L Hexagonal Perovskite Ir oxide Ba4BiIr3O12	KAZUYUKI MATSUHIRA	Kyushu Institute of Technology	Masaya Inoue	物質合成室
2	202207-MCBXU-0101	巨大な創発電磁場を伴う新規スキルミオン物質の開拓	高木 里奈	東京大学物性研究所		Exploration of new materials with magnetic skyrmions generating large emergent electromagnetic fields	Takagi Rina	ISSP The University of Tokyo		化学分析室
3	202203-MCBXU-0043	電気トロイダル秩序候補物質Ca5Ir3O12の単結晶構造解析	松平 和之	九州工業大学	花手 洋樹	Crystal Structure Analysis of Electric Toroidal Ordering Candidate Ca5Ir3O12	KAZUYUKI MATSUHIRA	Kyushu Institute of Technology	Hiroki Hanate	X線測定室

4	202203-MCBXU-0044	巨大異常ネルンスト効果を示す新規トポロジカル磁性体開発	酒井 明人	東京大学	王 陽明 Feng Zili 松尾 拓海 上杉 良太 梶原 悠人	Search for new topological magnets exhibiting the giant anomalous Nernst effect	Akito Sakai	The University of Tokyo	Yangming Wang Zili Feng Takumi Matsuo Ryota Uesugi yuto kajiwara	電子顕微鏡室
5	202204-MCBXU-0045	超伝導体転移温度に対する軸性圧力効果の検証	栗原 綾佑	東京理科大学	矢口 宏 小暮 琉介 高橋 龍生	Pressure dependence of superconducting transition temperatrue	Ryosuke Kurihara	Tokyo University of Science	Hiroshi Yaguchi Ryusuke Kogure Ryusei Takahashi	電磁気測定室
6	202205-MCBXU-0051	5d電子系における多極子物性の研究	平井 大悟郎	名古屋大学		Multipolar physics in 5d electron systems	Daigorou Hirai	Nagoya University		電磁気測定室、光学測定室

国際超強磁場科学施設 / International MegaGauss Science Laboratory

No.	課題番号	課題名	氏名	所属	分担者	Title	Name	Organization	Member of reseach project	担当所員
1	202111-HMBXX-0001	希土類金属間化合物および金属超伝導体の結晶育成と強磁場物性研究	海老原 孝雄	静岡大学	篠田 高志 エスティアク アフメド	Physical Properties at high magnetic fields in rare earth intermetallic compounds and metallic super conductors	Takao Ebihara	Shizuoka University	Takashi Shinoda Esteaque Ahmed	金道 浩一
2	202112-HMBXX-0020	λ型有機導体における強磁場超伝導状態の探索と超音波測定を用いた臨界終点の研究	福岡 脩平	北海道大学		Search for a superconducting state under high magnetic fields and study of the critical endpoint using ultrasound measurements in λ-type organic conductors	Shuhei Fukuoka	Hokkaido University		金道 浩一
3	202112-HMBXX-0022	カゴメ格子反強磁性フッ化物と層状遍歴磁性体の強磁場磁化過程	道岡 千城	京都大学	森山 広大 吉永 公平	High field magnetizations in kagome lattice antiferromagnetic fluorides and layered itinerant magnets	Michioka Chishiro	Kyoto University	Kodai Moriyama Kohei YOSHINAGA	金道 浩一
4	202112-HMBXX-0024	有機ラジカルからなるフラストレート磁性体の強磁場物性	山口 博則	大阪公立大学		High-field magnetic properties of frustrated materials composed of organic radicals	Hironori Yamaguchi	Osaka Metropolitan University		金道 浩一
5	202112-HMBXX-0026	有機超伝導体λ-(BETS)2GaCl4のフィリング制御によるフェルミ面の変化の検証	小林 拓矢	埼玉大学	小梁川 響子 安村 乃絵瑠	Investigation of the change of Fermi surface in organic superconductor λ-(BETS)2GaCl4 by filling control	Takuya Kobayashi	Saitama University	Kyoko Koyanagawa Noeru Yasumura	金道 浩一
6	202112-HMBXX-0028	乱れを導入した有機超伝導体における強磁場超伝導状態	杉浦 栞理	東北大学 金属材料研究所		High-field superconductivity in organic superconductors with artificially introduced disorders	Shiori Sugiura	Institute for Materials Research, Tohoku University		金道 浩一
7	202112-HMBXX-0031	カゴメ反強磁性体CaCu3(OH)6Cl2•0.6H2Oの超強磁場磁化測定	吉田 紘行	北海道大学		Ultra-high-field magnetization measurement on quantum kagome antiferromagnet CaCu3(OH)6Cl2•0.6H2O	Hiroyuki Kura Yoshida	Hokkaido University		松田 康弘
8	202111-HMBXX-0009	高磁場・低温におけるThCr2Si2型Eu化合物の磁化特性	酒井 英明	大阪大学	湯浅 直輝	High-field magnetic properties for ThCr2Si2-type Eu-based compounds	Hideaki Sakai	Osaka University	Naoki Yuasa	徳永 将史

9	202111-HMBXX-0018	希土類化合物RERu2Si2の強磁場磁化過程	原 嘉昭	国立高等専門学校機構　茨城工業高等専門学校	矢野 一雄（筑波大学） 喜多 英治（筑波大学） 雨海 有佑（室蘭工業大学）	High field magnetization process in rare-earth compound RERu2Si2	Yoshiaki Hara	National Institute of Technology (KOSEN), Ibaraki College	kazuo yano (University of Tsukuba) Eiji Kita (University of Tsukuba) Yusuke Amakai(Muroran Institute of Technology)	徳永 将史
10	202111-HMBXX-0019	励起子絶縁体候補物質Ta2NiSe5における強磁場下電気抵抗測定	広瀬 雄介	新潟大学	土田 駿	High-field magnetoresistance of excitonic insulator Ta2NiSe5	Yusuke Hirose	Niigata University	Shun Tsuchida	徳永 将史
11	202112-HMBXX-0021	V-Vダイマーを持つイルメナイト型バナジウム酸化物の電子相転移	山本 孟	東北大学	上山 幸子	Electronic phase transition in ilmenite-type vanadates possessing V-V dimers	Hajime Yamamoto	多元物質科学研究所	Kamiyama Sachiko	徳永 将史
12	202112-HMBXX-0023	新規ラクナスピネル化合物の強磁場下での物性	香取 浩子	東京農工大学	原口 祐哉 伊東 賢佑	Physical properties of novel lacunar spinel compounds under high magnetic fields	Hiroko Katori	Tokyo University of Agriculture and Technology	Yuya Haraguchi Kensuke Ito	徳永 将史
13	202112-HMBXX-0034	反強磁性体UPt3Al15の強磁場下磁化測定	本多 史憲	九州大学アイソトープ統合安全管理センター		High-field magnetization measurement on a new antiferromagnet UPt3Al5	Fuminori Honda	Central Institute of Radioisotope Science and Safety Management, Kyushu University		徳永 将史
14	202112-HMBXX-0029	擬多重項系近藤合金(Lu,Yb)Rh2Zn20における磁気異方性	北澤 崇文	東北大学	池田 陽一	Magnetic anisotropy in quasi-degenerate Kondo alloy (Lu,Yb)Rh2Zn20	Kitazawa Takafumi	Tohoku university	Yoichi Ikeda	小濱 芳允
15	202203-HMBXX-0036	パルス強磁場中c軸抵抗率測定による銅酸化物高温超伝導体における前駆クーパー対形成の検証	渡辺 孝夫	弘前大学	藤井 武則（低温科学研究センター）	Observation of preformed Cooper pairing in high-Tc cuprates using out-of-plane resistivity measurements of Bi(Pb)-2212 single crystals under high pulsed magnetic fields	Takao Watanabe	Hirosaki University	Takenori Fujii (Cryogenic Research Center)	金道 浩一
16	202204-HMBXX-0039	CoOナノ結晶の比熱測定	石渡 洋一	佐賀大学		Heat capacity measurements of CoO nanocrystals	Yoichi Ishiwata	Saga University		金道 浩一
17	202206-HMBXX-0084	Identifying magnetization plateaus in the Kagome antiferromagnet YCu3(OD)6+xBr3-x	Choi Kwang-Yong	Sungkyunkwan University	Lee Chanhyeon (Chung-Ang University) Jeon Sungmin Lee Seung-Yeol	Identifying magnetization plateaus in the Kagome antiferromagnet YCu3(OD)6+xBr3-x	Kwang-Yong Choi	Department of Physics, Sungkyunkwan University, Republic of Korea	Chanhyeon Lee (Chung-Ang University) Sungmin Jeon Seung-Yeol Lee	松田 康弘
18	202202-HMBXX-0035	強磁場下でのキラリティ誘起スピン偏極	宍戸 寛明	大阪公立大学		Chirality induced spin polarization under high magnetic fields	Hiroaki Shishido	Osaka metropolitan university		徳永 将史
19	202204-HMBXX-0042	PPMSを使った極低温イメージングシステムの開発	志村 恭通	広島大学	渡邊 寛大	Development of Very-Low Temperature Imaging System in PPMS	Yasuyuki Shimura	Hiroshima University	Kanta Watanabe	徳永 将史
20	202204-HMBXX-0043	パルス強磁場下超音波計測による強相関電子系の磁場中量子状態	栗原 綾佑	東京理科大学	矢口 宏 小峰 智弥 島根 恭汰	Ultrasonic study of quantum states in strongly-correlated electron systems under pulsed-magnetic fields	Ryosuke Kurihara	Tokyo University of Science	Hiroshi Yaguchi Tomoya Komine Kyota Shimane	徳永 将史
21	202204-HMBXX-0046	単一分子磁石の磁場誘起分極変化	呉 樹旗	九州大学　先導物質化学研究所	徐 文煌	Magnetic Field-Induced Polarization Change in Single-Molecule Magnets	Shu-Qi Wu	Institute for Materials Chemistry and Engineering, Kyushu University	Wenhuang Xu	徳永 将史
22	202205-HMBXX-0059	Exploring the origin of giant anomalous Hall effect in noncoplanr magnetic state of electron doped kagome magnet Mn3Sn	Nayak Ajaya	National Institute of Science Education and Research		Exploring the origin of giant anomalous Hall effect in noncoplanr magnetic state of electron doped kagome magnet Mn3Sn	Ajaya Kumar Nayak	National Institute of Science Education and Research		徳永 将史

23	202207-HMBXX-0085	High-field magnetization and magnetocaloric-effect measurements of a spin-chain compound	WANG Zhe	TU Dortmund University		High-field magnetization and magnetocaloric-effect measurements of a spin-chain compound	WANG Zhe	TU Dortmund University		小濱 芳允

大阪大学大学院理学研究科附属先端強磁場科学研究センター / Center for Advanced High Magnetic Field Science, Graduate School of Science, Osaka University

No.	課題番号	課題名	氏名	所属	分担者	Title	Name	Organization	Member of reseach project	担当所員
1	202111-HMOXX-0002	スピン磁気モーメントのみのEuとGd化合物の特異な磁性と強磁場物性	竹内 徹也	大阪大学	大貫 惇睦（東京都立大学）	Characteristic magnetic properties and high-field magnetism in the S-state Eu and Gd compounds.	Tetsuya Takeuchi	Osaka University	Yoshichika Onuki (Tokyo Metropolitan University)	萩原 政幸（大阪大学）
2	202111-HMOXX-0003	量子スピン系の電場励起ESRと方向二色性	木村 尚次郎	東北大学		Electric dipole active ESR and nonreciprocal directional dichroism in quantum spin systems	Shojiro Kimura	Tohoku University		萩原 政幸（大阪大学）
3	202111-HMOXX-0005	FCCフラストレート磁性体RInCu4のパルス強磁場下ホール抵抗測定	和氣 剛	京都大学	塩谷 太基	Pulse High-field Hall resistivity of FCC frustrated magnets RInCu4	Takeshi Waki	Kyoto University	Taiki Shiotani	萩原 政幸（大阪大学）
4	202111-HMOXX-0006	パルス強磁場用極低温実験装置の開発	野口 悟	大阪公立大学	吉田 勝一	Development of the cryostat for pulsed high magnetic field	Satoru Noguchi	Osaka Metropolitan University	Shoichi Yoshida	萩原 政幸（大阪大学）
5	202111-HMOXX-0007	種々の新型磁気力ブースターの性能試験	牧 祥	岡山理科大学		Performance test of various types of new magnetic force boosters	Syou Maki	Okayama University of Science		萩原 政幸（大阪大学）
6	202111-HMOXX-0011	ハニカムネットワークを持つ超伝導物質の開発	工藤 一貴	大阪大学		Development of novel superconductors with honeycomb networks	Kazutaka Kudo	Osaka University		萩原 政幸（大阪大学）
7	202111-HMOXX-0012	CdI2型構造を持つ超伝導体の物質開発	工藤 一貴	大阪大学		Development of novel superconductors with a CdI2-type structure	Kazutaka Kudo	Osaka University		萩原 政幸（大阪大学）
8	202111-HMOXX-0013	強いスピン-軌道相互作用を活かした酸化物スピントロニクス	松野 丈夫	大阪大学	塩貝 純一 上田 浩平	Oxide spintronics utilizing strong spin-orbit coupling	Jobu Matsuno	Osaka University	Junichi Shiogai Kohei Ueda	萩原 政幸（大阪大学）
9	202112-HMOXX-0014	パルス強磁場を用いた高圧下ESR装置の開発と圧力セルの最適化	櫻井 敬博	神戸大学	赤木 暢（東北大学）	Development of high-pressure ESR system used in pulsed high fields and optimization of pressure cell	Takahiro Sakurai	Kobe University	Mitsuru Akaki (Tohoku University)	萩原 政幸（大阪大学）
10	202112-HMOXX-0017	電荷密度波磁性半導体の異方的な磁気抵抗効果の研究	村川 寛	大阪大学		Study for the anisotropic magnetoresistance in chargedensity wave semiconductor	Hiroshi Murakawa	Osaka University		萩原 政幸（大阪大学）
11	202112-HMOXX-0027	有機無機層状磁性体の圧力下における磁性	本多 善太郎	埼玉大学		Magnetic properties of organic-inorganic layered magnets under pressure	Zentaro Honda	Saitama University		萩原 政幸（大阪大学）
12	202112-HMOXX-0030	非従来型超伝導体微細構造のパルス強磁場下輸送特性	掛谷 一弘	京都大学		Transport measurements on micro-structured unconventional superconductors under pulsed high magnetic fields	Itsuhiro Kakeya	Kyoto University		萩原 政幸（大阪大学）

強磁場コラボラトリー / The High Magnetic Field Collaboratory

No.	課題番号	課題名	氏名	所属	分担者	Title	Name	Organization	Member of reseach project	担当所員
1	202204-HMBXX-0040	光駆動型有機FET界面におけるフェルミオロジーと強磁場超伝導相	木俣 基	東北大学		Fermiology and high-field superconducting phase in photo-induced organic FET interface	Motoi Kimata	Tohoku University		徳永 将史
2	202112-HMCXX-0025	強磁場NMR測定によるカゴメ遍歴磁性体における磁場誘起磁気相の研究	井原 慶彦	北海道大学大学院		High-field NMR study for field-induced magnetic states in itinerant kagome magnets	Yoshihiko Ihara	Hokkaido University		小濱 芳允

3	202204-HMCXX-0041	定常・準定常・パルス強磁場下における精密熱輸送測定系の開発	木原 工	岡山大学異分野基礎科学研究所		Development of a thermal transport measurement system in the steady, quasi-steady, and pulsed high magnetic fields	Takumi Kihara	Research Institute for Interdisciplinary Science, Okayama University		小濱 芳允

留学研究課題（External Research Project Long / Short -term）

No.	課題番号	課題名	氏名	所属	分担者	Title	Name	Organization	Member of reseach project	担当所員
1	202111-VSBXS-0001	ホタルルシフェラーゼ環境下における AkaLumine の吸光度測定	大澤 敬太	群馬大学院理工学府		In situs absorption spectra for AkaLumine in firefly luciferase	Osawa Keita	Gunma University		秋山 英文
2	202111-VSBXS-0002	DEACM-ケージドルシフェリン光解離におけるUV光条件	松永 大輝	群馬大学		Study for UV irradiation condition on the photodissociation of DEACM caged D-luciferin	Hiroki Matsunaga	Gunma University		秋山 英文

2022年度　共同利用課題一覧（後期）/ Joint Research List 2022 (Latter Term)

※実施課題一覧、所属は申請時のデータ

嘱託課題 / Comission Research Project

No.	課題番号	課題名	氏名	所属	分担者	Title	Name	Organization	Member of reseach project	担当所員
1	202206-CMBXX-0125	ハライドペロブスカイト単結晶薄膜を用いたレーザー開発	高橋 竜太	日本大学		Development of Halide Perovskite Single Crystal Film Laser	Ryota Takahashi	Nihon University		Mikk Lippmaa
2	202206-CMBXX-0111	高圧下Ｘ線回折法の開発	江藤 徹二郎	久留米工業大学		Development of High Pressure X-ray diffraction measurements	Tetsujiro Eto	Kurume Institute of Technology		上床 美也
3	202206-CMBXX-0112	極低温下の磁気特性	鳥塚 潔	千葉工業大学		Development of magnetic measurement method	Kiyoshi Torizuka	Chiba Institute of Technology		上床 美也
4	202206-CMBXX-0113	低次元有機物質の圧力下物性研究	糸井 充穂	日本大学		Study on pressure induced superconductivity of low dimension organic conductor	Miho Itoi	Nihon University		上床 美也
5	202206-CMBXX-0114	3d遷移化合物に関する圧力効果	鹿又 武	東北学院大学工学総合研究所		Effect of pressure on the 3d transition compounds	Takeshi Kanomata	Research Institute for Engineering and Technology, Tohoku Gakuin University		上床 美也
6	202206-CMBXX-0117	希釈冷凍機温度での高圧発生装置の開発	松林 和幸	電気通信大学		Development of high pressure apparatus for low temperature	Kazuyuki Matsubayashi	The University of Electro-Communications		上床 美也
7	202206-CMBXX-0118	高圧下量子振動観測システムの開発	摂待 力生	新潟大学		Development of quantum oscillation under high pressure	Rikio Settai	Niigata University		上床 美也
8	202206-CMBXX-0119	圧力下NMR測定法に関する開発	藤原 直樹	京都大学		Development of NMR measurement method under high pressure	Naoki Fujiwara	Kyoto University		上床 美也
9	202206-CMBXX-0120	希土類化合物の良質試料作製	繁岡 透	山口大学		Preparation of high-quality samples of rare earth compounds	Toru Shigeoka	Yamaguchi University		上床 美也
10	202206-CMBXX-0121	低温物性測定法の開発	辺土 正人	琉球大学		Development of low temperature physical property measurement method	Masato Hedo	University of the Ryukyus		上床 美也
11	202206-CMBXX-0122	良質静水圧下での物性測定法の開発	村田 恵三	大阪公立大学		Development of a method for measuring physical properties under high-quality hydrostatic pressure	Keizo Murata	Osaka Metropolitan University		上床 美也
12	202206-CMBXX-0126	マルチアンビル圧力装置の調整	高橋 博樹	日本大学		Adjustment of Multi-anvil pressure apparatus	Hiroki Takahashi	Nihon University		上床 美也
13	202205-CMBXX-0069	4Gにおける共同利用推進(A)	佐藤 卓	東北大学		Research and Support of General-Use at 4G(A)	Taku J Sato	Tohoku University		眞弓 皓一
14	202205-CMBXX-0070	4Gにおける共同利用推進(C)	那波 和宏	東北大学		Research and Support of General-Use at 4G(C)	Kazuhiro Nawa	Tohoku University		眞弓 皓一
15	202205-CMBXX-0071	６G、T1-2、T1-3における共同利用推進(A)	藤田 全基	東北大学		Research and Support of General-Use at 6 G, T1-2 and T1-3(A)	Masaki Fujita	Tohoku University		眞弓 皓一
16	202205-CMBXX-0072	６G、T1-2、T1-3における共同利用推進(B)	南部 雄亮	東北大学		Research and Support of General-Use at 6 G, T1-2 and T1-3(B)	Yusuke Nambu	Tohoku University		眞弓 皓一
17	202205-CMBXX-0073	６G、T1-2、T1-3における共同利用推進(C)	池田 陽一	東北大学金属材料研究所		Research and Support of General-Use at 6 G, T1-2 and T1-3(C)	Yoichi Ikeda	Institute for materials research, Tohoku university		眞弓 皓一
18	202205-CMBXX-0074	６G、T1-2、T1-3における共同利用推進(D)	谷口 貴紀	東北大学		Research and Support of General-Use at 6 G, T1-2 and T1-3(D)	Takanori Taniguchi	Tohoku University		眞弓 皓一
19	202205-CMBXX-0082	T2-2における共同利用推進(B)	坂倉 輝俊	東北大学多元物質科学研究所		Research and Support of General-Use at T2-2(B)	Terutoshi Sakakura	Institute of Multidisciplinary Research for Advanced Materials, Tohoku University		眞弓 皓一

20	202205-CMBXX-0084	C1-2における共同利用推進(A)	杉山 正明	京都大学		Research and Support of General-Use at C1-2(A)	Masaaki Sugiyama	Kyoto University		眞弓 皓一
21	202205-CMBXX-0085	C1-2、C2-3-1における共同利用推進	井上 倫太郎	京都大学		Research and Support of General-Use at C1-2 and C2-3-1	Rintaro Inoue	Kyoto University		眞弓 皓一
22	202205-CMBXX-0086	C1-2における共同利用推進(B)	守島 健	京都大学		Research and Support of General-Use at C1-2(B)	Ken Morishima	Kyoto University		眞弓 皓一
23	202205-CMBXX-0088	C3-1-2における共同利用推進(A)	日野 正裕	京都大学		Research and Support of General-Use at C3-1-2(A)	Masahiro Hino	Kyoto University		眞弓 皓一
24	202205-CMBXX-0091	C3-1-2における共同利用推進(D)	中村 吏一朗	京都大学複合原子力科学研究所		Research and Support of General-Use at C3-1-2(D)	Riichiro Nakamura	Department of Nuclear Engineering, Kyoto University		眞弓 皓一
25	202205-CMBXX-0068	超強磁場におけるスピン格子強結合系の研究	池田 暁彦	電気通信大学		Study of the strongly spin-lattice-coupled systems in ultrahigh magnetic fields	Akihiko Ikeda	University of Electro-Communications		松田 康弘
26	202205-CMBXX-0100	光スピントロニクスに向けたスピン軌道ダイナミクスの研究	黒田 健太	広島大学		Studying spin-orbit dynamics for opt-spintronics	Kenta Kuroda	Hiroshima University		近藤 猛
27	202205-CMBXX-0103	レーザースピン角度分解光電子分光による表面電子状態の研究	矢治 光一郎	物質・材料研究機構		SARPES studies of atomic layer materials at surfaces	Koichiro Yaji	National Institute for Materials Science		近藤 猛
28	202205-CMBXX-0109	三次元nanoESCAによる実デバイスのオペランド電子状態解析	永村 直佳	物質・材料研究機構		Operando analysis of the electronic structure of actual devices by 3DnanoESCA	Naoka NAGAMURA	National Institute for Materials Science		原田 慈久

一般課題 / General Research Project

No.	課題番号	課題名	氏名	所属	分担者	Title	Name	Organization	Member of reseach project	担当所員
1	202204-GNBXX-0089	単一成分分子性導体における交換相互作用及び磁気特性に与えるアルキル基変調・伸長効果の研究	横森 創	立教大学		Study of effects of a modulation/extension of alkyl groups on magnetic properties and exchange interactions in single-component molecular conductors	So Yokomori	Rikkyo University		森 初果
2	202204-GNBXX-0090	高いプロトン伝導度を示すスルホン酸有機塩の創製	岡 弘樹	大阪大学	赤井 亮太	Sulfonic Acid Organic Salts with High Proton Conductivity	Kouki Oka	Osaka University	Ryota Akai	森 初果
3	202205-GNBXX-0101	脱プロトン型の新規分子性伝導体の磁性・電気伝導性の解明	上田 顕	熊本大学	藤井 雄也	Elucidation of magnetic and electrical properties of novel deprotonated molecular conductors	Akira Ueda	Kumamoto University	Yuya Fujii	森 初果
4	202210-GNBXX-0163	自己組織化ペプチド導入ニッケル錯体の電子物性評価	若林 里衣	九州大学		Investigation of electronic properties of nickel complexes modified with self-assembly peptides	Rie Wakabayashi	Kyushu University		森 初果
5	202210-GNBXX-0168	キタエフスピン液体候補物質α-RuCl3の結晶構造に関する研究	橋本 顕一郎	東京大学	今村 薫平 難波 隆一	Study on crystal structure of the Kitaev spin liquid candidate α-RuCl3	Kenichiro Hashimoto	The University of Tokyo	Kumpei Imamura Ryuichi Namba	森 初果
6	202205-GNBXX-0102	磁気トルクに強い小型高感度磁化測定装置の開発とベンチマーク測定	河野 洋平	中央大学	湯淺 翔平	Development of a miniaturized high-precision magnetometer robust to magnetic torque and measurements for its performance	Yohei Kono	Chuo University	Shohei Yuasa	山下 穣
7	202205-GNBXX-0109	シャストリーサザーランド四面体格子Ce5Si3とCe5Ga2Geの極低温磁化測定	小林 理気	琉球大学	植田 大地（高エネルギー加速器研究機構） 清水 悠晴（東北大学金属材料研究所）	Low-temperature magnetization measurements of Shastry-Sutherland tetrahedron lattice Ce5Si3 and Ce5Ga2Ge	Riki Kobayashi	University of the Ryukyus	Daichi Ueta (High Energy Accelerator Research Organization)Yusei Shimizu (Tohoku University)	山下 穣

8	202210-GNBXX-0164	UTe2の純良単結晶試料を中心とするスピン三重項超伝導体の磁化・比熱・磁歪測定	清水 悠晴	東北大学金属材料研究所		Magnetization, heat-capacity, and magnetostriction measurements on spin-triplet superconductors: studies using high-quality UTe2 single crystalline samples	Yusei Shimizu	Tohoku University, Institute for Materials Research		山下 穣
9	202205-GNBXX-0093	希土類金属間化合物および金属超伝導体の結晶育成と低温電子物性	海老原 孝雄	静岡大学	荒川 尚也	Crystal Growth and Physical Properties at low temperatures in rare earth intermetallic compounds and metallic superconductors	Takao Ebihara	Shizuoka University	Naoya Arakawa	大谷 義近
10	202209-GNBXX-0160	カゴメ格子超伝導体におけるトポロジーと対称性の破れに関する研究	橋本 顕一郎	東京大学	石原 滉大 広瀬 夏彦 六本木 雅生 劉 蘇鵬	Study of topology and symmetry breaking in kagome superconductors	Kenichiro Hashimoto	The University of Tokyo	Kota Ishihara Natsuhiko Hirose Masaki Roppongi SUPENG LIU	大谷 義近
11	202205-GNBXX-0096	エッジ制御したグラフェン素子における量子伝導	原 正大	熊本大学		Quantum transport in edge-controlled graphene devices	Masahiro Hara	Kumamoto University		勝本 信吾
12	202205-GNBXX-0105	二次元銅酸化物のホール係数測定 VII	神戸 士郎	山形大学	内藤 聖羅 加藤 貴大 荻野 拓哉	Hall coefficient measurement of 2D cuprates VII	Shiro Kambe	Graduate School of Science and Engineering, Yamagata University	Seira Naito Takahiro Kato OGINO TAKUYA	勝本 信吾
13	202206-GNBXX-0131	グラフェン/超伝導炭化物/SiCの低温電気伝導測定	乗松 航	名古屋大学	大塚 康平	Electrical measurements of graphene/superconducting-carbide/SiC	Wataru Norimatsu	Nagoya University	Otsuka Kohei	勝本 信吾
14	202209-GNBXX-0165	ハライドペロブスカイト薄膜を用いたレーザー開発	高橋 竜太	日本大学	太宰 卓朗	Development of halide perovskite film laser	Ryota Takahashi	Nihon University	Takuro Dazai	勝本 信吾
15	202205-GNBXX-0098	SiC基板上に成長したグラフェンへのFeインターカレーション	中辻 **寛**	東京工業大学	小森 文夫 竹村 晃一	Intercalation of Fe into graphene grown on a SiC substrate	Kan Nakatsuji	Tokyo Institute of Technology	Fumio Komori Koichi Takemura	吉信 淳
16	202205-GNBXX-0112	金属表面上へ担持した金属クラスターの触媒作用の機能探索	塚原 規志	群馬工業高等専門学校		Exploration of the catalytic property of the metal clusters on metal surfaces	Noriyuki Tsukahara	National Institute of Technology, Gunma College		吉信 淳
17	202205-GNBXX-0115	リグニンの有用化合物への変換を可能にする固体触媒及び反応条件の検討（4）	布浦 鉄兵	東京大学環境安全研究センター	堂脇 大志	Study of solid catalysts and reaction conditions enabling lignin conversion into valuable chemicals (4)	Teppei Nunoura	Environmental Science Center, the University of Tokyo	Taishi Dowaki	吉信 淳
18	202205-GNBXX-0117	二硫化モリブデンナノシートの製造に及ぼす超臨界二酸化炭素の影響（3）	布浦 鉄兵	東京大学環境安全研究センター	カン ジシン	Effect of supercritical carbon dioxide on fabrication of molybdenum disulfide nanosheets (3)	Teppei Nunoura	Environmental Science Center, the University of Tokyo	HAN Zixin	吉信 淳
19	202212-GNBXX-0172	異種二分膜におけるプロトン移動の実証と物性制御	加藤 浩之	大阪大学		Investigation of Proton Transfer and Property Control for Hetero-Bilayer	Hiroyuki S. Kato	Osaka University		吉信 淳
20	202205-GNBXX-0100	水溶液におけるseMpaiの吸収特性	樋山 みやび	群馬大学	原田 昌拓	Absorption spectra of seMpai in aqueous solution	Miyabi Hiyama	Gunma University	masahiro harada	秋山 英文
21	202205-GNBXX-0103	エルビウムドープIII-V族化合半導体の発光特性	矢口 裕之	埼玉大学	矢野 裕子 伊藤 駿平	Luminescence properties of Er doped III-V compound semiconductors	Hiroyuki Yaguchi	Saitama University	Yuko Yano Shunpei Ito	秋山 英文
22	202205-GNBXX-0123	新奇ケージドルシフェリン化合物の光解離測定	樋山 みやび	群馬大学	勝見 渓太	Study of photodissociation for a new caged compound	Miyabi Hiyama	Gunma University	katsumi keita	秋山 英文
23	202210-GNBXX-0169	プラズモニックデバイスの光学特性の解明	米谷 玲皇	東京大学	大岩 達典	Optical characteristic evaluations of plasmonic devices	Reo Kometani	The University of Tokyo	Tatsunori Oiwa	秋山 英文
24	202205-GNBXX-0116	二硫化モリブデンナノシートの製造に及ぼす超臨界二酸化炭素の影響（2）	布浦 鉄兵	東京大学環境安全研究センター	カン ジシン	Effect of supercritical carbon dioxide on fabrication of molybdenum disulfide nanosheets (2)	Teppei Nunoura	Environmental Science Center	HAN Zixin	三輪 真嗣
25	202206-GNBXX-0125	超伝導体/強磁性体界面で発現する新奇超伝導状態に関する研究	志賀 雅亘	九州大学	寺本 翼	Study of a novel superconductivity emerged at superconductor/ferromagnet interface	Masanobu Shiga	Environmental Science Center, the University of Tokyo	TSUBASA TERAMOTO	三輪 真嗣

26	202205-GNBXX-0104	超低温トポケミカル合成したスピン軌道結合磁性体の物性研究	原口 祐哉	東京農工大学	石北 大悟	Physical Properties of Spin-Orbit Coupled Magnets Synthesized by Ultralow Temperature Topochemical Manipulation	Yuya Haraguchi	Tokyo University of Agriculture and Technology	Daigo Ishikita	広井 善二
27	202205-GNBXX-0091	CeMnSiの高圧下における電気抵抗	川村 幸裕	室蘭工業大学	西山 紗恵	Electrical Resistivity of CeMnSi under high pressure	Yukihiro Kawamura	Muroran Institute of Technology	Sae Nishiyama	上床 美也
28	202205-GNBXX-0092	CeMnSiの高圧下における単結晶X線構造解析	川村 幸裕	室蘭工業大学	西山 紗恵	X-ray structural analysis of CeMnSi single crystal under high pressure	Yukihiro Kawamura	Muroran Institute of Technology	Sae Nishiyama	上床 美也
29	202205-GNBXX-0121	単結晶Eu3Bi2S4F4における圧力効果の研究	石垣 賢卯	東京理科大学		Research of single crystal Eu3Bi2S4F4 in high pressure	Kento Ishigaki	Tokyo University of Science		上床 美也
30	202205-GNBXX-0122	圧力媒体の混合効果	村田 惠三	大阪公立大学	上床 美也（東京大学物性研究所）	Mixing Effect of Pressure Medium	Keizo Murata	Osaka Metropolitan University	Yoshiya Uwatoko (ISSP The University of Tokyo)	上床 美也
31	202205-GNBXX-0149	多型化合物RIr2Si2(R=希土類)の磁気特性7	内間 清晴	学校法人沖縄キリスト教学院・沖縄キリスト教短期大学	繁岡 透（山口大学）	Magnetic characteristics of polymorphic compounds RIr2Si2(R=Rare earth) 7	Kiyoharu Uchima	Okinawa Christian Institute Okinawa christian junior College	Toru Shigeoka (Yamaguchi University)	上床 美也
32	202205-GNBXX-0150	CeNiC2の結晶育成と物質評価 2	繁岡 透	山口大学	内間 清晴（学校法人沖縄キリスト教学院・沖縄キリスト教短期大学）	Crystal growth and characterization of CeNiC2 2	Toru Shigeoka	Yamaguchi University	Kiyoharu Uchima (Okinawa Christian Institute Okinawa christian junior College)	上床 美也
33	202205-GNBXX-0151	擬三元化合物 Ce1- x La x NiC2の結晶育成と物質評価 4	繁岡 透	山口大学	内間 清晴（学校法人沖縄キリスト教学院・沖縄キリスト教短期大学）	Crystal growth and characterization of pseudo-ternary compounds Ce1- x La x NiC2 4	Toru Shigeoka	Yamaguchi University	Kiyoharu Uchima (Okinawa Christian Institute Okinawa christian junior College)	上床 美也
34	202206-GNBXX-0119	新ガスケット方式による対向アンビル型高圧装置の開発III	久田 旭彦	徳島大学	髙木 拓海	Development of opposed-type anvil apparatus with new gasket system III	Akihiko Hisada	Tokushima University	Takumi Takagi	上床 美也
35	202206-GNBXX-0126	(Ce1-xRx)PtGe2の単結晶育成と磁気的性質	中野 智仁	新潟大学	武藤 颯人	Single crystals growth of (Ce1-xRx)PtGe2 and thier magnetic properties	Tomohito NAKANO	Faculty of Engineering, Niigata University	Hayato Muto	上床 美也
36	202206-GNBXX-0130	ホイスラー化合物Fe3-xMnxSiの圧力下磁気相転移	廣井 政彦	鹿児島大学	赤石 幸起 髙本 翼	Magnetic phase transitions under pressure in Heuser compounds Fe3-xMnxSi	Masahiko HIROI	Kagoshima University	Kouki Akaishi Tsubasa Takamoto	上床 美也
37	202206-GNBXX-0132	Ni2In型強磁性体の自発磁化の圧力効果	安達 義也	山形大学		Pressure effects on the spontaneous magnetization for Ni2In-type ferromagnets	Yoshiya Adachi	Yamagata University		上床 美也
38	202206-GNBXX-0134	MnCoGe-MnFeGe系の磁気特性評価	小山 佳一	鹿児島大学	尾中 朱莉	Basic magnetic properties of MnCoGe-MnFeGe system	Keiichi KOYAMA	Kagoshima University	Akari Onaka	上床 美也
39	202206-GNBXX-0135	Ta2NiSe5のTaサイト置換物質の高圧力下電気抵抗測定	広瀬 雄介	新潟大学	土田 駿	Electrical resistivity measurement under pressure of Ta site substituted Ta2NiSe5	Yusuke Hirose	Niigata University	Shun Tsuchida	上床 美也
40	202206-GNBXX-0137	強誘電体および反強誘電体における圧力下量子臨界現象の研究	橋本 顕一郎	東京大学	劉 蘇鵬	Study of pressure-induced quantum critical phenomena in ferroelectric and antiferroelectric materials	Kenichiro Hashimoto	The University of Tokyo	SUPENG LIU	上床 美也
41	202206-GNBXX-0141	不定比化合物DyCrxGe2の単結晶育成	藤原 哲也	山口大学	五反田 礼	Single crystal growth of non stoichiometric compounds DyCrxGe2	Tetsuya Fujiwara	Yamaguchi University	Rei Gotanda	上床 美也
42	202206-GNBXX-0142	不定比化合物HoCrxGe2の単結晶育成	藤原 哲也	山口大学	新谷 怜和	Single crystal growth of non stoichiometric compounds HoCrxGe2	Tetsuya Fujiwara	Yamaguchi University	reo niiya	上床 美也
43	202206-GNBXX-0143	不定比化合物DyCrxGe2単結晶の磁化測定	藤原 哲也	山口大学	新谷 怜和	Magnetization measurements of non stoichiometric DyCrxGe2 single crystals	Tetsuya Fujiwara	Yamaguchi University	reo niiya	上床 美也

44	202206-GNBXX-0146	MxM'1-xZnSb (M, M':3d遷移金属)の磁気特性	三井 好古	鹿児島大学	長野 杜春	Magnetic properties of MxM'1-xZnSb (M, M':3d transition metal)	Yoshifuru MITSUI	Kagoshima University	Moriharu Nagano	上床 美也
45	202206-GNBXX-0147	遷移金属カルコゲナイドTiSe2の圧力下 dHvA 効果の研究	摂待 力生	新潟大学	出井 和樹	dHvA effect in transition metal dichalcogenides TiSe2 under pressure	Rikio Settai	Niigata University	Kazuki Idei	上床 美也
46	202206-GNBXX-0148	高スピン分極ホイスラー合金における圧力誘起量子臨界現象の探索	重田 出	鹿児島大学	青島 英樹	Search for pressure-induced quantum critical phenomenon in highly spin polarized Heusler alloys	Iduru Shigeta	Kagoshima University	Aoshima Hideki	上床 美也
47	202206-GNBXX-0152	片側末端にプロピレン基を持つ非対称TTF誘導体からなる有機伝導体の超高圧下物性研究	谷口 弘三	埼玉大学	小林 拓矢 小梁川 響子 佐藤 慧一	High pressure studies on physical properties of organic conductors based on asymmetrical TTF derivatives with a propylene group at one end	Hiromi Taniguchi	Saitama University	Takuya Kobayashi Kyoko Koyanagawa Keiichi Sato	上床 美也
48	202206-GNBXX-0153	反強磁性体Eu-Ru-Ge化合物の高圧下における電子状態の研究	本多 史憲	九州大学アイソトープ統合安全管理センター		Electronic properties of an antiferromagnetic Eu-Ru-Ge compound under high pressures	Fuminori Honda	Central Institute of Radioisotope Science and Safety Management, Kyushu University		上床 美也
49	202206-GNBXX-0154	ウラン化合物の磁性の圧力効果	本多 史憲	九州大学アイソトープ統合安全管理センター		Effect of Pressure on the magnetism of uranium compounds	Fuminori Honda	Central Institute of Radioisotope Science and Safety Management, Kyushu University		上床 美也
50	202209-GNBXX-0162	S置換したFeSeの高圧低温下NMR測定	藤原 直樹	京都大学	Yu Zhongyu	NMR studies on S-substituted FeSe at high pressures and low temperatures	Naoki Fujiwara	Kyoto University	Zhongyu Yu	上床 美也
51	202210-GNBXX-0166	立方晶Ho3AlCの低温比熱	松本 圭介	愛媛大学	宮本 諒人	Specific heat study of Ho3AlC	Keisuke Matsumoto	Ehime University	Makoto Miyamoto	上床 美也
52	202210-GNBXX-0167	Gd2CuO4の比熱へのNi/Zn添加効果	松本 圭介	愛媛大学	宮本 諒人 小椋 隆平	Specific heat study of Ni/Zn doped Gd2CuO4	Keisuke Matsumoto	Ehime University	Makoto Miyamoto Ryuhei Ogura	上床 美也
53	202301-GNBXX-0174	超高圧下量子振動効果測定装置の開発	菅原 仁	神戸大学	薦田 拓也	Development of the quantum oscillation measuring system under the ultra high pressure	Hitoshi Sugawara	Kobe university	Takuya Komoda	上床 美也
54	202205-GNBXX-0114	リグニンの有用化合物への変換を可能にする固体触媒及び反応条件の検討（３）	布浦 鉄兵	東京大学環境安全研究センター	堂脇 大志	Effect of supercritical carbon dioxide on fabrication of molybdenum disulfide nanosheets (2)	Teppei Nunoura	Environmental Science Center, the University of Tokyo	Taishi Dowaki	山室 修
55	202205-GNBXX-0110	高エネルギーX線透過ラウエによる中性子非弾性散乱実験用単結晶のアセンブル	小林 理気	琉球大学	植田 大地（高エネルギー加速器研究機構）玉城 良仁 琉球大学	Assembly of single crystals for inelastic neutron scattering experiments using high-energy X-ray transmission Laue	Riki Kobayashi	University of the Ryukyus	Daichi Ueta (High Energy Accelerator Research Organization)Tamashiro Yoshihito	益田 隆嗣
56	202209-GNBXX-0161	新規トポロジカル磁性体の合成と磁気構造の解明	車地 崇	東京大学	有馬 孝尚 徳永 祐介 厳 正輝（理化学研究所）	Magnetic structure analysis of novel topological magnets	Takashi Kurumaji	The University of Tokyo	Taka-hisa Arima Yusuke Tokunaga Masaki Gen (RIKEN)	益田 隆嗣
57	202204-GNBXX-0087	レーザー誘起合金化のパルス時間幅依存性	富田 卓朗	徳島大学	古市 健人	Pulse duration dependence of laser induced metal alloying	Takuro Tomita	Tokushima University	Taketo Furuichi	小林 洋平
58	202205-GNBXX-0094	金属ナノ構造の超高速発光による研究	末元 徹	電気通信大学		Studies on nanostructured metals by ultrafast luminescence spectroscopy	Suemoto Tohru	The University of Electro-Communications		小林 洋平

59	202205-GNBXX-0099	次世代レーザーとレーザー加工の基礎技術研究	吉富 大	産業技術総合研究所	髙田 英行 奈良崎 愛子 小川 博嗣 寺澤 英知 澁谷 達則 佐藤 大輔 黒田 隆之助 田中 真人 丸 征那	Basic research on next generation laser systems and laser machining technology	Dai Yoshitomi	National Institute of Advanced Industrial Science and Technology	Takada Hideyuki Aiko Narazaki Hiroshi Ogawa Eichi Terasawa Tatsunori Shibuya Daisuke Satoh Ryunosuke Kuroda Masahito Tanaka Sena Maru	小林 洋平
60	202205-GNBXX-0107	紫外光レーザー光源を用いた加工応用研究	藤本 靖	千葉工業大学		Research on laser processing application by ultraviolet laser light source	Yasushi Fujimoto	Chiba Institute of Technology		小林 洋平
61	202206-GNBXX-0127	熱可塑性高分子におけるレーザー誘起構造変化	山口 誠	秋田大学		Laser-induced structural changes in thermoplastic polymers	Yamaguchi Makoto	Akita University		小林 洋平
62	202212-GNBXX-0173	超短パルスYbファイバーレーザー光源を用いた生体組織の分子振動イメージング	長島 優	浜松医科大学		Molecular vibrational imaging of biological tissues using Yb fiber-based ultrashort pulse laser source	Yu Nagashima	Hamamatsu University School of Medicine		小林 洋平
63	202206-GNBXX-0136	SmSの高強度中赤外パルス光を用いた光誘起相転移ダイナミクス	渡邊 浩	大阪大学		High power mid-infrared laser induced phase transition dynamics on SmS	Hiroshi Watanabe	Osaka University		板谷 治郎
64	202205-GNBXX-0124	金属表面に形成された水素結合有機フレームワークによって誘起される量子井戸状態の直接観測	金井 要	東京理科大学	馬上 怜奈	Direct observation of quantum well states induced by the hydrogen-bonded organic frameworks formed on metal surface	Kaname Kanai	Tokyo University of Science	Rena Moue	近藤 猛
65	202206-GNBXX-0128	Hex-Au(100)上グラフェンにおけるπバンドスピン構造の研究	伊藤 孝寛	名古屋大学	杉本 卓史 保科 拓海 三田 愛也 寺澤 知潮（日本原子力研究開発機構） 小山 正太郎 強 博文	Spin structure study of π band of Graphene on Hex-Au(100)	Takahiro Ito	Nagoya University	Takafumi Sugimoto Hoshina Takumi Mita Manaya Tomoo Terasawa (Japan Atomic Energy Agency) Koyama Shotaro Bowen Qiang	近藤 猛
66	202206-GNBXX-0138	4d強磁性酸化物SrRuO3薄膜における準粒子状態のスピン分極評価	小林 正起	東京大学	武田 崇仁	Elucidation of the spin polarization of the quasi-particle states in 4d ferromagnetic oxide SrRuO3	Masaki Kobayashi	The University of Tokyo	Takahito Takeda	近藤 猛
67	202206-GNBXX-0140	強磁性体基板上のグラフェンのスピン角度分解光電子分光	矢治 光一郎	物質・材料研究機構	永村 直佳 津田 俊輔 竹澤 伸吾（東京理科大学） 中村 友謙	SAREES study of graphene on ferromagnetic substrates	Koichiro Yaji	National Institute for Materials Science	Naoka NAGAMURA Shunsuke Tsuda Shingo Takezawa (Tokyo University of Science) Tomonori Nakamura	近藤 猛
68	202205-GNBXX-0095	カロリメトリによる金属試料の赤外吸収率測定	末元 徹	電気通信大学	森野 春樹（電気通信大学）	Measurement of infrared absorptivity on metal samples by calorimetry	Suemoto Tohru	The University of Electro-Communications	Haruki Morino (The university of Electro-Communications)	岡崎 浩三
69	202206-GNBXX-0139	励起子絶縁体Ta2NiSe5及び鉄系超伝導体FeSeにおける光誘起相転移の研究	久保田 雄也	理化学研究所		Investigation of the photo-induced phase transitions in an excitonic insulator Ta2NiSe5 and an Fe-based superconductor FeSe	Yuya Kubota	RIKEN		岡崎 浩三

70	202206-GNBXX-0155	高分解能レーザー励起光電子顕微鏡を用いた鉄系超伝導体の電子ネマティック状態の実空間観察VI	影山 遥一	東京大学	大西 朝登	Real-space observation of electronic nematicity in iron-based superconductors by using a high-resolution laser photoemission electron microscope VI	Yoichi Kageyama	The University of Tokyo	Asato Onishi	岡崎 浩三
71	202301-GNBXX-0175	赤外パルスレーザーにより励起したSmSにおける光誘起ダイナミクス	中村 拓人	大阪大学	陳 奕同	Photo-induced dynamics on SmS excited by infrared-pulse laser	Takuto Nakamura	Osaka University	Yitong CHEN	岡崎 浩三

物質合成・評価設備Gクラス / Materials Synthesis and Characterization G Class Research Project

No.	課題番号	課題名	氏名	所属	分担者	Title	Name	Organization	Member of reseach project	実験室
1	202205-MCBXG-0056	フェロアキシャル物質の探索	木村 剛	東京大学	林田 健志 荒川 慶人 木村 健太（大阪公立大学） 三澤 龍介 吉岡 知輝 永井 隆之 諸見里 真人 山岸 茂直	Exploration of ferroaxial materials	Tsuyoshi Kimura	東京大学	Takeshi Hayashida Keito Arakawa Kenta Kimura (Osaka Metropolitan University) Ryusuke Misawa Tomoki Yoshioka Takayuki Nagai Masato Moromizato Shigetada Yamagishi	物質合成室
2	202206-MCBXG-0078	新奇トポロジカル超伝導体候補物質の合成と物性評価	石原 滉大	東京大学	影山 遥一 広瀬 夏彦 六本木 雅生 小河 弘樹	Synthesis and characterization of novel topological superconductors	Kota Ishihara	東京大学	Yoichi Kageyama Natsuhiko Hirose Masaki Roppongi Koki Ogawa	物質合成室
3	202206-MCBXG-0086	奇パリティ磁気多極子秩序を持つ物質の単結晶育成と物性評価	阿部 伸行	日本大学	岩﨑 義己	Crystal growth and physical properties measurement in odd parity multipole ordering materials	Nobuyuki Abe	Nihon University	IWASAKI Yoshiki	物質合成室
4	202205-MCBXG-0060	リグニンの有用化合物への変換を可能にする固体触媒及び反応条件の検討	布浦 鉄兵	東京大学環境安全研究センター	堂脇 大志	Study of solid catalysts and reaction conditions enabling lignin conversion into valuable chemicals	Teppei Nunoura	Environmental Science Center, the University of Tokyo	Taishi Dowaki	化学分析室
5	202205-MCBXG-0059	廃混紡布の炭化による吸着材の生産に関する研究	布浦 鉄兵	東京大学環境安全研究センター	賈 琰瓊	Carbonization of waste blended fabric to produce carbon-based adsorbent	Teppei Nunoura	Environmental Science Center, the University of Tokyo	YANQIONG JIA	X線測定室
6	202205-MCBXG-0061	バイオマスの超臨界水ガス化におけるCuO-Ni触媒の適用可能性に関する検討	布浦 鉄兵	東京大学環境安全研究センター	党 博文	Applicability of CuO-Ni catalyst for supercritical water gasification of biomass	Teppei Nunoura	Environmental Science Center, the University of Tokyo	Bowen DANG	X線測定室
7	202205-MCBXG-0067	亜臨界水と固体塩基触媒の組み合わせによる新規有機合成プロセスの開発	王 一琦	東京大学	王 一琦	Development of novel organic synthesis process with a combination of subcritical water and solid base catalyst	Haoran Xu	The University of Tokyo	Yiqi Wang	X線測定室
8	202205-MCBXG-0068	連続式超臨界水熱合成法による銀ナノ粒子の調製	秋月 信	東京大学	李 琰琛	Preparation Of Silver Nanoparticles Via Continuous Supercritical Hydrothermal Synthesis Method	Makoto Akizuki	The University of Tokyo	LI Yanchen	X線測定室
9	202205-MCBXG-0069	高温高圧水中の有機合成の多段反応装置による高効率化	秋月 信	東京大学	沖田 優美	Highly efficient organic synthesis in high temperature and high pressure water using a multi-stage reactor	Makoto Akizuki	The University of Tokyo	Yumi Okita	X線測定室
10	202205-MCBXG-0070	超臨界メタノールと固体塩基触媒を用いたバイオディーゼル燃料合成	秋月 信	東京大学	東郷 宣弘	Synthesis of biodiesel fuels in supercritical methanol using solid base catalysts	Makoto Akizuki	The University of Tokyo	Nobuhiro TOGO	X線測定室

11	202205-MCBXG-0076	二硫化モリブデンナノシートの製造に及ぼす超臨界二酸化炭素の影響（1）	布浦 鉄兵	東京大学環境安全研究センター	カン ジシン	Effect of supercritical carbon dioxide on fabrication of molybdenum disulfide nanosheets (1)	Teppei Nunoura	Environmental Science Center, the University of Tokyo	HAN Zixin	X線測定室
12	202206-MCBXG-0079	合金ナノ粒子のキャラクタリゼーション	佐々木 岳彦	東京大学	張 凱朝 フェ ジシュン 徐 浩然	Characterization for alloy nanoparticles	Takehiko Sasaki	The University of Tokyo	KAICHAO ZHANG HE ZIXUAN Haoran Xu	X線測定室
13	202206-MCBXG-0087	六方晶ペロブスカイト型イリジウム酸化物Ba4BiIr3O12の単結晶育成	松平 和之	九州工業大学	井上 正弥	Single Crystal Growth of 12L Hexagonal Perovskite Ir oxide Ba4BiIr3O12	Takashi Kitao	Department of Applied Chemistry, Graduate School of Engineering	Masaya Inoue	X線測定室
14	202206-MCBXG-0094	Co基ホイスラー合金におけるマルテンサイト変態材料の探索	重田 出	鹿児島大学	青島 英樹	Search for materials with the Martensitic transformation in Co-based Heusler alloys	Teppei Nunoura	Environmental Science Center	Aoshima Hideki	X線測定室
15	202206-MCBXG-0097	極性と幾何学的フラストレーションを有する磁性体の電気磁気効果	有馬 孝尚	東京大学	木村 真栄 徳永 祐介 石崎 大悟 虎頭 大輔	Magnetoelectric Effect in Polar Magnets with Geometrical Frustration	Taka-hisa Arima	The University of Tokyo	Shin-Ei Kimura Yusuke Tokunaga Daigo Ishizaki Koto Daisuke	X線測定室
16	202204-MCBXG-0100	高度に制御された凝縮相と高圧非平衡プラズマの相互作用による金属等の表面改質および微粒子合成の研究	小池 健	東京大学	新田 魁洲 黒田 知暉 羽藤 健 小池 健	Surface modification of metals and synthesis of fine metal particles by interaction between highly controlled condensed phases and high-pressure non-equilibrium plasmas	Teppei Nunoura	The University of Tokyo	Kaishu Nitta Kuroda Tomoki Takeru Hato Takeru Koike	電子顕微鏡室
17	202205-MCBXG-0052	金属間化合物の構造解析	齋藤 哲治	千葉工業大学		Study of intermetallic compounds	Teppei Nunoura	Environmental Science Center		電子顕微鏡室
18	202205-MCBXG-0055	MOFを鋳型とした機能性ナノマテリアルの創製	北尾 岳史	東京大学	細野 暢彦 ビームスリー キート 葉 思遠 チャンド サンタヌ	Fabrication of functional nanomaterials using metal-organic frameworks	Makoto Akizuki	The University of Tokyo	Nobuhiko Hosono Keat Beamsley SIYUAN YE SANTANU CHAND	電子顕微鏡室
19	202205-MCBXG-0066	超臨界水熱法によるBaTiO3微粒子合成における粒径と欠陥の制御	秋月 信	東京大学	徐 思キ	Synthesis and growth control of BaTiO3 by supercritical hydrothermal method	Makoto Akizuki	The University of Tokyo	SIQI XU	電子顕微鏡室
20	202204-MCBXG-0046	電子不足型三量体転移を示す MTe2(M:V,Nb,Ta)の構造研究	片山 尚幸	名古屋大学	松田 悠大	Structural sturdy on MTe2 (M : V,Nb, Ta) which exhibit an electron deficient trimer transition	Naoyuki Katayama	Nagoya University	Matsuda Yudai	電磁気測定室
21	202204-MCBXG-0047	高圧下で超伝導-絶縁体転移を示すロジウムスピネルの放射光X線構造研究	片山 尚幸	名古屋大学	小島 慶太	Synchrotron X-ray diffraction study on Rhodium Spinel compounds which exhibit a superconductivity to insulator transition under pressure	Naoyuki Katayama	Nagoya University	Keita Kojima	電磁気測定室
22	202204-MCBXG-0048	Fe(Se,Te)薄膜の高機能化	飯田 和昌	日本大学		Improvement of the superconducting properties for Fe(Se,Te) thin films	Kazumasa Iida	Nihon University		電磁気測定室
23	202205-MCBXG-0050	Nd1-x(Ba0.25Sr0.25Ca0.50)xFeO3 (0.1≦x≦0.9) の高温における磁性と熱電特性に関する研究	中津川 博	横浜国立大学		Magnetism and thermoelectric properties at high temperature in Nd1-x(Ba0.25Sr0.25Ca0.50)xFeO3 (0.1≦x≦0.9))	Hiroshi Nakatsugawa	Yokohama National University		電磁気測定室
24	202205-MCBXG-0054	超伝導体転移温度に対する軸性圧力効果の検証	高橋 龍生	東京理科大学	矢口 宏 小暮 琉介 高橋 龍生	Pressure dependence of superconducting transition temperatrue	Ryusei Takahashi	Tokyo University of Science	Hiroshi Yaguchi Ryusuke Kogure Ryusei Takahashi	電磁気測定室
25	202205-MCBXG-0062	スピン液体"擬態"物質における磁気秩序の観測の試み	原口 祐哉	東京農工大学		An attempt to observe magnetic ordering in spin liquid "mimicries"	Yuya Haraguchi	Tokyo University of Agriculture and Technology		電磁気測定室
26	202205-MCBXG-0063	3d電子系におけるスピン軌道結合磁性の開拓	原口 祐哉	東京農工大学		Exploring spin-orbit coupled magnetism in 3d electron systems	Yuya Haraguchi	Tokyo University of Agriculture and Technology		電磁気測定室

27	202205-MCBXG-0064	二次元酸化物の磁化率測定III	荻野 拓哉	山形大学	内藤 聖羅 加藤 貴大 荻野 拓哉	Magnetic susceptibility measurement of 2D oxides III	Ogino Takuya	Yamagata University	Seira Naito Takahiro Kato OGINO TAKUYA	電磁気測定室
28	202206-MCBXG-0081	新規ラクナスピネル化合物の磁性	香取 浩子	東京農工大学	原口 祐哉 伊東 賢佑	Magnetism of novel lacunar spinel compounds	Hiroko Katori	Tokyo University of Agriculture and Technology	Yuya Haraguchi Kensuke Ito	電磁気測定室
29	202206-MCBXG-0083	ホイスラー化合物での反強磁性の研究	廣井 政彦	鹿児島大学	赤石 幸起 高本 翼	Study on antiferromagnetism in Heusler compounds	Masahiko HIROI	Kagoshima University	Kouki Akaishi Tsubasa Takamoto	電磁気測定室
30	202206-MCBXG-0093	高スピン分極ホイスラー合金の磁気特性のスピンゆらぎ理論による解析に関する研究	重田 出	鹿児島大学	青島 英樹	Study on analysis of magnetic properties for highly spin polarized Heusler alloys by the spin fluctuation theory	Iduru Shigeta	The University of Tokyo	Aoshima Hideki	電磁気測定室
31	202206-MCBXG-0099	ランダムネスがある系における磁場誘起マルチフェロイック相の開拓	有馬 孝尚	東京大学	渡辺 義人	Development of Magnetic-Field-Induced Multiferroic Phase in Random Spin Systems	Takahisa Arima	The University of Tokyo	Yoshito Watanabe	電磁気測定室
32	202205-MCBXG-0058	家庭用浄水のためのグラフェン膜の製造	布浦 鉄兵	東京大学環境安全研究センター	ラスロフ ディニス	Production of graphene membrane for household water purification	Teppei Nunoura	Environmental Science Center, the University of Tokyo	Dinis Rasulov	光学測定室
33	202206-MCBXG-0082	超臨界流体を用いたスクラップタイヤの脱硫化に関する検討	布浦 鉄兵	東京大学環境安全研究センター	楊 丹	Devulcanization of scrap tire using supercritical fluid	Teppei Nunoura	Environmental Science Center, the University of Tokyo	DAN YANG	光学測定室
34	202205-MCBXG-0073	重希土類および第13族元素を充填した新規スクッテルダイト型熱電材料の高圧合成	関根 ちひろ	室蘭工業大学	淡路 功太 新井 聖也 寺坂 聡志 長瀬 竜也	High-pressure synthesis of new skutterudite-type thermolectric materials filled with heavy rare earth and group 13 element	Chihiro Sekine	Muroran Institute of Technology	Awaji Kouta SEIYA ARAI Satoshi Terasaka Tatsuya Nagase	高圧合成室
35	202206-MCBXG-0088	ケイ素を含んだ鉄の水素化挙動の探索	森 悠一郎	東京大学	鍵 裕之	Investigation into Si effect on iron hydrogenation	Mori Yuichiro	The University of Tokyo	Hiroyuki Kagi	高圧合成室
36	202206-MCBXG-0090	新規3d遷移金属ケイ化物の超高温高圧合成と結晶化学	丹羽 健	名古屋大学	有賀 甚	Ultra-high-pressure and high-temperature synthesis and crystal chemistry of novel 3d transition metal silicides	Ken Niwa	Nagoya University	Aruga Jin	高圧合成室
37	202206-MCBXG-0092	高圧下における多成分遷移金属窒化物の合成	佐々木 拓也	名古屋大学	神崎 亮	High-pressure synthesis and characterization of multicomponent transition-metal nitrides	Takuya Sasaki	Nagoya University	Ryo Kanzaki	高圧合成室
38	202205-MCBXG-0072	ハニカム格子を持つRu(Br1-xIx)3の高圧合成	今井 良宗	東北大学	佐藤 楓貴	High pressure synthesis of Ru(Br1-xIx)3 with the honeycomb structure	Yoshinori Imai	Tohoku university	Fuki Sato	X線測定室、高圧合成室
39	202206-MCBXG-0098	ハニカム型反強磁性体における特異な熱伝導現象の起源の研究	上野 正人	東京大学	車地 崇 池田 凜太郎 上野 正人	Research on the origin of unique thermal transport in honeycomb antiferromagnets	Masato Ueno	The University of Tokyo	Takashi Kurumaji rintaro ikeda Masato Ueno	X線測定室、電磁気測定室
40	202206-MCBXG-0084	新奇量子スピン液体候補物質の合成と物性評価	橋本 顕一郎	東京大学	今村 薫平 ファン センジェ 劉 蘇鵬 吉田 悠生	Synthesis and characterization of novel quantum spin liquid materials	Kenichiro Hashimoto	The University of Tokyo	Kumpei Imamura Shengjie Fang SUPENG LIU Yusei Yoshida	物質合成室、X線測定室、電磁気測定室

物質合成・評価設備Uクラス / Materials Synthesis and Characterization U Class Research Project

No.	課題番号	課題名	氏名	所属	分担者	Title	Name	Organization	Member of reseach project	実験室
1	202209-MCBXU-0103	超伝導体 NbNx における結晶構造の温度依存性の観測	武田 崇仁	東京大学		Observation of the temperature dependence of the crystal structure of superconductor NbNx	Takahito Takeda	The University of Tokyo		X線測定室
2	202211-MCBXU-0106	強相関トポロジカル物質の物性評価	水上 雄太	東北大学	大野 綾太郎	Characterization of strongly correlated topological materials	Yuta Mizukami	Tohoku University	Ryotaro Ono	X線測定室

3	202209-MCBXU-0104	巨大異常ネルンスト効果を示す新規トポロジカル磁性体開発	梶原 悠人	東京大学	王 陽明 Feng Zili 黒沢 駿一郎 小池 祐樹	Search for new topological magnets exhibiting the giant anomalous Nernst effect	yuto kajiwara	The University of Tokyo	Yangming Wang Zili Feng Shunichiro Kurosawa Yuki Koike	電子顕微鏡室
4	202209-MCBXU-0102	新規トポロジカル磁性体の合成と物性開拓	車地 崇	東京大学	有馬 孝尚 徳永 祐介 厳 正輝（理化学研究所） 上野 正人	Materials development for novel topological magnets	Takashi Kurumaji	The University of Tokyo	Taka-hisa Arima Yusuke Tokunaga Masaki Gen (RIKEN) Masato Ueno	電磁気測定室
5	202210-MCBXU-0105	5d電子系における多極子物性の研究	平井 大悟郎	名古屋大学		Multipolar physics in 5d electron systems	Daigorou Hirai	Nagoya University		物質合成室、電磁気測定室、高圧合成室

国際超強磁場科学施設 / International MegaGauss Science Laboratory

No.	課題番号	課題名	氏名	所属	分担者	Title	Name	Organization	Member of reseach project	担当所員
1	202205-HMBXX-0048	希土類金属間化合物の強磁場物性研究	海老原 孝雄	静岡大学	大窪 悠太 エスティアク アフメド 小林 和	Physical Properties at high magnetic fields in rare earth intermetallic compounds	Takao Ebihara	Shizuoka University	Yuta Okubo Esteaque Ahmed Kazu Kobayashi	金道 浩一
2	202205-HMBXX-0052	四面体配位された3d電子系化合物における新規スピン軌道結合磁場誘起相の探索	原口 祐哉	東京農工大学	石北 大悟	Search for novel spin-orbit-entangled-magnetic-field-induced phases in transition metal materials with tetrahedrally coordinated 3d-electrons	Yuya Haraguchi	Tokyo University of Agriculture and Technology	Daigo Ishikita	金道 浩一
3	202205-HMBXX-0058	幾何学的フラストレート磁性体の強磁場磁化測定	菊池 彦光	福井大学		Magnetization measurements of the frustrated magnets	Hikomitsu Kikuchi	University of Fukui		金道 浩一
4	202206-HMBXX-0066	乱れを導入した有機超伝導体における強磁場超伝導状態	杉浦 栞理	東北大学 金属材料研究所		High-field superconductivity in organic superconductors with artificially introduced disorders	Shiori Sugiura	Institute for Materials Research, Tohoku University		金道 浩一
5	202206-HMBXX-0068	量子スピン液体候補物質κ-[(BEDT-TTF)1-x(BEDT-STF)x]2Cu2(CN)3の示す特異なMott転移に対する磁場効果	福岡 脩平	北海道大学		Magnetic field effects on the Mott transition in a quantum spin liquid candidate κ-[(BEDT-TTF)1-x(BEDT-STF)x]2Cu2(CN)3	Shuhei Fukuoka	Hokkaido University		金道 浩一
6	202206-HMBXX-0080	パルス強磁場磁化測定から観測するYb希薄系(Lu,Yb)Rh2Zn20の磁気異方性の回復過程	北澤 崇文	東北大学	池田 陽一	Recovery processes of the magnetic anisotropy in a diluted Yb system (Lu,Yb)Rh2Zn20 revealed by pulsed high field magnetization measurements	Kitazawa Takafumi	Tohoku university	Yoichi Ikeda	金道 浩一
7	202205-HMBXX-0053	Magnetism and anisotropy of uranium chalcogenides UOX (X = S, Se, Te) and U7Te12	Opletal Petr	日本原子力研究開発機構	芳賀 芳範	Magnetism and anisotropy of uranium chalcogenides UOX (X = S, Se, Te) and U7Te12	Petr Opletal	Japan Atomic Energy Agency	Yoshinori Haga	徳永 将史
8	202205-HMBXX-0054	キラル構造をもつ磁性体NdPt2Bの磁気相図	佐藤 芳樹	東京理科大学	岡崎 竜二 柴岡 歩 江口 恭平	Magnetic phase diagram of NdPt2B with a chiral structure	Yoshiki Sato	Tokyo University of Science	Ryuji Okazaki Ayumu Shibaoka Kyohei Eguchi	徳永 将史
9	202205-HMBXX-0061	鉄系超伝導体の磁気光学イメージングによる超伝導状態の観測	矢口 宏	東京理科大学	小暮 琉介 高橋 龍生 栗原 綾佑	Observations of superconducting states in iron-based superconductors using an MO imaging technique	Hiroshi Yaguchi	Tokyo University of Science	Ryusuke Kogure Ryusei Takahashi Ryosuke Kurihara	徳永 将史
10	202206-HMBXX-0063	パルス強磁場下超音波計測による強相関電子系の磁場中量子状態	栗原 綾佑	東京理科大学	矢口 宏 小峰 智弥 島根 恭汰	Ultrasonic study of quantum states in strongly-correlated electron systems under pulsed-magnetic fields	Ryosuke Kurihara	Tokyo University of Science	Hiroshi Yaguchi Tomoya Komine Kyota Shimane	徳永 将史

11	202206-HMBXX-0067	新規ラクナスピネル化合物の強磁場下での物性	香取 浩子	東京農工大学	原口 祐哉 伊東 賢佑	Physical properties of novel lacunar spinel compounds under high magnetic fields	Hiroko Katori	Tokyo University of Agriculture and Technology	Yuya Haraguchi Kensuke Ito	徳永 将史
12	202206-HMBXX-0079	構造相転移近傍の極性ディラック電子系物質の量子伝導現象	酒井 英明	大阪大学	近藤 雅起 湯浅 直輝 宮本 雄哉	Quantum transport for polar Dirac metals near a structural transition	Hideaki Sakai	Osaka University	Masaki Kondo Naoki Yuasa Yuya Miyamoto	徳永 将史
13	202205-HMBXX-0047	金属超伝導体の結晶育成と強磁場物性研究	エスティアク アフメド	静岡大学	小林 和	Crystal growth and physical Properties at high magnetic fields in metallic super conductors	Esteaque Ahmed	Shizuoka University	Kazu Kobayashi	小濱 芳允
14	202209-HMBXX-0088	極性磁性ワイル半金属候補物質のフェルミオロジー	車地 崇	東京大学	有馬 孝尚	Fermiology of polar magnetic Weyl semimetal candidate	Takashi Kurumaji	The University of Tokyo	Taka-hisa Arima	金道 浩一
15	202209-HMBXX-0089	六方晶QS型鉄酸化物 Ba2MeSn2Fe10O22 の強磁場磁気特性	神島 謙二	埼玉大学	原澤 秀明	Magnetic properties of hexagonal QS-type iron oxide Ba2MeSn2Fe10O22 under high magnetic fields	Kenji Kamishima	Saitama University	Harasawa Hideaki	徳永 将史
16	202301-HMBXX-0097	希土類化合物RERu2Si2の強磁場磁化過程	原 嘉昭	国立高等専門学校機構　茨城工業高等専門学校	矢野 一雄（筑波大学） 喜多 英治（筑波大学） 雨海 有佑（室蘭工業大学）	High field magnetization process in rare-earth compound RERu2Si2	Yoshiaki Hara	National Institute of Technology (KOSEN), Ibaraki College	Kazuo Yano (University of Tsukuba) Eiji Kita (University of Tsukuba)Yusuke Amakai (Muroran Institute of Technology)	徳永 将史
17	202302-HMBXX-0098	2重Dirac点を持つ層状トポロジカル物質の線形磁気抵抗	青木 勇二	東京都立大学大学院	東中 隆二 Ahmad Nazir Afzal Md Asif	Linear magnetoresistance in layered topological materials with double Dirac points	Yuji Aoki	Tokyo Metropolitan University	Ryuji Higashinaka Nazir Ahmad Md Asif Afzal	徳永 将史

大阪大学大学院理学研究科附属先端強磁場科学研究センター / Center for Advanced High Magnetic Field Science, Graduate School of Science, Osaka University

No.	課題番号	課題名	氏名	所属	分担者	Title	Name	Organization	Member of reseach project	担当所員
1	202204-HMOXX-0045	電気磁気反強磁性Cr2O3薄膜の界面磁化検出	白土 優	大阪大学		Detection of interfacial magnetic moment in magnetoelectric Cr2O3	Yu Shiratsuchi	Osaka University		萩原 政幸（大阪大学）
2	202205-HMOXX-0049	CdI2型構造を持つ超伝導体の物質開発	工藤 一貴	大阪大学		Development of novel superconductors with a CdI2-type structure	Kazutaka Kudo	Osaka University		萩原 政幸（大阪大学）
3	202205-HMOXX-0050	ハニカムネットワークを持つ超伝導物質の開発	工藤 一貴	大阪大学		Development of novel superconductors with honeycomb networks	Kazutaka Kudo	Osaka University		萩原 政幸（大阪大学）
4	202205-HMOXX-0051	空間反転対称性の破れや磁気フラストレーションに誘発された特異な磁性を持つ希土類化合物の強磁場物性	竹内 徹也	大阪大学	大貫 惇睦（東京都立大学）	Characteristic magnetic properties and high-field magnetism in rare-earth compounds without space inversion symmetry	Tetsuya Takeuchi	Osaka University	Yoshichika Onuki (Tokyo Metropolitan University)	萩原 政幸（大阪大学）
5	202205-HMOXX-0055	種々の新型磁気力ブースターの性能試験	牧 祥	岡山理科大学		Performance test of various types of new magnetic force boosters	Syou Maki	Okayama University of Science		萩原 政幸（大阪大学）
6	202205-HMOXX-0056	カゴメ反強磁性体の強磁場磁化測定	吉田 紘行	北海道大学		High-field magnetization measurements of kagome antiferromagnets	Hiroyuki Kura Yoshida	Hokkaido University		萩原 政幸（大阪大学）
7	202205-HMOXX-0057	偏光依存・強磁場ESR測定の開発とSr2CoSi2O7のエレクトロマグノン研究	赤木 暢	東北大学		Development of the ESR probe for light-polarization dependence measurement and study of the electromagnon in Sr2CoSi2O7	Mitsuru Akaki	Tohoku University		萩原 政幸（大阪大学）
8	202205-HMOXX-0060	強磁性ホイスラー合金Ni2MnGa系合金の磁気的機能性の研究	左近 拓男	龍谷大学		Research on magnetic functionalities of Ni2MnGa Heusler alloys	Takuo Sakon	Ryukoku University		萩原 政幸（大阪大学）

9	202205-HMOXX-0064	一次元反強磁性体CuX2•(γ-pic)2(X=Cl,Br)の高磁場多周波ESR	浅野 貴行	福井大学		High-field multi-frequency ESR in the one-dimensional antiferromagnets, CuX2•(γ-pic)2(X=Cl,Br)	Takayuki Asano	University of Fukui		萩原 政幸（大阪大学）
10	202205-HMOXX-0077	パルス強磁場を用いた高圧下ESR装置用圧力セルの最適化	櫻井 敬博	神戸大学		研究分野	Takahiro Sakurai	Kobe University		萩原 政幸（大阪大学）
11	202206-HMOXX-0071	強いスピン-軌道相互作用を活かした酸化物スピントロニクス	松野 丈夫	大阪大学	塩貝 純一 上田 浩平	Oxide spintronics utilizing strong spin-orbit coupling	Jobu Matsuno	Osaka University	Junichi Shiogai Kohei Ueda	萩原 政幸（大阪大学）
12	202206-HMOXX-0075	層状磁性半導体の巨大磁気抵抗効果の研究	村川 寛	大阪大学		Research for the giant magnetoresistance in layered magnetic semiconductors	Hiroshi Murakawa	Osaka University		萩原 政幸（大阪大学）
13	202206-HMOXX-0076	ディラック電子系NiTe2のドハースファンアルフェン効果	宮坂 茂樹	大阪大学		de Haas-van Alphen effect in Dirac material NiTe2	Shigeki Miyasaka	Osaka University		萩原 政幸（大阪大学）
14	202206-HMOXX-0078	ThCr2Si2型Eu化合物の多彩な磁気秩序の解明	酒井 英明	大阪大学		Study of complex antiferromagnetic orders in ThCr2Si2-type Eu-based compounds	Hideaki Sakai	Osaka University		萩原 政幸（大阪大学）
15	202206-HMOXX-0082	非従来型超伝導体微細構造のパルス強磁場下輸送特性	掛谷 一弘	京都大学		Transport measurements on micro-structured unconventional superconductors under pulsed high magnetic fields	Itsuhiro Kakeya	Kyoto University		萩原 政幸（大阪大学）
16	202209-HMOXX-0087	均一粒径クロミック材料の強磁場物性	浅野 貴行	福井大学		Magnetic properties of chromic materials with uniform particle size under high magnetic field	Takayuki Asano	University of Fukui		萩原 政幸（大阪大学）
17	202210-HMOXX-0092	FCCフラストレート磁性体RInCu4のパルス強磁場下ホール抵抗測定	和氣 剛	京都大学		Pulse High-field Hall resistivity of FCC frustrated magnets RInCu4	Takeshi Waki	Kyoto University		萩原 政幸（大阪大学）
18	202211-HMOXX-0095	パルス強磁場用極低温実験装置の開発	野口 悟	大阪公立大学	吉田 勝一	Development of the cryostat for pulsed high magnetic field	Satoru Noguchi	Osaka Metropolitan University	Shoichi Yoshida	萩原 政幸（大阪大学）

強磁場コラボラトリー / The High Magnetic Field Collaboratory

No.	課題番号	課題名	氏名	所属	分担者	Title	Name	Organization	Member of reseach project	担当所員
1	202205-HMBXX-0069	有機ラジカルからなるフラストレート磁性体の強磁場物性	山口 博則	大阪公立大学		High-field magnetic properties of frustrated materials composed of organic radicals	Hironori Yamaguchi	Osaka Metropolitan University		金道 浩一
2	202210-HMBXX-0090	光駆動型有機FET界面におけるフェルミオロジーと強磁場超電導相	木俣 基	東北大学		Fermiology and high-field superconducting phase in photo-induced organic FET interface	Motoi Kimata	Tohoku University		徳永 将史
3	202206-HMCXX-0070	強磁場NMR測定によるカゴメ遍歴磁性体における磁場誘起磁気相の研究	井原 慶彦	北海道大学大学院		High-field NMR study for field-induced magnetic states in itinerant kagome magnets	Yoshihiko Ihara	Hokkaido University		小濱 芳允

留学研究課題 / External Research Project Long / Short -term

No.	課題番号	課題名	氏名	所属	分担者	Title	Name	Organization	Member of reseach project	担当所員
1	202111-VSBXL-0003	超短パルスレーザー照射により誘起される微細構造変化の評価	高林 圭佑	秋田大学		Evaluation of structural changes induced by ultrashort pulsed laser	Keisuke Takabayashi	Akita University		小林 洋平

2022年度　中性子科学研究施設　共同利用課題一覧 / Joint Research List of Neutron Scattering Research Project 2022

※実施課題一覧、所属は申請時のデータ

No.	課題名	氏名	所属	分担者（共同研究者）	Title	Name	Organization	Member of research project	装置	ビームポート
1	GPTAS（汎用3軸中性子分光器）IRT課題	佐藤 卓	東北大学	那波 和宏, Wu Hung-Cheng, 村崎 遼, Pharit Piyawongwatthana, 横山 淳, 田畑 吉計, 下館 凌人	IRT project of GPTAS	Taku J Sato	Tohoku University	Kazuhiro Nawa, Wu Hung-Cheng, Ryo Murasaki, Pharit Piyawongwatthana, Makoto Yokoyama, Yoshikazu Tabata, Ryoto Shimodate	GPTAS	4G
2	PONTA（高性能偏極中性子散乱装置）IRT課題	中島 多朗	東京大学	齋藤 開, Seno Aji, 川崎 卓郎, 小林 尚暉, 車地 崇, 有馬 孝尚, 高阪 勇輔, 姜 佳良, 厳 正輝, 徳永 祐介, 石崎 大悟, Kamini Gautum	IRT project of PONTA	Taro Nakajima	The University of Tokyo	Hiraku Saito, Seno Aji, Takuro Kawasaki, Naoki Kobayashi, Takashi Kurumaji, Takahisa Arima, Yusuke Kosaka, Karyou Kyo, Masaki Gen, Yusuke Tokunaga, Daigo Ishizaki, Kamini Gautum	PONTA	5G
3	TOPAN（東北大理：３軸型偏極中性子分光器）IRT課題	池田 陽一	東北大学	藤田 全基, 北澤 崇文, 池内 和彦, 那波 和宏, 中島 多朗, 清水 悠晴, 高田 秀佐, 猪野 隆, Xie Peiao, Pang Xiaoqi, Wang Tong, 唐 一飛, Chen Yizhou, 大里 耕太郎, 北山 慎之介, 磯村 楓, 二見 采樹, 大亀 佑太, Zheng Jiajie, 岡部 博孝, 高田 秀佐, 足立 匡, 小宮山 陽太, 岡田 陸玖	IRT project of TOPAN	Yoichi Ikeda	Tohoku University	Masaki Fujita, Takahumi Kitazawa, Kazuhiko Ikeuchi, Kazuhiro Nawa, Taro Nakajima, Yusei Shimizu, Shusuke Takada, Takashi Ino, Xie Peiao, Pang Xiaoqi, Wang Tong, Ichito Tan, Chen Yizhou, Kotaro Osato, Shinnosuke Kitayama, Kaede Isomura, Saiki Futami, Yuta Ohki, Zheng Jiajie, Hirotaka Okabe, Shusuke Takada, Tadashi Adachi, Yota Komiyama, Riku Okada	TOPAN	6G
4	HERにおける量子物質の準粒子構造の研究	益田 隆嗣	東京大学	佐藤 卓, 中島 多朗, 横山 淳, 阿曽 尚文, 浅井 晋一郎, 齋藤 開, 寺田 典樹, 三宅 岳志, Liu Zheyuan, Wei Zijun	IRT project of HER	Takatsugu Masuda	The University of Tokyo	Taku J Sato, Tato Nakajima, Makoto Yokoyama, Naofumi Aso, Shinichiro Asai, Hiraku Saito, Noriki Terada, Takeshi Miyake, Liu Zheyuan, Wei Zijun	HER	C1-1
5	SANS-U(二次元位置測定小角散乱装置)IRT課題	眞弓 皓一	東京大学	小田 達郎, 井上 倫太郎, 守島 健, 土肥 侑也, 平田 芳信, Jakkrit Prateepkaew, 山田 悟史, 奥田 綾, 辻 優依, 中村 絵里佳, 櫻木 美菜, Lester Geonzon, 榎木 崇人, 橋本 慧, 貞包 浩一朗, 安部 美季, 木田 拓充, 高橋 倫太郎, 犬飼 海洋, 山本 勝宏	IRT project of SANS-U	Koichi Mayumi	The University of Tokyo	Tatsuro Oda, Rintaro Inoue, Ken Morishima, Yuya Doi, Yoshinobu Hirata, Jakkrit Prateepkaew, Norifumi Yamada, Aya Okuda, Yui Tsuji, Erika Nakamura, Mina Sakuragi, Lester Geonzon, Takato Enoki, Kei Hashimoto, Koichiro Sadakane, Miki Abe, Takumitsu Kida, Rintaro Takahashi, Mihiro Inukai, Katsuhiro Yamamoto	SANS-U	C1-2
6	iNSE（中性子スピンエコー分光器)IRT課題	小田 達郎	東京大学	眞弓 皓一, 遠藤 仁, 井上 倫太郎, 山田 悟史, 佐藤 節夫	IRT project of iNSE	Tatsuro Oda	The University of Tokyo	Koichi Mayumi, Hitoshi Endo, Rintaro Inoue, Norifumi Yamada, Setsuo Sato	iNSE	C2-3-1
7	AGNES（高分解能パルス冷中性子分光器）IRT課題	山室 修	東京大学	秋葉 宙, 大政 義典, 佐藤 創, Menghan Zhang, 佐藤 駿, Xuejun Wu, 中津 大貴, 辻 孝史, 田路 智也, 尾原 幸治, 池田 一貴	IRT project of AGNES	Osamu Yamamuro	The University of Tokyo	Hiroshi Akiba, Yoshinori Ohmasa, Hajime Sato, Menghan Zhang, Shun Sato, Xuejun Wu, Hiroki Nakatsu, Takashi Tsuji, Tomoya Taji, Koji Ohara, Kazutaka Ikeda	AGNES	C3-1-1
8	MINE（京大複合研：多層膜中性子干渉計・反射率計）IRT課題	日野 正裕	京都大学	小田 達郎, 北口 雅暁, 田崎 誠司, 中村 吏一朗, 奥野 泰希, 中野 貴之, 橋本 優作, 櫻井 辰大, 清水 裕彦, 奥平 琢也, 藤家 拓大, 奥野 泰希, 中野 貴之, 橋本 優作, 櫻井 辰大, 山田 悟史, 佐藤 節夫, 大下 英敏, 神谷 好郎, 西村 龍太郎	MINE (Multilayer neutron interferometer and reflectmeter)	Masahiro Hino	Kyoto University	Tatsuro Oda, Masaaki Kitaguchi , Seiji Tasaki, Riichiro Nakamura, Yasuki Okuno, Takayuki Nakano, Yusaku Hashimoto, Tatsuhiro Sakurai, Masahiro Shimizu, Takuya Okudaira, Takuhiro Fujiie, Norifumi Yamada, Setsuo Sato, Hidetoshi Ohshita, Yoshio Kamiya, Ryutaro Nishimura	MINE	C3-1-2

9	HQR(高分解能中性子散乱装置)IRT課題	大山 研司	茨城大学	岩佐 和晃, 桑原 慶太郎, 横山 淳, 伊賀 文俊, 中野 岳仁, 中島 多朗, 下田 愛海, 熊田 隆伸, 今関 啓雅, 黒澤 航海, 鈴木 陽太郎, 井能 楓, 上條 力, 内馬場 優太, 小林 龍珠, 大谷 良美, 紺谷 駿, 原島 周平, 高野 元輝, 菅野 友哉, 星 翔太, 小林 洋大, 富松 優花, 會澤 幸希, 川上 修汰, 平石 雅俊, 矢代 安澄, 小泉 遼介, 海老澤 秀明, 高橋 哲平	IRT project of HQR	Kenji Ohoyama	Ibaraki University	Kazuaki Iwasa, Keitaro Kuwahara, Makoto Yokoyama, Fumitoshi Iga, Takehito Nakano, Tato Nakajima, Ami Shimoda, Takanobu Kumada, Hiromasa Imazeki, Wataru Kurosawa, Yotaro Suzuki, Keade Ino, Riki Kamijo, Yuta Uchibaba, Ryuju Kobayashi, Yoshimi Otani, Shun Kontani, Syuhei Harashima, Motoki Takano, Tomoya Kanno, Shota Hoshi, Yodai Kobayashi, Yuka Tomimatsu, Koki Aizawa, Shuta Kawakami, Masatoshi Hiraishi, Azumi Yashiro, Ryosuke Koizumi, Hideaki Ebisawa, Teppei Takahashi	HQR	T1-1
10	AKANE（東北大金研：三軸型中性子分光器）IRT課題	谷口 貴紀	東北大学	藤田 全基, 南部 雄亮, 池田 陽一, 猪野 隆, 奥 隆之, 上床 美也, 山根 悠, 森 賢太郎, 渡邊 功雄, Utami Widyaiswari, Anita Eka Putri, Muhammad Abdan Syakuur, 磯村 楓, 二見 采樹, 大亀 佑太, Zheng Jiajie, 岡部 博孝, 高田 秀佐, 川本 陽, 梅本 好日古, Xie Peiao, Pang Xiaoqi, Wang Tong, 北澤 崇文, 唐 一飛, 川又 雅広, Chen Yizhou, 大里 耕太郎, 北山 慎之介	IRT project of AKANE	Takanori Taniguchi	Tohoku University	Masaki Fujita, Yusuke Nambu, Yoichi Ikeda, Takashi Ino, Takayuki Oku, Yoshiya Uwatoko, Yu Yamane, Kentaro Mori, Isao Watanabe, Utami Widyaiswari, Anita Eka Putri, Muhammad Abdan Syakuur, Kaede Isomura, Saiki Futami, Yuta Ohki, Zheng Jiajie, Hirotaka Okabe, Shusuke Takada, You Kawamoto, Yoshihiko Umemoto, Xie Peiao, Pang Xiaoqi, Wang Tong, Tamafumi Kitazawa, Ichito Tan, Masahiro Kawamata, Chen Yizhou, Kotaro Osato, Shinnosuke Kitayama	AKANE	T1-2
11	HERMES（東北大金研：中性子粉末回折装置）IRT課題	南部 雄亮	東北大学	藤田 全基, 池田 陽一, 谷口 貴紀, 大山 研司, 八島 正知, 藤井 孝太郎, 加藤 大地, 津森 竜也, 松崎 洋介, Tong Zhu, 田中 貴大, 原田 雅史, 斎藤 あゆみ, 井上 貴裕, 京谷 智裕, 奈木野 勇生, Song Subin, 瀧ケ平 隼輔, 岡部 博孝, 髙田 秀佐, 李 哲虎, 坂上 良介, Maxim Avdeev, 磯村 楓, 二見 采樹, 大亀 佑太, Zheng Jiajie, 川本 陽, 梅本 好日古, Xie Peiao, Pang Xiaoqi, Wang Tong, 北澤 崇文, 唐 一飛, 川又 雅広, Chen Yizhou, 大里 耕太郎, 北山 慎之介, 小野 圭吾	IRT project of HERMES	Yusuke Nambu	Tohoku University	Masaki Fujita, Yoichi Ikeda, Takanori Taniguchi, Kenji Ohoyama, Masatomo Yashima,Kotaro Fujii, Daichi Kato, Tatsuya Tsumori, Yosuke Matsuzaki, Tong Zhu, Takahiro Tanaka, Masafumi Harada, Ayumi Saito, Takahiro Inoue, Tomohiro Kyotani, Yuki Nagino, Song Subin, Shunsuke Takigahira, Hirotaka Okabe, Shusuke Takada, Chul-Ho Lee, Ryosuke Sakagami, Maxim Avdeev, Kaede Isomura, Saiki Futami, Yuta Ohki, Zheng Jiajie, You Kawamoto, Yoshihiko Umemoto, Xie Peiao, Pang Xiaoqi, Wang Tong, Tamafumi Kitazawa, Ichito Tan, Masahiro Kawamata, Chen Yizhou, Kotaro Osato, Shinnosuke Kitayama, Keigo Ono	HERMES	T1-3
12	FONDER(中性子4軸回折装置)IRT課題	木村 宏之	東北大学	坂倉 輝俊, 山本 孟, 上山 幸子, 高橋 慎吾, 満田 節生, 内原 猛, 小関 真, 藤原 理賀, 川口 泰知, 南部 雄亮, 川又 雅広	IRT proposal for FONDER (Neutron 4-circle diffractometer)	Hiroyuki Kimura	Tohoku University	Terutoshi Sakakura, Hajime Yamamoto, Sachiko Kamiyama, Shingo Takahashi, Setsuo Mitsuda, Takeru Uchihara, Makoto Ozeki, Masayoshi Fujiwara, Taichi Kawaguchi, Yusuke Nambu, Masahiro Kawamata	FONDER	T2-2
13	液体プロピレンカーボネートの部分構造因子	亀田 恭男	山形大学	強口 岬, 天羽 優子, 臼杵 毅	Partial Structure Factors of Liquid Propylene Carbonate	Yasuo Kameda	Yamagata University	Misaki Kowaguchi, Yuko Amo, Takeshi Usuki	GPTAS	4G
14	a-Cu2V2O7 における磁気モーメント方向の温度依存性	佐藤 卓	東北大学	Pharit Piyawongwatthana, 那波 和宏, 奥山 大輔, Wu Hung-Cheng	Temperature dependence of the moment canting angle in a-Cu2V2O7	Taku J Sato	Tohoku University	Pharit Piyawongwatthana, Kazuhiro Nawa, Daisuke Okuyama, Wu Hung-Cheng	GPTAS	4G
15	新しい量子三角格子磁性体Ba3Yb(BO3)3の短距離磁気相関	佐藤 卓	東北大学	松坂 信之介, 那波 和宏, 奥山 大輔, Wu Hung-Cheng	Short-range spin correlations in the new quantum triangular-lattice compound Ba3Yb(BO3)3	Taku J Sato	Tohoku University	Shinnosuke Matsuzaka, Kazuhiro Nawa, Daisuke Okuyama, Wu Hung-Cheng	GPTAS	4G

16	反強磁性量子臨界的挙動がもたらす異常超伝導物性 I	横山 淳	茨城大学	川崎 郁斗, 平山 堅理, 矢代 安澄, 井能 楓, 清水 悠晴	Anomalous superconducting properties coupled with antiferromagentic quantum criticality I	Makoto Yokoyama	Ibaraki University	Ikuto Kawasaki, Takatoshi Hirayama, Azumi Yashiro, Kaede Inou, Yusei Shimizu	GPTAS	4G
17	２等辺三角格子イジング磁性体CoNb2O6のワニエ状態における磁気相関	満田 節生	東京理科大学	小澤 竜也, 内原 猛, 玉造 博夢, 澤田 大地, 岡村 洸輝	Magnetic correlations at the Wannier point in isosceles triangular lattice Ising magnet CoNb2O6	Setsuo Mitsuda	Tokyo University of Science	Tatsuya Kozawa, Takeru Uchihara, Hiromu Tamatsukuri, Daichi Sawada, Kouki Okamura	GPTAS	4G
18	カゴメ格子反強磁性体におけるマグノンスピン-軌道角運動量ロッキング	那波 和宏	東北大学	佐藤 卓, Matan Kittiwit, 村崎 遼, Piyawongwatthana Pharit, 下館 凌人, 松坂 信之介	Magnon spin-momentum locking in kagome antiferromagnets	Kazuhiro Nawa	Tohoku University	Taku J Sato, Matan Kittiwit, Ryo Murasaki, Piyawongwatthana Pharit, Ryoto Shimodate, Shinnosuke Matsuzaka	GPTAS	4G
19	スピン1/2フラストレート正方格子磁性体2VOSO4_H2SO4_nH2Oの逐次相転移	那波 和宏	東北大学	柴田 将弥, 佐藤 卓, Wu Hung-Cheng, Pharit Piyawongwatthana	Successive phase transition in the spin-1/2 frustrated square lattice magnet 2VOSO4_H2SO4_nH2O	Kazuhiro Nawa	Tohoku University	Masaya Shibata, Taku J Sato, Wu Hung-Cheng, Pharit Piyawongwatthana	GPTAS	4G
20	Au64Ga22Tb14近似結晶の逐次相転移	那波 和宏	東北大学	鈴木 慎太郎, 田村 隆治, 佐藤 卓, 鈴木 慎太郎, Farid Labib, Wu Hung-Cheng, 村崎 遼	Successive phase transitions of the quasicrystal approximant Au64Ga22Tb14	Kazuhiro Nawa	Tohoku University	Shintaro Suzuki, Ryuji Tamura , Taku J Sato, Shintaro Suzuki, Farid Labib, Wu Hung-Cheng, Ryo Murasaki	GPTAS	4G
21	量子スピン液体の研究	門脇 広明	東京都立大学	佐藤 卓	Quantum spin liquid	Hiroaki Kadowaki	Tokyo Metoropolitan University	Taku J Sato	GPTAS	4G
22	有効スピン1/2のジグザグ鎖をもつ磁性半導体YbAgSe2における相転移の秩序変数	鬼丸 孝博	広島大学	水谷 宗一郎, 山本 理香子, 志村 恭通, 大山 研司, 小坂 昌史, 道村 真司, 草ノ瀬 優香, 菅野 友哉, 高野 元輝, 星 翔太, 小林 洋大, 富松 優花, 會澤 幸希, 川上 修汰	Order parameter of a phase transition in a magnetic semiconductor YbAgSe2 with an effective spin-1/2 zigzag chains	Takahiro Onimaru	Hiroshima University	Soichiro Mizutani, Rikako Yamamoto, Yasuyuki Shimura, Kenji Ohoyama, Masashi Kosaka, Shinji Michimura, Yuka Kusanose, Tomoya Kanno, Motoki Takano, Syota Hoshino, Yodai Kobayashi, Yuka Tomimatsu, Koki Aizawa, Syuta Kawakami	GPTAS	4G
23	立方晶PrCdNi4の非磁性基底二重項による相転移の秩序変数	鬼丸 孝博	広島大学	草ノ瀬 優香, 志村 恭通, 岩佐 和晃	Order parameter of the phase transition of a nonmagnetic ground state doublet in a cubic compound PrCdNi4	Takahiro Onimaru	Hiroshima University	Yuka Kusanose, Yasuyuki Shimura, Kazuaki Iwasa	GPTAS	4G
24	Search for non-coplanar magnetism in 2D van-der-Waals materials	ヒルシュベルガー マックス	東京大学	中島 多朗, 赤塚 駿	Search for non-coplanar magnetism in 2D van-der-Waals materials	Hirschberger Maximilian	The University of Tokyo	Nakajima Taro, Akatsuka Shun	PONTA	5G
25	van-der-Waals magnet HoTe3 with spin chirality: a magnetic structure study	ヒルシュベルガー マックス	東京大学	中島 多朗, 赤塚 駿	van-der-Waals magnet HoTe3 with spin chirality: a magnetic structure study	Hirschberger Maximilian	The University of Tokyo	Nakajima Taro, Akatsuka Shun	PONTA	5G
26	ハーフホイスラー型DyPtBiにおける一軸応力による磁気ドメイン制御	上田 健太郎	東京大学	黒川 亮	uniaxial pressure control of magnetic domains in half-Heusler DyPtBi	Kentaro Ueda	The University of Tokyo	Ryo Kurokawa	PONTA	5G
27	NiO酸化物の磁気相転移とスピンカレントに関する研究	古川 はづき	お茶の水女子大学	左右田 稔, 中村 琴美, Foley Edward	Contribution of magnetism on spin current in NiO	Hazuki Furukawa	Ochanomizu University	Minoru Soda, Kotomi Nakamura, Foley Edward	PONTA	5G
28	塑性歪みを加えたPt3Fe反強磁性体における強磁性ドメインの磁場中挙動	小林 悟	岩手大学	松尾 咲琴, 堀田 侑里, 西館 直樹, 中野 愛弓, 後藤 颯樹	Behavior of ferromagnetic domains under magnetic fields for plastically strained Pt3Fe antiferromagnet	Satoru Kobayashi	Iwate University	Sakoto Matsuo, Yuri Hotta, Naoki Nishidate, Ayumi Nakano, Satsuki Goto	PONTA	5G
29	キラルな立方晶磁性体Mn3IrSiの逐次磁気相転移	有馬 孝尚	東京大学	Gautam Kamini, 厳 正輝	Successive Magnetic Transitions in a Chiral Cubic Magnet Mn3IrSi	Takahisa Arima	The University of Tokyo	Gautam Kamini, Masaki Gen	PONTA	5G
30	CaBaCo4-xNixO7における巨大な電気磁気効果	有馬 孝尚	東京大学	徳永 祐介, 石崎 大悟, 車地 崇	Giant Magnetoelectric Effect in CaBaCo4-xNixO7	Takahisa Arima	The University of Tokyo	Yusuke Tokunaga, Daigo Ishizaki, Takashi Kurumaji	PONTA	5G
31	中性子回折による反強磁性体UPt3Al5の磁気構造の研究	本多 史憲	九州大学	本間 佳哉, 清水 悠晴, 青木 大	Magnetic structure study of an antiferromagnet UPt3Al5 using neutron diffraction	Fuminori Honda	Kyushu University	Yoshiya Homma, Yusei Shimizu, Dai Aoki	PONTA	5G
32	中性子回折による擬カゴメ構造化合物 URhSn の多極子秩序構造の研究	田端 千紘	京都大学	清水 悠晴, 今 布咲子, 網塚 浩, 中尾 裕則, 齋藤 開	Neutron diffraction study on multipole order in pseudo-Kagom? structure compound URhSn	Chihiro Tabata	Kyoto University	Yusei Shimizu, Fusako Kon, Hiroshi Amitsuka , Hironori Nakao, Hiraku Saito	PONTA	5G
33	励起子絶縁体候補物質Ca0.5Pr0.5CoO3の中性子散乱	益田 隆嗣	東京大学	浅井 晋一郎, 三宅 岳志, 菊地 帆高, Liu Zheyuan	Neutron Scattering Study for Excitonic Insulator Candidate Ca0.5Pr0.5CoO3	Takatsugu Masuda	The University of Tokyo	Shinichiro Asai, Takeshi Miyaka, Hodaka Kikuchi, Liu Zheyuan	PONTA	5G

34	Eu系ダイアモンド格子物質における磁場中偏極中性子散乱実験	車地 崇	東京大学	有馬 孝尚, 徳永 祐介, 中島 多朗, 齋藤 開	In field polarized neutron scattering on Eu-based diamond magnet	Takashi Kurumaji	The University of Tokyo	Takahisa Arima, Yusuke Tokunaga, Tato Nakajima, Hiraku Saito	PONTA	5G
35	UPt2X2 (X = Si, Ge)における電荷密度波と反強磁性の共存状態の研究	網塚 浩	北海道大学	今 布咲子, 日比野 瑠央, 田端 千紘, 清水 悠晴, 中尾 裕則, 齋藤 開, 中島 多朗	Study on the coexistence of CDW and AFM in UPt2X2 (X = Si, Ge)	Hiroshi Amitsuka	Hokkaido University	Fusako Kon, Ruo Hibino, Chihiro Tabata, Yusei Shimizu, Hironori Nakao, Hiraku Saito, Taro Nakajima	PONTA	5G
36	時間反転対称性の破れた反強磁性体の磁気構造解析	関 真一郎	東京大学	中島 多朗, 高木 里奈, 摂待 裕生	Magnetic structure analysis of antiferromagnets with broken time-reversal symmetry	Shinichiro Seki	The University of Tokyo	Taro Nakajima, Rina Takagi, Yuki Settai	PONTA	5G
37	異方的三角格子反強磁性体Ca3ReO5Cl2における非整合磁気構造	那波 和宏	東北大学	平井 大悟郎, 廣井 善二, 佐藤 卓, 村崎 遼, Wu Hung-Cheng, Piyawongwatthana Pharit	Incommensurate magnetic structure of nisotropic triangular lattice antiferromagnet Ca3ReO5Cl2	Kazuhiro Nawa	Tohoku University	Daigoro Hirai , Zenji Hiroi , Taku J Sato, Ryo Murasaki, Wu Hung-Cheng, Piyawongwatthana Pharit	PONTA	5G
38	フェリ磁性絶縁体Tb3Fe5O12 における音響マグノンモード の磁場依存性	南部 雄亮	東北大学	川本 陽	Magnetic field dependent acoustic mode in the ferrimagnetic insulator Tb3Fe5O12	Yusuke Nambu	Tohoku University	You Kawamoto	TOPAN	6G
39	偏極中性子散乱法によるEu(Al0.6Ga0.4)4の磁気構造解析	高木 里奈	東京大学	中島 多朗, 関 真一郎	Magnetic structure analysis of Eu(Al0.6Ga0.4)4 by polarized neutron scattering	Rina Takagi	The University of Tokyo	Taro Nakajima,Shinnichirou Seki	PONTA	5G
40	重い電子系超伝導体CeCu2Si2における価数クロスオーバー領域における結晶場電子状態	池田 陽一	東北大学	北澤 崇文, 藤田 全基, 梅本 好日古, 二見 采樹, 大亀 佑太	Crystalline electric field states around a valence crossover region in the heavy fermion superconductor CeCu2Si2	Yoichi Ikeda	Tohoku University	Takahumi Kitazawa, Masaki Fujita, Yoshihiko Umemoto, Saiki Futami, Yuta Ohki	TOPAN	6G
41	FeMn基Elinvar合金の非線形フォノン分散異常の研究	池田 陽一	東北大学	梅本 好日古, 藤田 全基, 北澤 崇文, 二見 采樹, 大亀 佑太	Study of anomalous non-linear phonon dispersion in an FeMn-based Elinvar alloy	Yoichi Ikeda	Tohoku University	Yoshihiko Umemoto, Masaki Fujita, Takafumi Kitazawa, Saiki Futami, Yuta Ohki	TOPAN	6G
42	Nonreciprocal magnon dispersion in a Dresselhaus antiferromagnet	南部 雄亮	東北大学	Pang Xiaoqi, 川又 雅広	Nonreciprocal magnon dispersion in a Dresselhaus antiferromagnet	Yusuke Nambu	Tohoku University	Pang Xiaoqi, Masahiro Kawamata	HER	C1-1
43	Nd3Co4Sn13のカイラル対称結晶構造相における磁気励起	岩佐 和晃	茨城大学	下田 愛海, 熊田 隆伸, 桑原 慶太郎, 今関 啓雅, 黒澤 航海, 鈴木 陽太郎	Magnetic excitations in chiral structure phases of Nd3Co4Sn13	Kazuaki Iwasa	Ibaraki University	Ami Shimoda, Takanobu Kumada, Keitaro Kuwahara, Hiromasa Imazeki, Wataru Kurosawa, Yotaro Suzuki	HER	C1-1
44	フラストレーション磁性体YbBaCo4O7における磁気散漫散乱	左右田 稔	お茶の水女子大学	鴇田 莉佳, 茂木 麻琴	Magnetic Diffuse Scattering in Frustrated Magnet YbBaCo4O7	Minoru Soda	Ochanomizu University	Rika Tokita, Makoto Mogi	HER	C1-1
45	スピンギャップ系KCuCl3の圧力誘起量子臨界点近傍における磁気励起	栗田 伸之	東京工業大学	田中 秀数, 益田 隆嗣	Magnetic excitation of spin gap system KCuCl3 in the vicinity of pressure-induced QCP	Nobuyuki Kurita	Tokyo Institute of Technology	Hidekazu Tanaka, Takatsugu Masuda	HER	C1-1
46	ワイル－近藤半金属物質Ce3Rh4Sn13のカイラル構造相での磁気ゆらぎ	岩佐 和晃	茨城大学	下田 愛海, 熊田 隆伸, 桑原 慶太郎, 今関 啓雅, 黒澤 航海, 鈴木 陽太郎	Magnetic fluctuation in chiral structure phases of the Weyl-Kondo semimetal Ce3Rh4Sn13	Kazuaki Iwasa	Ibaraki University	Ami Shimoda, Takanobu Kumada, Keitaro Kuwahara, Hiromasa Imazeki, Wataru Kurosawa, Yotaro Suzuki	HER	C1-1
47	イルメナイトNiTiO3におけるディラックマグノンの観測	益田 隆嗣	東京大学	浅井 晋一郎, Wei Jijun, 菊地 帆高, Liu Zheyuan	Dirac magnon in NiTiO3	Takatsugu Masuda	The University of Tokyo	Shinichiro Asai, Wei Jijun, Hodaka Kikuchi, Liu Zheyuan	HER	C1-1
48	Bi-2201系銅酸化物の超過剰ドープ領域における磁気ゆらぎ	足立 匡	上智大学	小宮山 陽太, 谷口 貴紀, 藤田 全基, 林 幹稀	Magnetic fluctuations in the heavily overdoped Bi-2201 cuprates	Tadashi Adachi	Sophia University	Yota Komiyama, Takanori Taniguchi, Masaki Fujita, Motoki Hayashi	HER	C1-1
49	スピン液体候補物質NaErSe2の中性子非弾性散乱	益田 隆嗣	東京大学	Ma Jie, 浅井 晋一郎, 菊地 帆高, Liu Zheyuan, Shu Mingfang, Jiao Jinlong	Inelastic neutron scattering study on spin liquid candidate NaErSe2	Takatsugu Masuda	The University of Tokyo	Ma Jie, Shinichiro Asai, Hodaka Kikuchi, Liu Zheyuan, Shu Mingfang, Jiao Jinlong	HER	C1-1
50	電気磁気交差相関現象を示すCe3TiX5(X=Bi, Sb)の長周期磁気構造	阿曽 尚文	琉球大学	本山 岳, 篠崎 真碩, 田中 真侑, 佐藤 滉太, 中川 敬太	Long-period magnetic structure in a heavy fermion antiferromagnet Ce3TiX5(X=Bi, Sb) exhibiting electromagnetic cross-correlation phenomenon	Naofumi Aso	University of the Ryukyus	Gaku Motoyama, Masahiro Shinozaki, Mayu Tanaka, Kota Sato, Keita Nakagawa	HER	C1-1
51	単結晶NdCo2Zn20における磁気分散と低エネルギー磁気励起の時空相関	鬼丸 孝博	広島大学	山本 理香子, 志村 恭通, 岩佐 和晃, 下田 愛海	Magnetic dispersion and the space-time correlation of low-energy excitations in single-crystalline NdCo2Zn20	Takahiro Onimaru	Hiroshima University	Rikako Yamamoto, Yasuyuki Shimura, Kazuaki Iwasa, Ami Shimoda	HER	C1-1

52	Structure characterization of model tetra-poly(acrylic acid) gel	Li Xiang	北海道大学	Gupit Caidric, 光上 義朗, 柴山 充弘, 辻 優依, 大平 征史	Structure characterization of model tetra-poly(acrylic acid) gel	Li Xiang	Hokkaido University	Gupit Caidric, Yoshiro Mitsukami, Mitsuhiro Shibayama, Yui Tsuji, Masashi Ohira	SANS-U	C1-2
53	スピン1/2フラストレート正方格子磁性体2VOSO4_H2SO4_nH2Oの磁気励起	那波 和宏	東北大学	柴田 将弥, 佐藤 卓, 村崎 遼, Piyawongwatthana Pharit, 下館 凌人, 松坂 信之介	Spin excitations of the spin-1/2 frustrated square lattice magnet 2VOSO4_H2SO4_nH2O	Kazuhiro Nawa	Tohoku University	Masaya Shibata, Taku J Sato, Ryo Murasaki, Piyawongwatthana Pharit, Ryoto Shimodate, Shinnosuke Matsuzaka	HER	C1-1
54	中性子散乱法によるコアシェル型超分子ナノシートの構造解析	上沼 駿太郎	東京大学	眞弓 皓一, 數實 治己	Structural analysis of supramolecular core-shell nanosheet	Uenuma Shuntaro	The University of Tokyo	Koichi Mayumi, Haruki Kazumi	SANS-U	C1-2
55	小角中性子散乱による高圧下のタンパク質の構造解析	井上 倫太郎	京都大学	裏出 令子, 杉山 正明, 貞包 浩一朗, 會澤 直樹	Strutural analysis of protein under high pressure as studied by small-angle neutron scattering	Rintaro Inoue	Kyoto University	Reiko Urade, Masaaki Sugiyama, Koichiro Sadakane, Naoki Aizawa	SANS-U	C1-2
56	コントラスト変調SANSによる小麦タンパク質の複合構造解析	佐藤 信浩	京都大学	裏出 令子, 奥田 綾, 清水 将裕, 杉山 正明, 井上 倫太郎, 守島 健	Structural analysis on wheat protein assembly by contrast variation SANS	Nobuhiro Sato	Kyoto University	Reiko Urade, Aya Okuda, Masahiro Shimizu, Masaaki Sugiyama, Rintaro Inoue, Ken Morishima	SANS-U	C1-2
57	制御された不均一性を導入した過渡的網目の構造と物性評価	Li Xiang	北海道大学	大平 征史, 酒井 崇匡	Structure and mechanical properties of transient polymer network with controlled heterogeneity	Li Xiang	Hokkaido University	Masashi Ohira, Takamasa Sakai	SANS-U	C1-2
58	中性子小角散乱実験によるSr2RuO4の異常金属状態の研究	古川 はづき	お茶の水女子大学	左右田 稔, 石田 茜, Foley Edward, 中村 琴美	Anomalous vortex state in Sr2RuO4 studied by SANS experiments	Hazuki Furukawa	Ochanomizu University	Minoru Soda, Akane Ishida, Foley Edward, Kotomi Nakamura	SANS-U	C1-2
59	空間反転対称性の破れた超伝導体のヘリカル磁束格子の観測	古川 はづき	お茶の水女子大学	左右田 稔, 伊藤 未希, Foley Edward	Herical vortex phase on non-centrosymmetric superconductors	Hazuki Furukawa	Ochanomizu University	Minoru Soda, Miki Ito, Foley Edward	SANS-U	C1-2
60	強磁性超伝導体における自発的磁束格子構造の研究	古川 はづき	お茶の水女子大学	左右田 稔, 植木 萌, Foley Edward	Spontaneous vortex phase in ferromagnetic superconductors	Hazuki Furukawa	Ochanomizu University	Minoru Soda, Moe Ueki, Foley Edward	SANS-U	C1-2
61	ナノ・サブナノ空隙へのゲスト分子の選択的吸蔵現象の解明	千葉 文野	慶應義塾大学	伊藤 大基, 岩瀬 裕希, 村重 博美, 榎本 優里香	Selective absorption phenomena of guest molecules in nano- and sub-nano pores	Ayano Chiba	Keio University	Hiroki Ito, Hiroki Iwase, Hiromi Murashige, Yurika Enomoto	SANS-U	C1-2
62	中性子散乱によるカタニオニック界面活性剤がつくる泡沫の構造解析	吉村 倫一	奈良女子大学	矢田 詩歩, 王 珊, 長濱 佑美, 渡邊 萌, 岩瀬 裕希	Structural analysis of foam formed by catanionic surfactants using neutron scattering	Tomokazu Yoshimura	Nara Women's University	Shiho Yada, Shan Wang, Yumi Nagahama, Moe Watanabe, Yuki Iwase	SANS-U	C1-2
63	小角中性子散乱法によるナノクレイ/高分子懸濁液中の温度変化に伴う構造変化の評価	土肥 侑也	名古屋大学	磯田 龍矢	Evaluation of structural change with temperature change in nanoclay/polymer suspensions studied by small-angle neutron scattering	Yuya Doi	Nagoya University	Ryuya Isoda	SANS-U	C1-2
64	小角中性子散乱測定による延伸過程で生じるPEの構造変化メカニズムの解明	木田 拓充	北陸先端科学技術大学院大学	土肥 侑也	Microscopic Deformation Mechanism of PE under Tensile Deformation Detected by SANS measurement	Takumitsu Kida	Japan Advanced Institute of Science and Technology	Yuya Doi	SANS-U	C1-2
65	中性子小角散乱によるアミノ酸ー糖ハイブリッド界面活性剤の ミセル—紐状ミセル—ゲル転移の構造解析	吉村 倫一	奈良女子大学	矢田 詩歩, 長濱 佑美, 渡邊 萌, 王 珊	Structural analysis of micelle - worm-like micelle - gel transition of amino acid - sugar hybrid surfactants using small-angle neutron scattering	Tomokazu Yoshimura	Nara Women's University	Shiho Yada, Yumi Nagahama, Moe Watanabe, Shan Wang	SANS-U	C1-2
66	スライドリング網目を有するイオンゲルの延伸中における網目構造変化	橋本 慧	東京大学	眞弓 皓一, 榎木 崇人	Strain-induced structural change of slide-ring network in ion gel	Kei Hashimoto	The University of Tokyo	Koichi Mayumi, Takato Enoki	SANS-U	C1-2
67	均一網目構造を有する過渡的網目における結合性・濃度と構造相関	片島 拓弥	東京大学	大平 征史, 安田 傑, Li Xiang, 酒井 崇匡	Effects of Connectivity and Concentration on Structure in Transient Homogeneous Reticulation	Takuya Katashima	The University of Tokyo	Masashi Ohira, Takashi Yasuda, Li Xiang, Takamasa Sakai	SANS-U	C1-2
68	コントラストマッチング中性子散乱法によるハイブリッドベシクル中の ポリマードメインの構造解析：ポリマー重合度とドメインサイズの相関	西村 智貴	信州大学	櫻木 美菜, 藤井 翔太	Structural Analysis of Polymer Domains in Hybrid Vesicles by Contrast-Matched Neutron Scattering: Relationship between Degree of polymerization and Domain Size	Tomoki Nishimura	Shinshu University	Mina Sakuragi, Shota Fujii	SANS-U	C1-2

69	中性子小角散乱によるマルチドメインタンパク質のドメイン配置解析	杉山 正明	京都大学	井上 倫太郎, 矢木-内海 真穂, 守島 健	Conformation analysis of multi-domain protein utilizing small-angle neutron scattering	Masaaki Sugiyama	Kyoto University	Rintaro Inoue, Maho Yagi-Utsumi, Ken Morishima	SANS-U	C1-2
70	高圧条件下における混合溶液系の新奇な臨界挙動と隠れた長距離相互作用の解明	貞包 浩一朗	同志社大学	眞弓 皓一, 小田 達郎, 吉良 康弘, 後藤 篤子	Novel critical behavior in a mixture of water/organic solvent under high-pressure condition	Koichiro Sadakane	Doshisha University	Koichi Mayumi, Tatsuro Oda, Yasuhiro Kira, Atsuko Goto	SANS-U	C1-2
71	界面活性剤が誘起する液-液相分離のメカニズムの解明	貞包 浩一朗	同志社大学	吉良 康弘, 後藤 篤子, 三桝 黎, 和田 竜誠	Phase separation induced by surfactants	Koichiro Sadakane	Doshisha University	Yasuhiro Kira, Atsuko Goto, Rei Mimasu, Ryusei Wada	SANS-U	C1-2
72	水と低分子有機溶媒のみの２成分混合溶液における臨界現象の平均場/3D-Isingクロスオーバー	貞包 浩一朗	同志社大学	吉良 康弘, 後藤 篤子, 高椋 利幸	Crossover from mean field to 3D-Ising critical behavior in water/organic solvent mixtures	Koichiro Sadakane	Doshisha University	Yasuhiro Kira, Atsuko Goto, Toshiyuki Takamuku	SANS-U	C1-2
73	小角中性子散乱による重合誘起ガラス化近傍での不均一性解析	鈴木 祥仁	大阪府立大学	土肥 侑也, 眞弓 皓一	Polymerization induced phase separation at the vicinity of vitrification investigated by SANS	Yasuhito Suzuki	Osaka Prefecture University	Yuya Doi, Koichi Mayumi	SANS-U	C1-2
74	中性子散乱法によるシンジオタクチックポリスチレン/アタクチックポリスチレンブレンドの結晶高次構造解析	西辻 祥太郎	山形大学	岩原 大輔, 武部 智明, 藤井 望, 森谷 太祐, 酒井 一帆	Crystalline structural analysis of syndiotakuctic polystyrene / atactic polystyrene blend by neutron scattering method	Shotaro Nishitsuji	Yamagata University	Daisuke Iwahara, Tomoaki Takebe, Nozomu Fujii, Taisuke Moritani, Kazuho Sakai	SANS-U	C1-2
75	SANS法による分子性液体中でのピリジニウム系イオン液体のモルフォロジー観測	高椋 利幸	佐賀大学	佐々木 魁斗, 筒井 奏, 樋熊 知紗, 山田 萌乃	SANS Study on Morphology of Pyridinium-based Ionic Liquids in Molecular Liquids	Toshiyuki Takamuku	Saga University	Kaito Sasaki, Sou Tsutsui, Chisa Higuma, Moeno Yamada	SANS-U	C1-2
76	イミダゾリウム系イオン液体中におけるエタノールクラスターの形成	高椋 利幸	佐賀大学	佐々木 魁斗, 筒井 奏, 樋熊 知紗, 山田 萌乃	Ethanol Cluster Formation in Imidazolium-based Ionic Liquids	Toshiyuki Takamuku	Saga University	Kaito Sasaki, Sou Tsutsui, Chisa Higuma, Moeno Yamada	SANS-U	C1-2
77	ポリアルキルスチレン類とポリイソプレンの相溶性評価と相溶化機構の検討	高野 敦志	名古屋大学	都築 侑奈, 北原 彩音, 土肥 侑也, 鈴木 海渡, 安田 悠真	Investigation of miscibility between polyalkylstyrenes and polyisoprene by SANS	Atsushi Takano	Nagoya University	Yuna Tsuzuki, Ayane Kitahara, Yuya Doi, Kaito Suzuki, Yuma Yasuda	SANS-U	C1-2
78	酸化ジルコニウムナノ流体の水のダイナミクス測定	吉田 亨次	福岡大学	永井 哲郎	Water dynamisc of zirconium oxide nanofluid	Koji Yoshida	Fukuoka University	Tetsuro Nagai	AGNES	C3-1-1
79	中性子・X線散乱法を利用した外部環境変化に伴う牛乳内カゼインミセル構造変化の研究	高木 秀彰	高エネルギー加速器研究機構		A study on the structural changes of casein micelles with the change of external environments using neutron and X-ray scattering	Hideaki Takagi	High Energy Accelerator Research Organization		SANS-U	C1-2
80	架橋高分子ゲルSephadex G25に吸着・内包された水の動的挙動	山室 憲子	東京電機大学	湊 広章, 柳 凌聖	Dynamic properties of water confined in cross-linked polymer gel Sephadex G-25	Noriko Yamamuro	Tokyo Denki University	Hiroaki Minato, Ryosei Yanagi	AGNES	C3-1-1
81	疎水性環境下における水クラスターのダイナミクスに関する研究	岡 弘樹	大阪大学	山室 修, 秋葉 宙	Study on the dynamics of water clusters in hydrophobic environment	Kouki Oka	Osaka University	Osamu Yamamuro, Hiroshi Akiba	AGNES	C3-1-1
82	中性子準弾性散乱法による糖溶液の凍結濃縮ガラス転移挙動の解明	川井 清司	広島大学	曽我部 知史, 中川 洋, 山田 武	Freeze-concentrated glass transition behavior of carbohydrate solutions by quasielastic neutron scattering	Kiyoshi Kawai	Hiroshima University	Tomochika Sogabe, Hiroshi Nakagawa, Takeshi Yamada	AGNES	C3-1-1
83	可塑剤が非晶質アミロペクチンの分子ダイナミクスに及ぼす影響	川井 清司	広島大学	曽我部 知史, 中川 洋, 山田 武, 加賀谷 勇生	Effect of plasticizer on the molecular dynamics of amorphous amylopectin	Kiyoshi Kawai	Hiroshima University	Tomochika Sogabe , Hiroshi Nakagawa, Takeshi Yamada, Yuki Kagaya	AGNES	C3-1-1
84	水和したアニオン交換型電解質膜のダイナミクス測定	吉田 亨次	福岡大学	犬飼 潤治, 川本 鉄平, 西山 博通, 白勢 裕登, Solomon Wekesa, Anna Kapulwa	Dynamics of hydrated anion exhange membrain	Koji Yoshida	Fukuoka University	Junji Inukai, Teppei Kawamoto, Hiromichi Nishiyama, Yuto Shirase, Solomon Wekesa, Anna Kapulwa	AGNES	C3-1-1
85	中性子準弾性散乱法による高水素配位錯イオンの動的挙動解析	高木 成幸	東北大学	山室 修, 大政 義典, 秋葉 宙, 折茂 慎一, 安達 淳	Quasi-elastic neutron scattering study of hydride complexes with high hydrogen coordination	Shigeyuki Takagi	Tohoku University	Osamu Yamamuro, Yoshinori Ohmasa, Hiroshi Akiba, Shinichi Orimo, Jun Adachi	AGNES	C3-1-1
86	中性子基礎物理実験のためのデバイス開発	北口 雅暁	名古屋大学	清水 裕彦, 奥平 琢也, 藤家 拓大, 奥泉 舞桜, 南部 太郎, 椿原 暖人, 長屋 沙優	Development of neutron devices for fundamental physics	Masaaki Kitaguchi	Nagoya University	Hirohiko Shimizu, Takuya Okudaira, Takuhiro Fujiie, Mao Okuizumi, Taro Nambu, Haruto Tsubakihara, Sayu Nagaya	MINE	C3-1-2
87	超冷中性子スピン解析器の開発	川崎 真介	高エネルギー加速器研究機構	三島 賢二, 市川 豪, 北口 雅暁, 樋口 嵩, 今城 想平, 赤塚 浩明, 畑中 吉治	Development of a Spin Analyzer for Ultra Cold Neutron	Shinsuke Kawasaki	High Energy Accelerator Research Organization	Kenji Mishima, Go Ichikawa, Masaaki Kitaguchi , Takashi Higuchi, Sohei Imajo, Hiroaki Akatsuka, Kichiji Hatanaka	MINE	C3-1-2

88	中性子反射率法による各種基油内における添加剤吸着層の構造解析	平山 朋子	京都大学	日野 正裕, 山下 直輝, 中村 吏一朗	Structural Analysis of Adsorbed Additive Layer in Various Base Oils by Neutron Reflectometry	Tomoko Hirayama	Kyoto University	Masahiro Hino, Naoki Yamashita, Riichiro Nakamura	MINE	C3-1-2
89	多層膜性中性子ミラーの高度化と集光デバイス開発	日野 正裕	京都大学	中村 吏一朗, 細畠 拓也, 小田 達郎, 奥野 泰希	Development of multilayer neutron mirrors and focusing devices	Masahiro Hino	Kyoto University	Riichiro Nakamura, Takuya Hosobata, Tatsuro Oda, Yasuki Okuno	MINE	C3-1-2
90	MOFガラスにおけるゲスト分子のダイナミクスに関する研究	秋葉 宙	東京大学	佐藤 創, Yin Zheng, Zeng Ming-Hua, 山室 修, 佐藤 駿, Zhang Menghan	Dynamics of guest molecules in MOF glass	Hiroshi Akiba	The University of Tokyo	Hajime Sato, Yin Zheng, Zeng Ming-Hua, Osamu Yamamuro, Shun Sato, Zhang Menghan	AGNES	C3-1-1
91	ガラスキャピラリープレートを用いた中性子イメージング検出器の開発	門叶 冬樹	山形大学	日野 正裕, 森谷 透, 武山 美麗, 高橋 貫太, 浅野 紘輝	Development of neutron imager based on hole-type MPGD with glass capillary plate	Fuyuki Tokanai	Yamagata University	Masahiro Hino, Toru Moriya, Mirei Takeyama, Kanta Takahashi, Hiroki Asano	MINE	C3-1-2
92	π電子反強磁性体RbO2の結晶構造および磁気構造解析	中野 岳仁	茨城大学	神戸 高志, 紺谷 駿, 大山 研司, 塩見 透慎	Magnetic and crystal structural studies on π-orbital antiferromagnet RbO2	Takehito Nakano	Ibaraki University	Takashi Kanbe, Shun Kontani, Kenji Ohoyama, Toma Shiomi	HQR	T1-1
93	特異な価数秩序を示すYbPdの最低温磁気構造解析	光田 暁弘	九州大学	大山 研司, 横枕 拓八	Magnetic structure at lowest temperatures of exotic valence-ordered YbPd	Akihiro Mitsuda	Kyushu University	Kenji Ohoyama, Takuya Yokomakura	HQR	T1-1
94	反強磁性量子臨界的挙動がもたらす異常超伝導物性II	横山 淳	茨城大学	川崎 郁斗, 平山 堅理, 矢代 安澄, 井能 楓, 清水 悠晴, 小泉 遼介, 海老澤 秀明, 高橋 哲平	Anomalous superconducting properties coupled with antiferromagentic quantum criticality II	Makoto Yokoyama	Ibaraki University	Ikuto Kawasaki, Takatoshi Hirayama, Azumi Yashiro, Kaede Inou, Yusei Shimizu, Ryosuke Koizumi, Hideaki Ebisawa, Teppei Takahashi	HQR	T1-1
95	中性子スピン干渉現象を用いた3次元偏極解析手法の開発	田崎 誠司	京都大学	安部 豊, 鈴木 雄也	3D polarization analysis using resonance neutron spin interferometry	Seiji Tasaki	Kyoto University	Yutaka Abe, Yuya Suzuki	MINE	C3-1-2
96	f電子系金属間化合物が持つフラストレーション効果の研究	谷口 貴紀	東北大学	藤田 全基, 南部 雄亮, 池田 陽一, 大里 耕太郎, 磯村 楓, Xie Peiao, Wang Tong, Chen Yizhou, 北山 慎之介	the frustrated effects on f electron system	Takanori Taniguchi	Tohoku University	Masaki Fujita, Yusuke Nambu, Yoichi Ikeda, Kotaro Osato, Kaede Isomura, Xie Peiao, Wang Tong, Chen Yizhou, Shinnosuke Kitayama	AKANE	T1-2
97	アンモニウム含有層状ハライドペロブスカイトの結晶と磁気構造の変化	Zhu Tong	京都大学	陰山 洋	Crystal and Magnetic Structural Evolutions of Layered Ammonium Halide Perovskites	Zhu Tong	Kyoto University	Hiroshi Kageyama	HERMES	T1-3
98	六方ペロブスカイト関連酸化物の結晶構造とイオン拡散経路	八島 正知	東京工業大学	藤井 孝太郎, 張 文鋭, 安井 雄太, 矢口 寛, 作田 祐一, 齊藤 馨, 森川 里穂, 上野 那智, 松崎 航平, 山田 大史	Crystal Structure and Ion Diffusion Path of Ion-Conducting Hexagonal Perovskite-Related Oxides	Masatomo Yashima	Tokyo Institute of Technology	Kotaro Fujii, Wenrui Zhang, Yuta Yasui, Hiroshi Yaugchi, Yuichi Sakuda, Kei Saito, Riho Morikawa, Nachi Ueno, Kohei Matsuzaki, Taishi Yamada	HERMES	T1-3
99	アニオン置換・挿入による層状ペロブスカイトのtilting制御	加藤 大地	京都大学	生方 宏樹, 陰山 洋, 松崎 洋介, 田畔 春紀, 津森 竜也	Tilting design of layered perovskite via anion insertion and substitution	Daichi Kato	Kyoto University	Hiroki Ubukata, Hiroshi Kageyama, Yosuke Matsuzaki, Haruki Taguro, Tatsuya Tsumori	HERMES	T1-3
100	Magnetic structure of the bilayered two-dimensional triangular antiferromagnet Fe2Ga2S5	南部 雄亮	東北大学	Tang Yifei	Magnetic structure of the bilayered two-dimensional triangular antiferromagnet Fe2Ga2S5	Yusuke Nambu	Tohoku University	Tang Yifei	HERMES	T1-3
101	中性子散乱法による高濃度界面含有複合体内Li伝導固体のLi状態解析	大野 真之	九州大学	岡崎 直斗, 柳原 祥馬	Exploration of structure-transport relationship in the vicinity of heterogeneous interfaces	Saneyuki Ohno	Kyushu University	Naoto Okazaki, Shoma Yanagihara	HERMES	T1-3
102	高圧合成によって得られる遷移金属ペロブスカイト酸水素化物の構造と組成	山本 隆文	東京工業大学	大河内 寛保, 英 遼太郎, 小菅 大輝	Structures and formula of transition metal oxyhydride synthesized under high pressure	Takafumi Yamamoto	Tokyo Institute of Technology	Hiroyasu Okochi, Ryotaro Hanabusa, Taiki Kosuge	HERMES	T1-3
103	単結晶中性子回折による三角格子反強磁性体面内磁気構造の同定	南部 雄亮	東北大学	川又 雅広	Magnetic structure refinement of triangular antiferromagnets under fields	Yusuke Nambu	Tohoku University	Masahiro Kawamata	AKANE	T1-2
104	Dion‐Jacobson型酸化物イオン伝導体の結晶構造とイオン拡散経路の解析	張 文鋭	東京工業大学	八島 正知, 藤井 孝太郎, 安井 雄太, 矢口 寛, 作田 祐一, 齊藤 馨, 森川 里穂, 上野 那智, 松崎 航平, 山田 大史	Crystal Structure Analysis and Oxide-Ion Diffusion Paths of Dion‐Jacobson type Oxide-ion Conductors	Wenrui Zhang	Tokyo Institute of Technology	Masatomo Yashima,Kotaro Fujii, Yuta Yasui, Hiroshi Yaugchi, Yuichi Sakuda, Kei Saito, Riho Morikawa, Nachi Ueno, Kohei Matsuzaki, Taishi Yamada	HERMES	T1-3

105	電気磁気交差相関現象が期待されるCe3TiSb5とCe3ZrSb5の磁気構造の比較	本山 岳	島根大学	阿曽 尚文, 篠崎 真碩, 中川 敬太, 佐藤 滉太	Magnetic structure comparison between Ce3TiSb5 and Ce3ZrSb5 of two candidate magnetoelectric materials	Gaku Motoyama	Shimane University	Naofumi Aso, Masahiro Shinozaki, Keita Nakagawa, Kota Sato	HERMES	T1-3
106	中性子回折法によるハイパーカゴメ反強磁性体ZnMgMn3O8の研究	気谷 卓	東京工業大学	川路 均	Neutron diffraction study on hyperkagome antiferromagnet ZnMgMn3O8	Suguru Kitani	Tokyo Institute of Technology	Hitoshi Kawaji	HERMES	T1-3
107	磁性半金属における磁気構造の解明	高橋 英史	大阪大学	南部 雄亮	Clarification of magnetic structure in magnetic semimetal	Hidefumi Takahashi	Osaka University	Yusuke Nambu	HERMES	T1-3
108	新規酸塩化物イオン伝導体の結晶構造解析とイオン伝導機構解明	藤井 孝太郎	東京工業大学	八島 正知, 張 文鋭, 安井 雄太, 矢口 寛, 作田 祐一, 齊藤 馨, 森川 里穂, 上野 那智, 松崎 航平, 山田 大史	Crystal Structure Analysis and Elucidation of Ion Conduction Mechanism of Novel Oxychloride Ion Conductors	Kotaro Fujii	Tokyo Institute of Technology	Masatomo Yashima, Wenrui Zhang, Yuta Yasui, Hiroshi Yaugchi, Yuichi Sakuda, Kei Saito, Riho Morikawa, Nachi Ueno, Kohei Matsuzaki, Taishi Yamada	HERMES	T1-3
109	T*構造銅酸化物の結晶構造に対する酸素アニール効果	藤田 全基	東北大学	谷口 貴紀, 池田 陽一, 陳 逸舟, 谢 佩翱, 王 彤, 北山 慎之介	Oxidation annealing effects on the crystal structure of T*-type cuprate oxides	Masaki Fujita	Tohoku University	Takanori Taniguchi, Yoichi Ikeda, Chen Yizhou, Xie Peiao, Wang Tong, Shinnosuke Kitayama	HERMES	T1-3
110	YbCu4Niの量子臨界性と結晶構造の関係	谷口 貴紀	東北大学	藤田 全基, 南部 雄亮, 池田 陽一, 大里 耕太郎, 鄭 家傑, 小宮山 陽太, 岡田　陸玖, Xie Peiao, Wang Tong, Chen Yizhou, 北山 慎之介	Quantum criticality and crystal structure on YbCu4Ni	Takanori Taniguchi	Tohoku University	Masaki Fujita, Yusuke Nambu, Yoichi Ikeda, Kotaro Osato, Zheng Jiajie, Yota Komiyama, Riku Okada, Xie Peiao, Wang Tong, Chen Yizhou, Shinnosuke Kitayama	HERMES	T1-3
111	Au72Si12.5Eu13.5近似結晶の磁気構造	那波 和宏	東北大学	鈴木 慎太郎, 田村 隆治, 佐藤 卓, 村崎 遼, Wu Hung-Cheng	Magnetic structure of the quasicrystal approximant Au72Si12.5Eu13.5	Kazuhiro Nawa	Tohoku University	Shintaro Suzuki, Ryuji Tamura , Taku J Sato, Ryo Murasaki, Wu Hung-Cheng	HERMES	T1-3
112	ハニカム格子様化合物Pb6Co9(TeO6)5の磁気構造	那波 和宏	東北大学	平岡 巧, 佐藤 卓	Magnetic structure of the honeycomb lattice like compound Pb6Co9(TeO6)5	Kazuhiro Nawa	Tohoku University	Takumi Hiraoka, Taku J Sato	HERMES	T1-3
113	ホイスラー合金Ru2CrSiの反強磁性状態	重田 出	鹿児島大学	廣井 政彦, 渕崎 員弘, 南部 雄亮	Antiferromagnetic state of Heusler alloy Ru2CrSi	Iduru Shigeta	Kagoshima University	Masahiko Hiroi, Kazuhiro Fuchizaki, Yusuke Nambu	HERMES	T1-3
114	Nd3T4Sn13 (T = Rh, Ir)のカイラル対称結晶構造相における反強磁気秩序	岩佐 和晃	茨城大学	下田 愛海, 熊田 隆伸, 今関 啓雅, 黒澤 航海, 鈴木 陽太郎	Antiferromagnetic ordered states in chiral structure phases of Nd3T4Sn13 (T = Rh, Ir)	Kazuaki Iwasa	Ibaraki University	Ami Shimoda, Takanobu Kumada, Hiromasa Imazeki, Wataru Kurosawa, Yotaro Suzuki	HERMES	T1-3
115	Estimate the DM interaction in a Dresselhaus magnet	南部 雄亮	東北大学	Pang Xiaoqi, 木村 宏之, 山本 孟, 川又 雅広	Estimate the DM interaction in a Dresselhaus magnet	Yusuke Nambu	Tohoku University	Pang Xiaoqi, Hiroyuki Kimura, Hajime Yamamoto, Masahiro Kawamata	FONDER	T2-2
116	塑性歪みを加えたPt3Fe反強磁性体の磁気構造解析	小林 悟	岩手大学	松尾 咲琴, 堀田 侑里, 西館 直樹, 中野 愛弓, 後藤 颯樹	Magnetic structural analysis of plastically strained Pt3Fe antiferromagnet	Satoru Kobayashi	Iwate University	Sakoto Matsuo, Yuri Hotta, Naoki Nishidate, Ayumi Nakano, Satsuki Goto	FONDER	T2-2
117	T'-type Pr2CuO4における結晶構造の還元効果	木村 宏之	東北大学	坂倉 輝俊, 山本 孟	Oxygen reduction effect on the crystal structure in the T'-structure of Pr2CuO4+y	Hiroyuki Kimura	Tohoku University	Terutoshi Sakakura, Hajime Yamamoto	FONDER	T2-2
118	マルチフェロイックEuMn2O5における強誘電相転移の起源	木村 宏之	東北大学	坂倉 輝俊, 山本 孟, 野田 幸男	Origin of ferroelectric phase transition in multiferroic EuMn2O5	Hiroyuki Kimura	Tohoku University	Terutoshi Sakakura, Hajime Yamamoto, Yukio Noda	FONDER	T2-2
119	Tb0.5Gd0.5Mn2O5の電気磁気効果の発現機構	石井 祐太	東北大学	木村 宏之, 野田 幸男, 山本 孟	Mechanism of Magneto-electric effect of Tb0.5Gd0.5Mn2O5	Yuta Ishii	Tohoku University	Hiroyuki Kimura, Yukio Noda, Hajime Yamamoto	FONDER	T2-2
120	typeIII 型反強磁性体 Pt-Mn における整合ー非整合磁気相転移	高橋 美和子	筑波大学	川崎 卓郎	Commensurate-Incommensurate Magnetic Phase Transition in Type-III Anti-ferromagnet Pt-Mn	Miwako Takahashi	University of Tsukuba	Takuro Kawasaki	FONDER	T2-2
121	導電性酸化物における極性-非極性構造相転移とその構造解析	高津 浩	京都大学	南部 雄亮, 村山 寛太郎, Tong Zhu	Polar-Nonpolar Phase Transition in Conductive Oxides and Their Structural Analysis	Hiroshi Takatsu	Kyoto University	Yusuke Nambu, Kantaro Murayama, Tong Zhu	HERMES	T1-3
122	二糖類水和物の結晶構造	高橋 美和子	筑波大学	川崎 卓郎, 片岡 邦光	Crystal structure of hydrate disaccharide	Miwako Takahashi	University of Tsukuba	Takuro Kawasaki, Kunimitsu Kataoka	FONDER	T2-2
123	正二十面体準結晶i-ZnMgYにおける光学フォノンモードの研究	柴田 薫	日本原子力研究開発機構	de Boissieu Marc, de Laitre Geoffroy	Optical Phonon Modes in the ZnMgY icosahedral quasicrystal	Kaoru Shibata	Japan Atomic Energy Agency	de Boissieu Marc, de Laitre Geoffroy	GPTAS	4G

124	価数揺動希土類化合物における電荷揺らぎとフェルミ面ネスティング	筒井 智嗣	高輝度光科学研究センター	李 哲虎, 光田 暁弘, 和田 裕文	correlation between valence fluctuation and Fermi surface nesting in a valence-fluctuating rare-earth compound	Satoshi Tsutsui	Japan Synchrotron Radiation Research Institute	Chul-Ho LEE, Akihiro Mitsuda, Hirofumi Wada	GPTAS	4G
125	三角格子反強磁性体CuFeO2の圧力誘起磁気相転移に伴う磁気励起の探査	寺田 典樹	物質材料研究機構		Pressure dependence of magnetic excitation in triangular lattice antiferromagnet CuFeO2	Noriki Terada	National Institute for Materials Science		HER	C1-1
126	Mg3Sb2のフォノンダイナミクス	李 哲虎	産業技術総合研究所	坂上 良介, 小野 圭吾, 長谷川 巧, 後藤 陽介	Phonon dynamics of Mg3Sb2	Chul-Ho LEE	National Institute of Advanced Industrial Science and Technology	Ryosuke Sakagami, Keigo Ono, Takumi Hasegawa, Yosuke Goto	HER	C1-1
127	水中で距離秩序構造を形成するイオン性ボトルブラシポリマーの構造解明	山内 祥弘	物質材料研究機構		Structural Analysis of Ionic Bottlebrush Polymers Forming Long-range Order in Water	Yoshihiro Yamauchi	National Institute for Materials Science		SANS-U	C1-2
128	グリセロール水溶液の低温における水のダイナミクスの研究	中川 洋	日本原子力研究開発機構	川井 清司, 曽我部 知史, 山田 武	Study of water dynamics in aqueous glycerol solutions at cryo-temperatures	Hiroshi Nakagawa	Japan Atomic Energy Agency	Kiyoshi Kawai, Tomochika Sogabe, Takeshi Yamada	AGNES	C3-1-1
129	分子構造の異なる澱粉の動的挙動とその加熱糊化による変化の解析	中川 洋	日本原子力研究開発機構	山田 武	Molecular dynamics of starches with different molecular structures and their changes by heating	Hiroshi Nakagawa	Japan Atomic Energy Agency	Takeshi Yamada	AGNES	C3-1-1
130	中性子非弾性散乱による出土琥珀の産地推定	山口 繁生	公益財団法人　元興寺文化財研究所	中川 洋, 植田 直見	Provenance study of excavated amber by inelastic neutron scattering.	Shigeo Yamaguchi	Gangoji institute for research of cultural property	Hiroshi Nakagawa, Naomi Ueda	AGNES	C3-1-1
131	液体イオウの光誘起重合転移における局所構造の研究II	坂口 佳史	総合科学研究機構		Investigations on the local structure of liquid sulfur at photo-induced polymerization transition II	Yoshifumi Sakaguchi	Comprehensive Research Organization for Science and Society		HERMES	T1-3
132	熱電材料143ジントル相の結晶構造	李 哲虎	産業技術総合研究所	坂上 良介, 小野 圭吾, 三浦 章, 出村 萌々香	Crystal structure of 143 Zintl phase thermoelectric compounds	Chul-Ho Lee	National Institute of Advanced Industrial Science and Technology	Ryosuke Sakagami, Keigo Ono, Akira Miura, Momoka Demura	HERMES	T1-3
133	中性子回折法による新奇フラストレート磁性体BaFe12Se7O6の磁気構造解析	辻本 吉廣	物質材料研究機構	南部 雄介, 林 浩章	Powder neutron diffraction study of a new spin-frustrated magnet BaFe12Se7O6	Yoshihiro Tsujimoto	National Institute for Materials Science	Yusuke Nambu, Hiroaki Hayashi	HERMES	T1-3
134	エルビウム鉄ガーネットの磁気補償温度での磁気構造異常	社本 真一	総合科学研究機構	山内 宏樹, 赤津 光洋, 松浦 直人, 坂倉 輝俊, 木村 宏之, 張 烈錚	Magnetic structure anomaly at the magnetic compensation temperature of erbium iron garnet	Shinichi Shamoto	Comprehensive Research Organization for Science and Society	Hiroki Yamauchi, Mitsuhiro Amatsu, Masato Matsuura, Terutoshi Sakakura, Hiroyuki Kimura, Lieh-Jeng Chang	FONDER	T2-2
135	三角磁気クラスターの面心立方格子による二重フラストレーション	社本 真一	総合科学研究機構	山内 宏樹, Chang Lieh-Jeng, 坂倉 輝俊, 木村 宏之	Double frustration with face-centered cubic lattice of triangular magnetic clusters	Shinichi Shamoto	Comprehensive Research Organization for Science and Society	Hiroki Yamauchi, Chang Lieh-Jeng, Terutoshi Sakakura, Hiroyuki Kimura	FONDER	T2-2

2022年度　軌道放射物性研究施設 共同利用課題一覧 / Joint Research List of Synchrotron Radiation Research Project 2022

※実施課題一覧、所属は申請時のデータ

播磨分室　BL07LSU/Harima Branch BL07LSU

No.	課題番号	課題名	氏名	所属	分担者（共同研究者）	Title	Name	Organization	Member of reseach project	担当所員
1	202103-SRBXS-0030	軟X線オペランド計測の高度化が拓く次世代触媒科学	山本　達	東北大学多元物質科学研究所		Next Generation Catalysis Science Opened by Sophistication of Operando Soft X-ray Spectroscopies	Susumu Yamamoto	Tohoku University		松田
2	202012-SRBXS-0009	次世代光源に向けた全反射ウォルターミラーを利用した新規X線イメージング技術の開発	木村 隆志	東京大学物性研究所	志村 まり（国立国際医療研究センター）、江川 悟（理化学研究所）、古谷 登、竹尾 陽子、櫻井 快	Development of Novel X-ray Imaging Technology using Total Reflection Walter Mirror for Next Generation Light Source.	Takashi Kimura	The Institute for Solid State Physics, The University of Tokyo	Mari Shimura, Satoshi Egawa, Noboru Frutani, Youko Takeo, Kai Sakurai	木村
3	202111-SRBXG-0005	CT-ptychographyによるI細胞内構造変化の解析	志村 まり	国立国際医療研究センター	江川 悟（理化学研究所・博士研究員）、古谷 登、竹尾 陽子、櫻井 快	Changes of cellular structures using CT-ptychography	Mari Shimura	National Center for Global Health and Medicine	Satoshi Egawa, Noboru Frutani, Youko Takeo, Kai Sakurai	木村
4	202112-SRBXG-0012	非磁性金属/酸化膜界面における軌道偏極の観測	金 俊延	理化学研究所	大谷 義近（東京大学物性研究所）、堀尾 眞史（東京大学物性研究所）、妹尾 共晃（東京大学物性研究所）	Observation of orbital polarization at non-magnetic metal/oxide interface	Kim Junyeon	Institute of Physical and Chemical Research	Yoshichika Otani, Masafumi Horio, Tomoaki Senou	松田
5	202112-SRBXG-0026	交流電流と位相検波を用いた高感度オペランドXMCD計測手法の開発: 特異な量子スピン輸送現象のオペランド分光	堀尾 眞史	東京大学物性研究所	妹尾 共晃、鷲見 寿秀	Development of a Highly-Sensitive Method for Operando-XMCD using AC Current and Phase Detection Technique: Operando-Spectroscopy of Exotic Quantum Spin Transport Phenomena	Masafumi Horio	The Institute for Solid State Physics, The University of Tokyo	Tomoaki Senou, Toshihide Sumi	松田
6	202112-SRBXP-0028	偏光可変軟X線による二次元単層ホウ化銅の電子状態の研究	近藤 剛弘	筑波大学	堀尾 眞史（東京大学物性研究所）、辻川 夕貴（東京大学物性研究所）	Electric states of 2D copper boride studied by polarization controlled soft X-ray	Takehiro Kondo	University of Tsukuba	Masafumi Horio, Yuki Tsujikawa	松田
7	202111-SRBXG-0001	ミクロ相分離水性二相系における水の電子状態	檜垣 勇次	大分大学理工学部	舛田 拓己、倉岡 直輝	Electronic structure of water confined in aqueous microphase two-phase systems	Yuji Higaki	Oita University	Takumi Masuda, Naoki Kurata	原田
8	202111-SRBXG-0003	分子間相互作用からなる細孔性結晶に形成した1次元水チャネルの電子状態解析	堀内 新之介	長崎大学大学院工学研究科	木内 久雄（東京大学物性研究所）、小倉 祥太、辰田 和穂（東京大学物性研究所）	Soft X-ray emission spectroscopic analysis of 1D water channel within a noncovalent porous crystal	Shinnosuke Horiuchi	Nagasaki University School of Engineering & Graduate School of Engineering	Hisao Kiuchi, Shouta Ogura, Kazuho Tatsuta	原田
9	202112-SRBXG-0006	オペランド軟X線吸収/発光分光分析によるアルカリ水電解酸素発生触媒の電子状態解析	辰田 和穂	東京大学物性研究所	木内 久雄	Electronic states analysis of oxygen evolution reaction catalyst for alkaline water electrolysis by Operando soft x-ray absorption and emission spectroscopy	Kazuo Tatsuta	The Institute for Solid State Physics, The University of Tokyo	Hisao Kiuchi	原田
10	202112-SRBXG-0007	共鳴非弾性X線散乱法を用いた全固体フッ化物電池窒化物正極の電子状態分析	山本 健太郎	奈良国立大学機構奈良女子大学研究院工学系	木内 久雄（東京大学物性研究所）	Study on the electronic structure of nitride cathode for all-solid-state fluoride ions batteries by resonant inelastic X-ray scattering	Kentaro Yamamoto	Nara Women's University	Hisao Kiuchi	原田

11	202112-SRBXG-0008	気相試料の軟X線発光角度異方性の研究	倉橋 直也	東京大学物性研究所	宮脇 淳（量子科学技術研究開発機構）、張 文雄、山添 康介、UGALINO RALPH（東京大学）、木内 久雄	Study of soft X-ray emission angular anisotropy of gas phase	Naoya Kurahashi	The Institute for Solid State Physics, The University of Tokyo	Jun Miyawaki, Wenxiong Zhan, Kosuke Yamazoe, Ugalino Ralph, Hisao Kiuchi	原田
12	202112-SRBXG-0010	顕微分光による新規合金系熱電材料"FAST材"の電子状態解析II	高際 良樹	物質・材料研究機構	尾嶋 正治（東京大学）、永村 直佳、小嗣 真人（東京理科大学）、吉成 朝子（東京理科大学）、竹澤 伸吾（東京理科大学）、津田 俊輔	Electronic state analysis of earth-abundant Fe–Al–Si thermoelectric (FAST) materials using scanning photoelectron microscopy (II)	Yoshiki Takagiwa	National Institute for Materials Science	Masaharu Oshima, Naoka Nagamura, Masato, Kotsugi, Asako Yoshinari, Shingo Takezawa, Shunsuke Tsuda	原田
13	202112-SRBXG-0011	グラフェン/強誘電体ヘテロ構造の時間分解光電子分光研究	松田 巌	東京大学物性研究所	山本 達（東北大学）、堀尾 眞史	Time-resolved photoemission investigation of graphene-ferroelectric heterostructure	Iwao Matsuda	The Institute for Solid State Physics, The University of Tokyo	Susumu Yamamoto, Masafumi Horio	松田
14	202111-SRBXG-0014	フラーレンに内包された水分子の電子状態解析	橋川 祥史	京都大学化学研究所	倉橋 直也（東京大学物性研究所）、木内 久雄（東京大学物性研究所）、貞井 俊平（京都大学）	Analysis of Electronic Configuration for a Water Molecule Encapsulated inside a Fullerene	Yoshifumi Hashikawa	Institute for Chemical Research, Kyoto University	Naoya Kurahashi, Hisao Kiuchi, Shunpei Sadai	原田
15	202112-SRBXG-0018	全固体リチウムイオン電池を用いた電極材料のオペランド軟X線発光分光 3	朝倉 大輔	産業技術総合研究所	細野 英司、石山 智大、小林 正起（東京大学）	Operando soft X-ray emission spectroscopy of electrode materials by using all-solid-state Li-ion battery 3	Daisuke Asakura	National Institute of Advanced Industrial Science and Technology	Eiji Hosono, Tomohiro Ishiyama, Masaki Kobayashi	原田
16	202112-SRBXG-0020	ニッケル錯体アニオン塩ベシクル膜と水和する中間水の軟X線電子状態解析	藤野 智子	東京大学物性研究所	伊藤 雅聡	Soft X-ray structural analysis of constrained water molecules on nickel-complex anion salt vesicles	Tomoko Fujino	The Institute for Solid State Physics, The University of Tokyo	Masatoshi Ito	原田
17	202112-SRBXG-0021	レーザー切断により作製したMoS2エッジ面および金属修飾面の電子状態と化学種のオペランド雰囲気光電子分光による研究	吉信 淳	東京大学物性研究所	向井 孝三、尾崎 文彦、田中 駿介	Operando ambient pressure X-ray photoelectron spectroscopy study of the electronic states and chemical properties of the clean and metal deposited MoS_2 edge planes fabricated by laser cutting	Jun Yoshinobu	The Institute for Solid State Physics, The University of Tokyo	Kozo Mukai, Fumihiko Ozaki, Tanaka Shunsuke	松田
18	202112-SRBXG-0024	その場光電子分光法によるリチウム過剰正極材料の熱挙動	張 文雄	東京大学物性研究所	朝倉 大輔（産業技術総合研究所）、細野 英司（産業技術総合研究所）、尾嶋 正治（東京大学）、永村 直佳（物質・材料研究機構）、木内 久雄	Thermal behavior of lithium-rich cathode material by in-situ photoemission spectroscopy	Zhang Wenxiong	The Institute for Solid State Physics, The University of Tokyo	Disuke Asakura, Eiji Hosono, Masaharu Oshima, Naoka Nagamura, Hisao Kiuchi	原田
19	202112-SRBXG-0025	酸化物界面における高移動度二次元キャリア気体の発現機構解明	小林 正起	東京大学大学院工学系研究科	武田 崇仁	Unveiling the mechanism of the appearance of high-mobility two-dimensional carrier gas states at an oxide SrTiO3 interface	Masaki Kobayashi	The University of Tokyo	Takahito Takeda	原田
20	202112-SRBXG-0029	Understanding the influence of surface charge induced by ultrafine water (UFW) on thereduction of the transepidermal water loss in the stratum corneum lipids by O K-edge XASand XES	Mustafa al Samarai	東京大学物性研究所		Understanding the influence of surface charge induced by ultrafine water (UFW) on the reduction of the transepidermal water loss in the stratum corneum lipids by O K-edge XAS and XES	Mustafa al Samarai	The Institute for Solid State Physics, The University of Tokyo		原田

21	202112-SRBXG-0031	Co 2p3d RIXSを用いた水酸化触媒用酸化コバルト電着自己修復薄膜の電子構造に対するFe添加効果の検討	Olaf Rudiger	Group Leader		Investigation of Fe Doping Effects on the Electronic Structure of Cobalt Oxide Electrodeposited Self-Repair Thin Films for Water Oxidation Catalysts using Co 2p3d RIXS	Olaf Rudiger	Max Planck Institute for Chemical Energy Conversation		原田

柏キャンパスE棟 / Laser and Synchrotron Radiation Laboratory in Kashiwa

No	課題番号	課題名	氏名	所属	分担者（共同研究者）	Title	Name	Organization	Member of reseach project	担当所員
1	202203-CMBXX-0067	トポロジカル絶縁体Bi2Te3薄膜におけるスピン軌道ダイナミクスの1研究	八田 振一郎	京都大学		Studying spin-orbit dynamics of topological insulator Bi2Te3 thin film	Shinichiro Hatta	Kyoto University		近藤　猛
2	202111-GNBXX-0024	Pb系トポロジカル絶縁体のスピン角度分解光電子分光	矢治 光一郎	物質・材料研究機構	永村直佳、津田俊輔	SARPES study of a Pb-based topological insulator	Koichiro Yaji	National Institute for Materials Science	Naoka Nagamura, Shunsuke Tsuda	近藤　猛
3	202111-GNBXX-0011	有機分子水素結合ネットワーク/貴金属界面におけるラシュバ分裂の増大	金井 要	東京理科大学	馬上怜奈	Enhancement of Rashba splitting on organic molecular hydrogen bond network/noble metal interface	Kaname Kanai	Tokyo University of Science	Reina Moue	近藤　猛
4	202112-GNBXX-0069	Zr3SnC2のスピン分解角度分光光電子分光	伊藤 孝寛	名古屋大学	杉本卓史、三田愛也	Spin- and Angle-resolved photoemission study of Zr3SnC2	Takahiro Ito	Nagoya University	takushi Sugimoto, Manaya Mita	近藤　猛
5	202112-GNBXX-0047	バルク敏感高分解能スピン分解角度分解光電子分光によるハーフメタル強磁性体La1-xSrxMnO3のNQP 状態の観測	横谷 尚睦	岡山大学	片岡範行、瀬戸口太朗	Observation of NQP state in half metal ferromagnet La1-xSrxMnO3 by bulksensitive high-resolution spin and angle resolved photoemissionspectroscopy	Takayoshi Yokoya	Okayama University	Noriyuki Kataoka, Taro Setoguchi	近藤　猛
6	所内	低エネルギー励起光電子強度分布における隠れたパラメータの探索	田中 宏明	東京大学物性研究所	川口海周	Unconventional angular distribution of photoemission intensity in low-energy angle-resolved photoemission spectroscopy	Hiroaki Tanaka	The Institute for Solid State Physics, The University of Tokyo	Kaishu Kawaguchi	近藤　猛
7	所内	Surface state spin polarization measurement of Co doped LaFeAsO	Huh Soonsang	東京大学物性研究所	森亮、川口海周	Surface state spin polarization measurement of Co doped LaFeAsO	Huh Soonsang	The Institute for Solid State Physics, The University of Tokyo	Ryo Mori, Kaishu Kawaguchi	近藤　猛
8	所内	トポロジカル絶縁体 Bi2Te3 薄膜におけるスピン偏極バンド構造の膜厚依存性	川口 海周	東京大学物性研究所	八田 振一郎（京都大学）	Thickness dependence of spin-polarized band structure in topological insulator Bi2Te3 thin films	Kaishu Kawaguchi	The Institute for Solid State Physics, The University of Tokyo	Shinichiro Hatta (Kyoto University)	近藤　猛
9	202205-GNBXX-0124	金属表面に形成された水素結合有機フレームワークによって誘起される量子井戸状態の直接観測	金井 要	東京理科大学	馬上怜奈	Direct observation of quantum well states induced by the hydrogen-bonded organic frameworks formed on metal surface	Kaname Kanai	Tokyo University of Science	Reina Moue	近藤　猛
10	202206-GNBXX-0128	Hex-Au(100)上グラフェンにおけるπバンドスピン構造の研究	伊藤 孝寛	名古屋大学	杉本卓史、保科 拓海、三田愛也、寺澤 知潮（日本原子力研究開発機構）、小山 正太郎、強 博文	Spin structure study of π band of Graphene on Hex-Au(100)	Takahiro Ito	Nagoya University	Takushi Sugimoto, Takumi Hoshina, Manaya Mita, Tomo-o Terasawa (JAEA), Shotaro Oyama, Bowen Qiang	近藤　猛

11	202206-GNBXX-0140	強磁性体基板上のグラフェンのスピン角度分解光電子分光	矢治 光一郎	物質・材料研究機構	永村直佳、津田俊輔、竹澤 伸吾（東京理科大学）、中村 友謙	SARPES study of graphene on ferromagnetic substrates	Koichiro Yaji	National Institute for Materials Science	Naoka Nagamura, Shunsuke Tsuda, Shingo Takezawa (Tokyo University of Science), Tomonori Nakamura	近藤　猛
12	202206-GNBXX-0138	4d強磁性酸化物SrRuO3薄膜における準粒子状態のスピン分極評価	小林 正起	東京大学	武田 崇仁	Elucidation of the spin polarization of the quasi-particle states in 4d ferromagnetic oxide SrRuO3	Masaki Kobayashi	The University of Tokyo	Takahito Takeda	近藤　猛
13	所内	Investigation of spin polarization of surface states in NbIrTe4	Huh Soonsang	東京大学物性研究所		Investigation of spin polarization of surface states in NbIrTe4	Huh Soonsang	The Institute for Solid State Physics, The University of Tokyo		近藤　猛

2022年度　スーパーコンピュータ共同利用課題一覧 / Joint Research List of Supercomputer System 2022

※採択課題一覧、所属は申請時のデータ

1. 第一原理計算 / First-Principles Calculation of Materials Properties

No.	課題番号	課題名	氏名	所属	Title	Name	Organization
1	2022-Ea-0007	密度汎関数理論と機械学習法による不均一触媒の動的過程の理論的研究	森川 良忠	大阪大学 大学院工学研究科 物理学系専攻	Theoretical study on dynamical processes in heterogeneous catalysis using density functional theory and machine learning methods	Yoshitada Morikawa	Department of Precision Engineering, Graduate School of Engineering, Osaka University
2	2022-Ea-0008	密度汎関数理論による物性予測	杉野 修	東京大学物性研究所	Prediction of material properties using the density functional theory	Osamu Sugino	Institute for Solid State Physics, University of Tokyo
3	2022-Ea-0003	量子論大規模計算による半導体薄膜成長とデバイス界面形成の微視的機構解明	押山 淳	名古屋大学未来材料・システム研究所	Clarification of Microscopic Mechanisms of Semiconductor Epitaxial Growth and Device-Interface Formation by Large-Scale Quantum-Theory-Based Computations	Atsushi Oshiyama	Institute of Materials and Systems for Sustainability
4	2022-Ea-0010	第一原理基高速計算フレームワークによる不規則材料系の構造・物性相関の解明	笠松 秀輔	山形大学学術研究院	Understanding structure-property relationships of disordered materials using first-principles based high-throughput simulation framework	Shusuke Kasamatsu	Academic Assembly, Yamagata University
5	2022-Ca-0065	表面、界面、欠陥等の複雑構造における原子構造と原子ダイナミク スに関する解析	渡邊 聡	東京大学大学院工学系研究科マテリアル工学専攻	Analyses related to atomic structures and atom dynamics at complex structures such as surfaces, interfaces and defects	Satoshi Watanabe	Department of Materials Engineering, School of Engineering, The University of Tokyo
6	2022-Ca-0095	第一原理電子状態・輸送特性計算コードRSPACEの開発と高機能界面のデザイン	小野 倫也	神戸大学大学院工学研究科電気電子工学専攻	Development of first-principles calculation code RSPACE and design of highly functional interface	Tomoya Ono	Department of Electrical and Electronic Engineering, Graduate School of Engineering, Kobe University
7	2022-Cb-0043	第一原理電子状態･輸送特性計算コードRSPACEの開発と高機能界面のデザイン	小野 倫也	神戸大学大学院工学研究科電気電子工学専攻	Development of first-principles calculation code RSPACE and design of highly functional interface	Tomoya Ono	Department of Electrical and Electronic Engineering, Graduate School of Engineering, Kobe University
8	2022-Ca-0049	三元系最密充填構造に基づく新物質探索	尾崎 泰助	東京大学物性研究所	Computational materials discovery based on densest ternary sphere packings	Taisuke Ozaki	Institute for Solid State Physics, The University of Tokyo
9	2022-Cb-0015	CeO2(100)面上でのWater-splittingによる水素生成	横 哲	東北大学材料科学高等研究所	Hydrogen production by water splitting on CeO2 (100) facet	Akira Yoko	WPI-AIMR, Tohoku University
10	2022-Cb-0051	原子層状物質における大規模電子輸送特性についての第一原理研究	江上 喜幸	北海道大学大学院工学研究院	First-principles study on electron-transport properties of large scale atomic layered materials	Yoshiyuki Egami	Faculty of Engineering, Hokkaido University
11	2022-Ca-0006	磁気異方性の界面歪みと界面電気分極による制御	合田 義弘	東京工業大学物質理工学院材料系	Control of magnetic anisotropy by strain and electric polarization at interfaces	Yoshihiro GOHDA	Department of Materials Science and Engineering, Tokyo Institute of Technology
12	2022-D-0001	ポリマーの多階層物理と深層学習を掛け合せたスーパーコンポジット電気絶縁材料の創成	佐藤 正寛	東京大学大学院工学系研究科	Discovery of Super-Composite Electrical Insulating Materials Based on Multiscale Physics and Deep Learning of Polymers	Masahiro Sato	Dept. of Eng., The University of Tokyo
13	2022-Ca-0103	光応答性機能材料の第一原理的研究	常行 真司	東京大学大学院理学系研究科物理学専攻	First-principle study of photoresponsive functional materials	Shinji Tsuneyuki	Department of Physics, University of Tokyo
14	2022-Ca-0059	2次元層状ヘテロ構造における第一原理電子輸送特性研究	江上 喜幸	北海道大学大学院工学研究院	First-principles electron-transport study on 2D layered material-based heterostructures	Yoshiyuki Egami	Faculty of Engineering, Hokkaido University
15	2022-Cb-0044	異常ホール効果を計算する正確で効率的な方法の開発	石井 史之	金沢大学ナノマテリアル研究所	Development of an accurate and efficient method for calculating the anomalous Hall effect	Fumiyuki Ishii	Kanazawa University
16	2022-Cb-0001	光起電力応用ナノクリスタルの第一原理計算による研究	ビュクール マリウス	国立研究開発法人産業技術総合研究所	First-principles computational study of nanocrystals for photovoltaic applications	Marius Buerkle	National Institute of Advanced Industrial Science and Technology
17	2022-Ca-0024	スピン注入磁化反転型磁気抵抗メモリ(STT-MRAM)の第一原理計算による研究	白石 賢二	名古屋大学　未来材料・システム研究所	First Principles Studies on Spin Tranfer Torque Magnetic Randum Access Memory (STT-MRAM)	Kenji Shiraishi	Institute of Materials and Systems for Sustainability, Nagoya University
18	2022-Ca-0040	格子振動に由来する負熱膨張材料の機構解明と設計指針創出	望月 泰英	東京工業大学物質理工学院	Elucidation and design principle of negative thermal expansion originating from lattice vibration	Yasuhide Mochizuki	School of Materials and Chemical Technology, Tokyo Institute of Technology
19	2022-Ca-0051	高圧力下における共有結合性液体･ガラスの構造と電子状態の第一原理計算	下條 冬樹	熊本大学大学院先端科学研究部	First-Principles Molecular-Dynamics Study of Structural and Electronic Properties of Covalent Liquids and Glasses under Pressure	Fuyuki Shimojo	Department of Physics, Kumamoto University

20	2022-Ca-0091	第一原理計算に基づく熱機能材料の開発	塩見 淳一郎	東京大学工学系研究科	Development of Thermal Functional Materials Based on First-principles Simulations	Junichiro Shiomi	School of Engineering, The University of Tokyo
21	2022-Ea-0011	第一原理計算に立脚したグリーンデバイスの提案：材料探索からデバイス作製まで	松下 雄一郎	東京工業大学	Proposal for Green Devices Based on First-Principles Calculations: From Material Exploration to Device Fabrication	Yu-ichiro Matsushita	Tokyo Institute of Technology
22	2022-Ca-0104	大規模第一原理電気伝導計算法による量子伝導理論	小林 伸彦	筑波大学 数理物質系　物理工学域	Quantum transport theory by large scale first-principles electron transport calculations	Nobuhiko Kobayashi	Department of Applied Physics, University of Tsukuba
23	2022-Cb-0030	燃料電池電極触媒とギ酸分解触媒の省貴金属化	坂口 紀史	北海道大学大学院工学研究院　附属エネルギー・マテリアル融合領域研究センター	Reduction of Rare Metals in Fuel Cell and Formic Acid Decomposition Catalysts	Norihito Sakaguchi	Center for Advanced Research of Energy and Materials, Faculty of Engineering, Hokkaido University
24	2022-Cb-0029	金属酸化物のプラズマ耐性に関する研究	浜口 智志	大阪大学工学研究科	Study on plasma resistance of metal oxides	Satoshi Hamaguchi	Graduate School of Engineering, Osaka University
25	2022-Ca-0027	第一原理分子動力学法に基づくガラスの静的構造に関する機械学習を用いた研究	高良 明英	熊本大学技術部	Machine learning study on static structure of glass materials based on {\it ab initio} molecular dynamics	Akihide Koura	Technical Division, Kumamoto University
26	2022-Ca-0043	電子論と古典溶液理論による界面反応の第一原理シミュレーション	大谷 実	筑波大学計算科学研究センター	First-principles simulation of interfacial reactions using density functional theory and classical liquid theory	Minoru Otani	Center for Computational Sciences, The University of Tsukuba
27	2022-Ca-0074	電場下の半導体pn接合界面でのトンネル電流の理論：第一原理計算に基づく研究	中山 隆史	千葉大学理学部物理学科	Theory of tunneling currents at semiconductor pn junctions in electric fields based on first-principles calculation	Takashi Nakayama	Department of Physics, Chiba University
28	2022-Cb-0010	第一原理計算による電子--フォノン結合を考慮した有機結晶のバンド計算	柳澤 将	琉球大学理学部物質地球科学科物理系	First-principles bandstructure calculation of organic crystals with the electron-phonon coupling	Susumu Yanagisawa	Department of Physics and Earth Sciences, Faculty of Science, University of the Ryukyus
29	2022-D-0005	第一原理計算を用いた熱伝導度データベース作成	中村 和磨	九州工業大学	Construction of thermal conductivity database from first principles	Kazuma Nakamura	Kyushu Institute of Technology
30	2022-Cb-0038	第一原理計算に基づく熱機能材料の開発	塩見 淳一郎	東京大学工学系研究科	Development of Thermal Functional Materials Based on First-principles Simulations	Junichiro Shiomi	School of Engineering, The University of Tokyo
31	2022-Cb-0031	高効率な酸素吸蔵材料と水素遮蔽材料の探索	國貞 雄治	北海道大学大学院工学研究院　附属エネルギー・マテリアル融合領域研究センター	Development of Efficient Oxygen Storage Materials and Hydrogen Permeation Barrier Materials	Yuji Kunisada	Center for Advanced Research of Energy and Materials, Faculty of Engineering, Hokkaido University
32	2022-Ca-0087	全電子混合基底法プログラムの改良と応用	大野 かおる	横浜国立大学大学院工学研究院	Improvement and application of all-electron mixed basis program	Kaoru Ohno	Graduate School of Engineering, Yokohama National University
33	2022-Ca-0107	原子層・トポロジカル物質の熱電性の第一原理計算	石井 史之	金沢大学ナノマテリアル研究所	First-principles calculation of thermoelectric properties in atomic-layer and topological materials	Fumiyuki Ishii	Kanazawa University
34	2022-Cb-0020	フラッシュメモリ応用を目指したSi-richアモルファスSiNの第一原理計算による研究	白石 賢二	名古屋大学　未来材料・システム研究所	First Principles Studies on Si-rich a-SiN for Flash Memory Application	Kenji Shiraishi	Institute of Materials and Systems for Sustainability, Nagoya University
35	2022-Cb-0024	密度汎関数理論を用いた金属表面上における分子吸着と反応の研究	濱田 幾太郎	大阪大学大学院工学研究科　物理学系専攻　精密工学コース	Density functional theory study of adsorption and reaction of molecules on metal surfaces	Ikutaro Hamada	Department of Precision Engineering, Graduate School of Engineering, Osaka University
36	2022-Ca-0008	人工ニューラルネットワーク力場を用いた多成分複雑系に対する熱伝導度計算	島村 孝平	熊本大学大学院先端科学研究部	Thermal Conductivity calculation with ANN potential for multi-component heterogeneous materials	Kohei Shimamura	Faculty of Advanced Science and Technology, Kumamoto University
37	2022-Ca-0120	第一原理による特異原子構造探索	幾原 雄一	東京大学大学院工学系研究科総合研究機構	Exploring singular atomic arrangements via first-principles calculations	Yuichi Ikuhara	Institute of Engineering Innovation, University of Tokyo
38	2022-Ca-0005	粒界－転位相互作用の微視的機構の解明に向けた高精度な機械学習型原子間ポテンシャルと大規模分子シミュレーション法の確立	横井 達矢	名古屋大学大学院工学研究科　物質科学専攻	High-accuracy machine-learning interactomic potential and massively large-scale molecular simulation for miscroscopic mechanisms of grain-boundary-dislocation interactions	Tatsuya Yokoi	Department of Materials Physics, Nagoya University

39	2022-Ca-0054	金属酸化物のプラズマ耐性に関する研究	浜口 智志	大阪大学工学研究科	Study on plasma resistance of metal oxides	Satoshi Hamaguchi	Graduate School of Engineering, Osaka University
40	2022-Ca-0061	結晶構造探索手法の開発と物質探索	山下 智樹	長岡技術科学大学	Development of crystal structure prediction method and material search	Tomoki Yamashita	Nagaoka University of Technology
41	2022-Ca-0115	モット絶縁体のキャリアドーピングの第一原理計算	レービガー ハンネス	横浜国立大学　大学院工学研究院　物理工学コース	First Principles calculation of carrier doping in Mott Insulators	Hannes Raebiger	Depertment Physics, Yokohama National University
42	2022-Ca-0010	準フォノニック結晶によるナノ熱輸送の究極の抑制	LIAO YUXUAN	東京大学機械工学専攻	Ultimate Suppression of Nanoheat Transport with Quasi-phononic Crystal	YUXUAN LIAO	Department of Mechanical Engineering, the University of Tokyo
43	2022-Ca-0047	熱活性化遅延蛍光分子の光学特性調査	野口 良史	静岡大学工学部	Investigation on optical properties of TADF molecules	Yoshifumi Noguchi	Graduate School of Engineering, Shizuoka University
44	2022-Ca-0016	磁性元素を含む材料表面・界面ナノ構造に関する第一原理的研究	立津 慶幸	名桜大学	Ab-initio research on nano structures of materials' surfaces and grain boundaries with magnetic elements	Yasutomi Tatetsu	Meio University
45	2022-Cb-0018	高機能スピントロニクス磁性材料の電子・磁気構造解析および準粒子自己無撞着GW法の並列化開発	小田 竜樹	金沢大学理工研究域数物科学系	Analyses on electronic and magnetic structure and parallelization development in quasi-particle self-consistent GW code	Tatsuki Oda	Faculty of Mathematics and Physics, Institute of Science and Engineering, Kanazawa University
46	2022-Cb-0047	機械学習ベースの熱機能材料用に最適化されたポリマー	許 斌	東京大学大学院機械工学専攻	Machine learning based optimized polymer for thermal function materials	Xu Bin	Department of Mechanical Engineering, The University of Tokyo
47	2022-Ca-0088	ナノグラフェン・デバイスにおける量子効果の理論的研究	草部 浩一	兵庫県立大学大学院理学研究科	Theoretical study of quantum effects in nanographene devices	Koichi Kusakabe	Graduate School of Science, University of Hyogo
48	2022-Eb-0005	第一原理計算に立脚したグリーンデバイスの提案：材料探索からデバイス作製まで	松下 雄一郎	東京工業大学	Proposal for Green Devices Based on First-Principles Calculations: From Material Exploration to Device Fabrication	Yu-ichiro Matsushita	Tokyo Institute of Technology
49	2022-Ca-0078	密度汎関数法と溶液理論を用いた電気化学反応の解析 4	春山 潤	東京大学物性研究所	Electrochemical reaction analysis using density functional calculation + implicit solvation model 4	Jun Haruyama	Institute for Solid State Physics, The University of Tokyo
50	2022-Ca-0086	密度汎関数理論を用いた分子・金属界面の研究	濱田 幾太郎	大阪大学大学院工学研究科　物理学系専攻　精密工学コース	Density functional theory study of molecule/metal interfaces	Ikutaro Hamada	Department of Precision Engineering, Graduate School of Engineering, Osaka University
51	2022-Ca-0026	新規蓄電デバイス材料の構造・電子状態に関する理論的解析	山田 淳夫	東京大学工学系研究科	Theoretical Analysis on Structure/Electronic State of Novel Energy Storage Materials	Atsuo Yamada	Faculty of Engineering, The University of Tokyo
52	2022-Ca-0118	エネルギー貯蔵用途のためのイオン液体の機械学習最適化	邵 成	東京大学機械工学塩見研究室	Machine-learning optimization of ionic liquids for energy storage application	Cheng Shao	Shiomi Lab, Mechanical engineering, The University of Tokyo
53	2021-D-0008	π電子－プロトン相関型分子性導体群の圧力下構造及び電子状態の系統的予測	出倉 駿	東北大学多元物質科学研究所	Systematic elucidation of structure and electronic state of π-electron-proton coupled molecular conductors under pressure	Shun Dekura	Institute of Multidisciplinary Research for Advanced Materials, Tohoku University
54	2022-Ca-0058	遷移電流密度を用いた非線形光学応答の第一原理的解析	佐藤 駿丞	筑波大学計算科学研究センター	First-principles analysis for nonlinear optical responses based on the transition current density	Shunsuke Sato	Center for Computational Sciences, University of Tsukuba
55	2022-Ca-0063	新奇トポロジカル物質の第一原理設計および異常ホール伝導度の評価	山内 邦彦	大阪大学工学研究科	First-principles design of novel topological materials and evaluation of anomalous Hall conductivity	Kunihiko Yamauchi	Graduate School of Engineering Osaka University
56	2022-Ca-0004	グラフェン層数に依存する水/グラフェン界面構造の理論研究	大戸 達彦	名古屋大学大学院工学研究科	First-principles study on the structure of water/graphene interfaces depending on the number of graphene layers	Tatsuhiko Ohto	Graduate School of Engineering, Nagoya University
57	2022-Ca-0019	高効率な酸素吸蔵材料と水素遮蔽材料の探索	國貞 雄治	北海道大学大学院工学研究院　附属エネルギー・マテリアル融合領域研究センター	Development of Efficient Oxygen Storage Materials and Hydrogen Permeation Barrier Materials	Yuji Kunisada	Center for Advanced Research of Energy and Materials, Faculty of Engineering, Hokkaido University

58	2022-Ca-0029	第一原理計算による有限温度下での電子--フォノン結合を考慮したバンド計算	柳澤 将	琉球大学理学部物質地球科学科物理系	First-principles band structure calculation with the electron-phonon coupling at finite temperature	Susumu Yanagisawa	Department of Physics and Earth Sciences, Faculty of Science, University of the Ryukyus
59	2022-Ca-0108	金属酸化物ナノクラスターの構造物性に関する理論計算	横 哲	東北大学材料科学高等研究所	Theoretical study for structure and property of metal oxide nanoclusters	Akira Yoko	WPI-AIMR, Tohoku University
60	2022-Cb-0036	フォノンデータベースを利用した熱機能材料の開発	大西 正人	東京大学機械工学専攻	Development of Thermal Materials Using Phonon Database	Masato Ohnishi	Department of Mechanical Engineering, The University of Tokyo
61	2022-Ca-0018	燃料電池電極触媒とギ酸分解触媒の省貴金属化	坂口 紀史	北海道大学大学院工学研究院　附属エネルギー・マテリアル融合領域研究センター	Reduction of Rare Metals in Fuel Cell and Formic Acid Decomposition Catalysts	Norihito Sakaguchi	Center for Advanced Research of Energy and Materials, Faculty of Engineering, Hokkaido University
62	2022-Ca-0070	機械学習を用いた環境発電用ポリマーエレクトレット材料の開発	鈴木 雄二	東京大学大学院工学系研究科機械工学専攻	Development of Polymer Electret Materials for Energy Harvesting Using Machine Learning	Yuji Suzuki	Dept. of Mechanical Engineering, The University of Tokyo
63	2022-Ca-0094	第一原理計算によるナノ物質の構造・機能の解明と予測	武次 徹也	北海道大学大学院理学研究院化学部門	Ab initio study on the structure and functions of nanomaterials	Tetsuya Taketsugu	Department of Chemistry, Faculty of Science, Hokkaido University
64	2022-Ca-0062	第一原理計算による有機強誘電体・圧電体の物性予測	石橋 章司	産業技術総合研究所	Prediction of properties of organic ferroelectrics and piezoelectrics by first-principles calculation	Shoji Ishibashi	National Institute of Advanced Industrial Science and Technology
65	2022-Ca-0125	第一原理分子動力学法を用いた固体酸化物触媒の機能解明	中山 哲	東京大学大学院工学系研究科化学システム工学専攻	First-principles molecular dynamics study for metal-oxide catalysis	Akira Nakayama	Department of Chemical System Engineering, The University of Tokyo
66	2022-Ca-0011	第一原理計算による光熱変換原理の解明	江目 宏樹	山形大学	Study of the principle of photothermal conversion by ab initio calculations	Hiroki Gonome	Yamagata University
67	2022-Ca-0090	フォノンデータベースを利用した熱機能材料の開発	大西 正人	東京大学機械工学専攻	Development of Thermal Materials Using Phonon Database	Masato Ohnishi	Department of Mechanical Engineering, The University of Tokyo
68	2022-Ca-0014	高機能スピントロニクス磁性材料の電子・磁気構造解析および準粒子自己無撞着GW法の並列化開発	小田 竜樹	金沢大学理工研究域数物科学系	Analyses on electronic and magnetic structure and parallelization development in quasi-particle self-consistent GW code	Tatsuki Oda	Faculty of Mathematics and Physics, Institute of Science and Engineering, Kanazawa University
69	2022-Cb-0008	第一原理計算による光熱変換原理の解明	江目 宏樹	山形大学	Study of the principle of photothermal conversion by ab initio calculations	Hiroki Gonome	Yamagata University
70	2021-D-0006	第一原理計算による銀(111)表面上ヘリセン吸着構造の数値的研究	濱本 雄治	大阪大学 大学院工学研究科 物理学系専攻	First principles study of the adsorption structure of helicene on the Ag(111) surface	Yuji Hamamoto	Department of Precision Engineering, Osaka University
71	2022-Ca-0084	多色レーザー場による誘電体光吸収の第一原理シミュレーション	篠原 康	東京大学工学系研究科附属光量子科学研究センター	First-principles simulations for optical absorption of dielectrics under multi-color laser field	Yasushi Shinohara	Photon Science Center, School of Engineering, the University of Tokyo
72	2022-Cb-0048	機械学習を用いた環境発電用ポリマーエレクトレット材料の開発	鈴木 雄二	東京大学大学院工学系研究科機械工学専攻	Development of Polymer Electret Materials for Energy Harvesting Using Machine Learning	Yuji Suzuki	Dept. of Mechanical Engineering, The University of Tokyo
73	2022-Ca-0119	ガウス過程回帰による銀(111)表面上シリセン安定構造の大域的探索	濱本 雄治	大阪大学 大学院工学研究科 物理学系専攻	Global search for metastable structures of silicene on the Ag(111) surface by Gaussian process regression	Yuji Hamamoto	Department of Precision Engineering, Osaka University
74	2022-Cb-0052	第一原理計算に基づく多層膜の安定性および物性評価	中村 和磨	九州工業大学	Ab initio calculations for structural stability and property of multilayer system	Kazuma Nakamura	Kyushu Institute of Technology
75	2022-Ca-0007	触媒表面基準RuTi合金触媒のメカニズム解明	BUI VANPHO	大阪大学大学院工学研究科	Study on the catalytic mechanism of RuTi alloy in catalyst referred etching method	VANPHO BUI	Graduate School of Engineering, Osaka University
76	2022-Ca-0089	第一原理計算による白金ナノ粒子の酸化・硫化の研究	佐々木 岳彦	東京大学　大学院新領域創成科学研究科	Study on oxidation and sulfurization of platinum nanoparticles	Takehiko Sasaki	Graduate School of Frontier Sciences, The University of Tokyo
77	2022-Cb-0045	非従来型分子性導体Cat-TTF類縁体におけるπ電子ープロトン相関物性の解明に向けた電子相関パラメータの第一原理計算	出倉 駿	東北大学多元物質科学研究所	First-principles calculations of electron correlation parameters to elucidate π-electron-proton coupled physical properties of the unconventional molecular conductors Cat-TTF analogues	Shun Dekura	Institute of Multidisciplinary Research for Advanced Materials, Tohoku University

78	2022-Ca-0124	2次元金属有機構造体および層状半導体の吸着状態と超高速動力学	首藤 健一	横浜国立大学・工学部	Ultrafast adsorption states of two-dimensional metal-organic-frameworks and semiconductors	Ken-ichi Shudo	Yokohama Nat'l Univ.
79	2022-Ca-0066	電子状態計算による触媒における電荷移動反応メカニズムの解析	城塚 達也	茨城大学	Analyzing Reaction Mechanism of Charge Transfer in Catalysis by Electronic Structure Calcutions	Tatsuya Joutsuka	Ibaraki University
80	2022-Cb-0042	金属間化合物の表面原子構造と化学的特性に関する第一原理計算	野澤 和生	鹿児島大学理学部物理科学科	First-principles study of surface atomic structure and chemical properties of intermetallic compounds	Kazuki Nozawa	Department of Physics and Astronomy, Kagoshima University
81	2022-Ca-0053	第一原理計算を活用した分子性結晶におけるプロトン互変異性に基づく高速プロトン伝導機構解明	出倉 駿	東北大学多元物質科学研究所	Elucidation of the mechanism of fast proton conduction based on proton tautomerism in molecular crystals by using first-principles calculations	Shun Dekura	Institute of Multidisciplinary Research for Advanced Materials, Tohoku University
82	2022-Ca-0020	照射損傷と格子間原子との相互作用の研究	大澤 一人	九州大学応用力学研究所	Study of interaction between radiation damage and interstitial atom	Kazuhito Ohsawa	Research Institute for Applied Mechanics, Kyushu University
83	2022-Ca-0021	不純物半導体の金属絶縁体転移のexponent puzzle	原嶋 庸介	奈良先端科学技術大学院大学	Exponent puzzle for metal-insulator transition in doped semiconductors	Yosuke Harashima	Nara Institute of Science and Technology
84	2022-Ca-0048	固体表面界面における構造的素励起の研究	影島 博之	島根大学大学院自然科学研究科	Study on structural elementary excitations at solid surfaces and interfaces	Hiroyuki Kageshima	Graduate School of Natural Science and Technology, Shimane University
85	2022-Ca-0077	電磁場と物質の相互作用の第一原理計算手法開発	加藤 洋生	東京大学光量子科学研究センター	Development of First Principles methods for Light-Matter Interaction	Hiroki Katow	Photon Science Center, the University of Tokyo
86	2022-Ca-0116	分子吸着表面上における波数空間分解光電子分光スペクトルの解析	二木 かおり	千葉大学	Analysis of wavenumber space-resolved photoelectron spectrum of molecules adsorbed on surface	Kaori Niki	Chiba University
87	2022-Cb-0025	鉄系材料表面におけるアンモニア分解反応機構のモデル化	李 敏赫	東京大学大学院工学系研究科機械工学専攻	Modeling of the Ammonia Decomposition Reaction on Iron-based Material Surfaces	Minhyeok Lee	Department of Mechanical Engineering, The University of Tokyo
88	2022-Ba-0046	第一原理LCPAO法を用いた大規模系におけるベリー位相を介した物性の効率的な評価手法の開発	山口 直也	金沢大学ナノマテリアル研究所	Development of Efficient Evaluation Methods of Berry-phase-mediated Physical Properties for Large Scale Systems Using the First-principles LCPAO Method	Naoya Yamaguchi	Nanomaterials Research Institute, Kanazawa University
89	2022-Ca-0113	光触媒Ba$_{2}$PrBiO$_{6}$の表面電子構造の研究	西館 数芽	岩手大学理工学部	Electronic structure investigation of the Ba$_{2}$PrBiO$_{6}$ photocatalyst	Kazume Nishidate	Faculty of Science and Engineering, IWATE University
90	2022-Cb-0026	ガウス過程回帰による銀(111)表面上シリセン安定構造の大域的探索	濱本 雄治	大阪大学 大学院工学研究科 物理学系専攻	Global search for metastable structures of silicene on the Ag(111) surface by Gaussian process regression	Yuji Hamamoto	Department of Precision Engineering, Osaka University
91	2022-D-0002	高熱伝導絶縁物質のための熱伝導率計算：第一原理計算	河野 翔也	九州工業大学	Thermal conductivity calculation for high thermal conductive insulator	Shoya Kawano	Kyushu Institute of Technology
92	2022-Bb-0001	第一原理量子輸送と深層学習を連携させ、仮想実験環境を構築	ビュクール マリウス	国立研究開発法人産業技術総合研究所	Combining first-principles quantum transport and deep learning to create a virtual experimental environment	Marius Buerkle	National Institute of Advanced Industrial Science and Technology
93	2022-Ba-0015	新たなナノスケール表面界面の電子物性に関する理論的研究	小林 功佳	お茶の水女子大学理学部物理学科	Theoretical study on electronic properties of new nanoscale surfaces and interfaces	Katsuyoshi Kobayashi	Department of Physics, Faculty of Science, Ochanomizu University
94	2022-Bb-0023	遷移金属炭窒化物の新規相探索	大久保 將史	早稲田大学	Exploration of transition-metal carbides and nitrides	Masashi Okubo	Waseda University
95	2022-Ca-0064	ナノカーボン系物質の原子構造・電子物性の解明	藤本 義隆	九州大学工学研究院	Atomic structures and electronic properties of nanocarbon-based materials	Yoshitaka Fujimoto	Faculty of Engineering, Kyushu University
96	2022-D-0006	ハイエントロピー合金と形状記憶合金の相平衡	御手洗 容子	東京大学新領域創成科学研究科	Phase equilibrium of high entropy alloys and shape memory alloys	Yoko Mitarai	Graduate School of Frontier Sciences, The University of Tokyo
97	2022-Ba-0008	表面合金データベース	小野 頌太	東北大学金属材料研究所	Surface Alloy Database	Shota Ono	Tohoku University
98	2022-Ba-0016	末端官能基を制御した層状遷移金属炭化物MXeneの電荷貯蔵機構	大久保 將史	早稲田大学	Charge storage mechanism of layered transition metal carbides with regulated terminal groups	Masashi Okubo	Waseda University

99	2022-Ba-0067	RSDFT計算による非接触原子間力顕微鏡で捉えた探針試料間に働く力の解析	新井 豊子	金沢大学	RSDFT calculation of the force acting between a tip and a sample detected by noncontact atomic force microscope	Toyoko Arai	Kanazawa University
100	2022-Bb-0011	ハイエントロピー合金の相安定性と力学特性	御手洗 容子	東京大学新領域創成科学研究科	Phase stability and mechanical properties of high-entropy alloys	Yoko Mitarai	Graduate School of Frontier Sciences, The University of Tokyo
101	2022-Bb-0015	第一原理計算を用いた金属とプラズマ処理したフッ素樹脂界面の接着メカニズムの解明	大久保 雄司	大阪大学大学院工学研究科	Clarification of atomistic mechanism application of process design for adhesion interface between metal and plasma-treated fluoropolymers using first principles calculation	Yuji Ohkubo	Graduate School of Engineering, Osaka University
102	2022-Bb-0009	しわ構造を持つグラフェンナノリボンの電子状態計算	有馬 健太	大阪大学 大学院 工学研究科	Calculation of electronic structures of graphene nanoribbons with wrinkles	Kenta Arima	Graduate School of Engineering, Osaka University
103	2022-Ba-0032	量子液晶の第一原理計算	池田 浩章	立命館大学理工学部物理科学科	first principles calculations in quantum liquid crystals	Hiroaki Ikeda	Department of Physics, Ritsumeikan University
104	2022-Ba-0035	ハイエントロピー合金の相変態	御手洗 容子	東京大学新領域創成科学研究科	Phase transformation of high-entropy alloys	Yoko Mitarai	Graduate School of Frontier Sciences, The University of Tokyo
105	2022-Ba-0058	ダイヤモンド表面のグラファイト化とその剥離プロセスの第一原理計算	稲垣 耕司	大阪大学大学院工学研究科	First-principles calculation of graphitization of diamond surface and its exfoliation process	Kouji Inagaki	Graduate Scool of Engineering, Osaka University
106	2022-Ba-0061	狭いバンドギャップを持つ有機電荷移動錯体半導体の計算機による探索	島田 敏宏	北海道大学　大学院工学研究院	Computational search for narrow bandgap organic charge transfer complex	Toshihiro Shimada	Faculty of Engineering, Hokkaido University
107	2022-Bb-0018	異方的結晶構造を有する磁性材料の解析	小幡 正雄	金沢大学理工研究域	Analysis of magnetic materials with anisotropic crystal structures	Masao Obata	Institute of Science and Engineering, Kanazawa University
108	2022-Ba-0039	Pb系トポロジカル絶縁体のバルク絶縁性向上を目指したドーパント探索	徳本 有紀	東京大学生産技術研究所	Exploring dopants aiming at achieving high bulk insulation in Pb-based topological insulators	Yuki Tokumoto	Institute of Industrial Science, The University of Tokyo
109	2022-Ba-0040	絶縁体的基底状態を有する希土類酸化物の振動・磁気特性に関する第一原理計算	牧野 哲征	福井大学遠赤外領域開発研究センター	Ab-inition calculations for vibrational and magnetic properties of rare-earth monooxides with insulating ground states	Takayuki Makino	Research Center for Development of Far-Infrared Region, University of Fukui
110	2022-Ba-0028	異方的結晶構造を持つ磁性体の解析	小幡 正雄	金沢大学理工研究域	Analysis of magnetic material with an anisotropic crystal structure	Masao Obata	Institute of Science and Engineering, Kanazawa University
111	2022-Ba-0042	d電子系およびｄ電子系化合物の電子構造とフェルミオロジー	眞榮平 孝裕	琉球大学　理学部	Electronic Structure and Fermiology of d- and f-electron compounds	Takahiro Maehira	Faculty of Science, University of the Ryukyus
112	2022-Ba-0002	触媒インフォマティクスに向けた複雑酸化物の表面酸素空孔の安定性評価	日沼 洋陽	産業技術総合研究所	Evaluating surface oxygen vacancy stablity in complicated oxides for catalyst informatics	Yoyo Hinuma	National Institute of Advanced Industrial Science and Technology
113	2022-Ba-0026	新奇ボロン系二次元物質BSの電子状態と類縁物質の設計	豊田 雅之	東京工業大学　理学院物理学系	Electronic Structure of Novel 2D Boron Monosulfide and Design of Related Materials	Masayuki Toyoda	Department of Physics, School of Science, Tokyo Institute of Technology
114	2022-Ba-0027	第一原理計算を用いた金属とプラズマ処理したフッ素樹脂界面の接着メカニズムの解明	大久保 雄司	大阪大学大学院工学研究科	Clarification of atomistic mechanism application of process design for adhesion interface between metal and plasma-treated fluoropolymers using first principles calculation	Yuji Ohkubo	Graduate School of Engineering, Osaka University
115	2022-Ba-0056	酸化チタンTiO$_{2}$表面の酸素欠陥の第一原理計算	河野 翔也	九州工業大学	First-principles calculation of oxygen defects on the surface of titanium dioxide TiO$_{2}$	Shoya Kawano	Kyushu Institute of Technology
116	2022-Ca-0030	金属間化合物の表面原子構造と化学的特性に関する第一原理計算	野澤 和生	鹿児島大学理学部物理科学科	First-principles study of surface atomic structure and chemical properties of intermetallic compounds	Kazuki Nozawa	Department of Physics and Astronomy, Kagoshima University
117	2022-Ca-0093	第一原理計算に基づく多層膜の安定性評価	中村 和磨	九州工業大学	Ab initio calculations for stability of multilayer sysmte	Kazuma Nakamura	Kyushu Institute of Technology

118	2022-Ba-0023	金属表面と磁性金属フタロシアニン分子の相互作用	有賀 哲也	京都大学理学研究科化学専攻	Interaction of magnetic metal phthalocyanines with metal surfaces	Aruga Tetsuya	Dept. Chem., School of Science, Kyoto University
119	2022-Ba-0050	固体表面・界面、ナノ構造体の新規電子物性の探索と実現	稲岡 毅	琉球大学理学部	Search and realization of novel electronic properties of surfaces and interfaces and of nanostructures	Takeshi Inaoka	Department of Physics and Earth Sciences, Faculty of Science, University of the Ryukyus
120	2022-Bb-0006	共役π電子系分子の面内相互作用	有賀 哲也	京都大学理学研究科化学専攻	In-plane interaction of conjugated molecules	Aruga Tetsuya	Dept. Chem., School of Science, Kyoto University
121	2022-Ba-0001	金属表面上における有機ハロゲン分子およびその反応生成物に関するDFT計算	塚原 規志	群馬工業高等専門学校	DFT calculations of organic halogen molecules and their reaction products on metal surfaces	Noriyuki Tsukahara	National Institute for Technology, Gunma College
122	2022-Bb-0012	グラフェン基板上の2D金属の安定構造	小野 頌太	東北大学金属材料研究所	Stable structure of 2D metals on graphene substrate	Shota Ono	Tohoku University
123	2022-A-0001	光起電力応用ナノクリスタルの第一原理計算による研究	ビュクール マリウス	国立研究開発法人産業技術総合研究所	First-principles computational study of nanocrystals for photovoltaic applications	Marius Buerkle	National Institute of Advanced Industrial Science and Technology
124	2022-A-0002	第一原理計算によるメタン変換触媒の理論的研究	辻 雄太	九州大学総合理工学研究院	Theoretical study of methane conversion catalysts by first-principles calculations	Yuta Tsuji	Faculty of Engineering Sciences, Kyushu University
125	2022-A-0006	ハイパーマテリアルのバンド計算	竹森 那由多	大阪大学	Band calculation of hypermaterials	Nayuta Takemori	Osaka University
126	2022-A-0008	固体中・表面上でのジラジカル状態に関する理論研究	多田 幸平	国立研究開発法人　産業技術総合研究所	Theoretical study for diradicals in solids and on surfaces	Kohei Tada	National Institute of Advanced Industrial Science and Technology (AIST)
127	2022-A-0014	水和イオン液体の電子状態	高橋 修	広島大学大学院理学研究科	Electronic structure of aqueous ionic liquids	Osamu Takahashi	Graduate School of Science, Hiroshima University
128	2022-A-0024	量子化学計算によるポリマー設計	山本 小夜子	九州大学	Polymer Design by Quantum Chemical Calculation	Sayoko Yamamoto	Kyushu University

2. 強相関 / Strongly Correlated Quantum Systems

No.	課題番号	課題名	氏名	所属	Title	Name	Organization
1	2022-Eb-0001	遷移金属酸化物高温超伝導物質の網羅的第一原理計算	今田 正俊	早稲田大学理工学術院	Systematic ab initio studies on high temperature superconductivity of transition metal oxides	Masatoshi Imada	Research Institute for Science and Engineering, Waseda University
2	2022-Ea-0004	長距離クーロン相互作用が導くキタエフ量子スピン液体候補における相競合	山地 洋平	物質・材料研究機構	Phase competition induced by long-range Coulomb interactions in candidate materials of Kitaev's quantum spin liquid	Youhei Yamaji	National Institute for Materials Science
3	2022-Ea-0006	分光実験データと高精度大規模数値計算を組み合わせた強相関電子系のための統合分光研究	今田 正俊	早稲田大学理工学術院	Integrated spectroscopic studies by combining experimental data and high precision large-scale computation for strongly correlated electrons	Masatoshi Imada	Research Institute for Science and Engineering, Waseda University
4	2022-Cb-0013	第一原理計算と機械学習を援用した強相関トポロジカル物性の理論研究	求 幸年	東京大学大学院工学系研究科	Theoretical study of strongly-correlated topological phenomena by exploiting first-principles calculations and machine learning	Yukitoshi Motome	Department of Applied Physics, The University of Tokyo
5	2022-Ca-0056	第一原理計算と機械学習を援用した強相関トポロジカル物性の理論研究	求 幸年	東京大学大学院工学系研究科	Theoretical study of strongly-correlated topological phenomena by exploiting first-principles calculations and machine learning	Yukitoshi Motome	Department of Applied Physics, The University of Tokyo
6	2022-Ca-0098	擬一次元的電子状態を有する銅酸化物超伝導体の理論研究	黒木 和彦	大阪大学	Theoretical studies on cuprate superconductors with quasi-one-dimensional electronic structure	Kazuhiko Kuroki	Osaka University
7	2022-Ca-0068	多軌道強相関物質における非局所電子相関の研究	野村 悠祐	慶應義塾大学	Study on nonlocal correlations in multi-orbital strongly-correlated materials	Yusuke Nomura	Keio University
8	2022-Ca-0082	強相関電子系における動的感受率の第一原理計算	品岡 寛	埼玉大学理学部物理学科	First-principles calculations of dynamical susceptibilities for strongly correlated materials	Hiroshi Shinaoka	Department of Physics, Saitama University
9	2022-Ca-0015	光励起された一次元モット絶縁体の過渡吸収スペクトル	遠山 貴己	東京理科大学理学部応用物理学科	Transient absorption spectrum in photo-excited one-dimensional Mott insulator	Takami Tohyama	Department of Applied Physics, Tokyo University of Science

10	2022-Ca-0071	ホルミウムイオンに創出する3チャンネル近藤効果の研究	堀田 貴嗣	東京都立大学理学研究科物理学専攻	Research of Three-Channel Kondo Effect Emerging from Holmium Ions	Takashi Hotta	Department of Physics, Graduate School of Science, Tokyo Metropolitan University
11	2022-Ca-0012	トポロジカル磁性における光誘起現象の開拓	望月 維人	早稲田大学先進理工学部応用物理学科	Research for photoinduced phenomena in topological magnets	Masahito Mochizuki	Waseda university
12	2022-Cb-0014	磁性金属における光誘起トポロジカル電子状態の探索	望月 維人	早稲田大学先進理工学部応用物理学科	Research on photoinduced topological electronic states in metallic magnets	Masahito Mochizuki	Waseda university
13	2022-Ca-0045	近藤格子における強相関現象	ピータース ロバート	京都大学	Correlation induced phenomena in Kondo lattice systems	Robert Peters	Kyoto University
14	2022-Ca-0034	EDXTオリゴマー電荷移動塩の電子構造解析：分子内・分子間クーロン反発エネルギーの算出	藤野 智子	東京大学物性研究所	Electronic structures of EDXT oligomers in charge transfer salts: estimation of intramolecular and intermolecular Coulomb repulsion energy	Tomoko Fujino	Institute for Solid State Physics, The University of Tokyo
15	2022-Ba-0009	有機ディラック電子系における秩序状態の系統的解明	小林 晃人	名古屋大学　大学院理学研究科	Systematic elucidation of ordered states in organic Dirac electron systems	Akito Kobayashi	Graduate School of Science, Nagoya University
16	2022-Ba-0021	多バンド模型を用いた銅酸化物高温超伝導体の統一的記述	渡部 洋	立命館大学	Unified description of cuprate high-temperature superconductors using multiband models	Hiroshi Watanabe	Ritsumeikan University
17	2022-Bb-0017	強相関電子系の電子状態の数値的研究	柳沢 孝	産業技術総合研究所	Numerical study of electronic states of strongly correlated electron systems	Takashi Yanagisawa	National Institute of Advanced Industrial Science andTechnology
18	2022-Ba-0055	ホイスラー化合物の熱電性能に関する理論的研究：弱結合理論からのアプローチ	西口 和孝	神戸大学大学院システム情報学研究科	Theoretical study of thermoelectric properties in Heusler compounds: A weak-coupling approach	Kazutaka Nishiguchi	Graduate School of System Informatics, Kobe University
19	2022-Ba-0049	強相関電子系の電子状態の数値的研究	柳沢 孝	産業技術総合研究所	Numerical study of electronic states in strongly correlated electron systems	Takashi Yanagisawa	National Institute of Advanced Industrial Science andTechnology
20	2022-Ba-0036	遍歴磁性体における光誘起非平衡ダイナミクス	小野 淳	東北大学大学院理学研究科	Photoinduced nonequilibrium dynamics in itinerant magnets	Atsushi Ono	Department of Physics, Tohoku University
21	2022-A-0016	強磁性ドメイン壁の電流駆動による創発電場の数値計算	賀川 史敬	東京工業大学	Emergent Electric Field induced by current-driven ferromagnetic domain walls	Fumitaka Kagawa	Tokyo Institute of Technology

3. 巨視系の協同現象 / Cooperative Phenomena in Complex, Macroscopic Systems

No.	課題番号	課題名	氏名	所属	Title	Name	Organization
1	2022-Eb-0002	古典・量子統計力学モデルにおけるループ気体表現とテンソルネットワーク計算	川島 直輝	東京大学物性研究所	Loop-gas representation of classical and quantum statistical-mechanical models and its tensor-network calculation	Naoki Kawashima	Institute for Solid State Physics, University of Tokyo
2	2022-Ea-0001	全原子及び粗視化モデルによるソフトマターの大規模分子シミュレーション	篠田 渉	岡山大学異分野基礎科学研究所	Large-scale Molecular Simulation of Soft Materials using All-Atom and Coarse-Grained Model	Wataru Shinoda	Okayama University, Research Institute for Interdisciplinary Science
3	2022-Ea-0009	古典・量子統計力学モデルにおけるループ気体表現とテンソルネットワーク計算	川島 直輝	東京大学物性研究所	Loop-gas representation of classical and quantum statistical-mechanical models and its tensor-network calculation	Naoki Kawashima	Institute for Solid State Physics, University of Tokyo
4	2022-Eb-0003	全原子及び粗視化モデルによるソフトマターの大規模分子シミュレーション	篠田 渉	岡山大学異分野基礎科学研究所	Large-scale Molecular Simulation of Soft Materials using All-Atom and Coarse-Grained Model	Wataru Shinoda	Okayama University, Research Institute for Interdisciplinary Science
5	2022-Ca-0069	テンソルネットワークとサンプリングによる量子多体系のシミュレーション	藤堂 眞治	東京大学大学院理学系研究科物理学専攻	Simulation of quantum many-body systems by tensor network and sampling	Synge Todo	Department of Physics, University of Tokyo
6	2022-Ca-0039	生体膜の構造形成	野口 博司	東京大学物性研究所	structure formation of biomembrane	Hiroshi Noguchi	Institute for Solid State Physics, University of Tokyo
7	2022-Ca-0052	フラストレート磁性体の新規物性解明	大久保 毅	東京大学大学院理学系研究科知の物理学研究センター	Novel phenomena in frustrated magnets	Tsuyoshi Okubo	Institute for Physics of Intelligence, The University of Tokyo

8	2022-Cb-0050	分子動力学法を用いた界面構造の動的性質の解析	渡辺 宙志	慶応義塾大学理工学部	Molecular dynamics study of dynamic properties of interface structure	Hiroshi Watanabe	Faculty of Science and Technology Keio University
9	2022-Ca-0067	J1-J2フラストレートイジング模型の非平衡緩和解析	渡辺 宙志	慶応義塾大学理工学部	Non-equilibrium relaxation analysis on J1-J2 frustrated Ising model	Hiroshi Watanabe	Faculty of Science and Technology, Keio University
10	2022-Ca-0085	相転移を伴う複雑流体のマルチスケール流動シミュレーション	川勝 年洋	東北大学大学院理学研究科物理学専攻	Multiscale Flow Simulations on Complex Fluids Undergoing Phase Transition	Toshihiro Kawakatsu	epartment of Physics, Faculty of Science, Tohoku University
11	2022-Ca-0002	フラストレート磁性体における磁気スキルミオンを探索するための機械学習を併用した数値シミュレーション	速水 賢	北海道大学大学院理学研究院	Numerical simulations combined with machine learning to search for magnetic skyrmion in frustrated magnets	Satoru Hayami	Department of Physics, Hokkaido University
12	2022-Ca-0106	マルチスケールシミュレーションによる荷電リン脂質二重膜とイオン分布の相関	樋口 祐次	九州大学情報基盤研究開発センター	Correlation between the structure of charged phospholipid bilayer membrane and ion distribution by multi-scale simulation	Yuji Higuchi	Research Institute for Information Technology, Kyushu University
13	2022-Ca-0003	非エルミートランダム系の局在・非局在転移	大槻 東巳	上智大学理工学部	Localization-delocalization transition in non-Hermitian random system	Tomi Ohtsuki	Faculty of Science and Technology, Sophia University
14	2022-Ca-0100	相転移点近傍におけるスピンダイナミクスの大規模計算	諏訪 秀麿	東京大学大学院理学系研究科物理学専攻	Large-scale simulation of spin dynamics in the vicinity of a phase transition point	Hidemaro Suwa	Department of Physics, The University of Tokyo
15	2022-Cb-0012	フッ素樹脂の熱的・誘電特性に関するデータセットの構築	吉本 勇太	東京大学 大学院工学系研究科 機械工学専攻	Constructing a dataset of thermal and dielectric properties of fluoropolymers	Yuta Yoshimoto	Department of Mechanical Engineering, The University of Tokyo
16	2022-Cb-0034	自発的対称性の破れを伴う磁化プラトー	坂井 徹	兵庫県立大学大学院理学研究科	Magnetization Plateau with Spontaneous Symmetry Breaking	Toru Sakai	Graduate School of Science, University of Hyogo
17	2022-Cb-0049	荷電リン脂質二重膜と水分子の構造とダイナミクス	樋口 祐次	九州大学情報基盤研究開発センター	Structure and dynamics of charged phospholipid bilayer membrane and water molecules	Yuji Higuchi	Research Institute for Information Technology, Kyushu University
18	2022-Ca-0105	伸長流動下の高分子ダイナミクス	村島 隆浩	東北大学大学院理学研究科	Polymer Dynamics under Elongational Flow	Takahiro Murashima	東北大学大学院理学研究科
19	2022-Ca-0025	蛋白質物性に強く関与するソフトモードの効率的サンプリングシミュレー ション	北尾 彰朗	東京工業大学生命理工学院	Efficient sampling simulation of the soft modes significantly contribute to protein properties	Akio Kitao	Institute of Molecular and Cellular Biosciences,University of Tokyo
20	2022-Cb-0017	ゆらぎ交換近似を用いた有機電荷移動錯体の超伝導転移温度および超伝導対称性に関する研究	Jeschke Harald	岡山大学異分野基礎科学研究所	Fluctuation exchange approximation calculations for the superconducting transition temperatures and pairing symmetries of organic charge transfer salts	Harald Jeschke	Research Institute for Interdisciplinary Science Okayama University
21	2022-Cb-0028	機械学習ポテンシャルを用いた表面・界面・欠陥等の複雑構造における局所物性に関する解析	渡邉 聡	東京大学大学院工学系研究科マテリアル工学専攻	Analyses on local properties at complex structures such as surfaces, interfaces and defects via machine-learning potentials	Satoshi Watanabe	Department of Materials Engineering, School of Engineering, The University of Tokyo
22	2022-Ca-0060	広義のトポロジカル相とバルクエッジ対応の科学の数値的研究	初貝 安弘	筑波大学大学院数理物質科学研究科物理学専攻	Numerical studies for science of bulk-edge correspondence and topological phases	Yasuhiro Hatsugai	Institute of Physics, University of Tsukuba
23	2022-Ca-0036	キタエフ量子スピン液体におけるフラックス構造のマヨラナ励起への影響	古賀 昌久	東京工業大学	Effects of flux structures on Majorna excitations in Kitaev spin liquids	Akihisa Koga	Tokyo Institute of Technology
24	2022-Cb-0004	アクティブブラウン粒子系が示すモティリティ誘起相転移の数値的解析	中野 裕義	東京大学物性研究所	Numerical analysis of motility-induced phase transition in active Brownian particle system	Hiroyoshi Nakano	The Institute for Solid State Physics, The University of Tokyo
25	2022-Ca-0028	相界面の特異的性質と自由エネルギーの有限サイズ効果	中川 尚子	茨城大学理学部	Nontrivial properties of interface and finite size effects of free energies	Naoko Nakagawa	Department of Physics, Ibaraki University
26	2022-Ca-0041	分子動力学シミュレーションによる病気関連生体分子の研究	奥村 久士	自然科学研究機構生命創成探究センター	Molecular dynamics simulation of disease-related biomolecules	Hisashi Okumura	Exploratory Research Center on Life and Living Systems, Institute for Molecular Science
27	2022-Cb-0054	センサー材料のためのノイズを考慮した確率的量子混合計算シミュレーション	水上 渉	大阪大学 量子情報・量子生命研究センター	Simulations of stochastic quantum-classical-hybrid calculations for sensor materials with considering noise	Wataru Mizukami	Center for Quantum Information and Quantum Biology

28	2022-Cb-0021	結合分子誘起の相分離の分子動力学法による研究	福島 孝治	東京大学大学院総合文化研究科	Molecular dynamics study of phase separation induced by binding molecules	Koji Hukushima	Department of Basic Science, The University of Tokyo
29	2022-Ca-0037	HPCを基盤とした実験解析・シミュレーション・データ駆動科学の融合	星 健夫	鳥取大学大学院工学研究科機械宇宙工学専攻応用数理工学講座	HPC-based fusion of experiment analysis, simulation and data-driven science	Takeo Hoshi	Department of Applied Mathematics and Physics,Tottori University
30	2022-Ca-0097	ポリマー材料の周波数依存誘電特性に関するデータセットの構築	吉本 勇太	東京大学 大学院工学系研究科 機械工学専攻	Constructing a dataset of frequency-dependent dielectric properties of polymeric materials	Yuta Yoshimoto	Department of Mechanical Engineering, The University of Tokyo
31	2022-Ca-0109	摩擦の物理	松川 宏	青山学院大学理工学部	Physics of Friction	Hiroshi Matsukawa	Faculty of Science and Engineering, Aoyama Gakuin University
32	2022-Ca-0075	量子多体系における観測誘起相転移とカオス的ダイナミクス	手塚 真樹	京都大学大学院理学研究科物理学・宇宙物理学専攻	Measurement-induced phase transition and chaotic dynamics in quantum many-body systems	Masaki Tezuka	Department of Physics, Kyoto University
33	2022-Cb-0003	医療や産業への応用を指向した新規タンパク質の理論的設計	新井 宗仁	東京大学大学院総合文化研究科	Theoretical design of novel proteins for medical and industrial applications	Munehito Arai	Graduate School of Arts and Sciences, The University of Tokyo
34	2022-Ca-0001	熱伝導系が示す非平衡長距離相関	中野 裕義	東京大学物性研究所	Nonequilibrium long-range correlation in heat conduction systems	Hiroyoshi Nakano	The Institute for Solid State Physics, The University of Tokyo
35	2022-Ca-0046	分子動力学法を用いた熱硬化性樹脂多成分系における化学反応計算	大矢 豊大	東京理科大学先進工学部	Molecular dynamics simulation for chemical reactions in multicomponent systems of thermosetting resins	Yutaka Oya	Fuculty of Advanced Engineering, Tokyo University of Science
36	2022-Ca-0081	量子スピン系の低エネルギー状態に関する数値的研究	中野 博生	兵庫県立大学大学院理学研究科	Numerical study on low-energy states of quantum spin systems	Hiroki Nakano	Graduate School of Science, University of Hyogo
37	2022-Cb-0023	ガウス過程回帰を用いたゆらぎの緩和による臨界指数評価	尾関 之康	電気通信大学情報理工学研究科	Gauss process regression applied to relaxation of fluctuation for estimations of critical exponents	Yukiyasu Ozeki	Department of Applied Physics and Chemistry, The University of Electro-Communications
38	2022-Ca-0042	異方的相互作用を持つ蜂の巣格子Kitaev-Γ模型の動的性質	鈴木 隆史	兵庫県立大学　大学院工学研究科	Dynamical properties of the extended Kitaev-Γ model on a honeycomb lattice	Takafumi Suzuki	Graduate School of Engineering, University of Hyogo
39	2022-Ca-0110	疾患に関わるタンパク質間相互作用を阻害する新規抗体の理論的設計	新井 宗仁	東京大学大学院総合文化研究科	Theoretical design of novel antibodies that inhibit disease-related protein-protein interactions	Munehito Arai	Graduate School of Arts and Sciences, The University of Tokyo
40	2022-Ca-0035	大規模粒界構造探索と構造に基づく複数物性予測	藤井 進	大阪大学大学院工学研究科マテリアル生産科学専攻	Systematic searches for grain boundary structures and structure-based prediction of multiple properties	Susumu Fujii	Division of Materals and Manufucturing Science, Graduate School of Engineering, Osaka University
41	2022-Ca-0057	臨界現象研究のためのスケーリング解析の開発と応用	尾関 之康	電気通信大学情報理工学研究科	Development and applications of scaling analysis for critical phenomena	Yukiyasu Ozeki	Department of Applied Physics and Chemistry, The University of Electro-Communications
42	2022-Ca-0083	量子光に誘起された固体中協力現象の初期ダイナミクス理論	石田 邦夫	宇都宮大学工学部	Initial dynamics of photoinduced cooperativity by quantized light	Kunio Ishida	School of Engineering, Utsunomiya University
43	2022-Cb-0022	フラストレートした量子磁性体に対する熱ゆらぎの効果	下川 統久朗	沖縄科学技術大学院大学	Thermal effects on the frustrated magnets	Tokuro Shimokawa	Okinawa Institute of Science and Technology Graduate University
44	2022-Ca-0023	ハニカム格子スピン系における磁性の数値的研究	安田 千寿	琉球大学理学部	Numerical study of magnetism in the honeycomb-lattice spin systems	Chitoshi Yasuda	Department of Physics and Earth Sciences, University of the Ryukyus
45	2022-Ca-0101	フラストレートした量子磁性体に対する熱ゆらぎの効果	下川 統久朗	沖縄科学技術大学院大学	Thermal effects on quantum frustrated magnetisms	Tokuro Shimokawa	Okinawa Institute of Science and Technology Graduate University
46	2022-Ca-0099	テンソルくりこみ群によるランダムスピン系の研究	福島 孝治	東京大学大学院総合文化研究科	Tensor renormalization-group study of random spin systems	Koji Hukushima	Department of Basic Science, The University of Tokyo
47	2022-Ca-0033	新奇スピンネマティック相の数値的研究	坂井 徹	兵庫県立大学大学院理学研究科	Numerical Study on Novel Spin Nematic Phase	Toru Sakai	Graduate School of Science, University of Hyogo

48	2022-Ca-0117	センサー材料のためのノイズを考慮した確率的量子混合計算シミュレーション	水上 渉	大阪大学 量子情報・量子生命研究センター	Simulations of stochastic quantum-classical-hybrid calculations for sensor materials with considering noise	Wataru Mizukami	Center for Quantum Information and Quantum Biology
49	2022-Ca-0096	ランダム位相積状態法とニューラルネットワーク波動関数を使った量子多体系有限温度計算	飯高 敏晃	理化学研究所	Finite temperature calculation of quantum manybody system using random phase product state and neural network wavefunction	Toshiaki IITAKA	Riken
50	2022-Cb-0046	Ground state and dynamical properties of the J_1J_2K-Heisenberg model on the square lattice	ゴウケ マティアス	沖縄科学技術大学院大学	Ground state and dynamical properties of the J_1J_2K-Heisenberg model on the square lattice	Matthias Gohlke	Okinawa Institute of Science and Technology Graduate University
51	2022-Ca-0080	フラストレート磁性体における新奇秩序	川村 光	神戸大学分子フォトサイエンス研究センター	Novel order in frustrated magnets	Hikaru Kawamura	Molecular Photoscience Research Center, Kobe University
52	2022-Cb-0007	相転移キネティクスとポリアモルフィズム	渕崎 員弘	愛媛大学理工学研究科	Kinetics of phase transition and polyamorphism	Kazuhiro Fuchizaki	Department of Physics, Ehime University
53	2022-Cb-0055	分子動力学法によるペロブスカイト型酸化物粒界の研究	幾原 雄一	東京大学大学院工学系研究科総合研究機構	Molecular dynamics simulation of grain boundaries in perovskite oxide	Yuichi Ikuhara	Institute of Engineering Innovation, University of Tokyo
54	2022-Ca-0112	Ground state and dynamical properties of the J_1J_2K-Heisenberg model on the square lattice	ゴウケ マティアス	沖縄科学技術大学院大学	Ground state and dynamical properties of the J_1J_2K-Heisenberg model on the square lattice	Matthias Gohlke	Okinawa Institute of Science and Technology Graduate University
55	2022-Cb-0041	テンソルネットワークを用いたテンソルデータ解析	原田 健自	京都大学大学院情報学研究科	Tensor data analysis by tensor network	KENJI HARADA	Graduate school of Informatics, Kyoto University
56	2022-Ca-0017	クロソ化合物超イオン伝導体の無秩序化による相転移及び輸送機構の解明	佐藤 龍平	東北大学材料科学高等研究所	the study on super ionic conduction and phase transition by disordering of complex hydride	Ryuhei Sato	Advanced Institute for Materials Research, Tohoku University
57	2022-Ca-0038	相転移キネティクスとポリアモルフィズム	渕崎 員弘	愛媛大学理工学研究科	Kinetics of phase transition and polyamorphism	Kazuhiro Fuchizaki	Department of Physics, Ehime University
58	2022-Ca-0044	ブロックコポリマーの相分離構造の鎖交差禁止による効果の検討	萩田 克美	防衛大学校応用科学群応用物理学科	Effect of chain crossing prohibition on phase-separated structure of block copolymers	Katsumi Hagita	Department of Applied Physics, School of Applied Sciences, National Defense Academy
59	2022-Ca-0009	材料シミュレーションとインフォマティクスによる粒界アルカリイオン伝導機構の解析	中山 将伸	名古屋工業大学	Unveiling grain boundary alkaline ion conductivity by using materials simulation and	Masanobu Nakayama	Nagoya Institute of Technology
60	2022-D-0003	散逸のある超伝導回路素子におけるマイクロ波散乱の理論	山本 剛史	筑波大学	Theory of microwave scattering in a dissipative superconducting circuit element	Tsuyoshi Yamamoto	University of Tsukuba
61	2022-Bb-0004	テンソルネットワーク法によるKitaev模型のクエンチダイナミクスの研究	金子 隆威	早稲田大学 理工学術院総合研究所	Tensor-network study of the quench dynamics of the Kitaev model	Ryui Kaneko	Research Institute for Science and Engineering, Waseda University
62	2022-Cb-0033	フラストレート磁性体における新奇秩序	川村 光	神戸大学分子フォトサイエンス研究センター	Novelorderinfrustratedmagnets	Hikaru Kawamura	Molecular Photoscience Research Center, Kobe University
63	2022-Ba-0029	電子間クーロン相互作用を考慮したエリアシュベルグ方程式解法の実装	明石 遼介	量子科学技術研究開発機構	Solution of the Eliashberg equation with the electron-electron Coulomb interaction	Ryosuke Akashi	National Institutes for Quantum Science and Technology
64	2022-Bb-0007	荷電patchy粒子系における構造形成	寺尾 貴道	岐阜大学工学部	Structural formation of inverse patchy particles	Takamichi Terao	Faculty of Engineering, Gifu University
65	2022-Bb-0014	メタダイナミクス法と教師なし機械学習によるアモルファス一酸化シリコンの構造解析	灘 浩樹	鳥取大学	Structural Analysis of Amorphous Silicon Monoxide by a Metadynamics Method with Unsupervised Machine Learning	Hiroki Nada	Tottori University
66	2022-Ba-0060	異方的三角strip模型におけるgapless SPT相	押川 正毅	東京大学物性研究所	Gapless symmetry-protected topological phase in anisotropic triangle strips	Masaki Oshikawa	Institute for Solid State Physics, University of Tokyo
67	2022-Bb-0022	ブリージングカゴメ反強磁性体におけるトポロジカルカイラル秩序への磁場効果	青山 和司	大阪大学大学院理学研究科宇宙地球専攻	Magnetic field effect on a topological chiral order in breathing-kagome antiferromagnets	Kazushi Aoyama	Department of Earth and Space Science, Graduate School of Science, Osaka University

68	2022-Bb-0028	イジング計算機のための古典アルゴリズムの開発	白井 達彦	早稲田大学基幹理工学部	Quantum algorithm for an Ising machine	Tatsuhiko Shirai	School of Fundamental Science and Engineering, Waseda University
69	2022-Ba-0013	ボゾン系における量子多体傷跡状態の数値的研究	金子 隆威	早稲田大学 理工学術院総合研究所	Numerical study of quantum many-body scars in bosonic systems	Ryui Kaneko	Research Institute for Science and Engineering, Waseda University
70	2022-Ba-0017	動的架橋エラストマーのレオロジーシミュレーション	保田 侑亮	国立研究開発法人　産業技術総合研究所	Rheology Simulation of Dynamically Cross-linked Elastomers	Yusuke Yasuda	National Institute of Advanced Industrial Science and Technology
71	2022-Ba-0033	テンソルネットワーク法による普遍性クラスの同定	森田 悟史	慶應義塾大学大学院理工学研究科	Identification of universality classes by tensor network methods	Satoshi Morita	Faculty of Science and Technology, Keio University
72	2022-Ba-0045	磁性接合系におけるスピン輸送の数値研究	加藤 岳生	東京大学物性研究所	Numerical Study of Spin Transport in Magnetic Junctions	Takeo Kato	Institute for Solid State Physics, The University of Tokyo
73	2022-Ca-0079	テンソルネットワークを用いたテンソルデータ解析	原田 健自	京都大学大学院情報学研究科	Tensor data analysis by tensor network	KENJI HARADA	Graduate school of Informatics, Kyoto University
74	2022-Bb-0026	観測誘起相転移における普遍性クラスの数値的研究	藤 陽平	東京大学工学系研究科物理工学専攻	Numerical investigation of universality classes in measurement-induced phase transitions	Yohei Fuji	Department of Applied Physics, University of Tokyo
75	2022-Ba-0012	ホタル生物発光基質および関連分子の電子励起状態	樋山 みやび	群馬大学	Theoretical study for firefly bioluminescence substrate analogs and related molecules	Miyabi Hiyama	Gunma University
76	2022-Ba-0018	様々な架橋構造を持つ高分子網目の構造解析・力学物性シミュレーション	保田 侑亮	国立研究開発法人　産業技術総合研究所	Structural Analysis and Mechanical Properties Simulations of Polymer Networks with Various Network Structures	Yusuke Yasuda	National Institute of Advanced Industrial Science and Technology
77	2022-Ba-0022	ブリージングカゴメ反強磁性体で実現するトポロジカルカイラリティ秩序とその安定性	青山 和司	大阪大学大学院理学研究科宇宙地球専攻	Topological chirality order and its stability in breathing-kagome antiferromagnets	Kazushi Aoyama	Department of Earth and Space Science, Graduate School of Science, Osaka University
78	2022-Ba-0044	蓄電固体ホモ・ヘテロ界面におけるイオン伝導の分子動力学解析	小林 亮	名古屋工業大学	Molecular dynamics analyses of ion migration at electrode-electrolyte interfaces and grain boundaries in electrolytes	Ryo Kobayashi	Nagoya Institute of Technology
79	2022-Ba-0065	マルチスピンフリップ法を用いたイジング計算機の開発	白井 達彦	早稲田大学基幹理工学部	An Ising machine based on multi-spin flip method	Tatsuhiko Shirai	School of Fundamental Science and Engineering, Waseda University
80	2022-Bb-0005	ソフトマテリアルの秩序構造とそのダイナミクス，光学的性質の計算	福田 順一	九州大学　大学院理学研究院	Calculation of ordered structures, dynamics and optical properties of soft materials	Jun-ichi Fukuda	Faculty of Science, Kyushu University
81	2022-Ba-0006	荷電patchy粒子系における構造形成	寺尾 貴道	岐阜大学工学部	Structural formation of inverse patchy particles	Takamichi Terao	Faculty of Engineering, Gifu University
82	2022-Ba-0010	原子論的モデルによる永久磁石の保磁力機構研究	早坂 太志	物質・材料研究機構	Atomistic model study on the coercivity mechanism of permanent magnets	Hiroshi Hayasaka	National Institute for Materials Science
83	2022-Ba-0062	量子パイロクロア磁性体の研究	門脇 広明	東京都立大学 理学研究科 物理学専攻	quantum pyrochrole magnet	Hiroaki Kadowaki	Department of Physics, Tokyo Metropolitan University
84	2022-Ba-0066	情報統計力学におけるイジングモデルの解析	関 優也	慶應義塾大学	Analysis of Ising model in statistical-mechanical informatics	Yuya Seki	Keio University
85	2022-Ba-0003	空間構造をもつ一次元量子スピン系の数値的研究	利根川 孝	神戸大学大学院理学研究科	Numerical Study of the One-Dimensional Quantum Spin Systems	Takashi Tonegawa	Graduate School of Science, Kobe University
86	2022-Ba-0020	ANNポテンシャルを用いた大規模分子動力学シミュレーションによるシリカガラスの圧力誘起配位数変化の研究	若林 大佑	高エネルギー加速器研究機構物質構造科学研究所	Large-scale molecular-dynamics simulation of pressure-induced coordination change in silica glass with ANN potentials	Daisuke Wakabayashi	Institute of Materials Structure Science, High Energy Accelerator Research Organization (KEK)
87	2022-Ba-0030	ソフトマテリアルの秩序構造とそのダイナミクス，光学的性質の計算	福田 順一	九州大学　大学院理学研究院	Calculation of ordered structures, dynamics and optical properties of soft materials	Jun-ichi Fukuda	Faculty of Science, Kyushu University

88	2022-Ba-0034	極限環境下における破壊現象に関する分子動力学解析	三澤 賢明	福岡工業大学工学部知能機械工学科	Molecular dynamics study on destruction phenomena under extreme conditions	Masaaki Misawa	Department of Intelligent Mechanical Engineering, Fukuoka Institute of Technology
89	2022-Ba-0038	三角格子及びカゴメ格子上のハイゼンベルグ反強磁性体の熱力学特性，励起スペクトルの数値的研究	福元 好志	東京理科大学	Numerical studies on thermodynamics and excitation spectra in Heisenberg antiferromagnets on the triangular and kagome lattices	Fukumoto Yoshiyuki	Tokyo University of Science
90	2022-Bb-0003	空間構造をもつ一次元量子スピン系の数値的研究	利根川 孝	神戸大学大学院理学研究科	Numerical Study of the One-Dimensional Quantum Spin Systems	Takashi Tonegawa	Graduate School of Science, Kobe University
91	2022-Bb-0020	球体カゴメ系{W72V30}における磁化過程，帯磁率に対する大きなボンドランダムネスの効果の数値的研究	福元 好志	東京理科大学	Numerical study of the effect of large bond randomness on the magnetization process and magnetic susceptibility in the spherical Kagome system {W72V30}	Fukumoto Yoshiyuki	Tokyo University of Science
92	2022-Ca-0092	グリシンナノ結晶が示す多彩な結晶形の大規模メタダイナミクス計算解析	灘 浩樹	鳥取大学	Analysis of Various Crystal Forms of Glycine Nanocrystals by Large-Scale Metadynamics Simulations	Hiroki Nada	Tottori University
93	2022-Ca-0121	機械学習を用いた代替燃料の低温酸化反応モデル構築	李 敏赫	東京大学大学院工学系研究科機械工学専攻	Development of the Low-Temperature Oxidation Model for Alternative Fuels Using Machine Learning	Minhyeok Lee	Department of Mechanical Engineering, The University of Tokyo
94	2022-Ba-0064	観測誘起相転移における普遍性クラスの数値的研究	藤 陽平	東京大学工学系研究科物理工学専攻	Numerical investigation of universality classes in measurement-induced phase transitions	Yohei Fuji	Department of Applied Physics, University of Tokyo
95	2022-Ba-0031	加工用触媒としての機能性グラフェンシートの電子状態と反応性評価	有馬 健太	大阪大学 大学院 工学研究科	Understanding electronic structures and reactivity of functional graphene sheets toward machining catalyst	Kenta Arima	Graduate School of Engineering, Osaka University
96	2022-Ba-0025	１次元フラストレート量子スピン系の数値的研究	飛田 和男	埼玉大学大学院理工学研究科物質科学部門	Numerical Study of One Dimensional Frustrated Quantum Spin Systems	Kazuo Hida	Division of Material Science, Graduate School of Science and Engineering, Saitama University
97	2022-Ba-0057	非整合積層系の新奇物性：新物質の探索と電子状態解析	苅宿 俊風	物材機構	Novel phenomena in mismatched multilayer systems: Search for new candidate materials and analysis of electronic structures	Toshikaze Kariyado	NIMS
98	2022-Ba-0059	2DMATによる２次元ホウ素シートボロフェンの構造解析	高山 あかり	早稲田大学	Structure analysis of borophene by using 2DMAT	Akari Takayama	Waseda University
99	2022-Ba-0054	反転対称なハバード模型における多重Q秩序の磁気構造	内田 尚志	北海道科学大学	Magnetic structures of multiple-Q orders in inversion-symmetric Hubbard models	Takashi Uchida	Hokkaido University of Science
100	2022-Ba-0048	振動数解析に基づくLennard-Jonesクラスターの準安定構造マップ	小野 頌太	東北大学金属材料研究所	Metastable structure map of Lennard-Jones cluster based on vibrational frequency analysis	Shota Ono	Tohoku University
101	2022-Ca-0122	マクロな固体間摩擦の形状依存性	大槻 道夫	大阪大学基礎工学研究科	Shape dependence of macroscopic friction between solids	Michio Otsuki	Graduate school of engineering science
102	2022-A-0003	β''-(ET)$_2X$電荷移動錯体の感受率および超伝導に関するFLEXを用いた理論研究	Jeschke Harald	岡山大学異分野基礎科学研究所	FLEX computation of susceptibility and superconductivity of β''-(ET)$_2X$ charge transfer salts	Harald Jeschke	Research Institute for Interdisciplinary Science Okayama University
103	2022-A-0005	多波動力学的回折理論によるタンパク質結晶のX線回折強度の計算	沖津 康平	東京大学 大学院工学系研究科	Calculation of X-ray difffraction intensities from protein crystals based on the n-beam dynamical diffraction therory	Kouhei Okitsu	School of Engineering, University of Tokyo
104	2022-A-0007	ナノカーボン複合構造の分子動力学	小林 慶裕	大阪大学大学院工学研究科	Molecular dynamics of nanocarbon heterostructure	Yoshihiro Kobayashi	Graduate School of Engineering, Osaka University
105	2022-A-0009	トポロジカルネマティック超流動の非軸対称渦	正木 祐輔	東北大学	Non-axisymmetric vortices in topological nematic superfluids	Yusuke Masaki	Tohoku University
106	2022-A-0011	アクリレートポリマーにおける結合水に関する分子シミュレーション解析	金 鋼	大阪大学大学院基礎工学研究科	Molecular dynamics simulations for interfacial water in acrylate polymers	Kang Kim	Graduate School of Engineering Science, Osaka University
107	2022-A-0012	高密度コロイドガラスの脱ガラス化の起源とダイナミクス	柳島 大輝	京都大学理学研究科物理学・宇宙物理学専攻	Origin and dynamics of devitrification in dense colloidal glasses	Taiki Yanagishima	Division of Physics and Astronomy, Graduate School of Science, Kyoto University

108	2022-A-0015	高次元量子ウォークのダイナミクス	羽田野 直道	東京大学生産技術研究所	Dynamics of Quantum Walks in Higher Dimensions	Naomichi Hatano	Institute of Industrial Science, The University of Tokyo
109	2022-A-0020	多孔性金属錯体内における分子拡散の分子動力学シミュレーション	細野 暢彦	東京大学大学院工学系研究科応用化学専攻	Molecular Dynamics Simulation of Molecular Diffusion in Metal-Organic Frameworks	Nobuhiko Hosono	Department of Applied Chemistry, Graduate School of Engineering, The University of Tokyo
110	2022-Ba-0053	ゆっくり地震から高速地震への遷移時刻の見積もりとその数理的意義	鈴木 岳人	青山学院大学	Estimation of the transition time from slow to fast earthquakes and its mathematical implications	Takehito Suzuki	Aoyama Gakuin University
111	2022-Bb-0016	透水係数の空間変化に基づく前震－本震系列の繰り返し周期の決定	鈴木 岳人	青山学院大学	Determining the period of the mainshock repetition with foreshocks in terms of permeability profile	Takehito Suzuki	Aoyama Gakuin University

2022年度　CCMSスパコン共用事業枠課題一覧 / Supercomputing Consortium for Computational Materials Science Project List of Supercomputer System 2022

※共同利用ではなく共用事業の実施課題一覧。所属は申請時のデータ

前期課題 / The first half term

No.	課題名	氏名	所属	Title	Name	Organization
1	グラフニューラルネットワークによる分子動力学サンプリングの加速	芝　隼人	東京大学 情報基盤センター	Graph neural network accelerated MD sampling	Hayato Shiba	Information Technology Center, University of Tokyo
2	擬一次元有機物質TM系分子性導体に対する第一原理有効ハミルトニアンの網羅的解析	吉見 一慶	東京大学 物性研究所	A systematic *ab initio* study of quasi-one-dimensional molecular conductors TM salts	Kazuyoshi Yoshimi	Institute for Solid State Physics, University of Tokyo
3	大規模電子状態計算による有機光デバイスの励起子物性の解析	藤田　貴敏	量子科学技術研究開発機構	Exciton Properties in Organic Optoelectronic Devices from Large-Scale Electronic Structure Calculations	Takatoshi Fujita	National Institutes for Quantum Science and Technology
4	高温超伝導の機構解析	今田　正俊	早稲田大学/豊田理化学研究所	Analysis on Superconducting Mechanism of high-Tc Superconductors	Masatoshi Imada	Waseda University/Toyota Physical and Chemical Research Institute
5	省エネルギー次世代半導体デバイス開発のための量子論マルチシミュレーション	押山 淳	名古屋大学 未来材料・システム研究所	Quantum-theory-based multiscale simulation for next-generation power devices	Atsushi Oshiyama	Nagoya University
6	分子動力学シミュレーションを用いた長鎖高分子ブレンド相溶性の効率的な計算手法の開発	松林 伸幸	大阪大学 大学院基礎工学研究科 物質創成専攻 化学工学領域	Development of an efficient method for calculating miscibility of long-chain polymer blends using molecular dynamics simulations	Nobuyuki Matubayasi	Division of Chemical Engineering, Graduate School of Engineering Science, Osaka University
7	磁性界面における歪み効果	合田 義弘	東京工業大学 物質理工学院	Strain effects at magnetic interfaces	Yoshihiro Gohda	Tokyo Institute of Technology
8	富岳電池課題(B-1:燃料電池の電極界面反応)	杉野 修	東京大学 物性研究所	Fugaku Battery & Fuel-Cell (B-1：Electrode interface reaction in fuel cell)	Osamu Sugino	Institute for Solid State Physics, University of Tokyo
9	磁性材料を対象とした基盤的シミュレーションコードの開発	福島 鉄也	東京大学 物性研究所	Development of fundamental simulation code for magnetic materials	Tetsuya Fukushima	Institute for Solid State Physics, University of Tokyo
10	大規模計算とデータ駆動手法による高性能永久磁石の開発	三宅　隆	産業技術総合研究所	Development of high-performance permanent magnets by large-scale simulation and data-driven approach	Takashi Miyake	National Institute of Advanced Industrial Science and Technology
11	新規光触媒化合物の母構造および添加物に対するデータ駆動型研究(「富岳」を活用した革新的光エネルギー変換材料の実現)	藤井 幹也	奈良先端科学技術大学院大学	Data driven analysis for impurity effects on photocatalysts	Mikiya Fujii	Nara Institute of Science and Technology
12	第一原理計算による水素製造半導体光触媒の理論的研究	天能 精一郎	神戸大学大学院 科学技術イノベーション研究科/システム情報学研究科	Theoretical study of hydrogen-evolution semiconductor photocatalysts using first-principles calculations	Seiichiro L. Ten-no	Kobe University

後期課題 / The second half term

No.	課題名	氏名	所属	Title	Name	Organization
1	グラフニューラルネットワークによる液体分子動力学代理モデルの開発	芝　隼人	東京大学 情報基盤センター	Development of surrogate model for liquid molecular dynamics based on graph neural networks	Hayato Shiba	Information Technology Center, University of Tokyo
2	ベイズ最適化による有効模型推定ツールの開発	吉見 一慶	東京大学 物性研究所	Development of an effective model estimation tool by Bayesian optimization	Kazuyoshi Yoshimi	Institute for Solid State Physics, University of Tokyo

3	大規模電子状態計算と時間分解分光による有機光デバイスの励起子ダイナミクス	藤田　貴敏	量子科学技術研究開発機構	Exciton Dynamics in Organic Optoelectronic Devices from Large-Scale Electronic Structure Calculations and Time-Resolved Spectroscopy	Takatoshi Fujita	National Institutes for Quantum Science and Technology
4	多層系銅酸化物の第一原理系統解析	今田　正俊	早稲田大学/豊田理化学研究所	Systematic Analyses on Multi—Layer Copper Oxide Superconductors	Masatoshi Imada	Waseda University/Toyota Physical and Chemical Research Institute
5	省エネルギー次世代半導体デバイス開発のための量子論マルチシミュレーション	押山 淳	名古屋大学 未来材料・システム研究所	Quantum-theory-based multiscale simulation for next-generation power devices	Atsushi Oshiyama	Nagoya University
6	高性能磁性材料のマテリアルデザイン	福島 鉄也	東京大学 物性研究所	Materials design of high performance magnetic materials	Tetsuya Fukushima	Institute for Solid State Physics, University of Tokyo
7	大規模計算とデータ駆動手法による高性能永久磁石の開発	三宅 隆	産業技術総合研究所	Development of high-performance permanent magnets by large-scale simulation and data-driven approach	Takashi Miyake	National Institute of Advanced Industrial Science and Technology

The Institute for Solid State Physics (ISSP), The University of Tokyo

Address	5-1-5 Kashiwanoha, Kashiwa, Chiba, 277-8581, Japan
Phone	+81-4-7136-3207
Home Page	https://www.issp.u-tokyo.ac.jp